Universidad de Málaga

Facultad de Ciencias

Escuela de Doctorado

TESIS DOCTORAL

Design and Synthesis of Nanostructures to Study the Specific Molecular Recognition and Effector Cell Activation in the Immunological Responses to Amoxicillin.

Programa de doctorado: Química y Tecnologías Químicas. Materiales and Nanotecnología

Autor: Amene Tesfaye Ayane

Director: Dr María Isabel Montañez Vega

Málaga, 2021

This project has received funding from the European Union's Horizon 2020 research and innovation programme under the Marie Skłodowska-Curie, grant agreement No 7131721.

UNIVERSIDAD
DE MÁLAGA

AUTOR: Amene Tesfaye Ayane

https://orcid.org/0000-0003-0482-8895

EDITA: Publicaciones y Divulgación Científica. Universidad de Málaga

UNIVERSIDAD DE MÁLAGA

UNIÓN EUROPEA
Fondo Europeo de Desarrollo Regional

bionand
Centro Andaluz de Nanomedicina & Biotecnología

Doña **María Isabel Montañez Vega**, Doctora en Química e Investigadora del Centro Andaluz de Nanomedicina y Biotecnología (BIONAND) y del Instituto de Investigación Biomédica de Málaga (IBIMA),

CERTIFICA:

Que el trabajo que presenta Don **Amene Tesfaye Ayane**, con el título **"Design and Synthesis of Nanostructures to Study the Specific Molecular Recognition and Effector Cell Activation in the Immunological Responses to Amoxicillin",** adscrito al proyecto NANOMEDPhD (Nanomedicine Doctoral Programme) financiado por el programa Horizonte 2020 en investigación e innovación de la UE con Marie Skłodowska-Curie (No 7131721), ha sido realizado en el Centro Andaluz de Nanomedicina y Biotecnología-BIONAND bajo mi DIRECCIÓN y considero que tiene el contenido y rigor científico necesarios para ser sometido a juicio del tribunal que ha nombrado la Universidad de Málaga para optar al grado de Doctor.

Y para que así conste,

firmo el presente certificado en Málaga, a 28 de Septiembre de 2021.

Fdo. María Isabel Montañez Vega

UNIVERSIDAD DE MÁLAGA

UNIÓN EUROPEA
Fondo Europeo de Desarrollo Regional

bionand
Centro Andaluz de Nanomedicina & Biotecnología

Don **Ezequiel Pérez-Inestrosa de Villatoro**, Doctor en Química, Catedrático de Universidad del Departamento de Química Orgánica de la Universidad de Málaga,

CERTIFICA:

Que el trabajo que presenta Don **Amene Tesfaye Ayane**, con el título **"Design and Synthesis of Nanostructures to Study the Specific Molecular Recognition and Effector Cell Activation in the Immunological Responses to Amoxicillin"**, ha sido realizado en el Centro Andaluz de Nanomedicina y Biotecnología-BIONAND bajo mi TUTORIZACIÓN y considero que tiene el contenido y rigor científico necesario para ser sometido a juicio del tribunal que ha nombrado la Universidad de Málaga para optar al grado de Doctor.

Y para que así conste,

firmo el presente certificado en Málaga, a 28 de Septiembre de 2021.

Fdo. Ezequiel Pérez de Inestrosa Villatoro

UNIVERSIDAD DE MÁLAGA

UNIÓN EUROPEA
Fondo Europeo de Desarrollo Regional

bionand
Centro Andaluz de Nanomedicina & Biotecnología

Yo, **Amene Tesfaye Ayane**, estudiante del programa de doctorado "Química y Tecnologías Químicas. Materiales y Nanotecnología" de la Universidad de Málaga,

DECLARO QUE:

Soy autor del presente trabajo de investigación cuyo título es **"Design and Synthesis of Nanostructures to Study the Specific Molecular Recognition and Effector Cell Activation in the Immunological Responses to Amoxicillin"**, que ha sido realizado en el Centro Andaluz de Nanomedicina y Biotecnología-BIONAND bajo la dirección de Dña. **María Isabel Montañez Vega**, y la tutela de D. **Ezequiel Pérez-Inestrosa de Villatoro,** para la obtención del título de Doctor por la Universidad de Málaga.

La tesis presentada es una obra original que no infringe los derechos de propiedad intelectual ni los derechos de propiedad industrial u otros, conforme al ordenamiento jurídico vigente (Real Decreto Legislativo 1/1996, de 12 de abril, por el que se aprueba el texto refundido de la Ley de Propiedad Intelectual, regularizando, aclarando y armonizando las disposiciones legales vigentes sobre la materia), modificado por la Ley 2/2019, de 1 de marzo.

Igualmente asumo, ante la Universidad de Málaga y ante cualquier otra instancia, la responsabilidad que pudiera derivarse en caso de plagio de contenidos en la tesis presentada, conforme al ordenamiento jurídico vigente.

Y para que así conste, firmo en Málaga, a 28 de septiembre de 2021.

Fdo. Amene Tesfaye Ayane

Parts of the Contents Included in this Thesis Resulted in the Following Scientific Outcomes.

Publications:

1. **A. Tesfaye**, A. Rodríguez-Nogales, S. Benedé, T.D. Fernández, J.L. Paris, M.J. Rodriguez, I.M. Jiménez-Sánchez, G. Bogas, C. Mayorga, M.J. Torres, M.I. Montañez, Nanoarchitectures for Efficient IgE Cross-Linking on Effector Cells to Study Amoxicillin Allergy, Allergy. 2021;00:1–11.
2. N. Molina, A. Martin-Serrano, T.D. Fernandez, **A. Tesfaye**, F. Najera, M.J. Torres, C. Mayorga, Y. Vida, M.I. Montañez, E. Perez-Inestrosa, Dendrimeric antigens for drug allergy diagnosis: A new approach for basophil activation tests, Molecules. 23 (2018) 1–13.

Communication to Conferences:

1. María Isabel Montañez, **Amene Tesfaye**, Alba Rodriguez, Sara Benedé, Isabel María Jiménez, María José Torres. "Nanoarchitectures based on Dendrimers for the Diagnostic Approach of Drug Allergy" in the "Séptimo Encuentro sobre Dendrímeros" (EDEN7)13th-14th February 2020 in Málaga, Oral communication.
2. **Amene Tesfaye**, Sara Benedé ,Alba Rodriguez, Isabel María Jiménez, María José Torres, María Isabel Montañez. Flexible and rigid dendrimer- based nanostructures for cell effector studies in the context of amoxicillin allergy" in the European-Academy-of-Allergy-and-Clinical-Immunology (EAACI) Digital Congress. 6th-8th June 2020 in London, Oral communication. Published on Allergy. 2020;75 (Suppl. 109):5–99. https://doi.org/10.1111/all.14504
3. **Amene Tesfaye**, Sara Benedé, Alba Rodriguez, Isabel María Jiménez, María José Torres, María Isabel Montañez. Identifying the structural requirement in the cellular degranulation of allergic reactions to Betalactam antibiotics using polymeric bidendron antigen nanoarchitectures. Presented on the e-POSTER section of the digital platform of the European-Academy-of-Allergy-and-Clinical-Immunology (EAACI) Hybrid Congress 2021 in Krakow, Poland

4. Patent:

- PCT/ES2021/070103 (12th February 2021) **A. Tesfaye**, M.I. Montañez, C. Mayorga, Alba. Rodríguez, T.D. Fernández, E. Pérez-Inestrosa, Y. Vida, M.J. Torres. Nanoestructuras para el diagnóstico de alergias antibióticos betalactámicos, procedimientos de obtención y aplicaciones.

Funding information

The Present Study has been Supported by the Following Funding:

- Marie Skłodowska-Curie Programme, grant agreement No 7131721, funded from the European Union's Horizon 2020 research and innovation programme. To the author of the present thesis
- PI17/01237: "Application of synthetic nanoarchitectures to the study of basophil activation mechanisms and to the diagnosis of allergic reactions to amoxicillin" funded by the Spanish public health research institute (Instituto de Salud Carlos III, ISCIII); grants cofunded by European Regional Development Fund (ERDF), for developing the project. Principal Investigator: M.I. Montañez.
- RETICS ARADyAL RD16/0006/0001: Asthma, Adverse Drug Reactions and Allergy Network, which is a thematic network of translational cooperative health research (RETICS), funded by ISCIII. Coordinator: M.J. Torres

Acknowledgement

Consistency of effort over the long run is everything.

Angela Duckworth

My journey to this end of my life has been long and full of life adventures: the good and the bad. I consider myself very lucky to have nice and helpful people all along my ways. Finding myself at this junction of life would have not been possible without your contribution to my personal and professional development. For that, I immensely indebted and would like to say thank you to all friends and family who have positively contributed towards my achievement.

I could not find words that better satisfy to express the great contributions of my advisor Dr María Isabel Montañez for her unreserved guidance and friendly handling throughout the study period. This work would have not been completed without the great contribution of our group in the Hospital (thankful to all who participated) and Dr Sara (Madrid) and Dr Alba (Granada). I would also express my gratefulness to Professor Ezequiel Pérez-Inestrosa for being my academic tutor.

If this ride of my life has taught me anything, it is this: challenge in routine work is enormous and overcoming them requires primly not taking the work-related stress to home and bed. The other is enjoying every moment of life and sharing ideas with good people around. Any ride is good with people whom you hang on until the top will come again and shares life. In this regard, mentioning some friends and colleague individually seems important: Dr Noemi, Dr John, Dr Jonas, Dr Juan, Vladimir, Ashish, Anjara, Violeta, Desi, Patri, and Claudia, I thank you immensely for the good working environment in Bionand and memorable stay in Malaga. The recollections we shared will stay with me for life. I would like to thank all my colleagues from COFUND, all members of Professor Ezequiel Pérez-Inestrosa group and Bionand administrative staffs, specially Ainhoa, your contribution to settlement in Malaga was unforgettable. Maria (NMR) I thank you very much for being such a positive person to me in all my request for your help.

Dedication

To :

Getachew,

Meron,

Mama,

Butushu

Table of Contents

List of Tables

List of Figures

List of Abbreviations

ADR	Adverse Drug Reactions
ANOVA	One-way Analysis of Variance
AX	Amoxicillin
AXO	Amoxicilloyl
AXO-Bu	Amoxicilloyl -butylamine
BAT	Basophil Activation Test
BiAns	Bidendron Antigens
Boc	*Tert*-Butoxycarbonyl
BP	Benzylpenicillins
BPO	Benzylpenicilloyl
BP-OL	Benzylpenicilloyl-octa-L-Lysine
BSA	Bovine Serum Albumin
CDI	1,1′- Carbonyldiimidazole
CLV	Clavulanic Acid
CuAAC	Copper (I) -Catalyzed Azide/Alkyne Cycloaddition
DAT	Direct Antiglobulin Test
DCC	Dicyclohexylcarboiimide
DDC	Sodium Diethyldithiocarbamate
DeAns	Dendrimeric Antigens
DHRs	Drug Hypersensitivity Reactions
DNP	Dinitrophenyl
DOSY	Diffusion-Ordered Spectroscopy
EDC	1-ethyl-3-(3-dimethylaminopropyl Carboiimide)
ELISA	Enzyme-linked Immunosorbent Assay
ENDA	European Network for Drug Allergy
$Fc_{\varepsilon}RI$	High-Affinity Receptor
FEIA	Fluorescence Enzyme Immunoassay
G	Generation (Dendrimer)
GPC	Gel Permeation Chromatography
HOBt	1-Hydroxybenzotriazole Hydrate

HSA	Human Serum Albumin
iBuCOCl	Isobutyl chloroformate
IAT	Indirect Antiglobulin Test
IgE	Immunoglobulin E
IgG	Immunoglobulin G
IR	Immediate Reaction
K-S	Kolmogorov-Smirnov
LC	Liquid Chromatography
MALDI-TOF-MS	Matrix-Assisted Laser Desorption Ionization-Time of Flight Mass Spectrometry
MCs	Mast Cells
MDM	Minor Determinants Mixtures
MoAbs	Monoclonal Antibodies
MW	Molecular Weight
NHS	N-Hydroxy Succinimide
NIRs	Non-Immediate Reactions
NMM	N-methyl Morpholine
OpNS TEM	Optimized Negative-staining Transmission Electron Microscopy
PAMAM	PolyAmidoAmine
PEG	Polyethylene Glycol
PI	Pharmacological Interaction
PPh_3	Triphenylphosphine
PPL	Penicilloyl- poly-L-Lysine
PLL	Poly-L-Lysine
PPI	Polypropylenimine
RAST	Radioallergosorbent Test
RBL	Rat Basophil Leukemia
RIA	Radioimmunoassay
SAR	Structural Activity Relationship
SDS-PAGE	Sodium Dodecyl Sulfate-Polyacrylamide Gel Electrophoresis
SEC	Size Exclusion Chromatography
SEFT	Spin Echo Fourier Transform
SJS	Stevens-Johnson Syndrome

TBTA	Tris (benzyltriazoylmethyl) Amine
TsCl	4-toluenesulfonyl Chloride
TCEP	Tris (2-carboxyethyl) Phosphine
THPTA	Tris (3-hydroxypropyltrizolylmethyl) Amine
TLC	Thin-layer Chromatography
WHO	World Health Organization

Outline of the Thesis

This thesis is about the study of specific molecular recognition and modulation of the immunological responses to amoxicillin using synthetic nanostructures. The whole contents of the thesis are organized into seven chapters, among which, chapter three, four and five correspond to results and discussions of the conducted research.

The first chapter gives a general introduction to drug allergy, classifications, and diagnostic approaches. It also discusses the existing diagnostic techniques and their limitations and how nanostructures can be applied for the development of new tests or improving the existing ones. The chapter also briefly outlines the synthetic strategies in obtaining dendrimers and related structures as a promising scaffold to gain a better understanding of the structural requirement for effector cell degranulation in the case of the allergic reaction to amoxicillin.

The second chapter describes the hypothesis, justification, and objectives of the study. In this section, the general hypothetical aspiration of the current work and its scientific and theoretical explanations are coined based on previous knowledge documented in the scientific literature. To settle our hypothesis and attain the anticipated result, the general and specific objectives are enumerated in sequential order to help approach our goals.

The third chapter deals with a set of dendrimeric structures with an exponentially diverging number of antigenic determinants and a linear increase in size. The chapter gives the details of the synthesis, characterization, and biological evaluation of the structures. In the end, the effect of the variation in the number of antigenic determinants and size are discussed with the background of cell assays used for evaluation.

The fourth chapter focused on bidendronized structures constructed based on different length polymeric spacers and terminally displaying the same number of antigenic determinants. The design, synthesis, characterization, and immunological evaluation of the structures are discussed.

In chapter five, different design of bidendronized structures, with simultaneous variation in the length of the polymeric spacers and the number of antigenic determinants, through a more efficient synthetic strategy is described. Likewise, the synthetic strategy, characterization and biological evaluation are discussed in detail.

The experimental section of this thesis is compiled in chapter six. In this chapter, the materials and methods used to obtain the findings described in this thesis are detailed. Under the subsection of the methods, the synthetic strategies used to obtain every intermediate and final product are given.

The general conclusions of the work and future perspectives, highlighting short- and long-term activities as recommendations, for the complete realisation of the sought objectives, are given in chapter seven. To end, all the supporting information are attached as an Appendix.

Chapter 1: General Introduction

1.1. Background

An adverse drug reaction (ADR) is defined by the World Health Organization (WHO) as a noxious, unintended and undesired response to medicine that occurs when taken at a normal dose used for treatment, diagnosis and/or prophylaxis [1]. This definition excludes adverse drug events, therapeutic failure, accidental poisoning, and drug abuse [2]. It is one of the common problems in the clinical practice affecting close to 25 % and resulting in serious reactions in 7-13 % of patients [3]. The ADRs can be classified into two broad groups: Predictable (type A) and unpredictable (type B) reactions (Figure 1.1). The predictable type is the most common form of reactions that comprise up to 80 % of all ADR and usually linked to the pharmacological actions of the drugs. The type B reactions are generally not related to the pharmacological actions of the drugs and may include immunologically mediated drug hypersensitivity (drug allergy) or idiosyncratic reactions that are not immune-mediated [3–5].

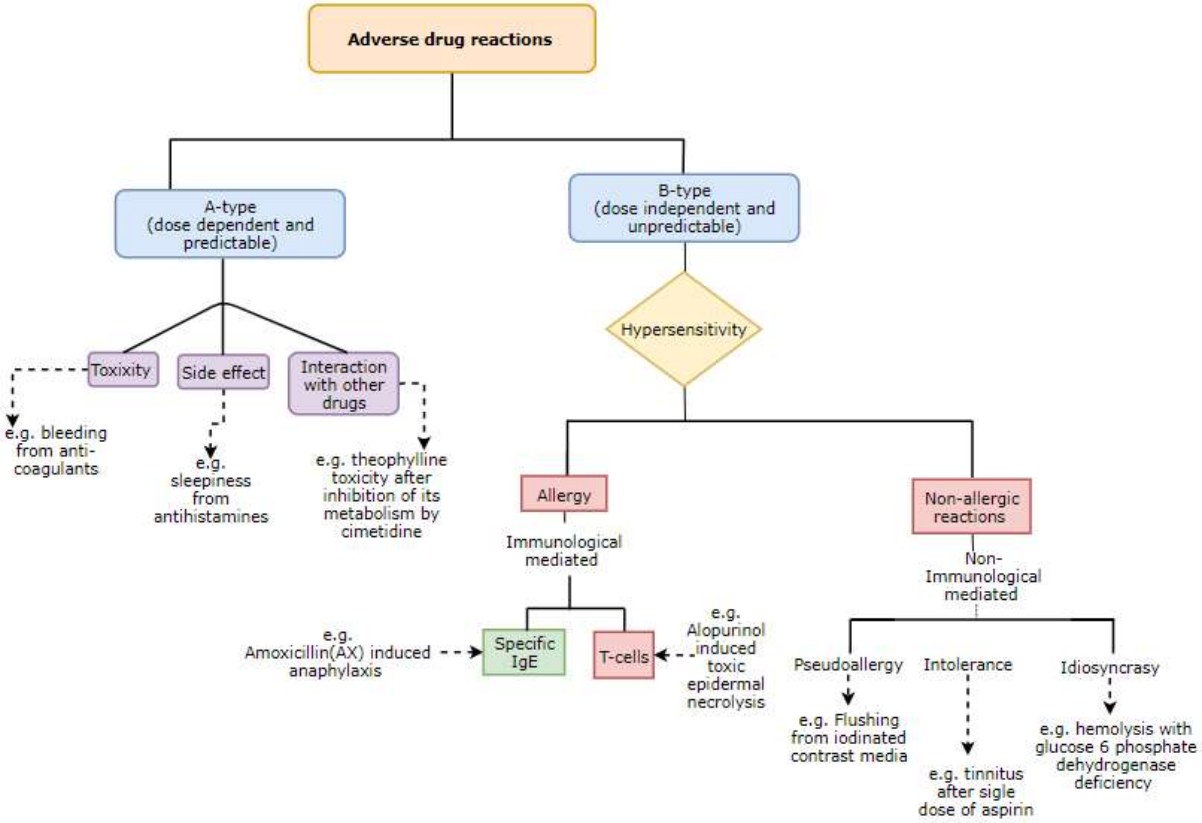

Figure 1. 1. Classification of ADRs. Adapted from [6].

Drug hypersensitivity reactions (DHRs) are the adverse effects of pharmaceutical formulations (including active drugs and excipients) that clinically resemble allergy. DHRs belong to type B ADRs [6]. Drug allergy is a subcategory of an unpredictable type of ADR that encompasses

immunologically mediated DHRS. It accounts for 5-10 % ADR that affects patient quality of life, increase morbidity, and might lead to mortality [3,4].

Table 1.1. Mechanisms of drug interaction with the immunological system in different types of DHRs [7]

	Hapten Hypothesis	**P-i Concept**	**Pseudoallergic**
	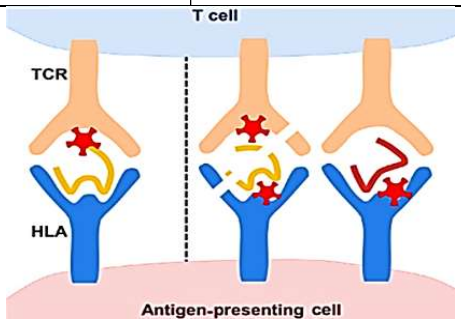		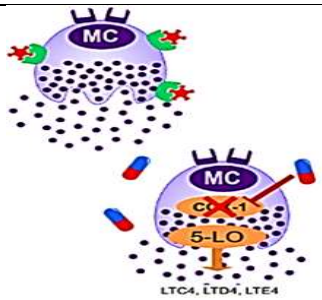
Types of Reactions	Immediate(IR)/ non-immediate (NIR)	NIR	IR
Clinical Entities	Urticaria, Anaphylaxis, Maculopapular exanthema, severe cutaneous adverse reactions	Maculopapular exanthema, severe cutaneous adverse reactions, drug-induced liver injury	Urticaria, Anaphylaxis, Angioedema, Respiratory symptoms
Drugs	β-lactams, Sulphanilamides, Metamizole, Radiocontrast media, Neuromuscular, blocking agent, Antineoplastics	β-lactams, Sulphanilamides, Metamizole, Quinolones, Radiocontrast media, Vancomycin, Anticonvulsants, Abacavir, Antineoplastics	Nonsteroidal anti-inflammatory drugs, Quinolones, Radiocontrast media, Neuromuscular blocking agent, Vancomycin

MC, mast cells; 5-LO, 5-lipoxygenase; LTC4, leukotriene C4; LTD4, leukotriene D4; LTE4, leukotriene E4; COX-1, cycloxigenase-1.

1.2. Immunochemical Basis of DHRs

The specific interaction of the immune system with the drugs or their metabolites could cause allergic reactions [8]. Based on the immunochemical basis, the DHRs are classified as allergic-immune, the pharmacological interaction (PI) and pseudo-allergic forms (Table 1.1) [7,9]. The allergic/immune stimulation is explained by the hapten hypothesis, which states that most drugs are too small with a molecular weight (MW) of less than 1000 Da, which cannot by themselves elicit an immune response. The immunogenic potential is only gained when the small molecules form a covalent conjugate with the tissue or plasma protein forming the drug-protein or metabolite-protein complex to create a complete antigen responsible for stimulation of the immune response (Figure 1. 2) [10,11].

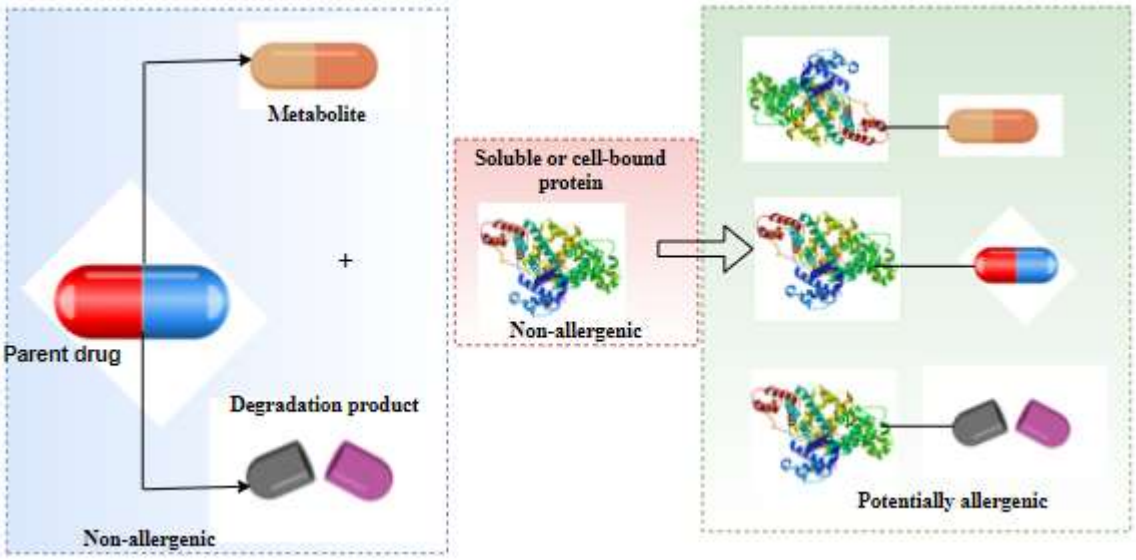

Figure 1. 2. Diagrammatic representation of potentially allergenic hapten-protein complexes that may form from the parent drug and/or its metabolite (s) and degradative product (s). Adapted from [13].

The P-i hypothesis, on the other hand, proposes that the drugs can directly stimulate the immune system by defying the formation of covalent hapten-carrier to gain immunogenicity, which is a well-established dogma in immunology [12]. It hypothesises that the non-covalent bonds (hydrogen bonds, electrostatic interactions, and Van der Waals forces) as responsible binding forces to the immune receptor proteins directly. This concept looks well-suited to explain the certain *off-target effect* of drugs and could be regarded as a bridge between immunology and pharmacology [9].

The pseudo-allergic, like that of the P-i, states that interaction of the drugs with receptors or enzymes of the effector cells occurs without covalently binding to the protein and involvement of the adaptive immune mechanism. This interaction will enhance the level of inflammatory mediators and leads to the pharmacological *off-target* activity of certain drugs [9].

1.3. Immunological and Clinical Classification of Drug Allergic Reactions

After the immunochemical sensitization phase with the culprit drugs, the second phase involves the T cells and antibodies to initiate the elicitation phase, corresponding to type I to IV immune reactions according to the Gell and Coombs classification, summarized in Table 1.2. The most frequently occurring drug allergies can be designated in type I and IV; whereas type II and III happen less frequently [11,13].

Type I reactions, immediate hypersensitivity reactions, comprise the Immunoglobulin E (IgE) mediated release of histamine and leukotrienes from the basophils and mast cells (MCs). Of all the four Gell and Coombs conception, this has depicted the most clear-cut immunopathological correlation. Hay fever or allergic asthma is the classical example of this class of reactions [14]. The immunological mechanism is triggered when a multivalently presented antigen reacts with the IgE system of the high-affinity receptor ($Fc_{\varepsilon}RI$) on the surface MCs and circulating basophils, resulting in intricate crosslinking of the $Fc_{\varepsilon}RI$ [15–17]. These crosslinking events initiate cascades of down cell signals that facilitate the release of preformed cytokines, chemokines, vasoactive amines, and other mediators to elicit acute phase of allergic responses [14,16].

Type II reactions, cytotoxic hypersensitivity reactions, are mediated by Immunoglobulin G (IgG) or IgE antibodies bound to cell surface antigens. An example is drug-induced hemolytic anemia. The primary mechanism is through direct activation of the macrophages, eosinophils and neutrophils that are linked to immunoglobulin coated target cells (basically the blood cells) through the Fcγ-receptor of the antibody. Alternatively, it could also occur through the complement-induced lysis and induction of the membrane by either binding to C3b or C3d on the target cells or C5b-C9 membrane complex [18,19].

Type III reactions, immune-complex reactions, involve the deposit of circulating antigen-antibody immune complexes at the postcapillary venules. The existence of these complexes coupled with recruited polymorphonuclear leukocytes by the complement activation results in

tissue injury and affect cellular functions. An example of this group of reaction includes serum sickness [14].

Type IV reactions, cell-mediated reactions, are delayed hypersensitivity reactions mediated by T-lymphocytes and macrophages rather than by antibodies. Several organ-specific autoimmune disorders are falling into this class of reactions. An example of this is contact dermatitis from poison ivy or nickel allergy [19].

Table 1. 2. Classification of allergic drug reactions, immune mechanisms, diagnostic tests, and clinical manifestation. Adapted from [3]

Immune reaction	Mechanisms	Diagnostic tests	Timing of reactions	Clinical manifestation
Type I (IgE-mediated)	IgE - basophils and/or MCs	Skin and intradermic tests, immunoassays, BAT, HRT	Minutes to hours after drug exposure	Anaphylaxis, urticaria, angioedema, bronchospasm
Type II (cytotoxic)	IgG and/or IgM - antigens in the cell membranes	Coombs' test (IAT, DAT)	Variable	Anemia, cytopenia, thrombocytopenia
Type III (immune complexes)	IgM and/or IgG complexes - soluble antigens	Complement (C3, C4), immunohistochemical test (IIF, DIF)	1 to 3 weeks after drug exposure	Serum sickness, vasculitis, fever, rash, arthralgia
Type IV (delayed, cell-mediated)	MHC presentation of drug molecules to T Cells with cytokine and inflammatory	Epidermal (patch) and intradermic test, *in-vitro* lymphocyte transformation, cytokines measures	2 to 7 days after cutaneous drug exposure	Contact sensitivity, skin rashes, organ- tissue damage

BAT, basophil activation test; HRT; histamine release test; IAT/DA; indirect antiglobulin test/direct antiglobulin test; IIF/DIF, indirect immunofluorescence/direct immunofluorescence test.

Allergic reactions have also been classified clinically into two groups based on the time interval between the administration and symptom onset as IR and NIR. Either can occur following the administration of drugs. IR usually occur within 1 hr after drug intake, NIR appears later than 1hr [7,20].

1.4. Antibiotics Frequently Involved in Allergic Reactions

Antibiotics are an important class of drug that can cause a life-threatening immune-mediated drug reaction. The burden of this problem is sometimes overestimated due to inaccurate

diagnosis, false-positive diagnosis, not properly documenting or being not remembered by patients. Only 10 to 30 % of reported allergic reactions can be confirmed [21]. This might result in the unnecessary use of alternative drugs that are broad-spectrum increasing adverse events and antibiotic resistance [22,23].

Antibiotics may be classified simply as β-lactam and non- β-lactam antibiotics [24]. β-lactam antibiotics are the most widely used classes of antibiotics frequently implicated in drug allergy. This includes specific drugs from penicillins, cephalosporins, carbapenems, monobactams and clavams as culprits [23,25]. The general population prevalence of allergic reactions to β-lactams ranges from 0.7 to 10 % [26]. Penicillin and cephalosporin are the two most frequently implicated antibiotics in drug allergy reactions due to the pattern of prescription and consumption [24,27].

Penicillins

Penicillins are the most widely used antibiotics for common infections and are still the treatment of choice for numerous conditions [28]. Depending on the specific population assessed, penicillin allergy remains a major drug allergy reported [29], with anaphylaxis occurring in 0.015 to 0.004 % cases [26]. The change in the pattern of consumption over time has gradually replaced Benzylpenicillin (BP) by AX alone or combined with clavulanic acid (CLV) as the main elicitor of immunologically mediated DHRs [20,30]. While there has been a decrease in the percentage of reactions attributed to penicillin (from 8 to 3.9 %), and cephalosporins (from 2.5 to 1.5 %), there is an increase in reactions attributed to AX-CLV (from 3.5 to 8.7 %) [21].

Cephalosporins

Cephalosporins are antibiotics most widely prescribed, and their use is increasing over time, with approximately 1-3 % of the general population reporting a cephalosporin allergy [31]. Numerous categories of hypersensitivity reactions have been reported with cephalosporins ranging from mild reactions to life-threatening anaphylaxis in patients with IgE mediated allergy [32]. The misdiagnosis and misunderstanding of the cross-reactivity among the β-lactams included within the cephalosporin class frequently lead to the change of therapy that represent safety issues to the patients and may lead to antibiotic resistance [31].

The non-β-lactams classes of antibiotics can also instigate hypersensitivity reaction in 1-3 % of the general population [33]. This class encompasses different drugs with dissimilar chemical structures and hence confer different immunogenicity [24]. Some of the examples of these types of antibiotics are described below.

Quinolones

Quinolones are synthetic antibiotics that are drugs of choice for the treatment of both Gram-positive and negative bacterial infections. The use of this class of drugs has gained importance in recent years for the treatment of bacterial infections in immunocompromised patients [34]. The prevalence of quinolones allergy in the general population is unknown [35]. A recent study has reported a hospital prevalence rate of 2 % with the most documented reactions being hives, rash, and nausea/vomiting [36]. This incidence rate is lower than that of β-lactams [37], nevertheless related to the change in the pattern of consumptions of these drugs, the prevalence of quinolones allergy has been rising over the past decade [38]. While drug allergy has been reported to all quinolones, moxifloxacin (63 %), ciprofloxacin (29 %) and levofloxacin (8 %) are the major culprits in inducing IR [39].

Sulphonamides

Sulphonamides are drugs carrying the SO_2NH_2 functional group and sulfamethoxazole, sulfadoxine and sulfapyridine are of allergenic importance [40]. The prevalence of sulphonamides allergy in the general population is approximately 3-8 % [41]. However, the prevalence of the reactions could as high as 40 and 60 % in patients with hematological malignancies and Acquired Immunodeficiency Syndrome (AIDS), respectively [20]. Rash and skin eruptions are the most frequently reported allergic reactions to these antimicrobials. More serious reactions like Stevens-Johnson Syndrome (SJS) could also occur with lower frequency but with significant morbidity and mortality [42].

Glycopeptides

Vancomycin is a tricyclic glycopeptide antibiotic used for the treatment of Gram-positive bacterial infections. The increase in the pattern of consumption vancomycin has led to various ADRs [43]. The prevalence of ADRs to vancomycin can reach up to 10 %. Vancomycin causes a red man syndrome, a reaction that is IgE-independent or pseudoallergic in nature, which

happens as a result of nonspecific MCs degranulation [44]. Vancomycin more rarely causes NIRs like SJS [43].

Aminoglycosides

Aminoglycosides are natural or semisynthetic antibiotics derived from actinomycetes [45]. They are the primary agent for the treatment of infections caused by Gram-negative pathogens [46]. Like β-lactam antibiotics, it can cause NIRs and with allergic reactions reported in less than 2 %. Streptomycin and neomycin are the two most common drugs causing allergic reactions from the group followed by gentamicin and amikacin [47].

Macrolides

Macrolides are a broad-spectrum antibiotic that consists of a large macrocyclic lactone ring to which one or more deoxy sugar is attached [48]. Macrolides can cause both IR and NIRs. Allergic reactions to macrolides occur infrequently (0.4–3 %). The common clinical manifestations include urticaria, angioedema and anaphylaxis [49].

1.5. IRs to β-lactams

IRs to drugs are mediated by specific IgE (sIgE) immune mechanisms usually occurring within the first hour after exposure to the culprit drug [26]. This involves ranges of clinical manifestations from rhinitis and urticaria/angioedema to anaphylaxis and death [50]. β-lactams are the drugs most frequently involved in these reactions. Of these, penicillins are the most studied antibiotics, due to their high consumption and the chemical stability of the conjugates that are formed, and it is for this reason that their immunochemistry is well known and serves as a model for the study of allergy to other drugs [51]. Various factors influence the foundation of the allergic reaction among which the chemical structure and its reactivity with proteins; cross-reactivity with other sensitizers are to be listed [51,52].

1.5.1. β-lactams Chemical Structures

Based on the chemical structure, β-lactams are classified as penicillins, cephalosporins, carbapenems, monobactams and clavams (Table 1.3). The basic structure across all group is the four-member β-lactam ring, which is core to antibacterial activity and as well as immunogenicity. All except monobactams are bicyclic consisting of another ring structure

fused to the β-lactam ring. In penicillins β-lactam is connected to a five-member sulphur ring (thiazolidine), in cephalosporins to six-member sulfur ring (dihydrothiazine), in carbapenems to a five-member ring (dihydropyrrole), and in clavams to a five-member oxygen ring (oxazolidine). In addition to the core or the nuclear parts of the structure, all β-lactams except clavams display sidechains or R substituents. The R and R^1 side chains are coupled to β-lactam ring in all cases excluding clavams. Moreover, the non-β-lactam rings display additional sidechains, in cephalosporins (R^2) and Carbapenems (R^2 and/or R^3) [53,54].

1.5.2. β-lactams as Haptens

β-lactams are assumed to be too small molecules to elicit an immune response [10]. The antigenicity of β-lactams is explained by the hapten hypothesis, which states that the immunogenic capacity of the drugs can only be gained by forming covalent conjugates with proteins [53]. The structural propensity of the β-lactam ring due to strain makes β-lactams highly reactive. The electrophilicity of the β-lactam carbonyl group enables binding to the protein via nucleophilic attack by primary amines, leading to the opening of the β-lactam ring and the formation of an amide bond to form a drug-protein adduct with increased size and multivalence [55,56].

The immunological recognition of such multivalently presented antigenic determinants on a conjugate by, at least, two adjacent IgE antibodies that are bound to their $Fc_{\varepsilon}RI$ on the surface of MCs and circulating basophils, results in the crosslinking of the $Fc_{\varepsilon}RI$ receptor [16,17,56,57]. The crosslinking would result in the degranulation and release of preformed vasoactive amines, cytokines, chemokines and other mediators, eliciting the acute phase of the allergic response [16,58]. The efficiency of the stimulation of the effector cell degranulation is dependent on many factors that include the structure of the drug antigenic determinant [54], its valency on the conjugate or complete antigen [59,60], the size of the complete [16,60], the proximity of the IgE epitopes [61] and the potential presence of the steric hindrance [62].

Table 1. 3. Chemical structures of β-lactams.

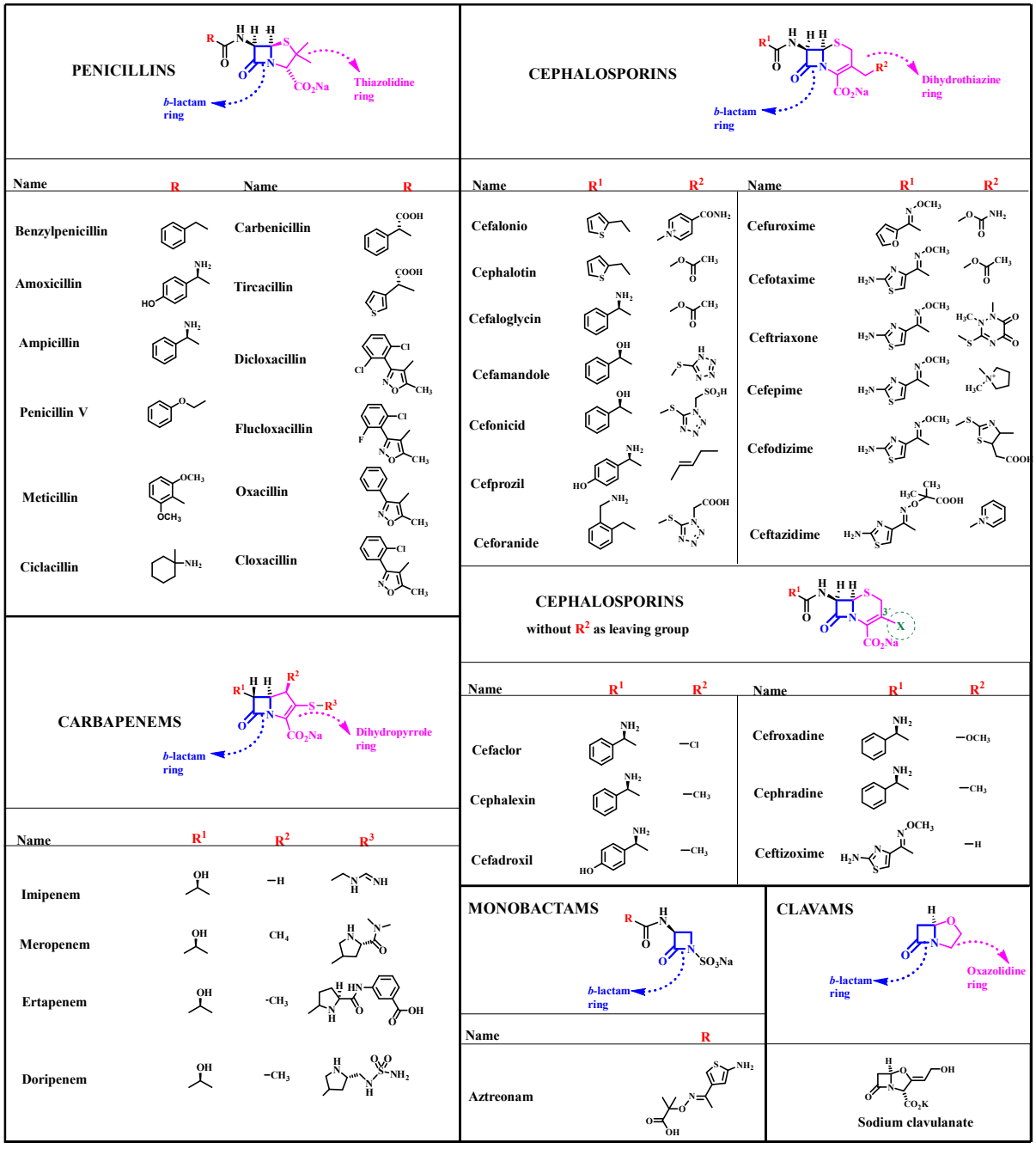

Penicillins are the first drugs to be described illustrating the formation of antigenic determinants [63]. The mechanism of antigenicity of this group of drugs is well established probably due to the historical pattern of prescription and consumption. Penicillins have very similar chemical structures only differing in the sidechain and BP is considered as a reference model to study allergy to β-lactams [64]. In penicillins, the haptenization process is spontaneous and efficient due to the high strain within the β-lactam ring as a result of its

condensation with the thiazolidine ring [65]. This process leads to the β-lactam ring opening with the formation of penicilloyl antigenic determinants. These structures are stable enough to be isolated and characterized by spectroscopic techniques [66].

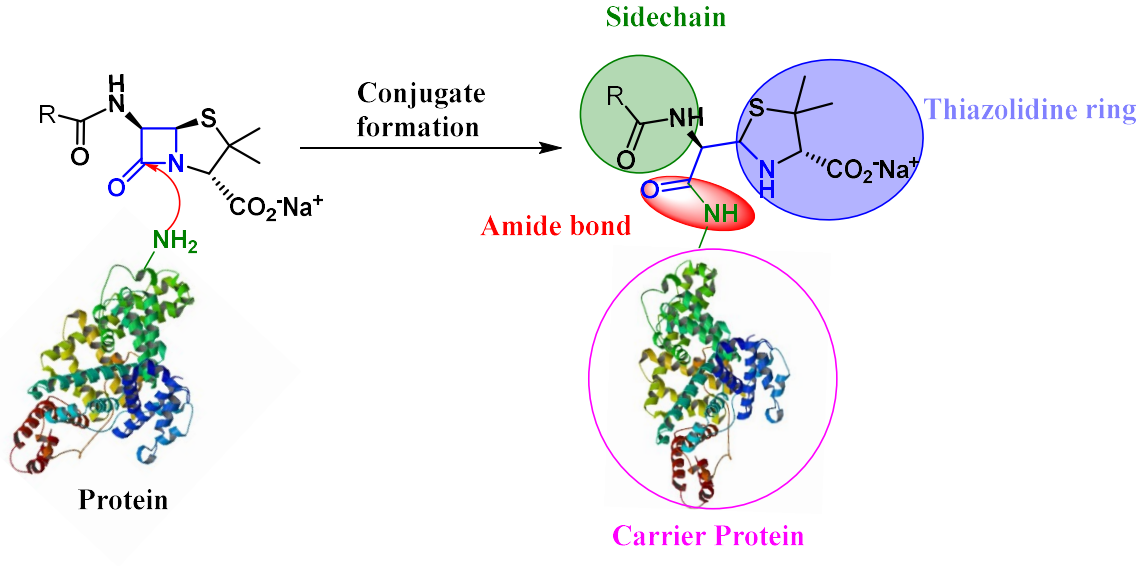

Figure 1. 3. Penicillins conjugation to carrier proteins and formation of major antigenic determinants. Different regions of recognition or epitopes are highlighted.

The *in vitro* haptenization and production of monoclonal antibodies (MoAb) helped to characterize the antigenic determinants of commonly used penicillins, where three epitopes are identified: the side chain, the thiazolidine ring and the amide bond formed as a result of β-lactam coupling to a protein carrier, although these regions can overlap [67] (Figure 1. 3). Protein conjugation to BP results in benzylpenicilloyl (BPO) as a major antigenic determinant in 95 % quantitative predominance [68]. The remaining 5 % of the structures are produced by degradation or metabolism that include benzylpenicilloic acid, benzylpenaldate, D-benzylpenicillamine, benzylpenicillenate, benzylpenicillanyl, benzylpenamaldate [54], which are not well described immunochemically and their involvement in allergic reactions are not well clear (Figure 1.4B) [54,69,70].

AX is the penicillin currently regarded as the main culprit in eliciting allergic reactions due to its recent consumption pattern [71,72]. The chemical structure of AX is similar to BP differing by the hydroxyl and amino group on the side chain, which helps to explain selective allergy to AX in patients tolerant to other β-lactams [55]. Likewise, to that of the BP, the straightforward opening of the β -lactam ring by the amino groups of the proteins, results in amoxicilloyl

(AXO) as a major antigenic determinant [73]. Other minor determinants of AX are formed by hydrolysis of the β-lactam ring, resulting in amoxicilloic acid, or intramolecular acylation by the amino group of the AX side chain, yielding diketopiperazine (Figure 1.4C). Contrasting to that of the BP, the stability of the AX minor determinants has allowed their chemical and immunological characterization. These two structures, however, are not able to bind to proteins, and therefore cannot be recognized by the sIgE from allergic patients as demonstrated in the skin and BAT [74]. In addition to protein adducts, AX polymers formed by AX-dimer were reported which could possess strong antigenic properties [75].

Cephalosporins can be classified according to their nucleophilic properties that enable binding to the protein. Although penicillins and cephalosporins share the β-lactam ring, their reactivity and stability of resulting structures differ. The lower tension in the β-lactam ring of cephalosporins, compared to that of penicillins, decrease acylation properties of the β-lactam carbonyl and slows the haptenization. Moreover, the R^2 chemical structure at position 3′ on clinically relevant cephalosporins can modulate the reactivity through the elimination of R^2 [65] (Figure 1.5). The conjugation of cephalosporin to proteins results in cephalosporoyl, a highly unstable structure. The determinants formed after conjugation with protein are quite different from those of penicillins, as cephalosporoyl undergoes fragmentation of the β-lactam and dihydrothiazine rings, complicating the understanding of the immunogenicity of the cephalosporins [54,65]. Irrespective of the reactivity of the R^2, the involvement of the R^1 side chain shared both by penicillins and cephalosporins seems to play a leading part in determining the immunologic reactions to cephalosporins and cross-reactivity [76–78]. Several studies based on structural activity relationship (SAR) aimed to identify the structures of antigenic determinants derived from different cephalosporins, from which different synthetic determinants based on cephalosporin degradation hypothesis have been described [78–80].

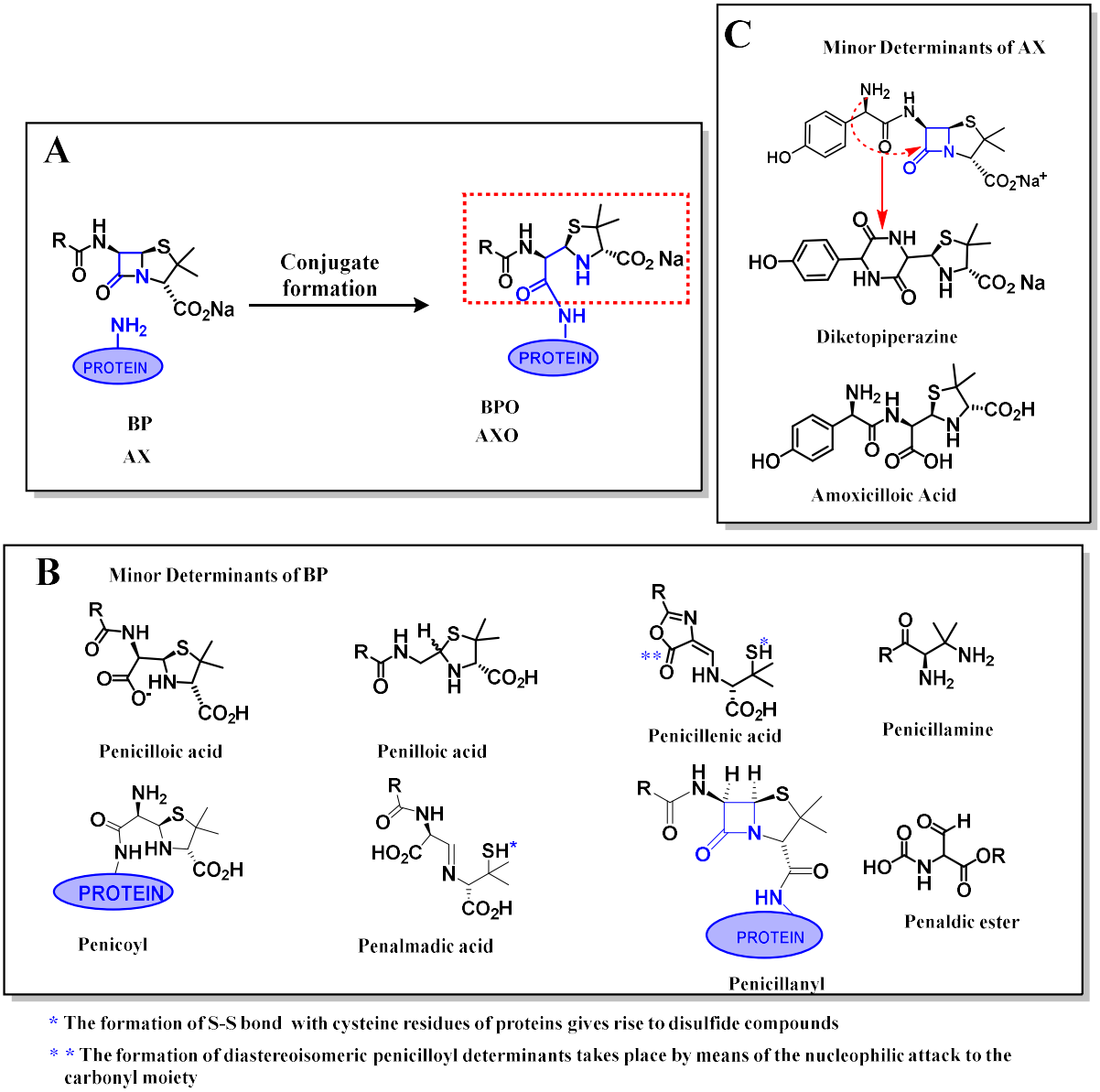

Figure 1. 4.The major and minor antigenic determinants of BP and AX.

Carbapenems are bicyclic structures with β-lactam and an unsaturated 5-membered ring containing carbon atom instead of sulfur [81]. The immunogenicity is gained by forming an adduct with protein and the stable dihydropyrrole ring gives the specificity of the response and higher epitope density for the conjugates [82].

Monobactams are monocyclic compounds, where β -lactam ring is not attached to another ring, unlike most β-lactam antibiotics. Aztreonam is the only commercially available monobactam and includes a similar sidechain to ceftazidime, a cephalosporin. This antibiotic does not show cross-reactivity with most β-lactams, except in some report with ceftazidime [83].

Clavams are antibiotics with weak antibacterial activity, nevertheless with potent inhibition capacity for the β -lactamases [84]. CLV is the only commercially available drug from the group and clinically used in combination with AX [85]. Despite the initial report that CLV present a very low immunogenic and allergenic potential [82], there have been growing pieces of evidence reporting its immunogenicity and that it can induce IgE-mediated reactions [30,84,86]. The mechanism of immunogenicity of CLV has not yet been well-established as a result of the instability of the structures after protein conjugation and multiple possible determinants due to degradation [73]. Nevertheless, our group has recently identified 3-oxopropanamide derivative as CLV antigenic determinant using SAR studies [87].

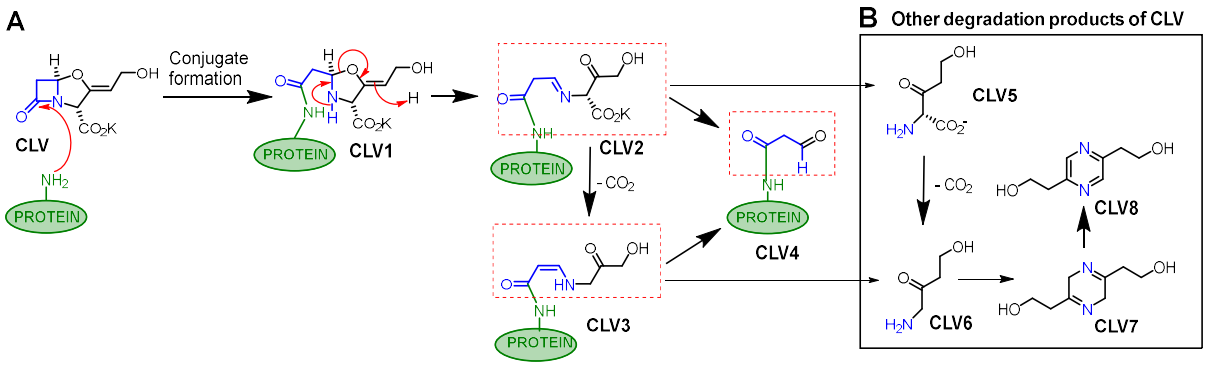

Figure 1. 5. Pathway to the formation of proposed antigenic determinant structures of CLV (dotted box) and other degradation products of CLV which do not bind to the protein. Adapted from [89].

1.5.3. Target Proteins for Haptenation by β-lactams

All β-lactams are small molecules (MW < 1000 Da) that by themselves do not have enough size to be processed by antigen-presenting cells to elicit an immune response [9]. This structural requirement is attained through haptenation, a process by which reactive drugs or their metabolites covalently modify the protein, an important process in ADRs [72]. The *in vivo* haptenation process and amplification mechanisms that cause an allergic reaction is not yet fully understood [53]. Identification and characterization of formed adducts help in understanding mechanisms of the protein haptenation by β-lactams, the ability to activate the immune system and subsequent pathogenic role [88,89]. The advancement of proteomic techniques has meaningfully enabled the identification of both the binding site of protein haptenation and several targets for haptenation of AX and other β-lactams [90].

Human serum albumin (HSA) is the most abundant single-chain and non-glycosylated serum protein that contains 585 amino acids with a MW of 66,500Da [91]. The role of this protein is to regulate colloidal osmotic pressure through depot or transport of endogenous and exogenous compounds [91,92]. It is a major binding protein for most acidic drugs [93]. The pioneering study to understand the pathogenic role of protein haptenization by β-lactams considered HSA as the main protein and therefore involved the characterization of penicilloyl-HSA adducts. This led to the identification of 6 Lys out of 59 (Lys 190, 195,199, 432, 541, and 545) as the main binding site for BPO from both serum samples of patients treated with BP and *in vitro* samples using high-performance liquid chromatography (Figure 1.6B) [94,95].

The advancement of analytical techniques through the coupling of the liquid chromatography system with mass spectrometry has facilitated the identification of HSA modification by various drugs including AX [75,88], BP [96,97], CLV [87], flucloxacillin [98], and piperacillin [99] from the serum of patient treated with drugs or *in vitro* samples. It was also reported that some lysine residue on HSA (Lys190, Ly199, and Lys541) are more reactive in forming protein adduct with β-lactams [75]. Although the factors that regulate the selectivity of which amino acids modified by β-lactams are not well known, recent molecular modelling studies proposed residues accessibility and the surrounding microenvironment as a plausible factor to enhance the intrinsic reactivity of the Lys residues [89]. Nevertheless, there are differences in the modification patterns between the β-lactam molecules probably due to structural differences or the incubation conditions that includes the concentration of the drug. The variation in samples from patients could also be due to the dissimilarities in the therapeutic conditions including dosage, route of administration, concomitant treatments or pathological conditions [89,100].

The involvement of HSA in the haptenation with BP and induction of immune response to this drug was reported in a study that detected penicilloylated HSA in penicillin treated patients, and the appearance of anti-penicilloyl antibodies in almost half of patients treated with BP [101]. Subsequently, transferrin was identified as another protein modified with ampicillin with a similar mechanism of acylation of the basic amino acid observed in HSA modification [102]. More recent immunological and proteomics studies by our group have identified HSA, transferrin, haptoglobin, and the light and heavy chain of immunoglobulin as target serum proteins for haptenation by AX [88,89] and/ or CLV [103]. In addition to protein adduct formation, the formation of AX-dimer was reported [75], which according to earlier observations the AX polymer could possess strong antigenic properties [104,105]. The reason

for the selective binding of β-lactam antibiotics to these proteins while other relatively abundant serum proteins did not show a detectable adduct is not yet fully understood [53]. Moreover, the binding of β-lactam antibiotics or derivatives with cellular membranes of macrophages, B-lymphoma cells, monocytes and intracellular protein are reported with a relatively slower rate of adduct formation than that of serum protein [72,106–109].

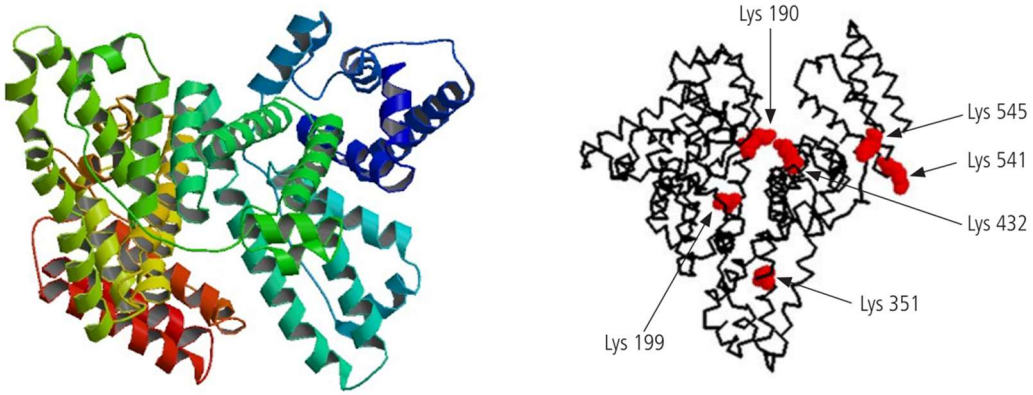

Figure 1. 6. Crystal structure of HSA taken from the protein database with a code of 1A06 and common Lys residues modified by β-lactams identified by mass spectrometry. Obtained from [55,112].

1.6. Diagnostic Approaches for Allergic Reactions to β-lactams

The complexity and overestimation of antibiotic allergy associated with diagnostic problems have led to the use of needless alternative drugs that are less effective, expensive, and potentially more toxic that could result in therapeutic failure [20]. To overcome these problems, there is a need for an improved diagnostic approach with enhanced accuracy avoiding both false-positive and false-negative results, to achieve optimal specificity and sensitivity, respectively. The diagnostic procedures depend on the drug involved and the type of DHRs, IR or NIR [7]. The detailed clinical history and careful physical examination are, therefore, essential steps toward an accurate diagnosis and establishment of the underlying mechanisms of allergic reactions [20].

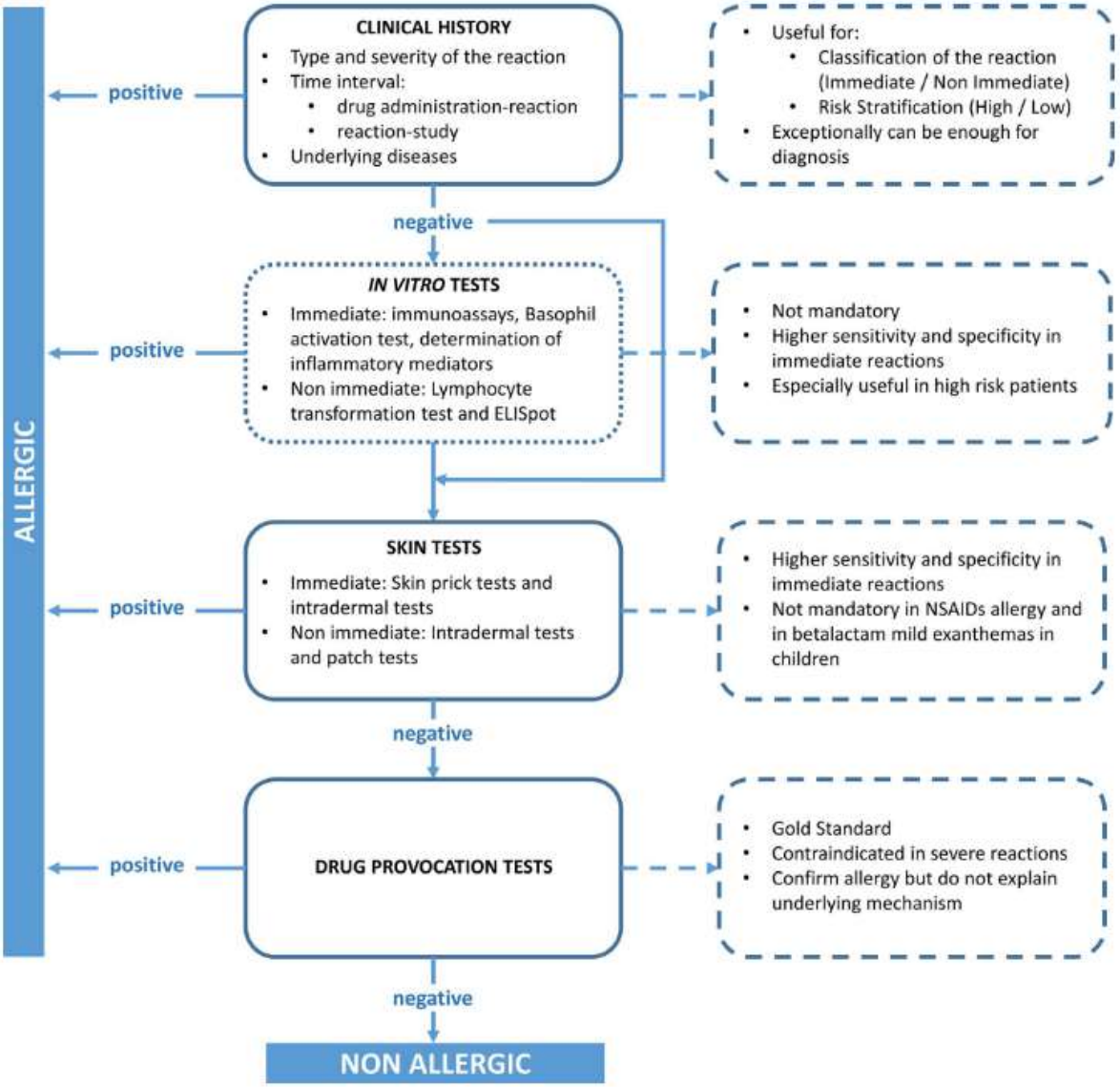

Figure 1. 7. Schematic illustration allergological workup for DHRs. Adapted from [113].

The allergological workups of a suspected drug allergy after the predictive model that is based only the clinical history, require the performance of different diagnostic tests: *in vivo* test that includes the skin test and the drug provocation tests; and the *in vitro* tests such as immunoassays and cellular assays [7] (Figure 1.7). Nevertheless, the clinical history is frequently not reliable, and the sensitivity of the skin test might not be optimal to establish an accurate diagnosis [110]. Although less sensitive, *in vitro* tests results are complementary to *in vivo* tests. Moreover, *in vitro* assays are the only alternative to *in vivo* tests and are recommended to be performed before in high-risk patients, such as patients with a history of life-threatening reactions.

1.6.1. *In vivo* Tests

Skin tests are one of the oldest *in vivo* diagnostic techniques and the well-validated method for the diagnosis of IR to β-lactams [111]. These tests are performed primarily by prick and followed by intradermal if the response is negative [112]. The diagnosis of an allergic reaction to penicillins uses the following skin test reagents: Nowadays, the commercial determinants in skin test reagents used are BPO-lysine polymer conjugates (benzylpenicilloyl-octa-L-lysine (BP-OL) or penicilloyl- poly-L-lysine (PPL), in Europe and the United States respectively) (Figure 1.8A), together with benzylpenicilloate as a minor determinant (only in Europe). However, it should be noted that commercial determinants availability depends on the country. Previous reagents included minor determinants mixtures (MDM) consisting of BP, benzylpenicilloate (hydrolysis product of BP), and benzylpenilloate (subsequent decarboxylation product) (Figure 1.8B) [113,114].

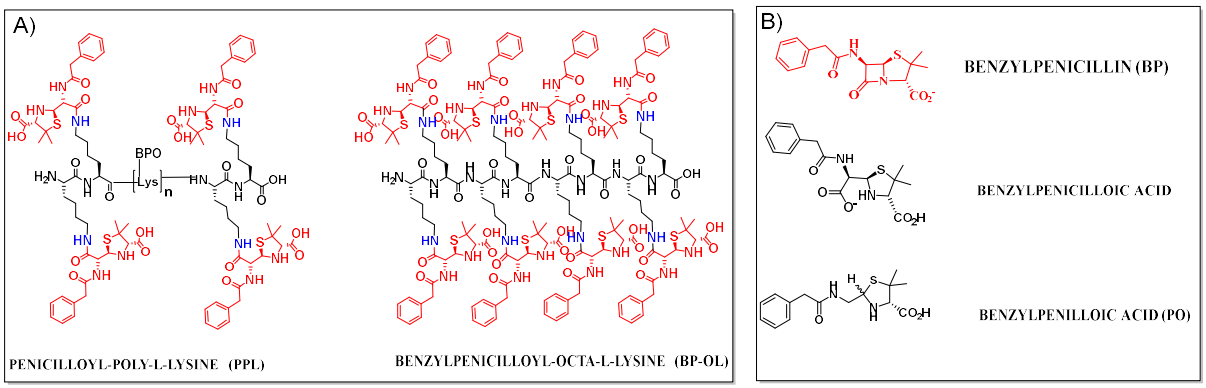

Figure 1.8.The Penicillins major determinants (A) and MDM (B).

Due to the change in the pattern of consumption and appearance of semisynthetic penicillins in clinical use, other determinants such as AX, ampicillin and cephalosporins were required to increase the sensitivity of the skin test. The relevance of benzylpenicilloate alone as an important hapten in IR to penicillin has declined and including AX increased the positivity of the skin test to 70 % [111,113,115]. Consequently, European Network for Drug Allergy (ENDA) recommended the use of PPL/BP-OL, BP minor determinant and AX, as the first reagents to be tested and in case of negative results, parent BP should be added [111]. Moreover, the use of AX-CLV combination in the clinical use posed another problem to the existing diagnostic procedure as both drugs can independently be involved in allergic reactions [73]. Therefore, including not only AX but also CLV in the diagnosis of allergic reactions to AX-CLV improve the test sensitivity in both skin-prick and intradermal testing [113] [116].

A drug provocation test is the controlled administration of drugs to diagnose DHRs, and it is the ultimate step in establishing an accurate diagnosis in the absence of alternative diagnostic methods. The procedure is time-consuming and performed under medical surveillance by trained personnel in a specialized center due to the potential risk to the patient [117,118]. This drug can be a structural/pharmacologically related drug, alternative, or the culprit drug itself [119]. Due to the non-optimal sensitivity of skin tests, drug provocation test is considered as the gold standard to establish the diagnosis, which is risky and is not recommended in patients with a history of life-threatening reactions [113,119].

1.6.2. *In vitro* Tests

In vitro tests are based on the principles of evaluating the cells and mediators released during the allergic reactions for the identification of the culprit drug based on the mechanisms and reaction kinetics involved [120]. These tests are mostly performed as an added means in the diagnostic algorithm of DHR. However, lately, it was highlighted that the complementary utilization of both *in vivo* and *in vitro* tests benefits considerably especially if the skin test is not confirmatory and the drug provocation test is contraindicated [7,121]. If reliable, and with acceptable sensitivity, *in vitro tests* improve the accuracy of the diagnosis of DHRs, with the added value of avoiding the potential risk to the patient [20,121]. The *in vitro* tests can further be classified based on the type of reactions as *in vitro test* for IR and NIR. A detailed review of *in vitro* test for NIR is given by Doña *et al* [20].

1.6.3. *In vitro* Tests for diagnosing IR

Albeit IRs can be IgE-mediated or off-target mechanism involving different mediators, the existing *in vitro* tests are only useful for IgE-mediated reactions, with the two commonly used being: immunoassays and BAT [7].

Immunoassay is a technique that uses (hapten)-carrier conjugates coupled to a solid surface for the quantification of sIgE in serum. The bound sIgE can be detected by different techniques after incubating the solid phase with patient serum including colorimetric enzyme (enzyme-linked immunosorbent assay (ELISA)), fluorescent enzyme (fluorescence enzyme immunoassay (FEIA)) and radioisotope (radioimmunoassay (RIA)) [20] based assays. The most widely used technique for diagnosing β-lactams allergy is the FEIA-based commercial ImmunoCAP. Nonetheless, this method is bestowed with false-positive results, low and variable sensitivity (0-50 %) and defiantly with astonishing high specificity (83 -100 %) [120].

The limited availability of ImmunoCAP to a few β-lactams and related issues of sensitivity and specificity has led to the use of in-house immunoassays including Sepharose-RIA and radioallergosorbent test (RAST) [120]. However, these methods can only be assayed in research laboratories and the use of isotopic reagents have the additional inconvenience of needing to manipulate radioactive materials.

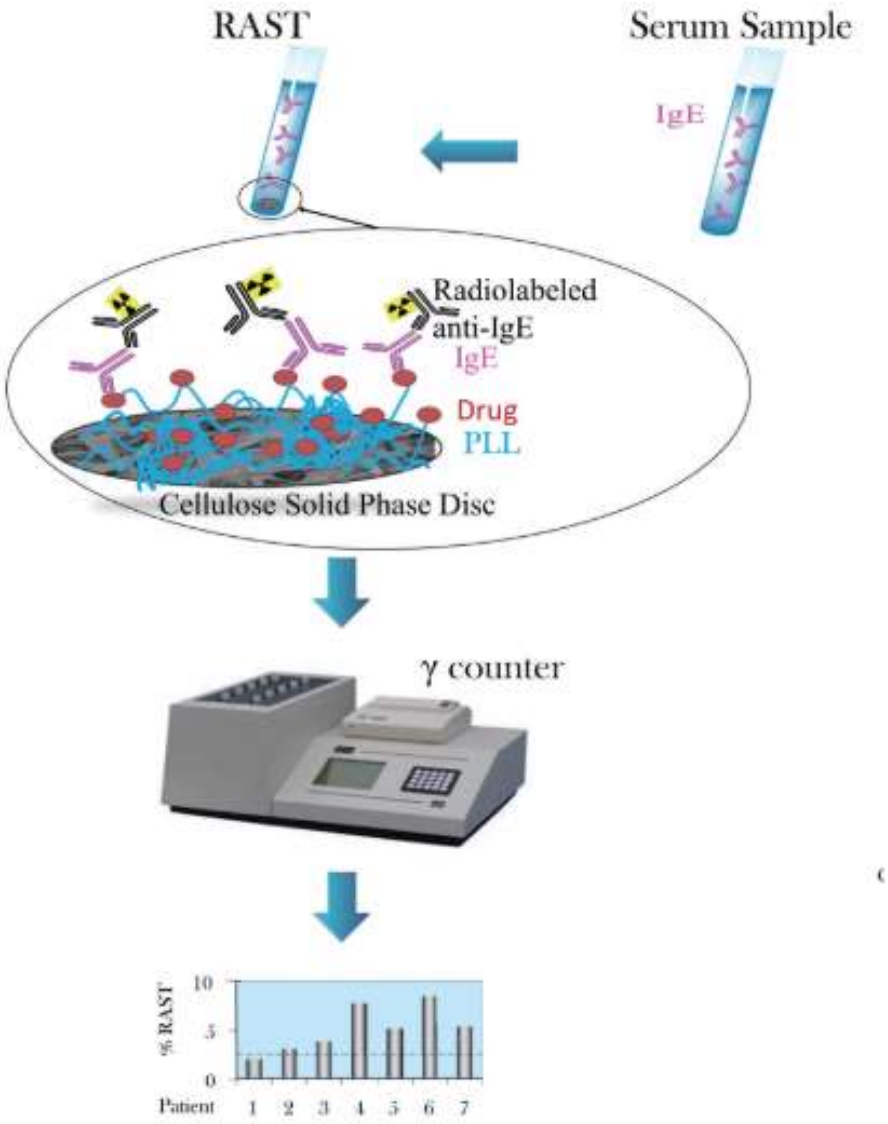

Figure 1. 9. Diagrammatic representation of the RAST. Adapted from [22].

RAST is a test for detecting allergen antibodies using a cellulose paper disc activated with cyanogen bromide and covalently coupled with carrier molecule (usually poly-L-Lysine (PLL) haptenized with the drug of interest [20,122]. The schematic description of the principle of RAST is given in Figure 1.9. In the first step, the solid-phase allergen is incubated with serum

and antibodies to the allergens will eventually bind. After washing steps to remove unbound antibodies, the second step involves the reaction between solid-phase allergen-antibody complex and radioiodinated secondary anti-human IgE antibody. After another washing step, radioactivity is measured. The measure of radioactivity from the solid phase is proportional to the quantity of IgE antibodies in the first step [122]. This in-house test shows higher sensitivity (43 -75 %) than ImmunoCAP and specificity ranges from 68 to 83 % [20]. The high correlation of RAST results with skin test (87-95 %) and drug provocation test (80 %) has signified the importance of this technique in measuring sIgE in the diagnosis of β-lactams allergy [113].

BAT is another commercially available *in vitro* test, performed in fresh blood, that measures the ability of IgE to induce the activation of basophils in the presence of allergen using flow cytometry (Figure 1.10) [123,124]. Different single-cell markers or a combination (anti-IgE, CCR3, CRTH2, and CD203c) are used to detect the basophils. Once basophils are selected, CD63 and CD203c are the two commonly detected marker of basophil activation after stimulation with the culprit drug [20]. The BAT performance range in sensitivity (50-78 %) and specificity (89 -97 %) for the diagnosis of β-lactams allergy signify its importance as a complementary technique to both *in vivo* and *in vitro* tests [125–127]. Nevertheless, the use of in-house techniques due to the absence of standard protocols related to markers, procedures and drug concentrations serve as a basis of variation among different laboratories [120].

Moreover, BAT has two inherent limitations: the need to be performed in the first 24 h after blood collection to avoid a decrease in the activation [128]; and the existence of a 10-15 % of subjects that have non-responder [128,129]. To circumvent this, passive BAT using basophils from donors sensitized with stored sera from patients have been recently described [130], in parallel to the measure of histamine release [131]. Application of the latter have been investigated for β-lactam allergy diagnosis, finding a sensitivity of 55 % and specificity of 85 % in the diagnosis of CLV allergy [131], and 79 % and 100 % respectively for AX when using AX-octalysine as a conjugate, improving the values obtained when using only AX (63 % sensitivity and 90 % specificity) [132].

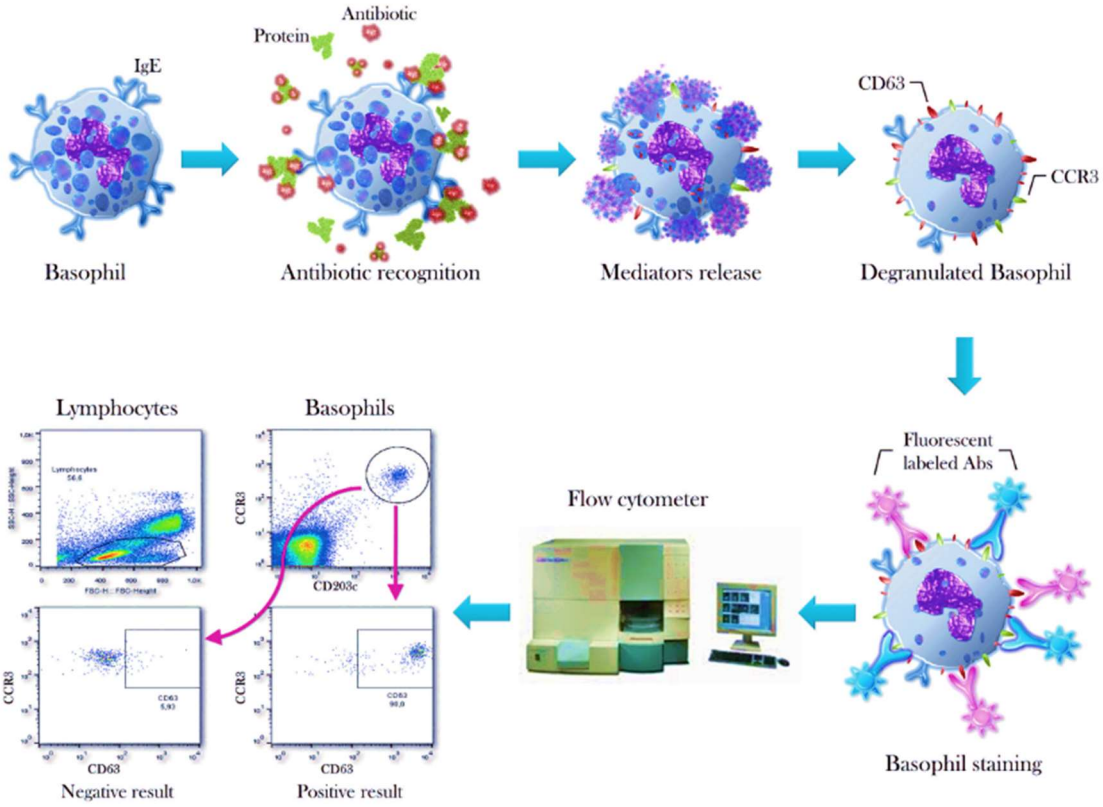

Figure 1. 10. Diagrammatic representation of BAT. Adapted from [22].

Despite these results and the possibility of use sera, this method presents the limitation of the need of a basophil donor, which must be available for blood collection during all the study, and the need of stripping the IgE already bound on donor basophils. Overcoming these issues, mast cell activation test (MAT) has emerged to complement BAT, especially in food allergy [130]. MAT uses a mast cell line grown in the laboratory that is sensitized with sera from the patients to mimic the patients' own MCs. These cells are then stimulated and analysed by flow cytometry for the expression of activation markers on their surface or the release of inflammatory mediators. Outside protein allergens, MAT has been recently used to diagnose IgE/FcεRI dependent allergy to small drug molecules, such as chlorhexidine [133] and platin [134]. These unique approaches have been performed either in derivatized human MC, LUVA cells or rat basophil leukemia (RBL) cell lines.

1.7. Limitation of Diagnostic Approaches for Allergic Reactions to β-lactams and Future Directions

Accurate diagnosis of DHRs not only identifies the culprit drug but also explore all cross-reactive structures for establishing a safer alternative. Hence, glitches with both underdiagnosis and overdiagnosis need to be circumvented to precisely categorize the subject as allergic or not. Misdiagnosis, particularly as false-negative, will severely impair patient safety, especially in those with severe reactions [121]. The current approach in the diagnosis of β-lactam allergy, *in vivo* and *in vitro* tests, is not without limitation. The *in vivo* tests, the uncontested approach to the diagnosis of β-lactam allergy, have major drawbacks depending on the drugs under enquiry. This is a time-consuming and expensive approach that is not without risk and require experienced personal and specialized facility [113]. To avoid these challenges, the best alternative could be reliable *in vitro* tests with optimal specificity and sensitivity. Nevertheless, the currently available tests do not fulfil these requirements.

In vitro tests aim to identify the culprit drug, by determining sIgE, either in serum by immunoassays or on basophil surface by functional BAT. The detailed advantages and limitations of *in vitro* diagnostic approach in DHRs have been reviewed by Mayorga *et al*.[121]. While the availability of diverse types of *in vitro* test is not a problem, the lack of experts' consensus on their diagnostic value is hampering their utility in routine clinical care [120]. The currently available immunoassays show issues more related to the low sensitivity, probably due to the extremely low levels of drug-sIgE (associated with DHR) or the use of an incorrect drug metabolite or drug conjugates. Besides, reported low specificity is explained by unspecific IgE binding to the solid phase. Another disadvantage is that they are available or described only for a limited number of drugs. On the other hand, BAT is a functional test that can be performed with any injectable drug without preparing hapten–carrier conjugates, although it is rarely thoroughly validated. One point of disagreement is related to the absence of methodologically sound studies implemented with significant numbers of well-characterized patients and control subjects that include a comparison with reference standard [26,121]. Consequently, there is a need of validating current methods, developing new *in vitro* methods and /or modification of the existing tests to improve sensitivity and specificity, for achieving a reliable diagnosis that eventually avoids the *in vivo* methods [113].

In recent decades, the diversity of *in vitro* tests is evolving offering numerous advantages in drug allergy diagnosis. To advance in this area, it is essential to gain a detailed understanding of different drug-conjugates and mechanisms of formation, chemical structures of the antigenic determinants, and the nature and features of the carrier protein. Moreover, diversifying the number of antibiotics, antigenic determinants and similar conjugated structures that mimic the *in vivo* molecular recognition *in vitro,* for their inclusion in the assays, would overcome the limitation of the existing tests and facilitate the development of a novel approach with the better performance [26].

The advancement of new technologies in the fields of immunology, proteomics, nanotechnology, and chemistry will add up to the understanding of hypersensitivity reactions to β-lactams and expand the array of the diagnostic approach by overcoming the limitations of the currently available tests. A summary of the ongoing advancement on the improvement of the diagnostic tests for allergic reactions, particularly the importance of using nanostructures in developing new diagnostic tests or improving the existing test is given in the section below.

1.8. Nanostructures in the Diagnosis of Allergy

Nanoscience and nanotechnology allow manipulating, assembling, manufacturing, and controlling matter at the nanometer scale level (1 to 100 nm) through a multidisciplinary approach [135]. It has led to the development of nanomaterials, which behave very differently from materials with larger scales. Moreover, their functionalization with ligands can tune their physicochemical properties and provide interaction with different targets [136]. The nanostructures differ in size, shape, and dimension [137], and can broadly be classified into four material-based categories: Organic, inorganic, composite and carbon-based [138]. This encompasses structures such as nanoparticles, nanopores, nanorods, nanowires, nanoribbons, nanotubes, nanoscaffolds, liposomes, polymers, dendrimers and nanogels as popular representatives [139,140]. The diversity in the physicochemical properties that depend mainly on the size, shape, composition, and functionalization of the system, can be modulated to achieve the desired biological properties for health applications including in early diagnosis, treatment and prevention of diseases [141].

Nanodiagnostics uses the principles of nanotechnology for diagnostic purposes and exploits the nanoscale properties derived from an interaction between the surface and biomolecules for

increasing the sensitivity, specificity and facilitate the earlier detection of the disease [142]. The precise control over the physicochemical properties of the nanostructures allows the construction of the nanometric system that can mimic the complex *in vivo* recognition in the i*n vitro* systems for both, immunoassays, and cellular tests.

1.8.1. Novel Approaches to Improve Immunoassays for Drug Allergy Diagnosis

There are a growing number of approaches based on using the advantages of nanomaterials to be able to detect and/or quantify sIgE. In this regard, various strategies including nanofluidics [143], or the use of nanostructures as carrier molecules [66,144–146] and/or solid supports [147,148] to capture antibodies, or as a detection tool to enhance and amplify the measurement signal (such as fluorescent, surface plasmon resonance (SPR), or electrochemical detection) for enhancing the test performances have been investigated.

The use of PolyAmidoAmine dendrimers (PAMAM) as hapten carrier allows the presentation of multivalent antigenic determinant that mimics the globular protein, named Dendrimeric Antigens (DeAns). This dendrimer platform has allowed the synthesis of three-dimensional structures with precise control over the size and number of antigenic determinants that permitted increasing the sensitivity, due to higher hapten density, and reproducibility of the diagnostic tests in penicillins-sIgE detection [136]. Moreover, this platform has allowed the inclusion of two different β-lactams on DeAn to create bi-epitope-DeAn that allowed the detection of sIgE from both selective and cross-reactive patients. This study also confirms the influence of the tri-dimensional distribution of a hapten in a carrier molecule in the IgE recognition process [66].

Different solid support scaffold anchored with nanostructures including dendrimerized cellulose [144], solid phases consisting of zeolites [148] and silica nanoparticles [147] have shown the increase in sensitivity in immunoassays through increasing the density of the nanoconjugates, which eventually result in the higher sensitivity of the test result. Another advantage is the reproducibility of the tests performed with reproducible and controlled materials. Likewise, another solid phase platform, nanoplasmonic biosensor, based on dendrimeric gold nanodisks have shown comparable test result to commercial ImmunoCAP test [146].

1.8.2. Novel Approaches to Get Insight into the Activation of Cellular Mechanisms or to Detect sIgE in Cellular Tests

Cellular tests, including those based on MCs and basophils, have not been sufficiently addressed to benefit from the unique physicochemical properties of the nanomaterials, to develop new diagnostic methodologies or improve the performance of existing ones. Given the complex cellular process, the design of precisely crafted nanostructures that mimic the hapten-protein conjugate (formed *in vivo*) is enormous [16]. In this context, different nanoarchitectures have been designed to evaluate the influence of different parameters on the degranulation of MCs using synthetic ligands/haptens supported on bi- or multivalent structures, which can be manipulated to control the occupation of the receptor and blockade of the cellular response [60]. The influence of size and multivalence has been demonstrated in a study using flexible polyethylene glycol (PEG) type spacers attached to model ligands, dinitrophenyl (DNP), for the stimulation of RBL cells with the multivalent antigen. Thus, it has been observed that a small dendrimer with 4 DNP blocks the activation of the cells caused by DNP- bovine serum albumin (BSA), while another larger dendrimer with 16 ligands causes the degranulation. They also show the influence of the size of flexible spacers, finding that those long spacers in the range of 100 Å inhibit the crosslinking of IgE due to the formation of cyclic monomers [60], while shorter spacers (<50 Å) are not able to stimulate degranulation of the mast cell due to the formation of cyclic dimers of IgE [149]. Regarding the use of nanostructures for the diagnosis of DHRs, through assessing the specific activation of effector cells, such as basophils or MCS, only a few studies have been reported. For instance, nanoallergens consisting of liposomes have been used as platforms for platin-based drugs metabolites displayed in a highly multivalent fashion in the detection of platin-induced allergies [134].These systems trigger significant degranulation responses from MCs-like cells (RBL-SX38) primed with serum IgE from patients.

1.9. Dendritic Structures in Drug Allergy Diagnosis

The structural features of these precise nanostructures for mimicking the carrier protein with the advantage of control over structural build-up and the number of hapten on the surface make them very attractive carriers for studies related to drug allergy. In the section above, it was mentioned that dendrimer-based structures have shown promising outcome in developing new *in vitro* tests for the diagnosis of allergy and shade light into establishing the understanding of

the complex effector cell activation. A brief introduction to the chemistry of the dendritic structures and their diversified application with a special interest in biomedicine is given below.

1.9.1. Introduction to Dendrimers and Dendrons

The term dendrimer is derived from the Greek words "dendron" (tree) and "meros" (parts), describing the tree-resembling features of these macromolecules [150]. Dendrimers are nanoscaled, highly branched, globular, multivalent, and mono-dispersed structures with synthetic elasticity and diverse applications [151–153]. Structurally, dendrimers are defined by three distinct features namely [150] (Figure 1.11):

- The core.
- The branching or arms.
- The end groups.

The core, the central part of the dendrimer unit, can be an atom or groups of atoms that serve as focal points where branches of carbon or other elements converge or diverge. The core is usually enclosed by extensive branching which generates numerous interior layers, which regulates the multiplicity and size of the structures [154,155]. Moreover, the core by itself could confer functionality as in the case of ferrocene core metallodendrimer with redox properties [156].

Dendron, a structural component of the parent dendrimer, informally called wedges, is simply the branching and peripheral groups of the dendrimer, but usually contains an active core moiety that can be further functionalized.

The reiterating synthetic steps result in numbers of branching points creating layers of repeat units (monomer)from the central core to the surface which are called dendrimer generation (G). For example, as can be seen from Figure 1.11, a dendrimer with three branching points is denoted as "third-generation", symbolised as G3 dendrimer. The flexibility and rigidity parameters of dendrimer are affected by the types of branching units [157].

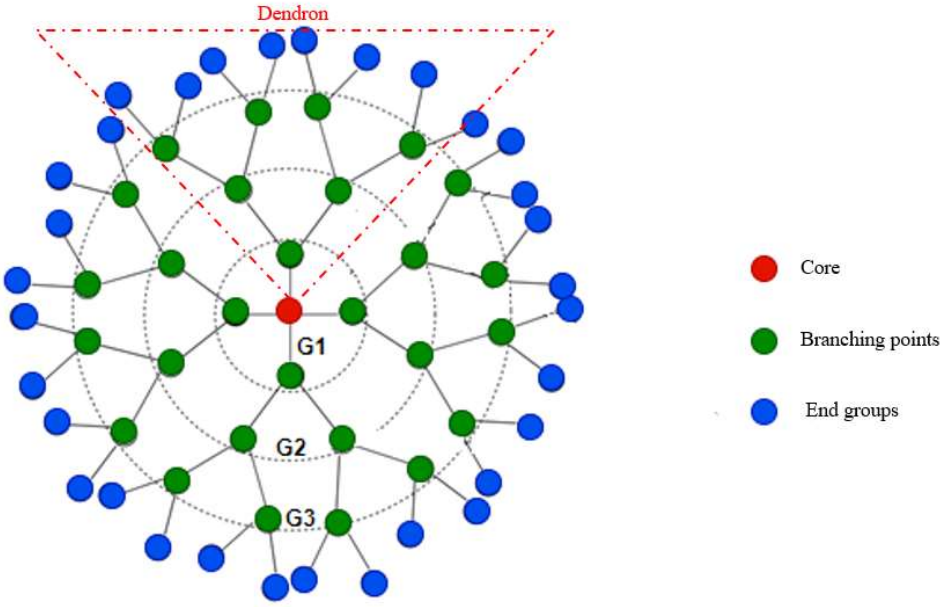

Figure 1. 11. Schematic representation of dendrimer and dendron (red highlight).

The end groups are the functional groups on the surface of the dendrimer. The number of end group is determined by dendrimer generation, reactive core group and branching points. Consequently, the physicochemical properties of the dendrimer are governed by the surface functional group in addition to the branching units. By selecting the proper end group, it is possible to fine-tune the characteristics of the dendrimer to diversified applications [154].

Polypropylenimine (PPI) is the first dendrimer-like compound synthesized in 1978, nonetheless, the synthetic approach used has encountered difficulties in synthesizing higher generation compounds [158]. Later, two independent groups, Newkome *et al.*[159] and Tomalia [160], have synthesized a well-defined dendrimer of higher generation by the mid-80s. Since the first disclosure, over 100 dendrimer compositions (families) and 1000 dendrimer surface modifications have been described. There are diverse types of dendrimers commercially available (Figure 1.12). The Tomalia-type PAMAM dendrimer and Fréchet-type polyether compositions are the two most widely studied families of dendrimers [161]. Another well-described dendritic material is a family of 2,2- bis(hydroxymethyl)propionic acid (bis-MPA) as a building block. The bis-MPA molecule, being an AB2 monomer, has successfully been explored for the construction of a large number of dendritic materials, ranging from monodisperse dendrons and dendrimers to polydisperse hyperbranched polymers and dendritic-linear hybrids [162].

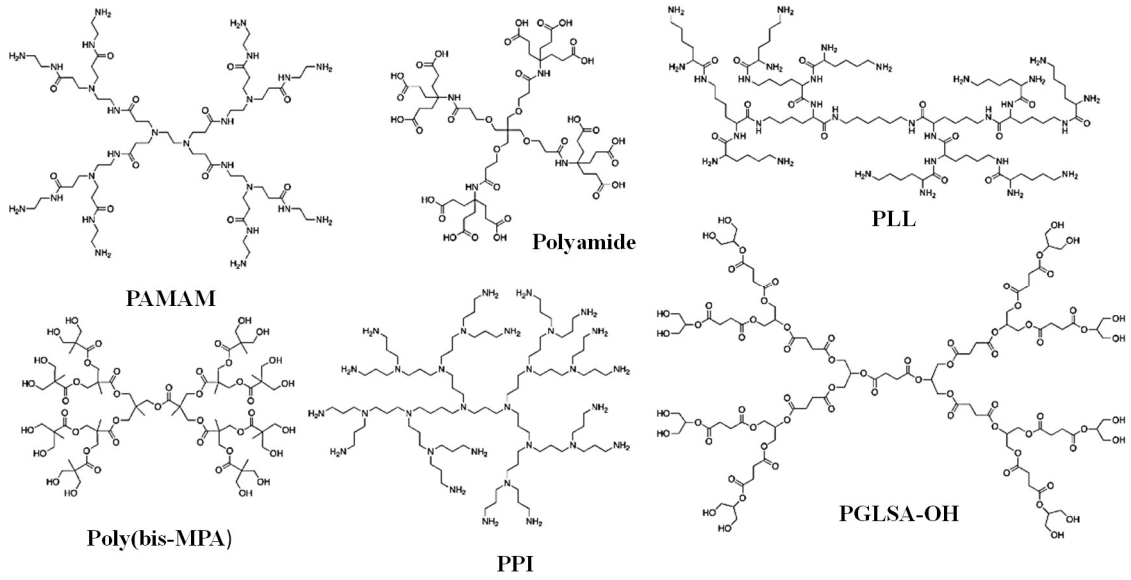

Figure 1. 12. Illustrative structures of common and commercially available dendrimer structures [162].

1.9.1.1. Dendrimer Synthesis: Divergent and Convergent Methods

The synthetic outlines for the preparation of dendrimer have control over the important parameters that include size, shape, surface/interior chemistry, flexibility, and topology. The synthesis of dendrimer relies on the application of both the well-known traditional and novel organic chemistry reactions, where efficient protection/ deprotection and coupling reactions are of primary importance. This approach enables in obtaining of dendritic macromolecules that have variable structures, that contain exclusively aliphatic, aromatic, or mixed structures [163]. There are two general strategies to accomplish the synthesis of dendrimers: divergent or convergent method [164].

The divergent synthetic strategy is one of the classic methods for the synthesis of dendrimer starting from the multifunctional core of molecule, B_n ($n \geq 2$), to the periphery, whose next dendrimer generations is built via the subsequent addition of monomer building blocks (Figure 1.14A) [154]. To achieve controlled growth of the dendrimer, an AB_n monomer is used where A-functional is a reactive group and B-functional is deactivated /protected group. The widely used monomer is AB_2 type trifunctional molecule that coupled to di, tri or tetra-functional core to result in the first-generation dendrimer. The next step is the activation of the B-functionalities of the first-generation dendrimer and coupling with a new set of monomers to

result in second-generation. The reiteration of these two steps will result in the desired higher generation of the dendrimer. The number of the generation corresponds to the number of branched layers from the core [154,163]. However, as the generation increases, so does the number of formed bonds in only one reaction step, which could result in the appearance of defective structures. Therefore, in this method of synthesis, it is very important to assure the completion of the reaction before the next step to avoid deficiency in the formed branches. To overcome this limitation, an excess of a monomer is usually used in the reaction which necessitates purification after each step and making the reaction tedious and time-consuming [158]. A prominent example of dendrimer synthesized by using the divergent strategy is the PAMAM dendrimer. This ethylenediamine core dendrimer was obtained up to the tenth generation via two iterative reactions: a Michael-type addition of amino groups to methyl acrylate followed by aminolysis of the resulting methyl ester with an excess of ethylenediamine [160].

The convergent synthetic approach is a strategic growth of the dendrimer that was developed to overcome the weaknesses of the divergent approach [165]. The convergent growth begins from the periphery of the dendrimer moving inwards to the core when wedges of sufficient size are achieved [166]. Analogous to the divergent strategy, the activation/deactivation steps are employed to construct the dendrons of desired size (Figure 1.13B). It is only after reaching the desired generation size that the dendron is coupled to a small polyfunctional core molecule. The final step of the synthesis involves the activation of the core, where two or more dendrons are joined, creating the dendrimer [167]. This approach sometimes referred to as the organic chemist`s approach due to greater structural control and stepwise assembly of the building blocks [166]. Convergent growth, unlike the divergent approach, allowed the synthesis of dendrimers without defect as it involves a limited number of reactions on the same molecule, going from generation one (or the core) to another significantly higher (usually up to 6^{th} generation) [163]. Nevertheless, the main drawback of this approach is the risk of structural defects within dendrons and dendrimers of higher generation due to both chemical and stereochemical factor. These include the reactivity, availability of the focal point and the steric hindrance shielding the multifunctional core from reacting.

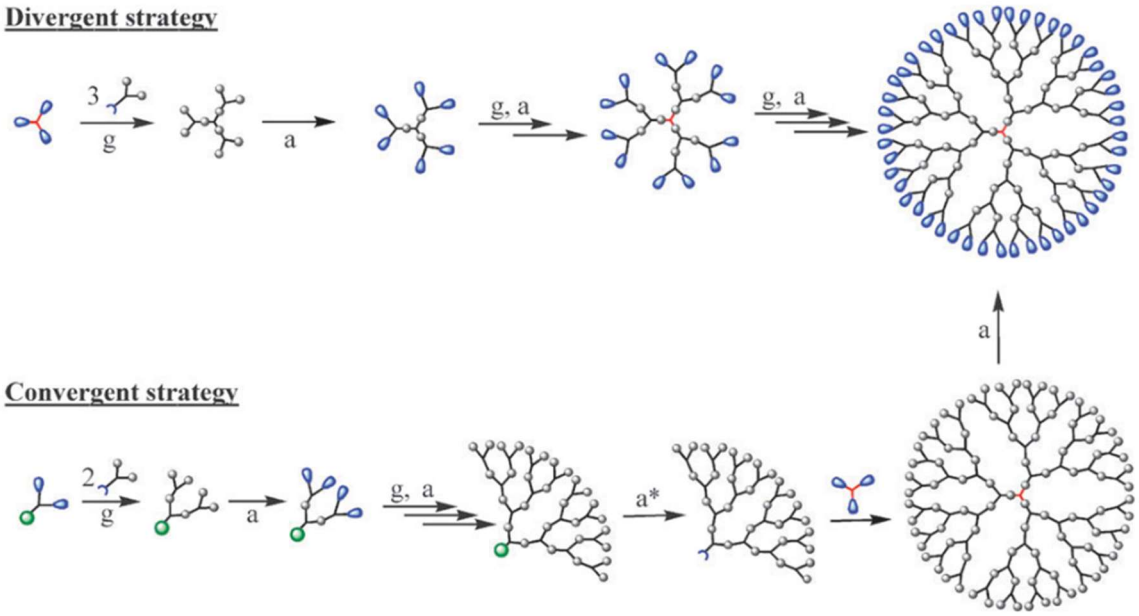

Figure 1. 13. Scheme for the synthesis of dendrimer Adapted from[171]: A) divergent strategy; B) convergent strategy. Descriptions of the conditions: (a) activation of the surface group; (a*) activation of the core; (g) dendritic growth

1.9.1.2. Chemistries in the Synthesis of Dendrimer: Brief Overview

The synthesis of dendritic structures without defect and preserved monodispersity requires the use of efficient and selective reactions that simplify or possibly avoid the difficulties in the purification steps. In these regards, there have been concerted efforts to improve the efficiency of the existing reactions or develop new protocols for the synthesis and functionalization of dendrimers [168]. Here, we present a brief introduction to the most common chemical reaction used in the synthesis of dendrimers.

Protection and deprotection strategy are undesired, still unavoidable type of reactions in the organic synthesis. In real scenarios, the importance of these strategies is ubiquitous in the synthesis of dendrimer to avoid side products while the multifunctional molecule reacts with only allowed group and maintaining the other part inert [169]. The incorporation of the orthogonal protecting group in the dendrimer synthesis provides opportunities for the systematic modification of the growing structures [170].

Amine protection/ deprotection is one of the commonly used strategies in the synthesis of dendrimer [170]. The *tert*-butoxycarbonyl(Boc) is one of the extensively used protective group

of amines [171]. As an example, the protection of amine with Boc facilitates the manipulation of the compound with benzyl ester and another carboxylic acid protective group through hydrogenation as the protected amine resists hydrogenation and strong alkali medium [172]. When the compound of interest attained or the extensions of the chain growth is desired, deprotection can readily be achieved using acids such as trifluoracetic acid and hydrochloric acid in dioxane [173]. Carboxylic acid protection and deprotection is another strategy in the synthesis and strategic growth of dendritic structure [172]. Carboxylic acids need to be protected as the acidic proton can interfere in the base-catalyzed reactions or prevent unnecessary nucleophilic addition reaction [174]. The sequential protection and deprotection of carboxylic acid are recently described in the synthesis of the amino-terminal dendrimer. In this synthesis, the use of mild condition to protect the carboxylic acid using benzyl bromide and sodium carbonate to form benzyl ester is described. The deprotection of the benzyl esters can be attained through hydrogenolysis using Pearlman's catalyst [172]. Boc group is perfectly stable under these conditions allowing selective protection and deprotection to strategically manage the synthesis of higher generation dendritic structures.

Another commonly used reactions in the synthesis of dendritic structures are the esterification or amide-forming types of reactions using different strategies. There are numerous kinds of these reactions: via the formation of acid chloride [175], or carbodiimide, using a different activating reagent that includes dicyclohexylcarboiimide (DCC) along with N-hydroxy succinimide (NHS)[176] or 1-hydroxybenzotriazole hydrate (HOBt) [177], 1-ethyl-3-(3-dimethylaminopropyl carboiimide) (EDC) [178] and fluoride-promoted esterification using 1,1′- carbonyldiimidazole as activation reagent (CDI) [179] are to be mentioned among the others.

A relatively new advancement in the synthesis of the dendrimer is the introduction of the click chemistry concept in the year 2001. The most widely studied "click" chemistry both in the divergent and convergent synthesis of the dendrimer is Copper (I) -catalyzed azide/alkyne cycloaddition (CuAAC) [180]. The presence of Cu (I) prevents the formation of 1,5-triazole, which constitutes around 50% of the products during Huisgen cycloaddition and results in regioselective 1,4-disubstituted 1,2,3-triazole heterocycles as a result of reactions between alkyne and azide [181] (Figure 1.14). In addition to the dramatic improvement of the regioselectivity of the reaction, the presence of the catalytic amount of Cu (I) increases the reaction rate up to 8 orders of magnitude higher compared to the uncatalyzed process [182].

This type of reaction presented an unprecedented advantage that includes flexibility, high enthalpy, high yields, and generates an inoffensive by-product [183].

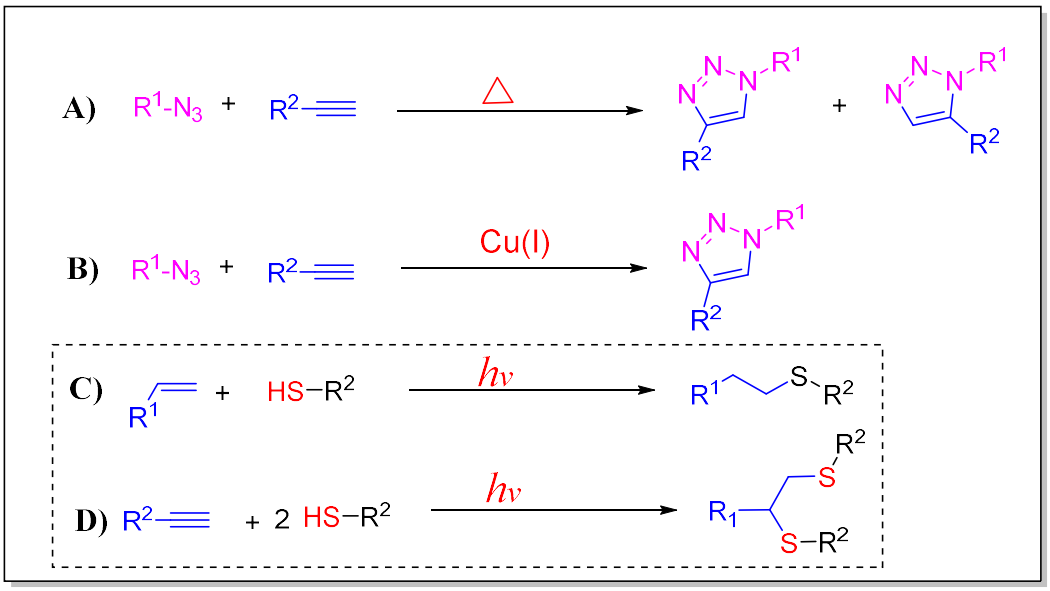

Figure 1. 14. Scheme for Huisgen 1,3-dipolar cycloaddition (A); Copper (I)-catalyzed 1,3-dipolar cycloaddition (B); radical thiol–ene coupling (C), and radical thiol–yne reaction (D).

The radical-mediated thiol-ene and thiol-yne are another "click" type reactions in the synthesis of dendritic structures [184]. The thiol-ene reaction is proved to be particularly useful for network formation, polymer functionalization and dendrimer synthesis for various applications [185]. This reaction is outstandingly efficient and importantly it can be carried out in the presence of oxygen at room temperature in the absence of a solvent or aqueous solvent [186]. Thiol-ene coupling has been proved to be a robust and efficient technique for the orthogonal synthesis of dendrimers [187]. The thiol–yne chemistry (Figure 1.14C) offers an outstanding benefit of being orthogonal with CuAAC while sharing its substrates, the alkynes, and is a robust and versatile method that tolerates a variety of functional groups. It gives an impression to be an ideal approach to construct multifunctional dendritic structures [188].

1.9.1.3. Dendrimers as Synthetic Carrier Molecules

The unique properties of dendrimers, such as a higher degree of branching, multivalency, globular architecture and well-defined MW, make them promising scaffolds for numerous applications [189]. The diversified use of dendrimers as a carrier in drug and gene delivery [151,190,191], imaging [192,193], scaffolds for tissue repair [194–196], optical oxygen

sensors [197,198] and DeAns [66,136] are to be mentioned among the greater use of these nanoarchitectures.

The multivalency of the dendrimer, perhaps, is the most exploited dendritic features in various applications. Below are examples of various properties of dendrimers modulated by multivalent end groups: i) the dendrimer solubility: hydrophobic core dendrimer solubility in water due to multiple hydrophilic end group and solubility of the compound with the hydrophilic interior in oil as a result of multiple hydrophobic peripheral moieties; ii) affixing multiple copies of ligands on the periphery of the molecules which promotes multivalent interactions between the ligand and the cells. Thus, having multiple weak binders on a dendrimer can turn it into a high-affinity reagent [199]. Furthermore, the core-shell effect that generates dissimilar nanoenvironment at the core and peripheries; the nanometer size and globular tri-dimensional shapes of the higher generation dendrimers to mimic some features of proteins, signifies the importance of this group of nanostructures in the field of biomedicine [200].

One of the problems in cellular-based allergy research is to obtain the optimal hapten-carrier conjugate that mimics the *in vivo* situation *in vitro*. For example, hapten-BSA is a commonly used conjugate system in the allergic model. This system, while usually used to prompt degranulation, it does not precisely mimic the complex situation of the natural allergens. The problem arises first from a lack of control on the number of conjugations and their molecular orientation on each BSA protein. Secondly, the hapten- BSA conjugates have a limited valency, (∼20, given the number of lysines for binding) which restricts their ability to stimulate degranulation [57,201]. HSA is another carrier protein used in antigenic hapten–carrier conjugate which presents the possibility of infections, difficulties in both the chemical handling and characterization of the haptenized protein. Additionally, PLL, the most widely used protein carrier in the development of diagnostic tests for drug allergy impedes problems related to its polydispersity that deter from the accurate chemical characterization, reproducibility, and medical interpretations [66].

Given the limitations of the existing hapten-carrier system, the development of a synthetic carrier with a well-defined structure and control over the number of hapten per carrier is urgently needed to develop diagnostic tests for drug allergies. The prospect of precise control over the features of the carrier through characterization and the multiplicity of the surface

would hasten the translation of these tests into clinical practice. In this regard, our group has demonstrated the importance of dendrimer based synthetic carrier with a multivalent display of hapten and its versatile features to be adapted into different solid support platforms (cellulose disks, zeolites and silica particles) in the determination of sIgE to β-lactams allergies [66,145,148,202–204]

Chapter 2: Hypothesis and Objectives

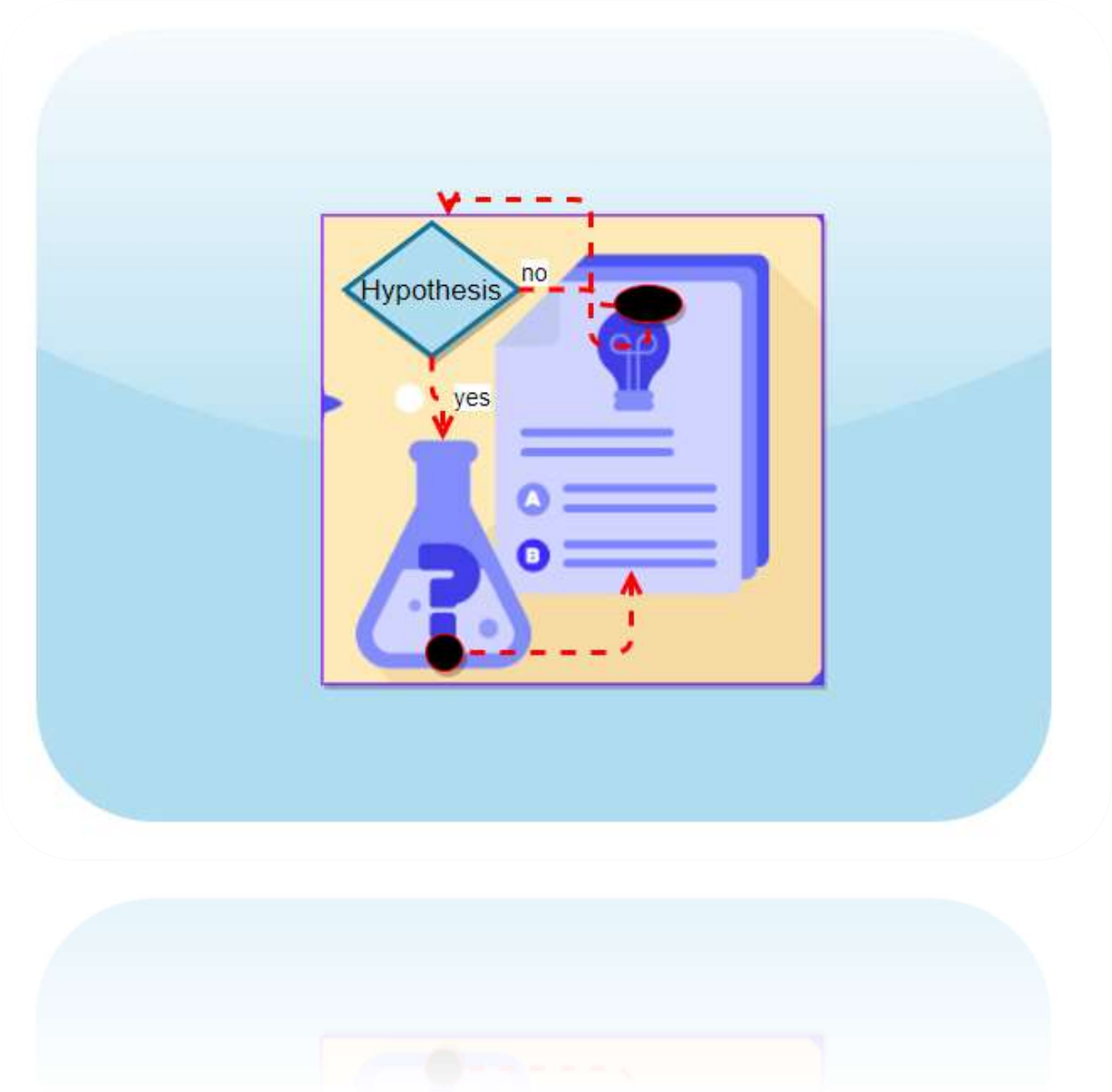

2.1. Hypothesis and Justification

β-lactam antibiotics are the first-choice treatment of many bacterial infections [205]; nevertheless, they are also the most frequent triggers of reactions, being their prevalence usually associated with consumption patterns [113]. Nowadays, AX, alone or in combination with CLV, is the most common elicitor [20,30,113]. β-lactam allergy can be induced by different immune mechanisms, among which the IgE antibodies-mediated one is the most common and better studied [30,50]. The diagnosis of IRs to AX in clinical practice is based mainly on *in vivo* and *in vitro* methods [120]. Due to the non-optimal sensitivity of skin tests, drug provocation test is considered the gold standard to establish the diagnosis, which is risky to the patient and not recommended in patients with a history of life-threatening reactions [113,119]. *In vitro* tests are based on the determination of sIgE (immunoassays), with the commercial ImmunoCAP only detecting 20 % of allergic patients, and on the quantification of basophil activation after stimulation with the culprit drug, showing sensitivity around 50 %. Among the factors affecting such low sensitivity could be the fact that correct antigenic determinant and/or conjugates are not incorporated into *in vitro* tests. An improved sensitivity can be only addressed using suitable structures.

Moreover, in the case of BAT understanding, cellular activation is essential. Besides BAT, a novel passive cellular tests, using basophil or mast cell lines, are being described as emerging *in vitro* methods for diagnosing allergy to allergens and drugs. These complex cellular and structural restrictions in the *in vitro* activation or inhibition of effector cells (*section 1.5.2*) requires sophisticated structures that are well-defined and characterized to facilitate the interpretation of results. Although different molecules have been designed to assess the influence of different parameters on the degranulation of MCs, using either sophisticated scaffold models for allergens or synthetic haptens (DNP, dansyl) linked on bi- or multi-valent structures, structures containing drugs have been hardly studied in this cellular process. Moreover, dissimilar optimal sizes have been reported for effective cross-linking as a consequence of the diverse features of the synthetic systems studied, such as the different density of haptens (or valency) [60,206], three-dimensional structure, and flexibility [60] or rigidity [16,206,207], affinity, cooperativity, and proximity of epitopes [17,61,208] of the synthetic systems.

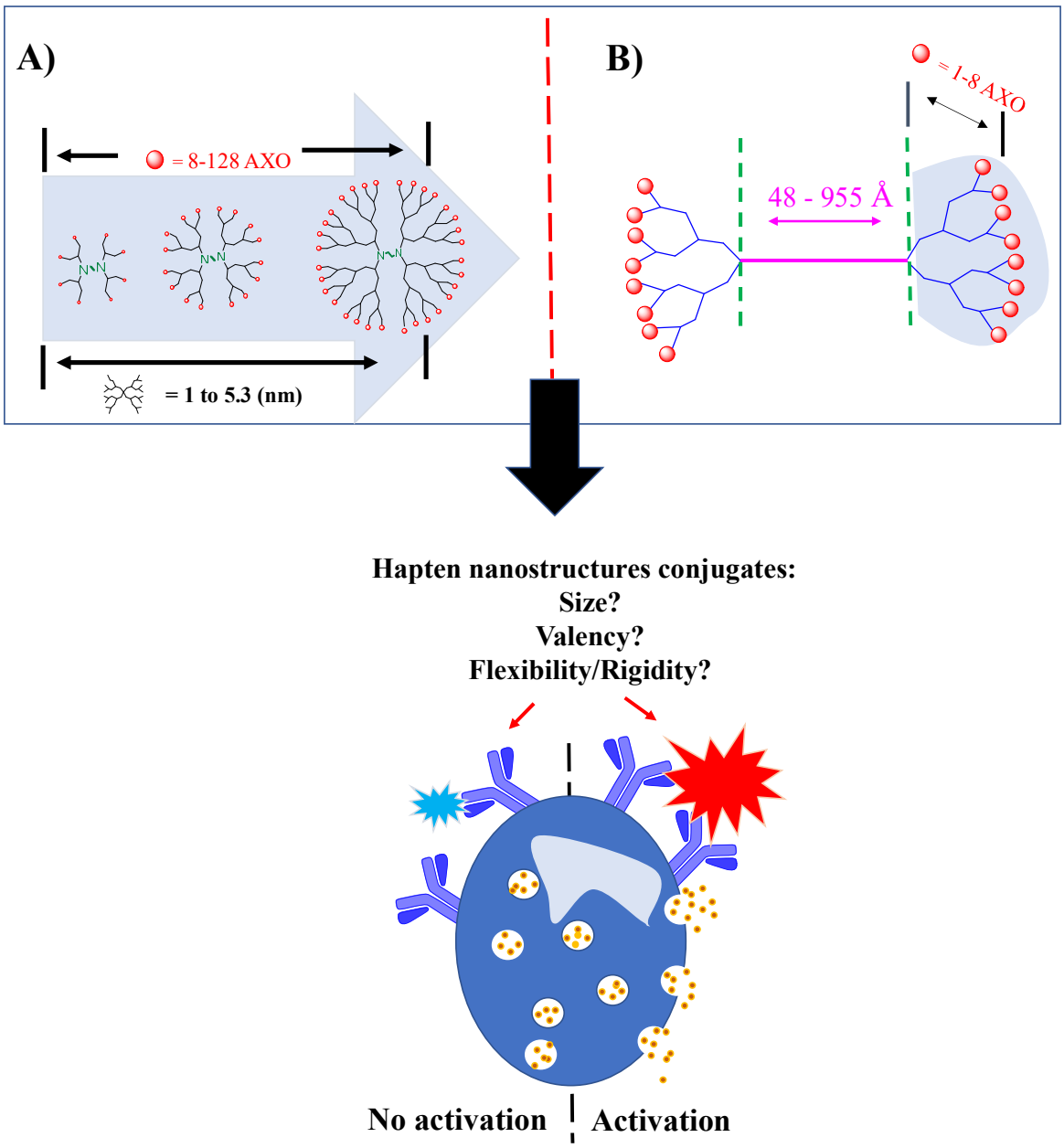

Figure 2.1. Schematic explanation of the proposed study: A) Schematic view of the DeAn of various end groups (8-128 AXO groups); B) Schematic representation of the parallel variation both in the spacer length (PEG600- 12000) and the number of end groups

Intending to investigate the structural requirements of conjugates to induce effector cell activation, we propose a SAR approach using nanostructures containing AX (real hapten) and samples from allergic patients (sIgE). AX is a small compound that requires protein haptenation to form multivalent conjugates with increased size to be immunogenic. We hypothesize that optimal structural requirement for promoting the activation of effector cells can be attained using well-precised multi-AX nanostructures, either of globular shape or that

also contain flexible polymeric spacers of enough length, in which the distance between epitopes may be relevant for the immune complex morphology and effector cell degranulation (Figure 2.1). Inspired by our previous design of DeAns that showed potential use for penicillin-sIgE quantification, we propose the design of three different sets of related nanoarchitectures to expand the interaction studies with the immune system. We will make use of dendrimer-based structures due to the controlled structure and multivalency that can be functionalized with the desired ligands, the antigenic determinant of AX, for the proper interaction with the immunological system.

In summary, we hypothesize that structural properties of conjugates can be nano-engineered to be appropriate for intra-molecular crosslinking of sIgE bound to FcεRI on basophils or MCs, considering:

- **Distance between two haptens**. The maximum distance between haptens would be: (i) the diameter of the nanostructure in a dendrimer globular structure; (ii) the length of the spaced linker with dendrons in bidendron-based structures.
- **Flexibility/Rigidity of structures**. PEG spacers can be used as flexible linkers whereas, dendrimers of lower generations (1 and 2) are marked by flexible scaffolding, and become bigger, more globular, and rigid with increasing generations.
- **Multivalence**. A haptenized dendron or dendrimer would enhance the probability of IgE recognition by displaying multiple haptens in its flexible scaffold, although in the case of dendron its dimension would be insufficient for the crosslinking process. Since degranulation is achieved by at least two IgEs, systems of bidendron antigens (BiAns) would be of interest.

Those molecules that present the structural requirements to activate cells, should increase the sensitivity of cellular diagnostic assays.

2.2. Objectives

2.2.1. General Objective

The long-term aim of this study is to increase *in vitro* test sensitivity to diagnose IRs to AX, by including in the assay nano-engineered multivalent structures that display the optimal size for crosslinking processes of effector cells. To generate knowledge of such structural requirements, we aim to design and synthesize a series of nanostructures decorated with AX, and to study the specific molecular recognition and effector cell Activation in the immunological responses to AX.

2.2.2. Specific Objectives

- Synthesis and structural characterization of a series of DeAns starting from PAMAM dendrimers of different generations (G1-G5) and terminally decorated with AX (number of end groups from 8 to 128).
- Synthesis and structural characterization of a series of symmetrical BiAns based on PEG linkers of different lengths (MW 600-12000 Da) and end-coupled with G2-PAMAM dendrons, each terminally functionalized with AX (number of end groups of each dendron 8).
- Synthesis and structural characterization of a series of symmetrical BiAns based on polyamide type dendron scaffolds, varying both the length of the polymeric spacer (MW 600-12000Da) and the number of the peripheral functionality with AX (2 to 16).
- Evaluation of the ability of AX-sIgE to recognize all designed nanostructures by competitive immunoassays.
- Study the influence of spacer length of the BiAns on the formation of immunocomplexes by transmission electron microscopy (TEM).
- Evaluation of the effects of nanostructures on cell viability, and on their allergenic activity using bone marrow-derived MCs passively sensitized with mouse anti-AX MoAb and humanized RBL-2H3 or LUVA cells sensitized with polyclonal antibodies from sera of AX-allergic patients. *These studies were performed in collaboration with Dr Alba Rodriguez-Nogales (Digestive Unit, University Hospital, Granada) and Dr Sara Benedé (Instituto de Investigación en Ciencias de la Alimentación, Madrid)*
- Evaluation of the inclusion of nanostructures in BAT for diagnostic, *which was performed by our research group.*

Chapter 3: Synthesis, Characterization, and Immunological Evaluation of Nanoarchitectures based on Dendrimers

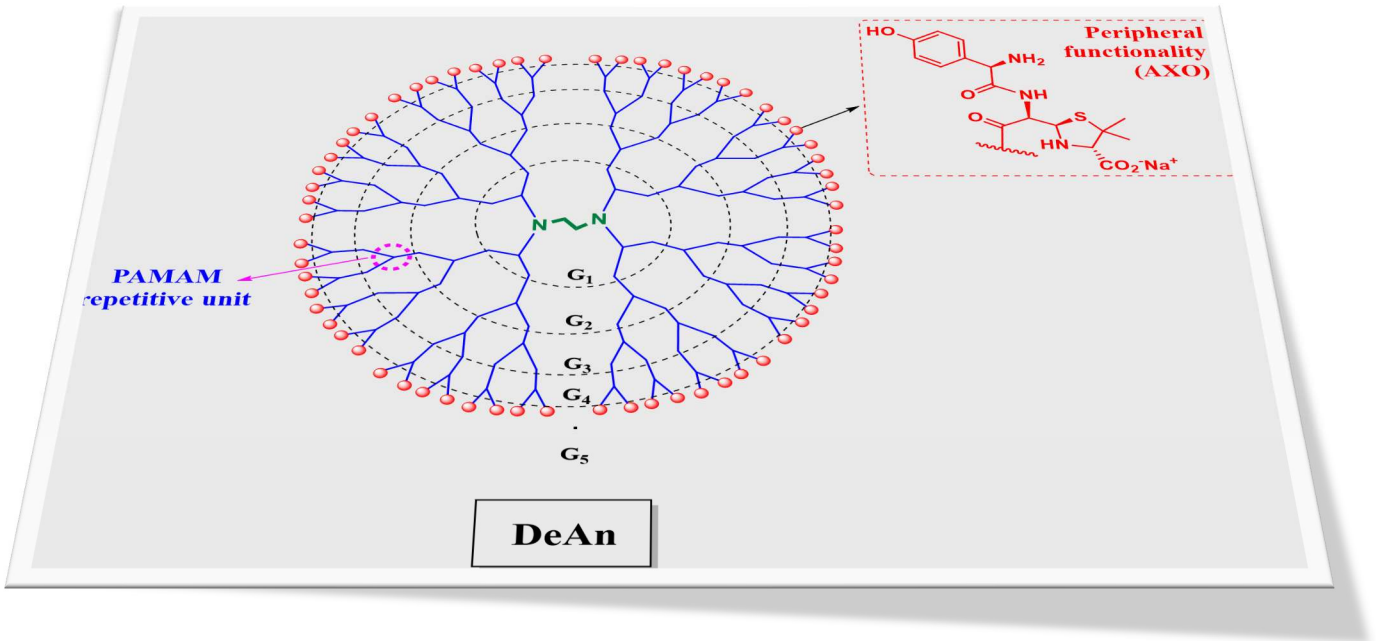

3.1. Introduction

Immediate hypersensitivity and allergic diseases are executed by the crosslinking of IgE bound to its $Fc_{\varepsilon}RI$, with multivalent antigen initiating the activation of the effector cells by promoting the aggregation of $Fc_{\varepsilon}RI$ [210]. The presence of multivalent antigen (allergen) of enough size to at least be able to bind two FcεRI-bound IgE is the minimal requirement. In this chapter, DeAns were used to generating knowledge regarding their structural features required for effector cell activation, in which the size may play a key role. We make use of the advantages of dendrimers as carrier molecules in achieving multivalent, and reproducible hapten-carrier conjugates which structures can precisely be characterized [66,203]. Although protein-based conjugates would be more similar to the conjugates formed *in vivo*, which are responsible for inducing allergic reactions, the main limitation of using these conjugates is the lack of control on both the haptenation number and their molecular orientation on the protein. Moreover, if thinking in a diagnostic application, their broad distribution of molecular weight makes it difficult to standardise the assays. In this context, to overcome the limitations of the lack of characterization of protein conjugates, a series of DeAns were employed as the first set of controlled structures with precise sizes and number of AXO moieties for SAR.

3.2. Design of DeAns

The design of DeAns involves the decoration of the PAMAM dendrimers with AXO peripheral units. These constructs would allow evaluating the influence of both dendrimer size and the number of determinants (valency), features given by each generation in cell activation (Figure 3.1). PAMAM dendrimers were chosen as common scaffold based on their commercial availability, aqueous solubility, the amino peripheral functionality that can emulate the reactivity of those in proteins lysines and previous studies showing that DeAns based on PAMAM are recognized by penicillin-sIgE. The size of starting PAMAM dendrimers of five generations (G1 to G5) (from 1 to 5.3 nm) with ethylenediamine core increases linearly as a function of added generations, at a rate of approximately 1 nm per generation, whereas the terminal functional groups proliferate exponentially at each generation (from 8 to 128 peripheral amino groups) [161,209].

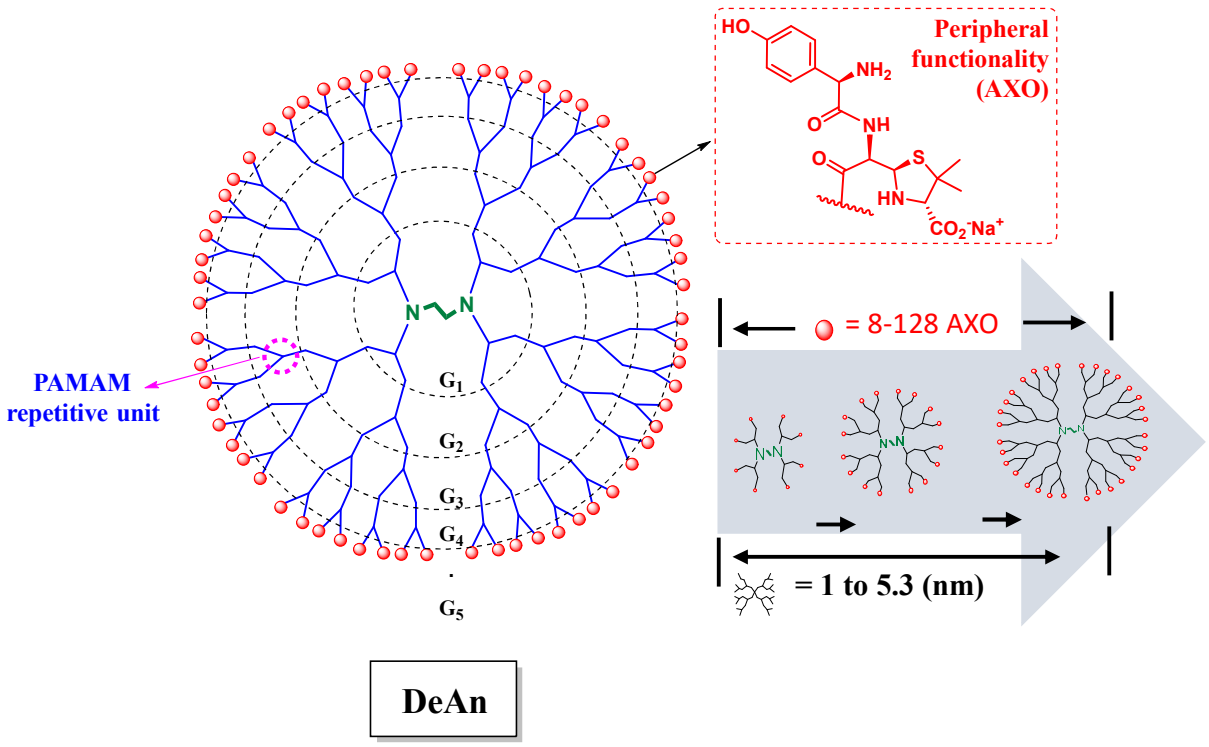

Figure 3.1. Schematic representation of DeAns. Structural variations among them consist of the increasing number of antigenic determinants (AXO), ranging from 8 to 128, and rising size depending on the growing generation (G1 to G5, with starting PAMAM dendrimer size ranging from 1 to 5.3 nm).

3.3. Synthesis and NMR Characterization of DeAns

DeAns were obtained through the nucleophilic reactions of the free amine on the periphery of dendrimers to the β-lactam ring of AX. Incubations of PAMAM dendrimers (with ethylenediamine core) of five generations (G1-G5) with an excess of AX were carried out in basic pH buffer (for ensuring peripheral amino groups to be deprotonated) at 4 °C. As a representative example, the synthesis scheme and ^{1}H NMR of G1- AXO are shown in Figure 3.2 and Figure 3.3, respectively. The low temperature was an important factor in obtaining fully functionalized molecules as a result of the reduced mobility of the substituted branch and a decrease in the steric hindrance as previously reported by our group [203]. Additionally, the incubation time needed for the complete functionalization increased for higher generations.

The purification was efficiently performed by gel filtration chromatography using Sephadex columns. Characterization and monitoring of the reactions were performed by ^{1}H and ^{13}C NMR, with the latter providing more information about the complete functionalization of

amine groups. Accordingly, the formation of the amide bond was confirmed by the shift of the terminal methylene proton of the dendrimer from around 2.72 to 3.26 ppm. The partial shift in this proton was used as a controlling method to decide whether the reaction needs to be refreshed with AX or not.

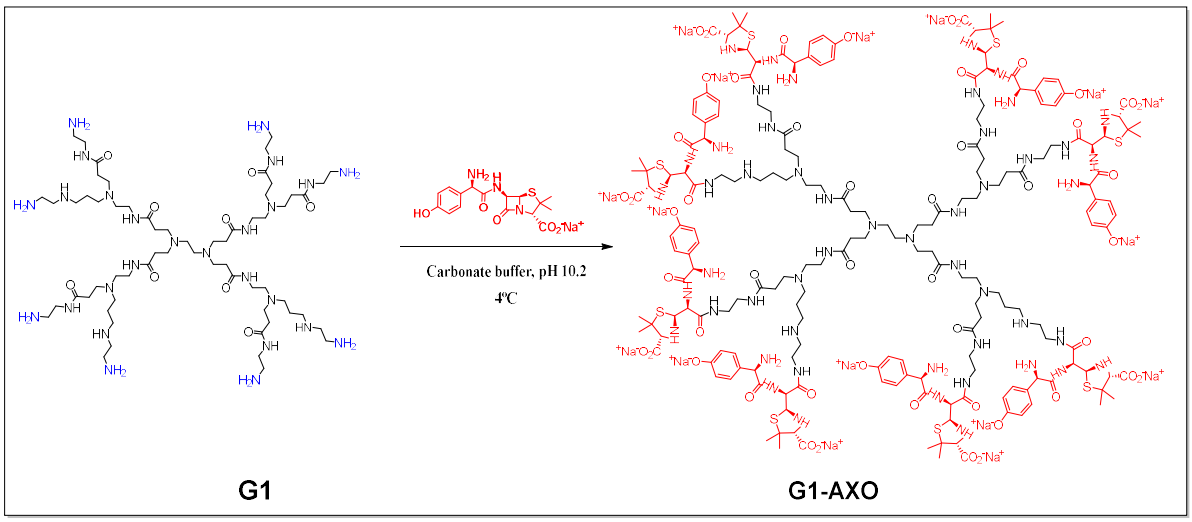

Figure 3.2. A representative schematic illustration of the synthesis of G1-AXO. The commercial PAMAM dendrimer (G1) was incubated with AX at aqueous basic pH and cold temperature until complete functionalization

Additionally, the presence of the opened form of the β-lactam attached to the dendrimer was evidenced by the shift and separation of β-lactam protons (H5 and H6) to a higher field compared to the shift in free AX (5.42 and 5.41 ppm). Finally, the confirmation of the completion of the reaction was attained by ^{13}C NMR observing the shift in the signal of the terminal ethylene residue due to condensation reaction. The shift in carbons (h) and (i) from around 41.9 and 40.0 ppm, respectively in G1 PAMAM dendrimer (Figure 3.4A) to 38.8 and 38.7 ppm in G1-AXO (Figure 3.4B) indicate the absence of signals for the carbon bonded to the unfunctionalized amino groups. Yield ranging from 69-82 % were obtained, the highest yield being for the lower and lowest for the higher generations of the dendrimers.

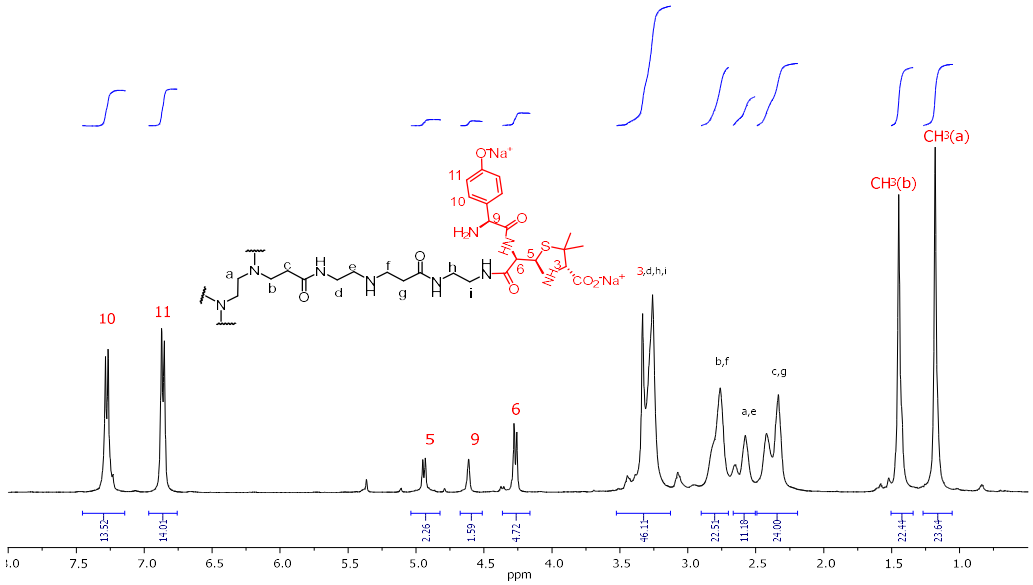

Figure 3.3. A representative example of ^{1}H NMR spectra of DeAns, a spectrum of G1-AXO in deuterium oxide(D_2O) with solvent signal suppression. The integration of the protons of the aromatic region and the methyl groups of the thiazolidine ring, which are not overlapped by others was used to estimate the functionalization with AXO.

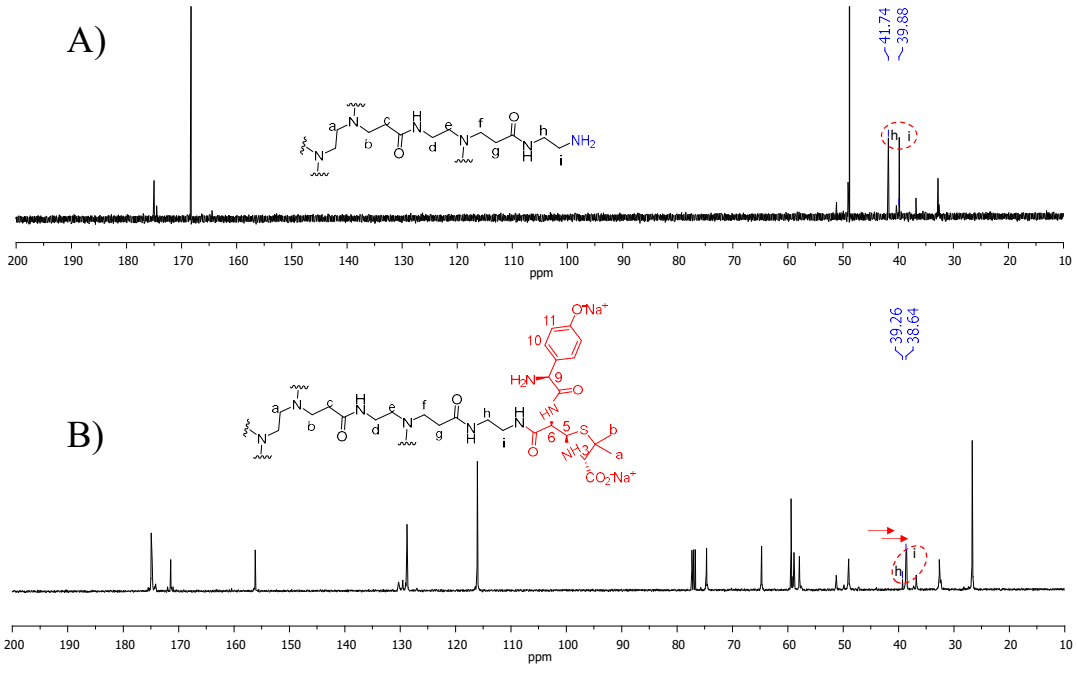

Figure 3.4. A representative example of ^{13}C NMR spectra of the starting G1 PAMAM dendrimer (A) and G1-AXO (B) in D_2O using a chemical shift of deuterated chloroform ($CDCl_3$) as reference. The shift in the signal of the terminal ethylene residue due to condensation reaction is highlighted and indicated by arrows.

The ^{1}H and ^{13}C spectra of all the DeAns are summarized in Table 3.1, 3.2 and 3.3. As can be seen, the spectra of all generations are quite similar indicating the symmetricity and monodisperse nature of the conjugates.

Table 3. 1. ^{1}H NMR data that corresponds to the AXO units in Gn-AXO, where n =1-5

Types of H		H-11	H-10	H-5	H6	H-9	H-3	CH_3(a)	CH_3(b)
δ (ppm)		7.28	6.86	4.94	4.27	4.59	3.33	1.18	1.45
Description		d J=8.1 Hz	d J=8.1 Hz	d J=7.8 Hz	d J=7.8 Hz	s	s	s	s
G1-AXO	*No of protons*	16	16	8	8	8	8	24	24
G2-AXO		32	32	16	16	16	16	48	48
G3-AXO		64	64	32	32	32	32	96	96
G4-AXO		128	128	64	64	64	64	192	192
G5-AXO		256	256	128	128	128	128	384	384

Table 3. 2. ^{1}H NMR data that corresponds to the dendritic skeleton in Gn-AXO, where n =1-5

Types of H		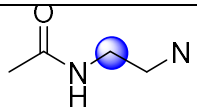	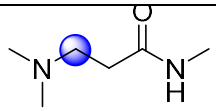	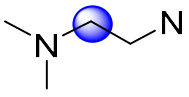	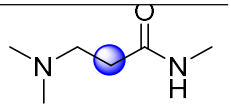
Range of δ (ppm)/description		3.48-3.12(*m*)	2.94-2.69(*m*)	2.67-2.49(*m*)	2.48.2.20(*m*)
G1-AXO	*No of protons*	40	24	12	24
G2-AXO		88	56	28	56
G3-AXO		184	120	60	120
G4-AXO		376	248	124	148
G5-AXO		760	504	252	404

Table 3. 3. ^{13} C NMR data that corresponds Gn-AXO, where n =1-5

δ range (ppm)	Types of Carbon
175.2-174.7	**C3**-$CO_2^-Na^+$
171.7-171.5	**C**O-NH, **C**O-NH
156.4-156.2	**C**O^-Na^+
130.0-129.6	Aromatic
129.1-128-7	Aromatic
116.4-115.9	Aromatic
75.1-74.6	C3
65.2-64.4	C5
59.7-59.4	C6
59.2-58.8	C2
58.4-57.9	Ph-**C**H
51.6-51.1	N-CH_2-**C**H_2-N
49.4-48.9	NHCO-CH_2-**C**H_2-N
39.1-38.5	**C**H_2-NH-CO
33.1-32.1	**C**H_2-CO-NH
27.0-26.5	(**C**H_3)$_2$-C2

3.4. Gel Permeation Chromatography (GPC) Analysis

The increase of the MW of dendrimers after conjugation with AX was confirmed GPC. The GPC measurements were performed on both the commercial PAMAM dendrimers (G1-G5), used as controls, and the final DeAns using calibration with Polyethylene glycol Standards Kit (with MW range from 100-100,000 Da) in DMF with 10 mM LiCl as mobile phase (Figure 3.5). Due to the inherent conflict of comparing the hydrodynamic volumes of linear polymer standards with globular polymer analytes, the GPC-based molecular weight determination was of limited use. However, the GPC traces analysis was useful to show the shifts of the peaks of conjugated products compared to the earlier elution times of starting materials, indicating the MW increment (Figure 3.5 B). The graph also clearly illustrates the difference in the MW among the dendrimer generations of both starting dendrimers and AXO-modified DeAns.

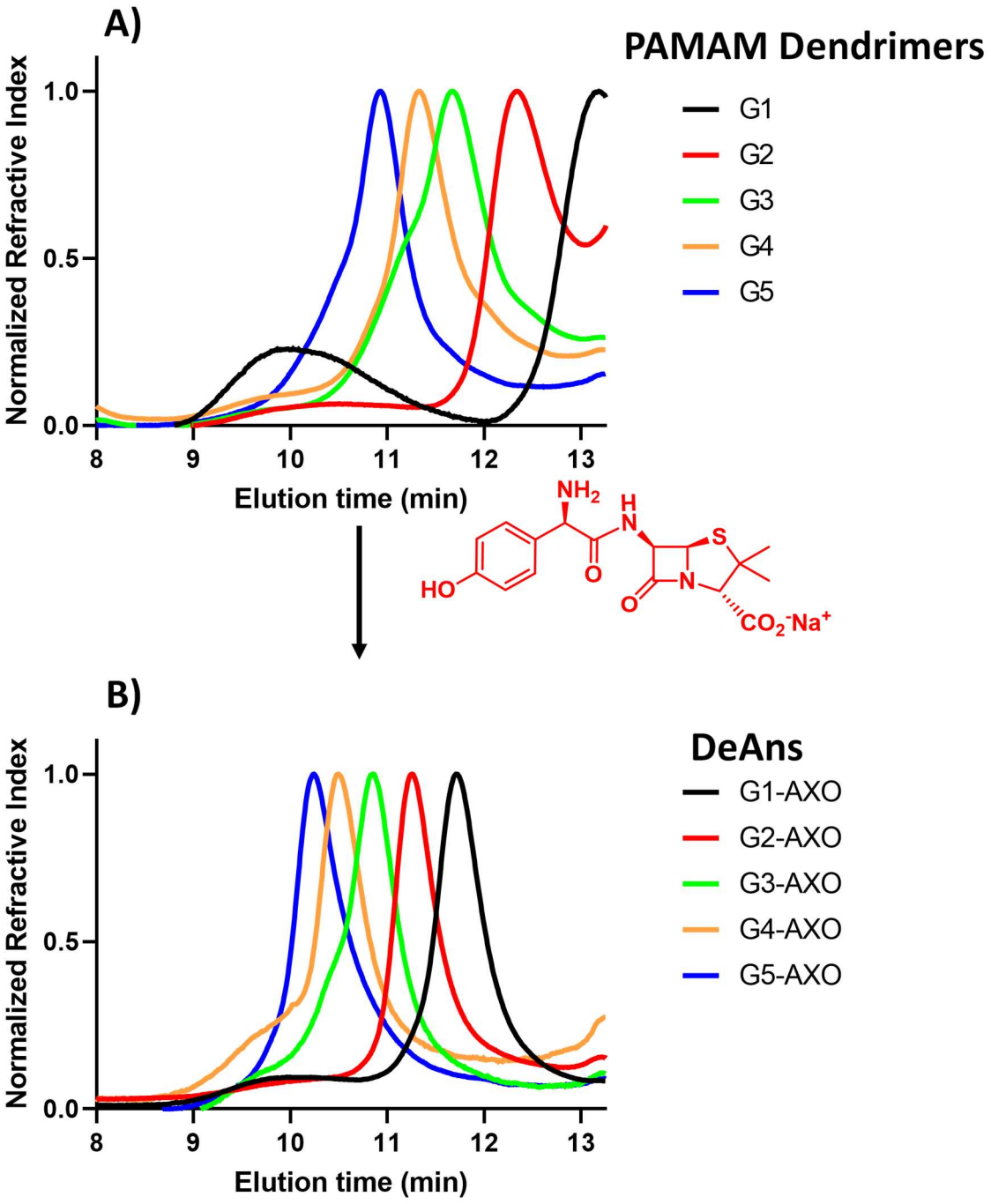

Figure 3.5. GPC traces of (A) unconjugated PAMAM dendrimer (controls) and (B) their corresponding DeAns obtained after conjugation with AX.

3.5. NMR Diffusion Experiments

The purity of the different DeAns was confirmed by Diffusion-Ordered Spectroscopy (DOSY) NMR experiments, sometimes also called NMR chromatography. It is a robust technique to separate the NMR spectra of components within a mixture, that can detect traces in a complex

mixture [211]. Their differentiation is based on the measurement of translational diffusion coefficients, which are linked to the size and shape of the molecule, depending on chemical shift and diffusion behaviour. Therefore, it can be used as an efficient method to detect impurity, unreacted monomer, residual homopolymers, or degradation products [211,212]. The stacked spectra of DeAns were processed via Bayesian transformation to yield the 2D DOSY map, representative DOSY maps of D1-AXO shown in Figure 3.6.

$$\ln\left(\frac{I}{Io}\right) = -\gamma^2\delta^2G^2\left(\Delta - \frac{\sigma}{3}\right)D$$

where G is the gradient strength, I intensity at a given value G, I_0 is the intensity at $G = 0$, γ is gyromagnetic constant, δ is gradient duration, Δ is echo delay, and D is diffusion coefficient.

Table 3. 4. Estimated and experimental values of the DeAn nanostructures.

Synthetic DeAns	Dendrimer Generations	Starting Dendrimer MW(Da)	Estimated DeAns MW(Da)	Hydrodynamic Diameter of Dendrimers (nm)*	D (m^2s^{-1})	Rh nm	Valency
G1-AXO	1	1429.9	4528.9	2.2	$1.49x10^{-10}$	1.4	8
G2-AXO	2	3256.2	9454.4	2.9	$1.21x10^{-10}$	1.7	16
G3-AXO	3	6908.8	19305.3	3.6	$1.05x10^{-10}$	1.9	32
G4-AXO	4	14214.2	39007.1	4.5	$9.97x10^{-11}$	2.0	64
G5-AXO	5	28824.8	78410.7	5.4	$9.22x10^{-11}$	2.1	128

* The hydrodynamic diameter of the dendrimers (nm) obtained from [213]

The DOSY map shows two well-separated peaks along the diffusion dimension, corresponding to the presence of trace amounts of water. As can be seen from the maps, the absence of other peaks different from the main peak that correspond to the DeAn shows that the product is free from impurities and other unreacted residuals of the starting materials, as free AX, amoxicilloic acid or PAMAM only partially functionalized. The diffusion coefficient (D) generally decreases with increasing MW (Table 3.4) as determined by Stejskal-Tanner equation [214] :

$$D = \frac{K_B T}{6\pi\eta Rh}$$

where K_B is the Boltzmann constant, T is temperature and η is the viscosity of the solution (1.0963 cP for D_2O viscosity) by assuming the viscosity of the solution is that of pure D_2O at T=300 K. The corresponding R_H value increases with MW for all structures (Table 3.4). However, the radii of the higher DeAns are not increasing likewise the smaller compounds. This could be due to the back folding of the dendrimer arms as previously reported [214,215].

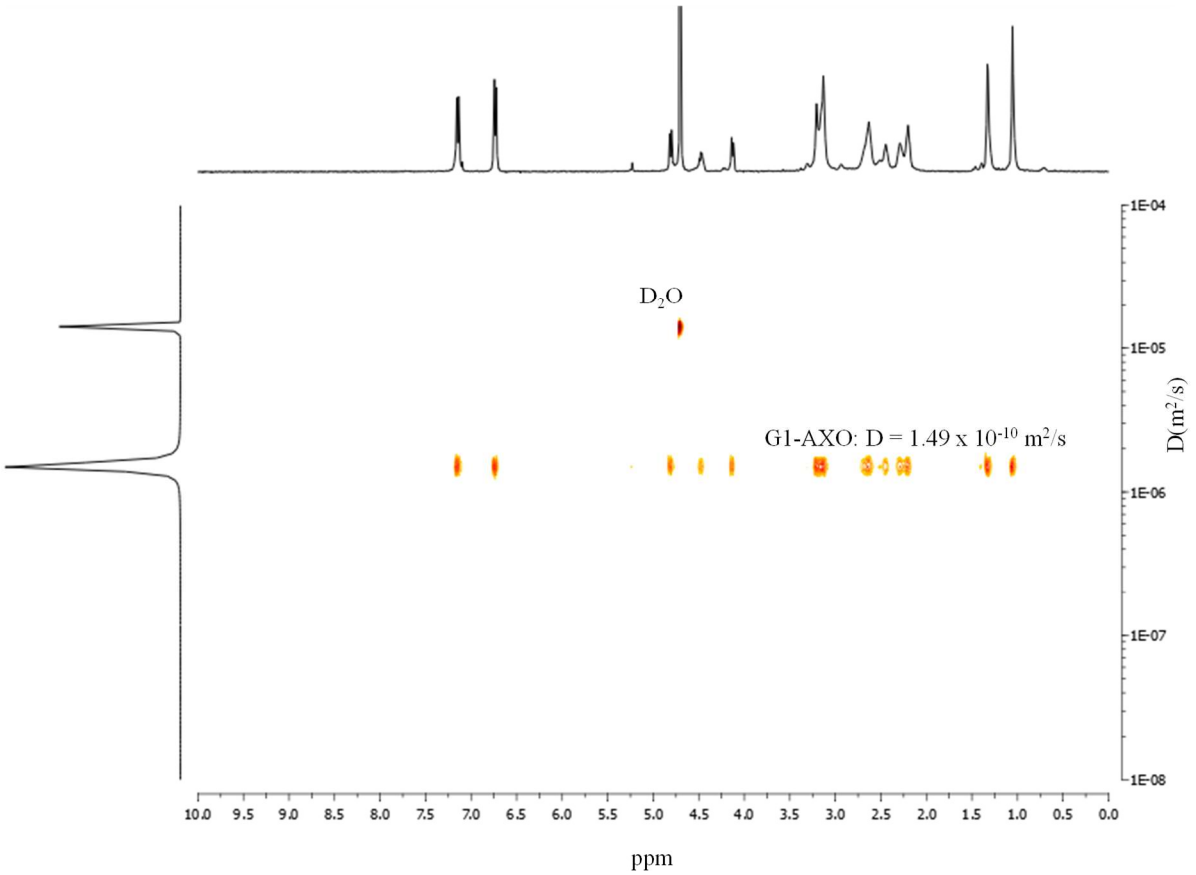

Figure 3.6. 2D DOSY map of G1-AXO in D_2O. The dotted lines show the average diffusion coefficients of A) D_2O; B) G1-AXO after Bayesian transformation. The translational diffusion coefficients correlate the chemical identity of different chemical species.

3.6. IgE Recognition of the DeAns

RAST inhibition study was carried out to compare the capacity of the DeAns to be recognized by AX-sIgE using a pool of sera from patients allergic to AX. This assay consists in competitive serum IgE recognition between the solid phase (PLL-AXO conjugate attached to cellulose discs) and the different inhibitors, DeAns, in the fluid phase, and results are represented as % inhibition IgE binding. To be able to compare the inhibition patterns of the DeAns, the inhibition was performed using an equivalent concentration of AXO units for each DeAn. For

this, three different concentration of the inhibitors (60, 30 and 6 mM), the lowest concentration being the 10-fold serial dilutions of the highest concentrations were evaluated. The monomer of butylamine (AXO-Bu) with the same molar concentration of AXO was used as a reference inhibitor [55].

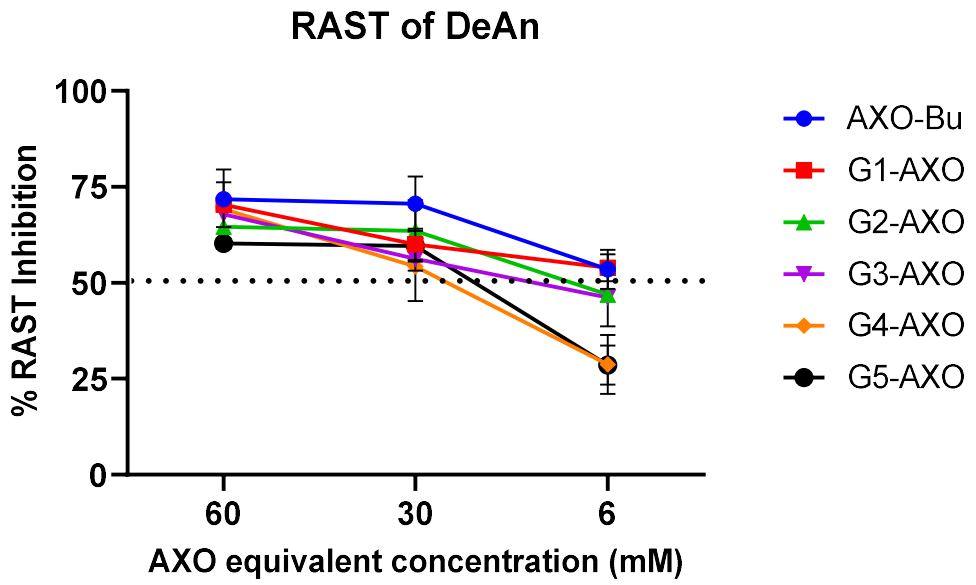

Figure 3.7. RAST inhibition assays performed with a pool of sera from patients allergic to AX, using the series of DeAns and AXO-Bu conjugate as inhibitors and cellulose discs modified with PLL-AXO as the solid phase. Specific IgE recognition is considered with an inhibition of ≥50%.

As can be seen in Figure 3.7, the structures are recognized by AX-sIgE in a concentration-dependent manner. All DeAns conjugates are recognized in the same way despite the difference in the number of AXO antigenic determinants displayed on the periphery. This indicates that the presence of at least one antigenic determinant specific to the antibody (the case of AXO-Bu) is the minimum requirement for the structures to be recognized by sIgE. It is worth noting that the monomeric conjugate (AXO-Bu) and G1-AXO have shown a higher percentage of inhibition (>50%) at all concentration evaluated signifying the absence (AXO-Bu) and a minimal level of steric hindrance between the arms of DeAns (G1-AXO) compared to other DeAns of increasing generations presenting higher density of epitopes.

3.7. Effects of DeAns on IgE Activation of Bone Marrow-derived Cells

Bone marrow-derived MCs were used to evaluate the capacity of the DeAns to induce IgE-dependent degranulation. For these experiments, HSA-AXO conjugates were prepared and their haptenation degree was characterized. In addition, hybridomae AO6.2, IgE isotype (specific to AX side chain) provided by Dr. Cristobalina Mayorga [216] was grown, produced and properly purified. Different experiments were needed to optimize these assays performed by Dr. Benedé, see experimental section. Different concentrations of the DeAns were incubated with cells sensitized with mouse anti-AX IgE MoAb. The β−hexosaminidase release was measured to determine the activation and subsequent degranulation of the cells.

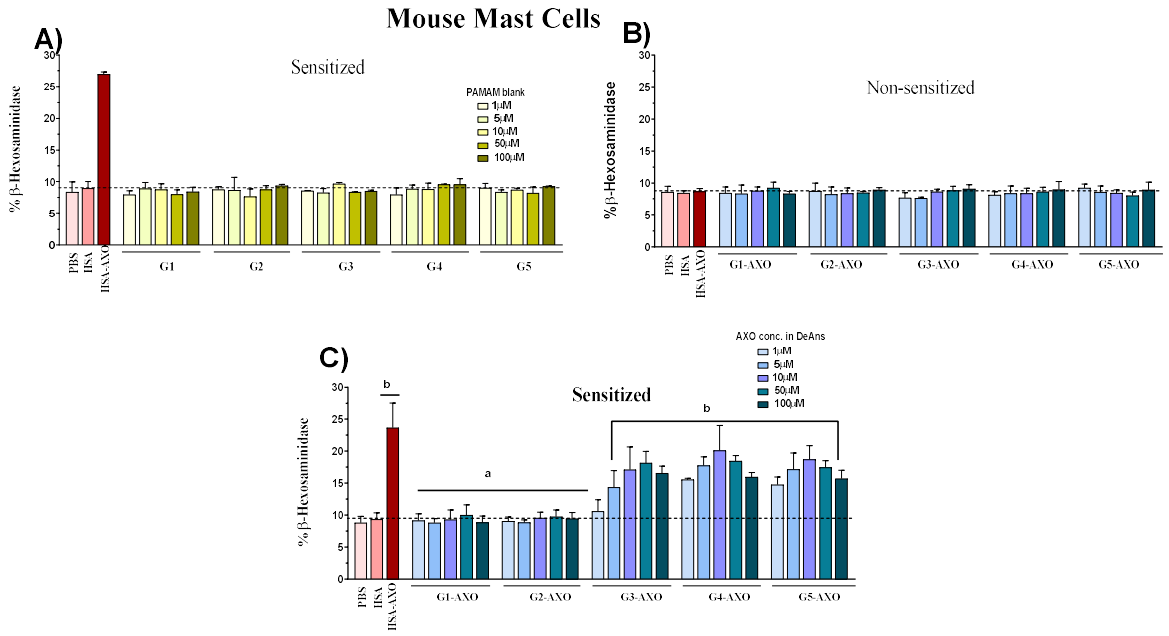

Figure 3.8. Degranulation assays after incubation of Mouse MCs with the series of DeAns at 1,5,10, 50, and 100 μM of AXO equivalents and PAMAM blank. A) Percentage of β-hexosaminidase release in sensitized bone marrow-derived MCs treated with PAMAM blank. B) Percentage of β-hexosaminidase release in unsensitized bone marrow-derived MCs treated with DeAns. C) Percentage of β-hexosaminidase release in sensitized bone marrow-derived MCs treated with DeAns. HSA and HSA-AXO (at 10 μM of AXO) were used as a negative and positive control, respectively. Data are expressed as means ± S.D and are representative of three independent experiments. Groups with different letters statistically differ ($P \leq 0.05$). For multiple comparisons of quantitative data, one-way analysis of variance (ANOVA) was used followed by Dunnett's multiple comparisons test.

Table 3.5. Clinical characteristics of allergic patients and *in vivo* tests used for the diagnosis.

Clinical Characteristics						*In vivo* Tests			
						Skin Tests			DPT
Case	Age	Sex	Clinical Reaction	Drugs Involved in the Reaction	*Grade Severity	BP-OL	MD	AX	AX
1	78	F	Anafilaxis	AX-CLV	II	ND	ND	ND	ND
2	39	F	Urticaria	AX-CLV	I	Neg	Neg	Pos (IDT)	ND
3	32	F	Anafilaxis	AX-CLV	II	Neg	Neg	Pos (SPT)	ND
4	59	M	Anafilaxis	AX-CLV	II	Neg	Neg	Pos (SPT)	ND
5	38	M	Anafilaxis	AX-CLV	III	Neg	Neg	Pos (SPT)	ND
6	50	M	Anafilaxis	AX-CLV	II	Neg	Neg	Pos (IDT)	ND
7	19	M	Anafilaxis	AX-CLV	II	Neg	Neg	Pos (IDT)	ND
8	55	F	Anafilaxis	AX-CLV	II	Neg	Neg	Pos (SPT)	ND
9	43	F	Urticaria/AE	AX-CLV	I	Neg	Neg	Pos (IDT)	ND
10	65	M	Urticaria	AX	I	Pos (IDT)	Neg	Neg	ND
11	58	M	Urticaria/AE	Cefuroxim	II	ND	ND	ND	ND
12	36	F	Urticaria	AX-CLV	I	Neg	Neg	Neg	Pos (AX-CLV)
13	45	F	Anafilaxis	AX-CLV	II	Neg	Neg	Pos (IDT)	ND
14	48	M	Anafilaxis	AX-CLV	II	Neg	Neg	Pos (SPT)	ND

Table 3.6. Clinical characteristics of allergic patients and in vitro tests used for the diagnosis.

	Clinical Characteristics					*In vitro* Tests							
						RIA		IMMUNOCAP-FEIA			BAT		
Case	Age	Sex	Clinical Reaction	Drugs Involved in the Reaction	*Grade Severity	BP-sIgE	AX-sIgE	BP-sIgE	AX-sIgE	Total IgE	BP	AX	AX/CLV
1	78	F	Anafilaxis	AX-CLV	II	Neg	Neg	0.22	0.08	12	Neg	Pos	Neg
2	39	F	Urticaria	AX-CLV	I	Neg	Neg	0.01	0.09	91	ND	Pos	ND
3	32	F	Anafilaxis	AX-CLV	II	Neg	Pos	0.13	0.71	93	Pos	Pos	Pos
4	59	M	Anafilaxis	AX-CLV	II	Neg	Pos	0.26	0.25	505	ND	ND	ND
5	38	M	Anafilaxis	AX-CLV	III	Neg	Pos	0.02	0.26	918	ND	Neg	ND
6	50	M	Anafilaxis	AX-CLV	II	Neg	Pos	0.01	1.82	2337	Neg	Neg	ND
7	19	M	Anafilaxis	AX-CLV	II	Neg	Pos	0.44	3.14	2442	ND	ND	ND
8	55	F	Anafilaxis	AX-CLV	II	Neg	Neg	0.27	0.83	591	Neg	Neg	ND
9	43	F	Urticaria/AE	AX-CLV	I	Neg	Neg	0	0.48	≥5000	ND	ND	ND
10	65	M	Urticaria	AX	I	Pos	Pos	3.03	0.26	388	ND	Neg	ND
11	58	M	Urticaria/AE	Cefuroxim	II	Pos	Pos	0.24	0.89	214	ND	Neg	ND
12	36	F	Urticaria	AX-CLV	I	Neg	Neg	0	2.04	105	Neg	Pos	Pos
13	45	F	Anafilaxis	AX-CLV	II	Neg	Pos	0	0.05	155	Neg	Neg	Neg
14	48	M	Anafilaxis	AX-CLV	II	Neg	Neg	0.4	0.13	35	Neg	Pos	Pos

*AX: Amoxicillin; CLV: potassium clavulanate; DPT: drug provocation test; F: Female; IDT: intradermal test; M: male; Neg: negative; Pos: positive; NP, not performed. *Grading system for generalized hypersensitivity reactions: I, mild (skin and subcutaneous issues only); II, moderate (features suggesting respiratory, cardiovascular, or gastrointestinal involvement); III, severe (hypoxia, hypotension, or neurologic compromise). REF: Brown SG. Clinical features and severity grading of anaphylaxis* [217].

The positive control, HSA-AXO, induced around 20 % of β-hexosaminidase release at 10 μM of AXO moieties concentration, lowest concentration evaluated for the DeAns (Figure 3.8B). The nanostructures constructed with lower generation dendrimers, G1- AXO and G2-AXO, did not result in the activation of the cells. However, the DeAns bearing a higher number of AXO units (based on G3 and above) and associated size have induced the release of β-

hexosaminidase release, with no significant difference, compared to the positive control (HSA-AXO) at all the concentrations apart from with G5-AXO (100 μM). This brings out the importance of the size of the nanostructures as a relevant factor in addition to the multivalent presentation of the antigenic determinants. None of the unsensitized cells (Figure 3.8A) treated with DeAns or the positive control (HSA-AXO) resulted in the degranulation, indicating that activation occurs through an IgE-mediated mechanism.

3.8. Effects of DeAns on IgE-Induced Degranulation in RBL-2H3

The capacity of IgE to bind to DeAns and cross-link specific IgE on effector cells was investigated in a more realistic scenario using a series of sera from allergic patients to AX and tolerant subjects. To evaluate this, the humanized RBL-2H3 cell line which shares characteristics with both MCs and basophils, and expressing FcεRI) [218] was passively sensitized with sera from 14 allergic patients and sera from 11 tolerant subjects to AX. Subsequently, the primed cells were treated with four different concentrations of DeAns (in terms of the same equivalents of AXO determinants) and the blank structures (PAMAM G1-G5). The degranulation was measured in RBL-2H3 cells as total β -hexosaminidase release. Patients' characteristics are described in Table 3. 5 and 3.6.

The results in cell sensitized with AX-allergic patients (containing sIgE) demonstrate that only DeAns of higher generations (G3 and above), and hence size and valency, have resulted in a dose-dependent degranulation, compared with a negative control group (PBS). Higher degranulation was obtained with cells stimulated with G5-AXO, with the highest valency (128 AXO units) and biggest size, at all concentrations and showing a maximum response at 100 μM (Figure 3.9B). Even at the lowest concentration (10μM of AXO units), G5-AXO, bearing the highest multivalent (128 AXO units) and size structure, induced a release of around 26 % of β-hexosaminidase, signifying it as the most effective cross-linker. Blank structure controls (PAMAM dendrimers) did not induce cell degranulation. Examining the degranulation responses in RBL-2H3 cells primed with the sera from tolerant subjects treated with structures, none of them (DeAns, blank dendrimers or HSA-AXO control structures) did induce cell degranulation (Figure 3.9A).

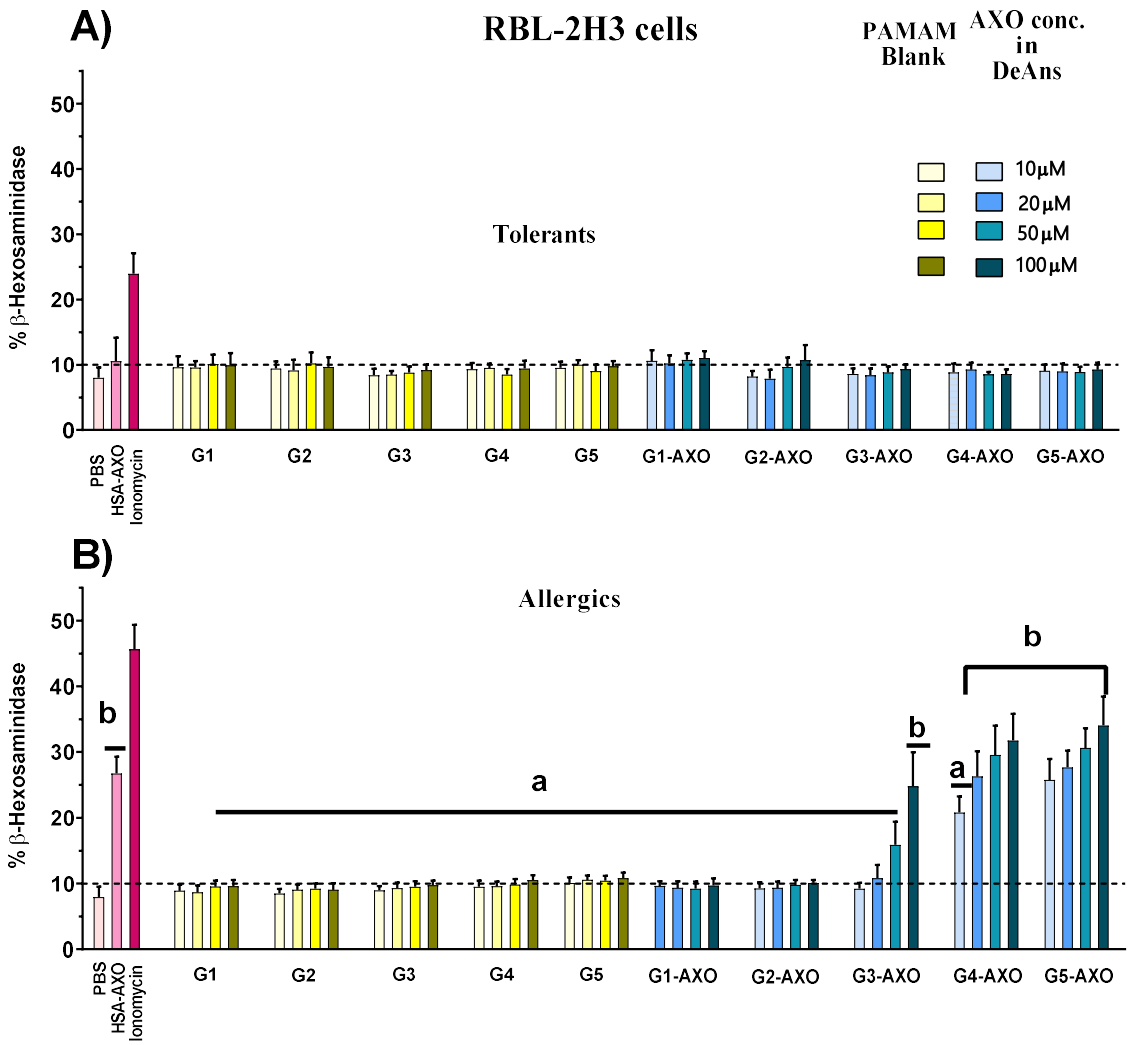

Figure 3.9. Impact of DeAns on RBL-2H3 cells degranulation at different concentrations (10 µM, 20 µM, 50 µM, 100 µM of AXO, in blue) and the equivalent concentration of PAMAM (without functionalization with AX, in yellow) as negative controls. **A**) Percentage of β-hexosaminidase release after incubation with different nanoarchitectures on sensitized cells with sera from 11 tolerant subjects; **B**) Percentage of β-hexosaminidase release after incubation with nanostructures on sensitized cells with 14 different sera from AX-allergic patients. PBS and HSA-AXO were used as negative and positive control respectively and ionomycin was used to lyse cells and determine maximum response. Data are expressed as means ± S.D. Groups with different letters statistically differ ($P \leq 0.05$). For multiple comparisons of quantitative data, ANOVA was used followed by Bonferroni's multiple comparisons test. $P<0.05$ considered indicating a statistically significant difference.

3.9. Effects of DeAns on IgE-Induced Degranulation in LUVA cells

To strengthen our observation with the two types of cells described above, the effects of DeAns were further evaluated on LUVA cells. LUVA cells are immortalized human MC displaying high levels of FcεRI receptor [219].

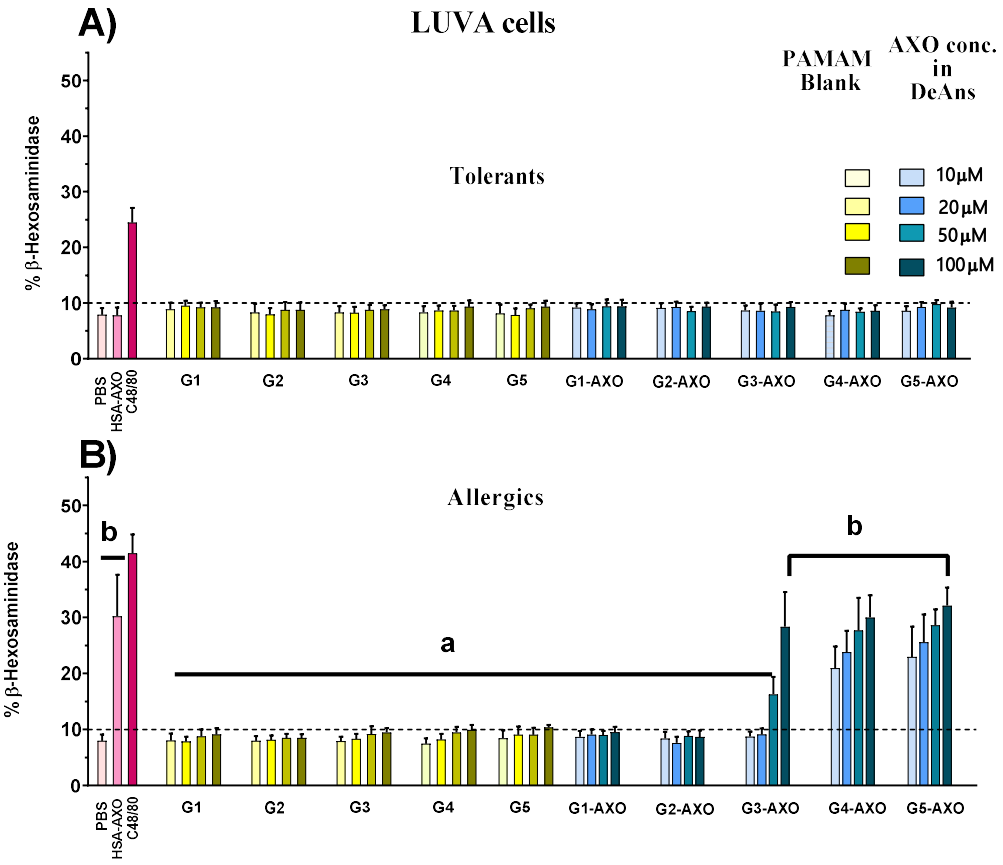

Figure 3.10. LUVA cell degranulation in response to DeAns at different concentrations (10 µM, 20 µM, 50 µM, 100 µM of AXO, in blue) and the equivalent concentration of free PAMAM structures (blank, in yellow). A) LUVA cells were primed with sera from tolerant subjects and exposing to free PAMAM structures and DeAns. Degranulation is expressed as a percentage of β-hexosaminidase release; B) LUVA cells were primed with sera from allergic patients to AX and incubated with free PAMAM structures and DeAns. PBS and HSA-AXO were used as negative and positive control respectively and a mast cell activator (C48/80) was used to lyse cells and determine maximum response. Data are expressed as means ± S.D. Groups with different letters statistically differ ($P \leq 0.05$). For multiple comparisons of quantitative data, ANOVA was used followed by Bonferroni's multiple comparisons test. $P<0.05$ considered indicating a statistically significant difference.

Like that of the RBL-2H3 cells, the LUVA cells were primed with sera from allergic patients and tolerant subjects and exposed to different concentrations of the DeAns and the control structures omitting the AXO units. Stimulated exocytotic release of the granule marker, β-hexosaminidase was measured. As can be seen in Figure 3.10B, and consistent with the two cell studies described above, only DeAns based on higher generation PAMAM (G3 and above) resulted in the degranulation of cells in a dose-dependent manner for LUVA cells. Markedly, G4-AXO (64 AXO units) and G5-AXO (128 AXO units) stimulated degranulation response with no statistical significance difference with HSA-AXO even at the lowest concentration evaluated (10 μM). Under conditions in which multivalent HSA-AXO stimulates a maximal response of ~30 % granular release, none of the structures omitting the AXO units and DeAns of lower generation G1-AXO (8 AXO units) and G2-AXO (16 AXO units) stimulated degranulation (Figure 3.10B). This signifies the importance of the size considering that the HSA-AXO conjugate used in this experiment bears approximately 14 AXO units (as estimated from the MALDI-TOF data, Figure S2), which is comparable with the 16 AXO units displaying G2-AXO that did not result in the degranulation. As expected, all structures did not result in degranulation in cells primed with sera from tolerant subjects (Figure 3.10A).

3.10. Preliminary BAT results

Before performing all described evaluation in the different cell lines, we assessed the ability of two different generations of DeAn (G2-AXO and G4-AXO) to activate basophils as a proof of concept. This was achieved by performing BAT with blood samples from three AX-allergic patients and two individuals tolerant to this drug. Patient characteristics are shown in Table 3.7 and indicate the patient 1 is selective to AX whereas patients 2 and 3 are cross-responders to BP and AX. BAT results (Figure 3.11) were considered positive when the stimulation index (SI) was greater than two.

SI was calculated as the ratio between the percentage of activated basophils with the different immunogens (free drugs and DeAns), compared to the percentage activated with the negative control. The DeAns were able to induce activation in a selective and specific way in basophils from allergic patients following the observed pattern regarding generation: G4-AXO produces higher SI than G2-AXO; this could be due to the size, valence, or proximity between epitopes in the immunogen.

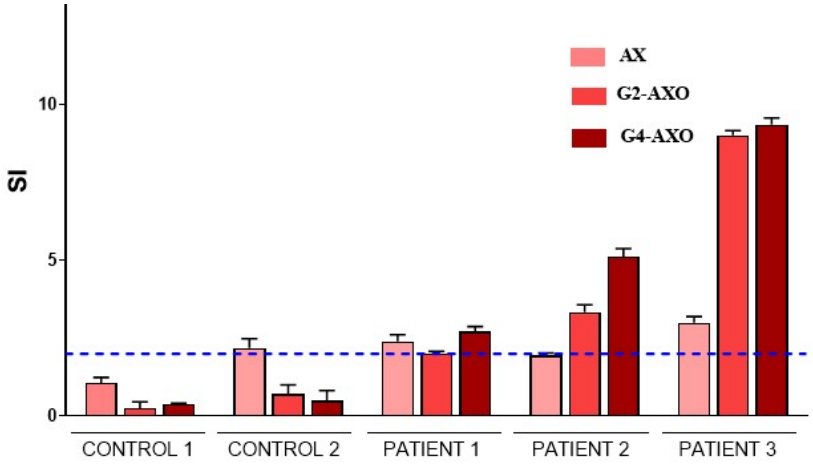

Figure 3.11. Evaluation of BAT performed with different immunogens (AX, G2-AXO, and G4-AXO). Individual BAT results expressed as SI of each structure for patients and controls. BAT represents the mean of five determinations plus the mean + SEM (Standard Error of the Mean).

Table 3.7. Classification and clinical characteristics of controls and patients diagnosed with an immediate allergic reaction to AX included in the study.

Subject	Sex	Age (Years)	Reaction	Responsible Drug	Int R-S	Skin Test				RAST	
						BP-OL	MD	AX	+to other Drug	BPO-PLL	PLL-AXO
Contr1	F	43	Urticaria/AE	Cefaclor	5	-	-	-	Cefaclor	-	-
Contr2	F	48	Anaphylaxis	Cefur	3	-	-	-	Cefur	-	-
Pat 1	M	28	Anaphylaxis	AX	5	-	-	-	nd	-	-
Pat 2	M	30	Anaphylaxis	AX	5	nd	nd	nd	nd	+	+
Pat 3	F	18	Anaphylaxis	BP	6	+	-	+	nd	+	+

Abbreviations. Contr: Control; Pat: Patient; F: female; M: male; AE: Angioedema; AX: Amoxicillin; BP: Benzylpenicillin; Cefur: Cefuroxime; Int R-S: Time interval between reaction and in vitro study (months); BP-OL: benzylpenicilloyl-octa-L-lysine; MD: benzylpenicillin minor determinant; (−): negative; (+): positive; ND: not determined; RAST: Radioallergosorbent test; BPO-PLL: benzylpenicilloyl-poly-L-lysine; PLL-AXO: amoxicilloyl-poly-L-lysine.

3.11. Discussion

This study took the advantage of PAMAM structures, permitting the simultaneous variation of the size (linear) and end-groups (exponential) for SAR studies. Considering the changes of approximately 1 nm in the molecular diameter between each generation of PAMAM [213] (Table 3.4), it would be logical to assume that the complete functionalization of the amino groups with AX will result in DeAn with a size of at least one generation higher than the parent structure. The findings observed in all cell lines experiments were consistent, indicating that DeAn structures of G3 and above generations resulted in IgE-mediated degranulation. The schematic representation for DeAns with and without cellular restriction is given in Figure 3.12. The current study was limited to only structures based on G5 and lower, considering the diverging surface amino groups for higher generation dendrimers (256 NH2 groups for G6 and exponentially increasing for higher generations), where the complete functionalization of larger structures might not be attainable because of steric hindrance. This phenomenon can be explained by steric congestion [220] which states that for generations higher than 6 there are tight conformations of the terminal groups above which a sterically inhibited reaction rate would be observed [221]. Thus, the number of antigenic determinants coupled to the dendrimers of such higher generations would be difficult to control, due to incomplete functionalization of the peripheral amino groups, preventing the study of the influence of relevant parameters, size and valence.

Activation of the effector cells degranulation was observed starting with the structure of G3-AXO (estimated molecular diameter of 4.6 nm). The incapacity of the other two DeAn structures, G1-AXO (8 AXO units, an estimate of 3.2 nm in diameter) and G2-AXO (16 AXO units, an estimate of 3.9 nm in diameter) could be attributed to the small size that fails to induce intermolecular crosslinking with IgE on FcεRI. Sometimes such intermolecular process can be inhibited by intramolecular crosslink with IgE, which can be excluded considering the average distance between the two binding sites on a single IgE (~10 nm)[60] and the estimated diameter of G1-AXO and G2-AXO, too small to occupy the two IgE binding sites. The observed inability of these two DeAns of lower generations to stimulate the cells suggests that the absence of intermolecular crosslinking could be attributed to either the smaller size of the conjugate or the lower number of exhibited AXO moieties. Such explanation related to the size of the conjugate can also be strengthened by the fact that HSA-AXO (used as positive control) and G2-AXO (that failed to activate the degranulation) display approximately the same number

of AXO units. This might be related to the combined effect of the optimal size and the better accessibility of AXO moieties on HSA-AXO that could allow the crosslinking of more than two IgE with a single molecule, resulting in activation of cells.

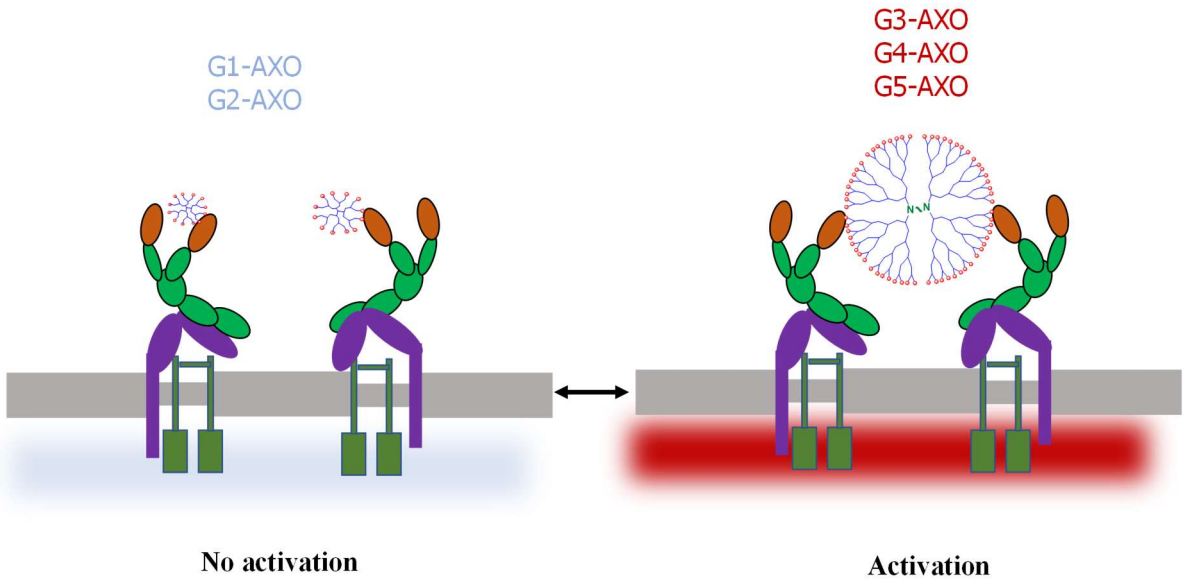

Figure 3.12. Illustration of cellular response with two types of nanoarchitectures based on the structural features. The low generation-DeAns, G1-AXO and G2-AXO, did not induce the crosslinking of FcεRI and hence no activation of the cellular response. The higher generation-DeAns, G3-AXO, G4-AXO, and G5-AXO, however, resulted in IgE-mediated crosslinking and activation (degranulation) of the effector cells.

DeAn structures starting with a size of approximately ≥ 4.6 nm and the number of antigenic determinants (≥ 32 AXO units) are identified as a minimum requirement where the stimulation of cellular degranulation is activated. This is in agreement with a study with bivalent DNP ligands based on a double-stranded DNA spacer where stimulation of the degranulation was observed in the size range of 4.5-5 nm [60]. Interestingly, in RBL-2H3 and LUVA cells, the overall degranulation response increases with doses with the highest β-hexosaminidase release measured at 100 µM (AXO units) of G3-AXO, G4-AXO and G5-AXO (Figure 3.10B and Figure 3.11B).

However, as can be seen in Figure 3.9B, in the MCs primed with IgE MoAb against AX and treated with different concentrations of DeAns, the maximum degranulation occurred at 10 µM of the AXO units of structures based on G3 and above, showing a decrease in the level of β-

hexosaminidase at higher concentrations. This is matched with a similar observation suggesting that the decrease in degranulation at high allergen concentrations is caused by active inhibitory pathways [222]. In fact, both behaviours are in agreement with a model which states that the degree of IgE crosslinking increases up to a point when monovalent allergen-IgE interactions begin to dominate due to excess allergen [222,223].

In a more realistic scenario, the ability of DeAns to stimulate basophils was demonstrated in blood from patients with β-lactam allergy, with basophil response being associated with the size of the DeAn and density of haptens [202]. Therefore, these structures in BAT provide the possibility of both increasing the hapten density, because of their multivalent capacity, and presenting the appropriate size for having an optimal sIgE bridging on the basophil surface. These two factors are essential to improve the sensitivity of this cellular test. This preliminary study demonstrates that the inclusion of G4-AXO improves the sensitivity of the BAT technique using free AX as a stimulator.

However, BAT has two inherent limitations: the need to be performed into the first 24 h after blood collection to avoid a decrease in the activation; and the existence of a 10-15 % of subjects that transiently do not respond to stimulation through IgE dependent mechanisms for months. To circumvent this, passive cellular tests, using basophils or mast cells sensitized with stored sera from patients can be seen in the experiments performed with different cell lines, suggesting potential as a diagnostic tool in sera from patients whatever the level of sIgE, total IgE and value of the previous BAT.

3.12. Conclusion

This chapter describes how well-defined nanoarchitectures, with parallel variation in the size and numbers of antigenic determinants, enable an integrative approach to study the effector cells degranulation. The results demonstrated the structural constraints in crosslinking IgE receptor complexes and establish minimal structural requirement above which the stimulation of the effector cells occurs. Furthermore, preliminary utilization of G4-AXO that showed a positive response in all cellular activation assays also indicated a higher level of basophil activation in allergic patients in BAT. Moreover, these studies have opened the possibility of developing passive cellular test using these structures.

Chapter 4: Synthesis, Characterization, and Immunological Evaluation Bidendron Antigen Nanoarchitectures

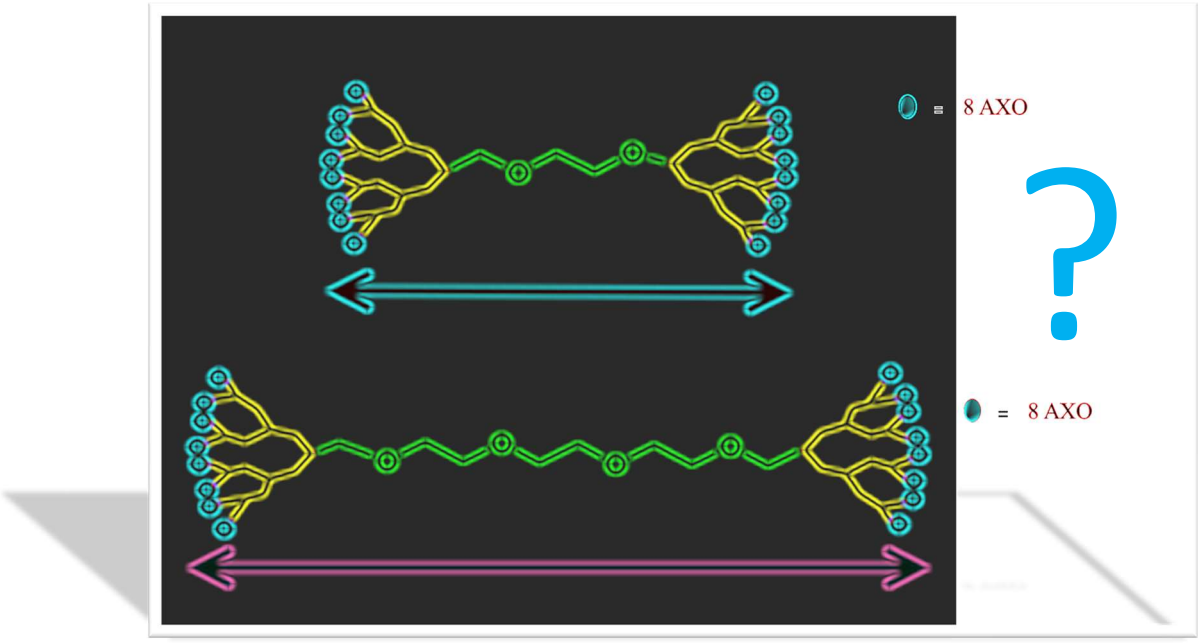

4.1. Introduction

In chapter 3, we described the effect of DeAns by controlling the multivalence (number of haptens), its three-dimensional structure and size. The findings depict those structures based on lower generations dendrimer, lower size, and the number of haptens, did not activate the cellular degranulation. However, those structures based on higher generation dendrimer, higher size, and the number of haptens, have resulted in degranulation of the effector cells. Therefore, to identify the effects of the size of the nanostructures while keeping the number of haptens unchanged, we propose structures that is based on the same number of haptens (16 AXO) analogous to the DeAn that did not activate the cellular degranulation. To achieve this, we propose to design and synthesis symmetrical bidendritic nanoarchitectures, called BiAns, decorated with multiple units of AXO and separated by flexible polymeric spacers of different lengths and evaluate the influence of the nanoarchitecture size for promoting the activation of effector cells that causes drug allergic reactions. This SAR study will help deeply understand the required distance between AXO determinants to activate basophils or MCs for improving the sensitivity of *in vitro* tests for diagnosing allergic reactions to AX.

4.2. Design of BiAns

To study the mechanisms of activation of effector cells in allergic reactions to AX, a novel set of symmetrical dendritic nanoarchitectures, BiAns, represented in Figure 4.1A was designed and synthesized.

The BiAns were constructed to display critical design features: (i) bearing multiple units of AX antigenic determinant on the periphery of the dendron scaffolds to support multivalent interaction with the target antibody; (ii) an homobifunctional flexible hydrophilic PEG spacer that provides a specific length between dendrons. The latter eventually promotes aqueous solubility [224] and reduces non-specific protein adsorption, immunogenicity, and antigenicity [60,225]. The PAMAM dendrimer was selected as a scaffold for obtaining conjugates covalently coupled to multiple drug units since peripheral amino functionality allowed the straightforward amidation with β-lactams. The second-generation (G_2) of PAMAM dendron was chosen as a common dendritic scaffold whereas PEG of different average MWs (from 600 Da to 12000 Da) were used as a spaced linker. Thus, the resulting BiAns encompass the same number of peripheral functionality (eight AXO units per dendron, and therefore 16 AXO per BiAns), differing only in the length of the hydrophilic spacer separating the dendrons. The

flory radius of starting PEG chains ranges from 17 to 101 Å, with the contour length span from 48 to 955 Å (Table 4.2).

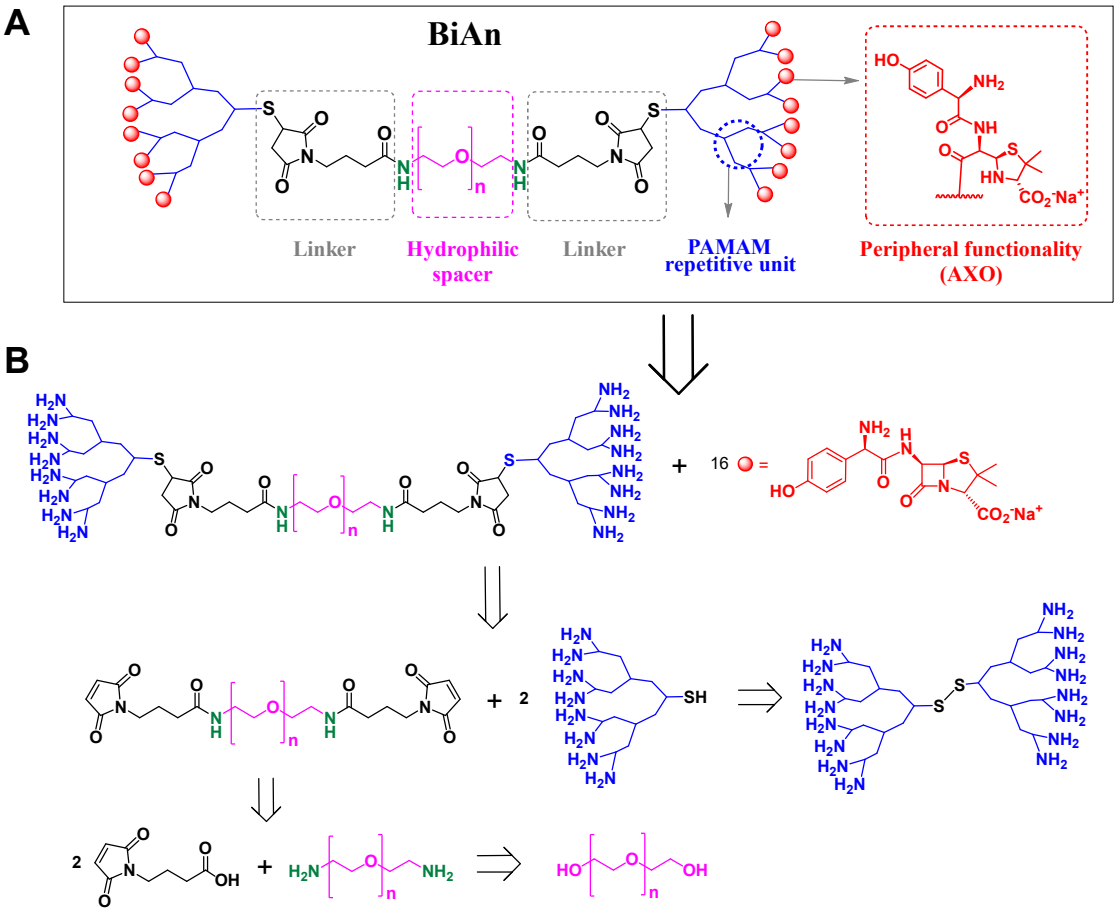

Figure 4.1. A) Schematic representation of BiAns nanoarchitectures bearing 16 AXO determinants. The structural variation among different BiAns depends on the PEG length (with n ranging from 14 to 273; B) General retrosynthetic analysis for proposed BiAns

4.3. Synthesis and Characterization of BiAns

To synthesize the series of BiAns, we followed the general retrosynthetic analysis described in Figure 4.1B. The fully AXO-functionalized BiAn can be readily prepared by modifying all amino terminals of the homobidendron PEG skeleton precursor using an excess of AX, which is reactive against amino groups. The disconnection of the thioether bonds leads to three synthons, the bismaleimide-activated PEG and two identical dendrons with a thiol group at the core. These dendrons can be obtained by the reduction of PAMAM dendrimer with a cystamine core.

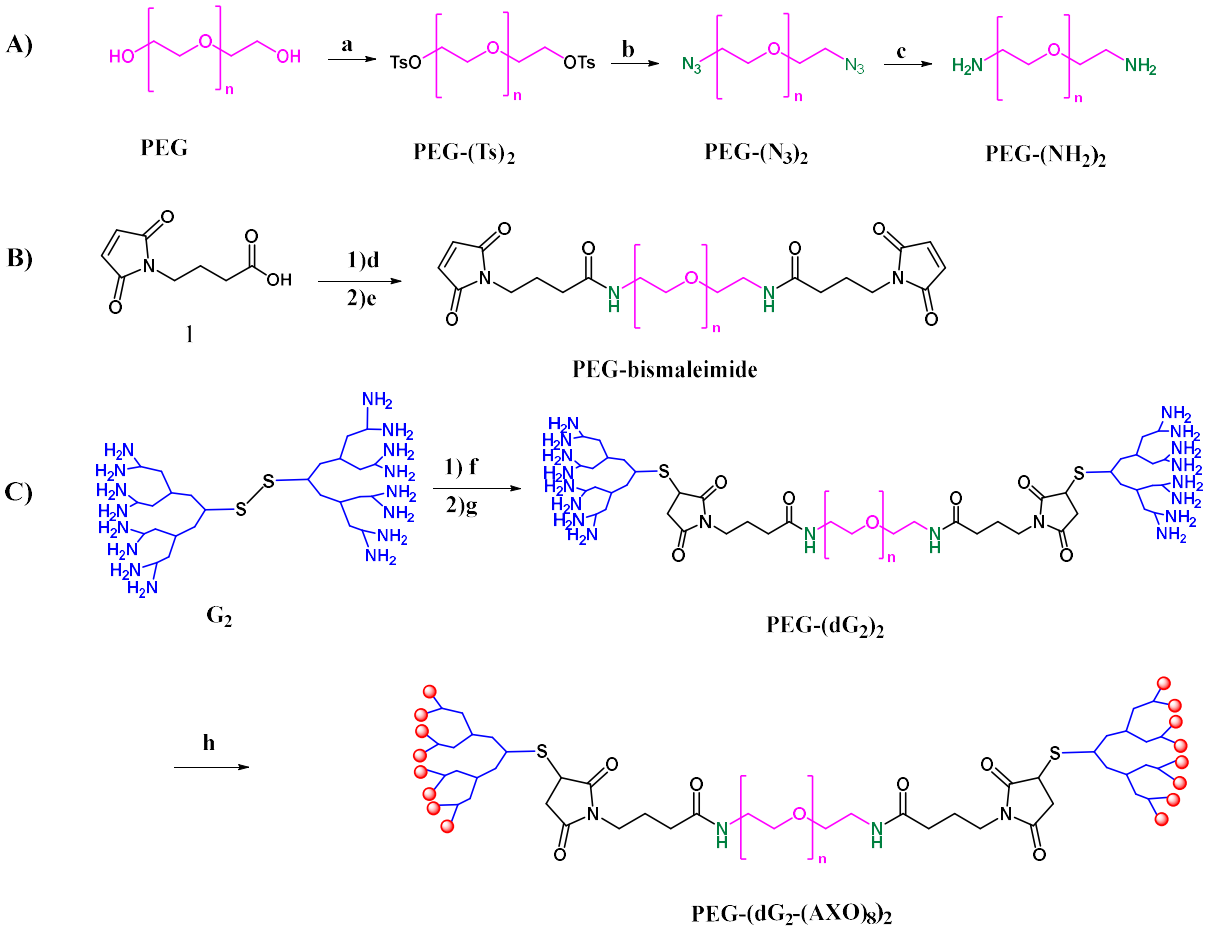

Figure 4.2. General synthetic scheme: A) the intermediate PEG diamine; B) the intermediate PEG-bismaleimide; and C) the final BiAns. Reaction conditions: (a) TsCl, CH_2Cl_2, KOH, 0 oC; (b) NaN_3, THF-H_2O (80:20), reflux at 70 ºC; (c) H_2, Pd/C, MeOH, (d) ^{i}BuCOCl, NMM, CH_2Cl_2, 0 oC; (e) PEG-$(NH_2)_2$, CH_2Cl_2; (f) PBS, pH 6.5, TCEP; (g) PEG-bismaleimide, H_2O, DMSO; (h) AX, carbonate buffer (0.05 M, pH 10.2).

The synthetic scheme and chemical structures used to obtain BiAns are illustrated in Figure 4.2. Briefly, the synthetic procedure consisted of obtaining bismaleimide-activated PEG compounds that allowed coupling between thiol-core dendrons (G_2), whose peripheral groups were eventually functionalized with AX. In building up this, a series of independent chemical reactions were followed, and the completion of the reactions was monitored by ^{1}H and ^{13}C NMR through the appearances and disappearances of distinctive signals. Eight PEG linkers of different lengths with MWs ranging from 600 to 12000 Da were used. Initially, amine transformation of the hydroxyl groups of PEG was obtained via three-step reactions (Figure 4.2A): First, activating the alcohol with tosyl chloride (TsCl) in the presence of KOH. Secondly, converting the PEG ditosylate (PEG-$(Ts)_2$) to PEG diazide (PEG-$(N_3)_2$) by reaction with NaN_3

in THF-H_2O (80:20) under reflux. As displayed in Figure 4.3A-B, the nucleophilic substitution of the tosylate leaving groups by azide is evidenced by the complete disappearance of peaks at around 7.78, 7.31, and 2.42 ppm, as well as the shift of the directly bonded methylene peak to the higher field (from around 4.12 to 3.37), indicating the successful synthesis of series of different MW PEG-$(N_3)_2$ with an average yield greater than 90 %.

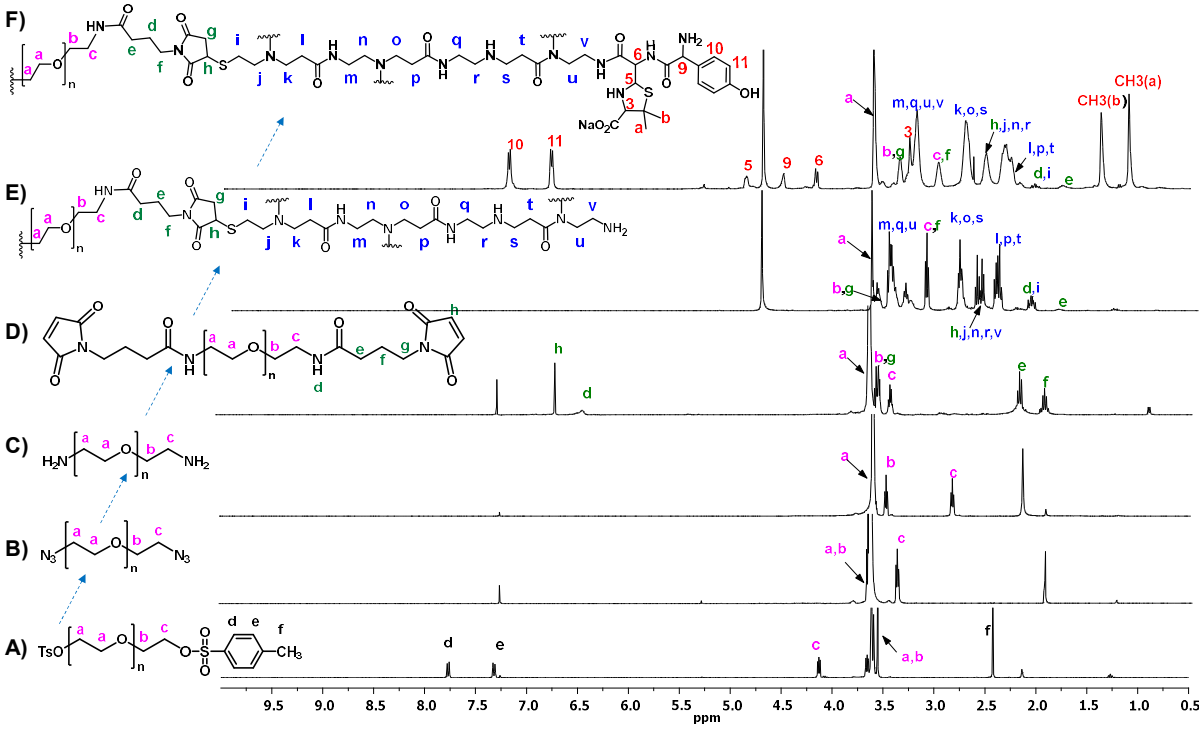

Figure 4.3. ^{1}H NMR spectra for monitoring the reactions by following the sequential appearance and disappearance of peaks characteristic of the respective functional groups.

Lastly, the PEG-$(N_3)_2$ was transformed to PEG diamine (PEG-$(NH_2)_2$) using palladium-catalyzed hydrogenation reaction in quantitative yields. The ^{1}H NMR confirms the transformation of azide to amine moieties by the shift of the two ethylene peaks in the extremes of PEG chains from around 3.65 and 3.38 ppm to 3.48 and 2.83 ppm, respectively (Figure 4.3C). On the other hand, the reduction of azides to amines was initially performed with the Staudinger reaction, which gave the desired product in a good yield for the corresponding lower MW PEG (up to MW 2000). However, the synthesis involving higher MW PEG posed two problems that resulted in low yields: incomplete reactions even after repeatedly refreshing with excess triphenylphosphine (PPh_3) reagent, and purification issues in which, after the necessary work up with water, significant portions of the product remained in the organic phase. On the contrary, the desired products for all MW were obtained with quantitative yields through

hydrogenation, whose completion time took longer (from hours to days) with increasing MW of PEG. This variation could be attributed to different degrees of steric hindrance, which increases with a higher MW polymeric chain, preventing the accessibility of the desired functional groups.

The subsequent conversion of amino groups into thiol-reactive maleimide was carried out by reacting with compound 1 through an anhydride coupling reaction (Figure 4.2B). This was confirmed by a shift in the methylene peaks directly bonded to amine from around 2.83 ppm to lower field (around 3.44 ppm), and the appearance of new peaks at 6.43 and 6.72 ppm, corresponding to the presence of amide protons and the alkene of maleimide, respectively (Figure 4.3D). As the next step, a slight excess of PAMAM G_2 dendrimer was precisely converted to the same half-dendron through reductive cleavage of the cystamine disulfide core using tris (2-carboxyethyl) phosphine (TCEP) and coupled with PEG-bismaleimide linker via thiol-maleimide ´click´ reactions, forming a stable thioether bond. The resulting symmetrical platform with 16 readily functionalizable terminal amine groups was confirmed by the disappearance of the alkene characteristic resonance at 6.72 ppm and the appearance of typical signals corresponding to dendron ranging from 2.27 to 3.50 ppm (Figure 4.3E).

Finally, the functionalization of the amino groups with AX was carried out through the nucleophilic reactions of the free amine on the periphery of dendrons to the β-lactam ring of AX. The bidendron constructs, PEG-$(dG_2)_2$ (Figure 4.2C), were incubated with an excess of AX in basic pH buffer (for ensuring peripheral amino groups to be deprotonated) at 4 °C to afford the desired BiAns. The low-temperature condition was a previously optimized factor for obtaining fully haptenized dendrimers as a result of the reduced mobility of the substituted branch and a decrease in the steric hindrance [66,203]. The resonance shift in the methylene protons of dendron linked to amine from 2.63 to 3.44 indicates the formation of an amide bond (Figure 4.3F).

Table 4.1. ^{1}H NMR assignments of the BiAns

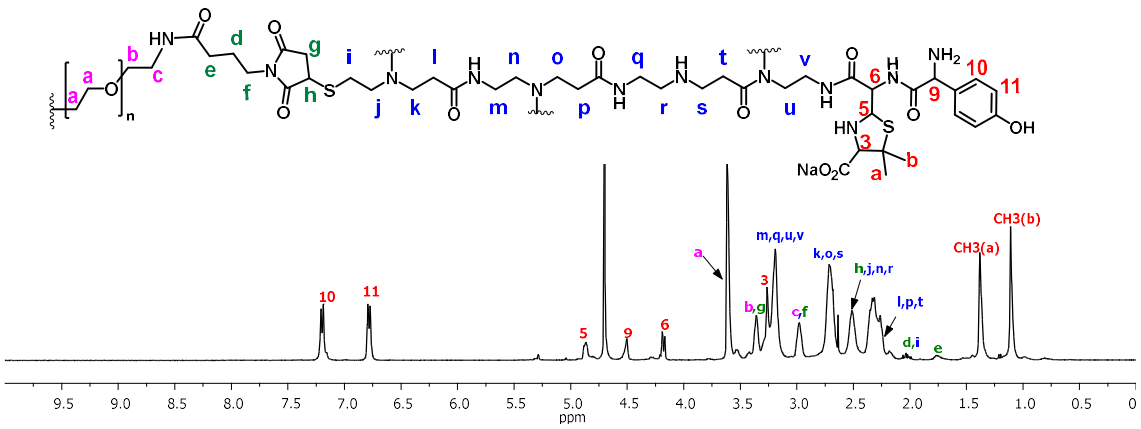

Description		Number of H							
Position	***δ(ppm)***	**BiAn (600)**	**BiAn (1000)**	**BiAn (2000)**	**BiAn (4000)**	**BiAn (6000)**	**BiAn (8000)**	**BiAn (10000)**	**BiAn (12000)**
a	3.88 3.57(*m*)	56	93	186	373	560	746	993	1120
b, g	3.56 – 3.51(*m*)	16	16	16	16	16	16	16	16
m,q,u,v	3.32 – 3.05 (*m*)	88	88	88	88	88	88	88	88
c,f	3.12 – 3.03(*m*)	8	8	8	8	8	8	8	8
K,o,s	2.89 – 2.69 (*m*)	56	56	56	56	56	56	56	56
h,j,n,r	2.66 – 2.51 (*m*)	30	30	30	30	30	30	30	30
l,p,t	2.48 – 2.26 (*m*)	56	56	56	56	56	56	56	56
d, i	2.18 –2.06 (*m*)	8	8	8	8	8	8	8	8
e	1.90– 1.77 (*m*)	4	4	4	4	4	4	4	4
CH_3(a)	1.47(*s*)	48	48	48	48	48	48	48	48
CH_3(b)	1.20 (*s*)	48	48	48	48	48	48	48	48
3	3.35 (*s*)	16	16	16	16	16	16	16	16
5	4.88(*d*, *J*=8.5Hz)	16	16	16	16	16	16	16	16
6	4.26(*d*, *J*=8.5Hz)	16	16	16	16	16	16	16	16
9	4.6 (*s*)	16	16	16	16	16	16	16	16
10	7.29(*d*, *J*=7.8 Hz)	32	32	32	32	32	32	32	32
11	6.89 (*d*, *J* =7.8 Hz)	32	32	32	32	32	32	32	32

Moreover, the presence of signals derived from AX confirmed its coupling in its AXO form, as the shift and separation of β-lactam proton (H5 and H6) peaks indicate the opening of this AX ring. The completion of the reactions has been confirmed by the shift in the carbons signal corresponding to the ethylene residue directly bonded to the primary amine from 42.1 and 40.2 ppm and the appearance of new peaks that correspond to the condensation reaction at 39.5 and 38.8 ppm. The pattern of assignation of ^{1}H NMR signals of all the BiAns is summarized in Table 4.1.

4.4. Determination of MW and Size Estimation

Wide-ranging analytical techniques have been used to characterize dendrimer or dendrimer-based structures [226,227]. Nevertheless, it is often challenging to obtain unswerving information about the molar mass of the dendritic polymer or related structures [228]. The difficulties arise from the chemical compositions of the structures like a high degree of branching, high MW, presence of chargeable groups and lack of appropriate standards [172,228,229]. The MW of dendritic structures can be determined by different methods, among which the size exclusion chromatography (SEC) [230,231], matrix-assisted laser desorption/ionization time-of-flight mass spectrometry (MALDI-TOF-MS) [232,233], polyacrylamide gel electrophoresis (PAGE) [234,235] are frequently used techniques.

4.4.1. Mass Spectrometry

The determination of the mass of the BiAns was performed by MALDI-TOF-MS with no valuable mass spectrum data obtained for the products. This might be due to the high positive charges of the fully AX functionalized structures because of the free amine (Ph-NH_2). The difficulty of characterizing dendrimers with high MW and charges have been previously reported [228]. More recently, a study reported a similar observation that it was not possible to obtain a mass spectrum of both the tert-butoxycarbonyl (Boc) protected dendrimer (GNHBoc derivatives) and free amine dendrimer (GNH_2 derivatives) as a result of the liability of the protecting group and the high degree of positive charges associated with free amine during measurement [172].

4.4.2. NMR Diffusion Experiments

Before performing different experiments involving interaction with components of the immune system, the purity of the different BiAns was confirmed by DOSY NMR. Indeed, the DOSY maps were efficiently used in detecting traces of impurities, incomplete haptenated bidendrons or starting materials, as they permit discriminating between the different component of a mixture by translational diffusion (depending on chemical shift and diffusion behaviour) [211][212].

As expected, the diffusion coefficient of BiAns decreased with increasing MW (Table 4.2). An example of the utility of this "NMR chromatography" is explained in Figure 4.4 and Figure 4.5. Here we presented two DOSY maps of BiAn based on PEG (MW 12000): The first one

(Figure 4.5) displays two spectra resembling closely similar, but with two different D: $1.17x10^{-6}$ m^2/s and $9.47x10^{-10}$ m^2/s. This indicates that there are two different compounds in the reaction with different MW, which might dictate that there is no complete functionalization or only one side of the dendron is functionalized.

Table 4.2. Estimated and experimental values of the BiAn nanostructures

Synthetic Antigen	Estimated MW (Da)	Linker PEG MW (Da)	$(C_2H_4O)_N$ where N is	Flory Radius (nm)*	Solution PEG length (nm)**	Extended PEG length: Contour Length(nm)***	D (m^2s^{-1})	Valency
BiAn 600	10471.9	600	14	1.68	3.36	4.8	$1.53x10^{-10}$	16
BiAn 1000	10871.9	1000	23	2.28	4.56	8.0	1.32x10-10	16
BiAn 2000	11871.9	2000	45	3.46	6.92	15.9	$1.29x10^{-10}$	16
BiAn 4000	13871.9	4000	91	5.24	10.48	31.8	$1.24x10^{-10}$	16
BiAn 6000	15871.9	6000	136	6.68	13.36	47.7	$1.09x10^{-10}$	16
BiAn 8000	17871.9	8000	182	7.94	15.88	63.6	$9.64x10^{-11}$	16
BiAn 10000	19871.9	10000	227	9.08	18.16	79.5	$9.57x10^{-11}$	16
BiAn 12000	21871.9	12000	273	10.13	20.26	95.5	$9.50x10^{-11}$	16

*The Flory radius (R_F) is calculated with $R_F = a.n^{3/5}$ (where a is the length of a monomer unit, and n is the number of repeating monomeric units. **The contour length is calculated as a product of the polymeric length (n) and length of the monomeric unit, 3.5 Å for PEG [236].

However, after refreshing the same reaction with excess AX and incubating for days, the second DOSY map (Figure 4.6) indicating the only presence of one molecule ($D=9.47x10^{-10}$ m^2/s) was obtained. This valuable experiment helps not only in obtaining the diffusion coefficient of the molecule but also gives information about the presence of impurities and residuals of unreacted starting material.

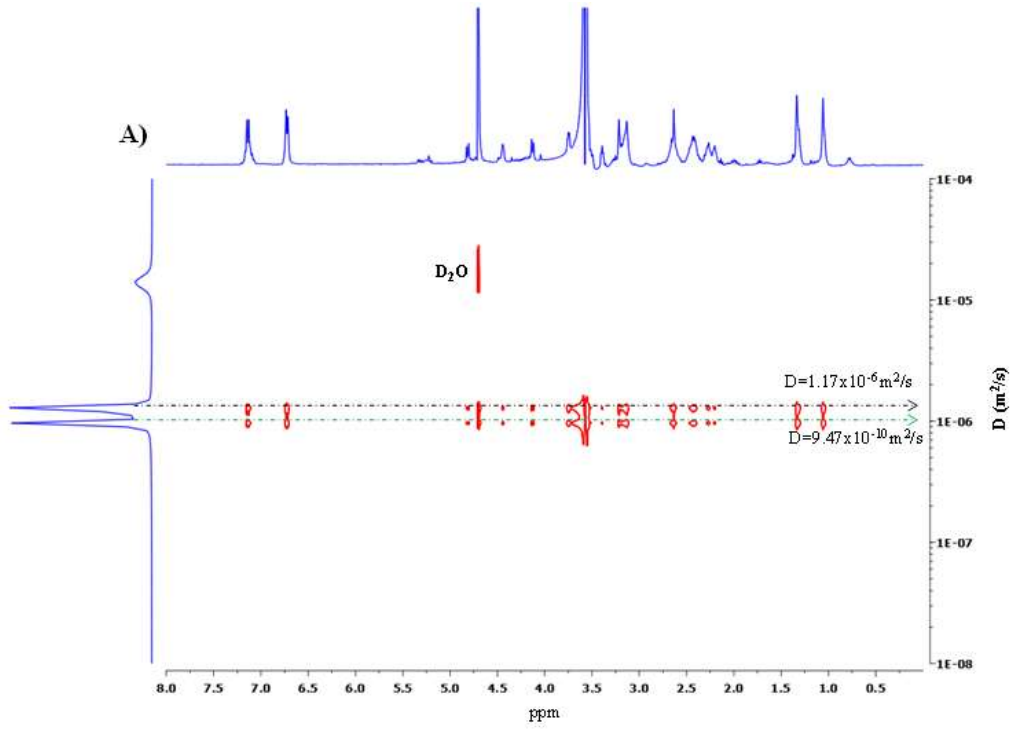

Figure 4.4. DOSY NMR spectra obtained at 300 K in D_2O. Spectra show two compounds with different diffusion coefficient indicating the incompletion of the functionalization of amino groups on the periphery of the structure with AX.

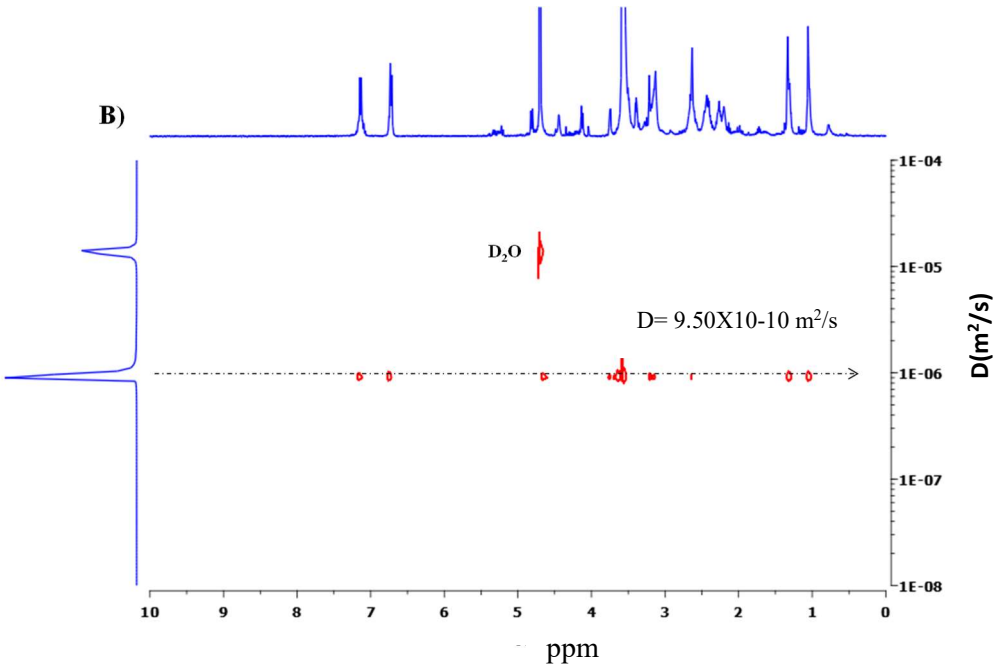

Figure 4.5. DOSY NMR spectra obtained at 300 K in D_2O. Spectra of a compound obtained after refreshing the reaction with an excess amount of AX on two occasions indicating the completion of the functionalization.

4.4.3. Dynamic Light Scattering (DLS)

To get an insight into the size of BiAns and determine whether they are aggregated in an aqueous solution, DLS experiment was performed. DLS provides information about the size of particles or colloids in solvents. For this experiment, we compared the sizes of the different PEG (parent molecules) and the corresponding BiAns (Figure 4.6). Even though DLS is not optimal for this kind of sample (and therefore, the sizes obtained might deviate from the expected theoretical values), the sizes are reasonable and fit relatively well with the results reported by others [237,238]. Correlation between the MW of the compound and the measured hydrodynamic diameter. The most important information obtained here is that the trend for both PEG and BiAn samples is very similar, with a certain gap between both (around 3-4 nm, close to the expected size of the AXO- functionalized G2 PAMAM dendrimer [209]. From these DLS data, it would not be expected that the BiAn molecules to aggregate into micelles or other supramolecular structures.

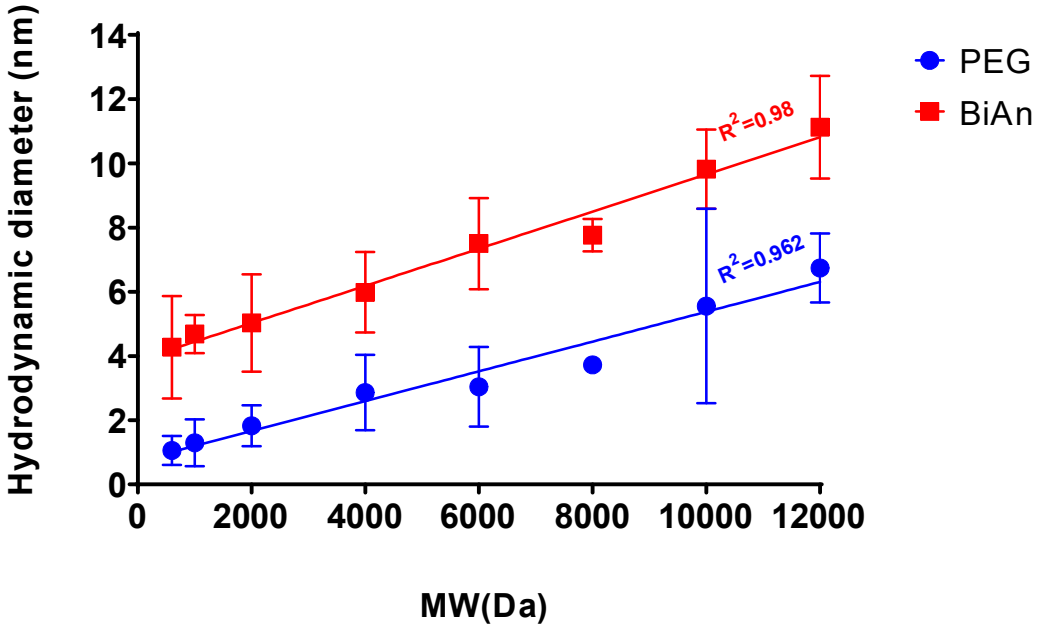

Figure 4.6. Variation of the hydrodynamic diameter with the MW of PEG (blue) and BiAn.

4.4.4. IgE Recognition of BiAns

The ability of AX-sIgE to recognize BiAn conjugates was evaluated by competitive RAST inhibition immunoassays using a pool of sera from patients allergic to AX (Table 4.3). The monomeric conjugate (AXO-Bu) was also employed as a control inhibitor already evaluated [55]. Assays were performed at equimolar amounts of AXO for all BiAns and the monomeric conjugate, with a maximum concentration not higher than 30 mM of AXO, due to solubility issues at higher concentrations of BiAns. At such maximum concentration, sera were inhibited by all BiAns. *In vitro* IgE recognition is generally considered meaningful when the inhibition percentage is higher than 50 %. In general, inhibition dropped at low concentrations of inhibitors (3 and 0.3 mM of AXO).

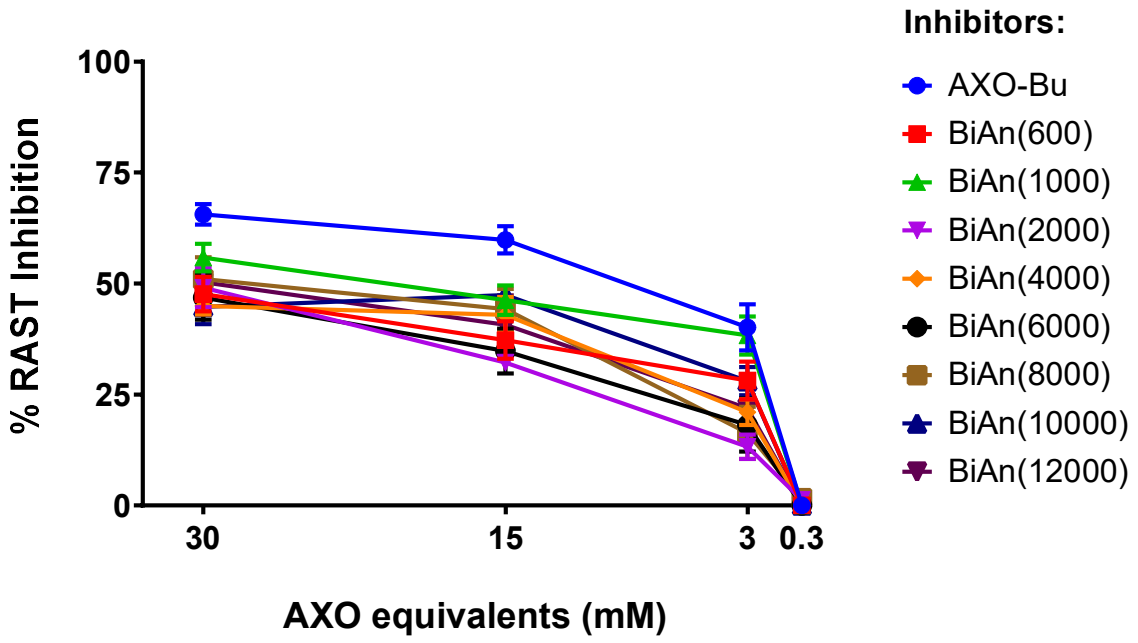

Figure 4.7. RAST inhibition assays performed with a pool of sera from patients allergic to AX, using the series of BiAns and AXO-Bu conjugate as inhibitors and cellulose discs modified with PLL-AXO as the solid phase. Specific IgE recognition is considered with an inhibition of ≥50%.

The presented data support that all compounds are recognized by AX-sIgE in a concentration-dependent manner, with no differences in the degree of IgE recognition among the different BiAns, as they present the same number of AXO equivalents (Figure 4.7). All the 8 AXO determinants exposed in each extreme dendron of PEG cannot be simultaneously involved in

an IgE-molecular recognition process because of the minor distance between determinants. Moreover, PEG chains could also contribute to a steric hindrance to the IgE binding. Therefore, the increased inhibition obtained with the monomeric AXO-Bu, compared with BiAns, can be attributed to the absence of steric interactions for sIgE binding to AXO moieties in this small conjugate. Moreover, a higher concentration of AXO is expected to increase the extent of inhibition, a pattern already reported with the monomeric AXO-conjugate [55] and DeAns with different penicillin determinants [66,145].

Table 4.3. Clinical characteristics of allergic patients and skin test results with penicillin antigenic determinants and *in vitro* determination of AX-sIgE by RAST.

	Clinical Characteristics					*In vivo* tests				*In vitro* tests
						Skin Tests			DPT	
Case	**Age**	**Sex**	**Clinical reaction**	**Drugs involved in the reaction**	**Grade severity ***	**BP-OL**	**MD**	**AX**	**AX**	**AX-sIgE (% RAST)**
1	51	F	Anaphylactic shock	AX	III	Neg	Neg	Pos (IDT)	NP	55
2	40	M	Anaphylaxis	AX	II	Neg	Neg	Pos (IDT)	NP	66
3	29	F	Urticaria	AX	I	Neg	Neg	Pos (SPT)	NP	7
4	35	F	Urticaria and Angioedema	AX-CLV	I	Neg	Neg	Neg	Pos	12
5	43	F	Anaphylaxis	AX	II	Neg	Neg	Pos (IDT)	NP	7
6	59	M	Anaphylaxis	AX-CLV	I	Neg	Neg	Pos (SPT)	NP	29
7	60	F	Anaphylaxis	AX-CLV	II	Neg	Pos (IDT)	Neg	Pos	36
8	46	F	Anaphylactic shock	AX-CLV	III	Neg	Neg	Pos (IDT)	NP	73
9	61	F	Anaphylactic shock	AX-CLV	III	Neg	Neg	Pos (IDT)	NP	33
10	61	F	Anaphylactic shock	AX	III	Neg	Neg	Pos (IDT)	NP	10
11	25	M	Anaphylaxis	AX-CLV	II	Neg	Neg	Pos (IDT)	NP	12
12	49	M	Anaphylaxis	AX-CLV	II	Neg	Neg	Neg	Pos	33
13	44	M	Anaphylactic shock	AX	III	Neg	Neg	Pos (SPT)	NP	7
14	40	F	Anaphylaxis	AX-CLV	II	Pos (SPT)	Neg	Neg	Pos	7

*AX: Amoxicillin; CLV: potassium clavulanate; BP-OL: benzylpenicilloyl-octa-L-lysine; F: female; IDT: intradermal test; M: male; MD: Minor Determinant; Neg: negative; NP, not performed; Pos: positive; SPT: skin prick test. *Grading system for generalized hypersensitivity reactions: I, mild (skin and subcutaneous issues only); II, moderate (features suggesting respiratory, cardiovascular, or gastrointestinal involvement); III, severe (hypoxia, hypotension, or neurologic compromise). REF: Brown SG. Clinical features and severity grading of anaphylaxis* [217].

4.4.5. Antibody-nanoarchitecture Complexes

In order to visualize IgE binding to the BiAn nanoarchitectures and the shape of the resulting immune complex, Optimized Negative-staining (OpNS) TEM was performed, allowing a high-

resolution image at nanoscale level [239,240]. The staining and imaging conditions were first optimized MoAb alone, AO3.2, which is specific to AXO structure. Afterwards, different MoAbs to BiAn ratios was tested to optimize the conditions, from which a molar ratio of 8:1 was found to be the optimal condition. Consequently, this ratio was used to incubate MoAbs with **BiAn (600)**, **BiAn (6000),** and **BiAn (10000)** to evaluate differences in the obtained complexes as a function of the employed nanoarchitecture.

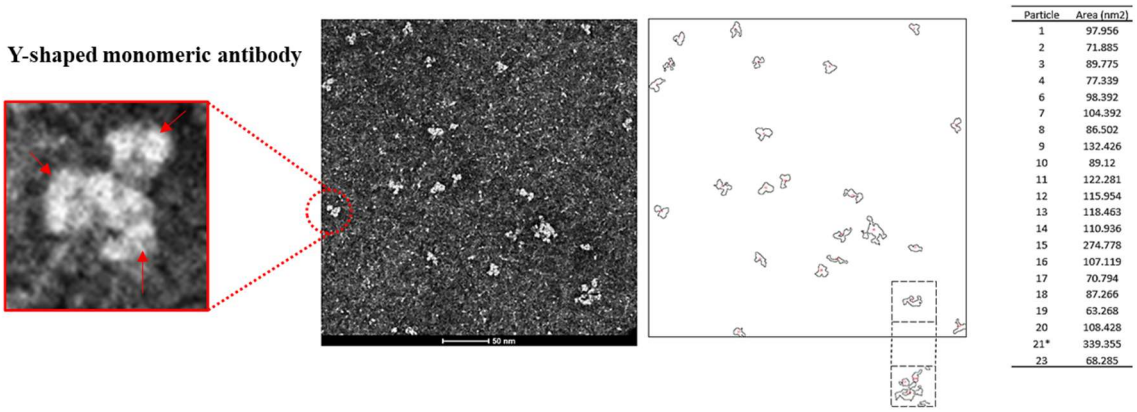

Figure 4.8. A representative example of the software-based identification and area estimation of the antibody-nanoarchitecture complex. The red highlight shows the zoomed-in views of selected individual antibody images. The arrows indicate the three different parts of an antibody.

Images were processed using Image J software, determining the negatively stained area of each complex (a minimum of 230 particles were measured per condition). Then, the number of MoAbs per complex was estimated by comparing the obtained area for each complex with the average area occupied by individual MoAbs not incubated with the nanostructures (57 ± 12.7 nm^2). A representative image of the software identified complex and area estimation is shown in Figure 4.8. Clear Y-shaped monomeric antibodies in different orientations, which serve as a working reference, are observed (Figure 4.9A). The three different parts corresponding to the two F_{ab} and one F_c domains are identifiable (Figure 4.9B). To study the influence of spacer length of the BiAns on the formation of immune complexes, various nanoarchitectures (BiAn (600), BiAn (6000), and BiAn (10000)) were incubated with the antibodies prior to evaluation of the complexes by OpNS TEM. To saturate the epitopes and evaluate the number of antibodies that bind to a nanostructure, an excess of MoAbs was incubated with nanostructures.

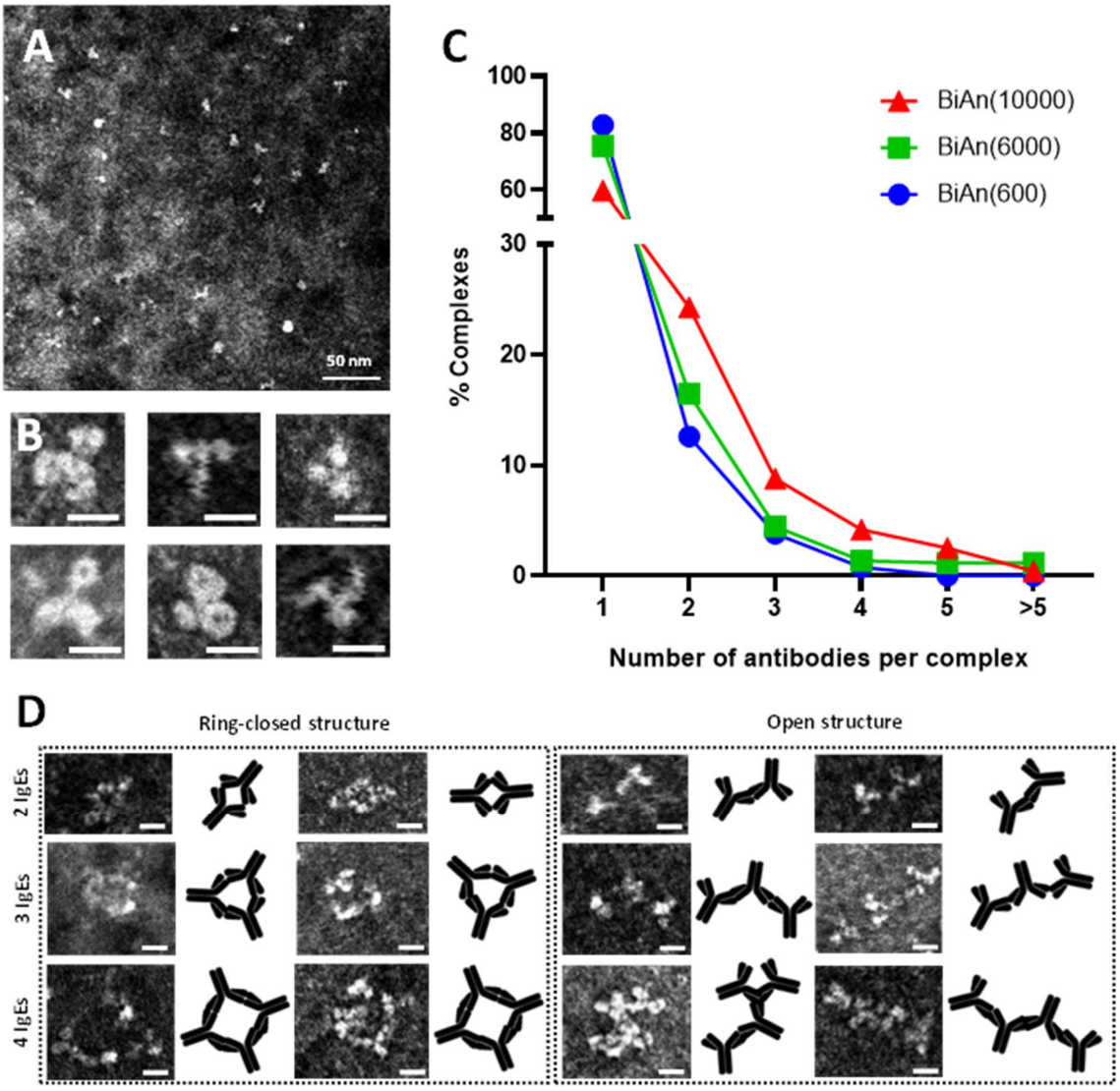

Figure 4.9. Transmission electron micrograph of negatively stained MoAbs: A) unbound MoAbs; Zoomed-in views of selected individual antibody images. Scale bars represent 10 nm; C) Number of MoAbs per complex after incubation with BiAn (600), BiAn (6000),or BiAn (10000); D) Zoomed-in views of selected individual complex images showing different open and ring-closed structures. Bars represent 10 nm.

A molar ratio of 8:1 was found to be the optimal condition for the study. Since 16 AXO determinants (or epitopes) are available on a single nanostructure (8 epitopes in each dendron extreme), this would correspond to half of the theoretical antibody molar ratio needed to completely saturate the AXO determinants of the nanoarchitecture. However, due to the proximity among the AXO units attached to the same dendron moiety, no more than 2 MoAbs are expected to bind to each dendron extreme.

In all cases, the immunocomplex formation followed a similar pattern, with most of the observed particles corresponding to individual antibodies (60-83 %). Since only the antibodies were detectable (and not the attached nanoarchitectures), it was not possible to distinguish monomeric complexes from non-complexed antibodies. Considering only structures with more than one antibody per particle, the most predominant configuration corresponded to dimeric complexes, which appeared to be the most energetically favored structure (Figure 4.9C, Table 4.5).

Table 4.5. Number (and percentage) of complexes with the different number of antibodies per complex as a function of the employed nanostructure.

Samples	Type of Immune Complexes					
	Monomeric	**Dimeric**	**Trimeric**	**Tetrameric**	**Pentameric**	**Others**
BiAn(600)	217 (82.8%)	33 (12.6%)	10 (3.8%)	2 (0.8%)	-	-
BiAn(6000)	389 (75.4%)	85 (16.5%)	23 (4.5%)	7 (1.4%)	6 (1.2%)	6 (1.2%)
BiAn(10000)	143 (59.8%)	58 (24.3%)	21 (8.8%)	10 (4.2%)	6 (2.5%)	1 (0.4%)

As it can be observed in Figure 4.9C, since the length of the PEG spacer in the BiAn increased (PEG 10000 > 6000 > 600), the percentage of complexes with 2 or more than 2 antibodies also increased. This might be ascribed to a larger steric hindrance in the structures with shorter PEG spacer, where the two AXO-dendrons are much closer to each other, preventing the binding of other antibodies to form the immune-complex. Interestingly, the BiAn (10000) showed a larger percentage of complexes with 3 or more antibodies per complex. This could be explained by the larger floury radius of the polymeric spacer (91Å) in the solution that separates the antigenic dendron and could allow additional antibodies to approach the complex by reducing the steric clash.

Besides the number of antibodies per complex, other differences could be also detected regarding the morphology of the complexes as a function of the studied molecule. As it can be seen in the examples shown in Figure 4.9D, for complexes involving 4 antibodies with an open structure, up to three different antibodies could be found to bind on a common spot (which could contain both dendron extremes of one nanostructure). For larger complexes, conformational elucidation becomes extremely challenging due to the superposition of several antibodies. It is important to bear in mind that the antibody saturation conditions of the

experiment may favor the formation of ring-closed complexes, and therefore minimize crosslinking potential. In this context, it is worth noting that all the complexes observed with BiAn(600), containing the shortest spacer, presented an open or linear structure (Figure 4.9D). This might correlate with the length of the spacer (4.8 nm in the extended conformation) between both antigenic dendrons in BiAn (600) being too short to allow the simultaneous interaction with both recognition sites of a single antibody (Table 4.2). The estimated average distance between the two Fabs domains of the antibody is 11-13 nm [241]. On the other hand, and although open structures were still predominant, Figure 4.9D also shows some examples of ring-closed complexes with different numbers of antibodies per complex that were observed with the other two nanoarchitectures tested (6.3 % of the complexes presented ring-closed conformation for BiAn (6000), and 6.2 % for BiAn (10000)).

4.4.6. Cellular Assays

4.4.6.1. Toxicity Assay

Effect of BiAns on cell viability was evaluated by MTS assay to ensure that the observed impact was not due to the cell death in each condition.

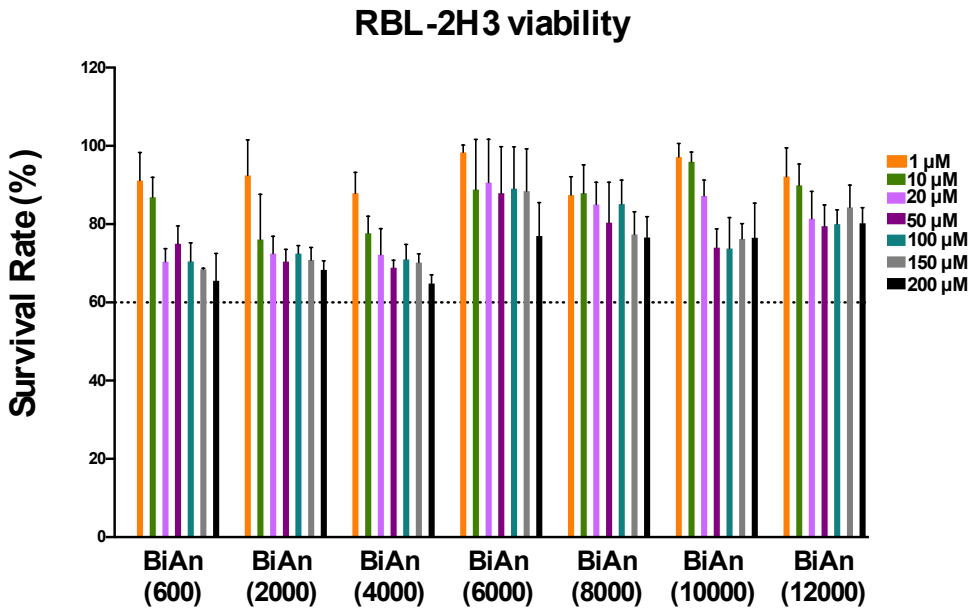

Figure 4.10. Effect of BiAns on RBL-2H3 cell viability. Cells were treated with indicated concentrations of BiAns for 24 h. The cellular viability was determined from the absorbance value and compared with untreated control cells Each value represents the mean ± S.D. of three independent experiments.

Treatment with the different concentrations of BiAns for 24 h revealed that the survival rate was greater than 70 % at most concentrations assayed. Only the highest one (200 μM) in BiAn (2000) and BiAn (4000) reduced the HumRBL-2H3 viability of up to 64 % (Figure 4.10).

4.4.6.2. Effects of BiAns on IgE Activation of Bone Marrow-derived MCs

The concentration of the anti-AX IgE MoAb and HSA-AXO (positive control) used in the MCs sensitization assay was optimized before the actual experiment. Figure 4.11 illustrates 1μg/mL of anti-AX IgE MoAb and 50 μg/mL of HSA-AXO were selected as optimal concentration to proceed for the degranulation study. The capacity of nanoarchitectures to induce IgE-dependent degranulation of bone marrow-derived MCs was evaluated. For this, cells were sensitized with IgE MoAb against AX (specific to the side chain of AX) and then treated with different concentrations of BiAns.

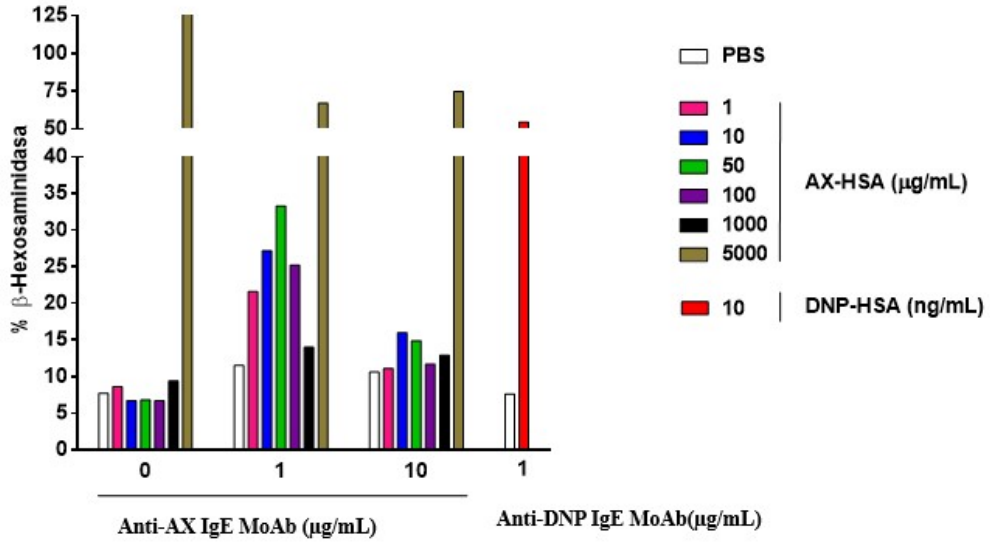

Figure 4.11. Conditions for the optimization of the concentration of anti-AX IgE MoAb for the sensitization of the MCs and selection of the concentration of the positive control. The anti-DNP IgE MoAb and DNP-HSA were used as references in the optimization phases.

The β−hexosaminidase degranulation assay was performed to determine the degree of activation (Figure 4.12A). Stimulation of cells with HSA-AXO exhibiting approximately 14 AXO units (Figure S2) (10 μM of AXO moieties) induced 25 % of β-hexosaminidase release. However, cell stimulation with BiAns using an equivalent concentration of AXO only caused activation with the BiAn (10000), inducing 17 % of β-hexosaminidase release. BiAns constructed with PEG of MW ≥ 6000 Da induced cell degranulation, showing up to 19 % of β-

hexosaminidase released at higher concentrations (50 μM and 100 μM of AXO moieties), and bringing out the importance of the polymeric spacer length to achieve cell activation. None of the BiAns tested induced cell degranulation on unsensitized cells (Figure 4.12A), indicating that they are not able to induce activation through an IgE independent mechanism.

4.4.6.3. Effect of BiAns on IgE-Induced Degranulation in RBL-2H3 cells.

Next, we chose the HumRBL-2H3 cell line, which shares some characteristics with both MCs and basophils, and expresses FcεRI [218].

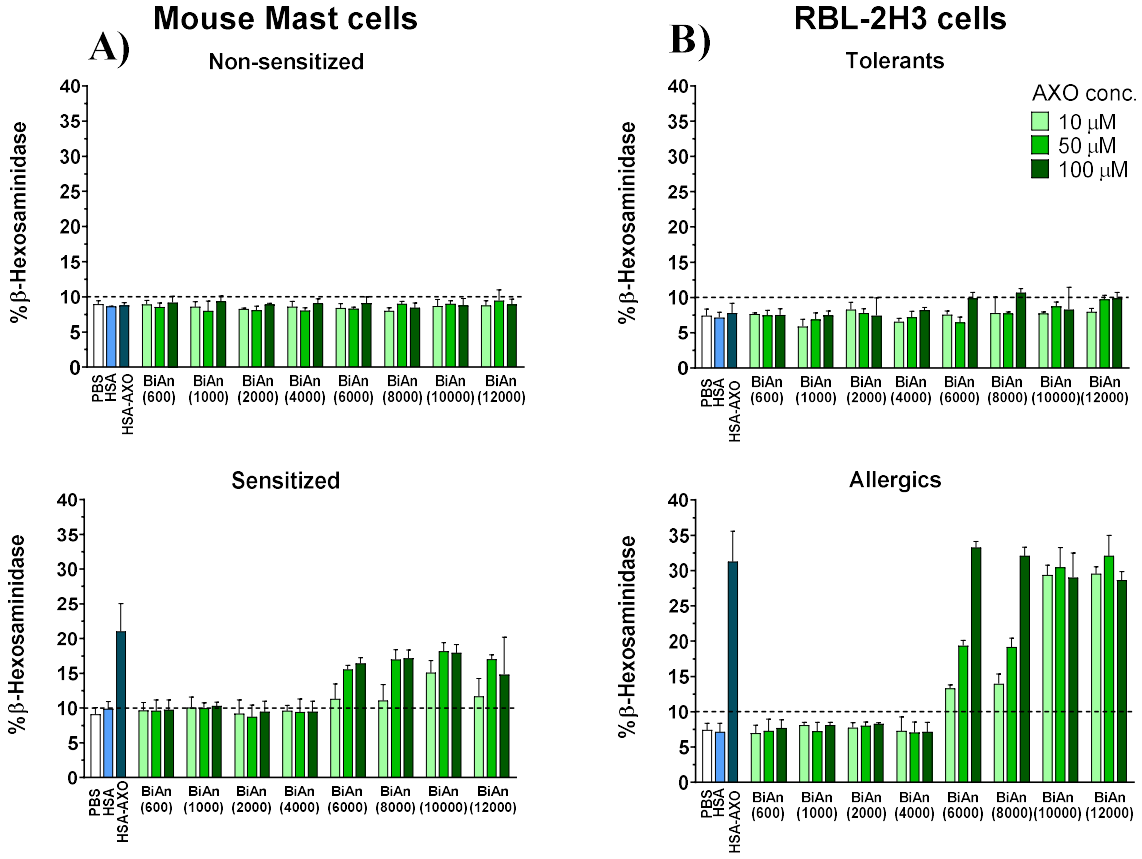

Figure 4.12. Degranulation assays after incubation of cells with the series of BiAns at 10, 50, and 100 μM of AXO equivalents. HSA and HSA-AXO (at 10 μM of AXO) were used as a negative and positive control, respectively. A) Percentage of β-hexosaminidase release in unsensitized (top) and sensitized (bottom) bone marrow-derived MCs; B) Percentage of β-hexosaminidase released by sensitized cells with sera from tolerant subjects (top) or with sera from AX allergic patients (bottom). Data are expressed as means ± S.D. The baseline of the percentage of β-hexosaminidase release is represented by the dotted horizontal line.

Cells were primed with polyclonal antibodies from sera of AX-allergic patients (Table 4.4) to enable patient-specific assessment of BiAn immunogenicity at the cellular level, rather than only assessing binding interactions as in immunoassays. Sensitized RBL-2H3 cells, with serum from AX allergic patients and tolerant subjects, were treated with different concentrations of BiAns to compare their effect in terms of the same equivalents of AXO determinants. The same PEG molecules but without AXO functionalization were used as blank structure controls. Results showed that sensitized cells with sera from allergic patients and stimulated with BiAns designed with PEG of MW ≥ 6000 Da significantly induced the β-hexosaminidase release in a concentration-dependent manner, compared with negative control groups (PBS and HSA activated cells) (Figure 4.12B bottom, Figure 4.13). Moreover, the highest concentrations of BiAns with MW ≥ 6000 Da induced a release of 33 % of β-hexosaminidase, like the one induced by HSA-AXO (at 10 μM conc of AXO) (Figure 4.13B).

Table 4.4. Clinical characteristics of allergic patients and skin test results with penicillin antigenic determinants and *in vitro* determination of AX-sIgE and BP.

	Clinical characteristics					*In vivo* test				*In vitro* test						
						Skin Tests			DPT	IgE determination				Basophil activation test		
Case	Age	Sex	Clinical reaction	Drugs involved in the reaction	Grade Severity*	BP-OL	MD	AX	AX	RAST (%)		ImmunoCAP (kU/L)		BP	AX	AX/ CLV
										BP-sIgE	AX-sIgE	AX-sIgE	Total IgE			
15	54	F	Urticaria and angiodema	AX/CLV	I	Neg	Neg	Pos (IDT)	NP	15	19	1.95	392	Pos	Pos	Pos
16	56	F	Anaphylaxis	AX/CLV	II	Neg	Neg	Pos (IDT)	NP	26	21	3.72	1158	Neg	Neg	Neg
17	50	F	Anaphylactic shock	Unknown	III	Pos (IDT)	Neg	Neg	Pos	16	19	4.33	3802	Neg	Neg	Neg

*AX: Amoxicillin; CLV: potassium clavulanate; DPT: drug provocation test; F: Female; IDT: intradermal test; M: male; MDM: Minor Determinants Mixture; Neg: negative; PPL: benzylpenicilloyl poly-L-lysine; Pos: positive; NP, not performed. *Grading system for generalized hypersensitivity reactions: I, mild (skin and subcutaneous issues only); II, moderate (features suggesting respiratory, cardiovascular, or gastrointestinal involvement); III, severe (hypoxia, hypotension, or neurologic compromise). REF: Brown SG. Clinical features and severity grading of anaphylaxis* [217].

Among these, BiAn (10000) and BiAn (12000) are the most effective intermolecular cross-linker as they induced above 27 % of β-hexosaminidase release at 10, 50, and 100 μM of AXO, although at lower concentration (1 μM); only BiAn (10000) induced substantial β-hexosaminidase release (Figure 4.13). No significant differences were observed in these BiAns treatments when the cells were sensitized with sera from tolerant subjects (Figure 4.13B top),

and on unsensitized cells included as control of IgE activation (data not shown); whereas a more specific dose-response effect was observed when the cells were sensitized with sera from patients. The fact that none of the BiAns induced cell degranulation on unsensitized cells excludes direct activation by off-target occupancy of cell surface receptors.

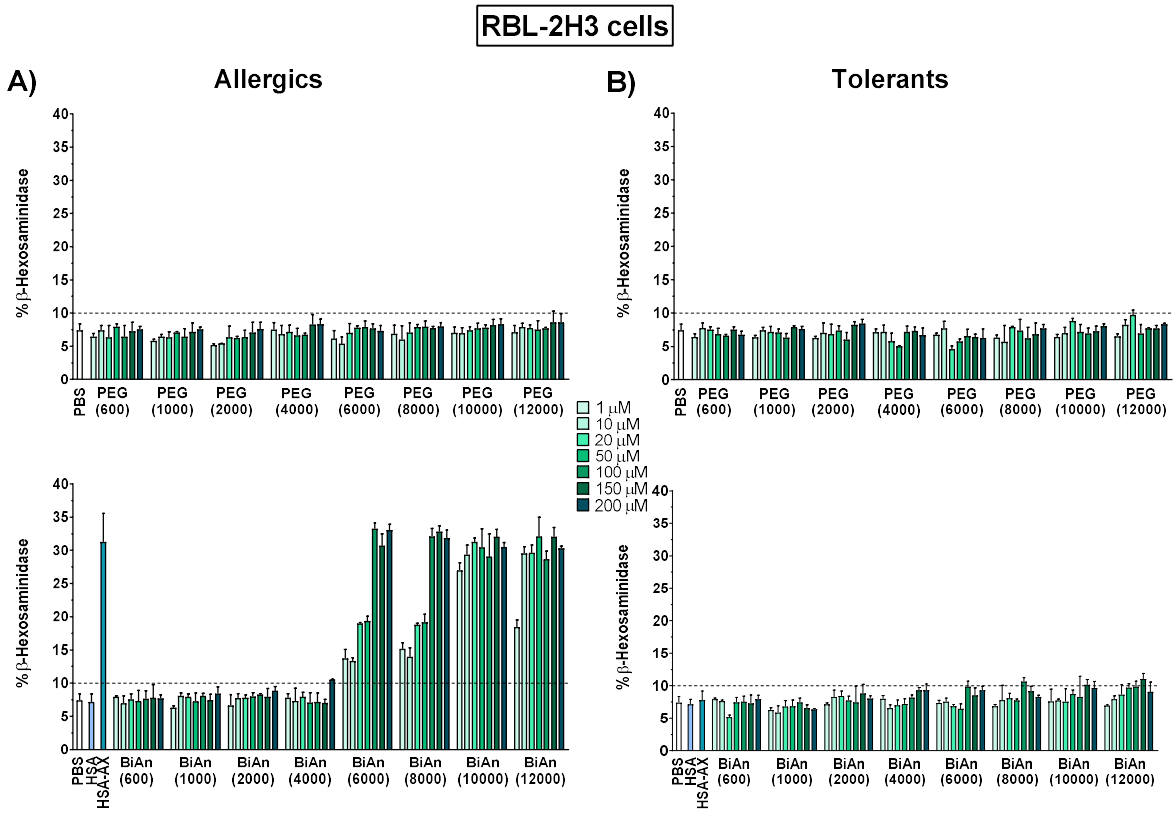

Figure 4.13. Impact of BiAns on RBL-2H3 degranulation at different concentrations (1 μM, 10 μM, 20 μM, 50 μM, 100 μM, 150 μM, 200 μM).A) Percentage of β-hexosaminidase release after incubation with PEG (without functionalization with AX) as negative controls (top) and BiAns (bottom) on sensitized cells with sera from allergic subjects. B) Percentage of β-hexosaminidase produced after incubation with PEG (without functionalization with AX) as negative controls (top) and BiAns (bottom) on sensitized cells with sera from tolerant subjects. HSA and HSA-AXO were used as a negative and positive control, respectively. Data are expressed as means ± S.D and are representative of three independent experiments. Groups with different letters statistically differ ($P \leq 0.05$). All statistical analysis was performed using GraphPad Software Prism 8 (version 8.4.2). For multiple comparisons of quantitative data, ANOVA was used followed by Tukey´s post-hoc test. $P < 0.05$ considered indicating a statistically significant difference.

4.4.6.4. Effect of BiAns on HMC1.2 Cell Line Degranulation.

To further exclude the non-IgE dependent effects, in addition to experiments with unsensitized cells and sensitized cells with tolerant subjects in RBL cells and unsensitized Bone Marrow-derived MCs, another degranulation assay was performed using HMC1.2 cell line by sensitizing with serum from 3 tolerant and 6 allergic patients before the incubation with the BiAns. HMC 1.2 cell line, exhibited a similar phenotype to that of human MCs, expressing IgG receptor (FcγR) but not FcεR [241]. As can be seen from Figure 4.14, none of the cells sensitized with the serum from the allergics and tolerant subjects and treated with BiAns has shown activation. The absence of activation observed in parallel experiments with the HMC 1.2 cell line, demonstrated that the BiAns do not trigger degranulation by an IgG-mediated pathway suggesting that BiAns stimulate the degranulation on HumRBL-2H3 through an IgE pathway.

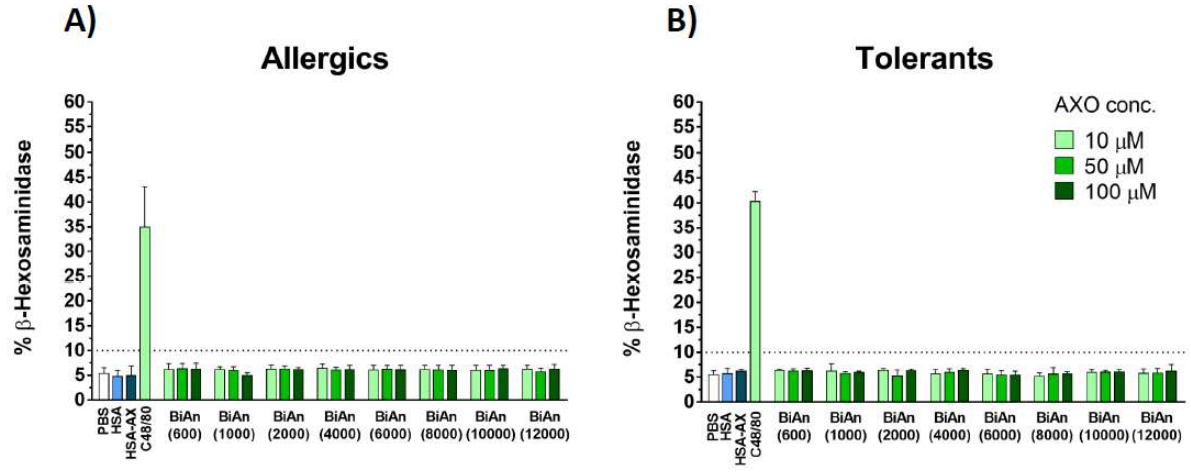

Figure 4.14. Impact of BiAns on HMC 1.2 degranulation at different concentrations (10 μM, 50 μM, 100 μM).A) Percentage of β-hexosaminidase release after incubation with BiAns on sensitized cells with sera from allergic subjects. B) Percentage of β-hexosaminidase produced after incubation with BiAns on sensitized cells with sera from tolerant subjects. HSA and HSA-AXO were used as negative controls and C48/80 as a positive control. No statistically significant difference was found.

4.5. Discussion

Our SAR study with well-characterized BiAns shows that the size and the proximity of AXO-determinants on these conjugates influence the number and shape of immunocomplexes and their subsequent ability to activate *in vitro* effector cells in an IgE-dependent mechanism. Through competitive immunoassays, it could be shown that all BiAn were recognized by AX-sIgE from patients. The higher concentration of determinants (AXO) increased the extent of inhibition, a pattern already reported with the monomeric AXO-Bu conjugate [55] and Dendrimeric Antigens with different penicillin determinants [66,145]. The increased inhibition obtained with the monomeric AXO-Bu, compared with BiAns, can be attributed to the absence of steric interactions for sIgE binding to AXO moieties in this small conjugate. In BiAn, PEG chains could contribute to a steric hindrance to the IgE binding, and also the high proximity of the eight AXO determinants exposed in each dendron would hinder their simultaneous IgE recognition. Using OpNS TEM, immunocomplexes could be visualized for different BiAn sizes. Assessment of BiAn immunogenicity at cellular level reveal that IgE-mediated degranulation of bone marrow derived-MCs and HumRBL-2H3 cells with BiAns is polymeric spacer length dependent. In both cellular assays, dose-dependent activation responses were observed with all BiAn containing flexible linkers above a critical size (PEG 6000). Although these PEG polymers take on a spherical equilibrium configuration in an aqueous environment (for instance 13 nm for PEG 6000 in its folded conformation), their chain units move freely [242] and both ends could be at any position within the contour length of the polymer chain (~48 nm) (Table 1).

The data shown in Figure 4.10C and in Table 4.5 classifies the raw data obtained (surface area per complex) in discrete categories based on the expected number of antibodies per complex. This was done to ease the interpretation of the data and to show the deeper reasoning behind measuring the surface area of each complex observed in the TEM grids. To make this classification, we first obtained the average surface area of single antibodies (using a control sample without nanostructures). Then, based on this value, we classified the complexes observed in the samples based on the estimated number of antibodies per complex. We considered that complexes with a surface area below 1.5 times that of the average single antibody only had one antibody per complex, those between 1.5 and 2.5 times this area were classified as having 2 antibodies per complex, and so on. This data processing method greatly improved the objectivity of the analysis compared to trying to estimate the number of

antibodies per complex manually. However, this processing method also presented some limitations. The two main limitations lie in the possibility of imperfect negative staining in some areas of the sample, and in the differences in the 2 dimensional projected negatively stained areas of the 3-dimensional antibodies. Both sources of error could lead to some of the complexes being incorrectly classified regarding their number of antibodies (by underestimating this number). For this reason, a new statistical analysis employing raw, uncategorized data has been included. We have compared the raw area per complex data between the different experimental groups, by means of the Kolmogorov-Smirnov (K-S) Test. The K-S Test determines sample distribution within populations without making specific distributional assumptions (it is a non-parametric test). First, the results show that the distribution of surface area per complex for sample BiAn(600) and BiAn(6000) was not significantly different ($p=0.089$; $D<$critical value (n scaled) for $\alpha=0.05$). However, when comparing the surface area per complex of both samples (BiAn(600) and BiAn(6000)) with BiAn(10000), in both cases, the distributions were significantly different ($p<<<0.05$; $D>$critical value (n scaled) for $\alpha=0.05$).

The OpNS TEM data support cellular activation results, since the BiAn that leads to a greater proportion of immunocomplexes, and the largest number of antibodies per complex, was also the most successful one in activating cellular responses, in agreement with reported potent degranulation achieved by synthetic allergens with a valency ≥ 3 [206,207,243]. The schematic illustration of the effect of the polymeric spacer length on the effector cell and *in vitro* immune complex formation is given in Figure 4.15. The failure of BiAn containing PEG ≤ 4000 to stimulate degranulation indicates that, despite their recognition by AX-sIgE, they are inefficient at cross-linking cell surface IgE, which could be explained by a relatively low abundance of extended conformation of the PEG polymers in aqueous solution. BiAn containing the larger PEG length, and bearing equal valency, facilitates this interaction, presenting BiAn (6000) the minimal distance between haptens that can induce cell degranulation. The most potent stimulator BiAn (10000) is effective at all studied concentrations in both cell lines, MC and RBL-2H3 (as low as 1 µM for RBL-2H3) (Figure 4.13), indicating that an estimated distance of ~ 18 nm between haptens seems to be optimal for cross-linking the receptors. Consistent with the literature, this ~ 20 nm dimension was found to be the optimal distance between DNP haptens on a rigid nanoparticle system to induce MC degranulation [206]. However, this is not in agreement with the pattern observed in DNP divalent and trivalent systems, in which rigid spacers of 4–5 nm stimulate stronger

degranulation responses compared with those possessing spacing greater than 7–10 nm [16,207]. Our findings indicate that not only the size and multivalence of nanostructures are important factors for inducing degranulation, but also their flexibility.

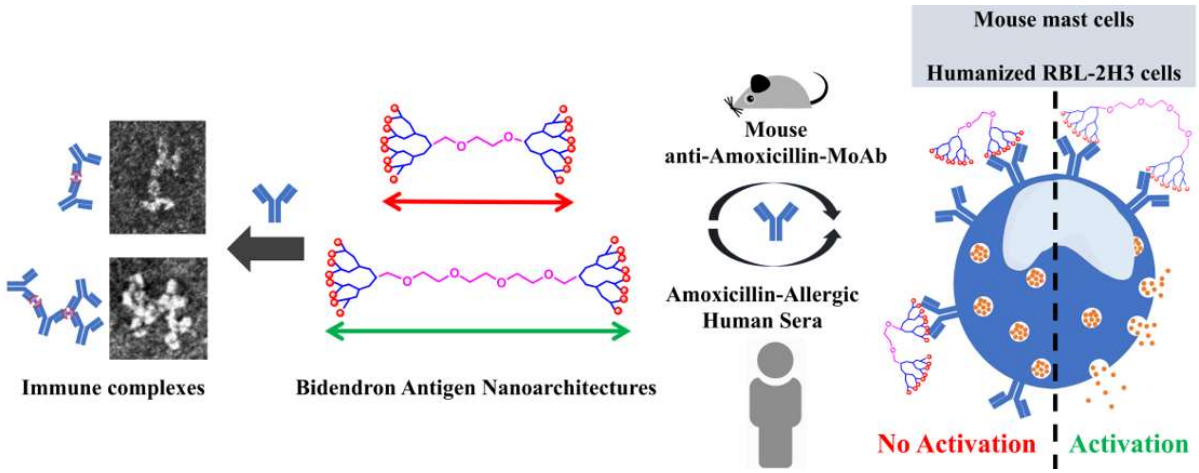

Figure 4.15. Graphical illustration of the effect of polymeric spacer length on the effector cell and in vitro immune complex formation

Overall, these results suggest that BiAn nanoarchitectures containing longer PEG chains (MW range: 6000-12000 Da) are effective triggers, whereas bivalent structures of DNP, in which haptens are also separated by flexible PEG of different lengths (MW range: 400-10000 Da), were reported not to activate MC, but to behave as inhibitors [60]. This inhibition was explained by a preferential formation of intramolecular cross-linking of antibody by bivalent DNP of sufficient PEG length (10 nm) (stable 1:1 complexes) [60], or formation of cyclic dimmers of IgE- FcεRI on the cell surface with shorter linkers (< 5 nm) [149] Comparisons in terms of chemical structure between BiAn and DNP-PEG systems [60] points to multivalent vs. bivalent hapten presentation as the main difference. Likely, the multivalence of the dendron in BiAn favoured IgE interaction, upon dendritic or synergetic effect, and therefore the degranulation. This is in agreement with cell activation induced by other multivalent systems: dendrimers presenting 16 units of DNP induced MCs degranulation in DNP studies interaction [60]; different penicillin DeAns activated basophils from patients, with increased stimulation index observed for those displaying higher valence (64 vs. 16 haptens) [202]; other rigid systems, nanoparticles (≥ 19.8 nm) functionalized with multiple DNP, showed to be very effective effectors, however, a reduced hapten density inhibited degranulation [206].

The scenario for MC and basophil degranulation is very complex, and the use of defined nanoarchitectures has allowed the identification of the minimal requirements for their activation in a realistic model. In this regard, multivalent dendritic- presentation and distance between the haptens in BiAn constructed with PEG MW range 6000-12000 fulfilled the optimal requirement to overcome the intricate cellular preconditions leading to cell activation. The optimal distance between AXO determinants for effective cross-linking is observed in BiAn (10000).

4.6. Conclusion

The scenario for MC and basophil degranulation is very complex, and the use of precisely controlled architectures, within the nanoscale, has allowed the identification of the minimal requirements for the release of mediators in a realistic model. The capacity of the BiAn construct based on PEG MW ≥ 6,000 to stimulate the cellular degranulation indicates that the structures have fulfilled the optimal requirement to overcome the intricate cellular preconditions. In this regard, multivalent dendritic presentation, and distance between the haptens larger than 6.7 nm result in intermolecular crosslinking leading to activation of the cells. The optimal distance between AXO determinants for effective crosslinking is around 9 nm, as observed in BiAn (10000) experiments.

In summary, using multivalent AXO-dendrons spaced by flexible PEG polymers, this study sheds light on the mechanism of the effector cells activation from a unique realistic perspective, using real human samples and haptens in routine clinical use. Moreover, the synthesis of BiAn platform is versatile and could apply to different drug haptens or allergen epitopes. Understanding the biology and nanoscale organization of the cell membrane receptors can lead to the development of novel diagnostic and therapeutic tools for drug allergy. Additionally, these results can serve as guidelines for designing nanoarchitectures to study other cellular responses beyond allergy

Chapter 5: Synthesis, Characterization, and Immunological Evaluation Bidendron Antigen Nanoarchitectures with Varying Numbers of Peripheral Functionalities

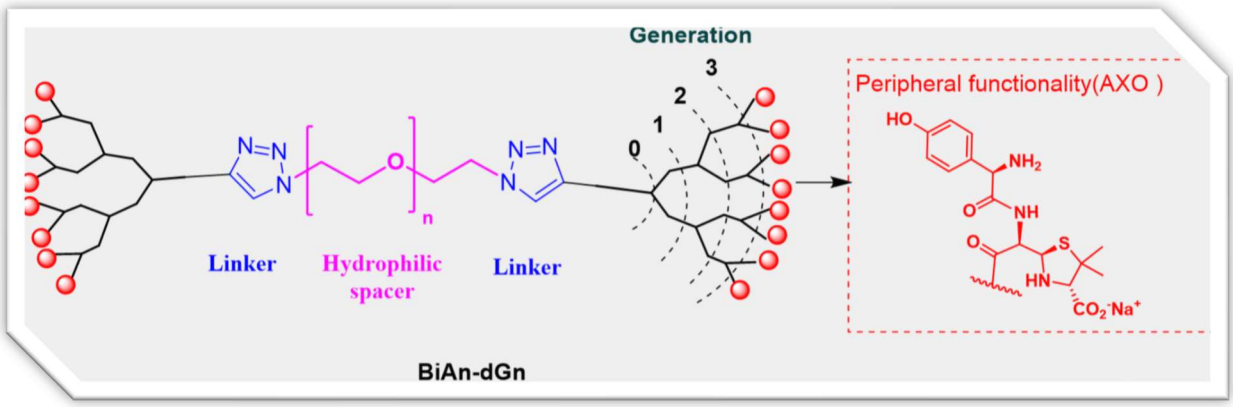

5.1. Introduction

In the previous chapter, we reported the effect of the architectural features of PEG-based nanostructures, BiAns, constructed based on PAMAM dendron, that terminally functionalized with the same number of peripheral functionality (16 units of AXO) on effector cell degranulation. Inspired by the finding regarding the importance of adduct size and distance between determinants to promote effector cell activation, we capitalize on mutually varying the length of the polymeric spacer and the number of the peripheral functionality to also study the influence of valence to promote effector cell activation in an allergic response to AX.

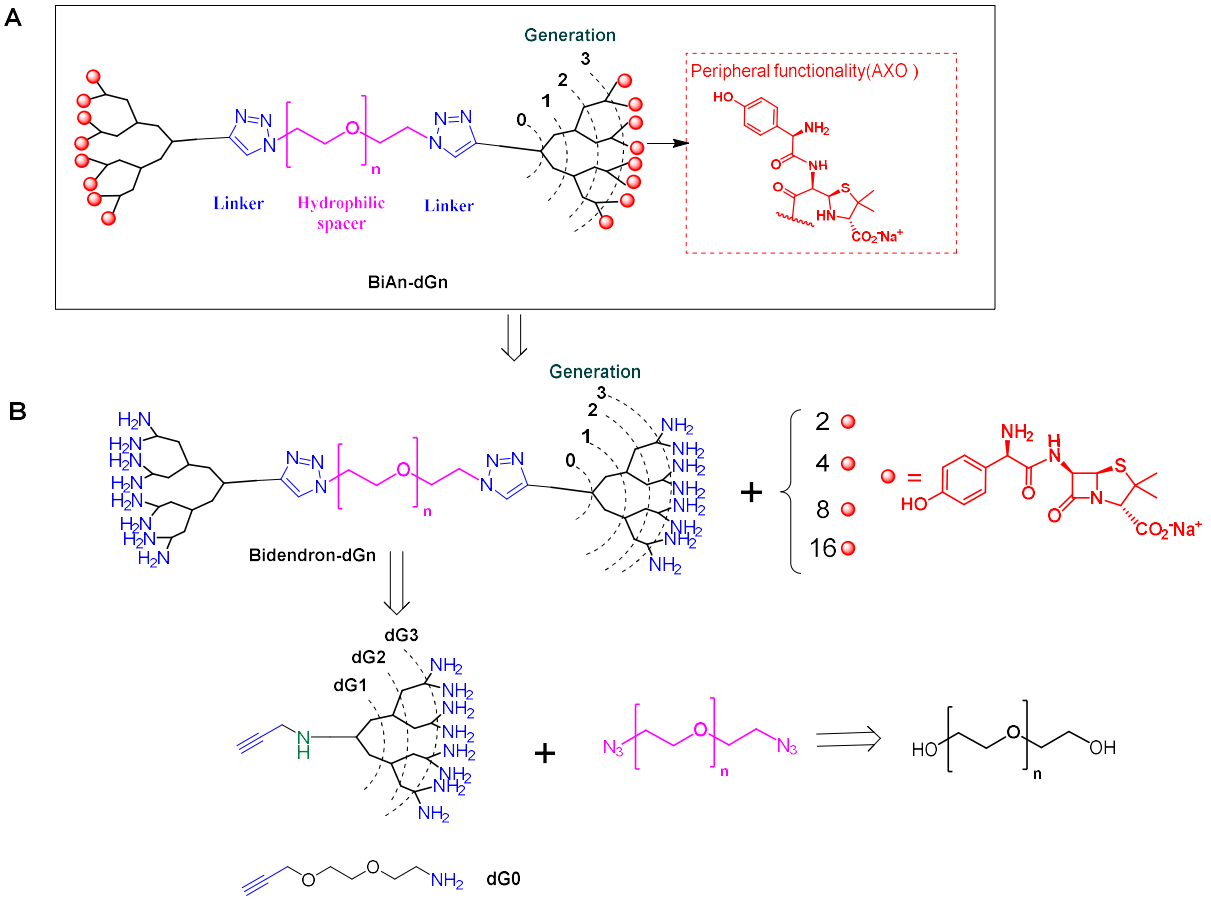

Figure 5.1. Schematic representation of multi-peripheral functional BiAn-dGn nanoarchitectures. The structures differ from each other by PEG length (n ranging from 14 to 273), monovalent PEG-alkyne amine (dG0 is 1 peripheral functionality) and dendron generations scaffold (dG1, dG2, dG3 with 2, 4 and 8 peripheral functionalities, respectively).

This is a more ambitious aim involving the synthesis and immunological evaluation of 32 nanoarchitectures. Since the whole synthetic process for achieving BiAns have been very

tedious, time-consuming, and involving many synthetic steps, a faster and more efficient procedure has been optimized for the construction of the second set of BiAns (which we call BiAn-dGn, where n denotes the generation of dendrons) using click chemistry and customized polyamide-based dendrons of different generations (first-generation (dG1), second-generation (dG2) and third-generation (dG3)) and an equivalent monovalent molecule (dG0). Unlike the library of BiAn described in the previous chapter, the current strategy focuses on designing a new library of BiAns (BiAn-dGn), that besides varying length of the polymeric spacer, display different valences: two (BiAn-dG0), four (BiAn-dG1), eight (BiAn-dG2) and sixteen (BiAn-dG3) peripheral functionalities, for further evaluation in the degranulation process of effector cells.

5.2. Synthesis and Characterization of BiAn-dGn Nanoarchitectures

The overall retrosynthetic representation is illustrated in Figure 5.1. The AXO decorated nanoarchitectures can be obtained through the nucleophilic attack of the amino groups of the homobidendron PEG skeleton precursor towards the β-lactam ring of the AX. The disconnection of the triazole linking results in three synthons: two identical units of alkyne-functional molecules bearing peripheral amino groups (either monovalent molecule or multivalent dendrons) and PEG diazide. Different PEG-$(N_3)_2$ based on PEG of different lengths were synthesized to readily click-couple with alkyne bearing compounds. The conversion of the hydroxyl groups at the ends of the PEG chains to azide groups has been carried out by treatment with tosyl chloride (introduction of leaving group), followed by reaction with sodium azide (bimolecular nucleophilic substitution). To obtain the BiAn-dG0, 2-(2-(prop-2-yn-1-yloxy) ethoxy) ethan-1-amine (Alkyne-PEG2-Amine) was carefully chosen to contain short hydrophilic arm permitting in bi-AXO functionalized structures. The other structures were constructed based on propargyl core polyamide dendrons of different generations containing a diverging number of amine termini. The dendrons (dG1, dG2 and dG3) were kindly received from the group of Professor Pérez-Inestrosa. Both the dendrons and Alkyne-PEG2-Amine (monovalent molecules) allows chemoselective orthogonal reactions in which alkyne functionality reacts only with azides, whereas the peripheral amine functionality remains unmodified until haptenation process. As a general procedure for BiAn-dGn synthesis, successive reactions involving two different chemistries were followed: (i) the attachment of both azide groups in the extremes of the polymeric spacer to alkyne functional molecules (Alkyne-PEG2-Amine and propargyl-functionalized dendrons) using CuAAC

"click" chemistry; (2) the formation of the amide linkage between the amine-terminated scaffold and the strained β-lactam ring of the AX. The CuAAC is a robust synthetic reaction commonly used in preparing functionalized macromolecular architectures [167]. The success of this "click" reaction is attributed to the ease to carry out, mild reaction condition, efficient use of a wide variety of functional groups and solvents, including aqueous media [244,245]. The method regio-specifically unites azides and terminal acetylenes to give only 1,4-disubstituted 1,2,3-triazoles in high yields using a variety of Cu (I) catalysts or precursors of Cu (I) catalysts [246]. Besides NMR techniques, the infrared (IR) was also used to monitor the completion of the reaction, with the disappearances of asymmetric stretching absorption of azide at 2100 cm^{-1} indicating complete consumption of the azide groups for the triazole ring formation (Figure 5.2). The MW estimate and number of expected antigenic determinants (valence) is given in Table 5.1.

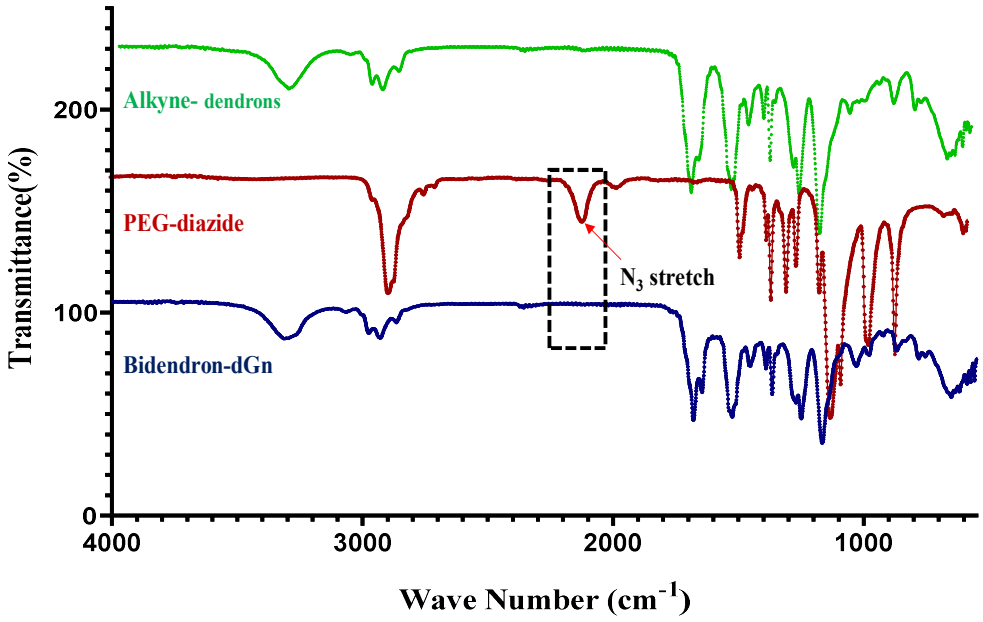

Figure 5.2. IR spectra of Alkyne-dendrons (green), PEG-$(N_3)_2$ (dark red) and Bidendron-dGn indicating the complete consumption of the azide in the reaction (evidenced by the absence of azide stretching at 2100 cm^{-1}).

Table 5.1. Descriptions of the BiAn-dGn Nanoarchitectures

Synthetic Antigen	Linker PEG MW(Da)	$(C_2H_4O)N$ Where N is	Estimated MW (Da)	Valency
	BiAn-dG0 			
BiAn-dG0(600)	600	14	1323.8	2
BiAn-dG0(1000)	1000	23	1723.8	2
BiAn-dG0(2000)	2000	45	2723.8	2
BiAn-dG0(4000)	4000	91	4723.8	2
BiAn-dG0(6000)	6000	136	6723.8	2
BiAn-dG0(8000)	8000	182	8723.8	2
BiAn-dG0(10000)	10000	227	10723.8	2
BiAn-dG0(12000)	12000	273	12723.8	2
	BiAn-dG1 			
BiAn-dG1(600)	600	14	2622.2	4
BiAn-dG1(1000)	1000	23	3022.2	4
BiAn-dG1(2000)	2000	45	4022.2	4
BiAn-dG1(4000)	4000	91	6022.2	4
BiAn-dG1(6000)	6000	136	8022.2	4
BiAn-dG1(8000)	8000	182	10022.2	4
BiAn-dG1(10000)	10000	227	12022.2	4
BiAn-dG1(12000)	12000	273	14022.2	4
	BiAn-dG2 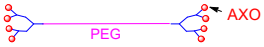			
BiAn-dG2(600)	600	14	4796.7	8
BiAn-dG2(1000)	1000	23	5196.7	8
BiAn-dG2(2000)	2000	45	6196.7	8
BiAn-dG2(4000)	4000	91	8196.7	8
BiAn-dG2(6000)	6000	136	10196.7	8
BiAn-dG2(8000)	8000	182	12196.7	8
BiAn-dG2(10000)	10000	227	14196.7	8
BiAn-dG2(12000)	12000	273	16196.7	8
	BiAn-dG3 			
BiAn-dG3(600)	600	14	9145.6	16
BiAn-dG3(1000)	1000	23	9545.6	16
BiAn-dG3(2000)	2000	45	10545.6	16
BiAn-dG234000)	4000	91	12545.6	16
BiAn-dG3(6000)	6000	136	14545.6	16
BiAn-dG238000)	8000	182	16545.6	16
BiAn-dG3(10000)	10000	227	18545.6	16
BiAn-dG3(12000)	12000	273	20545.6	16

5.2.1. Synthesis and Characterization of BiAn-dG0

For designing the simpler nanoarchitectures, BiAn-dG0, the monovalent-amine molecule containing alkyne group was chosen to react with the extremes of PEG, so similar methodology and structural features to compare all set of BiAn-dGn. The synthesis followed the general procedure for the reaction between azide and alkyne, the scheme described in Figure 5.3. For performing the CuAAC reaction, a solution of PEG-$(N_3)_2$ and dG0 (an alkyne) in THF-H_2O (1:1) was stirred with $CuSO_4$/sodium ascorbate (to generate Cu (I)) at room temperature overnight. A slight surplus of alkyne was used to guarantee the complete functionalization of the PEG-$(N_3)_2$. The elimination of copper from the reaction was achieved by QuadraSil triamine(QuadraSil® TA)metal scavenger and the final products were further purified by size exclusion chromatography. The ^{1}H NMR confirms the formation of the 1,2,3-triazole ring evidenced by the resonance of the triazole peak between 7.96 and 8.14 ppm (d in Figure 5.4 C) and the shift of the adjacent methylene from 4.29 ppm (e in Figure 5.4 B) to 4.67 ppm (e in Figure 5.4 C). Furthermore, the complete consumption of the PEG-$(N_3)_2$ in the reaction was evidenced by a shift of the peak around 3.56 ppm(c in Figure 5.4A), corresponding to the adjacent methylene (-CH_2-N_3), to the lower field (around 4.74 ppm, c in Figure 5.4 B). A quantitative yield was obtained for all the products regardless of the variation in the length of the polymeric spacer used.

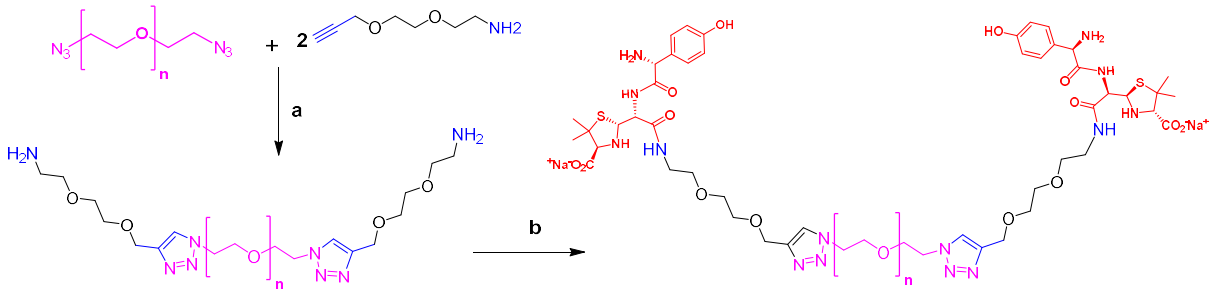

Figure 5.3. The synthetic scheme of BiAn-G0 bearing 2 AXO determinants. The structural variation depends on the PEG length (with n ranging from 14 to 273). Reaction conditions:(a) CuSO4.5H2O, sodium ascorbate, THF-H2O (1:1); (b) AX, carbonate buffer (0.05 M, pH 10.2), room temperature, overnight.

The final product was obtained through the nucleophilic reaction of the amine-terminated scaffold towards the β-lactam ring of the AX. To ensure the completion of the reactions, an excess of AX was used in a basic pH buffer. Unlike the structures constructed based on

different generation dendrons, the reaction of the BiAn-dG0 was carried out at room temperature and complete overnight as evidenced by a shift in the methylene (-CH_2-NH_2) from 3.24 to 3.40 ppm indicating the formation of amide linkage (i in Figure 5.4 C-D). The absence of steric hindrance in this reaction allowed in obtaining fully functionalized products at room temperature unlike in haptenized dendrimer derived structures, in which adjacent flexible arm requires low-temperature incubating condition. Moreover, the presence of peaks confirming the opened ring of AX evidenced by the shift and separation of the β-lactam proton, H5 (4.99 ppm) and H6 (4.35 ppm), signifies the attachment of AXO to the scaffold.

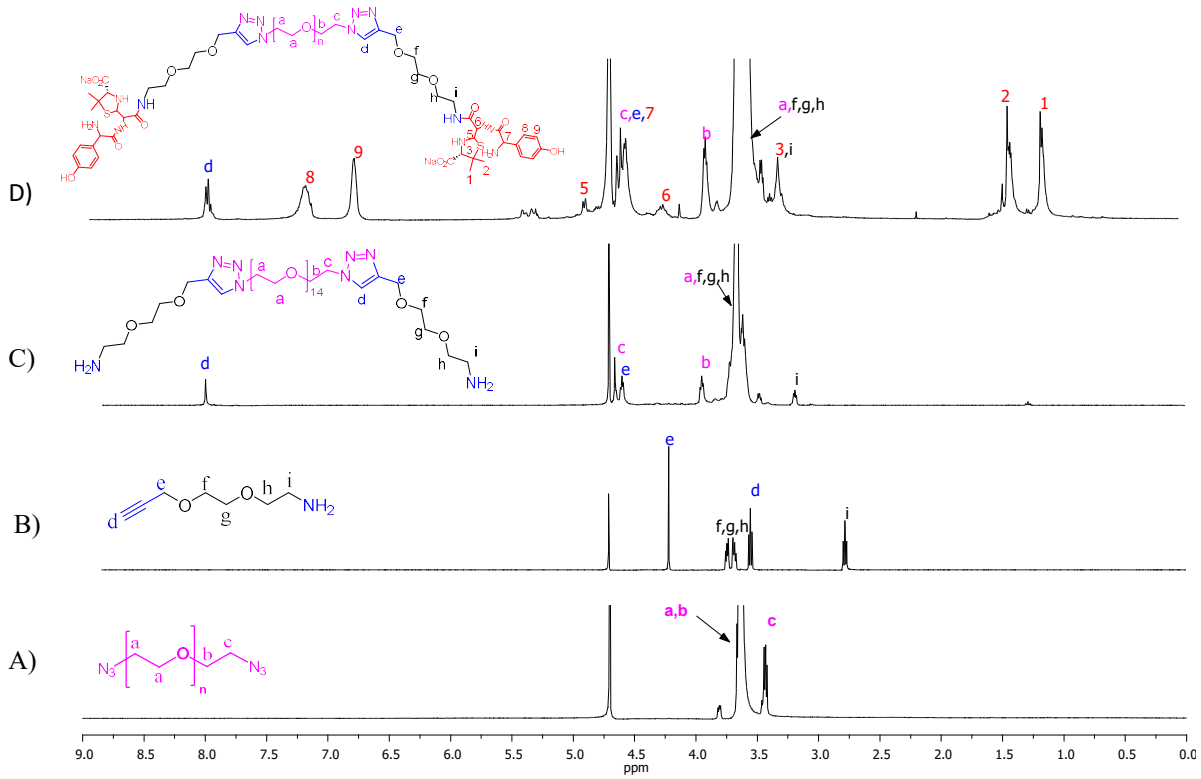

Figure 5.4. Representative ^{1}H NMR spectra in D_2O for monitoring the reactions to obtain the BiAn-G0 by following the sequential appearance, disappearance, and chemical shifts in the peaks

5.2.2. Synthesis and Characterization of BiAn-dGn

Three different alkyne core dendrons: dG1NH_2, dG2NH_2 and dG3NH_2 with two, four and eight amine-termini, respectively were used to construct nanostructures with a varying number of peripheral functionalities. Briefly, this dual alkyne and amino-functionalized dendrons were click-coupled with PEG-$(N_3)_2$ of different polymeric length and terminally functionalized with

varying number of AXO units on both sides of the Bidendron-dGn, resulting in symmetric structures separated by a flexible polymeric spacer (Figure 5.5).

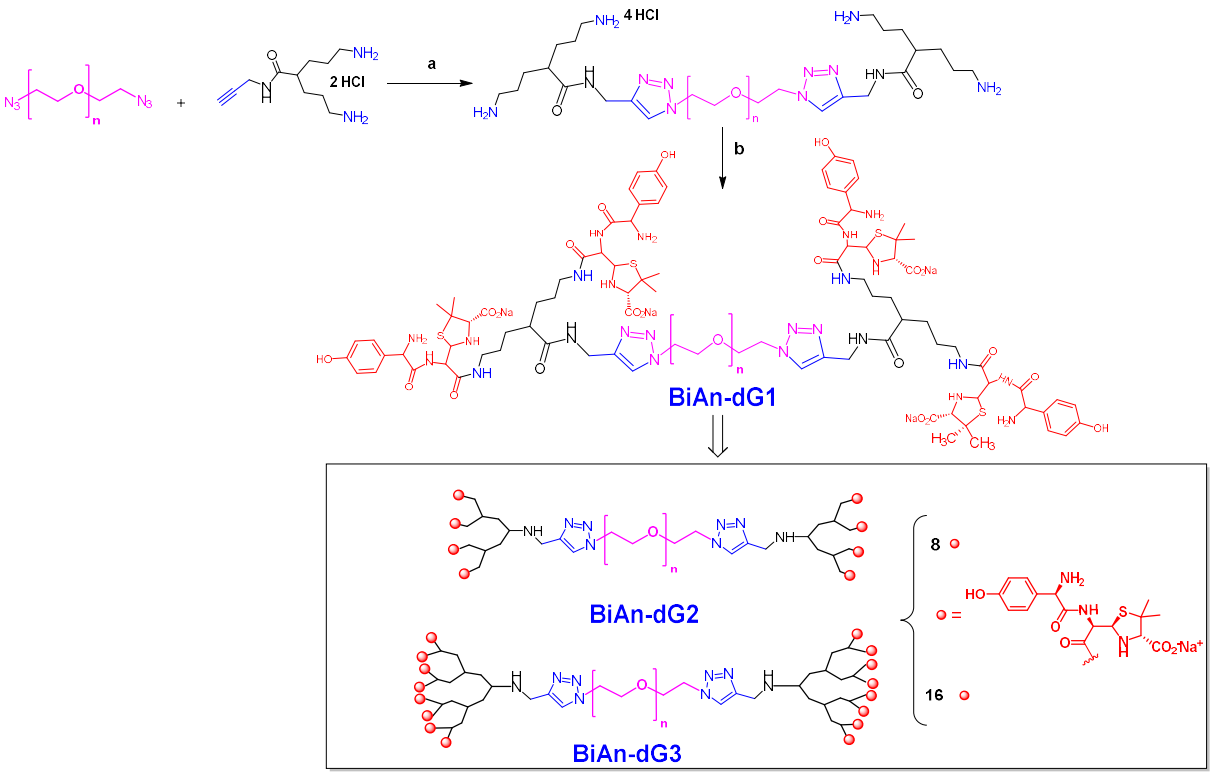

Figure 5.5.The synthetic scheme for BiAn-dGn, specifically BiAn-dG1Reaction conditions:(a) $CuSO_4.5H_2O$, sodium ascorbate, THF-H_2O (1:1); (b) AX, carbonate buffer (0.0 5 M, pH 10.2) at 4 ºC. The scheme for the final structures of BiAn-dG2 and BiAn-dG3 are represented within the square.

The synthetic scheme to obtain BiAn-dG1, BiAn-dG2, BiAn-dG3 followed general procedures both for the click and nucleophilic reactions. The reactions proceed by click-coupling the different polymeric length PEG with the MWs ranging from 600 to 12000 Da, terminally bi-functionalized with azide, together with acetylene core dendrons displaying amine HCl salt functionality. The CuAAC reaction was carried out in THF-H_2O (1:1) at room temperature. It was observed that both the length of the polymeric spacers and the generation of the dendrons affect the time needed to the completion of the reactions. The reaction between dG1, dG2 and the lower polymeric spacers PEG (up to MW 4000 Da) presented to completion over 24 h at room temperature. Nonetheless, the reactions involving the higher MW PEG spacers took up to 36 h to reach completion. Contrasting to the first two generations, the click with dG3 did not complete over 24 h even for those involving lower MW polymeric spacers as reactants. The

procedures with the lower MW PEG compounds (up to 4000 Da) were completed after 48 h, and with the higher MW PEG compounds took up to 72 h. This variation could be attributed to both the steric hindrance related to the polymeric spacers and reduced accessibility of acetylene core of higher generation dendron. Moreover, QuadraSil® TA metal scavenger used to remove traces coordinated coper (the process that was optimized as indicated in section 5.2.3) In all cases, the neutralization of protonated peripheral amine was performed by Amberlite ion exchange resin (as needed before the reaction with AX) and the resulting PEG-bidendrons were purified by size exclusion chromatography to afford all products in a yield greater than 87 %. The formation of 1,2,3-triazole was confirmed by the resonance of triazole proton between 7.88 and 8.03 ppm (d in Figure 5.6 C) and adjacent methylene shifting to the lower field from around 3.97 (e in Figure 5.6 B) to 4.48 ppm (e in Figure 5.6 C). The complete consumption of PEG-$(N_3)_2$ was confirmed by the shift in the methylene peak (-CH_2-N_3) to around 4.64 ppm (c in Figure 5.6 C).

Similar to previously described haptenation procedures, the AX was coupled to an amine-terminated scaffold through nucleophilic reaction. This is evidenced by the complete shift in terminal methylene peaks (-CH_2-NH_2) from 3.00 ppm (q in Figure 5.6 C) to 3.17 ppm (q in Figure 5.6 D) showing the successful formation of the amide linkage. Furthermore, the separation of the chemical shifts of H5 and H6 protons (Figure 5.6 D) compared to that of AX, together with the appearance of other peaks corresponding to AXO, indicate the successful coupling of AXO to the dendritic scaffold. The yield of this reaction step was greater than an average of 93 %, and the overall yield to obtain the BiAn-dGn starting from PEG-$(N_3)_2$ was greater than 81 %.

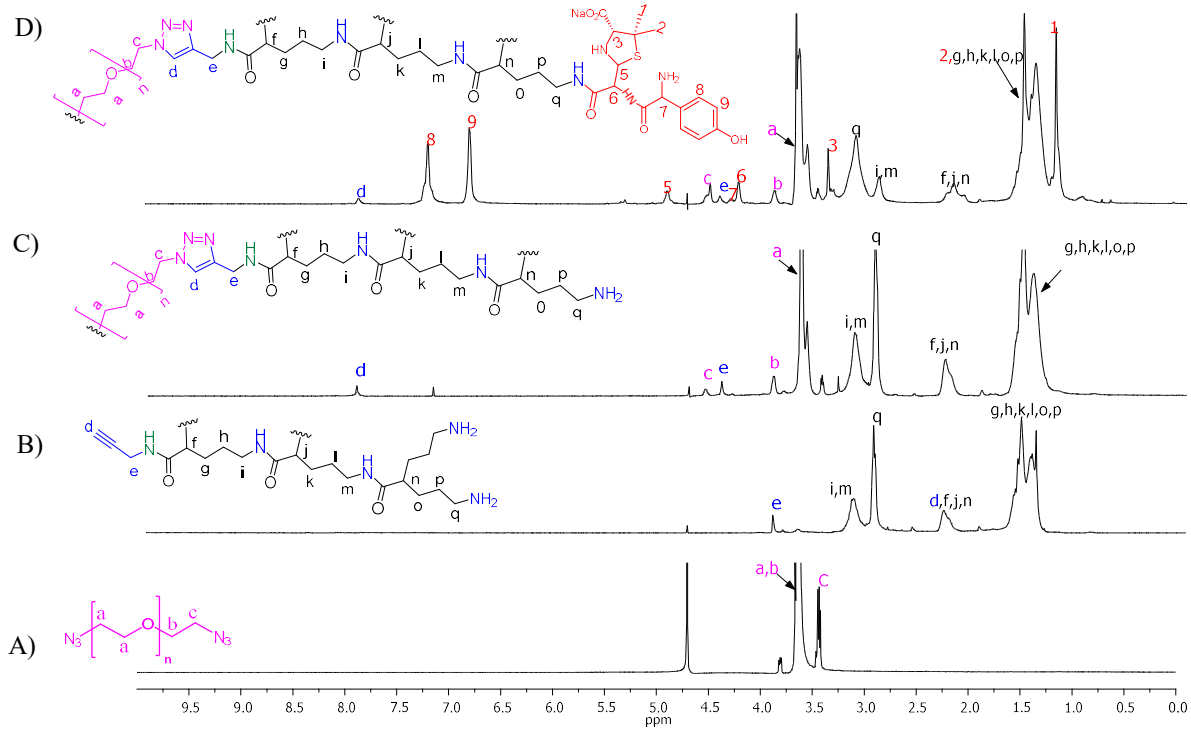

Figure 5.6. Representative ^{1}H NMR spectra in D_2O for monitoring the reactions to obtain the BiAn-dG3 by following the sequential appearance, disappearance, and chemical shifts in the peaks.

5.2.3. Elimination of Cu from Cu-Coordinating Nanostructures

The CuAAC is a versatile, selective, and highly efficient technique of growing interest in various fields such as medicinal chemistry, organic chemistry, catalysis and polymer science, amongst others, for the synthesis and ligation of molecules [247,248]. Thus, it has become a technique of preference in conjugation and functionalization of complex macromolecule in a facile way, affording high-yield product under mild conditions with few or no by-products [249,250]. However, one drawback of CuAAC is the high toxicity of Cu traces that induces changes in cellular metabolism [251]. Therefore, we investigated how to eliminate adequately traces of Cu from the product. The coordination of Cu with both nitrogens (the primary and tertiary amino) of PAMAM [252], and polytriazole containing molecules [251,253,254] have been reported.

There are numerous methods used for the removal of Cu from reactions including NH_4Cl/NH_4OH washes, EDTA washes, KCN washes, dialysis or the use of chelated sources of Cu such as tris (3-hydroxypropyltrizolylmethyl) amine (THPTA) and tris

(benzyltriazoylmethyl) amine (TBTA) [253]. However, the complete elimination of Cu from polar macromolecules comprising N-donor motifs such as in PAMAM, chitosan and 2-ureido-4H- pyrimidone units, is hampered by stronger coordination of the Cu with N-motifs [251,254].

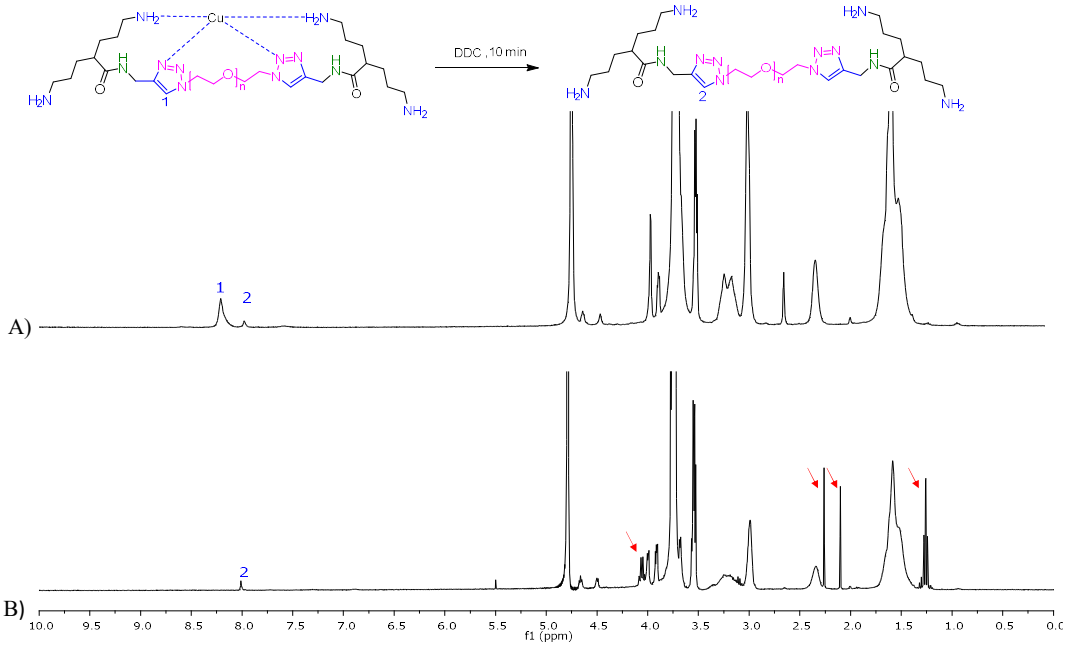

Figure 5.7. ^{1}H NMR spectra in D_2O of the bidendron-dGn: (A) purified by only size exclusion chromatography, showing Cu-coordinated and free triazole rings ; (B) after treating the sample with DDC for 10 min and Cu removal by filtration. The red arrows (B) indicate impurities incorporated after treatment with DDC.

The elimination was qualitatively monitored observing the broadening peaks and shift of the resonance signals of the triazole proton from 7.96−8.28 ppm (Figure 5.7 A and Figure 5.7 A-B). The presence of Cu (I) or its paramagnetic Cu (II) produces a change in the NMR spectra by broadening the signal or chemical shift dispersions [248,254]. In the current study, two approaches are shown to be enormously effective for the elimination of the N-motif coordinated Cu. First, is the use of sodium diethyldithiocarbamate (DDC) to precipitate sequestered Cu from a water solution of the macromolecule (Figure 5.7). This technique is rapid and has been reported with an efficiency of removing more than 99.9 % of Cu from Cu-binding polymers to a level below the detection limit [251]. This strategy, however, involves a filtering step to remove the DDC-Cu precipitate additional purification steps like dialysis via ultrafiltration to remove any excess DDC. Figure 5.7 B illustrates (red arrows) that even after

a couple of ultrafiltration, the excess DDC was not eliminated requiring further filtration steps. Second, the use of triamine functionalized silica-based metal scavenger, QuadraSil TA. As it can be seen from the NMR spectra the disappearance of the broad peak at 8.28 ppm (Figure 5.8 A) and the increase of the peak at around 7.96 ppm (Figure 5.8 C) indicate the removal of the N-motif coordinated Cu within 30 min under agitation. Finally, this strategy was adopted for the removal of Cu from all the reactions involving the use of Cu as catalyst due to the simplicity of purification step, since a simple filtration removes the metal scavenger and associated Cu.

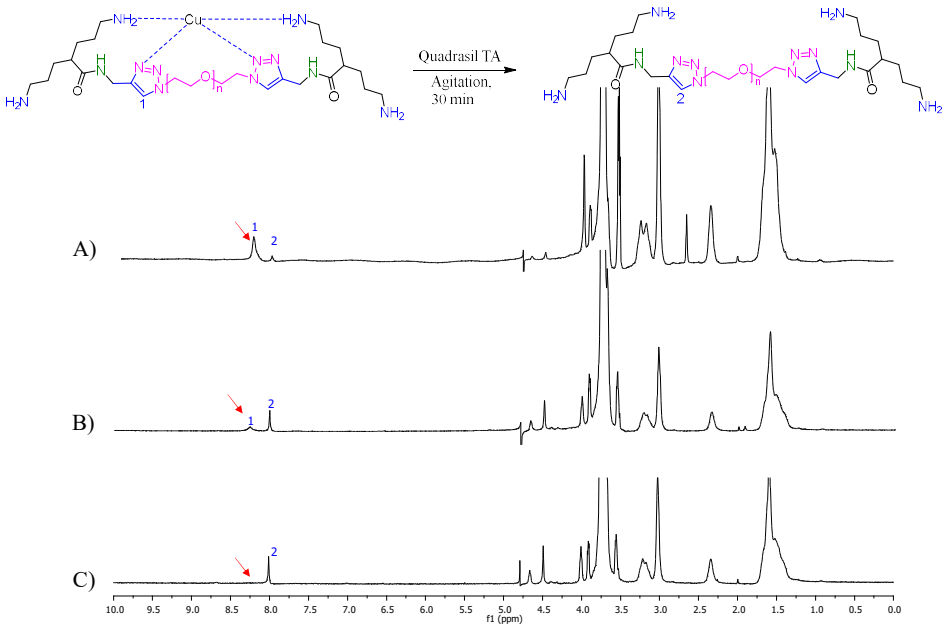

Figure 5.8. ^{1}H NMR spectra in D_2O of the bidendron-dGn: (A) purified by only size exclusion chromatography, showing Cu-coordinated and free triazole rings ; (B) after treating the sample with QuadraSil TA 10 min and Cu removal by filtration; (C) after treating the sample with QuadraSil TA for 30 min and Cu removal by filtration, indicating a free triazole ring.

5.2.4. IgE Recognition of BiAns-dGn

Competitive RAST inhibition immunoassays using sera from patients allergic to AX (with high RAST levels, >7 % of RAST using PLL-AXO) was performed to study the *in vitro* recognition of the different structures towards AX-sIgE antibodies. For this, PLL-AXO cellulose discs (as solid phase) and the different inhibitors (BiAn-dG0, BiAn- dG1, BiAn- dG2, BiAn- dG3 and AXO-Bu) in the fluid phase were used in the experiments. Figure 5.9 shows the inhibition

curves of all the BiAn-dGn as a function of the concentration of AXO moieties for comparison of the BiAn-dGn–AX-sIgE recognition pattern.

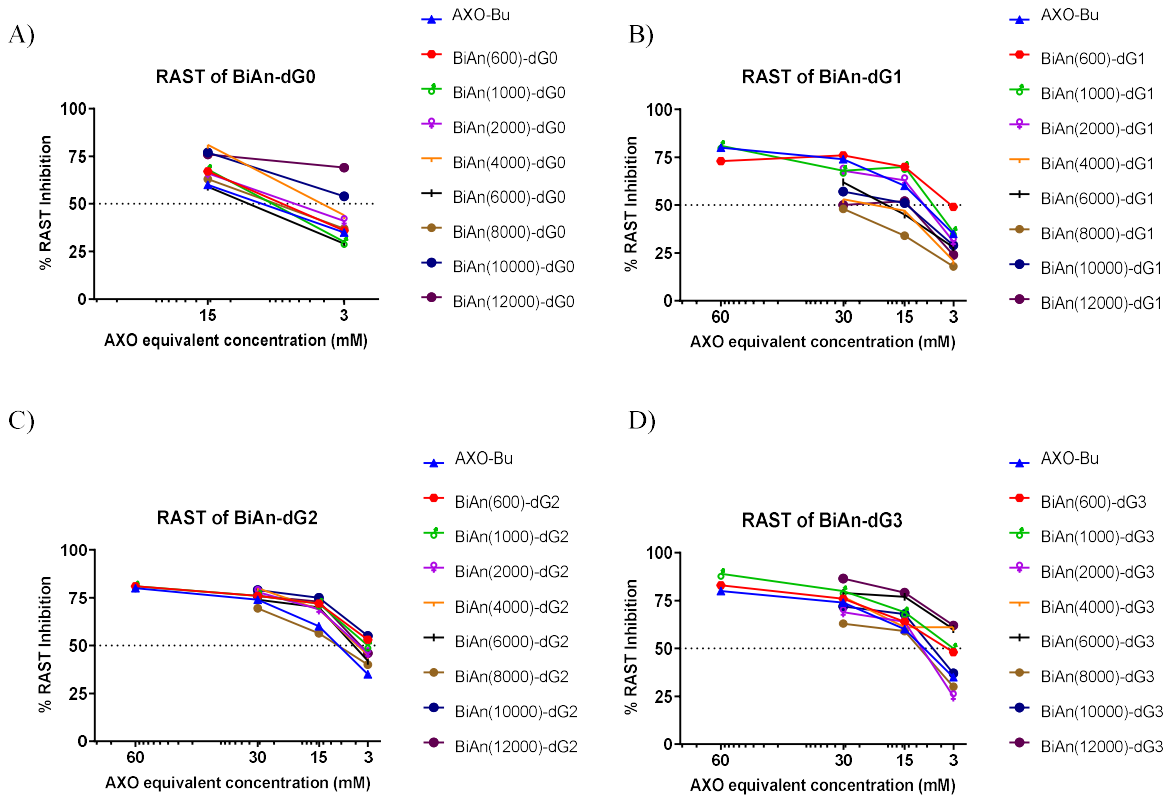

Figure 5.9. RAST inhibition assays performed with a pool of sera from patients allergic to AX, using BiAn-dG0 (A), BiAn- dG1(B), BiAn- dG2(C), BiAn- dG3 (D) constructed based on different polymeric length spacers and AXO-Bu as inhibitors. The PLL-AXO modified cellulose discs were used as Solid-phase. Specific IgE recognition is considered with an inhibition of ≥50 %.

More concentrated solutions of inhibitors were only possible for these compounds with lower MW due to solubility issues with those of higher MW at higher concentrations. As seen, in general, all structures at the higher concentration tested (30 mM or 15 mM) have shown a percentage of inhibition greater than 50 %, signifying that they are recognized by sIgE from patients allergic to AX. Overall, inhibition dropped at a lower concentration of AXO (3 mM) for all the inhibitors. The presented data supports that all compounds are recognized by AX-sIgE in a concentration-dependent manner, with no differences among the different BiAn-dGn if they present the same number of AXO equivalents.

5.2.5. Effects of BiAns-dGn on IgE Activation of Bone Marrow-derived MCs

The ability of different polymeric-spaced BiAn-dGn with various multivalence to stimulate MCs degranulation were assessed using sensitized bone marrow-derived MCs and then treated with different concentrations (10, 50 and 100 μM of AXO moieties) of BiAn-dGn (Figure 5.10). Due to technical issues, structures based on BiAn-dG2 could not be appropriately evaluated and experiments will be further performed. In allergic responses resulting in the release of inflammatory mediators, IgE targeting a nearly vast variety of antigens may be implicated. To simplify experiments, IgE MoAb against AX was used to sensitize the MCs, and multivalent antigens (≥ 2 AXO units) were used to stimulate degranulation of the effector cells. Then, the granule marker, β-hexosaminidase, was measured as a result of the exocytotic degranulation of MCs**.** Under sensitized cell conditions in which multivalent HSA-AXO, at 10 μM of AXO moieties, stimulated a maximal response of approximately 28 % granular release, none of the BiAn-dGn structures containing the shorter spacers and the PEG blank structures did induce degranulation. However, the BiAn-dGn structures containing the longest spacers were able to activate cellular degranulation. Astonishingly, regardless of the difference in the number of antigenic determinants, all tested nanostructures based on the longest polymeric spacer induced cell degranulation: BiAn-dG0 (with 2 AXO units) containing PEG MW ≥ 10000 Da, as well as both BiAn-dG1(with 4 AXO units) and BiAn-dG3 (with 16 AXO units) based on PEG MW ≥ 8000 Da. None of the blank PEG structures and BiAn-dGn treatment on unsensitized MCs resulted in degranulation different from the negative control. This absence of degranulation in unsensitized cells excludes the non-IgE dependent activation.

This indicates that the simpler structures, which is bivalent, are able to bind two IgE on cell FcεRI receptors resulting in MCs degranulation. The findings show that structures bearing at least two AXO moieties minimally distanced ∼18 nm are resulting in MCs degranulation (Figure 5.10 D). Two factors can contribute to shorter BiAn-dGn (n=1,3) structures-based on PEG MW 8000 Da to activate: (i) the contribution of the dendron dimensions to the overall size; (ii) the exhibition of more AXO units.

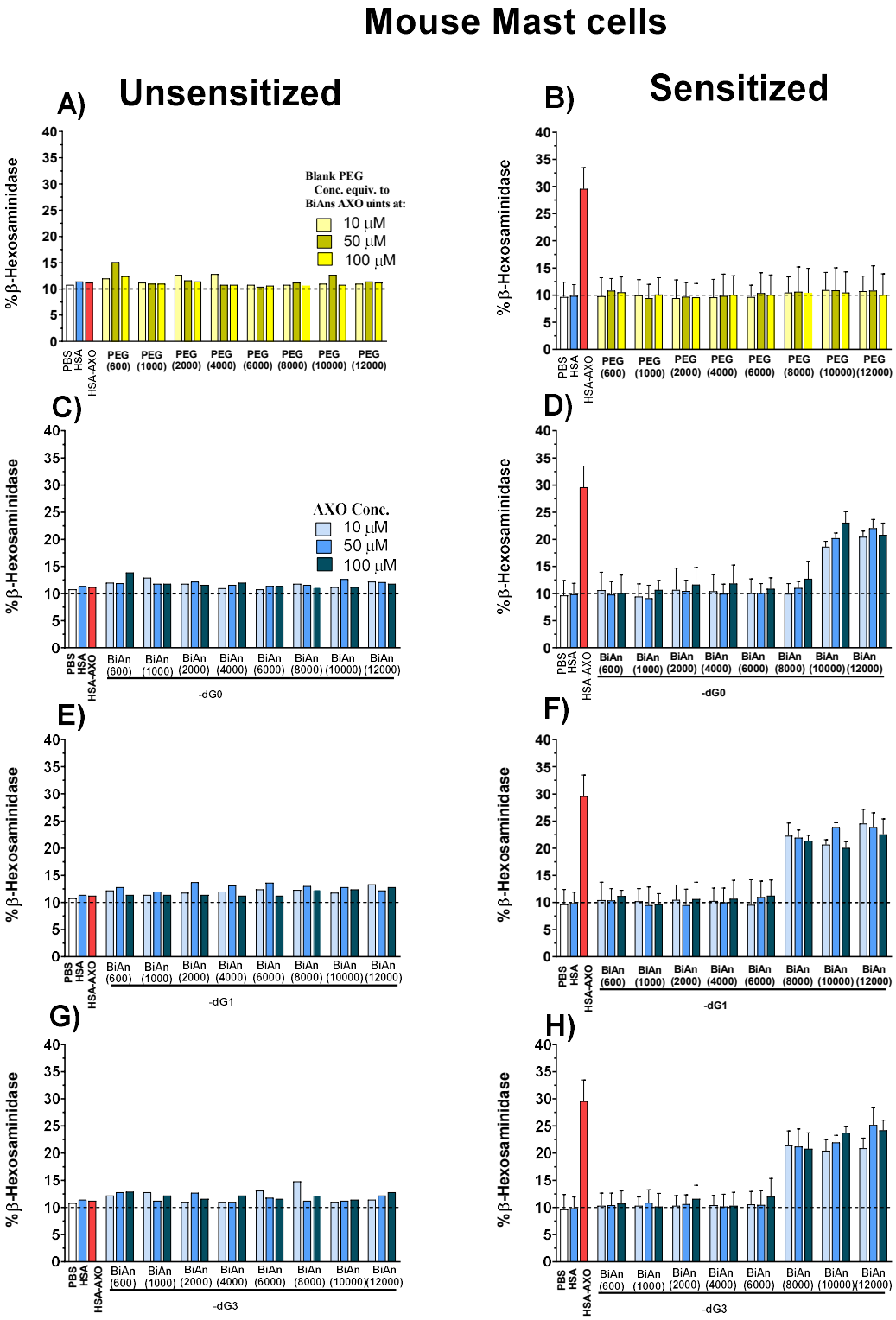

Figure 5.10. Degranulation assays after incubation of cells with the series of BiAn-dGn at 10, 50, and 100 μM of AXO equivalents. HSA and HSA-AXO (at 10 μM of AXO) were used as a negative and positive control, respectively. A) Percentage of β-hexosaminidase release in

unsensitized MCs treated with blank PEG structures, using equal concentrations to BiAn-dGn with 10, 50 and 100 μM of AXO; B) Percentage of β-hexosaminidase release in sensitized MCs treated with blank PEG structures; C) Percentage of β-hexosaminidase released by unsensitized cells treated with BiAn-dG0; D) Percentage of β-hexosaminidase released by sensitized cells treated with BiAn-dG0; E) Percentage of β-hexosaminidase released by unsensitized cells treated with BiAn-dG1; F) Percentage of β-hexosaminidase released by sensitized cells treated with BiAn-dG1;G) Percentage of β-hexosaminidase released by unsensitized cells treated with BiAn-dG3; H) Percentage of β-hexosaminidase released by sensitized cells with BiAn-dG3.. Data are expressed as means ± S.D. The baseline of the percentage of β-hexosaminidase release is represented by the dotted horizontal line.

5.3. Discussion

Herein we described the CuAAC reaction as a preferred conjugation strategy compared to the thiol-maleimide conjugation chemistry described in chapter 4. The preferences could be explained for the ease and lesser steps (two steps) for the conjugation between the PEG-$(N_3)_2$ and dendrons. Comparing the alkyne-azide vs thiol-maleimide approach, the first uses directly PEG-$(N_3)_2$ for dendron conjugation, whereas the thiol-maleimide strategy involves several steps. First, the reduction of PEG-$(N_3)_2$ to PEG-$(NH_2)_2$ using either palladium-catalyzed hydrogenation or Staudinger reaction. The formal is associated with longer time to the completion in the reaction involving higher MW (greater than MW 6000) and the latter associated with the incomplete reactions, even after repeatedly refreshing with excess PPh_3 reagent, and associated decrease in the yield of the reaction. The following conversion of the amino groups into maleimide through an anhydride coupling reaction is a step that necessitates chromatography purification (silica gel or gel permeation chromatography using Bio-Beads™ S-X1), which is time-consuming and resulted in a lowered yield of the products. However, the synthetic approach described in this chapter overcome these drawbacks. The CuAAC method allows the efficient coupling of PEG-$(N_3)_2$ with alkyne terminated dendrons that can readily be purified by trapping the Cu by a metal scavenger, filtration, and size-exclusion chromatography.

In the previous two chapters we have addressed the role of either the variation in valency or polymeric-spacer size for allergenic structures in MCs degranulation; however, the simultaneous variations of both parameters have not been evaluated. In this section, we designed a well-defined model nanostructure to investigate these two parameters in allergic reactions to AX. As such, the design would better reflect the complexity of IgE-hapten interactions observed in natural allergy systems. Having precise control over the valency and size of the model scaffold enabled us to establish the minimal structural requirement in the degranulation of effector cells, without other confounding factors.

The *in vitro* recognition of the BiAn-dGn towards AX-sIgE antibodies, assessed through competitive immunoassays using real samples of allergic patients indicated that all structures are recognized in a AXO-concentration dependent manner, a pattern already reported with the monomeric AXO-conjugate [55]. This is in agreement with results described for DeAns and

BiAns, in chapters 3 and 4, for which the higher concentration of AXO increased the extent of inhibition.

The effect of BiAn-dGn on sensitized effector cells indicated that the structures with enough length are able to induce activation. Our results demonstrated HSA-AXO to be potent stimulators of degranulation triggering a slightly stronger response than BiAn-dGn of sufficient size. This might be related to the globular presentation of the hapten that may increase the affinity between the haptens and the IgEs, where both correlate with an increase in the cellular responses. However, the use of this type of protein conjugate is associated with significant heterogeneity in both the number of haptens per protein and the sites of hapten conjugation, which may complicate the interpretation of the test results [223]. It is well-known that the structure of an antigen is vital for its activity particularly when designing multivalent ligands to bind to cell surface receptors. In an endeavour to elucidate the properties of allergens, a few reports used molecularly uniform synthetic allergens and were able to identify the minimum number of haptens needed to stimulate a cellular response [17]. In this regard, trivalent antigens are reported to form larger, highly branched aggregates leading to strong responses by IgE-FcεRI presenting cells unlike the bivalent ligands that unable to activate strong cellular responses [255]. Contrary to this observation, our finding suggests that structures bearing bivalent antigenic determinants (BiAn-dG0) activate the MCs degranulation starting with a structure based on the polymeric spacer of 10000 Da and above (Figure 5.10D). This is not in agreement with previously reported DNP bivalent structures based on PEG MW 10000 Da that fails to stimulate degranulation [60]. This spacer (MW 10000 Da) offers a solution length of ~18 nm and an extended length of 80 nm, providing this maximum separation between haptens.

The capacity of nanostructures based on PEG 10000 Da to stimulate degranulation regardless of the difference in the valency indicates that sufficient hapten binding and intermolecular crosslinking can occur when the required size is attained. Although there is a clear difference between the structures based on the valency, we consistently observe almost similar levels of activation (approximately above 20 % β-hexosaminidase release) for BiAn-dG0, BiAn-dG1 and BiAn-dG3 based on spacer of PEG MW ≥ 10000 Da. While these observations may seem surprising, they were not completely unexpected and determine the presence of two antigenic determinants, on the structures that fulfil the size requirement, as a minimal precondition to crosslink two IgEs on FcεRI of effector cells. Of note, the smaller BiAn-dG1 and BiAn-dG3 structures able to activate the cells contain a PEG spacer of MW 8000 (solution length of the

spacer ≥ 15 nm), suggesting that this length crosslinked the neighbouring IgE molecules on MCs rather than the two Fab arms on a single IgE (11–13 nm) [257].

When analyzing equivalent structures in terms of PEG MW and number of AXO groups for structures synthesized in chapter 4 versus those synthesized in chapter 5, we found that behaviors are similar while the synthetic step is optimized. Unlike the BiAns displaying 16 AXO (chapter 4) [256], for which the MCs activation took place with spacers based on PEG MW ≥ 6000 Da, in the cases of BiAn-dG3 with the same number of antigenic determinants (16 AXO units) (chapter 5) the cellular activation occurred with a structure based on PEG MW ≥ 8000 Da. This means that slightly longer PEG chains are needed to link two polyamide dendron units, via click chemistry, than to link two PAMAM dendrons, via maleimide-thiol reaction, to give rise to structures with dimensions capable of activating the cells. This might be related to the different chemical structures and monomer in which dendrimer synthesis was based on, a more compact polyamide based-dendron compared to PAMAM dendron, conferring the corresponding sizes to the arms of the dendrons and their contribution to the overall size of the antigenic structures in the aqueous environment. The BiAn-dG1 and BiAn-dG3 structures able to activate the cells contain a spacer of PEG MW 8000. The greater degranulation obtained with BiAn(10000) in chapter 4 involved 18% of β-hexosaminidase release whereas slightly higher values were obtained with structures synthesized in chapter 5: 23% of β-hexosaminidase release with BiAn(10000)-dG0 and ~25% of β-hexosaminidase with BiAn(12000)-dG1 and BiAn(12000)-dG3.

5.4. Conclusions

This chapter describes the development of well-defined structures with simultaneous variation both in the number of antigenic determinants and the polymeric length spacing between the hapten by bringing an integrative approach to study MCs degranulation in the allergic reaction of clinical importance. In summary, crosslinking of FcεRI on the cell membrane of effector cells requires structures that possess minimally two antigenic determinates fulfilling the requirement of distance between them.

Chapter 6: Conclusions and Future Perspectives

6.1. Conclusions

1. PAMAM dendrimers functionalized in their periphery with AXO, are recognized by sIgE in a concentration-dependent manner, as synthetic antigenic conjugates, mimicking conjugates formed *in vivo* with natural proteins. Therefore, the use of dendrimers of different generations (from G1 to G5, displaying from 8 to 128 peripheral AXO, along with linearly increasing size) allows the preparation of synthetic DeAns with well-defined structures from the chemical point of view.
2. Only the DeAns based on the third generation (G3, with 32 AXO) and above can induce degranulation of effector cells. These results were consistent in different effector cells (bone marrow derived-MCSs, RBL-2H3 and LUVA cells) sensitized with sIgE (mouse monoclonal or polyclonal from allergic patients), indicating that the bigger size and increasing valence favored the cell activation.
3. A series of symmetrical BiAns, based on two moieties of PAMAM dendrons of second generation (G2) functionalized with 8 AXO (per dendron) and linked to each other with PEG spacers of different lengths (PEG 600 – PEG 12000) can be successfully obtained as well-defined structures from the chemical point of view, by performing a series of synthetic reactions including thiol-maleimide ´click´ for binding dendrons to PEG. These structures are recognized by AX-sIgE in a concentration-dependent manner, with no differences in the degree of IgE recognition among the different BiAns.
4. From the SAR study of BiAns, in their evaluation using different effector cells (bone marrow derived-MCs and RBL-2H3) sensitized with sIgE (mouse monoclonal or polyclonal from allergic patients), it can be deduced that only BiAns based on PEG MW ≥ 6000 stimulate the cellular degranulation thorough an IgE-dependent mechanisms. The optimal structure being the BiAn based on PEG MW ≥ 10000, which reflects the influence of the drug-conjugate size in the IgE crosslinking process. In fact, the DeAn, based on the scaffold of second generation (G2) PAMAM dendrimer, do not activate effector cells, but can be converted to activator through incorporating only polymeric spacers of appropriate size, which highlights the importance of the distance between antigenic determinants.
5. Greater proportion of immunocomplexes and number of antibodies per complex are involved for those BiAn structures that best induce cellular responses, compared to

the other counterpart studied (BiAn (10000) > BiAn (6000) > BiAn (600), as visualized by TEM).

6. A library of symmetrical BiAns functionalized with AXO, BiAn-dGn, varying both parameters: the dendron generation (Gn 0-3, displaying 1, 2, 4 and 8 groups of AXO per dendron) and spacer length (PEG MW 600-12000), can be efficiently achieved through a simple protocol involving CuAAC "click" chemistry for binding bis-azide-PEG with customized polyamide dendrons. These BiAn-dGn structures are recognized by AX-sIgE in an AXO concentration-dependent manner.
7. From the SAR study of BiAn-dGn, in their evaluation with bone marrow derived-MCs sensitized with mouse monoclonal IgE against AX, it can be deduced that BiAn-dGn (n=1,3) only based on PEG MW ≥ 8000 stimulate the cellular degranulation, whereas for BiAn-dG0 a longer spacer, based on PEG MW ≥ 10000, is needed for the cellular activation.

As final remarks, the following general statements are coined:

- The immunological evaluation of different synthetic antigens, based on dendrimeric structures, with well-defined structures have established the minimal structural requirements for which both the IgE recognition and the stimulation of the effector cells occur in the context of AX allergy.
- The sIgE recognition to determinants of AX can take place in all structures displaying at least one AXO moiety that is available to the antibody. This IgE-binding process occurs whatever the size of the antigen structure, although greater proportion of immunocomplexes and number of antibodies per complex are involved for bigger structures that best induce cellular responses.
- Activation of cellular response to AX can happen with an antigen structure bearing at least two AXO moieties (antigenic determinants) separated by the optimal minimal distance between them, which highlights the importance of the antigen size.

6.2. Future Perspectives

The current study has signified the importance of size and the number of antigenic determinants to overcome the complex cellular requirements in the process of effector cell degranulation. It has creatively reflected on new approaches of constructing nanostructures of different size and multivalency involving a hapten in routine clinical practice, with a precise control over the final structures. Consequently, it was possible to establish optimal structures that activate or not the effector cell degranulation in different cellular assays. However, due to the limitations of time, some important studies which would have contributed significantly to our understanding in this area have not been performed. Based on the findings of the present work, further studies on the following future directions are recommended:

- The structures that did not activate the cellular degradation should be studied for inhibition assay.
- Identify potential inhibitor and evaluate the therapeutic potential of selective inhibitor in animal model.
- Identified structures without restriction to activation should be evaluated for improving the sensitivity of cellular diagnostic tests.

Chapter 7: Experimental

7.1. Materials

All chemicals, reagents, and solvents were purchased from Sigma-Aldrich (St. Louis, USA), VWR (Leuven, Belgium), PanReac (Darmstadt, Germany), or Merck (Darmstadt, Germany),Water ™ (Milford, USA), Polymer Standards Service (Mainz, Germany) and used without further purification unless otherwise stated. D_2O (99.96 % D) and $CDCl_3$ (99.80 % D) were used to obtain the NMR spectra. Water was purified with a Milli-Q purification system from Millipore. Prepacked column of Sephadex G-10 (PD MidiTrap G-10), Sephadex G-25 (PD MidiTrap G-25) and Sephadex® G-10 from GE-Healthcare (Buckinghamshire, UK), and Bio-beadsTM S-X1(200-400 mesh) from Bio-Rad (Hercules, USA) were packed in columns and used for the purification of the nanostructures by size exclusion chromatography. Column chromatography was also performed on silica gel 60 from Merck (0.040-0.063mm). Thin-layer chromatography (TLC) analysis was carried out on pre-coated TLC sheets (0.20mm) from Macherey-Nagel (Duren, Germany), visualized with staining ($KMnO_4$, Ninhydrin and Ellman's reagent) and UV light. Amicon ultra-4 3K centrifugal filter from Merck Millipore (Billerica, USA), NAb Protein A/G Spin Kit, and Pierce™ Coomassie Plus (Bradford) Assay Kit from Thermo Fisher Scientific (Rockford, USA) were used to concentrate, purify, and measure the total protein concentration, respectively.

7.2. Instrumentation and Characterization Methods

7.2.1. Monodimensional NMR

^1H NMR and ^{13}C NMR spectra were recorded in D_2O and $CDCl_3$ on a Bruker Ascend^{TM} 400 MHz spectrometer (Rheinstetten, Germany) equipped with a 5 mm BBFO^{PLUS} probe with ^2H "lock" channel and z gradient. All chemical shifts (δ) are reported in parts per million (ppm) using deuterated solvent resonance as an internal standard. The spectra were analysed using Mestre Nova version 12.0.3-1284 from Mestrelab Research (Santiago de Compostela, Spain).

7.2.2. NMR Diffusion Experiments

DOSY experiments were performed on samples of 1mM concentration (within reported infinite dilution ranges of related samples at 0.1−2.1 mM) in D_2O. The spectra were recorded on a Bruker Ascend 400^{TM} MHZ spectrometer equipped with a temperature control unit ranging from -50 to 50 ºC. The temperature was calibrated to 300 K using CD_3OD. The gradient strength was set by measuring the diffusion rate of the residual HDO in D_2O. For all

experiments, ^{1}H NMR was recorded before the DOSY experiments. A total of 16 scans with 10 s relaxation delay were recorded by setting the gradient pulse duration to 3 ms and diffusion delay to 100 ms. The spectra were processed in the Mestre Nova DOSY package by baseline correction, phase correction, spectral alignment and diffusion of the nanostructures were obtained by fitting the signal decay into the Stejskal-Tanner equation [214].

7.2.3. GPC

The estimation of the change in the MW and distribution of the DeAns were made by GPC using JASCO LC-Net II/ADC equipped with UV, RI detector and high-resolution Styragel HR columns (5 µm, 7.8 mm X 300 mm) with MW resolving a range of 50–100,000 Da. The measurements were made using DMF with 10 mM LiCl (1mL/min). Analytes were dissolved in DMF/LiCl solvent (1mg /mL), and the resulting solutions were filtered with 0.2 µm polyamide filter before analysis. PEG Standards Kit (with MW range from 100-100,000 Da) were used to calibrate the columns. The unconjugated commercial PAMAM dendrimers were used to estimate the change in mass after conjugation with AX.

7.2.4. DLS

The DLS experiments were performed by dissolving the BiAns and PEG standards in Milli-Q H_2O at concentration 1mg/ml and sonicated for 5 min before measurement. The hydrodynamic radius of conjugates was measured at conjugate concentration of 0.5 mg/ml. Measurements were performed in triplicate and the correlation between the MW of the compounds and hydrodynamic diameters were estimated from the calibration curve. Addition of an organic salts (NaCl, Na_2HPO_4) did not change results of hydrodynamic radius.

7.2.5. Sample Preparation for TEM and Micrograph Acquisition

The samples were prepared according to OpNS [258]. Briefly, 15 µg/mL of MoAb (AO3.2) at different molar ratios were incubated with BiAns for 90 min at room temperature. Aliquots (5 µL) of the samples adhered on carbon-film copper grids, which made hydrophilic by glow-discharge for 15 s, at 1 mbar. After incubating for 15 min at 4 ºC, grids were dried on a filter paper to remove an excess sample and washed with 30 µL of Milli-Q water for a few seconds. The excess water was dried, and samples were exposed to 15 µL of 1% (w/v) uranyl formate for 20-30 s protected from light at 4 ºC. Finally, the excess uranyl formate solution was removed with filter paper and left to dry at room temperature. The acquisitions of the images

were performed using Talos F200X 200 kV D6368 XTwin electron microscope operating at 80 KV. Magnification was set at 450000X to obtain the data with STEM nP SA zoom diffraction mode. From the different tested MoAb to BiAn ratios, a molar ratio of 8:1 was found to be the optimal condition. Consequently, this ratio was used to incubate MoAbs with BiAn (600), BiAn (6000) and BiAn (10000) to evaluate differences in the obtained complexes as a function of the employed nanoarchitecture. Images were processed using Image J software, determining the negatively stained area of each complex (a minimum of 230 particles were measured per condition). Then, the number of MoAbs per complex was estimated by comparing the obtained area for each complex with the average area occupied by individual MoAbs not incubated with the nanostructures (57 ± 12.7 nm^2).

7.3. Preparation of Protein/Polymer-Antibiotic Conjugates

7.3.1. PLL-AXO Conjugate

The PLL-AXO conjugate was prepared as described [67]. Briefly, molar excess of AX at 200 mg/mL dissolved in carbonate buffer (0.05 M, pH 10.2) and PLL at 50 mg/mL dissolved in PBS (1x, pH 7.4) were mixed and incubated at 37 ^oC for 48 h. The product was lyophilized and dissolved in 12 mL of distilled water and purified with a 3 K Amicon filter. Once the excess AX was meaningfully removed through ultrafiltration, the final touch of purification was performed by size exclusion chromatography using Sephadex G-10. The product was characterized by MALDI-TOF MS (Figure S1).

7.3.2. HSA-AXO Conjugate

HSA-AXO conjugate was prepared as previously described [55] by dissolving HSA (20 mg/mL) in PBS (1x, pH 7.4) and mixing with AX (200 mg/mL) in carbonate buffer (0.05M, pH 10.2). The resulting mixture was incubated at 37^oC for 48 h and purified by size exclusion chromatography using Sephadex G-10. The HSA control sample was also prepared in the same conditions without AX. The product was characterized by MALDI-TOF MS.

7.4. Production and Purification of anti-AXO MoAbs

Two different hybridomae: AO3.2, IgG_{2a} isotype, and AO6.2, IgE isotype, were produced according to the previously reported method [216]. After concentrating the hybridomae supernatants with Amicon ultra-4 3 K centrifugal filter, the purification of the anti-AXO MoAbs (AO6.2), an IgE isotype, was performed by affinity chromatography using cyanogen

bromide-activated sepharose [216,259]. and can be summarized into consecutive steps shown in Figure 7.1.

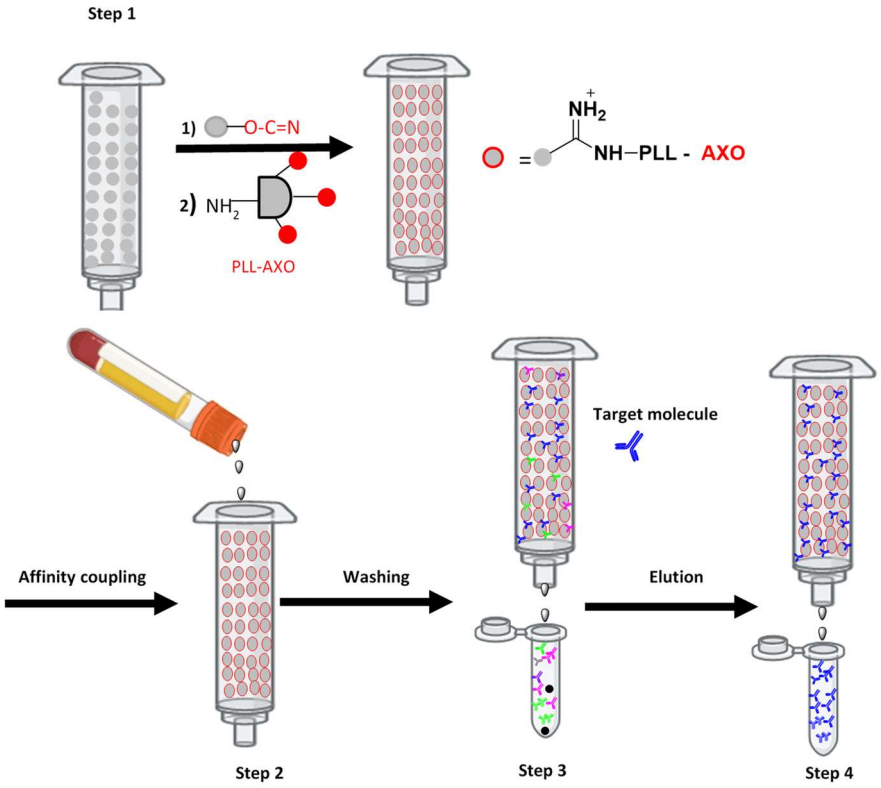

Figure 7.1. Schematic representation of the general steps for the affinity purification of IgE.

Briefly, sepharose was activated by 1 mM HCl at 4 ºC for 30 min and packed into a column. The column was conditioned with 5mL of borate-saline buffer (pH 8.3). The PLL-AXO conjugate in 5 mL of borate-saline buffer (pH 8.3) was added to the column and incubated for 2 h at room temperature under agitation. The excess and uncoupled PLL-AXO was eliminated by adding 25 mL of borate-saline buffer (pH 8.3). The unreacted group was blocked with 5mL of 50 mM bicarbonate-ethanolamine buffer. The blocking solution was removed with an extensive wash, first with borate-saline buffer (pH 8.3), then with acetate buffer (0.1 M, pH 4) containing 0.5 M NaCl. These wash cycles of high and low pH buffer solutions were repeated five times. Then, the column was washed with PBS (25 mL) and 25 mL of Tris buffer (0.1 M)-HCl (2 M).

The hybridoma supernatant was filtered with a 0.2 µm filter. The filtered supernatant (60mL) was mixed with 4 mL Tris buffer (1.5M, pH 8.8), 40mL Tris buffer (0.1 M)-HCl (2 M) pH 8.6,

and 7.012 g of NaCl. The resulting mixture was passed through the column. The first 2 mL of the eluent was discarded as it might contain Tris buffer. The other portions of the collected fractions were re-eluted through the column. Another 25 mL of Tris buffer (0.1 M)-HCl (2 M) was passed through the column to remove the traces of the supernatant and excess antibody remained unattached. Finally, 10 mL of diethylamine (50 mM) was added to collect an eluent of 1 mL volume in a vial containing 300 µL of Tris buffer (1 M, pH 6.8). The fractions containing the antibody were collected after measuring the absorbance at 280 nm and dialysed against PBS at 4 ºC for 72 h (changing PBS every 24 h) to eliminate the diethylamine. Likewise, the purification of AO3.2 was performed through affinity chromatography using Protein A/G agarose following the manufacturer guideline for NAb Protein A/G Spin Kit.

7.5. Immunoassays

7.5.1. RAST Assay

Radioimmunoassays were performed by RAST as previously described [260] using PLL cellulose solid phases conjugated to AX. Briefly, PLL was conjugated to cyanogen bromide-activated cellulose discs and then AX was conjugated to the PLL coupled to the cellulose discs, yielding PLL-AXO cellulose discs. RAST to AX was performed in duplicate by incubating 30 µL of patient serum with PLL-AXO cellulose discs for 3 h. After three washes, radiolabeled anti-IgE antibody (kindly provided by Thermo Fisher Scientific and radiolabeled in our laboratory following previously described methods) [79] was added and allowed to incubate overnight before washing to remove non-specifically bound anti-IgE. Radioactivity was measured using a multi-gamma counter as counts per minute (cpm). Results were calculated as a percentage (% RAST) obtained from the mean of duplicate values for each condition divided by the mean of the maximum cpm and considered positive if they were higher than 2.5 % of label uptake, which was the mean ± 2 SD of the negative control group.

$$\%\ \text{RAST} = \frac{\text{cpm PLL\_AXO} - \text{cpmPLL}}{\text{cpm maximum}}\ \text{x}\ 100$$

7.5.2. RAST Inhibition Assay

To evaluate the recognition of the different synthetic structures by AX-sIgE, competitive inhibition immunoassays were carried out with a pool of the 14 selected sera. The assay consists in the competition of IgE recognition between a solid phase (PLL-AXO) and the

inhibitors AXO-Bu and nanostructures) in a fluid phase. RAST inhibition was undertaken in the fluid phase using the sera from the patients incubated with different concentrations of the nanostructures (in terms of AXO equivalents) given in Table 6.1. For BiAns the higher concentrations were not assayed due to solubility issues. The monomeric conjugate AXO-Bu was included for comparison as its inhibition pattern at different concentrations has been previously reported (higher concentration of this conjugate increased inhibition without inducing nonspecific binding [55]. After 18 h of incubation at room temperature, PLL-AXO-functionalized solid-phase discs were added, followed by the previous procedure described for IgE determination. Results were calculated as the percentage of inhibition using the non-inhibited serum as a control. Specific IgE recognition was considered positive when % of inhibition was greater than 50 %.

Table 6.1. The concentration of the nanostructures (in terms of AXO equivalents) for RAST inhibition assay.

Name of the Nanostructures	Concentration in terms of AXO equivalents (mM)
DeAns	60,30,6
BiAns	30,15,30,0.3
BiAn-dGn (n=0,1,2,3)	60,30,15,3

$$\%\text{Inhibition} = \frac{(\%\ \text{RAST non} - \text{inhibited} - \%\ \text{RAST inhibited})}{\%\ \text{RAST non} - \text{inhibited}}\ \text{x}\ 100$$

7.6. Cell Assays

Cell assays were performed by other researchers collaborating in this study: Dr. Sara Benedé from CIAL, CSIC-UAM, performed experiments with bone marrow derived MCs, and Dr. Alba Rodriguez-Nogales from Universidad de Granada, performed cell viability and RBL-2H3 and LUVA cells studies.

7.6.1. Cell Viability Assay

The effects different nanostructures on cell viability were assessed using a non-radioactive assay performed according to the manufacturer's instructions (CellTiter 96 RAQueous One

Solution Cell Proliferation Assay, Promega, Wisconsin, USA). HumRBL-2H3 and LUVA cells were seeded into 96-well plates ($2x10^5$ cells/well) and incubated for 24 h with different concentrations of DeAns, BiAns, (ranges from 1-200 μM, in terms of AXO equivalents). Cells incubated only with the medium were included as a control group. Later, MTS ([3-(4,5-dimethylthiazol-2-yl)-5-(3-carboxymethoxyphenyl)-2-(4-sulfophenyl)-2H-tetrazolium) was added to each well and incubated for 3 h. The absorbance was measured at 490 nm. Cellular viability was determined by comparing the absorbance values obtained for nanostructures with those from untreated control cells.

7.6.2. Optimization of the Activation Studies in Mouse MCs.

In collaboration with Dr. Sara Benedé, MCs have been generated from mouse bone marrow, which have been passively sensitized with anti-AX MoAbs with IgE isotype, to evaluate activation with AX or nanostructures. To optimize these experiments, MCs have been sensitized with different concentrations of anti-AX IgE antibody (0.01-100 μg / mL) and activated with AX (0.1-250 μg / mL). According to our results, the optimal concentration range for sensitization is 0.1-1 μg / mL of antibody. For activation, incubation with AX induced low β-hexosaminidase secretion. Subsequently, more experiments have been carried out using different incubation times with the anti-AX antibody and using the HSA-AXO-conjugate, instead of the free drug, to activate the cells, showing optimal results in the production of β-hexosaminidase. Finally, the selected conditions have been sensitization with anti-AX: 1 μg / mL (4 h); and activation with HSA-AXO: 50 μg / mL (1 h), which implies a concentration of 10 μM of AXO.

7.6.3. Bone Marrow-derived MCs Activation Assay

Bone marrow cells were collected from femurs of Balb/c mice (4-6 weeks of age) from Charles River Laboratories (Saint Germain sur l´Arbresle, Rhône, France) and cultured in DMEM with glucose and L-glutamine, fetal bovine serum, penicillin/streptomycin, and sodium pyruvate (all from Gibco, Life Technologies), plus recombinant murine SCF, IL-3, IL-9, and TGF-β (all cytokines and growth factors were from Peprotech, Rocky Hill, NJ) to differentiate into MCs as previously described [261]. MCs were cultured for a minimum of 4 weeks and up to 8 weeks before they were used for functional assays. For activation through cross-linking of the IgE receptor, MCs were initially sensitized for 4 h with 1 μg/mL of mouse anti-AX IgE MoAb. After washing, MCs were resuspended in Tyrode´s buffer and activated with the different

nanostructures: DeAns at 1, 5, 10, 50, and 100 μM; and BiAns and BiAn-dGn at 10, 50, and 100 μM (concentration of AXO units) for 1 h. A conjugate of HSA-AXO at 50 μg/mL (0.7μM of HSA-AXO, corresponding to 9.7 μM of AXO) was used as a positive control. β-hexosaminidase was detected by an enzymatic colorimetric assay as described previously [262]. The percentage of β-hexosaminidase release was calculated as a percentage of the total β-hexosaminidase content. All protocols involving animals followed the European legislation (Directive 2010/63/EU) and were approved by Comunidad de Madrid (Ref PROEX 089/15).

7.6.4. Humanized RBL-2H3 Cells Activation Assay

HumRBL-2H3 cells were seeded in 96 well plates at a density of $2x10^5$ cells/well. Confluent growing HumRBL-2H3 cells were then sensitized with serum (50 % v/v) from AX allergic patients (n=3 for BiAns and n=14 DeAns) and tolerant subjects (n=3 for BiAns and n=11 for DeAns) for 48 h at 37 ºC. Unsensitized cells were used as controls. Subsequently, cells were stimulated with the series of DeAns (10 μM, 20 μM, 50 μM, 100 μM) and BiAns at different concentrations of AXO units (1 - 200 μM) for 2 h. In parallel experiments, cells were stimulated with the corresponding PEG linkers and PAMAM (without functionalization), structures without conjugated AXO, as negative controls. The HSA-AXO conjugate (at 10 μM concentration of AXO) was used as a positive control of degranulation induction. The degranulation response of the HumRBL-2H3 cells was quantified by measuring the level of β-hexosaminidase released in culture supernatants.

7.6.5. HMC.1.2 Cell Activation Assays

The human mast cell line HMC-1.2 cell line was obtained from Cell Culture Unit of the University of Granada (Granada, Spain). HMC-1 cells were cultured in Dulbecco´s modified Eagle medium (Invitrogen, Grand Island, USA) supplemented with 10 % heat-inactivated fetal bovine serum, 100 μg/mL penicillin, and 100 U/mL streptomycin, in a humidified 5 % CO2 atmosphere at 37 ºC. Cells were seeded in 96 well plates at a density of $2x10^5$ cells/well. Confluent growing HMC-1.2 cells were then sensitized with serum (50 % v/v) from AX allergic patients (n=3) and tolerant subjects (n=6) for 48 h at 37 ºC. Unsensitized cells were used as controls. Subsequently, cells were stimulated with the series of BiAns at different concentrations of AXO units (10, 50,100 μM) for 2h. In parallel experiments, cells were stimulated with the corresponding PEG (structures without dendron-AXO), as negative

controls. The HSA-AXO conjugate (at 10 µM concentration of AXO) and C48/80 (30 µg/mL) were used as positive controls of degranulation induction.

7.6.6. LUVA Cells Activation Assay

Human Mast cell line (LUVA) was cultured in Dulbecco´s modified Eagle medium (Invitrogen, Grand Island, USA) supplemented with StemPro-34 SFM (500 mL) (Thermo Fisher), L-glutamine (2 mM), 100 µg/mL penicillin, 100 U/mL streptomycin and 50 mg/ml primocin (Invitrogen), in a humidified 5 % CO_2 atmosphere at 37 ºC. Cells were seeded in 96 well plates at a density of $2x10^5$ cells/well. Confluent growing LUVA cells were then sensitized with serum (50 % v/v) from AX allergic patients (n=11) and tolerant subjects (n=7) for 48 h at 37 ºC. Unsensitized cells were used as controls. Subsequently, cells were stimulated with the series of DeAns at different concentrations of AXO units (10, 20, 50 and 100 µM) for 2 h. In parallel experiments, cells were stimulated with the corresponding blank PAMAM (structures without dendron-AXO), as negative controls. The HSA-AXO conjugate (at 10 µM concentration of AXO), Ionomycin (10 µM) and C48/80 (30 µg/ml) (Sigma-Aldrich) were used as positive controls of degranulation induction.

7.6.7. Cell Degranulation Assay (LUVA, HMC-1 and RBL-2H3 cells)

This was determined by measuring the release of b-hexosaminidase. Following the activation of cell degranulation, the cells were separated by centrifugation at 150 xg for 5 min at 4 ºC and then the supernatants were incubated in citrate buffer supplemented with 1 mM 4-nitrophenyl N-acetyl-β-D-glucosaminide at 37 °C for 1 h. Cell pellets were lysed with Tyrode's buffer containing 1% Triton X-100 and the reaction was stopped by adding 150 µL stop solution (0.1 M Na_2CO_3-$NaHCO_3$; pH 10). Absorbance was measured at 405 nm using the microplate reader (ELX808; BioTek Instruments, Inc., Winooski, VT, USA).

7.7. Synthetic Protocols

7.7.1. Synthesis of 4-(2,5-dioxo-2,5-dihydro-1H-pyrrol-1-yl)butanoic acid (Mal-COOH) (1)

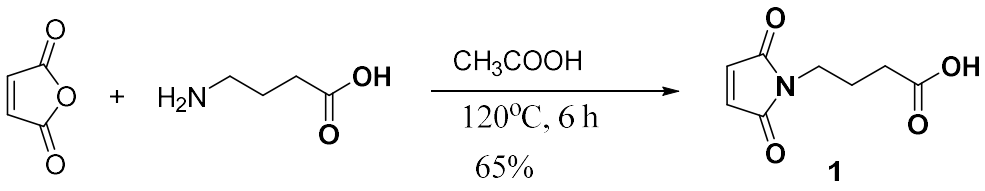

In a round bottom flask, γ-aminobutyric acid (6 g, 58.2 mmol) and maleic anhydride (6.8 g, 69.9 mmol) were dissolved under string in 120 mL of glacial acetic acid at 120 ºC for 6 h. The reaction was cooled to room temperature before pouring into 50 mL of water and extracted with 50 mL of ethyl acetate on three occasions. The collected organic layers were combined and dried on anhydrous $MgSO_4$. The solvent was removed under reduced pressure by rotary evaporation. Purification was performed by recrystallization of the crude product four times in 1:1 hexane: ethyl acetate to obtain **compound 1** with a 65 % yield. ^{1}H NMR (400 MHz, $CDCl_3$) δ: 10.81 (s, 1H), 6.71 (s, 2H), 3.60 (t, J = 6.8 Hz, 2H), 2.37 (t, J = 7.3 Hz, 2H), 1.93 (qt, J = 7.1 Hz, 2H). ^{13}C NMR (101 MHz, $CDCl_3$) δ: 178.3, 170.9, 134.2, 37.1, 31.2, 23.6.

7.7.2. Synthesis of Chapter 3: DeAns

General Synthetic Protocols for DeAns

PAMAM dendrimers (G1 to G5) was dissolved in 0.05 M carbonate buffer, pH 10.9 after removing the methanol under vacuum. A molar excess of AX (2 mol per NH_2 group) was added to the solution. The mixture was stirred for 7 days at 4ºC. The reactions were refreshed with 20 % of the initial mass of AX on three different occasions. The products were purified by gel filtration chromatography using Sephadex G-10 followed by lyophilizing the fractions containing the desired products.

G1-AXO (2).

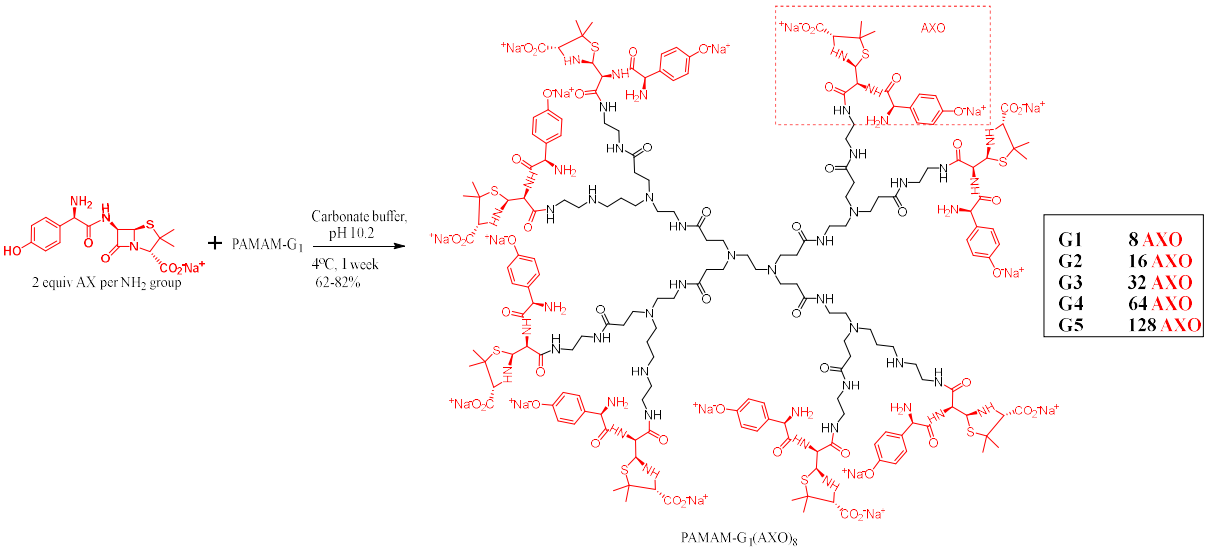

G1-PAMAM (100 mg, 0.067 mmol) was dissolved in 2 mL of carbonate buffer (0.05 M, pH 10.2) after evaporating MeOH under vacuum. An excess of AX (433 mg, 1.12 mmol) corresponding to 16 equivalences was added to the above solution and reacted at 4 ºC under magnetic stirring for 7 days. The reaction was refreshed with 20 % of the initial mass of AX on three different occasions. The purification was performed by gel filtration chromatography using Sephadex G-10 columns by collecting the product in small fractions. The product was isolated as a yellow power with 88 % yield. ^{1}H NMR (400 MHz, D_2O) δ 7.27 (d, J = 8.1 Hz, 16H), 6.85 (d, J = 8.1 Hz, 16H), 4.93 (d, J = 7.8 Hz, 8H), 4.61 (s, 8H), 4.26 (d, J = 7.8 Hz, 8H), 3.33 (s, 8H), 3.31 – 3.06 (m, 40H), 2.87 – 2.71 (m, 24H), 2.62 –2.50 (m, 12H), 2.46-227 (m, 24H), 1.45 (s, 24H), 1.18 (s, 24H).^{13}C NMR (101 MHz, D_2O) δ 174.8, 174.7, 174.1, 171.3, 160.3, 156.0, 130.2, 129.4, 128.7, 115.9, 74.6, 64.6, 59.3, 59.1, 58.8, 57.8, 51.1, 48.9, 39.2, 38.5, 36.7, 32.5, 26.6.

G2-AXO (3)

Obtained by dissolving G2-PAMAM (100 mg, 0.031 mmol) in 2 mL of carbonate buffer (0.05 M, pH 10.2) to which AX (380.7 mg, 0.98 mmol) was added to react for 7 days at 4 ºC. The reaction was refreshed with 20 % of the initial amount of AX on three different occasions. The purification was performed by gel filtration chromatography using Sephadex G-10. A yellow powder with 84 % yield was collected as a product. ^{1}H NMR (400 MHz, D_2O) δ 7.28 (d, J = 8.1 Hz, 32H), 6.86 (d, J = 8.1 Hz, 32H), 4.96 (d, J = 7.8 Hz, 16H), 4.57 (s, 16H), 4.26 (d, J =

7.8 Hz, 16H), 3.35(s,16H), 3.31 – 3.19 (m, 88H), 2.85 – 2.68 (m, 56H), 2.66 –2.51 (m, 28H), 2.45-2.24 (m, 56H), 1.46 (s, 48H), 1.19 (s, 48H). ^{13}C NMR (101 MHz, D_2O) δ 175.2, 175.0, 174.6, 171.7, 161.1, 156.7, 131.0, 129.8, 128.9, 116.3, 74.9, 64.9, 59.6, 59.5, 59.1, 58.3, 51.5, 49.2, 38.9, 37.0, 32.9, 27.0.

G3-AXO (4)

G3-PAMAM (100 mg, 0.0145 mmol) was dissolved in 2 mL of carbonate buffer (0.05 M, pH 10.2) and reacted with AX (360 mg, 0.93 mmol) for 7 days at 4 ºC. On three different occasions the reaction was refreshed with 20 % of the initial amount of AX. Gel filtration chromatography using Sephadex G-10 was used to purify the product to obtain a yellowish powder with 73% of yield. ^{1}H NMR (400 MHz, D_2O) δ 7.30 (d, J = 8.1 Hz, 64H), 6.88 (d, J = 8.1 Hz, 64H), 4.95 (d, J = 7.8 Hz, 32H), 4.65 (s, 32H), 4.27 (d, J = 7.8 Hz, 32H), 3.32(s, 32H), 3.30 – 3.18 (m, 184H), 2.89 – 2.71 (m, 120H), 2.64 –2.54 (m, 60H), 2.47-2.27 (m, 120H), 1.43 (s, 96H), 1.18 (s, 96H). ^{13}C NMR (101 MHz, D_2O) δ 175.1, 174.9, 174.5, 171.6, 160.6, 156.4, 130.1, 129.7, 129.1, 116.3, 75.0, 65.0, 59.6, 59.4, 59.1, 58.0, 51.5, 49.3, 39.5, 38.8, 36.9, 32.8, 26.9.

G4-AXO (5)

G4-PAMAM (100 mg, 0.0074 mmol) was dissolved in 2 mL of carbonate buffer (0.05 M, pH 10.2) and reacted with AX (367 mg, 0.947 mmol) for 7 days at 4ºC. On three different occasions, the reaction was refreshed with 20 % of the initial amount of AX and purified with gel filtration chromatography using Sephadex G-10. A yellow powder with 78 % yield was collected as a product. ^{1}H NMR (101 MHz, D_2O) δ 7.26 (d, J = 8.1 Hz, 128H), 6.84 (d, J = 8.1 Hz, 128H), 4.95 (d, J = 7.8 Hz, 64H), 4.57 (s, 64H), 4.27 (d, J = 7.8 Hz, 64H), 3.36 (s, 64H), 3.33 – 3.15 (m, 376H), 2.92 – 2.69 (m, 248H), 2.66 –2.50 (m, 124H), 2.47-2.27 (m,248H), 1.47 (s, 192H), 1.20 (s, 192H). ^{13}C NMR (400 MHz, D_2O) δ 175.3, 174.8, 174.6, 171.3, 159.5, 156.3, 130.6, 129.4, 128.5, 116.0, 74.6, 64.7, 59.3, 59.1, 58.8, 58.0, 51.2, 48.9, 38.6, 38.4, 36.6, 32.6, 26.6.

G5-AXO (6)

G5-PAMAM (100 mg, 0.0035 mmol) was dissolved in 2 mL of carbonate buffer (0.05M, pH10.2) and reacted with AX (348 mg, 0.896 mmol) for 7 days at 4 ºC. The reaction was refreshed with 20 % of the initial amount of AX on three different occasions. The purification

was performed by gel filtration chromatography using Sephadex G-10. A yellow powder with 73 % yield was collected as a product. ^{1}H NMR (400 MHz, D_2O) δ 7.25(d, J = 8.1 Hz, 256H), 6.83 (d, J = 8.1 Hz, 256H), 4.94 (d, J = 7.8 Hz, 128H), 4.58 (s, 8H), 4.26 (d, J = 7.8 Hz, 128H), 3.35(s,128H), 3.31 – 3.07 (m, 760 H), 2.90 – 2.66 (m, 504H), 2.64 –2.48 (m, 252H), 2.45-2.22 (m, 504H), 1.45 (s, 384H), 1.18 (s, 384H). ^{13}C NMR (101 MHz, D_2O) δ 175.2, 174.9, 174.6, 171.7, 161.5, 156.6, 130.8, 129.7, 129.0, 116.4, 75.0, 65.1, 59.7, 59.5, 59.1, 58.3, 51.6, 49.3, 39.6, 38.8, 37.1, 32.9, 27.

7.7.3. Synthesis of Chapter 4: BiAns

General Synthetic Protocols for BiAns

Synthesis of PEG-$(Ts)_2$. ***(Procedure A)***

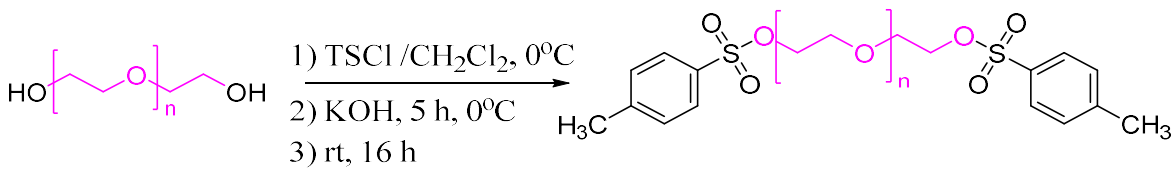

PEG (1 equiv.) dissolved in anhydrous CH_2Cl_2 and TsCl (3 equiv.) were placed in a 250 mL round-bottom flask, sparged with N_2, and ice-cooled to 0 ºC. Powdered KOH (4 equiv.) was added in small portions in order to maintain the temperature of the mixture below 5 ºC. After stirring for 5 h at 0 ºC, the reaction took place at room temperature overnight. After a washing step with H_2O, the organic layer was separated, and the aqueous phase was extracted with CH_2Cl_2 (3x15 mL). The combined organic layer was dried over anhydrous $MgSO_4$, filtered, and the solvent removed by a rotary evaporator to obtain a product.

Synthesis of PEG-$(N_3)_2$. ***(Procedure B)***

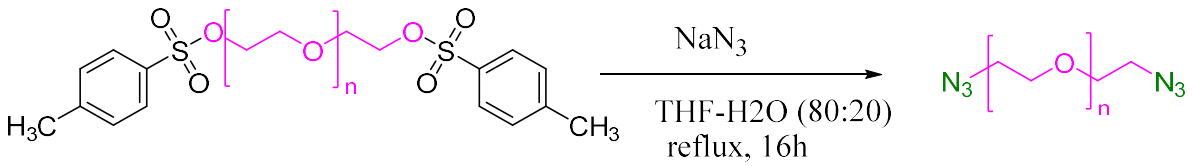

PEG–$(Ts)_2$ (1 equiv.) was dissolved in 50 mL of H_2O: THF (80:20), and NaN_3 (3 equiv.) was added to the dissolved product and refluxed at 70 ºC overnight. After cooling the reaction to room temperature, the solvent was removed under reduced pressure and the dried product was dissolved in CH_2Cl_2. The product was cleaned by washing with H_2O (3x30 mL), 1M HCl (10

mL), and brine. The collected organic layer was dried over anhydrous $MgSO_4$, filtered, and the solvent removed under reduced pressure to obtain a crude product.

Synthesis of PEG-$(NH_2)_2$. ***(Procedure C)***

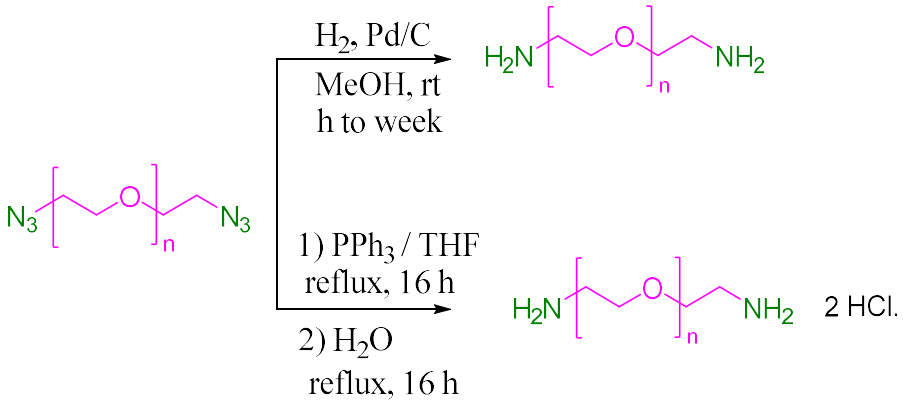

To a solution containing a weighed amount of PEG-$(N_3)_2$ in 15 mL of MeOH, 20 wt. % of 10 % Pd/C was added. The resulting suspension was stirred at 300 rpm under hydrogen gas (H_2, 50 bar) at room temperature. The reaction was monitored by ^1H NMR by the presence of the peak pertaining to *CH_2-N_3*. When the reaction reached completion, the catalyst was removed by filtering through MeOH-washed Celite, and the solvent was evaporated to yield the desired bisamine product in quantative amount.

Or

PEG-$(N_3)_2$ (1 equiv.) was dissolved in THF (20 mL) and placed in an ice bath. PPh_3 (3 equiv.) was dissolved in THF (10 mL) and added dropwise to the previous solution. The mixture was left under reflux in a heat block for 16 h. Afterwards, 2 mL of H_2O added to the mixture and the reaction was left under reflux for another day. Then, THF was removed under vacuum and the product was dissolved in HCl (1M, 10 mL). The aqueous phase was washed with CH_2Cl_2 (3 x30 mL). The resulting residue was concentrated under reduced pressure to obtain the desired product as a white solid.

Synthesis of PEG-bismaleimide. ***(Procedure D)***

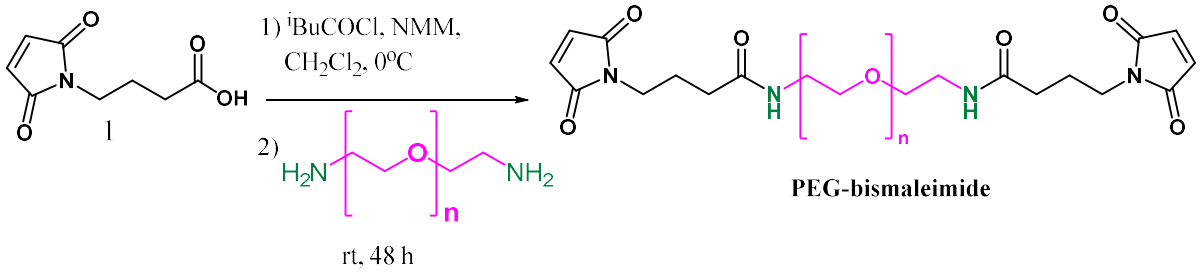

To a stirred solution of compound 1 (2.2 equiv.) in anhydrous CH_2Cl_2 at 0 ºC, NMM (2.3 equiv.) and ^{i}BuCOCl (2.3 equiv.) were sequentially added dropwise. After 1 h, PEG-$(NH_2)_2$ (1 equiv.) dissolved in anhydrous CH_2Cl_2 (15 mL) was added. The reaction was slowly warmed to room temperature and run for 48 h. The product was washed with H_2O, 5 % HCl aqueous solution, H_2O and 10% $NaHCO_3$ aqueous solution. The collected organic layer was dried over anhydrous $MgSO_4$, filtered, and the solvent removed under reduced pressure. The crude product was purified by gel permeation chromatography using Bio-Beads™ S-X1 support (200-400 mesh, Bio-Rad) with THF as eluent.

Synthesis of PEG-$(dG_2)_2$. ***(Procedure E)***

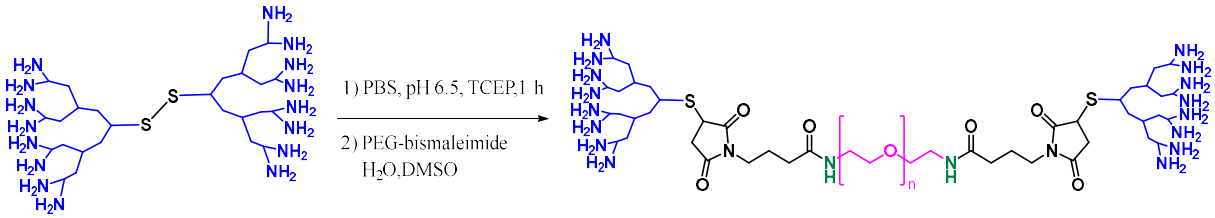

PAMAM dendrimer, cystamine core, generation 2 (G_2) (1.1 equiv.) in PBS (1x, pH 6.5) was deoxygenated by purging with N_2 gas. Then TCEP (10 equiv.) was added, and the mixture was stirred. The reduction of the disulfide bond was monitored by TLC using Ellman's and ninhydrin as reagents. When reduction was completed, PEG-bismaleimide (1 equiv.) was dissolved in 5 mL of distilled H_2O with few drops of DMSO as cosolvent and flushed with N_2 gas, added to the above solution, and the mixture was stirred overnight. The resulting residue was concentrated under reduced pressure, re-dissolved in distilled H_2O for purifying the product by gel filtration chromatography using Sephadex-10 and PD MidiTrap G-25.

Synthesis of PEG-(dG$_2$-(AXO)$_8$)$_2$. *(Procedure F)*

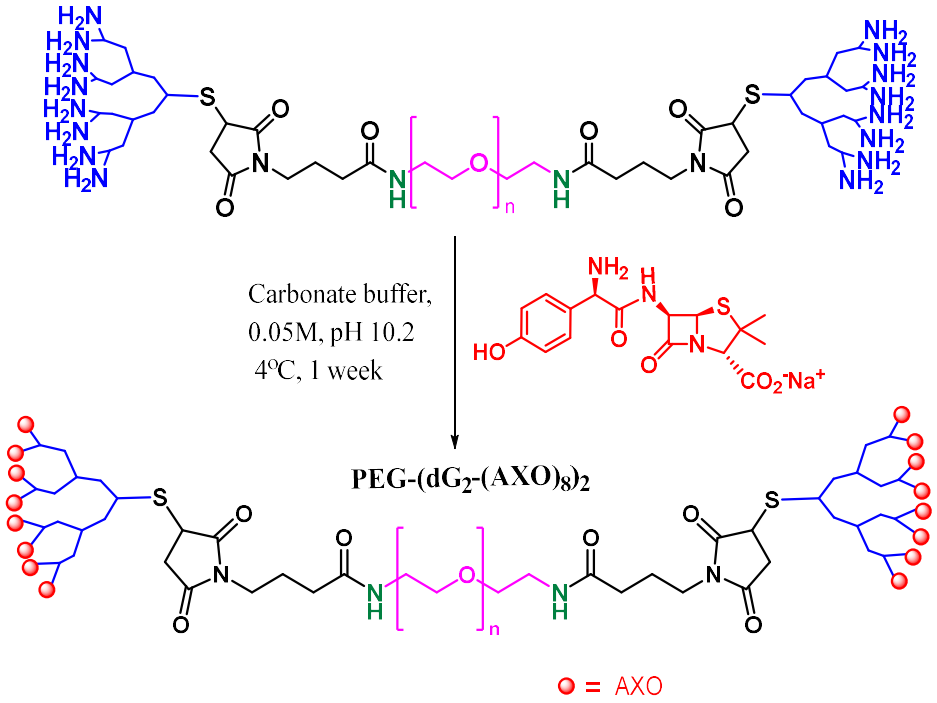

An excess of AX (32 equiv.) was added to a solution of PEG-(dG$_2$)$_2$ (1 equiv. of nanoarchitecture, 16 equiv. NH_2 group) in carbonate buffer (0.05 M, pH 10.2), and the mixture was cooled at 4 ºC under magnetic stirring for 7 days with refreshing on three different occasions with 20 % of the initial mass of AX. The purification was performed by gel filtration chromatography using Sephadex G-10 columns.

PEG (600)- (Ts)$_2$ (7)

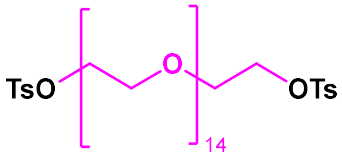

Synthesized according to general procedure A. PEG (MW~ 600 Da) (9 g, 15 mmol), CH_2Cl_2 (30 mL), TsCl (8.5 g, 45 mmol) and KOH (3.4 g, 60 mmol) were used in the reaction. The crude product was purified by column chromatography using CH_2Cl_2: MeOH (15:1 v/v) as an eluting solvent to obtain a white semisolid product with 93 % yield. ^{1}H NMR (400 MHz, $CDCl_3$) δ 7.78 (d, J = 8.2 Hz, 2H), 7.31 (d, J = 8.2 Hz, 2H), 4.12 (t, 4H), 3.67 – 3.55 (m, 56H), 2.42 (s, 6H). ^{13}C NMR (101 MHz, $CDCl_3$) δ 144.8, 133.0, 129.8, 128.0, 70.6, 69.3, 68.7, 21.7.

PEG (600) -$(N_3)_2$ (8)

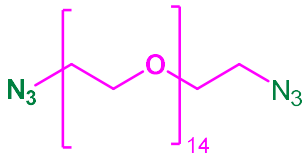

This was obtained according to general procedure B. **Compound 7** (8.4 g, 9.24 mmol), 50 mL of distilled H_2O: THF (80:20 % v/v) and NaN_3 (1.8 g, 27.6 mmol) were used in the reaction. As a final point, the product was purified by silica gel column chromatography using CH_2Cl_2: MeOH (9:1 v/v) as eluent (84 % yield). ^{1}H NMR (400 MHz, $CDCl_3$) δ 3.82 – 3.37 (m, 56H), 3.32 (t, J = 5.1 Hz, 4H). ^{13}C NMR (101 MHz, $CDCl_3$) δ 70.7, 70.0, 50.6.

PEG (600) -$(NH_2)_2$ (9)

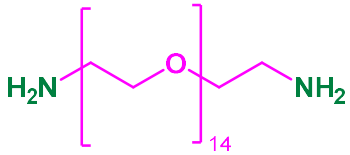

This was obtained according to general procedure C. **Compound 8** (500 mg, 0.76 mmol), 15 mL of MeOH, Pd/C (100 mg) were used. The reaction was stirred for 6 h to obtain a white semisolid product with 84 % of yield. ^{1}H NMR (400 MHz, $CDCl_3$) δ 3.67 – 3.57 (m, 56H), 3.48 (t, J = 5.2 Hz, 4H), 2.83 (t, J = 5.2 Hz, 4H). ^{13}C NMR (101 MHz, $CDCl_3$) δ 73.3, 70.6, 70.3, 41.7.

PEG (600) -(maleimide)$_2$ (10)

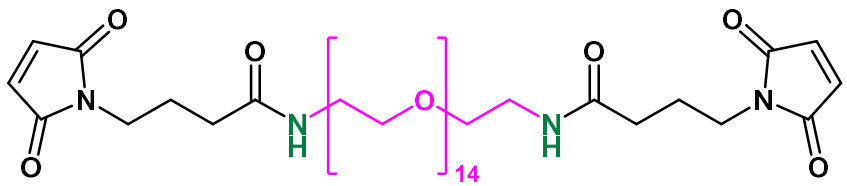

This is synthesized according to general procedure D. **Compound 1** (314 mg, 1.72 mmol),CH_2Cl_2 (15 mL), NMM (200.74 mg,1.79 mmol), ^{i}BuCoCl (234 mg,1.79 mmol.) and **compound 9** (466 mg, 0.78 mmol) dissolved in 15 mL CH_2Cl_2 were used to obtain a product with 60 % of yield. ^{1}H NMR (400 MHz, $CDCl_3$) δ 6.70 (s, 4H), 6.43 (s, 2H), 3.67 – 3.61 (m,

56H), 3.51–3.45 (m, 8H), 3.44 (t, J = 5.2 Hz, 4H), 2.17 (t, J = 7.2 Hz, 4H), 1.97 – 1.88 (m, 4H). ^{13}C NMR (101 MHz, $CDCl_3$) δ 172.3, 171.2, 134.6, 70.9, 70.6, 70.3, 39.7, 37.7, 25.1.

PEG (600)-[dG$_2$]$_2$(11)

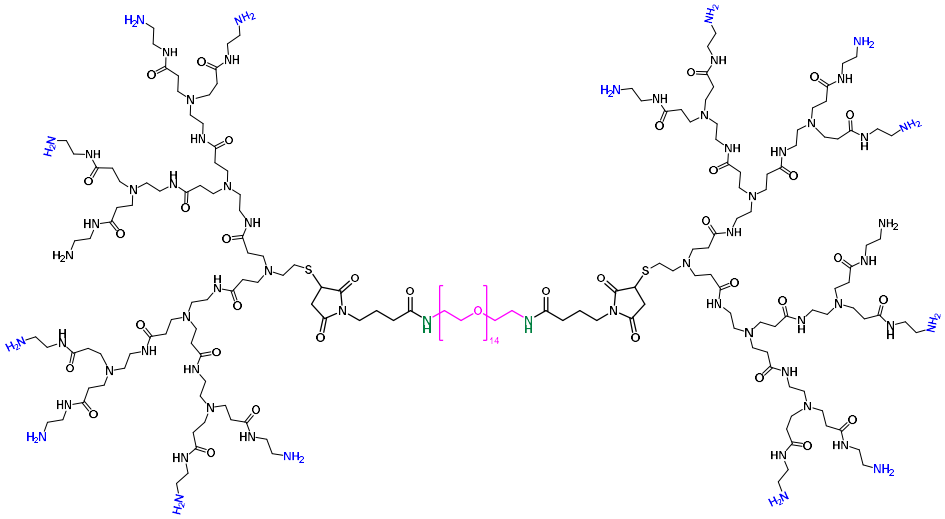

This was synthesized according to general procedure E. G_2 (614 mg, 0.18 mmol), 5 mL of PBS (1x, pH 6.5), TCEP (525 mg, 1.83 mmol), **compound 10** (150 mg, 0.166 mmol), 5 mL of H_20 and few drops of DMSO were used. The purification was performed gel filtration chromatography using PD MidiTrap G-10 columns and collecting the fractions of small volumes with 77 % of yields. ^{1}H NMR (400 MHz, D_2O) δ 3.73 – 3.67 (m, 56H), 3.66– 3.59 (m, 8H), 3.55 – 3.26 (m, 88H), 3.15 (t, J = 6.0 Hz, 8H), 2.87 – 2.76 (m, 56H), 2.68 – 2.56 (m, 30H), 2.50 – 2.39 (m, 56H), 2.17 – 2.08 (m, 8H), 1.92 – 1.83 (m, 4H). ^{13}C NMR (101 MHz, D_2O) δ 179.7, 178.7, 172.9, 172.6, 69.7, 69.6, 69.0, 51.9, 49.7, 49.5, 39.1, 37.0, 34.5, 30.2, 29.0, 28.4, 23.5, 22.9.

BiAn(600): PEG (600)-[dG$_2$-(AXO)$_8$]$_2$ (12)

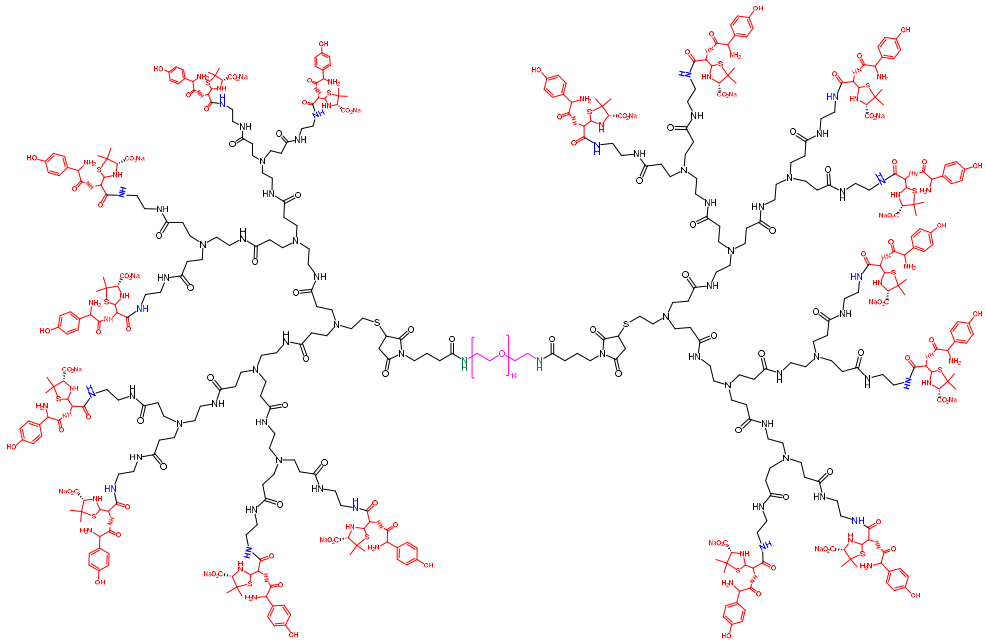

This was obtained by following general procedure F. **Compound 11** (81 mg, 0.021mmol) and AX (252 mg, 0.65 mmol) were reacted. The reaction was refreshed with 51 mg of AX on three different occasions. After purification, the product was collected as yellowish powder with 59 % of yield. ^{1}H NMR (400 MHz, D_2O) δ 7.29 (d, J = 7.8 Hz, 32H), 6.87 (d, J = 7.8 Hz, 32H), 4.96 (d, J = 8.0 Hz, 16H), 4.59 (s, 16H), 4.27 (d, J = 8.0 Hz, 16H), 3.75 – 3.55 (m, 56H), 3.62 – 3.57(m, 8H), 3.35(s,16H), 3.33 – 3.18 (m, 88H), 3.12 – 3.01 (m, 8H), 2.86 – 2.69 (m, 56H), 2.67 – 2.51 (m, 30H), 2.49 – 2.32 (m, 56H), 2.18– 2.05(m, 8H),1.97 – 1.75(m,4H), 1.47 (s, 48H), 1.20 (s, 48H). ^{13}C NMR (101 MHz, D_2O) δ 175.6, 175.1, 174.6, 171.6, 160.5, 156.2, 129.7, 128.8, 115.9, 74.9, 69.8, 69.6, 68.9, 64.9, 59.5, 59.1, 58.2, 51.4, 49.1, 39.4, 38.9, 38.7, 36.9, 36.9, 3.7, 28.9, 28.2, 26.8, 23.6, 23.0.

PEG (1k)- (Ts)$_2$ (13)

Synthesized according to general procedure A. PEG (MW~ 1000 Da) (10 g, 10 mmol), CH_2Cl_2 (30 mL), TsCl (5.7 g, 30 mmol) and KOH (2.2 g, 40 mmol) were used in the reaction. The crude product was purified by column chromatography using CH_2Cl_2: MeOH (9:1 v/v) as an eluting solvent to obtain a white powder product with 97 % yield. ^{1}H NMR (400 MHz, $CDCl_3$) δ 7.77 (d, J = 8.2 Hz, 2H), 7.32 (d, J = 8.2 Hz, 2H), 4.14 (t, 4H), 3.68 – 3.54 (m, 93H), 2.43(s, 6H). ^{13}C NMR (101 MHz, $CDCl_3$) δ 144.7, 133.1, 129.7, 127.9, 70.6, 69.3, 68.7, 21.7.

PEG (1k) -$(N_3)_2$ (14)

This was obtained according to general procedure B. **Compound 13** (8.7 g, 6.65 mmol), 50 mL of distilled H_2O: THF (80:20 % v/v) and NaN_3 (1.3 g, 19.95 mmol) were used in the reaction. As a final point, the product was purified by silica gel column chromatography using 9:1(v/v) CH_2Cl_2: MeOH as an eluent to obtain a white powder of 93 % of yield. ^{1}H NMR (400 MHz, $CDCl_3$) δ 3.64 – 3.56 (m, 93H), 3.34 (t, J = 5.1 Hz, 4H). ^{13}C NMR (101 MHz, $CDCl_3$) δ 70.5, 70.0, 50.6.

PEG (1k) -$(NH_2)_2$ (15)

This was obtained according to general procedure C. **Compound 14** (200 mg, 0.19 mmol), 15 mL of MeOH, Pd/C (40 mg) were used. The reaction took place for 12 h to obtain a product with 88 % yield. ^{1}H NMR (400 MHz, $CDCl_3$) δ 3.65 – 3.55 (m, 93H), 3.46 (t, J = 5.2 Hz, 4H), 2.81 (t, J = 5.2 Hz, 4H), 2.22(s, 4H). ^{13}C NMR (101 MHz, $CDCl_3$) δ 73.3, 70.5, 70.2, 41.7.

PEG (1k) -(maleimide)$_2$ (16)

This was synthesized according to general procedure D. **Compound 1** (80 mg, 0.44 mmol), NMM (54 mg, 0.46 mmol), ^{i}BuCoCl (62.8 mg, 0.46mmol.) and **compound 15** (200 mg, 0.2 mmol) and 15 mL CH_2Cl_2 were used to obtain a product with 75 % of yield. ^{1}H NMR (400 MHz, $CDCl_3$) δ 6.69 (s, 4H), 6.52 (s, 2H), 3.68 – 3.59 (m, 93 H), 3.57-3.51 (m, 8H), 3.44 (t, J = 5.2 Hz, 4H), 2.17(t, J = 7.2 Hz, 4H), 1.93 – 1.88 (m, 4H). ^{13}C NMR (101 MHz, $CDCl_3$) δ 172.0, 171.0, 134.2, 70.7, 70.6, 70.3, 39.4, 37.4, 24.8.

PEG (1k)-[dG$_2$]$_2$ (17)

This was synthesized according to general procedure E. G_2 (100 mg, 0.075 mmol), 5 mL of PBS (1x, pH 6.5), TCEP (237 mg, 1.83mmol), **Compound 16** (276 mg, 0.083 mmol) dissolved in 5 mL of H_20 and few drops of DMSO. The purification was performed gel filtration chromatography using PD MidiTrap G-10 columns and collecting the fractions of small volumes. The product was isolated as white powder with 72 % yield.^{1}H NMR (400 MHz, D_2O) δ 3.75 – 3.68 (m, 93H), 3.67– 3.59 (m, 8H), 3.56 – 3.22 (m, 88H),3.17 (t, J = 6.0 Hz, 8H), 2.87 – 2.74 (m, 56H), 2.73 – 2.55 (m, 30H), 2.52 – 2.41 (m, 56H), 2.22-2.08 (m, 8H), 1.92 – 1.83 (m, 4H). ^{13}C NMR (101 MHz, D_2O) δ 179.7, 179.5, 173.0, 172.7, 69.8, 69.6, 69.6, 51.9, 49.7, 49.4, 39.2, 38.9, 37.0, 34.5, 29.6, 29.1, 28.5, 23.5, 22.9.

PEG(1k)-[dG$_2$-(AXO)$_8$]$_2$ (18) : **BiAn(1000)**

This was obtained by following general procedure F. **Compound 17** (96 mg, 0.021mmol) and AX (256 mg, 0.65 mmol) were reacted. The reaction was refreshed with 51 mg of AX on three different occasions. After purification, the product was collected as yellowish powder with 76 % of yield. ^{1}H NMR (400 MHz, D_2O) δ 7.29 (d, J = 7.8 Hz, 32H), 6.87 (d, J = 7.8 Hz, 32H), 4.96 (d, J = 8.0 Hz, 16H), 4.59 (s, 16H), 4.27 (d, J = 8.0 Hz, 16H), 3.75 – 3.55 (m, 93H), 3.62 – 3.57(m,8H), 3.35(s,16H), 3.33 – 3.18 (m, 88H), 3.12 – 3.01 (m, 8H), 2.86 – 2.69 (m, 56H), 2.67 – 2.51 (m, 30H), 2.49 – 2.32 (m, 56H), 2.18 – 2.05(m, 8H),1.84 – 1.72(m,4H), 1.47 (s, 48H), 1.20 (s, 48H). ^{13}C NMR (101 MHz, D_2O) δ 176.0, 175.4, 175.0, 172.0, 160.8, 156.6, 130.0, 129.1, 116.5, 75.1, 70.1, 69.9, 69.3, 65.2, 59.94, 59.4, 58.5, 51.7, 49.5, 39.8, 39.1, 37.2, 33.1, 29.2, 28.5, 27.2, 23.5, 23.4.

PEG (2k)- (Ts)$_2$ (19)

Synthesized according to general procedure A. PEG (MW~ 2000 Da) (10 g, 5 mmol), CH_2Cl_2 (30mL), TsCl (2.8 g, 15 mmol) and KOH (2.24 g, 40 mmol) were used in the reaction. The crude product was purified by column chromatography using CH_2Cl_2: MeOH (9:1 v/v) as an eluting solvent to obtain a white solid product with 78 % yield. ^{1}H NMR (400 MHz, $CDCl_3$) δ 7.76 (d, J = 8.2 Hz, 2H), 7.33 (d, J = 8.2 Hz, 2H), 4.12 (t, J = 5.6 Hz, 4H), 3.67 – 3.54 (m, 184H), 2.42(s, 6H).^{13}C NMR (101 MHz, $CDCl_3$) δ 144.7, 133.1, 129.6, 128.0, 77.1, 70.3, 69.3, 68.7, 21.5.

PEG (2k) -(N$_3$)$_2$ (20)

This was obtained according to general procedure B. **Compound 19** (10.7 g, 4.6 mmol), 50 mL of distilled H_2O: THF (80:20 %v/v) and NaN_3 (900 mg, 13.8 mmol) were used in the reaction. As a final point, the product was purified by silica gel column chromatography using 9:1(v/v) CH_2Cl_2: MeOH as an eluent to obtain a white powder with 93 % of yield. ^{1}H NMR (400 MHz, $CDCl_3$) δ 3.67 – 3.54 (m, 186H), 3.39 (t, J = 5.1 Hz, 4H). ^{13}C NMR (101 MHz, $CDCl_3$) δ 70.6, 70.0, 50.7.

PEG (2k) -$(NH_2)_2$ (21)

This was obtained according to general procedure C. **Compound 20** (200 mg, 0.097 mmol), 15 mL of MeOH, Pd/C (40 mg) were used. The reaction was stirred for 12 h to obtain a product with 89 %. ^{1}H NMR (400 MHz, $CDCl_3$) δ 3.73 – 3.55 (m, 186H), 3.52 (t, J = 5.2 Hz, 4H), 2.88 (t, J = 5.2 Hz, 4H), 1.95(s, 4H). ^{13}C NMR (101 MHz, $CDCl_3$) δ 73.6, 70.7, 70.4, 41.7.

PEG (2k) -(maleimide)$_2$ (22)

This is synthesized according to general procedure D. **Compound 1** (101 mg, 0.56 mmol), NMM (151 mg, 1.3 mmol), ^{i}BuCOCl (176 mg, 1.3 mmol) and **compound 21** (500 mg, 0.25 mmol) and 15 mL CH_2Cl_2 were used to obtain a white solid product with 80 % of yield. ^{1}H NMR (400 MHz, $CDCl_3$) δ 6.70 (s, 4H), 6.39 (s, 2H), 3.70 – 3.59 (m, 186 H), 3.58-3.53 (m, 8H), 3.45 (t, J = 5.2 Hz, 4H), 2.16 (t, J = 7.2 Hz, 4H), 1.98 – 1.90 (m, 4H). ^{13}C NMR (101 MHz, $CDCl_3$) δ 172.0, 171.0, 134.2, 70.7, 70.6, 70.3, 39.4, 37.4, 24.8.

PEG (2k)-[dG_2]$_2$ (23)

This was synthesized according to general procedure E. G_2 (157 mg, 0.047 mmol), 5 mL of PBS (1x, pH 6.5), TCEP (135 mg, 0.47 mmol), **Compound 22** (100 mg, 0.043 mmol) dissolved in 5 mL of H_20 and few drops of DMSO. The purification was performed gel filtration chromatography using Sephadex G-10 columns. The product was isolated as white powder with 64 % yield.^{1}H NMR (400 MHz, D_2O) δ 3.77 – 3.66 (m, 186H), 3.62– 3.48 (m, 8H), 3.46 – 3.19 (m, 88H),3.17 (t, J = 6.0 Hz, 8H), 2.85 – 2.68 (m, 56H), 2.67 – 2.53 (m, 30H), 2.50 – 2.40 (m, 56H), 2.17-2.06 (m, 8H), 1.92 – 1.77 (m, 4H). ^{13}C NMR (101 MHz, D_2O) δ 179.8, 178.6, 173.0, 172.8, 69.9, 69.7, 69.1, 52.1, 49.8, 49.6, 39.3, 39.0, 37.2, 34.7, 29.2, 28.6, 23.7, 23.0.

BiAn(2000) : PEG(2k)-[dG_2-$(AXO)_8$]$_2$ (24)

This was obtained by following general procedure F. **Compound 23** (98 mg, 0.017 3mmol) and AX (214 mg, 0.554 mmol) were reacted. The reaction was refreshed with 43 mg of AX on three different occasions. After purification, the product was collected as yellowish powder with 71 % of yield. ^{1}H NMR (400 MHz, D_2O) δ 7.30 (d, J = 7.8 Hz, 32H), 6.88 (d, J = 7.8 Hz, 32H), 4.95 (d, J = 8.0 Hz, 16H), 4.67 (s, 16H), 4.27 (d, J = 8.0 Hz, 16H), 3.89 – 3.56 (m, 186H),

3.54 – 3.43(m, 8H), 3.35(s,16H), 3.33 – 3.20 (m, 88H), 3.16 – 3.11 (m, 8H), 2.90 – 2.69 (m, 56H), 2.68 – 2.53 (m, 30H), 2.50 – 2.29 (m, 56H), 2.27 –2.09 (m, 8H),1.92– 1.71(m, 4H), 1.46 (s, 48H), 1.20 (s, 48H). ^{13}C NMR (101 MHz, D_2O) δ 175.7, 175.1, 174.9, 171.6, 160.4, 156.3, 129.7, 129.0, 116.2, 74.9, 69.8, 69.6, 69.0, 64.9, 59.6, 59.1, 57.9, 51.4, 49.1, 39.4, 38.7, 37.3, 32.7, 28.9, 28.2, 26.8, 23.7, 23.1.

PEG (4k) -$(Ts)_2$ (25)

Synthesized according to general procedure A. PEG (MW~ 4000 Da) (10 g, 2.5 mmol), CH_2Cl_2 (30 mL), TsCl (1.43 g, 7.5 mmol) and KOH (1.68 g, 3 mmol) were used in the reaction. The crude product was purified by column chromatography using CH_2Cl_2: MeOH (9.5:0.5 v/v) as an eluting solvent to obtain a white powder product with 84 % yield. ^{1}H NMR (400 MHz, $CDCl_3$) δ 7.77 (d, J = 8.2 Hz, 2H), 7.34 (d, J = 8.2 Hz, 2H), 4.14 (t, 4H), 3.68 – 3.54 (m, 373H), 2.43(s, 6H). ^{13}C NMR (101 MHz, $CDCl_3$) δ 144.8, 132.9, 129.6, 128.0, 77.1, 70.6, 69.3, 68.7, 21.5.

PEG (4k) -$(N_3)_2$ (26)

This was obtained according to general procedure B. **Compound 25** (9 g, 2.1 mmol), 50 mL of distilled H_2O: THF (80:20 %v/v) and NaN_3 (0.41 g, 6.34 mmol) were used in the reaction. As a final point, the product was purified by silica gel column chromatography using 9:1(v/v) CH_2Cl_2: MeOH as an eluent to obtain a white powder of 91 % of yield. ^{1}H NMR (400 MHz, $CDCl_3$) δ 3.85 – 3.44 (m, 373H), 3.38 (t, J = 5.1 Hz, 4H). ^{13}C NMR (101 MHz, $CDCl_3$) δ 70.6, 70.2, 50.8.

PEG (4k) -$(NH_2)_2$ (27)

This was obtained according to general procedure C. **Compound 26** (200 mg, 0.049 mmol), 15 mL of MeOH, Pd/C (40 mg) were used. The reaction was stirred for 12 h to obtain product with 96 % yield. ^{1}H NMR (400 MHz, $CDCl_3$) δ 3.73 – 3.54 (m, 373H), 3.51 (t, J = 5.2 Hz, 4H), 2.86 (t, J = 5.2 Hz, 4H), 1.74(s, 4H). ^{13}C NMR (101 MHz, $CDCl_3$) δ 73.6, 70.7, 70.4, 41.9.

PEG (4k) -(maleimide)$_2$ (28)

This is synthesized according to general procedure D. **Compound 1** (46 mg, 0.256 mmol), NMM (61 mg, 0.526 mmol), ^{i}BuCoCl (72 mg, 0.526 mmol.) and **Compound 27** (500 mg, 0.125 mmol) and 15 mL CH_2Cl_2 were used to obtain a product with 76 % of yield. ^{1}H NMR (400 MHz, $CDCl_3$) δ 6.70 (s, 4H), 6.50 (s, 2H), 3.68 – 3.60 (m, 373 H), 3.59-3.53 (m, 8H), 3.45 (t, J = 5.2 Hz, 4H), 2.35(t, J = 7.2 Hz, 4H), 1.97 – 1.86 (m, 4H). ^{13}C NMR (101 MHz, $CDCl_3$) δ 172.0, 171.3, 134.2, 70.7, 70.3, 70.0, 39.3, 37.5, 33.63, 24.5.

PEG (4k)-[dG$_2$]$_2$ (29)

This was synthesized according to general procedure E. G_2 (84 mg, 0.0253 mmol), 5 mL of PBS (1x, pH 6.5), TCEP (73 mg, 0.253 mmol), **Compound 28** (100 mg, 0.023 mmol) dissolved in 5 mL of H_20 and few drops of DMSO. The purification was performed gel filtration chromatography using PD MidiTrap G-25columns. The product was isolated as white powder with 83 % yield. ^{1}H NMR (400 MHz, D_2O) δ 3.83 – 3.68 (m, 373 H), 3.68– 3.59 (m, 8H), 3.58 – 3.22 (m, 88H), 3.17 (t, J = 6.0 Hz, 8H), 2.92 – 2.79 (m, 56H), 2.78 – 2.59 (m, 30H), 2.58 – 2.44 (m, 56H), 2.22– 2.11 (m, 8H), 1.91 – 1.80 (m, 4H). ^{13}C NMR (101 MHz, D_2O) δ 178.5, 178.4, 172.9, 172.5, 69.9, 69.7, 69.1, 52.1, 49.9, 49.6, 39.3, 39.0, 37.1, 34.6, 29.7, 29.0, 27.6, 23.2, 22.6.

BiAn(4000) : PEG(4k)-[dG$_2$-(AXO)$_8$]$_2$ (30)

This was obtained by following general procedure F. **Compound 29** (94 mg, 0.0122 mmol) and AX (151 mg, 0.39 mmol) were reacted. The reaction was refreshed with 30 mg of AX on three different occasions. After purification, the product was collected as yellowish powder with 57 % of yield. ^{1}H NMR (400 MHz, D_2O) δ 7.30 (d, J = 7.8 Hz, 32H), 6.87 (d, J = 7.8 Hz, 32H), 4.96 (d, J = 8.0 Hz, 16H), 4.59 (s, 16H), 4.27 (d, J = 8.0 Hz, 16H), 3.85 – 3.62 (m, 373H), 3.57 – 3.49(m, 8H), 3.36 (s,16H), 3.34 – 3.12 (m, 88H), 3.11 – 3.01 (m, 8H), 2.88 – 2.67 (m, 56H), 2.66 – 2.49 (m, 30H), 2.47 – 2.29 (m, 56H), 2.18 – 2.08(m, 8H),1.91 – 1.73(m, 4H), 1.48 (s, 48H), 1.21 (s, 48H). ^{13}C NMR (101 MHz, D_2O) δ 174.3, 174.2, 173.9, 170.9, 160.1, 155.6, 129.1, 128.2, 115.5, 74.0, 69.0, 68.9, 68.7, 64.1, 58.8, 58.3, 57.5, 51.6, 48.2, 38.2, 38.0, 36.2, 32.0, 28.1, 27.53, 26.1, 23.05, 22.4.

PEG (6k) -$(Ts)_2$ (31)

Synthesized according to general procedure A. PEG (MW~ 6000 Da) (10 g, 1.67 mmol), CH_2Cl_2 (30 mL), TsCl (960 mg, 5 mmol) and KOH (840 mg, 15 mmol) were used in the reaction. The crude product was purified by column chromatography using CH_2Cl_2: MeOH (9.5:0.5 v/v) as an eluting solvent to obtain a white solid product with 82 % yield. ^{1}H NMR (400 MHz, $CDCl_3$) δ 7.79 (d, J = 8.2 Hz, 2H), 7.34 (d, J = 8.2 Hz, 2H), 4.14 (t, J = 5.6 Hz, 4H), 3.68 – 3.52 (m, 560H), 2.42(s, 6H).^{13}C NMR (101 MHz, $CDCl_3$) δ 144.7, 133.1, 129.9, 128.1, 70.6, 69.35, 68.7, 21.6.

PEG (6k) -$(N_3)_2$ (32)

This was obtained according to general procedure B. **Compound 31** (8.5g, 1.35 mmol), 50 mL of distilled H_2O: THF (80:20 %v/v) and NaN_3 (263 mg, 4.04 mmol) were used in the reaction. As a final point, the product was purified by silica gel column chromatography using 9.5:0.5(v/v) CH_2Cl_2: MeOH as an eluent to obtain a white powder with 95 % of yield. ^{1}H NMR (400 MHz, $CDCl_3$) δ 3.69 – 3.49 (m, 560H), 3.34 (t, J = 5.1 Hz, 4H). ^{13}C NMR (101 MHz, $CDCl_3$) δ 70.5, 70.0, 50.5.

PEG (6k) -$(NH_2)_2$ (33)

This was obtained according to general procedure C. **Compound 32** (200 mg, 0.033 mmol), 15 mL of MeOH, Pd/C (40 mg) were used. The reaction was stirred for 24 h to obtain a product with 96 %. ^{1}H NMR (400 MHz, $CDCl_3$) δ 3.72 – 3.59 (m, 560H), 3.48 (t, J = 5.2 Hz, 4H), 2.88 (t, J = 5.2 Hz, 4H), 1.92(s, 4H). ^{13}C NMR (101 MHz, $CDCl_3$) δ 73.5, 70.5, 70.3, 41.6.

PEG (6k) -(maleimide)$_2$ (34)

This is synthesized according to general procedure D. **Compound** 1 (33 mg, 0.183 mmol), NMM (49 mg, 0.421 mmol), ^{i}BuCOCl (57.5 mg, 0.421 mmol.) and **Compound 33** (500 mg, 0.083 mmol) and 15 mL CH_2Cl_2 were used to obtain a white solid product with 62 % of yield. ^{1}H NMR (400 MHz, $CDCl_3$) δ 6.69 (s, 4H), 6.39 (s, 2H), 3.79 – 3.54 (m, 560 H), 3.61-3.53 (m, 8H), 3.47 (t, J = 5.2 Hz, 4H), 2.33(t, J = 7.2 Hz, 4H), 1.98 – 1.88 (m, 4H). ^{13}C NMR (101 MHz, $CDCl_3$) δ 172.2, 170.9, 134.0, 70.7, 70.3, 69.9, 39.1, 37.2, 33.6, 24.7.

PEG (6k)-[dG$_2$]$_2$ (35)

This was synthesized according to general procedure E. G_2 (58 mg, 0.017 mmol), 5 mL of PBS (1x, pH 6.5), TCEP (45 mg, 0.158 mmol), **Compound 34** (100 mg, 0.016 mmol) dissolved in 5 mL of H_20 and few drops of DMSO. The purification was performed gel filtration chromatography using PD MidiTrap G-25 columns. The product was isolated as white powder with 66 % yield.^{1}H NMR (400 MHz, D_2O) δ 3.74 – 3.69 (m, 560H), 3.68– 3.60 (m, 8H), 3.57–3.28 (m, 88H), 3.18 (t, J = 6.0 Hz, 8H), 2.91 – 2.80 (m, 56H), 2.79 – 2.70 (m, 30H), 2.60 – 2.47 (m, 56H), 2.22– 2.13 (m, 8H), 1.93 – 1.80 (m, 4H). ^{13}C NMR (101 MHz, D_2O) δ 178.5, 177.6, 173.0, 172.6, 69.9, 69.8, 69.2, 52.0, 49.7, 49.6, 39.3, 39.0, 37.2, 34.6, 29.4, 29.4, 29.1, 23.2, 22.5.

BiAn(6000) : PEG(6k)-[dG$_2$-(AXO)$_8$]$_2$ (36)

This was obtained by following general procedure F. **Compound 35** (100 mg, 0.0103 mmol) and AX (128 mg, 0.554 mmol) were reacted. The reaction was refreshed with 27 mg of AX on three different occasions. After purification, the product was collected as yellowish powder with 48 % of yield. ^{1}H NMR (400 MHz, D_2O) δ 7.27 (d, J = 7.8 Hz, 32H), 6.86 (d, J = 7.8 Hz, 32H), 4.97 (d, J = 8.0 Hz, 16H), 4.59 (s, 16H), 4.26 (d, J = 8.0 Hz, 16H), 3.79 – 3.67 (m, 560H), 3.56 – 3.50 (m,8H), 3.35 (s,16H), 3.33 – 3.12 (m, 88H), 3.10 – 2.99 (m, 8H), 2.90 – 2.70 (m, 56H), 2.66 – 2.49 (m, 30H), 2.45 – 2.27 (m, 56H), 2.18 –2.07 (m, 8H),1.97– 1.70 (m,4H), 1.47 (s, 48H), 1.20 (s, 48H). ^{13}C NMR (101 MHz, D_2O) δ 175.2, 174.7, 171.8, 161.0, 156.5, 129.8, 128.9, 116.3, 74.9, 69.9, 69.8, 65.0, 59.7, 59.2, 58.4, 51.6, 49.3, 38.8, 37.0, 33.0, 29.1, 27.9, 27.0, 23.9, 23.0.

PEG (8k) -(Ts)$_2$ (37)

Synthesized according to general procedure A. PEG (MW~ 8000 Da) (10 g, 1.25 mmol), CH_2Cl_2 (30 mL), TsCl (710 mg, 3.75 mmol) and KOH (210 mg, 3.75 mmol) were used in the reaction. The crude product was purified by column chromatography using CH_2Cl_2: MeOH (7:1 v/v) as an eluting solvent to obtain a white solid product with 86 % yield. ^{1}H NMR (400 MHz, $CDCl_3$) δ 7.76 (d, J = 8.2 Hz, 2H), 7.33 (d, J = 8.2 Hz, 2H), 4.14 (t, J = 5.6 Hz, 4H), 3.76 – 3.51 (m, 746H), 2.42(s, 6H).^{13}C NMR (101 MHz, $CDCl_3$) δ 144.6, 133.0, 129.8, 127.8, 70.6, 69.2, 68.7, 21.7.

PEG (8k) -$(N_3)_2$ (38)

This was obtained according to general procedure B. **Compound 37** (8.8 g, 1.06 mmol), 50 mL of distilled H_2O: THF (80:20 %v/v) and NaN_3 (210 mg, 3.18 mmol) were used in the reaction. As a final point, the product was purified by silica gel column chromatography using (7:1 v/v) CH_2Cl_2: MeOH as an eluent to obtain a white powder with 8 % of yield. ^{1}H NMR (400 MHz, $CDCl_3$) δ 3.68 – 3.44 (m, 746H), 3.27 (t, J = 5.1 Hz, 4H). ^{13}C NMR (101 MHz, $CDCl_3$) δ 70.4, 69.9, 50.5.

PEG (8k) -$(NH_2)_2$ (39)

This was obtained according to general procedure C. using **Compound 38** (200 mg, 0.025 mmol), 15 mL of MeOH and Pd/C (40 mg). The reaction was stirred for 72 h to obtain a product with 85 % of yield. ^{1}H NMR (400 MHz, $CDCl_3$) δ 3.78 – 3.57 (m, 746H), 3.46 (t, J = 5.2 Hz, 4H), 2.87 (t, J = 5.2 Hz, 4H), 1.83(s, 4H). ^{13}C NMR (101 MHz, $CDCl_3$) δ 73.6, 70.6, 69.9, 41.7.

PEG (8k) -(maleimide)$_2$ (40)

This is synthesized according to general procedure D. **Compound 1** (5 mg, 0.0275 mmol), NMM (7 mg, 0.0616 mmol), ^{i}BuCOCl (8 mg, 0.0616 mmol.) and **Compound 39** (100 mg, 0.0125 mmol) and 15 mL CH_2Cl_2 were used to obtain a white solid product with 68 % of yield. ^{1}H NMR (400 MHz, $CDCl_3$) δ 6.70 (s, 4H), 6.32 (s, 2H), 3.80 – 3.52 (m, 746H), 3.62-3.53 (m,8H), 3.48 (t, J = 5.2 Hz, 4H), 2.33(t, J = 7.2 Hz, 4H), 1.98 – 1.83 (m, 4H).^{13}C NMR (101 MHz, $CDCl_3$) δ 171.8, 170.9, 134.2, 70.6, 70.3, 70.0, 39.1, 37.2, 33.4, 24.7.

PEG (8k)-[dG_2]$_2$ (41)

This was synthesized according to general procedure E. Using G_2 (31 mg, 0.0092 mmol), 5 mL of PBS (1x, pH 6.5), TCEP (24 mg, 0.084 mmol), **Compound 40** (70 mg, 0.0084 mmol) dissolved in 5 mL of H_20 and few drops of DMSO. The purification was performed gel filtration chromatography using PD MidiTrap G-25 columns. The product was isolated as white powder with 57 % yield. ^{1}H NMR (400 MHz, D_2O) δ 3.75 – 3.69 (m, 746H), 3.68– 3.61 (m, 8H), 3.59– 3.25 (m, 88H), 3.18 (t, J = 6.0 Hz, 8H), 2.92 – 2.80 (m, 56H), 2.79 – 2.69 (m, 30H), 2.61 – 2.47 (m, 56H), 2.23– 2.14 (m, 8H), 1.96 – 1.81 (m, 4H). ^{13}C NMR (101 MHz, D_2O) δ

178.3, 177.5, 172.6, 172.2, 69.7, 69.6, 69.0, 51.8, 49.7, 49.4, 39.1, 38.8, 36.9, 34.4, 29.2, 29.2, 28.9, 23.0, 22.3, 15.5, 15.0.

BiAn(8000) : PEG(8k)-[dG$_2$-(AXO)$_8$]$_2$ (42)

This was obtained by following general procedure F. **Compound 41** (47 mg, 0.004 mmol) and AX (50 mg, 0.129 mmol) were reacted. The reaction was refreshed with 10 mg of AX on three different occasions. After purification, the product was collected as yellowish powder with 45 % of yield. ^{1}H NMR (400 MHz, D_2O) δ 7.31 (d, J = 7.8 Hz, 32H), 6.87 (d, J = 7.8 Hz, 32H), 4.94 (d, J = 8.0 Hz, 16H), 4.62 (s, 16H), 4.29 (d, J = 8.0 Hz, 16H), 3.80 – 3.61 (m, 746H), 3.56 – 3.44 (m, 8H), 3.34(s, 16H), 3.32 – 3.05 (m, 88H), 3.14 – 3.02 (m, 8H), 2.90 – 2.71 (m, 56H), 2.68 – 2.50 (m, 30H), 2.47 – 2.26 (m, 56H), 2.18 –2.08 (m, 8H),1.90– 1.72(m,4H), 1.46 (s, 48H), 1.19 (s, 48H). ^{13}C NMR (101 MHz, D_2O) δ 175.1, 175.0, 174.6, 171.6, 160.9, 156.3, 129.7, 128.8, 116.2, 74.8, 69.8, 69.6, 69.6, 64.9, 59.5, 59.0, 58.2, 51.3, 49.1, 39.4, 38.8, 36.9, 32.8, 28.9, 26.8, 23.7, 23.1.

PEG (10k) -(Ts)$_2$ (43)

Synthesized according to general procedure A. PEG (MW~ 10000 Da) (10 g, 1 mmol), CH_2Cl_2 (30mL), TsCl (570 mg, 3 mmol) and KOH (168 mg, 3 mmol) were used in the reaction. The crude product was purified by column chromatography using CH_2Cl_2: MeOH (6:1 v/v) as an eluting solvent to obtain a white solid product with 71 % yield. ^{1}H NMR (400 MHz, $CDCl_3$) δ 7.80 (d, J = 8.2 Hz, 2H), 7.32 (d, J = 8.2 Hz, 2H), 4.14 (t, J = 5.6 Hz, 4H), 3.74 – 3.45 (m, 933H), 2.44(s, 6H).^{13}C NMR (101 MHz, $CDCl_3$) δ 144.9, 133.1, 129.9, 128.1, 70.6, 69.3, 68.7, 21.8.

PEG (10k) -(N$_3$)$_2$ (44)

This was obtained according to general procedure B. **Compound 43** (7.2 g, 0.7 mmol), 50 mL of distilled H_2O: THF (80:20 %v/v) and NaN_3 (136 mg, 2.1 mmol) were used in the reaction. As a final point, the product was purified by silica gel column chromatography using (6:1 v/v) CH_2Cl_2: MeOH as an eluent to obtain a white powder with 90 % of yield. ^{1}H NMR (400 MHz, $CDCl_3$) δ 3.62 – 3.41 (m, 933H), 3.27 (t, J = 5.1 Hz, 4H).^{13}C NMR (101 MHz, $CDCl_3$) δ 70.2, 69.7, 50.3.

PEG (10k) -$(NH_2)_2$ (45)

This was obtained according to general procedure C. Using **Compound 44** (100 mg, 0.00995 mmol), 15 mL of MeOH, and Pd/C (20 mg). The reaction was stirred for 96 h to obtain a product with 84 %. ^{1}H NMR (400 MHz, $CDCl_3$) δ 3.74 – 3.58 (m, 933H), 3.45 (t, J = 5.2 Hz, 4H), 2.87 (t, J = 5.2 Hz, 4H), 1.78 (s, 4H). ^{13}C NMR (101 MHz, $CDCl_3$) δ 73.6, 70.6, 69.9, 41.9.

PEG (10k) -(maleimide)$_2$ (46)

This is synthesized according to general procedure D. **Compound 1** (4 mg, 0.021 mmol), NMM (6 mg, 0.0475 mmol), ^{i}BuCOCl (7 mg, 0.0475 mmol.) and **Compound 45** (94 mg, 0.0094 mmol) and 15 mL CH_2Cl_2 were used to obtain a white solid product with 55 % of yield. ^{1}H NMR (400 MHz, $CDCl_3$) δ 6.70 (s, 4H), 6.32 (s, 2H), 3.79 – 3.61 (m, 933H), 3.62-3.53 (m,8H), 3.47 (t, J = 5.2 Hz, 4H), 2.33 (t, J = 7.2 Hz, 4H), 1.99 – 1.87 (m, 4H).^{13}C NMR (101 MHz, $CDCl_3$) δ 172.01, 170.9, 134.2,70.7, 70.3, 70.0, 39.3, 37.2, 33.4, 24.9.

PEG (10k)-[dG$_2$]$_2$ (47)

This was synthesized according to general procedure E. Using G_2 (18 mg, 0.0055 mmol), 5 mL of PBS (1x, pH 6.5), TCEP (16 mg, 0.055 mmol), **Compound 46** (52 mg, 0.0084 mmol) dissolved in 5 mL of H_20 and few drops of DMSO. The purification was performed gel filtration chromatography using PD MidiTrap G-25 columns. The product was isolated as white powder with 60 % yield.^{1}H NMR (400 MHz, D_2O) δ 3.74 – 3.69 (m, 993H), 3.68– 3.61 (m, 8H), 3.58– 3.28 (m, 88H), 3.18 (t, J = 6.0 Hz, 8H), 2.91 – 2.82 (m, 56H), 2.80 – 2.69 (m, 30H), 2.61 – 2.46 (m, 56H), 2.25– 2.14 (m, 8H), 1.93 – 1.81 (m, 4H). ^{13}C NMR (101 MHz, D_2O) δ 178.2, 178.1, 172.8, 172.5, 69.8, 69.8, 69.5, 51.9, 49.7, 49.6, 39.1, 39.1, 38.9, 38.9, 34.4, 29.2, 29.2, 28.9, 23.03, 22.3.

BiAn(10000) : PEG (10k)-[dG$_2$-(AXO)$_8$]$_2$ (48)

This was obtained by following general procedure F. Using **Compound 47** (40 mg, 0.0029 mmol) and AX (36 mg, 0.095 mmol) were reacted. The reaction was refreshed with 7 mg of AX on three different occasions. After purification, the product was collected as yellowish powder with 45 % of yield. ^{1}H NMR (400 MHz, D_2O) δ 7.29 (d, J = 7.8 Hz, 32H), 6.89 (d, J

= 7.8 Hz, 32H), 4.94 (d, *J* = 8.0 Hz, 16H), 4.63 (s, 16H), 4.29 (d, *J* = 8.0 Hz, 16H), 3.88 – 3.57 (m, 993H), 3.56 – 3.51(m, 8H), 3.34(s,16H), 3.32 – 3.05 (m, 88H), 3.12 – 3.03 (m, 8H), 2.89 – 2.69 (m, 56H), 2.66 – 2.51 (m, 30H), 2.48 – 2.26 (m, 56H), 2.18 –2.06 (m, 8H),1.90– 1.77 (m,4H), 1.46 (s, 48H), 1.19 (s, 48H). ^{13}C NMR (101 MHz, D_2O) δ 175.1, 174.6, 171.6, 160.7, 156.3, 129.7, 128.9, 116.2, 74.8, 69.8, 64.9, 59.6, 59.0, 58.1, 51.4, 49.3, 49.2, 39.4, 38.6, 36.9, 32.9, 28.9, 26.8, 26.7, 23.99, 23.0.

PEG (12k) -$(Ts)_2$ (49)

Synthesized according to general procedure A. PEG (MW~ 12000 Da) (10 g, 0.83 mmol), CH_2Cl_2 (30 mL), TsCl (480 mg, 2.5 mmol) and KOH (140 mg, 2.5 mmol) were used in the reaction. The crude product was purified by column chromatography using CH_2Cl_2: MeOH (5:1 v/v) as an eluting solvent to obtain a white solid product with 70 % yield. ^{1}H NMR (400 MHz, $CDCl_3$) δ 7.79 (d, *J* = 8.2 Hz, 2H), 7.32 (d, *J* = 8.2 Hz, 2H), 4.14 (t, *J* = 5.6 Hz, 4H), 3.78 – 3.49 (m, 1120H), 2.43(s, 6H). ^{13}C NMR (101 MHz, $CDCl_3$) δ 144.8, 133.5, 129.9, 128.1, 70.6, 69.3, 68.7, 21.6.

PEG (12k) -$(N_3)_2$ (50)

This was obtained according to general procedure B. **Compound 49** (7.2 g, 0.585 mmol), 50 mL of distilled H_2O: THF (80:20 %v/v) and NaN_3 (114 mg, 1.75 mmol) were used in the reaction. As a final point, the product was purified by silica gel column chromatography using (5:1 v/v) CH_2Cl_2: MeOH as an eluent to obtain a white powder with 81 % of yield. ^{1}H NMR (400 MHz, $CDCl_3$) δ 3.73 – 3.44 (m, 1120H), 3.34 (t, *J* = 5.1 Hz, 4H).^{13}C NMR (101 MHz, $CDCl_3$) δ 70.5, 70.0, 50.6.

PEG (12k) -$(NH_2)_2$ (51)

This was obtained according to general procedure C. Using **Compound 50** (100 mg, 0.0083 mmol), 15 mL of MeOH, and Pd/C (20 mg). The reaction was stirred for 5 days to obtain a product with 96 %. ^{1}H NMR (400 MHz, $CDCl_3$) δ 3.74 – 3.58 (m, 1120H), 3.45 (t, *J* = 5.2 Hz, 4H), 2.87 (t, *J* = 5.2 Hz, 4H), 1.78 (s, 4H). ^{13}C NMR (101 MHz, $CDCl_3$) δ 73.6, 70.6, 69.9, 41.9

PEG (12k) -(maleimide)$_2$ (52)

This is synthesized according to general procedure D. **Compound 1** (3 mg, 0.0174 mmol), NMM (2 mg, 0.0182 mmol), ^{i}BuCOCl (3 mg, 0.0182 mmol.) and **Compound 52** (95 mg, 0.0079 mmol) and 15 mL CH_2Cl_2 were used to obtain a white solid product with 58 % of yield. ^{1}H NMR (400 MHz, $CDCl_3$) δ 6.70 (s, 4H), 6.32 (s, 2H), 3.79 – 3.61 (m, 1120H), 3.62-3.53 (m,8H), 3.47 (t, J = 5.2 Hz, 4H), 2.33 (t, J = 7.2 Hz, 4H), 1.99 – 1.87 (m, 4H). ^{13}C NMR (101 MHz, $CDCl_3$) δ 172.0, 170.9, 134.2,70.7, 70.3, 70.0, 39.3, 37.2, 33.4, 24.9.

PEG (12k)-[dG$_2$]$_2$ (53)

This was synthesized according to general procedure E.G_2 (30 mg, 0.0089 mmol), 5 mL of PBS (1x, pH 6.5), TCEP (26 mg, 0.089 mmol), **Compound 52** (100 mg, 0.0081 mmol) dissolved in 5 mL of H_20 and few drops of DMSO. The purification was performed gel filtration chromatography using PD MidiTrap G-25 columns. The product was isolated as white powder with 51% yield. ^{1}H NMR (400 MHz, D_2O) δ 3.81 – 3.61 (m, 1120H), 3.66– 3.60 (m, 8H), 3.58– 3.25 (m, 88H), 3.17 (t, J = 6.0 Hz, 8H), 2.91 – 2.82 (m, 56H), 2.80 – 2.69 (m, 30H), 2.61 – 2.46 (m, 56H), 2.23– 2.14 (m, 8H), 1.92 – 1.81 (m, 4H). ^{13}C NMR (101 MHz, D_2O) δ 179.17, 178.95, 172.84, 172.84, 172.42, 77.48, 77.16, 77.16, 76.84, 69.8, 69.8, 51.9, 49.7, 49.5, 39.1, 38.9, 37.0, 34.4, 30.4, 28.9, 27.7, 22.8, 22.1.

BiAn(12000) : PEG (12k)-[dG$_2$-(AXO)$_8$]$_2$ (54)

This was obtained by following general procedure F. **Compound 53** (64 mg, 0.0041 mmol) and AX (51 mg, 0.131 mmol) were reacted. The reaction was refreshed with 10 mg of AX on three different occasions. After purification, the product was collected as yellowish powder with 54 % of yield. ^{1}H NMR (400 MHz, D_2O) δ 7.29 (d, J = 7.8 Hz, 32H), 6.89 (d, J = 7.8 Hz, 32H), 4.94 (d, J = 8.0 Hz, 16H), 4.63 (s, 16H), 4.29(d, J = 8.0 Hz, 16H), 3.88 – 3.57 (m, 1120H), 3.56 – 3.51(m,8H), 3.34(s,16H), 3.32 – 3.05 (m, 88H), 3.12 – 3.03 (m, 8H), 2.89 – 2.69 (m, 56H), 2.66 – 2.51 (m, 30H), 2.48 – 2.26 (m, 56H), 2.18 –2.06 (m, 8H),1.90– 1.77 (m,4H), 1.46 (s, 48H), 1.19 (s, 48H). ^{13}C NMR (101 MHz, D_2O) δ 175.6, 175.1, 174.6, 171.6, 156.2, 129.7, 128.8, 115.9, 77.1, 74.9, 69.8, 69.6, 68.9, 64.9, 59.5, 59.1, 58.2, 39.4, 38.9, 38.7, 36.9, 36.9, 32.7, 28.9, 28.2, 26.8, 23.6, 23.0.

7.7.4. Synthesis of Chapter 5: BiAns-dGn

General Procedure for Click Reactions

PEG-$(N_3)_2$ (1 equiv), alkyne compounds (1.1 equiv per azido group), copper (II) sulphate 5-hydrate (0.2 equiv per azido group) were dissolved in 2 mL of H_2O:THF (1:1). L(+)-ascorbic acid sodium salt (0.4 equiv per azido group) was added to the solution and the mixture was stirred overnight at room temperature. The completion of the reaction was confirmed by monitoring the IR spectra of the azide moieties. The resulting mixture was diluted to 5mL and 50mg/mL of QuadraSil® TA metal scavenger was added and agitated for 1 hr. The scavenger was removed by filtration and the products were purified by size exclusion chromatography using PD MidiTrap G-10 and G-25.

General Procedure for the functionalization of the Structures with AX

The functionalization of amino terminals with the AX was obtained by dissolving the starting materials in the carbonate buffer (0.05 M, pH 10.2), adding an excess of AX (2 equiv. per NH_2 group) and incubating overnight and 7 days at 4 °C under magnetic stirring for the monomer and dendrons-based synthesis, respectively. The reactions were refreshed by 20 % the initial mass of AX on two different occasions. The products were purified by Sephadex PD MidiTrap G-10 column

7.7.4.1. BiAn-dG0

PEG (600) -(*m*)$_2$ (55)

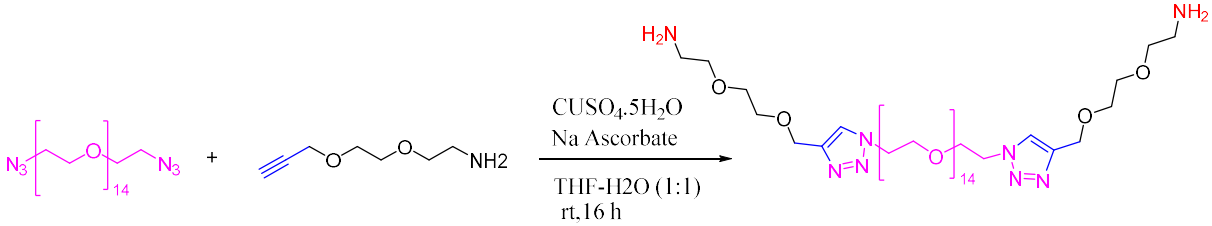

PEG (600)-$(N_3)_2$ (50 mg, 0.077 mmol), Alkyne-PEG2-Amine (25 mg, 0.177 mmol), $CUSO_4.5H_2O$ (8 mg, 0.031 mmol), and L(+) - ascorbic acid sodium salt (12 mg, 0.062 mmol) in 2 mL(1:1) THF-H_2O were used to perform the click reaction. The solvents were removed under reduced pressure. The concentrate was dissolved in 2 mL H_2O and purified using PD MidiTrap G-10 by collecting in small fractions. The eluent was lyophilized to obtain a

yellowish semisolid product with 74 % yield. ^{1}H NMR (400 MHz, D_2O) δ 8.12 (s, 2H), 4.72 (s, 4H), 4.67 (t, J = 5.0 Hz, 4H), 4.00 (t, J = 5.0 Hz, 4H), 3.81 – 3.58 (m, 56H), 3.52 (t, J = 5.0 Hz, 1H), 3.20 (t, J = 5.0 Hz, 4H). ^{13}C NMR (101 MHz, D_2O) δ 144.0, 125.6, 71.9, 69.9, 69.5, 69.2, 69.0, 63.2, 60.6, 50.3, 39.4.

BiAn-G0(600) : PEG (600) -(*m*-(AXO)$_1$)$_2$ (56)

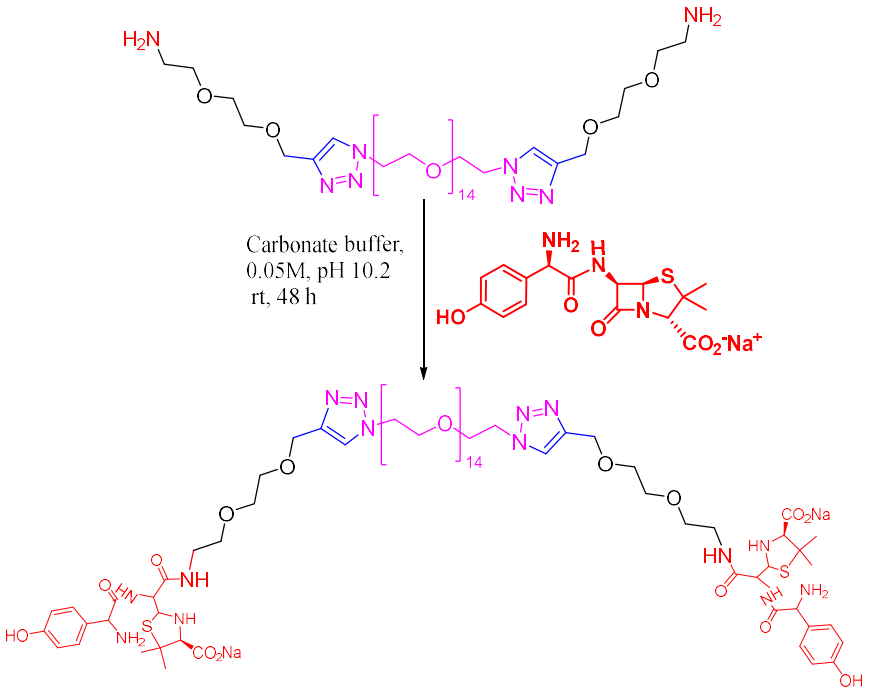

Following general procedure for the functionalization with AX **, Compound 55** (74 mg, 0.008 mmol) was dissolved in 2 mL of carbonate buffer (0.05 M, pH 10.2), adding an excess of AX (4 equiv, 122 mg) and stirring at room temperature for 48 h. The purification was performed by PD MidiTrap G-10 to obtain a yellowish powder with 62 % of yield .^{1}H NMR (400 MHz, D_2O) δ 8.12 (s, 2H), 7.24 (d, J = 7.8 Hz, 4H), 6.83 (d, J = 7.8 Hz, 4H), 4.91 (d, J = 8.0 Hz, 2H), 4.72 (s, 4H), 4.67 (t, J = 5.0 Hz, 4H), 4.29 (s, 2H), 4.25 (d, J = 8.0 Hz, 2H), 4.00 (t, J = 5.0 Hz, 4H), 3.81 – 3.58 (m, 58H), 3.52 (t, J = 5.0 Hz, 1H), 3.20 (t, J = 5.0 Hz, 4H), 1.41 (s, 6H), 1.14 (s, 6H). ^{13}C NMR (101 MHz, D_2O) δ 174.8, 172.3, 171.0, 156.2, 144.2, 129.7, 125.6, 116.2, 77.5, 76.8, 70.7, 69.8, 69.7, 69.4, 68.9, 65.1, 63.0, 60.6, 59.7, 6.6, 50.4, 50.2, 38.9, 26.8.

PEG (1k) -(*m*)$_2$ (57)

PEG (1k)-(N_3)$_2$ (50 mg, 0.048 mmol), Alkyne-PEG2-Amine (16 mg, 0.11 mmol), $CUSO_4.5H_2O$ (5 mg, 0.019 mmol), and L(+)-ascorbic acid sodium salt (8 mg, 0.038 mmol) in

2 mL(1:1) THF-H_2O were used to perform the click reaction. The solvents were removed under reduced pressure. The concentrate was dissolved in 2 mL H_2O and purified PD MidiTrap G-10. The eluent was lyophilized to obtain a yellowish powder with 70 % yield. ^{1}H NMR (400 MHz, D_2O) δ 8.14 (s, 2H), 4.74 (s, 4H), 4.67 (t, J = 5.0 Hz, 4H), 4.00 (t, J = 5.0 Hz, 4H), 3.85 – 3.58 (m, 93H), 3.52 (t, J = 5.0 Hz, 1H), 3.20 (t, J = 5.0 Hz, 4H). ^{13}C NMR (101 MHz, D_2O) δ 144.0, 125.8, 72.0, 69.7, 69.5, 69.2, 69.0, 66.6, 63.2, 60.6, 50.3, 39.4.

BiAn-G0(1000) : PEG (1k) -(*m*-(AXO)$_1$)$_2$ (58)

Following general procedure for the functionalization with AX**, Compound 57** (61mg, 0.079 mmol) was dissolved in 2 mL of carbonate buffer (0.05 M, pH 10.2), adding an excess of AX (4 equiv,71 mg) and stirring at room temperature 48 h. The purification was performed by PD MidiTrap G-10 to obtain a yellowish powder with 62 % of yield. ^{1}H NMR (400 MHz, D_2O) δ 8.10 (s, 2H), 7.31 (d, J = 7.8 Hz, 4H), 6.92 (d, J = 7.8 Hz, 4H), 4.91 (d, J = 8.0 Hz, 2H), 4.72 (s, 4H), 4.67 (t, J = 5.0 Hz, 4H), 4.29 (s, 2H), 4.25 (d, J = 8.0 Hz, 2H), 4.00 (t, J = 5.0 Hz, 4H), 3.81 – 3.58 (m, 95H), 3.52 (t, J = 5.0 Hz, 1H), 3.20 (t, J = 5.0 Hz, 4H),1.48 (s, 6H), 1.21(s, 6H).^{13}C NMR (101 MHz, D_2O) δ 174.8, 172.2, 171.2, 156.3, 144.0, 129.5, 128.6, 125.49, 116.0, 74.5, 71.8, 69.6, 69.5, 69.3, 69.0, 68.8, 64.6, 63.1, 60.4, 50.2, 50.1, 38.9, 26.6.

PEG (2k) -(*m*)$_2$ (59)

PEG (2k)-$(N_3)_2$ (50 mg, 0.024 mmol), Alkyne-PEG2-Amine (8 mg, 0.056 mmol), $CUSO_4.5H_2O$ (2.4 mg, 0.01 mmol), and L(+)-ascorbic acid sodium salt (3.9 mg, 0.02 mmol) in 2 mL(1:1) THF-H_2O were used to perform the click reaction. The solvents were removed under reduced pressure. The concentrate was dissolved in 2 mL H_2O and purified using PD MidiTrap G-10 by collecting in small fractions. The eluent was lyophilized to obtain a yellowish powder with 75 % yield.^{1}H NMR (400 MHz, D_2O) δ 8.14 (s, 2H), 4.74 (s, 4H), 4.68 (t, J = 5.0 Hz, 4H), 4.02 (t, J = 5.0 Hz, 4H), 3.82 – 3.62 (m, 186H), 3.50 (t, J = 5.0 Hz, 1H), 3.24 (t, J = 5.0 Hz, 4H). ^{13}C NMR (101 MHz, D_2O) δ 144.0, 125.8, 72.0, 69.7, 69.5, 69.2, 69.0, 66.6, 63.2, 60.6, 50.3, 39.4.

BiAn-G0(2000) : PEG (2k) -(*m*-(AXO)$_1$)$_2$ (60)

Following general procedure for the functionalization with AX**, Compound 59** (59 mg, 0.025 mmol) was in 2 mL of carbonate buffer (0.05 M, pH 10.2), adding an excess of AX (4 equiv,

39 mg) and stirring at room temperature 48 h. The purification was performed by PD MidiTrap G-10 to obtain a yellowish powder with 62 % of yield. ^{1}H NMR (400 MHz, D_2O) δ 8.12 (s, 2H), 7.32 (d, J = 7.8 Hz, 4H), 6.93 (d, J = 7.8 Hz, 4H), 4.99 (d, J = 8.0 Hz, 2H), 4.72 (s, 4H), 4.67 (t, J = 5.0 Hz, 4H), 4.29 (s, 2H), 4.25 (d, J = 8.0 Hz, 2H), 4.00 (t, J = 5.0 Hz, 4H), 3.81 – 3.58 (m, 188H), 3.52 (t, J = 5.0 Hz, 1H), 3.20 (t, J = 5.0 Hz, 4H),1.48 (s, 6H), 1.21(s, 6H). ^{13}C NMR (101 MHz, D_2O) δ 175.7, 175.2, 171.4, 156.0, 144.2, 129.4, 128.5, 125.6, 116.0, 72.0, 68.97, 63.2, 60.4, 59.4, 50.3, 39.4, 26.6.

PEG (4k) -(*m*)$_2$ (61)

PEG (4k)-(N_3)$_2$ (50 mg, 0.012 mmol), Alkyne-PEG2-Amine (4 mg, 0.028 mmol), $CUSO_4.5H_2O$ (1.2 mg, 0.005 mmol), and L(+)-ascorbic acid sodium salt (2 mg, 0.01 mmol) in 2 mL(1:1) THF-H_2O were used to perform the click reaction. The solvents were removed under reduced pressure. The concentrate was dissolved in 2 mL H_2O and purified using PD MidiTrap G-10 by collecting in small fractions. The eluent was lyophilized to obtain a yellowish powder with 85 % yield. ^{1}H NMR (400 MHz, D_2O) δ 8.14 (s, 2H), 4.74 (s, 4H), 4.68 (t, J = 5.0 Hz, 4H), 4.02 (t, J = 5.0 Hz, 4H), 3.82 – 3.62 (m, 373H), 3.50 (t, J = 5.0 Hz, 1H), 3.24 (t, J = 5.0 Hz, 4H). ^{13}C NMR (101 MHz, D_2O) δ 144.0, 125.5, 72.0, 69.7, 69.5, 69.2, 69.0, 66.6, 63.2, 60.6, 50.3, 39.4.

BiAn-G0(4000) : PEG (4k) -(*m*-(AXO)$_1$)$_2$ (62)

Following general procedure for the functionalization with AX **, Compound 61** (55 mg, 0.013 mmol) was dissolved in 2 mL of carbonate buffer (0.05 M, pH 10.2), adding an excess of AX (4 equiv, 20 mg) and stirring at room temperature 48 h. The purification was performed by PD MidiTrap G-10 to obtain a yellowish powder with 62 % of yield. ^{1}H NMR (400 MHz, D_2O) δ 8.11 (s, 2H), 7.30 (d, J = 7.8 Hz, 4H), 6.92 (d, J = 7.8 Hz, 4H), 4.99 (d, J = 8.0 Hz, 2H), 4.73 (s, 4H), 4.67 (t, J = 5.0 Hz, 4H), 4.29 (s, 2H), 4.21 (d, J = 8.0 Hz, 2H), 4.01 (t, J = 5.0 Hz, 4H), 3.81 – 3.58 (m, 375H), 3.52 (t, J = 5.0 Hz, 1H), 3.20 (t, J = 5.0 Hz, 4H),1.48 (s, 6H), 1.21(s, 6H). ^{13}C NMR (101 MHz, D_2O) δ 175.7, 175.2, 171.4, 156.0, 144.2, 129.4, 128.5, 125.6, 116.0, 72.0, 68.97, 63.2, 60.4, 59.4, 50.3, 39.4, 26.6.

PEG (6k) -(*m*)$_2$ (63)

PEG (6k)-$(N_3)_2$ (50 mg, 0.008 mmol), Alkyne-PEG2-Amine (2.7 mg, 0.019 mmol), $CUSO_4.5H_2O$ (0.8 mg, 0.003 mmol), and L(+)-ascorbic acid sodium salt(1.3 mg, 0.007 mmol) in 2 mL(1:1) THF-H_2O were used to perform the click reaction. The solvents were removed under reduced pressure. The concentrate was dissolved in 2 mL H_2O and purified using PD MidiTrap G-10 by collecting in small fractions. The eluent was lyophilized to obtain a yellowish powder with 74 % yield.^{1}H NMR (400 MHz, D_2O) δ 8.15 (s, 2H), 4.74 (s, 4H), 4.69 (t, J = 5.0 Hz, 4H), 4.02 (t, J = 5.0 Hz, 4H), 3.94 – 3.61 (m, 560H), 3.49 (t, J = 5.0 Hz, 1H), 3.26 (t, J = 5.0 Hz, 4H). ^{13}C NMR (101 MHz, D_2O) δ 144.0, 125.5, 71.7, 69.6, 69.5, 69.2, 68.8, 66.4, 63.0, 60.4, 50.1, 39.2.

BiAn-G0(6000) : PEG (6k) -(*m*-(AXO)$_1$)$_2$ (64)

Following general procedure for the functionalization with AX **, Compound 63** (44 mg, 0.007 mmol) was dissolved in 2 mL of carbonate buffer (0.05 M, pH 10.2), adding an excess of AX (4 equiv, 11 mg) and stirring at room temperature 48 h. The purification was performed by PD MidiTrap G-10 to obtain a yellowish powder with 62 % of yield.^{1}H NMR (400 MHz, D_2O) δ 8.14 (s, 2H), 7.36 (d, J = 7.8 Hz, 4H), 6.94 (d, J = 7.8 Hz, 4H), 4.99 (d, J = 8.0 Hz, 2H), 4.73 (s, 4H), 4.68 (t, J = 5.0 Hz, 4H), 4.29 (s, 2H), 4.21 (d, J = 8.0 Hz, 2H), 4.01 (t, J = 5.0 Hz, 4H), 3.81 – 3.58 (m, 562H), 3.52 (t, J = 5.0 Hz, 1H), 3.20 (t, J = 5.0 Hz, 4H),1.48 (s, 6H), 1.22(s, 6H).^{13}C NMR (101 MHz, D_2O) δ 175.7, 175.2, 171.4, 156.0, 144.2, 129.4, 128.5, 125.6, 116.0, 72.0, 68.97, 63.2, 60.4, 59.4, 50.3, 39.4, 26.6.

PEG (8k) -(*m*)$_2$ (65)

PEG (8k)-$(N_3)_2$ (50 mg, 0.006 mmol), Alkyne-PEG2-Amine (2 mg, 0.014 mmol), $CUSO_4.5H_2O$ (0.6 mg, 0.002 mmol), and L(+)-ascorbic acid sodium salt (1 mg, 0.005 mmol) in 2 mL(1:1) THF-H_2O were used to perform the click reaction. The solvents were removed under reduced pressure. The concentrate was dissolved in 2 mL H_2O and purified using PD MidiTrap G-10 by collecting in small fractions. The eluent was lyophilized to obtain a yellowish powder with 67 % yield.^{1}H NMR (400 MHz, D_2O) δ 8.14 (s, 2H), 4.74 (s, 4H), 4.67 (t, J = 5.0 Hz, 4H), 4.02 (t, J = 5.0 Hz, 4H), 3.94 – 3.61 (m, 746H), 3.49 (t, J = 5.0 Hz, 1H), 3.26 (t, J = 5.0 Hz, 4H). ^{13}C NMR (101 MHz, D_2O) δ 144.0, 125.5, 71.7, 69.6, 69.5, 69.2, 68.8, 66.4, 63.0, 60.4, 50.1, 39.2.

BiAn-G0(8000) : PEG (8k) -(*m*-(AXO)$_1$)$_2$ (66)

Following general procedure for the functionalization with AX**, Compound 65** (43 mg, 0.005 mmol) in 2 mL of carbonate buffer (0.05 M, pH 10.2), adding an excess of AX (4 equiv, 8 mg) and stirring at room temperature 48 h. The purification was performed by PD MidiTrap G-10 to obtain a yellowish powder with 62 % of yield. ^{1}H NMR (400 MHz, D_2O) δ 8.14 (s, 2H), 7.33 (d, J = 7.8 Hz, 4H), 6.92 (d, J = 7.8 Hz, 4H), 4.99 (d, J = 8.0 Hz, 2H), 4.73 (s, 4H), 4.68 (t, J = 5.0 Hz, 4H), 4.29 (s, 2H), 4.21 (d, J = 8.0 Hz, 2H), 4.01 (t, J = 5.0 Hz, 4H), 3.81 – 3.58 (m, 748H), 3.52 (t, J = 5.0 Hz, 1H), 3.20 (t, J = 5.0 Hz, 4H),1.48 (s, 6H), 1.22(s, 6H).^{13}C NMR (101 MHz, D_2O) δ 175.7, 175.2, 171.4, 156.0, 144.2, 129.4, 128.5, 125.6, 116.0, 72.0, 68.97, 63.2, 60.4, 59.4, 50.3, 39.4, 26.6.

PEG (10k) -(*m*)$_2$ (67)

PEG (10k)-(N_3)$_2$ (50 mg, 0.005 mmol), Alkyne-PEG2-Amine (1.6 mg, 0.011 mmol), $CUSO_4.5H_2O$ (0.5 mg, 0.002 mmol), and L(+)-ascorbic acid sodium salt(0.8 mg, 0.004 mmol) in 2 mL(1:1) THF-H_2O were used to perform the click reaction. The solvents were removed under reduced pressure. The concentrate was dissolved in 2 mL H_2O and purified using PD MidiTrap G-10 by collecting in small fractions. The eluent was lyophilized to obtain a yellowish powder with 70 % yield. ^{1}H NMR (400 MHz, D_2O) δ 8.14 (s, 2H), 4.74 (s, 4H), 4.67 (t, J = 5.0 Hz, 4H), 4.02 (t, J = 5.0 Hz, 4H), 3.94 – 3.61 (m, 933H), 3.49 (t, J = 5.0 Hz, 1H), 3.26 (t, J = 5.0 Hz, 4H). ^{13}C NMR (101 MHz, D_2O) δ 144.0, 125.5, 71.7, 69.6, 69.5, 69.2, 68.8, 66.4, 63.0, 60.4, 50.1, 39.2.

BiAn-G0(10000) : PEG (10k) -(*m*-(AXO)$_1$)$_2$ (68)

Following general procedure for the functionalization with AX **, Compound 67** (45 mg, 0.004 mmol) was dissolved in 2 mL of carbonate buffer (0.05 M, pH 10.2), adding an excess of AX (4 equiv, 7 mg) and stirring at room temperature overnight. The purification was performed by PD MidiTrap G-10 to obtain a yellowish powder with 62 % of yield.^{1}H NMR (400 MHz, D_2O) δ 8.14 (s, 2H), 7.33 (d, J = 7.8 Hz, 4H), 6.92 (d, J = 7-8 Hz, 4H), 4.99 (d, J = 8.0 Hz, 2H), 4.73 (s, 4H), 4.68 (t, J = 5.0 Hz, 4H), 4.29 (s, 2H), 4.21 (d, J = 8.0 Hz, 2H), 4.01 (t, J = 5.0 Hz, 4H), 3.81 – 3.58 (m, 935H), 3.52 (t, J = 5.0 Hz, 1H), 3.20 (t, J = 5.0 Hz, 4H),1.48 (s, 6H), 1.22(s, 6H).^{13}C NMR (101 MHz, D_2O) δ 175.7, 175.2, 171.4, 156.0, 144.2, 129.4, 128.5, 125.6, 116.0, 72.0, 68.97, 63.2, 60.4, 59.4, 50.3, 39.4, 26.6.

PEG (12k) -(*m*)$_2$(69)

PEG (12k)-(N_3)$_2$ (50 mg, 0.004 mmol), Alkyne-PEG2-Amine (1.4 mg, 0.01 mmol), $CUSO_4.5H_2O$ (0.4 mg, 0.002 mmol), and L(+)-ascorbic acid sodium salt (0.7 mg, 0.003 mmol) in 2 mL (1:1) THF-H_2O were used to perform the click reaction. The solvents were removed under reduced pressure. The concentrate was dissolved in 2 mL H_2O and purified using PD MidiTrap G-10 by collecting in small fractions. The eluent was lyophilized to obtain a yellowish powder with 62 % yield.^{1}H NMR (400 MHz, D_2O) δ 8.15 (s, 2H), 4.73 (s, 4H), 4.68 (t, J = 5.0 Hz, 4H), 4.01 (t, J = 5.0 Hz, 4H), 3.94 – 3.61 (m, 1120H), 3.49 (t, J = 5.0 Hz, 1H), 3.26 (t, J = 5.0 Hz, 4H). ^{13}C NMR (101 MHz, D_2O) δ 144.0, 125.5, 69.6, 69.5, 69.2, 68.8, 66.4, 63.0, 60.4, 50.1, 39.2.

BiAn-G0(12000) : PEG (12k) -(*m*-(AXO)$_1$)$_2$ (70)

Following general procedure for the functionalization with AX **, Compound 69** (44 mg, 0.004 mmol) was dissolved in 2 mL of carbonate buffer (0.05 M, pH 10.2), adding an excess of AX (4 equiv, 6 mg) and stirring at room temperature 48 h. The purification was performed by PD MidiTrap G-10 to obtain a yellowish powder with 62 % of yield. ^{1}H NMR (400 MHz, D_2O) δ 8.15 (s, 2H), 7.33 (d, J = 7.8 Hz, 4H), 6.94 (d, J = 7.8 Hz, 4H), 4.99 (d, J = 8.0 Hz, 2H), 4.72 (s, 4H), 4.67 (t, J = 5.0 Hz, 4H), 4.29 (s, 2H), 4.21 (d, J = 8.0 Hz, 2H), 4.01 (t, J = 5.0 Hz, 4H), 3.85 – 3.57 (m, 1122H), 3.52 (t, J = 5.0 Hz, 1H), 3.20 (t, J = 5.0 Hz, 4H),1.47 (s, 6H), 1.25(s, 6H). ^{13}C NMR (101 MHz, D_2O) δ 175.7, 175.2, 171.4, 156.0, 144.2, 129.4, 128.5, 125.6, 116.0, 72.0, 68.9, 63.2, 60.4, 59.4, 50.3, 39.4, 26.7.

7.7.4.2. BiAn-dG1

PEG (600) -(dG1)$_2$ (71)

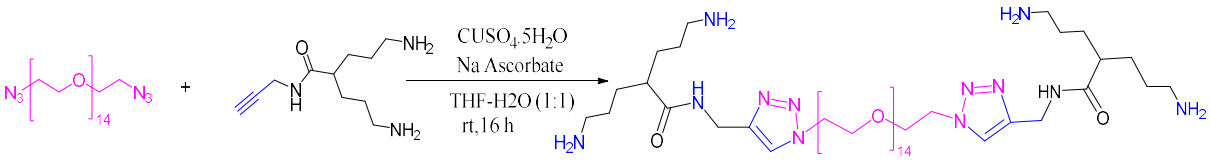

PEG (6k)-(N_3)$_2$ (50 mg, 0.077 mmol), dG1NH_2-alkyne (37 mg, 0.177 mmol), copper (II) sulphate 5-hydrate(7.7 mg, 0.031 mmol), and L(+)-ascorbic acid sodium salt (12 mg, 0.062 mmol) in 2 mL (1:1) THF-H_2O were to perform the click reaction. The solvents were removed under reduced pressure. The concentrate was dissolved in 2 mL H_2O and purified PD MidiTrap

G-10 by collecting in small fractions. The eluent was lyophilized to obtain a yellowish semisolid product with 76 % yield. ^{1}H NMR (400 MHz, D_2O) δ 8.03 (s, 2H), 4.66 (t, J = 5.0 Hz, 4H), 4.51 (s, 4H), 4.00 (t, J = 5.0 Hz, 4H), 3.85 – 3.56 (m, 56H), 3.08 – 2.85 (m, 8H), 2.37 (br s, 2H), 1.71 – 1.45 (m, 16H). ^{13}C NMR (101 MHz, D_2O) δ 177.9, 145.2, 124.7, 69.8, 69.7, 69.5, 68.9, 68.9, 50.4, 45.8, 39.4, 34.5, 29.0, 24.9.

BiAn-dG1(600) : PEG (600) -(dG1-(AXO)$_2$)$_2$ (72)

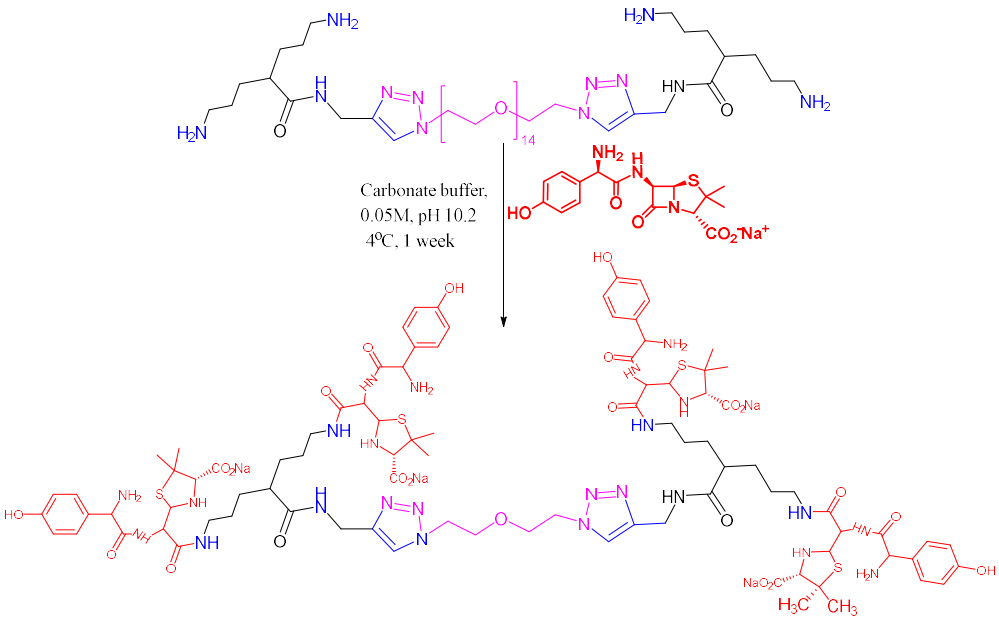

This was obtained by adding an excess, 8 equiv, of AX (182 mg, 0.47mmol) to a solution containing **compound 71** (63 mg, 0.059 mmol,) in carbonate buffer (0.05 M, pH 10.2) and incubating at 4 ^{o}C under magnetic stirring for 7 days. The reaction was refreshed with 20 % of the initial mass of AX in two different occasion and purified by PD MidiTrap G-10 columns to obtain a yellowish powder with 58 % of yield. ^{1}H NMR (400 MHz, D_2O) ^{1}H NMR (400 MHz, D_2O) δ 7.90 (s, 2H), 7.24 (d, J = 7.8 Hz, 8H), 6.84 (d, J = 7.8 Hz, 8H), 4.94 (d, J = 8.0 Hz, 4H), 4.44 (s, 4H), 4.25 (d, J = 8.0 Hz, 4H), 3.92 (s, 4H), 3.84 – 3.54 (m, 56H), 3.40 (s, 4H), 3.28 – 2.73 (m, 8H), 2.19 (br s, 2H), 1.50 (s, 12H), 1.49-1.27 (m, 16), 1.21 (s, 12H). ^{13}C NMR (101 MHz, D_2O) δ 175.2, 175.1, 171.2, 171.1, 156.5, 144.8, 129.7, 128.8, 124.5, 116.2, 74.7, 69.8, 69.5, 69.0, 67.9, 64.9, 60.6, 59.6, 59.2, 50.4, 50.2, 45.9, 39.5, 39.3, 34.5, 29.5, 27.1, 26.9.

PEG (1k) -(dG1)$_2$ (73)

PEG (1k)-(N_3)$_2$ (50 mg, 0.048 mmol), dG1NH_2-alkyne (23 mg, 0.11 mmol), $CUSO_4.5H_2O$ (4.8 mg, 0.019 mmol), and L(+)-ascorbic acid sodium salt (7.5 mg, 0.038 mmol) in 2 mL (1:1) THF-H_2O were to perform the click reaction. The solvents were removed under reduced pressure. The concentrate was dissolved in 2 mL H_2O and purified PD MidiTrap G-10 by collecting in small fractions. The eluent was lyophilized to obtain a yellowish powder with 80 % yield. ^{1}H NMR (400 MHz, D_2O) δ 8.03 (s, 2H), 4.64 (t, J = 5.0 Hz, 4H), 4.49 (s, 4H), 4.00 (t, J = 5.0 Hz, 4H), 3.88 – 3.58 (m, 93H), 3.28 – 2.73 (m, 8H), 2.39 (br s, 2H), 1.81 – 1.44 (m, 16H). ^{13}C NMR (101 MHz, D_2O) δ 177.6, 144.9, 124.6, 69.6, 69.7, 69.5, 68.9, 68.9, 50.2, 45.6, 39.2, 34.3, 28.9, 24.7.

BiAn-dG1(1000) : PEG (1k) -(dG1-(AXO)$_2$)$_2$ (74)

This was obtained by adding an excess, 8 equiv, of AX (118 mg, 0.304 mmol) to a solution containing **compound 73** (56 mg, 0.038 mmol) in carbonate buffer (0.05 M, pH 10.2) and incubating at 4 ºC under magnetic stirring for 7 days. The reaction was refreshed with 20 % of the initial mass of AX in two different occasions and purified by PD MidiTrap G-10 columns to obtain a yellowish powder with 57 % of yield. ^{1}H NMR (400 MHz, D_2O) δ 7.90 (s, 2H), 7.29 (d, J = 7.8 Hz, 8H), 6.83 (d, J = 7.8 Hz, 8H), 4.94 (d, J = 8.0 Hz, 4H), 4.44 (s, 4H), 4.25 (d, J = 8.0 Hz, 4H), 3.93 (s, 4H), 3.84 – 3.54 (m, 93H), 3.40 (s, 4H), 3.28 – 2.73 (m, 8H), 2.19 (br s, 2H), 1.51 (s, 12H), 1.50-1.27 (m, 16), 1.22 (s, 12H). ^{13}C NMR (101 MHz, D_2O) δ 175.2, 175.1, 171.2, 171.1, 156.5, 144.8, 129.7, 128.8, 124.5, 116.2, 74.7, 69.8, 69.5, 69.0, 67.9, 64.9, 60.6, 59.6, 59.2, 50.4, 50.2, 45.9, 39.5, 39.3, 34.5, 29.5, 27.1, 26.9.

PEG (2k) -(dG1)$_2$ (75)

PEG (2k)-(N_3)$_2$ (50 mg, 0.024 mmol), dG1NH_2-alkyne (12 mg, 0.056 mmol), $CUSO_4.5H_2O$ (2.4 mg, 0.01 mmol), and L(+)-ascorbic acid sodium salt (4 mg, 0.02 mmol) in 2 mL (1:1) THF-H_2O were to perform the click reaction. The solvents were removed under reduced pressure. The concentrate was dissolved in 2 mL H_2O and purified PD MidiTrap G-10 by collecting in small fractions. The eluent was lyophilized to obtain a yellowish powder with 85 % yield. ^{1}H NMR (400 MHz, D_2O) δ 8.01 (s, 2H), 4.66 (t, J = 5.0 Hz, 4H), 4.52 (s, 4H), 4.01 (t, J = 5.0 Hz, 4H), 3.85 – 3.61 (m, 186H), 3.17 – 2.94 (m, 8H), 2.40 (br s, 2H), 1.79 – 1.42 (m, 16H). ^{13}C

NMR (101 MHz, D_2O) δ 177.7, 144.5, 124.7, 69.6, 69.7, 69.5, 68.9, 68.9, 50.2, 45.8, 39.4, 34.4, 29.1, 24.9.

BiAn-dG1(2000) : PEG (2k) -(dG1-(AXO)$_2$)$_2$ (76)

This was obtained by adding an excess, 8 equiv, of AX (64 mg, 0.165 mmol) to a solution containing **compound 75** (51 mg, 0.021 mmol) in carbonate buffer (0.05 M, pH 10.2) and incubating at 4°C under magnetic stirring for 7 days. The reaction was refreshed with 20% of the initial mass of AX in two different occasions and purified by PD MidiTrap G-10 columns to obtain a yellowish powder with 75 % of yield. ^{1}H NMR (400 MHz, D_2O) δ 7.90 (s, 2H), 7.24 (d, J = 7.8 Hz, 8H), 6.84 (d, J = 7.8 Hz, 8H), 4.94 (d, J = 8.0 Hz, 4H), 4.43 (s, 4H), 4.25 (d, J = 8.0 Hz, 4H), 3.93 (s, 4H), 3.84 – 3.53 (m, 186 H), 3.41 (s, 4H), 3.28 – 2.73 (m, 8H), 2.19 (br s, 2H), 1.50 (s, 12H), 1.49-1.27 (m, 16), 1.21 (s, 12H). ^{13}C NMR (101 MHz, D_2O) δ 175.2, 175.1, 171.2, 171.1, 156.5, 144.8, 129.7, 128.7, 124.5, 116.2, 74.7, 69.8, 69.5, 69.0, 67.9, 64.9, 60.6, 59.6, 59.2, 50.4, 50.2, 45.9, 39.5, 39.3, 34.5, 29.5, 27.1, 26.7.

PEG (4k) -(dG1)$_2$ (77)

PEG (4k)-(N_3)$_2$ (50 mg, 0.012 mmol), dG1NH_2-alkyne (6 mg, 0.028 mmol), $CUSO_4.5H_2O$ (1.2 mg, 0.005 mmol), and L(+)-ascorbic acid sodium salt (2 mg, 0.01 mmol) in 2 mL (1:1) THF-H_2O were used to perform the click reaction. The solvents were removed under reduced pressure. The concentrate was dissolved in 2 mL H_2O and purified PD MidiTrap G-10 by collecting in small fractions. The eluent was lyophilized to obtain a yellowish powder with 89 % yield. ^{1}H NMR (400 MHz, D_2O) δ 8.02 (s, 2H), 4.67(t, J = 45.0 Hz, 4H), 4.52 (s, 4H), 4.02 (t, J = 5.0 Hz, 4H), 3.89 – 3.60 (m, 373H), 3.13 – 2.90 (m, 8H), 2.40 (br s, 2H), 1.78 – 1.44 (m, 16H). ^{13}C NMR (101 MHz, D_2O) δ 177.7, 144.5, 124.5, 69.8, 69.7, 69.5, 68.9, 68.9, 50.2, 45.8, 39.4, 34.4, 29.0, 24.6.

BiAn-dG1(4000) : PEG (4k) -(dG1-(AXO)$_2$)$_2$ (78)

This was obtained by adding an excess, 8 equiv, of AX (34 mg, 0.088 mmol) to a solution containing **compound 77** (49 mg, 0.011 mmol) in carbonate buffer (0.05 M, pH 10.2) and incubating at 4 °C under magnetic stirring for 7 days. The reaction was refreshed with 20 % of the initial mass of AX in two different occasions and purified by PD MidiTrap G-10 columns to obtain a yellowish powder with 86 % of yield. ^{1}H NMR (400 MHz, D_2O) δ 7.92 (s, 2H),

7.24 (d, *J* = 7.8 Hz, 8H), 6.84 (d, *J* = 7.8 Hz, 8H), 4.94 (d, *J* = 8.0 Hz, 4H), 4.44 (s, 4H), 4.25 (d, *J* = 8.0 Hz, 4H), 3.90 (s, 4H), 3.84 – 3.54 (m, 373H), 3.41 (s, 4H3.28 – 2.73 (m, 8H), 2.19 (br s, 2H), 1.52 (s, 12H), 1.49-1.27 (m, 16), 1.21 (s, 12H). ^{13}C NMR (101 MHz, D_2O) δ 175.2, 175.1, 171.2, 171.1, 156.5, 144.8, 129.7, 128.7, 124.5, 116.2, 74.7, 69.8, 69.5, 69.0, 67.9, 64.9, 60.6, 59.6, 59.2, 50.4, 50.2, 45.9, 39.5, 39.3, 34.5, 29.5, 27.1, 26.7.

PEG (6k) -(dG1)$_2$ (79)

PEG (6k)-(N_3)$_2$ (50 mg, 0.008 mmol), dG1NH_2-alkyne (4 mg, 0.019 mmol), $CUSO_4.5H_2O$ (0.8 mg, 0.003 mmol), and L(+)-ascorbic acid sodium salt (1.3 mg, 0.007 mmol) in 2 mL (1:1) THF-H_2O were used to perform the click reaction. The solvents were removed under reduced pressure. The concentrate was dissolved in 2 mL H_2O and purified PD MidiTrap G-25. The eluent was lyophilized to obtain a yellowish powder with 80 % yield. ^{1}H NMR (400 MHz, D_2O) δ 7.98 (s, 2H), 4.67 (t, *J* = 5.0 Hz, 4H), 4.53 (s, 4H), 4.02 (t, *J* = 5.0 Hz, 4H), 3.91 – 3.61 (m, 560H), 3.17 – 2.90 (m, 8H), 2.32 (br s, 2H), 1.90 – 1.38 (m, 16H). ^{13}C NMR (101 MHz, D_2O) δ 177.7, 144.5, 124.5, 69.8, 69.7, 69.5, 68.9, 68.9, 50.2, 45.8, 39.4, 34.4, 29.0, 24.6.

BiAn-dG1(6000) : PEG (6k) -(dG1-(AXO)$_2$)$_2$ (80)

This was obtained by adding an excess, 8 equiv, of AX (21 mg, 0.053 mmol) to a solution containing **compound 79** (43 mg, 0.007 mmol) in carbonate buffer (0.05 M, pH 10.2) and incubating at 4 ºC under magnetic stirring for 7 days. The reaction was refreshed with 20 % of the initial mass of AX in two different occasions and purified by PD MidiTrap G-10 columns to obtain a yellowish powder with 86 % of yield. ^{1}H NMR (400 MHz, D_2O) δ 7.86 (s, 2H), 7.21 (d, *J* = 7.8 Hz, 8H), 6.82 (d, *J* = 7.8 Hz, 8H), 4.92 (d, *J* = 8.0 Hz, 4H), 4.44 (s, 4H), 4.25 (d, *J* = 8.0 Hz, 4H), 3.92 (s, 4H), 3.81 – 3.54 (m, 560 H), 3.40 (s, 4H), 3.28 – 2.73 (m, 8H), 2.19 (br s, 2H), 1.50 (s, 12H), 1.49-1.27 (m, 16), 1.22 (s, 12H). ^{13}C NMR (101 MHz, D_2O) δ 175.2, 175.1, 171.2, 171.1, 156.5, 144.8, 129.7, 128.7, 124.5, 116.2, 74.7, 69.8, 69.5, 69.0, 67.9, 64.9, 60.6, 59.6, 59.2, 50.4, 50.2, 45.9, 39.5, 39.3, 34.5, 29.5, 27.1, 26.7.

PEG (8k) -(dG1)$_2$ (81)

PEG (8k)-(N_3)$_2$ (50 mg, 0.006 mmol), dG1NH_2-alkyne (3 mg, 0.014 mmol), $CUSO_4.5H_2O$ (0.6 mg, 0.002 mmol), and L(+)-ascorbic acid sodium salt (1 mg, 0.005 mmol) in 2 mL (1:1) THF-H_2O were used to perform the click reaction. The solvents were removed under reduced

pressure. The concentrate was dissolved in 2 mL H_2O and purified PD MidiTrap G-25. The eluent was lyophilized to obtain a yellowish powder with 78 % yield. ^{1}H NMR (400 MHz, D_2O) δ 8.03 (s, 2H), 4.67(t, J = 5.0 Hz, 4H), 4.52 (s, 4H), 4.01 (t, J = 5.0 Hz, 4H), 3.89 – 3.59 (m, 746H), 3.17 – 2.89 (m, 8H), 2.40 (br s, 2H), 1.80 – 1.45 (m, 16H). ^{13}C NMR (101 MHz, D_2O) δ 177.7, 144.5, 124.7, 69.8, 69.7, 69.5, 68.9, 68.9, 50.4, 45.8, 39.4, 34.2, 29.1, 24.9.

BiAn-dG1(8000) : PEG (8k) -(dG1-(AXO)$_2$)$_2$ (82)

This was obtained by adding an excess, 8 equiv, of AX (15 mg, 0.039 mmol) to a solution containing **compound 81** (41 mg, 0.005 mmol) in carbonate buffer (0.05M, pH 10.2) and incubating at 4 ºC under magnetic stirring for 7 days. The reaction was refreshed with 20 % of the initial mass of AX in two different occasions and purified by PD MidiTrap G-25 columns to obtain a yellowish powder with 68 % of yield. ^{1}H NMR (400 MHz, D_2O) δ 7.91 (s, 2H), 7.23 (d, J = 7.8 Hz, 8H), 6.84 (d, J = 7.8 Hz, 8H), 4.94 (d, J = 8.0 Hz, 4H), 4.45 (s, 4H), 4.26 (d, J = 8.0 Hz, 4H), 3.92 (s, 4H), 3.84 – 3.54 (m, 746H), 3.40 (s, 4H), 3.28 – 2.73 (m, 8H), 2.19 (br s, 2H), 1.50 (s, 12H), 1.49-1.27 (m, 16), 1.21 (s, 12H). ^{13}C NMR (101 MHz, D_2O) δ 175.2, 175.1, 171.2, 171.1, 156.5, 144.8, 129.7, 128.7, 124.5, 116.2, 74.7, 69.8, 69.5, 69.0, 67.9, 64.9, 60.6, 59.6, 59.2, 50.4, 50.2, 45.9, 39.5, 39.3, 34.5, 29.5, 27.1, 26.7.

PEG (10k) -(dG1)$_2$ (83)

PEG (10k)-(N_3)$_2$ (50 mg, 0.005 mmol), dG1NH_2-alkyne (2.4 mg, 0.011 mmol), $CUSO_4.5H_2O$ (0.6 mg, 0.002 mmol), and L(+)-ascorbic acid sodium salt (0.8mg, 0.004 mmol) in 2 mL (1:1) THF-H_2O were used to perform the click reaction. The solvents were removed under reduced pressure. The concentrate was dissolved in 2 mL H_2O and purified PD MidiTrap G-25. The eluent was lyophilized to obtain a yellowish powder with 69 % yield. ^{1}H NMR (400 MHz, D_2O) δ 8.03 (s, 2H), 4.65(t, J = 5.0 Hz, 4H), 4.51 (s, 4H), 4.01 (t, J = 5.0 Hz, 4H), 3.90 – 3.60 (m, 933H), 3.14 – 2.94 (m, 8H), 2.40 (br s, 2H), 1.79 – 1.43 (m, 16H). ^{13}C NMR (101 MHz, D_2O) δ 177.7, 144.5, 124.7, 69.8, 69.7, 69.5, 68.9, 68.9, 50.4, 45.8, 39.4, 34.2, 29.1, 24.9.

BiAn-dG1(10000) : PEG (10k) -(dG1-(AXO)$_2$)$_2$ (84)

This was obtained by adding an excess, 8 equiv, of AX (11 mg, 0.028 mmol) to a solution containing **compound 83** (36 mg, 0.003 mmol) in carbonate buffer (0.05 M, pH 10.2) and incubating at 4 ºC under magnetic stirring for 7 days. The reaction was refreshed with 20 % of

the initial mass of AX in two different occasions and purified by PD MidiTrap G-25 columns to obtain a yellowish powder with 70 % of yield. ^{1}H NMR (400 MHz, D_2O) δ 7.91 (s, 2H), 7.24 (d, J = 7.8 Hz, 8H), 6.84 (d, J = 7.8 Hz, 8H), 4.94 (d, J = 8.0 Hz, 4H), 4.44 (s, 4H), 4.25 (d, J = 8.0 Hz, 4H), 3.93 (s, 4H), 3.84 – 3.54 (m, 933H), 3.40 (s, 4H), 3.28 – 2.73 (m, 8H), 2.19 (br s, 2H), 1.50 (s, 12H), 1.50-1.27 (m, 16), 1.22 (s, 12H). ^{13}C NMR (101 MHz, D_2O) δ 175.2, 175.1, 171.2, 171.1, 156.5, 144.8, 129.7, 128.7, 124.5, 116.2, 74.7, 69.8, 69.5, 69.0, 67.9, 64.9, 60.6, 59.6, 59.2, 50.4, 50.2, 45.9, 39.5, 39.3, 34.5, 29.5, 27.1, 26.7.

PEG (12k) -(dG1)$_2$ (85)

PEG (12k)-(N_3)$_2$ (50 mg, 0.004 mmol), dG1NH_2-alkyne (2 mg, 0.01 mmol), $CUSO_4.5H_2O$ (0.4 mg, 0.002 mmol), and L(+)-ascorbic acid sodium salt (0.7 mg, 0.003 mmol) in 2 mL (1:1) THF-H_2O were used to perform the click reaction. The solvents were removed under reduced pressure. The concentrate was dissolved in 2 mL H_2O and purified PD MidiTrap G-25. The eluent was lyophilized to obtain a yellowish powder with 62 % yield. ^{1}H NMR (400 MHz, D_2O) δ 7.91 (s, 2H), 4.60 (t, J = 5.0 Hz, 4H), 4.51 (s, 4H), 4.01 (t, J = 5.0 Hz, 4H), 3.90 – 3.60 (m, 1120H), 3.14 – 2.94 (m, 8H), 2.31 (br s, 2H), 1.73 – 1.34 (m, 16H). ^{13}C NMR (101 MHz, D_2O) δ 177.7, 144.5, 124.7, 69.8, 69.7, 69.5, 68.9, 68.9, 50.4, 45.8, 39.4, 34.2, 29.1, 24.9.

BiAn-dG1(12000) : PEG (12k) -(dG1-(AXO)$_2$)$_2$ (86)

This was obtained by adding an excess, 8 equiv, of AX (8 mg, 0.021 mmol) to a solution containing **compound 85** (32 mg, 0.003 mmol) in carbonate buffer (0.05M, pH 10.2) and incubating at 4 ºC under magnetic stirring for 7 days. The reaction was refreshed with 20 % of the initial mass of AX in two different occasions and purified by PD MidiTrap G-25 columns to obtain a yellowish powder with 63 % of yield. ^{1}H NMR (400 MHz, D_2O) δ 7.86 (s, 2H), 7.22 (d, J = 7.8 Hz, 8H), 6.81 (d, J = 7.8 Hz, 8H), 4.93 (d, J = 8.0 Hz, 4H), 4.44 (s, 4H), 4.25 (d, J = 8.0 Hz, 4H), 3.92 (s, 4H), 3.84 – 3.54 (m, 1120H), 3.40 (s, 4H), 3.28 – 2.73 (m, 8H), 2.15 (br s, 2H), 1.51 (s, 12H), 1.49-1.27 (m, 16), 1.21 (s, 12H). ^{13}C NMR (101 MHz, D_2O) δ 175.2, 175.1, 171.2, 171.1, 156.5, 144.8, 129.7, 128.7, 124.5, 116.2, 74.7, 69.8, 69.5, 69.0, 67.9, 64.9, 60.6, 59.6, 59.2, 50.4, 50.2, 45.9, 39.5, 39.3, 34.5, 29.5, 27.1, 26.7.

7.7.4.3. BiAn-dG2

PEG (600) -(dG2)$_2$ (87)

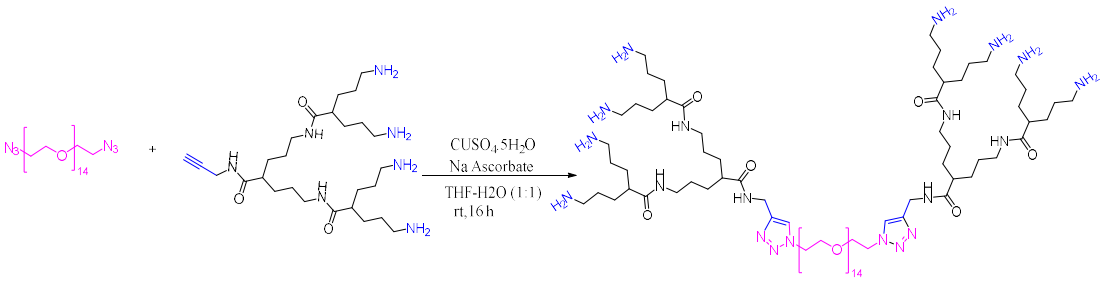

PEG (600)-(N_3)$_2$ (50 mg, 0.077 mmol), dG2NH_2-alkyne (93 mg, 0.177 mmol), $CUSO_4.5H_2O$ (8 mg, 0.031 mmol), and L(+)-ascorbic acid sodium salt (12 mg, 0.062 mmol) were dissolved in 2 mL (1:1) THF-H_2O. The reaction run overnight at room temperature. The solvents were removed under reduced pressure, re-dissolved in 2 mL of H_2O and purified by PD MidiTrap G-10, collecting the eluent in small fractions. The collected fractions were separately lyophilized and checked by NMR before combing fractions with same contents to obtain a semisolid product with 53 % yield. ^{1}H NMR (400 MHz, D_2O) δ 8.01 (s, 2H), 4.67 (t, J = 5.0 Hz, 4H), 4.49 (s, 4H), 4.01 (t, J = 5.0 Hz, 4H), 3.86 – 3.59 (m, 56H), 3.37 – 2.88 (m, 24H), 2.30 (br s, 6H), 1.81 – 1.25 (m, 48H). ^{13}C NMR (101 MHz, D_2O) δ 178.6, 177.7, 144.7, 124.7, 69.8, 69.7, 60.6, 50.2, 46.1, 39.5, 39.3, 34.4, 29.9, 29.1, 26.7, 24.9.

BiAn-dG2(600) : PEG (600) -(dG2-(AXO)$_4$)$_2$ (88)

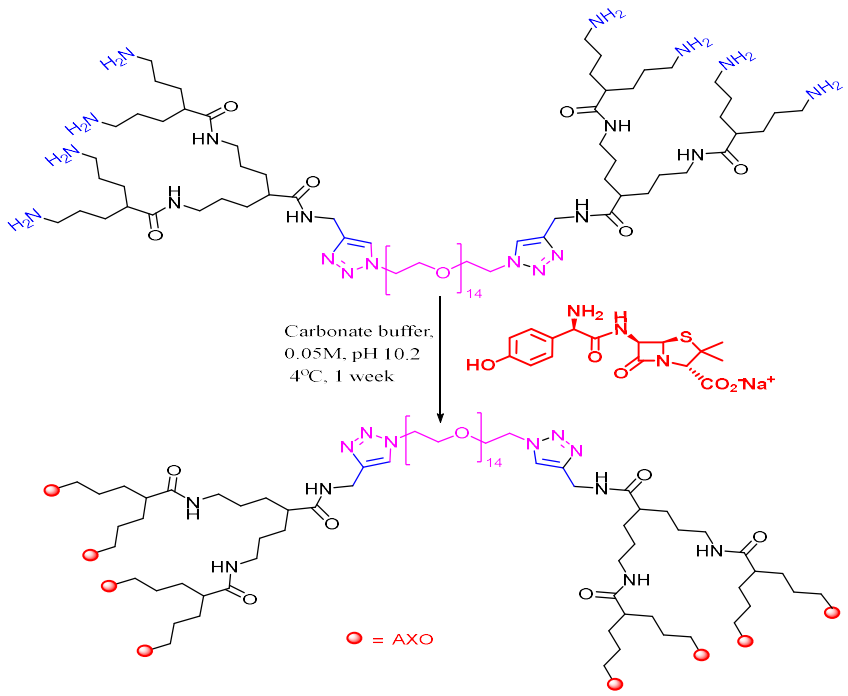

PEG (1k) -(dG2)$_2$ (89)

PEG (1k)-(N$_3$)$_2$ (50 mg, 0.048 mmol), dG2NH$_2$-alkyne (57 mg, 0.11 mmol), CUSO$_4$.5H$_2$O (5 mg, 0.019 mmol), and L(+)-ascorbic acid sodium salt (5 mg, 0.019 mmol) were dissolved 2 mL (1:1) THF-H$_2$O. The reaction run overnight at room temperature. The solvents were removed under reduced pressure, re-dissolved in 2 mL of H$_2$O and purified by PD MidiTrap G-10, collecting the eluent in small fractions. The collected fractions were separately lyophilized and checked by NMR before combing fractions with same contents to obtain a product with 65 % yield. ^{1}H NMR (400 MHz, D$_2$O) δ 8.03 (s, 2H), 4.67 (t, J = 5.0 Hz, 4H), 4.50 (s, 4H), 4.01 (t, J = 5.0 Hz, 4H), 3.89 – 3.63 (m, 93H), 3.40– 2.84 (m, 24H), 2.30 (br s, 6H), 1.79 – 1.32 (m, 48H). ^{13}C NMR (101 MHz, D$_2$O) δ 178.6, 177.7, 144.7, 124.7, 69.8, 69.7, 60.6, 50.4, 46.1, 39.5, 39.3, 34.4, 29.9, 29.1, 26.8, 24.9.

BiAn-dG2(1000) : PEG (1k) -(dG2-(AXO)$_4$)$_2$ (90)

To a solution containing compound **89** (45 mg, 0.021 mmol) in carbonate buffer (0.05 M, pH 10.2), an excess AX (16 equiv, 0.34 mmol, 133 mg) was added. The mixture was incubated at 4 °C under magnetic stirring for 7 days, while refreshing on two different occasions with 20 % the initial amount of AX. The product was purified by PD MidiTrap G-10 and lyophilized to

obtain a product with 67 % of yield. ^{1}H NMR (400 MHz, D_2O) δ 7.91 (s, 2H), 7.24 (d, J = 7.8 Hz, 16H), 6.83 (d, J = 7.8 Hz, 16H), 4.94 (d, J = 8.0 Hz, 8H), 4.44 (s, 4H), 4.25 (d, J = 8.0 Hz, 8H), 3.92 (s, 4H), 3.84 – 3.54 (m, 93H), 3.41 (s, 8H), 3.35 – 3.30 (m, 16H), 2.99 – 2.73 (m, 8H), 2.19 (br s, 6H), 1.50 (s, 24H), 1.49-1.27 (m, 48), 1.23 (s, 24H). ^{13}C NMR (101 MHz, D_2O) δ 175.1, 175.1, 171.2, 171.1, 156.4, 144.6, 129.9, 128.8, 124.8, 116.3, 74.7, 69.8, 69.5, 69.0, 67.9, 64.9, 60.6, 59.6, 59.2, 50.4, 50.2, 45.9, 39.5, 39.1, 34.5, 29.5, 26.9, 26.7.

PEG (2k) -(dG2)$_2$ (91)

PEG (2k)-(N_3)$_2$ (50 mg, 0.024 mmol), dG2NH_2-alkyne (29 mg, 0.056 mmol), $CUSO_4.5H_2O$ (2.4 mg, 0.01 mmol), and L(+)-ascorbic acid sodium salt (4 mg, 0.02 mmol) were dissolved 2 mL (1:1) THF-H_2O. The reaction run overnight at room temperature. The solvents were removed under reduced pressure, re-dissolved in 2 mL of H_2O and purified by PD MidiTrap G-10, collecting the eluent in small fractions. The collected fractions were separately lyophilized and checked by NMR before combing fractions with same contents to obtain a product with 64 % yield. ^{1}H NMR (400 MHz, D_2O) δ 8.01 (s, 2H), 4.67 (t, J = 5.0 Hz, 4H), 4.50 (s, 4H), 4.06 (t, J = 5.0 Hz, 4H), 3.89 – 3.63 (m, 186H), 3.40– 2.84 (m, 24H), 2.30 (br s, 6H), 1.79 – 1.35 (m, 48H). ^{13}C NMR (101 MHz, D_2O) δ 178.7, 177.6, 144.7, 124.7, 69.8, 69.7, 60.6, 50.4, 46.2, 39.5, 39.3, 34.5, 29.9, 29.1, 26.8, 24.9.

BiAn-dG2(2000) : PEG (2k) -(dG2-(AXO)$_4$)$_2$ (92)

To a solution containing compound **91**(43 mg, 0.014 mmol) in carbonate buffer (0.05 M, pH 10.2), an excess AX (16 equiv, 0.22 mmol, 86 mg) was added. The mixture was incubated at 4 ^{o}C under magnetic stirring for 7 days, while refreshing on two different occasions with 20 % the initial amount of AX. The product was purified by PD MidiTrap G-10 and lyophilized to obtain a product with 64 % of yield. ^{1}H NMR (400 MHz, D_2O) δ 7.90 (s, 2H), 7.24 (d, J = 7.8 Hz, 16H), 6.84 (d, J = 7.8 Hz, 16H), 4.94 (d, J = 8.0 Hz, 8H), 4.43 (s, 4H), 4.24 (d, J = 8.0 Hz, 8H), 3.92 (s, 4H), 3.81 – 3.53 (m, 186H), 3.40 (s, 8H), 3.35 – 3.31 (m, 16H), 2.99 – 2.73 (m, 8H), 2.19 (br s, 6H), 1.50 (s, 24H), 1.49-1.27 (m, 48), 1.21 (s, 24H). ^{13}C NMR (101 MHz, D_2O) δ 175.7, 175.1, 171.2, 171.1, 156.5, 144.6, 129.7, 128.8, 124.8, 116.3, 74.7, 69.8, 69.5, 69.0, 67.9, 64.9, 60.6, 59.6, 59.2, 50.4, 50.2, 45.9, 39.5, 39.1, 34.5, 29.5, 26.5, 26.9.

PEG (4k) -(dG2)$_2$ (93)

PEG (4k)-(N_3)$_2$ (50 mg, 0.012 mmol), dG2NH_2-alkyne (15 mg, 0.028 mmol), $CUSO_4.5H_2O$ (1.2 mg, 0.005 mmol), and L(+)-ascorbic acid sodium salt (2 mg, 0.01 mmol) were dissolved 2 mL (1:1) THF-H_2O. The reaction run overnight at room temperature. The solvents were removed under reduced pressure, re-dissolved in 2 mL of H_2O and purified by PD MidiTrap G-25 to obtain a product with 73 % yield. ^{1}H NMR (400 MHz, D_2O) δ 8.01 (br s, 2H), 4.67 (t, J = 5.0 Hz, 4H), 4.49 (s, 4H), 4.06 (t, J = 5.0 Hz, 4H), 3.89 – 3.63 (m, 373H), 3.37– 2.88 (m, 24H), 2.30 (s, 6H), 1.81 – 1.25 (m, 48H). ^{13}C NMR (101 MHz, D_2O) δ 178.6, 177.7, 144.6, 124.7, 69.8, 69.7, 60.6, 50.2, 46.2, 39.5, 39.3, 34.4, 29.9, 29.1, 26.8, 24.9.

BiAn-dG2(4000) : PEG (4k) -(dG2-(AXO)$_4$)$_2$ (94)

To a solution containing compound **93** (46 mg, 0.009 mmol) in carbonate buffer (0.05 M, pH 10.2), an excess AX (16 equiv, 0.14 mmol, 56 mg) was added. The mixture was incubated at 4 ^{o}C under magnetic stirring for 7 days, while refreshing on two different occasions with 20 % the initial amount of AX. The product was purified by PD MidiTrap G-25 and lyophilized to obtain yellowish powder with 62 % of yield. ^{1}H NMR (400 MHz, D_2O) δ 7.86 (s, 2H), 7.21 (d, J = 7.8 Hz, 16H), 6.84 (d, J = 7.8 Hz, 16H), 4.94 (d, J = 8.0 Hz, 8H), 4.44 (s, 4H), 4.25 (d, J = 8.0 Hz, 8H), 3.92 (s, 4H), 3.84 – 3.54 (m, 373H), 3.42 (s, 8H), 3.35 – 3.31 (m, 16H), 2.99 – 2.72 (m, 8H), 2.19 (br s, 6H), 1.51 (s, 24H), 1.49-1.27 (m, 48), 1.21 (s, 24H). ^{13}C NMR (101 MHz, D_2O) δ 175.7, 175.3, 171.2, 171.1, 156.5, 144.6, 129.7, 128.8, 124.8, 116.3, 74.7, 69.8, 69.5, 69.0, 67.9, 64.9, 60.6, 59.5, 59.2, 50.4, 50.2, 45.9, 39.5, 39.1, 34.5, 29.5, 26.5, 26.9.

PEG (6k) -(dG2)$_2$ (95)

PEG (6k)-(N_3)$_2$ (50 mg, 0.008 mmol), dG2NH_2-alkyne (10 mg, 0.019 mmol), $CUSO_4.5H_2O$ (0.8 mg, 0.003 mmol), and L(+)-ascorbic acid sodium salt (1.3 mg, 0.007 mmol) were dissolved 2 mL (1:1) THF-H_2O. The reaction run overnight at room temperature. The solvents were removed under reduced pressure, re-dissolved in 2 mL of H_2O and purified by PD MidiTrap G-25 to obtain a product with 59 % yield. ^{1}H NMR (400 MHz, D_2O) δ 8.01 (br s, 2H), 4.66 (t, J = 5.0 Hz, 4H), 4.49 (s, 4H), 4.01 (t, J = 5.0 Hz, 4H), 3.90 – 3.60 (m, 560H), 3.37– 2.88 (m,

24H), 2.30 (s, 6H), 1.84 – 1.11 (m, 48H). ^{13}C NMR (101 MHz, D_2O) δ 178.6, 177.7, 144.6, 124.7, 69.8, 69.7, 60.6, 50.2, 46.2, 39.5, 39.3, 34.4, 29.9, 29.1, 26.8, 24.9.

BiAn-dG2(6000) : PEG (6k) -(dG2-(AXO)$_4$)$_2$ (96)

To a solution containing compound **95 (**35 mg, 0,005 mmol) in carbonate buffer (0.05 M, pH 10.2), an excess AX (16 equiv, 0.08 mmol, 31 mg) was added. The mixture was incubated at 4 ºC under magnetic stirring for 7 days, while refreshing on two different occasions with 20 % the initial amount of AX. The product was purified by PD MidiTrap G-10 and lyophilized to obtain yellowish powder with 63 % of yield. ^{1}H NMR (400 MHz, D_2O) δ 7.91 (s, 2H), 7.23 (d, J = 7.8 Hz, 16H), 6.84 (d, J = 7.8 Hz, 16H), 4.93 (d, J = 8.0 Hz, 8H), 4.44 (s, 4H), 4.25 (d, J = 8.0 Hz, 8H), 3.92 (s, 4H), 3.84 – 3.54 (m, 560H), 3.40 (s, 8H), 3.35 – 3.30 (m, 16H), 2.99 – 2.73 (m, 8H), 2.19 (br s, 6H), 1.50 (s, 24H), 1.51-1.27 (m, 48), 1.21 (s, 24H). ^{13}C NMR (101 MHz, D_2O) δ 175.2, 175.3, 171.2, 171.1, 156.4, 144.6, 129.6, 128.9, 124.8, 116.3, 74.8, 69.8, 69.5, 69.0, 67.9, 64.9, 60.6, 59.5, 59.2, 50.4, 50.2, 45.9, 39.5, 39.3, 34.5, 29.5, 26.5, 26.7.

PEG (8k) -(dG2)$_2$ (97)

PEG (8k)-(N_3)$_2$ (50 mg, 0.006 mmol), dG2NH_2-alkyne (7 mg, 0.014 mmol), $CUSO_4.5H_2O$ (0.6 mg, 0.002 mmol), and L(+)-ascorbic acid sodium salt (1 mg, 0.005 mmol) were dissolved 2 mL (1:1) THF-H_2O. The reaction run overnight at room temperature. The solvents were removed under reduced pressure, re-dissolved in 2 mL of H_2O and purified by PD MidiTrap G-25 to obtain a product with 67 % yield. ^{1}H NMR (400 MHz, D_2O) δ 8.01 (br s, 2H), 4.66 (t, J = 5.0 Hz, 4H), 4.49 (s, 4H), 4.01 (t, J = 5.0 Hz, 4H), 3.90 – 3.60 (m, 746H), 3.37– 2.88 (m, 24H), 2.30 (s, 6H), 1.84 – 1.11 (m, 48H). ^{13}C NMR (101 MHz, D_2O) δ 178.6, 177.7, 144.6, 124.7, 69.8, 69.7, 60.6, 50.2, 46.2, 39.5, 39.3, 34.4, 29.9, 29.1, 26.8, 24.9

BiAn-dG2(8000):PEG (8k) -(dG2-(AXO)$_4$)$_2$ (98)

To a solution containing compound **97** (38 mg, 0.004 mmol) in carbonate buffer (0.05 M, pH 10.2), an excess AX (16 equiv, 0.08 mmol, 26 mg) was added. The mixture was incubated at 4 ºC under magnetic stirring for 7 days, while refreshing on two different occasions with 20 % the initial amount of AX. The product was purified by PD MidiTrap G-10 and lyophilized to obtain yellowish powder with 66 % of yield. ^{1}H NMR (400 MHz, D_2O) δ 7.91 (s, 2H), 7.21 (d, J = 7.8 Hz, 16H), 6.84 (d, J = 7.8 Hz, 16H), 4.91 (d, J = 8.0 Hz, 8H), 4.44 (s, 4H), 4.25 (d, J =

8.0 Hz, 8H), 3.92 (s, 4H), 3.84 – 3.54 (m, 746H), 3.40 (s, 8H), 3.35 – 3.30 (m, 16H), 2.99 – 2.73 (m, 8H), 2.19 (br s, 6H), 1.50 (s, 24H), 1.49-1.27 (m, 48), 1.22 (s, 24H). ^{13}C NMR (101 MHz, D_2O) δ 175.2, 175.3, 171.2, 171.1, 156.4, 144.6, 129.6, 128.9, 124.8, 116.3, 74.8, 69.8, 69.5, 69.0, 67.9, 64.9, 60.6, 59.5, 59.2, 50.4, 50.2, 45.9, 39.5, 39.3, 34.5, 29.5, 26.5, 26.7.

PEG (10k) -(dG2)$_2$ (99)

PEG (10k)-$(N_3)_2$ (50 mg, 0.005 mmol), dG2NH_2-alkyne (6 mg, 0.011 mmol), $CUSO_4.5H_2O$ (0.5 mg, 0.002 mmol), and L(+)-ascorbic acid sodium salt (0.8 mg, 0.004 mmol) were dissolved 2 mL (1:1) THF-H_2O. The reaction run overnight at room temperature. The solvents were removed under reduced pressure, re-dissolved in 2 mL of H_2O and purified by PD MidiTrap G-25 to obtain a product with 65 % yield. ^{1}H NMR (400 MHz, D_2O) δ 8.02 (br s, 2H), 4.67 (t, J = 5.0 Hz, 4H), 4.49 (s, 4H), 4.01 (t, J = 5.0 Hz, 4H), 3.87 – 3.59 (m, 933H), 3.33– 2.82 (m, 24H), 2.34 (s, 6H), 1.83 – 1.18 (m, 48H). ^{13}C NMR (101 MHz, D_2O) δ 178.6, 177.7, 144.6, 124.7, 69.8, 69.7, 60.6, 50.2, 46.2, 39.5, 39.3, 34.4, 29.9, 29.1, 26.8, 25.0.

BiAn-dG2(10000) : PEG (10k) -(dG2-(AXO)$_4$)$_2$ (100)

To a solution containing compound **99** (36 mg, 0.003 mmol) in carbonate buffer (0.05 M, pH 10.2), an excess AX (16 equiv, 0.05 mmol, 20 mg) was added. The mixture was incubated at 4 ^{o}C under magnetic stirring for 7 days, while refreshing on two different occasions with 20 % the initial amount of AX. The product was purified by PD MidiTrap G-10 and lyophilized to obtain yellowish powder with 63 % of yield. ^{1}H NMR (400 MHz, D_2O) δ 7.90 (s, 2H), 7.20 (d, J = 7.8 Hz, 16H), 6.84 (d, J = 7.8 Hz, 16H), 4.94 (d, J = 8.0 Hz, 8H), 4.44 (s, 4H), 4.25 (d, J = 8.0 Hz, 8H), 3.92 (s, 4H), 3.84 – 3.54 (m, 933H), 3.40 (s, 8H), 3.35 – 3.30 (m, 16H), 2.97 – 2.73 (m, 8H), 2.19 (br s, 6H), 1.50 (s, 24H), 1.49-1.28 (m, 48), 1.23 (s, 24H). ^{13}C NMR (101 MHz, D_2O) δ 175.2, 175.3, 171.2, 171.1, 156.4, 144.6, 129.6, 128.9, 124.8, 116.3, 74.8, 69.8, 69.5, 69.0, 67.9, 64.9, 60.6, 59.5, 59.2, 50.4, 50.2, 45.9, 39.5, 39.3, 34.5, 29.5, 26.5, 26.7.

PEG (12k) -(dG2)$_2$ (101)

PEG (12k)-$(N_3)_2$ (50 mg, 0.004 mmol), dG2NH_2-alkyne (5 mg, 0.01 mmol), $CUSO_4.5H_2O$ (0.4 mg, 0.002 mmol), and L(+)-ascorbic acid sodium salt (0.7 mg, 0.003 mmol) were dissolved 2 mL (1:1) THF-H_2O. The reaction run overnight at room temperature. The solvents were removed under reduced pressure, re-dissolved in 2 mL of H_2O and purified by PD MidiTrap

G-25 to obtain a product with 58 % yield. ^{1}H NMR (400 MHz, D_2O) δ 8.03 (br s, 2H), 4.64 (t, J = 5.0 Hz, 4H), 4.48 (s, 4H), 4.02 (t, J = 5.0 Hz, 4H), 3.89 – 3.60 (m, 1120H), 3.40– 2.84 (m, 24H), 2.35 (s, 6H), 1.92 – 1.27 (m, 48H). ^{13}C NMR (101 MHz, D_2O) δ 178.6, 177.7, 144.4, 124.7, 69.8, 69.7, 60.6, 50.2, 46.2, 39.5, 34.3, 29.9, 29.2, 26.8, 25.1

BiAn-dG2(12000) : PEG (12k) -(dG2-(AXO)$_4$)$_2$ (102)

To a solution containing compound **101**(32 mg, 0.002 mmol) in carbonate buffer (0.05 M, pH 10.2), an excess AX (16 equiv, 0.04 mmol, 15 mg) was added. The mixture was incubated at 4 ^{o}C under magnetic stirring for 7 days, while refreshing on two different occasions with 20 % the initial amount of AX. The product was purified by PD MidiTrap G-10 and lyophilized to obtain yellowish powder with 68 % of yield. ^{1}H NMR (400 MHz, D_2O) δ 7.89 (s, 2H), 7.23(d, J = 7.8 Hz, 16H), 6.84 (d, J = 7.8 Hz, 16H), 4.94 (d, J = 8.0 Hz, 8H), 4.44 (s, 4H), 4.25 (d, J = 8.0 Hz, 8H), 3.92 (s, 4H), 3.83 – 3.55 (m, 1120H), 3.41 (s, 8H), 3.35 – 3.30 (m, 16H), 2.98 – 2.74 (m, 8H), 2.19 (br s, 6H), 1.50 (s, 24H), 1.49-1.27 (m, 48), 1.21 (s, 24H). ^{13}C NMR (101 MHz, D_2O) δ 175.2, 175.3, 171.2, 171.1, 156.4, 144.6, 129.7, 128.9, 124.8, 116.2, 74.7, 69.8, 69.5, 69.0, 67.9, 64.9, 60.6, 59.5, 59.2, 50.4, 50.2, 45.9, 39.5, 39.3, 34.5, 29.5, 26.5, 26.9.

7.7.4.4. BiAn-dG3

PEG (600) -$(dG3)_2$ (103)

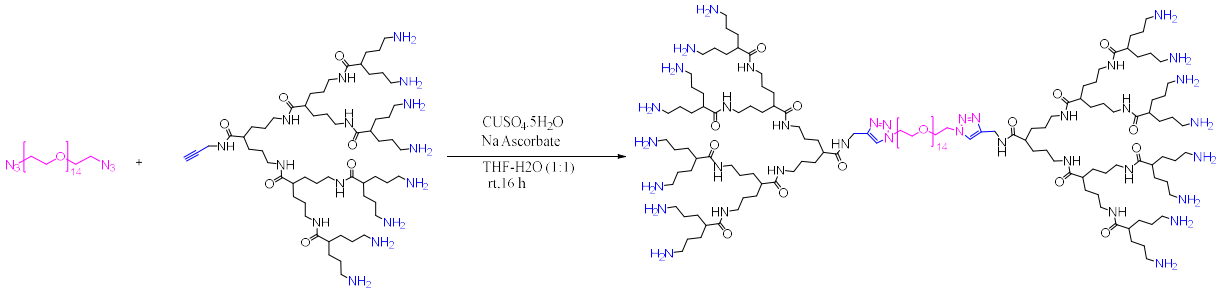

PEG (600) -$(N_3)_2$ (15 mg, 0.023 mmol), dG3NH_2-alkyne (61 mg, 0.053 mmol) were dissolved in 2 mL (1:1) THF-H_2O. $CUSO_4.5H_2O$ (2.3 mg, 0.009 mmol) and L(+)-ascorbic acid sodium salt (3.7 mg, 0.018 mmol) were added to the reaction sequentially. The mixture was left to react at room temperature overnight. The solvents were removed under reduced pressure, re-dissolved in H_2O and purified by PD MidiTrap G-10, by collecting the eluents in small fraction to obtain a product with 81 % yield. ^{1}H NMR (400 MHz, D_2O) δ 7.99 (s, 2H), 4.70 – 4.59 (m, 4H), 4.48 (s, 4H), 4.02 – 3.93 (m, 4H), 3.84 – 3.54 (m, 56H), 3.45 – 2.86 (m, 58H), 2.32 (br s, 14H), 1.81 – 1.29 (m, 112H). ^{13}C NMR (101 MHz, D_2O) δ 178.41, 177.71, 124.4, 76.8, 69.8, 69.5, 50.4, 46.4, 46.1, 39.4, 29.9, 29.1, 26.77, 24.9.

BiAn-dG3(600) : PEG (600) -(dG3-(AXO)$_8$)$_2$ (104)

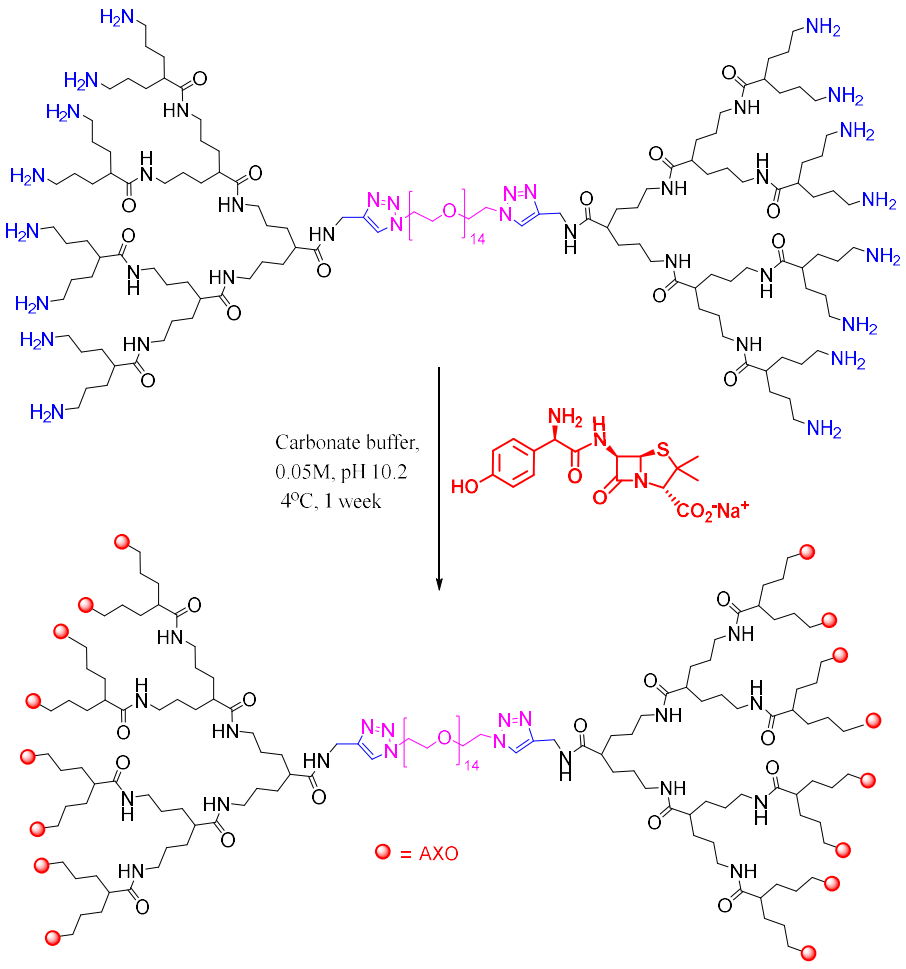

Obtained following the general procedure by dissolving compound **103** (55 mg, 0.019 mmol) in carbonate buffer (0.05 M, pH 10.2), adding an excess AX (32 equiv, 0.6 mmol, 231 mg) and incubating the mixture at 4 ºC under magnetic stirring for 7 days, while refreshing on two different occasions with 20 % the initial amount of AX. The product was purified by PD MidiTrap G-10 to obtain a product with 71 % yield. ^{1}H NMR (400 MHz, D_2O) δ 7.90 (s, 2H), 7.24 (d, J = 7.8 Hz, 32H), 6.84 (d, J = 7.8 Hz, 32H), 4.94 (d, J = 8.0 Hz, 16H), 4.44 (s, 4H), 4.25 (d, J = 8.0 Hz, 16H), 3.92 (s, 4H), 3.84 – 3.54 (m, 56H), 3.40 (s, 16H), 3.35 – 3.30 (m, 32H), 2.99 – 2.73 (m, 16H), 2.19 (br s, 14H), 1.50 (s, 48H), 1.49-1.27 (m, 112), 1.21 (s, 48H). ^{13}C NMR (101 MHz, D_2O) δ 178.2, 175.9, 175.1, 171.1, 156.7, 144.8, 129.7, 128.7, 124.5, 116.3, 77.5, 76.8, 74.7, 69.8, 69.5, 69.0, 64.9, 59.6, 59.2, 58.5, 50.4, 46.2, 39.5, 39.2, 34.5, 29.9, 27.2, 26.9, 25.2.

PEG (1k) -(dG3)$_2$ (105)

PEG (1k) -(N_3)$_2$ (25 mg, 0.024 mmol), dG3NH_2-alkyne (63 mg, 0.055 mmol) were dissolved in 2 mL (1:1) THF-H_2O. $CUSO_4.5H_2O$ (2.4 mg, 0.01 mmol) and L(+)-ascorbic acid sodium salt (3.8 mg, 0.019 mmol) were added to the reaction sequentially. The mixture was left to react at room temperature overnight. The solvents were removed under reduced pressure, re-dissolved in H_2O and purified by PD MidiTrap G-10, by collecting the eluents in small fraction to obtain a product with 84 % yield. ^{1}H NMR (400 MHz, D_2O) δ 7.88 (s, 2H), 4.71 – 4.56 (m, 4H), 4.48 (s, 4H), 4.02 – 3.93 (m, 4H), 3.84 – 3.55 (m, 93H), 3.45 – 2.73 (m, 58H), 2.33 (br s, 14H), 1.78 – 1.13 (m, 112H). ^{13}C NMR (101 MHz, D_2O) δ 178.41, 177.71, 124.4, 76.8, 69.8, 69.5, 50.4, 46.4, 46.1, 39.5, 39.3, 29.9, 29.1, 26.77, 24.9.

BiAn-dG3(1000) : PEG (1k) -(dG3-(AXO)$_8$)$_2$ (106)

Obtained following the general procedure by dissolving compound **105** (67 mg, 0.020 mmol) in carbonate buffer (0.05 M, pH 10.2), adding an excess AX (32 equiv, 0.6 mmol, 231 mg) and incubating the mixture at 4 ºC under magnetic stirring for 7 days, while refreshing on two different occasions with 20 % the initial amount of AX. The product was purified by PD MidiTrap G-10 to obtain a product with 79 % yield. ^{1}H NMR (400 MHz, D_2O) δ 7.89 (s, 2H), 7.23 (d, J = 7.8 Hz, 32H), 6.84 (d, J = 7.8 Hz, 32H), 4.94 (d, J = 8.0 Hz, 16H), 4.44 (s, 4H), 4.25 (d, J = 8.0 Hz, 16H), 3.92 (s, 4H), 3.84 – 3.54 (m, 56H), 3.40 (s, 16H), 3.37 – 3.29 (m, 32H), 2.90 – 2.71 (m, 16H), 2.20 (br s, 14H), 1.50 (s, 48H), 1.49-1.27 (m, 112), 1.21 (s, 48H).^{13}C NMR (101 MHz, D_2O) δ 178.2, 175.9, 175.1, 171.1, 156.7, 144.8, 129.7, 128.7, 124.5, 116.3, 77.5, 76.8, 74.7, 69.8, 69.5, 69.0, 64.9, 59.6, 59.2, 58.5, 50.4, 46.2, 39.5, 39.2, 34.5, 29.9, 27.2, 26.9, 25.2.

PEG (2k) -(dG3)$_2$ (107)

PEG (2k) -(N_3)$_2$ (60 mg, 0.029 mmol), dG3NH_2-alkyne (77 mg, 0.067 mmol) were dissolved in 2 mL (1:1) THF-H_2O. $CUSO_4.5H_2O$ (2.9 mg, 0.012 mmol) and L(+)-ascorbic acid sodium salt (4.6 mg, 0.023 mmol) were added to the reaction sequentially. The mixture was left to react at room temperature overnight. The solvents were removed under reduced pressure, re-dissolved in H_2O and purified by PD MidiTrap G-10, by collecting the eluents in small fraction

to obtain a product with 53 % yield. ^{1}H NMR (400 MHz, D_2O) δ 7.99 (s, 2H), 4.70 – 4.56 (m, 4H), 4.48 (s, 4H), 4.02 – 3.93 (m, 4H), 3.84 – 3.55 (m, 186H), 3.45 – 2.74 (m, 58H), 2.27 (br s, 14H), 1.73 – 1.10 (m, 112H). ^{13}C NMR (101 MHz, D_2O) δ 178.6, 177.71, 124.4, 69.8, 69.5, 50.4, 46.4, 46.1, 39.5, 39.3, 34.5, 39.4, 29.9, 29.1, 26.8, 25.0

BiAn-dG3(2000) : PEG (2k) -(dG3-(AXO)$_8$)$_2$ (108)

Obtained following the general procedure by dissolving compound **107** (67 mg, 0.015 mmol) in carbonate buffer (0.05 M, pH 10.2), adding an excess AX (32 equiv, 0.49 mmol, 191mg) and incubating the mixture at 4 ºC under magnetic stirring for 7 days, while refreshing on two different occasions with 20 % the initial amount of AX. The product was purified by PD MidiTrap G-10 to obtain a product with 73 % yield. ^{1}H NMR (400 MHz, D_2O) δ 7.89 (s, 2H), 7.23 (d, J = 7.8 Hz, 32H), 6.84 (d, J = 7.8 Hz, 32H), 4.94 (d, J = 8.0 Hz, 16H), 4.45 (s, 4H), 4.25 (d, J = 8.0 Hz, 16H), 3.92 (s, 4H), 3.84 – 3.54 (m, 93H), 3.40 (s, 16H), 3.37 – 3.29 (m, 32H), 2.90 – 2.71 (m, 16H), 2.20 (br s, 14H), 1.50 (s, 48H), 1.49-1.28 (m, 112), 1.23 (s, 48H). ^{13}C NMR (101 MHz, D_2O) δ 178.2, 175.9, 175.1, 171.1, 156.7, 144.8, 129.7, 128.7, 124.5, 116.3, 77.5, 76.8, 74.7, 69.8, 69.5, 69.0, 64.9, 59.6, 59.2, 58.5, 50.4, 46.2, 39.5, 39.2, 34.5, 29.9, 27.2, 26.9, 25.2.

PEG (4k) -(dG3)$_2$ (109)

PEG (4k) -(N_3)$_2$ (80 mg, 0.020 mmol), dG3NH_2-alkyne (52 mg, 0.045 mmol) were dissolved in 2 mL (1:1) THF-H_2O. $CUSO_4.5H_2O$ (2 mg, 0.008 mmol) and L(+)-ascorbic acid sodium salt (3 mg, 0.016 mmol) were added to the reaction sequentially. The mixture was left to react at room temperature overnight. The solvents were removed under reduced pressure, re-dissolved in H_2O and purified by PD MidiTrap G-25, by collecting the eluents in small fraction to obtain a product with 62 % yield. ^{1}H NMR (400 MHz, D_2O) δ 8.01 (s, 2H), 4.70 – 4.56 (m, 4H), 4.48 (s, 4H), 4.02 – 3.93 (m, 4H), 3.84 – 3.55 (m, 373H), 3.45 – 2.74 (m, 58H), 2.35 (br s, 14H), 1.80 – 1.07 (m, 112H). ^{13}C NMR (101 MHz, D_2O) δ 178.5, 177.6, 124.4, 69.8, 69.5, 50.4, 46.4, 46.1, 39.5, 39.3, 34.5, 39.4, 29.9, 29.1, 26.8, 25.0

BiAn-dG3(4000) : PEG (4k) -(dG3-(AXO)$_8$)$_2$ (110)

Obtained following the general procedure by dissolving compound **109** (78 mg, 0.012 mmol) in carbonate buffer (0.05 M, pH 10.2), adding an excess AX (32 equiv, 0.39 mmol, 152 mg)

and incubating the mixture at 4 ºC under magnetic stirring for 7 days, while refreshing on two different occasions with 20 % the initial amount of AX. The product was purified by PD MidiTrap G-10 to obtain a product with 69 % yield. ^{1}H NMR (400 MHz, D_2O) δ 7.91 (s, 2H), 7.23 (d, J = 7.8 Hz, 32H), 6.83 (d, J = 7.8 Hz, 32H), 4.94 (d, J = 8.0 Hz, 16H), 4.44 (s, 4H), 4.24 (d, J = 8.0 Hz, 16H), 3.92 (s, 4H), 3.84 – 3.54 (m, 373H), 3.40 (s, 16H), 3.37 – 3.29 (m, 64H), 2.90 – 2.71 (m, 32H), 2.20 (br s, 14H), 1.50 (s, 48H), 1.49-1.27 (m, 112), 1.21 (s, 48H). ^{13}C NMR (101 MHz, D_2O) δ 178.2, 175.1, 171.1, 160.9, 156.5, 144.7, 129.7, 128.7, 124.6, 116.2, 74.7, 69.8, 69.5, 69.0, 64.9, 59.6, 59.1, 58.5, 50.4, 50.2, 46.4, 39.5, 39.2, 38.9, 34.5, 29.8, 29.2, 28.4, 27.7, 26.9, 26.5, 25.2.

PEG (6k) -(dG3)$_2$ (111)

PEG (6k) -(N_3)$_2$ (80 mg, 0.013 mmol), dG3NH_2-alkyne (34 mg, 0.03 mmol) were dissolved in 2 mL (1:1) THF-H_2O. $CUSO_4.5H_2O$ (1.3 mg, 0.005 mmol) and L(+)-ascorbic acid sodium salt (2 mg, 0.011 mmol) were added to the reaction sequentially. The mixture was left to react at room temperature overnight. The solvents were removed under reduced pressure, re-dissolved in H_2O and purified by PD MidiTrap G-25, by collecting the eluents in small fraction to obtain a product with 58 % yield. ^{1}H NMR (400 MHz, D_2O) δ 8.05 (s, 2H), 4.70 – 4.56 (m, 4H), 4.52 (s, 4H), 4.02 – 3.93 (m, 4H), 3.84 – 3.55 (m, 560H), 3.45 – 2.74 (m, 58H), 2.35 (br s, 14H), 1.85 – 1.09 (m, 112H). ^{13}C NMR (101 MHz, D_2O) δ 178.4, 177.7, 124.6, 69.8, 69.5, 50.4, 46.4, 46.1, 39.5, 39.3, 34.5, 39.4, 29.9, 29.1, 26.8, 25.0

BiAn-dG3(6000) : PEG (6k) -(dG3-(AXO)$_8$)$_2$ (112)

Obtained following the general procedure by dissolving compound **111**(64 mg, 0.008 mmol) in carbonate buffer (0.05 M, pH 10.2), adding an excess AX (32 equiv, 0.25 mmol, 95 mg) and incubating the mixture at 4 ºC under magnetic stirring for 7 days, while refreshing on two different occasions with 20 % the initial amount of AX. The product was purified by PD MidiTrap G-10 to obtain a product with 68 % yield. ^{1}H NMR (400 MHz, D_2O) δ 7.89 (s, 2H), 7.23 (d, J = 7.8 Hz, 32H), 6.81 (d, J = 7.8 Hz, 32H), 4.94 (d, J = 8.0 Hz, 16H), 4.44 (s, 4H), 4.25 (d, J = 8.0 Hz, 16H), 3.92 (s, 4H), 3.84 – 3.54 (m, 560H), 3.40 (s, 16H), 3.37 – 3.29 (m, 32H), 2.92 – 2.73 (m, 16H), 2.20 (br s, 14H), 1.50 (s, 48H), 1.49-1.28 (m, 112), 1.21 (s, 48H). ^{13}C NMR (101 MHz, D_2O) δ 178.2, 175.1, 171.1, 160.9, 156.6, 144.7, 129.7, 128.8, 124.6,

116.2, 74.9, 69.8, 69.5, 69.0, 64.9, 59.6, 59.1, 58.5, 50.4, 50.2, 46.4, 39.5, 39.2, 38.9, 34.4, 29.8, 29.2, 28.4, 27.7, 26.9, 26.5, 25.2.

PEG (8k) -(dG3)$_2$ (113)

PEG (8k) -(N$_3$)$_2$ (80 mg, 0.01 mmol), dG3NH$_2$-alkyne (26 mg, 0.023 mmol) were dissolved in 2 mL (1:1) THF-H$_2$O. CUSO$_4$.5H$_2$O (1 mg, 0.004 mmol) and L(+)-ascorbic acid sodium salt (1.6 mg, 0.008 mmol) were added to the reaction sequentially. The mixture was left to react at room temperature overnight. The solvents were removed under reduced pressure, re-dissolved in H$_2$O and purified by PD MidiTrap G-25, by collecting the eluents in small fraction to obtain a product with 61 % yield. ^{1}H NMR (400 MHz, D$_2$O) δ 8.04 (s, 2H), 4.70 – 4.56 (m, 4H), 4.53 (s, 4H), 4.02 – 3.93 (m, 4H), 3.84 – 3.58 (m, 746H), 3.45 – 2.74 (m, 58H), 2.34 (br s, 14H), 1.78 – 1.15 (m, 112H). ^{13}C NMR (101 MHz, D$_2$O) δ 178.4, 177.7, 124.6, 69.8, 69.5, 50.4, 46.4, 46.1, 39.5, 39.3, 34.5, 29.9, 29.1, 26.8, 25.0.

BiAn-dG3(8000) : PEG (8k) -(dG3-(AXO)$_8$)$_2$ (114)

Obtained following the general procedure by dissolving compound **113** (63 mg, 0.006 mmol) in carbonate buffer (0.05M, pH 10.2), adding an excess AX (32 equiv, 0.19 mmol, 76 mg) and incubating the mixture at 4 ^{o}C under magnetic stirring for 7 days, while refreshing on two different occasions with 20 % the initial amount of AX. The product was purified by PD MidiTrap G-10 to obtain a product with 73 % yield. ^{1}H NMR (400 MHz, D$_2$O) δ 7.87 (s, 2H), 7.22 (d, J = 7.8 Hz, 32H), 6.83 (d, J = 7.8 Hz, 32H), 4.94 (d, J = 8.0 Hz, 16H), 4.44 (s, 4H), 4.25 (d, J = 8.0 Hz, 16H), 3.92 (s, 4H), 3.84 – 3.54 (m, 746H), 3.40 (s, 16H), 3.37 – 3.29 (m, 32H), 2.90 – 2.71 (m, 16H), 2.21 (br s, 14H), 1.50 (s, 48H), 1.49-1.27 (m, 112), 1.21 (s, 48H). ^{13}C NMR (101 MHz, D$_2$O) δ 178.4, 175.1, 170.8, 160.9, 157.4, 145.1, 130.3, 129.6, 123.8, 116.6, 74.8, 69.8, 69.5, 69.0, 64.9, 59.7, 59.1, 58.5, 50.4, 50.2, 46.2, 39.5, 39.2, 38.9, 34.4, 29.8, 29.2, 28.4, 27.7, 26.9, 26.9, 25.1.

PEG (10k) -(dG3)$_2$ (115)

PEG (10k) -(N$_3$)$_2$ (80 mg, 0.008 mmol), dG3NH$_2$-alkyne (21 mg, 0.018 mmol) were dissolved in 2 mL (1:1) THF-H$_2$O. CUSO$_4$.5H$_2$O (1 mg, 0.003 mmol) and L(+)-ascorbic acid sodium salt (2 mg, 0.006 mmol) were added to the reaction sequentially. The mixture was left to react at room temperature overnight. The solvents were removed under reduced pressure, re-dissolved

in H_2O and purified by PD MidiTrap G-25, by collecting the eluents in small fraction to obtain a product with 61 % yield. ^{1}H NMR (400 MHz, D_2O) δ 8.05 (s, 2H), 4.70 – 4.56 (m, 4H), 4.53 (s, 4H), 4.02 – 3.93 (m, 4H), 3.85 – 3.67 (m, 933H), 3.51 – 2.87 (m, 58H), 2.31(br s, 14H), 1.78 – 1.30 (m, 112H). ^{13}C NMR (101 MHz, D_2O) δ 178.4, 177.7, 144.9, 124.6, 69.8, 69.5, 50.4, 46.5, 46.1, 39.5, 39.3, 34.5, 29.9, 29.1, 26.8, 25.0.

BiAn-dG3(10000) : PEG (10k) -(dG3-(AXO)$_8$)$_2$ (116)

Obtained following the general procedure by dissolving compound **115** (60 mg, 0.005 mmol) in carbonate buffer (0.05 M, pH 10.2), adding an excess AX (32 equiv, 0.16 mmol, 60 mg) and incubating the mixture at 4 ºC under magnetic stirring for 7 days, while refreshing on two different occasions with 20 % the initial amount of AX. The product was purified by PD MidiTrap G-10 to obtain a product with 62 % yield. ^{1}H NMR (400 MHz, D_2O) δ 7.90 (s, 2H), 7.23 (d, J = 7.8 Hz, 32H), 6.83 (d, J = 7.8 Hz, 32H), 4.94 (d, J = 8.0 Hz, 16H), 4.44 (s, 4H), 4.25 (d, J = 8.0 Hz, 16H), 3.93 (s, 4H), 3.84 – 3.54 (m, 933H), 3.40 (s, 16H), 3.37 – 3.29 (m, 32H), 2.90 – 2.71 (m, 16H), 2.20 (br s, 14H), 1.50 (s, 48H), 1.50-1.27 (m, 112), 1.22 (s, 48H). ^{13}C NMR (101 MHz, D_2O) δ 178.3, 175.1, 171.1, 160.9, 156.2, 146.7, 129.8, 128.9, 123.8, 116.2, 74.7, 69.8, 69.5, 69.0, 59.7, 59.1, 58.5, 50.4, 50.2, 46.2, 39.3, 39.2, 38.9, 34.4, 29.8, 29.2, 28.4, 27.7, 26.9, 26.7, 25.1.

PEG (12k) -(dG3)$_2$ (117)

PEG (12k) -(N_3)$_2$ (80 mg, 0.007 mmol), dG3NH_2-alkyne (18 mg, 0.015 mmol) were dissolved in 2 mL (1:1) THF-H_2O. $CUSO_4.5H_2O$ (1 mg, 0.003 mmol) and L(+)-ascorbic acid sodium salt (2 mg, 0.005 mmol) were added to the reaction sequentially. The mixture was left to react at room temperature overnight. The solvents were removed under reduced pressure, re-dissolved in H_2O and purified by PD MidiTrap G-25, by collecting the eluents in small fraction to obtain a product with 61 % yield. ^{1}H NMR (400 MHz, D_2O) δ 7.90 (s, 2H), 4.70 – 4.56 (m, 4H), 4.53 (s, 4H), 4.02 – 3.93 (m, 4H), 3.85 – 3.67 (m, 1120H), 3.35 – 2.81 (m, 58H), 2.32 (br s, 14H), 1.80 – 1.24 (m, 112H). ^{13}C NMR (101 MHz, D_2O) δ 178.2, 177.7, 144.9, 124.6, 69.8, 69.5, 50.4, 46.5, 46.3, 39.5, 39.0, 34.5, 29.9, 29.1, 26.8, 25.0.

BiAn-dG3(12000) : PEG (12k) -(dG3-(AXO)$_8$)$_2$ (118)

Obtained following the general procedure by dissolving compound **117** (60 mg, 0.004 mmol) in carbonate buffer (0.05 M, pH 10.2), adding an excess AX (32 equiv, 0.13 mmol, 52 mg) and incubating the mixture at 4ºC under magnetic stirring for 7 days, while refreshing on two different occasions with 20 % the initial amount of AX. The product was purified by PD MidiTrap G-10 to obtain a product with 61 % yield. ^{1}H NMR (400 MHz, D_2O) δ 7.88 (s, 2H), 7.22 (d, J = 7.8 Hz, 32H), 6.84 (d, J = 7.8 Hz, 32H), 4.93 (d, J = 8.0 Hz, 16H), 4.44 (s, 4H), 4.25 (d, J = 8.0 Hz, 16H), 3.92 (s, 4H), 3.84 – 3.54 (m, H), 3.41 (s, 16H), 3.37 – 3.29 (m, 32H), 2.93 – 2.74 (m, 16H), 2.21 (br s, 14H), 1.50 (s, 48H), 1.49-1.27 (m, 112), 1.21 (s, 48H). ^{13}C NMR (101 MHz, D_2O) δ 178.0, 175.1, 171.1, 160.9, 156.2, 146.7, 129.8., 128.9, 123.8, 116.2, 74.7, 69.8, 69.5, 69.0, 59.7, 59.1, 58.5, 50.4, 50.2, 46.2, 39.3, 39.2, 38.9, 34.4, 29.8, 29.2, 28.4, 27.7, 26.9, 27.

Resumen

Capítulo 1. INTRODUCCIÓN

Antecedentes de la Alergia a Amoxicilina (AX), Mecanismos y Diagnóstico

Las reacciones inmediatas a fármacos están inducidas por mecanismos inmunológicos mediados por IgE específicas, y suelen producirse en la primera hora tras la exposición al fármaco responsable [26]. Esto implica una serie de manifestaciones clínicas que van desde la rinitis y la urticaria/angioedema hasta la anafilaxia y la muerte [50]. Los antibióticos β-lactámicos son los fármacos más frecuentemente implicados en estas reacciones, y entre ellos la penicilina es el grupo más estudiado. Debido a su elevado consumo y a la estabilidad química de los conjugados que se forman con las penicilinas, su inmunoquímica es bien conocida y sirve de modelo para el estudio de la alergia a otros fármacos [51]. Diversos factores influyen en el fundamento de la reacción alérgica fármacos, entre los que cabe citar la estructura química y su reactividad con proteínas, y la reactividad cruzada con otras estructuras similares [51,52].

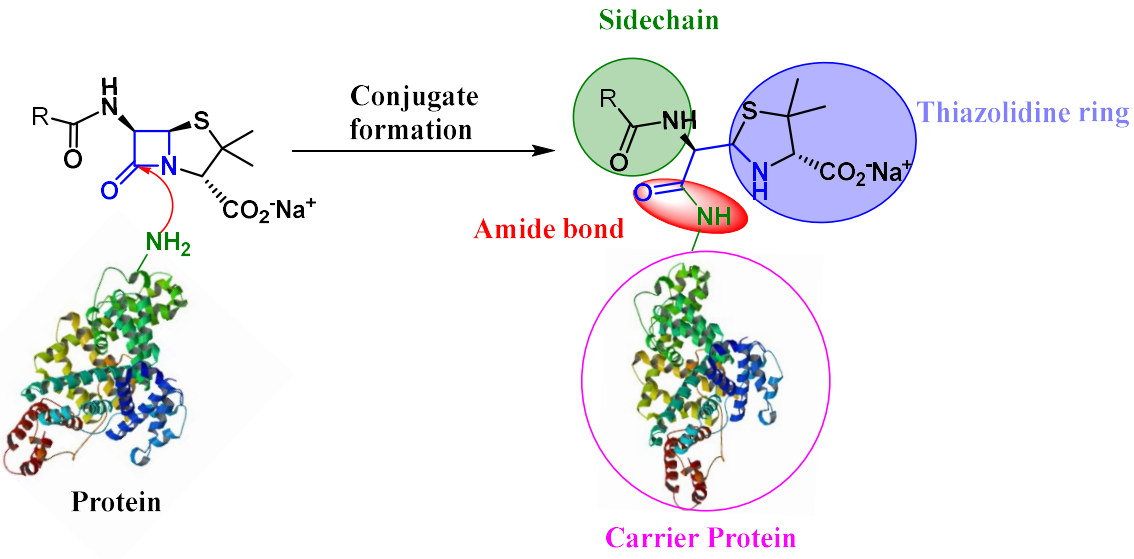

Figura R1. Conjugación de penicilinas con proteínas portadoras y formación de los principales determinantes antigénicos. Se indican diferentes regiones de reconocimiento o epítopos.

Se asume que las β-lactams son moléculas demasiado pequeñas para provocar una respuesta inmunológica [10]. Su antigenicidad se explica por la hipótesis del hapteno, que afirma que la

capacidad inmunogénica de los fármacos sólo puede obtenerse formando conjugados covalentes con proteínas [55]. La tensión estructural del anillo β-lactámico provoca que las β-lactamas sean altamente reactivas. La electrofilia del grupo carbonilo de la β-lactama permite la unión a la proteína mediante el ataque nucleofílico de sus aminas primarias, lo conduce a la apertura del anillo de la β-lactama y a la formación de un enlace amida para formar un aducto fármaco-proteína con mayor tamaño y multivalencia [55,56] (Figure R1).

El reconocimiento inmunológico de dichos determinantes antigénicos presentados de forma multivalente en un conjugado por, al menos, dos anticuerpos IgE adyacentes que se unen a su receptor de alta afinidad (FcεRI) en la superficie de los mastocitos y los basófilos circulantes, da lugar a la reticulación del receptor FcεRI [16,17,56,57]. El entrecruzamiento provoca la degranulación y la liberación de aminas vasoactivas preformadas, citocinas, quimiocinas y otros mediadores, provocando la fase aguda de la respuesta alérgica [16,58]. La eficacia de la estimulación de la degranulación de las células efectoras depende de muchos factores que incluyen la estructura del determinante antigénico del fármaco [54], su valencia en el conjugado o antígeno completo [16,60], el tamaño de la estructura completa [59,60], la proximidad de los epítopos de IgE [61] y la posible presencia de impedimento estérico [62].

La amoxicilina (AX) es la penicilina considerada actualmente como la principal responsable de provocar reacciones alérgicas debido a su reciente patrón de consumo [71,72]. La estructura química de la AX es similar a la de la bencilpenicilina, diferenciándose por el grupo hidroxilo y amino de la cadena lateral, lo que ayuda a explicar la alergia selectiva a la AX en pacientes tolerantes a otras β-lactamas [55]. Del mismo modo que en el caso de la bencilpenicilina, la apertura directa del anillo β-lactámico por los grupos amino de las proteínas da lugar al amoxiciloilo (AXO) como determinante antigénico mayor [73]. Otros determinantes menores de AX se forman por hidrólisis del anillo β-lactámico, dando lugar al ácido amoxiciloico, o a la acilación intramolecular por el grupo amino de la cadena lateral de AX, dando lugar a la dicetopiperazina (Figura R2). A diferencia de la bencilpenicilina, la estabilidad de los determinantes menores de la AX ha permitido su caracterización química e inmunológica. Sin embargo, estas dos estructuras no son reactivas frente a proteínas y, por lo tanto, no pueden ser reconocidas por la IgE específica (IgE específicas) del fármaco presente en los pacientes alérgicos, como se ha demostrado en las pruebas de activación de la piel y de los basófilos [74]. Además de los aductos proteicos, se ha descrito la existencia de polímeros formados por dímeros de AX que podrían poseer fuertes propiedades antigénicas [75].

El diagnóstico de las reacciones inmediatas a antibióticos betalactámicos en la práctica clínica se basa principalmente en métodos *in vivo* e *in vitro* [120]. Debido a la sensibilidad no óptima de las pruebas cutáneas, la prueba de provocación del fármaco se considera el gold estándar para establecer el diagnóstico, lo cual es arriesgado para el paciente y no se recomienda en pacientes con antecedentes de reacciones potencialmente mortales [113,119]. Las pruebas in vitro se basan en la determinación de la IgE específicas (inmunoensayos), en la que el ImmunoCAP comercial sólo detecta el 20% de los pacientes alérgicos, y en la cuantificación de la activación de los basófilos tras la estimulación con el fármaco responsable, mostrando una sensibilidad en torno al 50%. Entre los factores que influyen en esta baja sensibilidad La prueba de activación de basófilos (BAT) es otra prueba *in vitro* disponible comercialmente, realizada en sangre fresca, que mide la capacidad de la IgE para inducir la activación de los basófilos en presencia de alérgenos mediante citometría de flujo (Figura R.3) [123,124]. Se utilizan diferentes marcadores celulares o una combinación (anti-IgE, CCR3, CRTH2 y CD203c) para detectar los basófilos. Una vez seleccionados los basófilos, CD63 y CD203c son los dos marcadores de activación de basófilos que se detectan habitualmente tras la estimulación con el fármaco responsable [20]. Los valores aceptables del BAT en cuanto a sensibilidad (50-78%) y especificidad (89 -97%) para el diagnóstico de la alergia a los β-lactámicos explican su importancia como técnica complementaria a las pruebas *in vivo* e *in vitro* [125–127]. No obstante, debido a la ausencia de protocolos estándares relacionados con los marcadores, los procedimientos y las concentraciones de fármacos, con lo que existe variación en la realización de la técnica entre los distintos laboratorios [120].

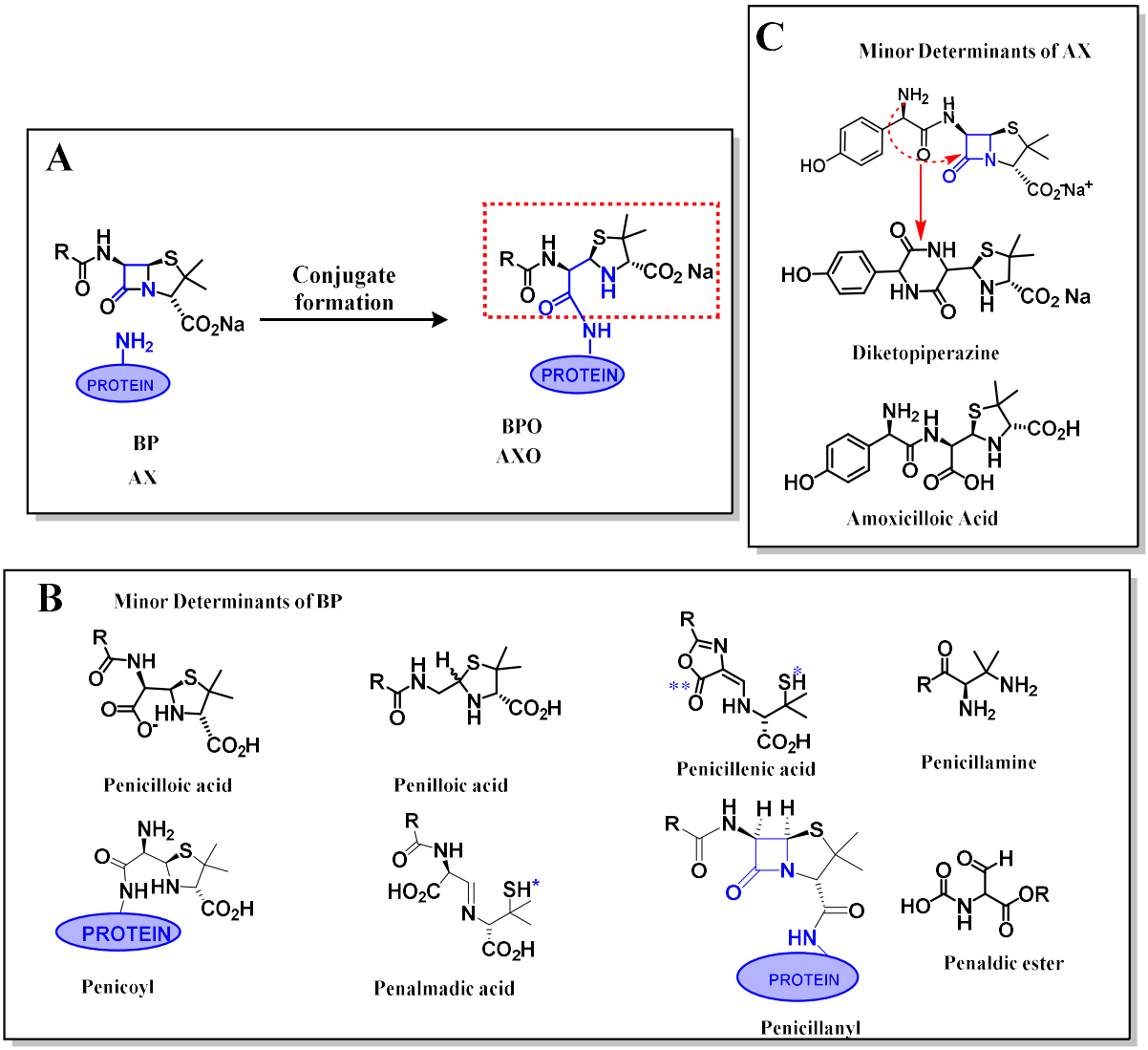

Figura R2. Los determinantes antigénicos mayores y menores de bencilpenicilina (BP) y AX.

podría estar el hecho de que no se incorpore el determinante antigénico correcto y/o los conjugados a las pruebas *in vitro*. Por lo tanto, la alternativa ideal sería el uso de pruebas *in vitro* no invasivas con una sensibilidad mejorada.

Además, el BAT tiene dos limitaciones inherentes: la necesidad de realizarlo en las primeras 24 h tras la extracción de sangre para evitar una disminución de la activación [128]; y la existencia de un 10-15% de sujetos que no responden [128,129]. Para evitar esto, se ha descrito recientemente un BAT pasivo utilizando basófilos de donantes sensibilizados con sueros de pacientes [130] en paralelo a la medida de la liberación de histamina [131]. Se ha investigado

la aplicación de esta última para el diagnóstico de la alergia a β-lactámicos, encontrando una sensibilidad del 55% y una especificidad del 85% en el diagnóstico de la alergia al ácido clavulánico (CLV) [131], y del 79% y el 100% respectivamente para AX cuando se utiliza AX-octalisina como conjugado, que mejora los valores obtenidos cuando se utiliza sólo AX (con 63% de sensibilidad y 90% de especificidad) [132].

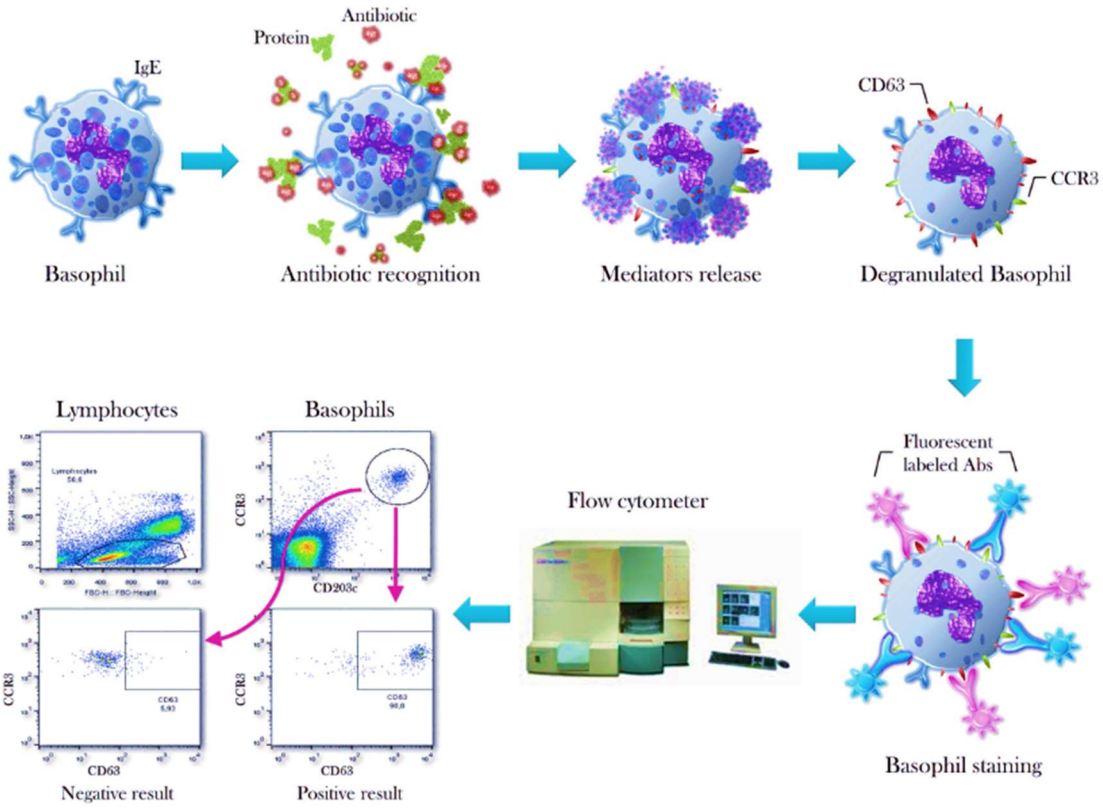

Figura R3. Representación esquemática del BAT. Adaptado de [20].

A pesar de estos resultados y de la posibilidad de utilizar sueros, este método presenta la limitación de la necesidad de un donante de basófilos, que debe estar disponible para la extracción de sangre durante todo el estudio, y la necesidad de eliminar la IgE ya unida a los basófilos del donante. Para superar estas limitaciones, ha surgido la prueba de activación de mastocitos (MAT) para complementar al BAT, especialmente en la alergia alimentaria [130]. La MAT utiliza una línea de mastocitos cultivada en el laboratorio que se sensibiliza con sueros de los pacientes para imitar los propios mastocitos de los pacientes. A continuación, estas células se estimulan y se analizan mediante citometría de flujo para determinar la expresión de marcadores de activación en su superficie o la liberación de mediadores inflamatorios. Más allá de las alergias hacia los alérgenos proteicos, la MAT se han utilizado recientemente para

diagnosticar la alergia dependiente de IgE/FcεRI a moléculas pequeñas o fármacos, como la clorhexidina [133] y los fármacos derivados del platino [134]. Estos diferentes enfoques se han realizado en líneas celulares derivadas de mastocitos humanos, LAD2 o RBL.

Nanoestructuras en el diagnóstico de la alergia

La nanociencia y la nanotecnología permiten manipular, ensamblar, fabricar y controlar la materia a escala nanométrica (de 1 a 100 nm) mediante un enfoque multidisciplinar [135]. Esto ha conducido al desarrollo de nanomateriales, que se comportan de forma muy diferente a los materiales de mayor escala. Además, su funcionalización con diferentes ligandos puede afinar sus propiedades fisicoquímicas y proporcionar interacción con diferentes receptores [136]. Las nanoestructuras difieren en tamaño, forma y dimensión [137], y pueden clasificarse a grandes rasgos en cuatro categorías basadas en materiales: orgánicos, inorgánicos, compuestos y basados en el carbono [138]. Esto engloba estructuras como las nanopartículas, los nanoporos, los nanorods, los nanohilos, los nanotubos, los liposomas, los polímeros, los dendrímeros y los nanogeles entre otros [139,140]. La diversidad de las propiedades fisicoquímicas, que dependen principalmente del tamaño, la forma, la composición y la funcionalización del sistema, puede modularse para conseguir las propiedades biológicas deseadas para aplicaciones sanitarias, incluyendo el diagnóstico precoz, el tratamiento y la prevención de enfermedades [141].

El nanodiagnóstico utiliza los principios de la nanotecnología con fines diagnósticos y explota las propiedades de la nanoescala derivadas de la interacción entre la superficie y las biomoléculas para aumentar la sensibilidad, la especificidad y facilitar la detección temprana de la enfermedad [142]. El control preciso de las propiedades fisicoquímicas de las nanoestructuras permite la construcción del sistema nanométrico que puede imitar el complejo reconocimiento *in vivo* en los sistemas *in vitro*, tanto para los inmunoensayos como para las pruebas celulares.

En la actualidad un creciente número de aproximaciones basadas en las ventajas de los nanomateriales están emergiendo para poder detectar y/o cuantificar IgE específicas. En este sentido, se han investigado diversas estrategias, como la nanofluídica [143], o el uso de nanoestructuras como moléculas portadoras [66,144–146] y/o soportes sólidos [147,148] para capturar anticuerpos, o como herramienta de detección para mejorar y amplificar la señal de

detección (fluorescente, de resonancia de plasmón superficial o electroquímica) para mejorar la sensibilidad de los inmunoensayos.

El uso de dendrímeros de poliamidoamina (PAMAM) como portadores de haptenos ha permitido la presentación de determinantes antigénicos de manera multivalente, mimetizando a los conjugados que se forman con proteínas globulares. Estos conjugados sintéticos se denominan Antígenos Dendriméricos (DeAn). Los dendrímeros son estructuras nanoescaladas, altamente ramificadas, globulares a altas generaciones, multivalentes con valencia definida, monodispersas, con versatilidad sintética y diversas aplicaciones [151–153] (Figura R4). El empleo de dendrímeros ha permitido la síntesis de estructuras tridimensionales con un control preciso sobre el tamaño y el número de determinantes antigénicos, que han logrado aumentar la sensibilidad, debido a la mayor densidad de haptenos, y la reproducibilidad de las pruebas de diagnóstico en la detección de IgE específicas a penicilinas [136]. Además, esta plataforma ha permitido la inclusión de dos antibióticos β-lactámicos diferentes en DeAn para crear DeAn-bi-epítopos que sirven para la detección de IgE específicas tanto de pacientes selectivos como aquellos con reactividad cruzada a ambos fármacos. Este estudio también confirma la influencia de la distribución tridimensional de un hapteno o determinante antigénico en la molécula portadora durante el proceso de reconocimiento de IgE específicas [66].

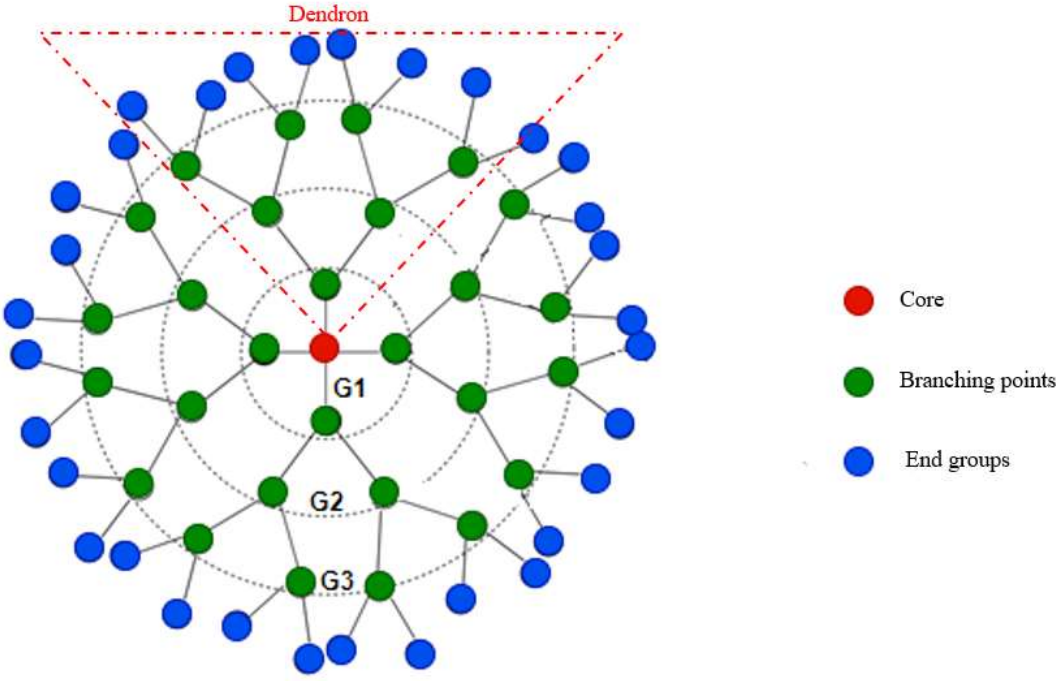

Figura R4. Representación esquemática del dendrímero y del dendrón (resaltado en rojo).

Capítulo 2. HIPÓTESIS Y OBJETIVOS

HIPÓTESIS Y JUSTIFICACIÓN

Los antibióticos β-lactámicos son el tratamiento de primera elección para combatir muchas infecciones bacterianas [205]; sin embargo, también son los desencadenantes más frecuentes de reacciones alérgicas, estando su prevalencia habitualmente asociada a los patrones de consumo [113]. En la actualidad, la AX, sola o en combinación con el CLV, es el inductor más común [20,30,113]. La alergia a los β-lactámicos puede ser inducida por diferentes mecanismos inmunológicos, entre los cuales el mediado por anticuerpos IgE es el más común y mejor estudiado [30,50]. El diagnóstico de las reacciones inmediatas a AX en la práctica clínica se basa principalmente en los métodos *in vivo* e *in vitro* [120]. Debido a que la sensibilidad de las pruebas cutáneas no es óptima, la prueba de provocación controlada (o de exposición) con el fármaco es el único método disponible para confirmar el diagnóstico, aunque es arriesgado para el paciente y no se recomienda en pacientes con antecedentes de reacciones potencialmente severas [113,119]. Las pruebas *in vitro* se basan en la determinación de la IgE específicas en suero (mediante inmunoensayos), o sobre receptores de basófilos en sangre (BAT). El inmunoensayo comercial disponible actualmente, ImmunoCAP, sólo detecta el 20% de los pacientes alérgicos. En el caso del BAT, la técnica muestra una sensibilidad en torno al 50%. Entre los factores que influyen en la sensibilidad tan baja de las pruebas *in vitro* podría estar el hecho de que no se incorporan los determinantes antigénicos y/o conjugados correctos en las pruebas *in vitro* para una apropiada interacción con el anticuerpo específico. Una mejora de la sensibilidad sólo puede abordarse utilizando estructuras adecuadas.

Además, para entender y poder mejorar la técnica del BAT, es esencial conocer los mecanismos de la activación celular. Aparte del BAT, que es la técnica celular más utilizada, se están describiendo nuevos ensayos celulares pasivos, que utilizan líneas de basófilos o mastocitos, como métodos *in vitro* emergentes para diagnosticar la alergia a alérgenos y fármacos. El estudio de las complejas restricciones celulares y estructurales en la activación o inhibición *in vitro* de las células efectoras requieren de estructuras sofisticadas bien definidas y caracterizadas para facilitar la interpretación de los resultados. Aunque se han diseñado diferentes moléculas para evaluar la influencia de distintos parámetros en la degranulación de los mastocitos (MCs), utilizando andamios sofisticados para alérgenos o haptenos sintéticos (dinitrofenilo, dansilo) enlazados en estructuras bi o multivalentes, no se han descrito

estructuras que contienen fármacos para estudiar este proceso celular. Además, se han descrito tamaños óptimos diferentes para el entrecruzamiento de IgE en la superficie de los mastocitos como consecuencia de las diversas características de los sistemas sintéticos estudiados, como la diferente densidad de los haptenos (o valencia) [60,206], la estructura tridimensional y la flexibilidad [60] o la rigidez [16,206,207], la afinidad, la cooperatividad y la proximidad de los epítopos [17,61,208] de los sistemas sintéticos.

Con la intención de investigar los requisitos estructurales de los conjugados para inducir la activación de las células efectoras, proponemos un estudio de relación estructura-actividad (SAR) utilizando nanoestructuras que contienen AX (hapteno real) y muestras séricas de pacientes alérgicos (donde se encuentra la IgE específicas). La AX es un compuesto pequeño que requiere de la unión covalente a proteínas para formar conjugados multivalentes con un tamaño mayor para ser inmunogénico. Hipotetizamos que los requisitos estructurales óptimos para promover la activación de las células efectoras se pueden investigar utilizando nanoestructuras multi-AX bien definidas, bien con forma globular o que también contengan espaciadores poliméricos flexibles de longitud suficiente, en los que la distancia entre epítopos puede ser relevante tanto para la morfología del inmunocomplejo como para la degranulación de las células efectoras (Figura R5). Inspirándonos en nuestro diseño anterior de DeAns, que mostraron potencial para el reconocimiento y la cuantificación de IgE específicas a bencilpenicilina, proponemos el diseño de tres conjuntos diferentes de nanoarquitecturas relacionadas para ampliar los estudios de interacción con el sistema inmunológico. Haremos uso de estructuras basadas en dendrímeros debido a su estructura controlada en la nanoescala, y multivalencia para ser funcionalizadas con el ligando de interés, el determinante antigénico de AX, para la correcta interacción con el sistema inmunológico. En resumen, hipotetizamos que las propiedades estructurales de los conjugados pueden ser nano-diseñadas para que sean apropiadas en el proceso de entrecruzamiento de las IgE específicas unidas a los receptores FcεRI de basófilos y mastocitos, considerando:

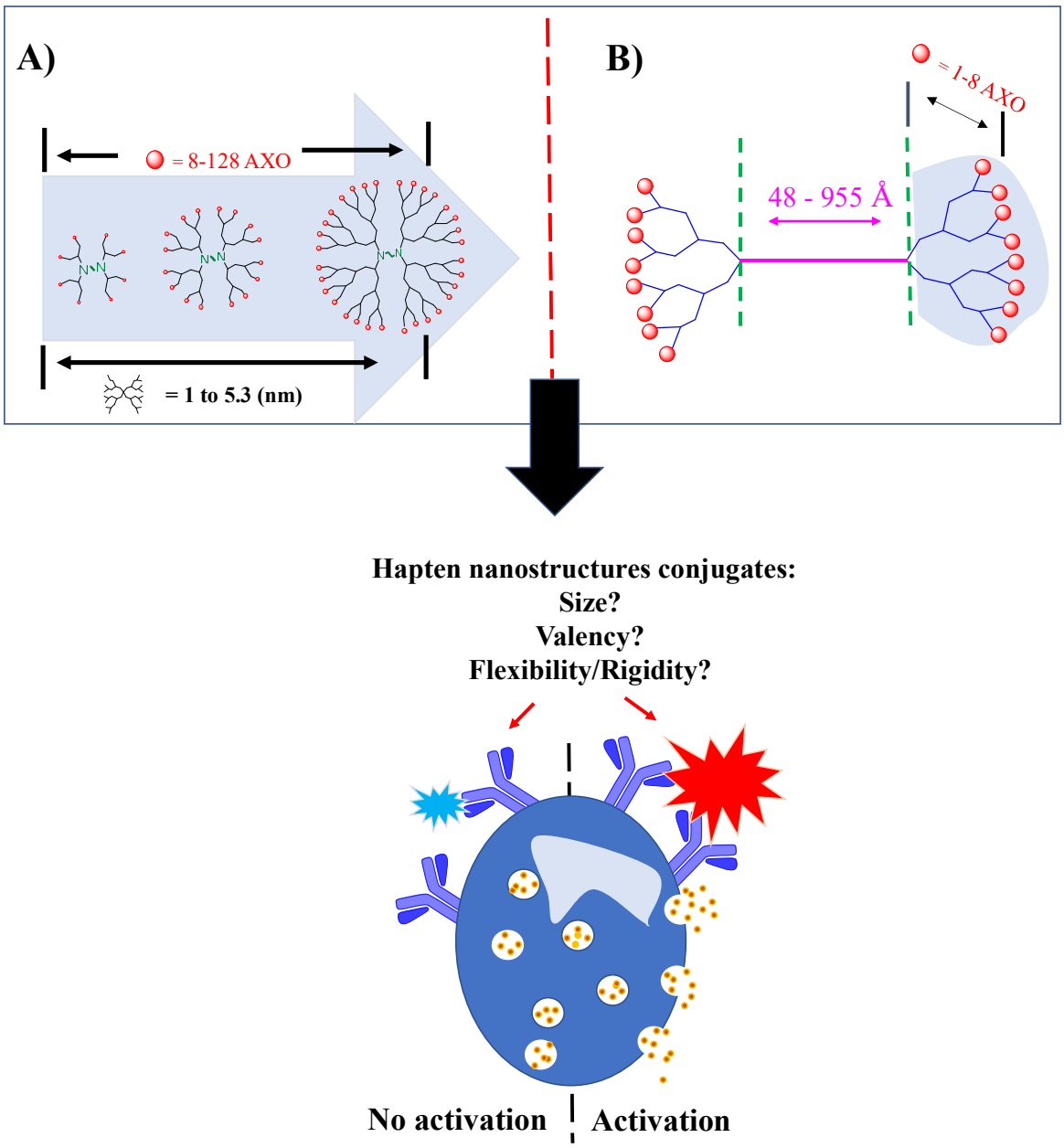

Figura R5. Explicación esquemática del estudio propuesto: A) Vista esquemática de los DeAn con diferentes grupos terminales (8-128 grupos AXO); B) Representación esquemática de nanoestructuras que varían tanto de la longitud del espaciador (PEG 600- 12000) como la del número de grupos terminales de cada dendrón (1-8 grupos AXO).

1. **Distancia entre dos haptenos.** La distancia máxima entre haptenos sería: (i) el diámetro de la nanoestructura en una estructura globular de dendrímeros; (ii) la longitud del espaciador nexo entre los dendrones en las estructuras basadas en bidendrones.

2. **Flexibilidad/rigidez de las estructuras.** Los espaciadores de PEG pueden utilizarse como espaciadores flexibles, mientras que los dendrímeros de generaciones inferiores (1 y 2) se caracterizan por un andamiaje flexible, y al incrementar el tamaño con el aumento de las generaciones, se vuelven más globulares, y cada vez más rígidos.

3. **Multivalencia.** Un dendrón o dendrímero haptenizado aumentaría la probabilidad de reconocimiento de la IgE específicas al presentar múltiples haptenos en su estructura flexible, aunque en el caso del dendrón su dimensión sería insuficiente para el proceso de entrecruzamiento. Dado que la degranulación se consigue mediante el entrecruzamiento de al menos dos IgE específicas, los sistemas de Antígenos Bidendron (BiAns) serían de interés.

Estas moléculas que presenten los requisitos estructurales para activar las células efectoras, serían de interés para aumentar la sensibilidad de los ensayos celulares de diagnóstico.

OBJETIVOS

Objetivo general

El objetivo de este estudio, a largo plazo, es aumentar la sensibilidad del ensayo *in vitro* para diagnosticar las reacciones inmediatas a AX, mediante la inclusión en el ensayo de nanoestructuras multivalentes que presenten el tamaño óptimo para que ocurran los procesos de reticulación de las células efectoras. Para generar conocimiento sobre tales requisitos estructurales, nos proponemos diseñar y sintetizar una serie de nanoestructuras decoradas con AX, para estudiar el reconocimiento molecular específico de estas estructuras y evaluar la activación que producen en células efectoras en el contexto de las respuestas alérgicas a AX.

Objetivos Específicos

1. Síntesis y caracterización estructural de una serie de DeAns a partir de dendrímeros PAMAM de diferentes generaciones (G1-G5) y decorados con AX (de 8 a 128 grupos terminales).
2. Síntesis y caracterización estructural de una serie de BiAns simétricos basados en espaciadores PEG de diferentes longitudes (MW 600-12000 Da) acoplados por ambos extremos con dendrones PAMAM-G2, decorados con AX (8 grupos por cada dendrón).

3. Síntesis y caracterización estructural de una serie de BiAns simétricos basados en andamios de dendrones tipo poliamida, variando tanto la longitud del espaciador polimérico (MW 600-12000 Da) como el número de grupos funcionales periféricos en la molécula o dendrón decorados con AX (de 1 a 8 por dendrón).
4. Evaluación de la capacidad de IgE específica a AX para reconocer todas las nanoestructuras diseñadas mediante inmunoensayos competitivos.
5. Estudiar la influencia de la longitud del espaciador de los BiAns en la formación de inmunocomplejos mediante microscopía electrónica de transmisión (TEM).
6. Evaluación de los efectos de las nanoestructuras sobre la viabilidad celular y sobre su actividad alergénica utilizando MCs derivadas de médula ósea sensibilizadas pasivamente con IgE monoclonal de ratón contra AX y células RBL-2H3 o LUVA humanizadas sensibilizadas con anticuerpos policlonales de sueros de pacientes alérgicos a AX.
7. Evaluación de la inclusión de nanoestructuras en el BAT para el diagnóstico, realizado por miembros de nuestro grupo de investigación.

Los experimentos celulares del objetivo 6 se realizaron por la Dra. Alba Rodríguez-Nogales (Unidad de Digestivo, Hospital Universitario, Granada) y la Dra. Sara Benedé (Instituto de Investigación en Ciencias de la Alimentación, Madrid) como parte de un estudio colaborativo.

Los ensayos BAT fueron realizado por miembros de nuestro grupo de investigación.

RESULTADOS Y DISCUSIÓN

Capítulo 3. Diseño, Síntesis, Caracterización y Evaluación Inmunológica de los DeAns

El diseño de DeAns implica la decoración de dendrímeros PAMAM con unidades periféricas de amoxiciloilo (AXO). Estas construcciones permitirían evaluar la influencia tanto del tamaño del dendrímero como del número de determinantes conjugados (valencia), características dadas por la generación del dendrímero, en el reconocimiento inmunológico y en la activación celular (Figura R6). Se seleccionaron los dendrímeros PAMAM como plataforma común de partida debido a su disponibilidad comercial, solubilidad en disoluciones acuosas, la presencia de grupos aminos periféricos que pueden emular la reactividad de las lisinas de las proteínas y estudios previos que muestran que los DeAns basados en PAMAM son reconocidos por la IgE específica a penicilina. El tamaño de los dendrímeros PAMAM de partida de cinco generaciones (G1 a G5) (de 1 a 5,3 nm) con núcleo de etilendiamina aumenta linealmente en función de las generaciones añadidas, a razón de aproximadamente 1 nm por generación, mientras que los grupos funcionales terminales proliferan exponencialmente en cada generación (de 8 a 128 grupos amino periféricos) [161,209].

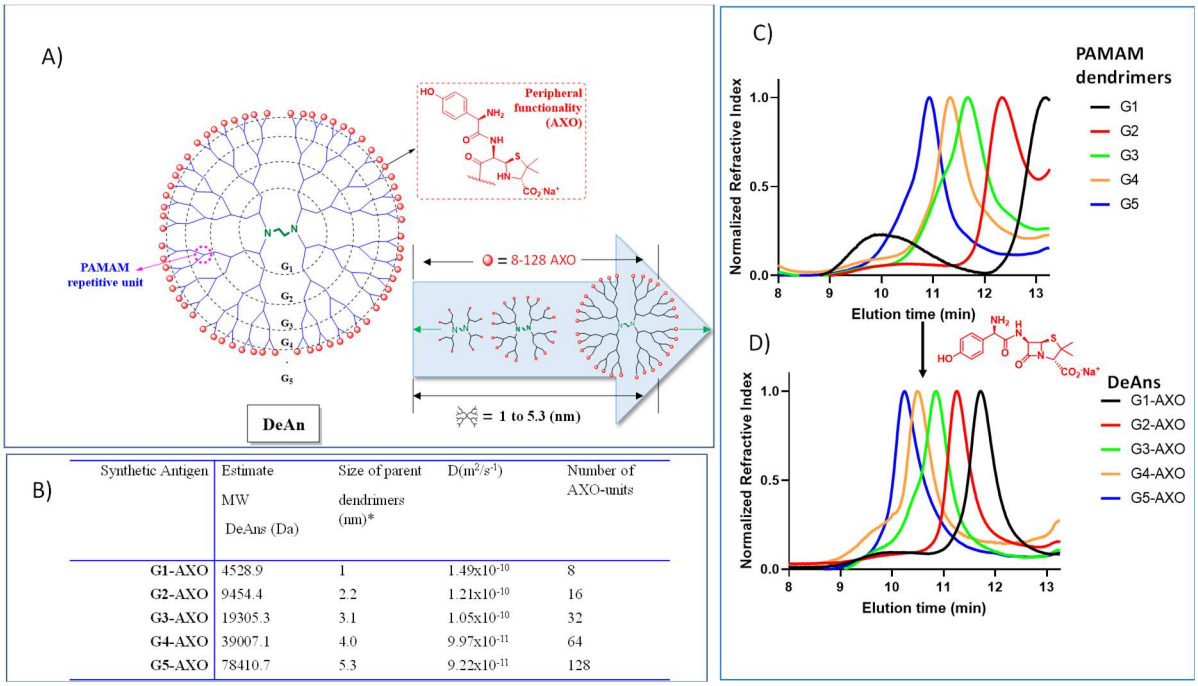

B)

Synthetic Antigen	Estimate MW DeAns (Da)	Size of parent dendrimers (nm)*	D(m^2/s^{-1})	Number of AXO-units
G1-AXO	4528.9	1	$1.49x10^{-10}$	8
G2-AXO	9454.4	2.2	$1.21x10^{-10}$	16
G3-AXO	19305.3	3.1	$1.05x10^{-10}$	32
G4-AXO	39007.1	4.0	$9.97x10^{-11}$	64
G5-AXO	78410.7	5.3	$9.22x10^{-11}$	128

Figura R6. Representación esquemática de las nanoarquitecturas dendríticas: A) La variación de tamaño depende de las generaciones (G1 a G5) en DeAn (con valencia de 8 a 128 AXO); B) Los datos descriptivos de todos los antígenos sintéticos se indican en la tabla del recuadro,

peso molecular teórico (MW), coeficiente de difusión (D) y el número de unidades AXO en la periferia de las estructuras; C) Cromatograma de Permeación en Gel (GPC) de los dendrímeros de partida, sin AXO; D) GPC de los DeAns después de conjugarlos con AX.

Los DeAns se obtuvieron mediante ataque nucleofílico de la amina libre en la periferia de los dendrímeros al anillo β-lactámico de AX. Las incubaciones de dendrímeros PAMAM (con núcleo etilendiamina) de cinco generaciones (G1-G5) con un exceso de AX se llevaron a cabo en tampón a pH básico (para asegurar la desprotonación de los grupos aminos periféricos) a baja temperatura, 4°C. Como ejemplo representativo, el esquema de síntesis y RMN-^{1}H de G1-AXO se muestran en la Figura R7 y la Figura R8, respectivamente. La baja temperatura fue un factor importante para la obtención de moléculas totalmente funcionalizadas, para reducir la movilidad de la ramas sustituidas y así disminuir el impedimento estérico, tal y como describió previamente nuestro grupo [203]. Además, el tiempo de incubación necesario para la funcionalización completa era mayor para las generaciones más altas.

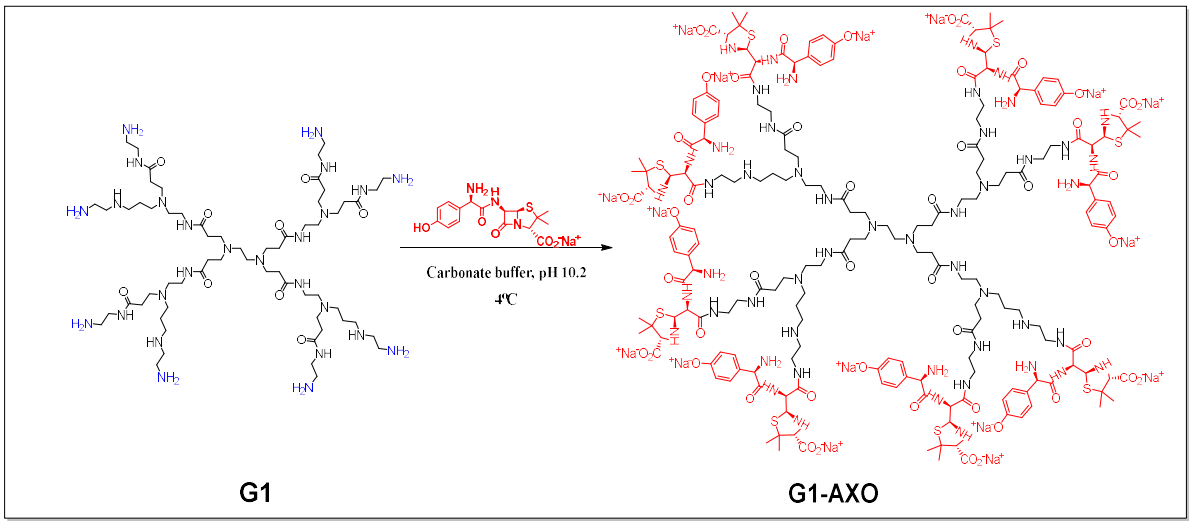

Figura R7. Ilustración esquemática representativa de la síntesis de G1-AXO. El dendrímero PAMAM comercial (G1) se incubó con AX en disolución acuosa a pH básico y a baja temperatura hasta su completa funcionalización.

La purificación se realizó de forma eficiente mediante cromatografía de filtración en gel utilizando columnas de Sephadex. La caracterización y monitorización de las reacciones se realizaron mediante RMN-^{1}H y ^{13}C, siendo esta última la que proporciona más información sobre la funcionalización completa de los grupos aminos. Así, la formación del enlace amida se confirmó por el desplazamiento de los protones de los metilenos terminales del dendrímero

de 2,72 a 3,26 ppm. El desplazamiento parcial de este protón se utilizó como método de control para decidir la necesidad de refrescar la reacción con AX.

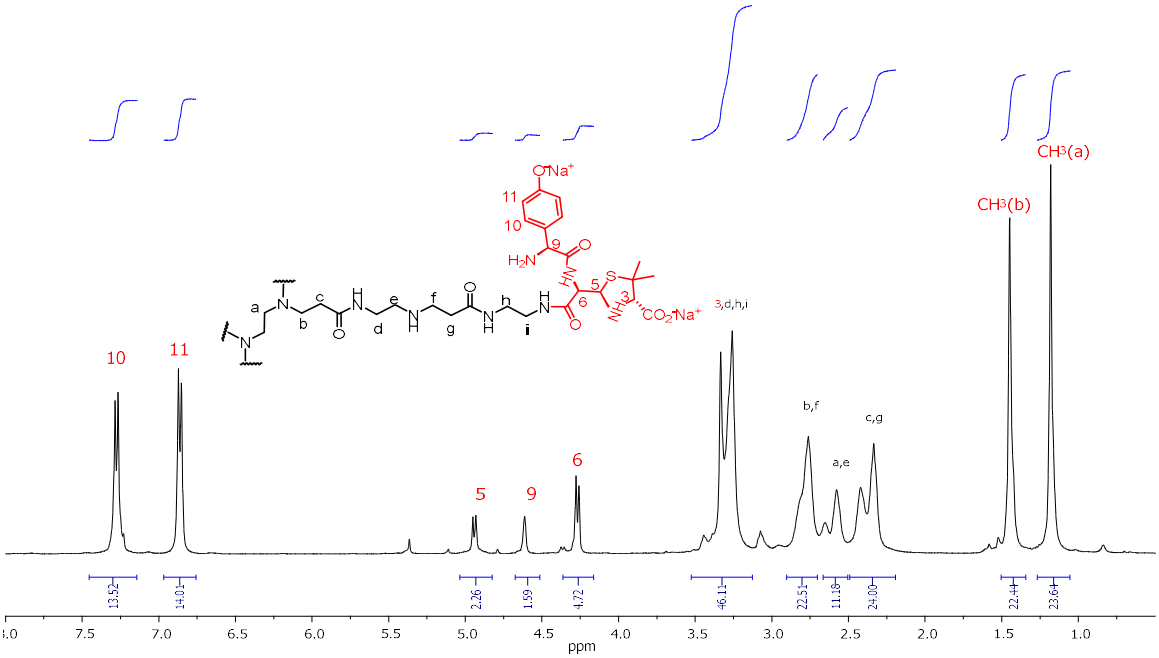

Figura R8. Ejemplo representativo de los espectros de RMN-^{1}H de DeAns: espectro de G1-AXO en óxido de deuterio (D_2O) con supresión de la señal del disolvente. La integración de los protones de la región aromática y de los grupos metilo del anillo de tiazolidina, que no se solapan con otros, se utilizó para estimar el grado de funcionalización con AXO.

Además, la presencia de la forma abierta de la β-lactama unida al dendrímero se evidenció por el desplazamiento y la separación de las señales correspondientes a los protones de la β-lactama (H5 y H6) a un campo más alto en comparación con el desplazamiento de la β-lactama cerrada en la AX libre (dobletes a 5,42 y 5,41 ppm). Por último, la confirmación de la finalización de la reacción se obtuvo mediante RMN-^{13}C observando el desplazamiento de la señal del residuo de etileno terminal debido a la reacción de condensación. El desplazamiento de los carbonos (h) e (i) (41,9 y 40,0 ppm, respectivamente) en el dendrímero PAMAM-G1 (Figura R9A) a campo alto (38,8 y 38,7 ppm) en G1-AXO (Figura R9B), indica la ausencia de señales para el carbono unido a los grupos aminos sin funcionalizar. Se obtuvieron rendimientos que oscilan entre el 69 y el 82 %, siendo el mayor rendimiento para las generaciones inferiores y el menor para las generaciones superiores de los dendrímeros.

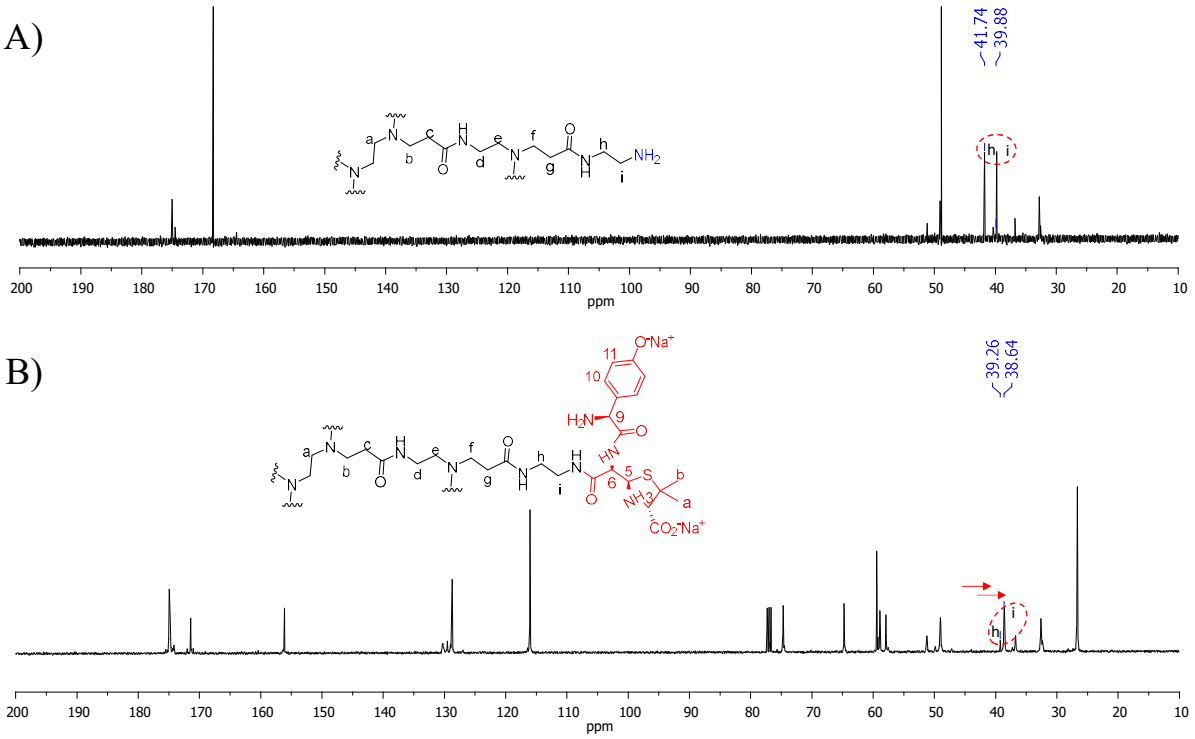

Figura R9. Ejemplo representativo de los espectros de RMN-^{13}C del dendrímero PAMAM-G1 inicial (A) y del G1-AXO (B) en D_2O utilizando el desplazamiento químico del cloroformo deuterado ($CDCl_3$) como referencia. Se señala (con flechas) el desplazamiento de la señal del residuo de etileno terminal debido a la reacción de condensación.

La capacidad de los DeAns de ser reconocidos por IgE específica a AX se evaluó mediante inmunoensayos competitivos (ensayos de inhibición de RAST –prueba de radioalergoadsorción–) empleando un pool de sueros de pacientes alérgicos a AX. Los resultados indican el reconocimiento por IgE específica a AX de todas las estructuras, de forma dependiente de la concentración de AXO (Figura R10). La capacidad de los DeAns para inducir la degranulación celular dependiente de IgE se evaluó empleando tres tipos diferentes de células: mastocitos de ratón derivados de la médula ósea, células RBL-2H3 y LUVA. Para estos experimentos, se prepararon conjugados HSA-AXO y se caracterizó su grado de haptenación.

Para los experimentos con mastocitos de ratón se cultivó, produjo y purificó adecuadamente un anticuerpo monoclonal (MoAb), hibridoma AO6.2 de ratón de isotipo IgE (específico de la cadena lateral AX) proporcionado por la Dra. Cristobalina Mayorga [216]. Todos los experimentos en mastocitos de ratón incluidos en esta tesis fueron realizados por la Dra. Benedé. Tras la puesta a punto de estos experimentos empleando el conjugado HSA-AXO

como antígeno (activador), se realizaron incubaciones a diferentes concentraciones de los DeAns con células (mastocitos de ratón) sensibilizadas con el MoAb anti-AX IgE de ratón.

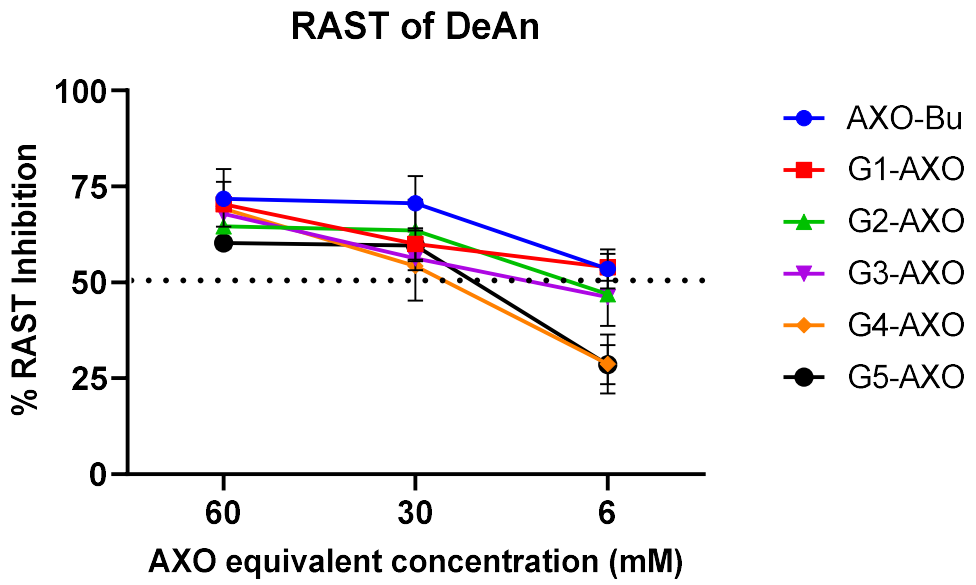

Figura R10. Ensayos de inhibición del RAST realizados con un pool de sueros de pacientes alérgicos a AX, utilizando la serie de DeAns y un conjugado de butilamina-AXO como inhibidores y discos de celulosa modificados con AXO-PLL como fase sólida. El reconocimiento de IgE específica se considera significativo con una inhibición ≥50%.

Se midió la liberación de β-hexosaminidasa para determinar la degranulación celular. El control positivo HSA-AXO, indujo alrededor de un 20% de liberación de β-hexosaminidasa, empleando una concentración de 10 µM de unidades AXO, la concentración más baja evaluada para los DeAns (Figura R11B). Los DeAns de menor generación, G1-AXO y G2-AXO, no dieron lugar a la activación de las células. Sin embargo, los DeAns de generaciones mayores (a partir de G3), mostrando un mayor número de grupos AXO así como un incremento de tamaño, han inducido la liberación de β-hexosaminidasa, sin diferencias significativas en comparación con el control positivo (HSA-AXO) en todas las concentraciones, excepto con G5-AXO (100µM). Esto pone de manifiesto la importancia del tamaño de las nanoestructuras como factor relevante, además de la presentación multivalente de los determinantes antigénicos. Ninguna de las células no sensibilizadas (Figura R11A) tratadas con DeAns o el control positivo (HSA-AXO) dio lugar a la degranulación, lo que indica que la activación se produce a través de un mecanismo mediado por IgE.

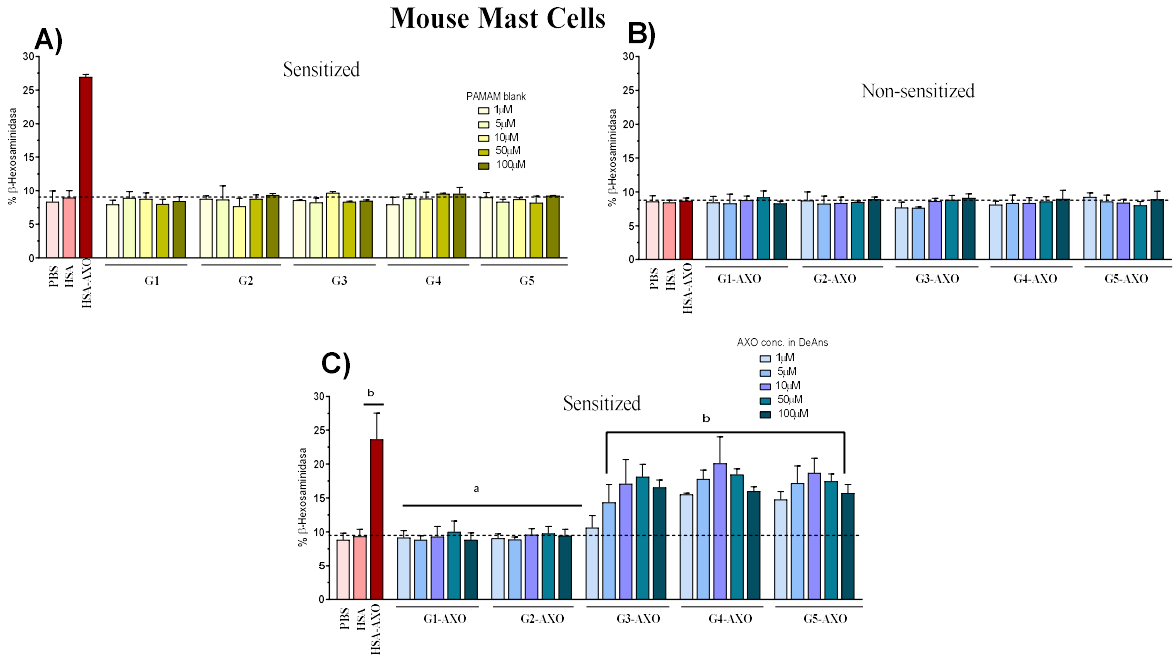

Figura R11. Ensayos de degranulación tras la incubación de MCs de ratón con la serie de DeAns a 1,5,10, 50, and 100 µM de equivalentes de AXO. A) Porcentaje de liberación de β-hexosaminidasa en MC derivados de la médula ósea sensibilizados tratados con blanco de PAMAM. B) Porcentaje de liberación de β-hexosaminidasa en MCs derivadas de médula ósea no sensibilizadas. C) Porcentaje de liberación de β-hexosaminidasa en MCs derivadas de médula ósea sensibilizadas. Se utilizaron HSA y HSA-AXO (a 10 µM de AXO) como control negativo y positivo, respectivamente. Los datos se expresan como media ± S.D. y son representativos de tres experimentos independientes. Los grupos con letras diferentes difieren estadísticamente ($P \leq 0,05$). Para las comparaciones múltiples de los datos cuantitativos, se utilizó un análisis de varianza (ANOVA) de una vía seguido de la prueba de comparaciones múltiples de Dunnett.

La capacidad de la IgE para unirse a los DeAns y entrecruzar las IgE específica en las células efectoras se investigó en un escenario más realista empleando sueros de pacientes alérgicos a AX (que contiene IgE específica) y de sujetos tolerantes. Para ello, la línea celular humanizada RBL-2H3, que comparte características tanto con los mastocitos como con los basófilos, y que expresa el receptor de IgE humano (FcεRI)] [218] se sensibilizó pasivamente con sueros de 14 pacientes alérgicos y sueros de 11 sujetos tolerantes a AX. Posteriormente, las células sensibilizadas se trataron con cuatro concentraciones diferentes de DeAns (en función de los mismos equivalentes de grupos AXO) y las estructuras blanco (sin funcionalizar con AXO,

PAMAM G1-G5). La degranulación en las células RBL-2H3 se midió como liberación total de β-hexosaminidasa. Los resultados en las células sensibilizadas con AX-alérgicos (que contienen IgE específica) demuestran que sólo los DeAns de generaciones más altas (G3 y superiores), y por tanto de mayor tamaño y valencia, han dado lugar a una degranulación dependiente de la concentración de AXO, comparado con un grupo de control negativo (PBS) (Figura R 12B). Se obtuvo una mayor degranulación con las células estimuladas con G5-AXO, con la mayor valencia (128 unidades AXO) y el mayor tamaño, en todas las concentraciones y mostrando una respuesta máxima a 100 μM (Figura R 12B). Cuando las células RBL-2H3 incubadas con los sueros de los sujetos tolerantes fueron tratados con todas las estructuras (DeAns, dendrímeros blanco -sin funcionalizar- o estructura de control HSA-AXO), ninguna de ellas indujo la degranulación celular (Figura R 12A).

Para reforzar nuestra observación con los dos tipos de células descritas anteriormente, se evaluaron además los efectos de los DeAns en células LUVA, que son células de mastocitos humanos inmortalizadas que presentan altos niveles de receptor FcεRI [219]. Al igual que las RBL-2H3, las LUVA se incubaron con sueros de pacientes alérgicos y de sujetos tolerantes y se expusieron a diferentes concentraciones de los DeAns y de las estructuras blanco (sin AXO). De nuevo se midió la liberación exocitótica estimulada del marcador de gránulos, β-hexosaminidasa. Los resultados de degranulación (Figura R13B) indican que sólo los DeAns basados en PAMAM de mayor generación (G3 y superiores) provocaron la degranulación de las células y que es dependiente de la concentración de AXO, en consonancia con los dos estudios celulares descritos anteriormente. Las estructuras derivadas de las generaciones más altas, G4-AXO (64 unidades AXO) y G5-AXO (128 unidades AXO) estimularon la respuesta de degranulación sin diferencia estadísticamente significativa con HSA-AXO, incluso a la concentración más baja evaluada (10 μM). En condiciones en las que el HSA-AXO multivalente estimula una respuesta máxima de ~30% de liberación granular, ninguna de las estructuras control (sin unidades AXO) ni los DeAns de menor generación, G1-AXO (con 8 unidades AXO) y G2-AXO (con 16 unidades AXO), estimularon la degranulación (Figura R13B). De aquí se deduce la importancia del tamaño si se tiene en cuenta que el conjugado HSA-AXO utilizado en este experimento tiene aproximadamente 14 unidades AXO (estimado a partir de los datos MALDI-TOF, Figura S2), que es comparable con las 16 unidades AXO presentes en G2-AXO, que no dió lugar a la activación celular. Como era de esperar, ninguna de las estructuras activó las células incubadas con sueros de sujetos tolerantes (Figura R13A).

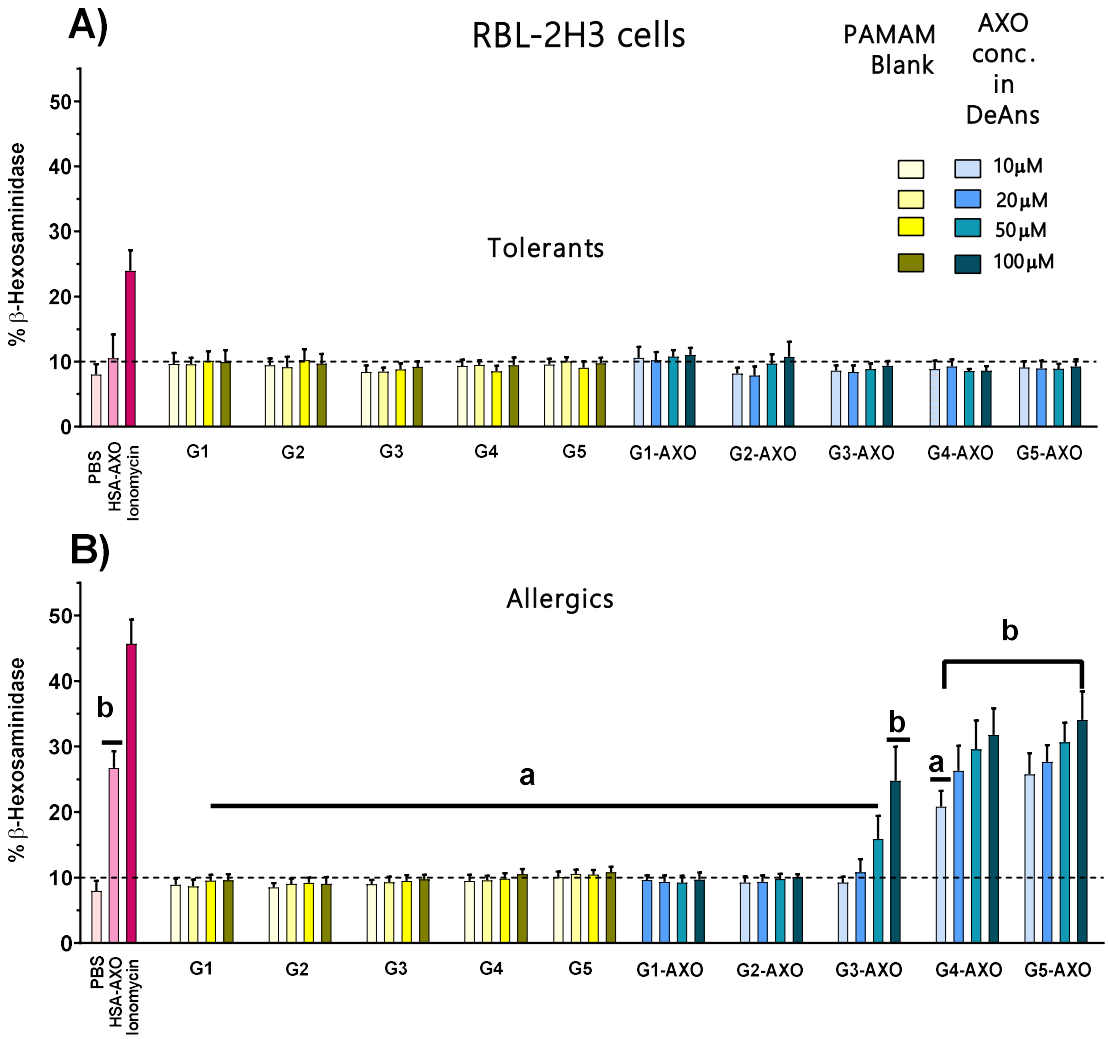

Figura R12. Impacto de los DeAns en la degranulación de las células RBL-2H3 a diferentes concentraciones (10 µM, 20 µM, 50 µM, 100 µM de AXO, en azul) y la concentración equivalente de PAMAM (sin funcionalización con AX, en amarillo) como controles negativos. A) Porcentaje de liberación de β-hexosaminidasa tras la incubación con diferentes nanoarquitecturas en células sensibilizadas con sueros de 11 sujetos tolerantes; B) Porcentaje de liberación de β-hexosaminidasa tras la incubación con nanoestructuras en células sensibilizadas con 14 sueros de diferentes pacientes alérgicos a AX. Se utilizaron PBS y HSA-AXO como control negativo y positivo respectivamente y se utilizó ionomicina para lisar las células y determinar la respuesta máxima. Los datos se expresan como medias ± S.D. Los grupos con letras diferentes difieren estadísticamente ($P \leq 0,05$). Para las comparaciones múltiples de los datos cuantitativos, se utilizó el ANOVA seguido de la prueba de comparaciones múltiples de Bonferroni. Se consideró que $P<0,05$ indicaba una diferencia estadísticamente significativa.

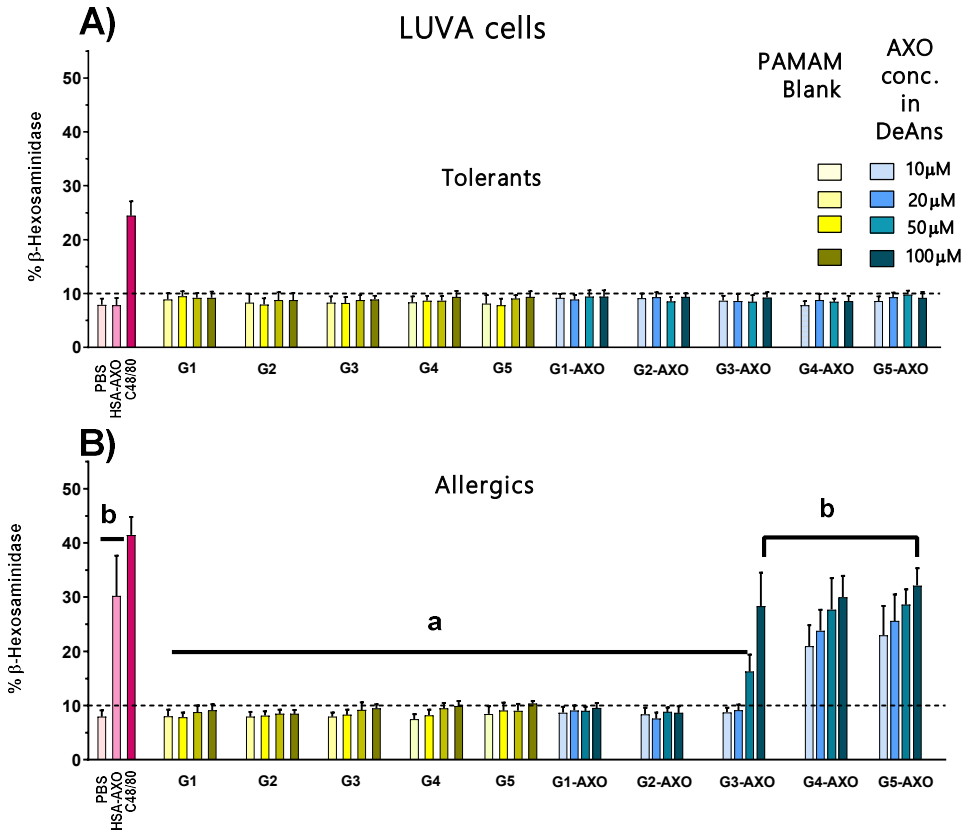

Figura R13. Degranulación de células LUVA en respuesta a DeAns a diferentes concentraciones (10 µM, 20 µM, 50 µM, 100 µM de AXO, en azul) y la concentración equivalente de estructuras PAMAM control (blanco, en amarillo). A) Las células LUVA se incubaron con sueros de sujetos tolerantes y se expusieron a estructuras PAMAM control y DeAns. La degranulación se expresa como porcentaje de liberación de β-hexosaminidasa; B) Las células LUVA se sensibilizaron con sueros de pacientes alérgicos a AX y se incubaron con estructuras PAMAM libres y DeAns. Se utilizaron PBS y HSA-AXO como control negativo y positivo respectivamente y se empleó un activador de mastocitos (C48/80) para lisar las células y determinar la respuesta máxima. Los datos se expresan como medias ± S.D. Los grupos con letras diferentes difieren estadísticamente ($P \leq 0,05$). Para las comparaciones múltiples de los datos cuantitativos, se utilizó el ANOVA seguido de la prueba de comparaciones múltiples de Bonferroni. Se consideró que $P<0,05$ indicaba una diferencia estadísticamente significativa.

En conclusión, este capítulo describe cómo las nanoarquitecturas bien definidas, con una variación paralela en el tamaño y el número de determinantes antigénicos, permiten evaluar la influencia de estos parámetros en la degranulación de las células efectoras (Figura R14).

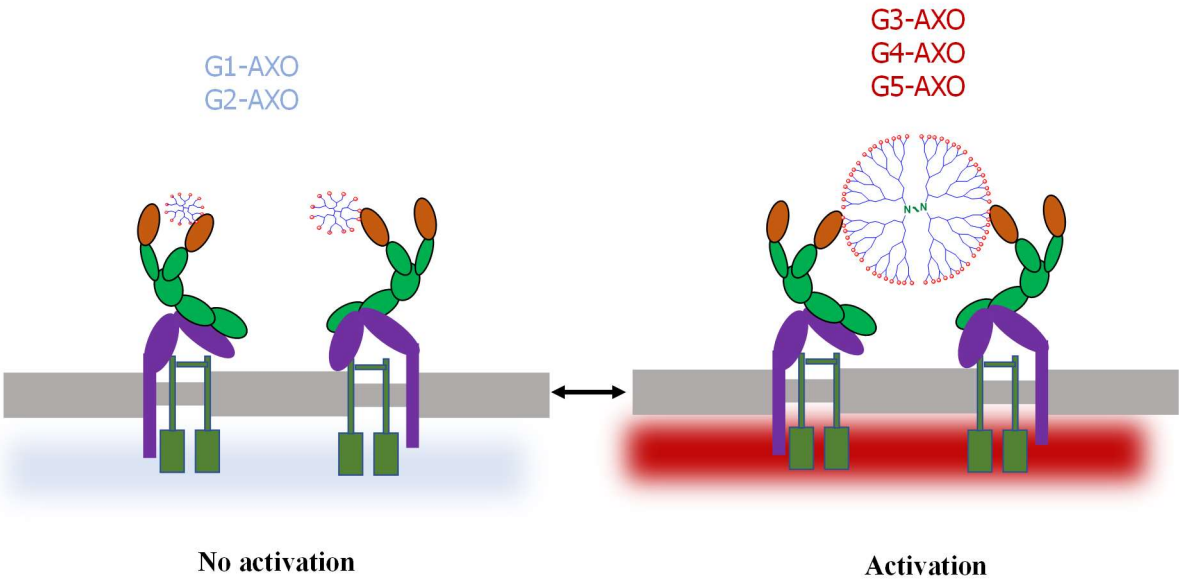

Figure R14. Ilustración de la respuesta celular con dos tipos de nanoarquitecturas con diferentes características estructurales. Los DeAns de baja generación, G1-AXO y G2-AXO, no indujeron el entrecruzamiento de FcεRI y, por tanto, no se observó ninguna activación de la respuesta celular. Sin embargo, los DeAns de mayor generación, G3-AXO, G4-AXO y G5-AXO, dieron lugar a dicho entrecruzamiento mediado por IgE, y a la consecuente activación de las células efectoras.

Los resultados demostraron las limitaciones estructurales en el entrecruzamiento de la IgE en los receptores celulares y establecieron un requisito estructural mínimo por encima del cual se produce la estimulación de las células efectoras. Además, la utilización preliminar de G4-AXO, que ha mostrado resultados positivos en todos los experimentos de activación celular pasiva, también produjo un mayor nivel de activación de basófilos en pacientes alérgicos en el BAT. Estos resultados óptimos han abierto la posibilidad de desarrollar ensayos celulares pasivos utilizando estas estructuras. Figure R14. Ilustración de la respuesta celular con dos tipos de nanoarquitecturas con diferentes características estructurales. Los DeAns de baja generación, G1-AXO y G2-AXO, no indujeron el entrecruzamiento de FcεRI y, por tanto, no se observó ninguna activación de la respuesta celular. Sin embargo, los DeAns de mayor generación, G3-AXO, G4-AXO y G5-AXO, dieron lugar a dicho entrecruzamiento mediado por IgE, y a la consecuente activación de las células efectoras.

Capítulo 4. Diseño, Síntesis, Caracterización y Evaluación Inmunológica de los BiAns

Las BiAns se diseñaron para mostrar características estructurales críticas (Figura R15): (i) mostrar múltiples unidades del determinante antigénico de AX en la periferia de los dendrones para favorecer la interacción multivalente con el anticuerpo diana; (ii) incluir un espaciador de PEG homobifuncional, hidrofílico y flexible, que proporciona una longitud específica entre los dendrones. Este último proporciona solubilidad en disoluciones acuosas [224] y reduce la adsorción inespecífica de proteínas, la inmunogenicidad y la antigenicidad [60,225].

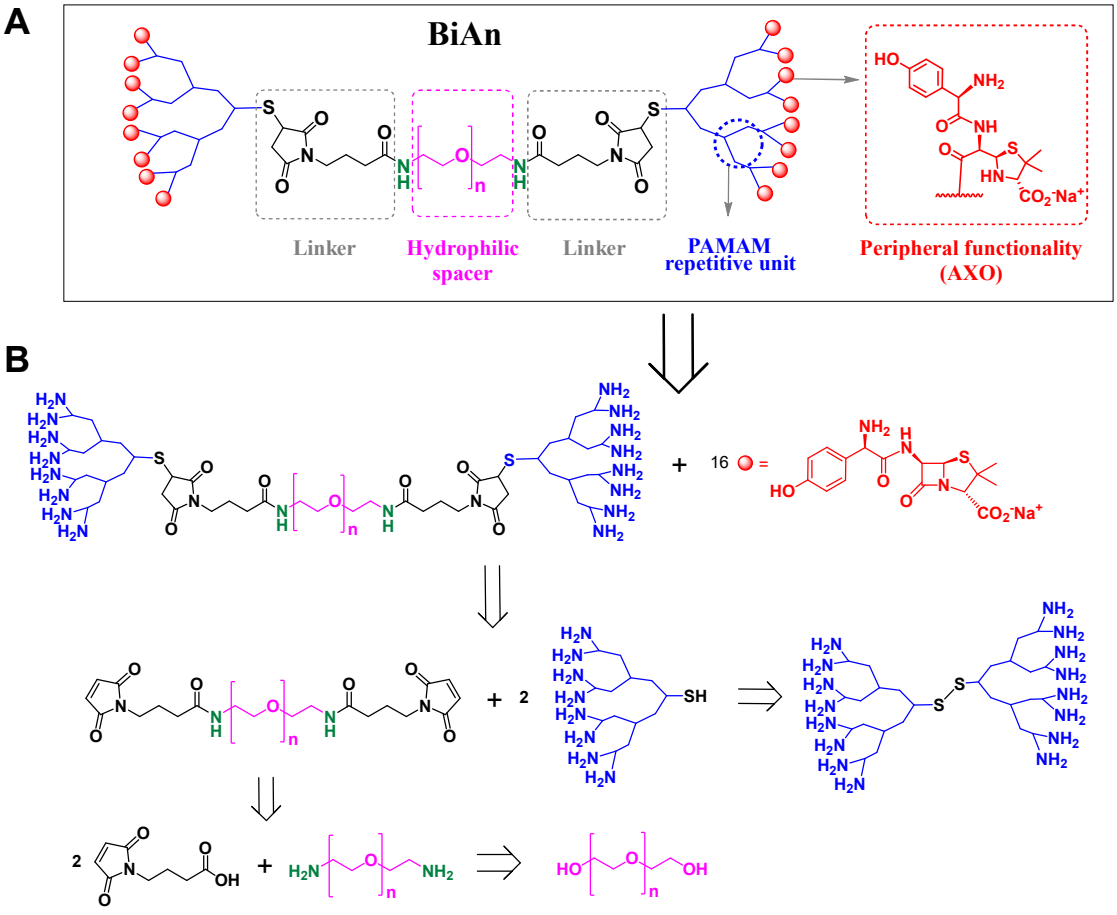

Figura R15. Representación esquemática de las nanoarquitecturas de BiAns con 16 determinantes AXO. La variación estructural entre los diferentes BiAns depende de la longitud del PEG (con n que va de 14 a 273; B) Análisis retrosintético general para los BiAns propuestos.

Se seleccionó estructuras PAMAM como andamio/plataforma para obtener conjugados acoplados covalentemente a múltiples unidades de fármacos, ya que la funcionalidad amino periférica permitía la amidación directa con β-lactamas. Se eligió la segunda generación (G2) del dendrón PAMAM como andamio dendrítico común, mientras que se utilizaron PEGs de diferentes promedios de MWs (de 600 Da a 12000 Da) como espaciador y conector. Así, los BiAns resultantes presentan el mismo número de grupos periféricos (ocho unidades AXO por dendrón, y por tanto 16 AXO por BiAns), diferenciándose únicamente en la longitud del espaciador hidrofílico que separa los dendrones. El radio de Flory de las cadenas de PEG de partida oscila entre 17 y 101 Å, y la longitud del contorno oscila entre 48 y 955 Å.

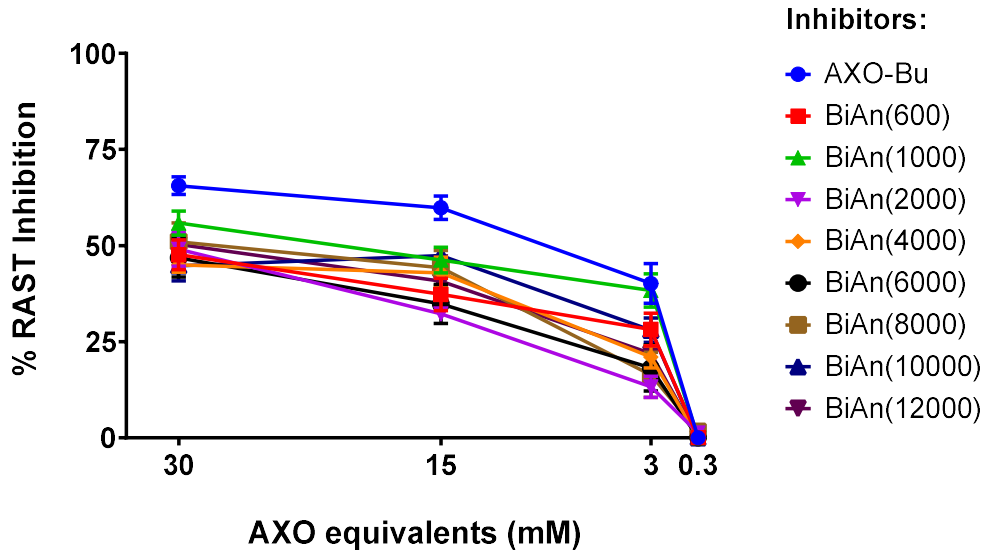

Figura R16. Ensayos de inhibición de RAST realizados con un pool de sueros de pacientes alérgicos a AX, utilizando como inhibidores la serie de BiAns y un conjugado de butilamina-AXO y empleando como fase sólida discos de celulosa modificados con AXO-PLL. El reconocimiento específico de la IgE se considera con una inhibición ≥50%.

Para sintetizar la serie de BiAns, nos basamos el análisis retrosintético general descrito en la Figura R 15B. El BiAn totalmente funcionalizado con AXO puede prepararse fácilmente modificando todos los aminos terminales del precursor del esqueleto de PEG homobidendrón utilizando un exceso de AX, que es reactivo frente a los grupos amino. La desconexión de los enlaces tioéter conduce a tres sintones, el PEG activado por bismaleimida y dos dendrones idénticos con un grupo tiol en el núcleo. Estos dendrones pueden obtenerse por reducción del dendrímero PAMAM con un núcleo de cistamina. El procedimiento sintético consistió en la

obtención de compuestos de PEG bismaleimida que permitieron el acoplamiento entre los dendrones (G2) con núcleo tiol, cuyos grupos periféricos fueron finalmente funcionalizados con AX.

El reconocimiento de los conjugados BiAns por parte de IgE específica a AX se evaluó mediante inmunoensayos de inhibición competitiva RAST utilizando un pool de sueros de pacientes alérgicos a AX (Figura R16). Los datos presentados indican que todos los compuestos son reconocidos por IgE específica a AX, de forma concentración-dependiente, sin que haya diferencias en el grado de reconocimiento de la IgE entre los distintos BiAns, ya que presentan el mismo número de equivalentes de AXO.

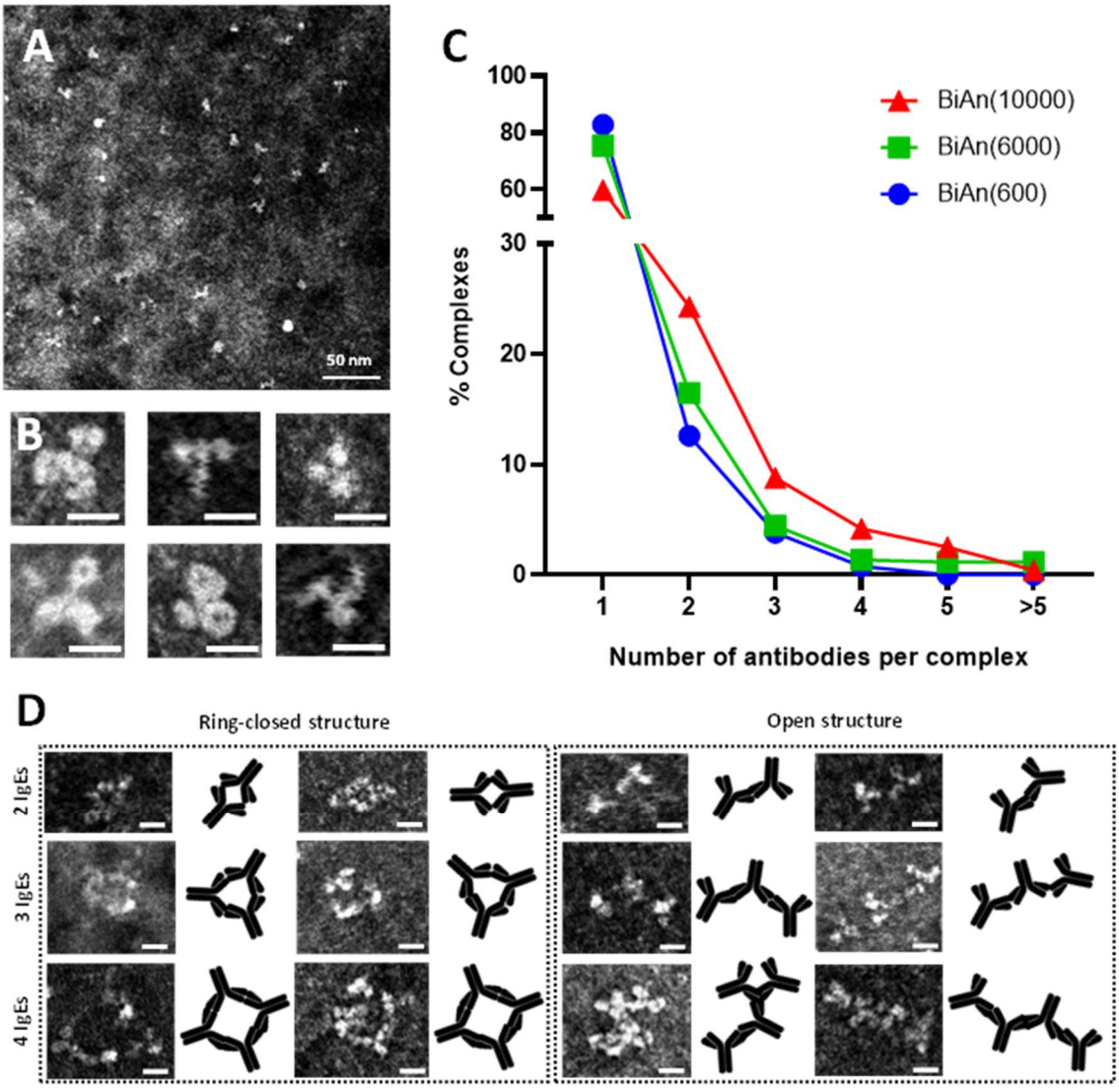

Figura R17. Micrografía electrónica de transmisión de MoAbs con tinción negativa: A) MoAbs (solo); Regiones ampliadas de imágenes de anticuerpos individuales seleccionados.

Las barras de escala representan 10 nm; C) Número de MoAbs por complejo tras la incubación con BiAn(600), BiAn(6000) o BiAn(10000); D) Regiones ampliadas de imágenes de complejos individuales seleccionados que muestran diferentes estructuras abiertas y cerradas en anillo. Las barras representan 10 nm.

Para estudiar la influencia de la longitud del espaciador de los BiAns en la formación de inmunocomplejos, se incubaron varias nanoarquitecturas (BiAn(600), BiAn(6000) y BiAn(10000)) con los anticuerpos previo a la evaluación de los complejos mediante microscopía electrónica de transmisión, con la técnica de tinción negativa. En todos los casos la formación de inmunocomplejos siguió un patrón similar, con la mayoría de las partículas observadas correspondiendo a anticuerpos individuales (60-83 %). Considerando sólo las estructuras con más de un anticuerpo por partícula, la configuración más predominante correspondía a complejos diméricos, que parecían ser la estructura más favorecida energéticamente (Figura R17C). Como puede observarse en la Figura R17C, al aumentar la longitud del espaciador de PEG en el BiAn (PEG 10000 > 6000 > 600), también aumentó el porcentaje de complejos formados por dos o más de dos anticuerpos.

Se evaluó la capacidad de las nanoarquitecturas para inducir la degranulación en mastocitos derivados de médula ósea de ratón. Para ello, se sensibilizaron las células con MoAb IgE contra AX (específico de la cadena lateral de AX) y luego se trataron con diferentes concentraciones de BiAns. La determinación de β-hexosaminidasa en la degranulación se realizó para determinar el grado de activación (Figura R18A). La estimulación de las células con HSA-AXO, que presentaba aproximadamente 14 unidades AXO (10 μM de elementos AXO), indujo un 25% de liberación de β-hexosaminidasa. Los BiAns construidos con PEG de MW ≥ 6000 Da indujeron la degranulación celular, mostrando hasta un 19% de β-hexosaminidasa liberada a concentraciones más altas (50 μM y 100 μM de grupos AXO), indicando la importancia de la longitud del espaciador polimérico para lograr la activación celular. Ninguno de los BiAns evaluados indujo la degranulación celular en células no sensibilizadas (Figura R18A), lo que indica que el mecanismo por el cual activan es dependiente de IgE.

Por otro lado, se utilizó la línea celular HumRBL-2H3, que comparte algunas características tanto con las MC como con los basófilos, y expresa el receptor de IgE humano (FcεRI) [218] para evaluar la capacidad de las nanoarquitecturas para inducir la degranulación dependiente de IgE. Las células RBL-2H3 sensibilizadas, con suero de pacientes alérgicos a la AX y de

sujetos tolerantes, se trataron con diferentes concentraciones de BiAns para comparar su efecto en función de los mismos equivalentes de los determinantes de la AXO. Las mismas moléculas de PEG pero sin funcionalización con AXO se utilizaron como estructuras control (blanco). Los resultados mostraron que las células sensibilizadas con sueros de pacientes alérgicos y estimuladas con BiAns diseñados con PEG de MW ≥ 6000 Da indujeron significativamente la liberación de β-hexosaminidasa de forma dependiente de la concentración de AXO, en comparación con los grupos de control negativo (PBS y células activadas con HSA) (Figura R18B inferior). Las concentraciones más altas de BiAns con MW ≥ 6000 Da indujeron una liberación del 33% de β-hexosaminidasa, como la inducida por HSA-AXO (a 10 µM conc de AXO) (Figura R18B).

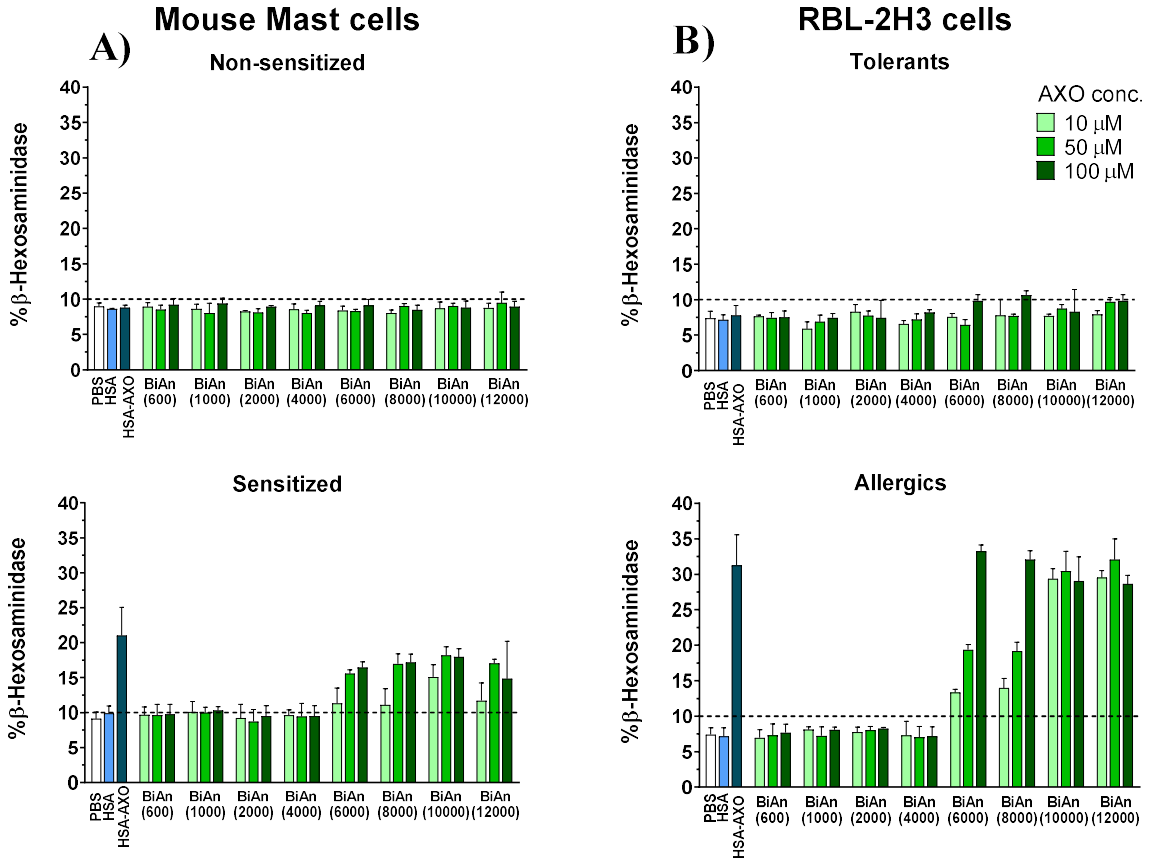

Figura R18. Ensayos de degranulación celular tras la incubación de diferentes células con la serie de BiAns a 10, 50 y 100 µM de equivalentes de AXO. Se utilizaron HSA y HSA-AXO (a 10 µM de AXO) como control negativo y positivo, respectivamente. A) Porcentaje de liberación de β-hexosaminidasa en MCs derivadas de médula ósea de ratón no sensibilizadas (arriba) y sensibilizadas (abajo); B) Porcentaje de β-hexosaminidasa liberada por células RBL-2H3 sensibilizadas con sueros de sujetos tolerantes (arriba) o con sueros de pacientes alérgicos

a AX (abajo). Los datos se expresan como media ± S.D. La línea horizontal de puntos representa la línea de base del porcentaje de liberación de β-hexosaminidasa.

Entre ellos, BiAn(10000) y BiAn(12000) son las estructuras que produjeron el entrecruzamiento de los FcεRI más eficaz, ya que indujeron más del 27% de liberación de β-hexosaminidasa a 10, 50 y 100 μM de AXO, aunque a una concentración más baja (1μM) sólo BiAn(10000) indujo una liberación sustancial de β-hexosaminidasa. No se observaron diferencias significativas en estos tratamientos con BiAns cuando las células se sensibilizaron con sueros de sujetos tolerantes (Figura R18B superior), y en células no sensibilizadas incluidas como control de la activación de IgE; mientras que se observó un efecto específico de respuesta a la concentración cuando las células se sensibilizaron con sueros de pacientes. El hecho de que ninguno de los BiAns indujera la degranulación celular en las células no sensibilizadas excluye la activación directa por la ocupación de otros receptores de la superficie celular. Además, la ausencia de activación observada en experimentos paralelos con la línea celular HMC 1.2, que presenta un fenotipo similar al de los mastocitos humanos expresando el receptor IgG (FcγR) pero no el receptor IgE de alta afinidad (FcεR), demostró que los BiAns no desencadenan la degranulación mediada por IgG (Figura S4), lo que sugiere que los BiAns estimulan la degranulación en HumRBL-2H3 a través de un mecanismo mediado por IgE.

En conclusión, de todas las estructuras BiAns evaluadas, solo aquellas basadas en PEG MW ≥6.000 tienen la capacidad para estimular la degranulación celular, indicando la importancia del tamaño del conjugado en la activación celular. A este respecto, la presentación dendrítica multivalente y la distancia entre los haptenos mayor de 6,7 nm dan lugar a un entrecruzamiento intermolecular que conduce a la activación de las células. La distancia óptima entre los determinantes AXO para un entrecruzamiento IgE eficaz es de unos 9 nm, como se observó en los experimentos de BiAn (10000).

Capítulo 5. Diseño, Síntesis, Caracterización y Evaluación Inmunológica de los BiAn-Gn

Se trata de un objetivo más ambicioso que implica la síntesis y evaluación inmunológica de 32 nanoarquitecturas. Dado que todo el proceso sintético para conseguir BiAns ha sido muy tedioso, ha consumido mucho tiempo y ha implicado muchos pasos sintéticos, se ha optimizado un procedimiento más rápido y eficiente para la construcción del segundo conjunto de BiAns (que llamamos BiAn-dGn, donde n denota la generación del dendrón) utilizando química click y dendrones basados en poliamida de diferentes generaciones (primera generación (dG1), segunda generación (dG2) y tercera generación (dG3)) y una molécula monovalente equivalente (dG0).

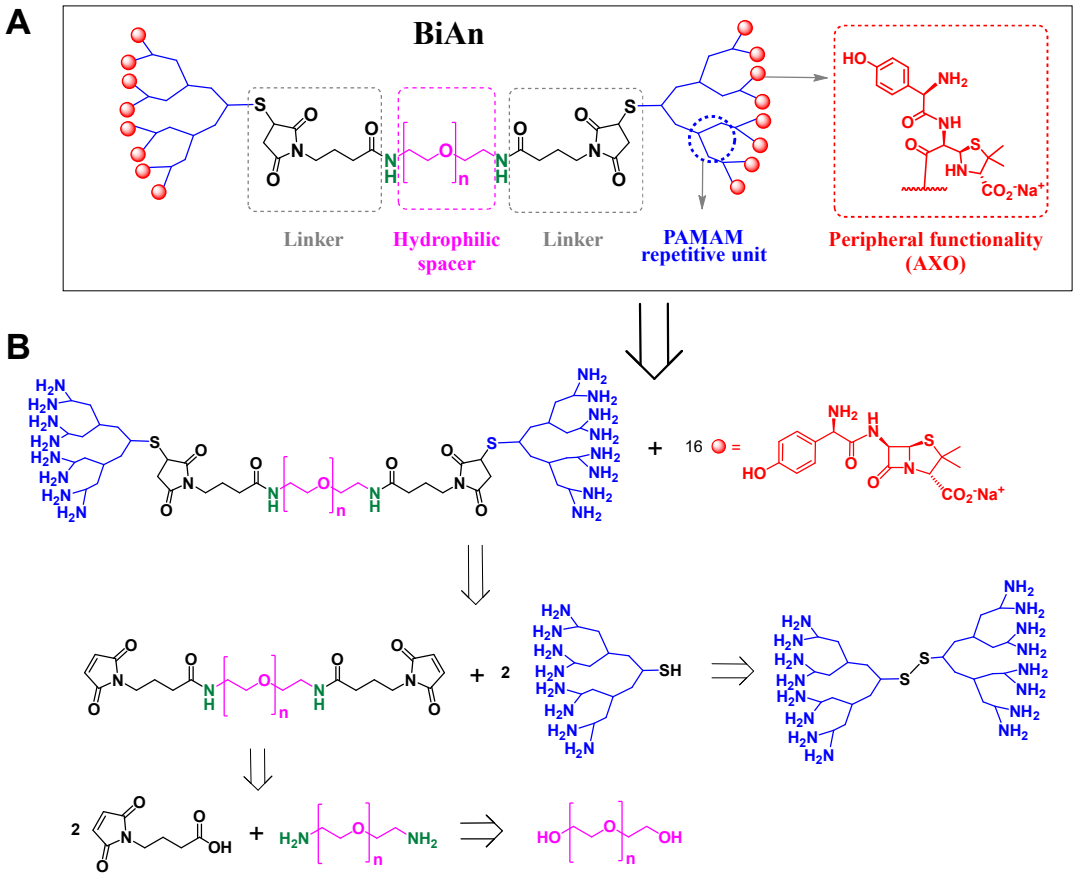

Figura R19. Representación esquemática de las nanoarquitecturas BiAn-dGn multivalentes. Los BiAn-dGn difieren entre sí por la longitud del PEG (n que va de 14 a 273) y por el número de grupos funcionales periféricos en cada extremo: la amina monovalente del propargyl-PEG2-amina (dG0 con 1 grupo funcional periférico) y los dendrones multivalentes (dG1, dG2, dG3 con 2, 4 y 8 grupos funcionales periféricos, respectivamente).

A diferencia de la librería de BiAn descrita en el capítulo anterior, la estrategia actual se centra en el diseño de una nueva librería de BiAns (BiAn-dGn), que además de variar la longitud del espaciador polimérico, presentan diferentes valencias: dos (BiAn-dG0), cuatro (BiAn-dG1), ocho (BiAn-dG2) y dieciséis (BiAn-dG3) grupos funcionales periféricos, para su posterior evaluación inmunológica.

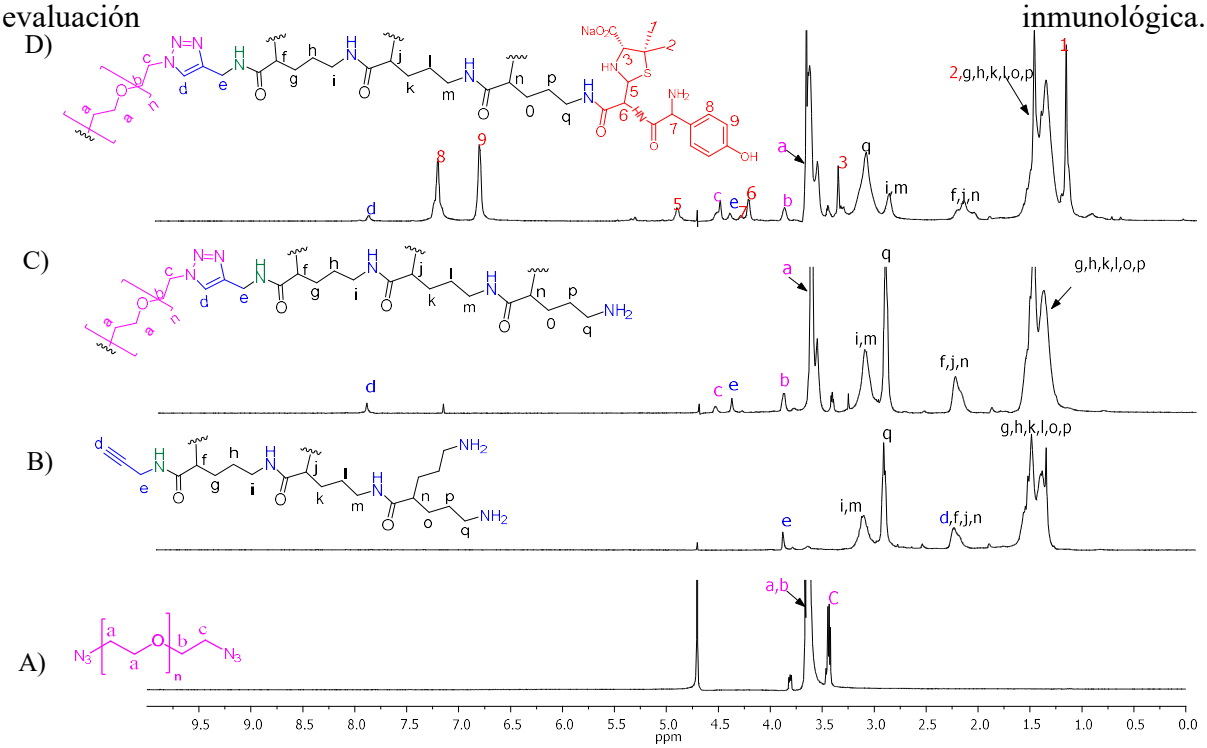

Figura R20. Espectros representativos de RMN-^{1}H en D_2O para la monitorización de las reacciones para la obtención del BiAn-dG2 donde se aprecia la aparición, desaparición y correspondiente desplazamiento químico secuencial asociado a los diferentes compuestos.

El esquema retrosintético general se ilustra en la Figura R19. Las nanoarquitecturas decoradas con AXO pueden obtenerse mediante el ataque nucleofílico de los grupos amino del precursor del esqueleto de PEG homobidendrón al anillo β-lactámico de la AX. La desconexión del enlace triazol da lugar a tres sintones: dos unidades idénticas de moléculas alquino-funcionales con grupos aminos periféricos (ya sea una molécula monovalente o dendrones multivalentes) y el PEG-diazida. Se sintetizaron diferentes PEG-$(N_3)_2$ basados en PEG de diferentes longitudes para acoplarse fácilmente con los compuestos alquinos. La conversión de los grupos hidroxilo de los extremos de las cadenas de PEG a grupos azida se ha llevado a cabo mediante el tratamiento con cloruro de tosilo (introducción del grupo saliente), seguido de la reacción con azida sódica (sustitución nucleofílica bimolecular). Para obtener el BiAn-dG0, se

seleccionó propargyl-PEG2-amina (alquino-PEG2- amina) para acoplar a ambos extremos del espaciador un brazo hidrofílico corto que permitiera funcionalización con AXO, dando lugar a estructuras funcionalizadas bi-AXO. Las otras estructuras se construyeron a partir de dendrones de poliamida con núcleo de propargilo de diferentes generaciones que contenían un número divergente de terminaciones de amina. Empleamos los dendrones (dG1, dG2 y dG3) preparados por el grupo del profesor Pérez-Inestrosa. Tanto los dendrones como los alquinos-PEG2-aminas (moléculas monovalentes) permiten reacciones ortogonales quimioselectivas en las que el grupo funcional alquino reacciona sólo con las azidas, mientras que la funcionalidad amina periférica permanece sin modificar hasta el proceso de haptenación.

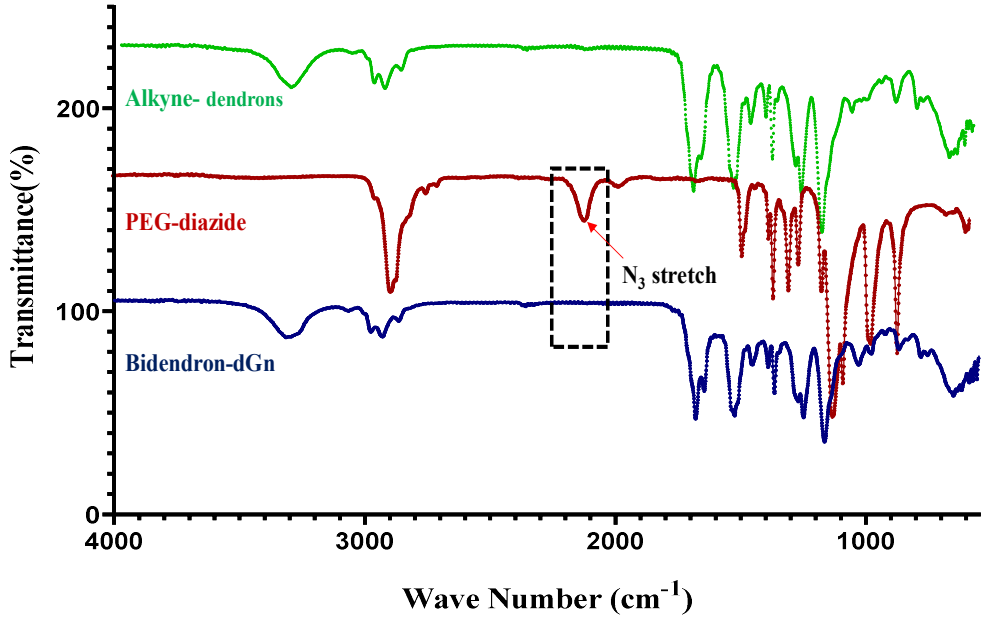

Figura R21. Espectros IR de alquinos-dendrones (verde), PEG-$(N_3)_2$ (rojo) y bidendrón-dGn que indican el consumo completo de la azida en la reacción (evidenciado por la ausencia de la banda de estiramiento de la azida en 2100 cm^{-1}).

Como procedimiento general para la síntesis de BiAn-dGn, se realizaron dos reacciones secuenciales basadas en químicas diferentes (i) la unión de ambos grupos azida en los extremos del espaciador polimérico a moléculas funcionales alquino (alquino-PEG2-amina y dendrones funcionalizados con propargilo) utilizando la química "click" CuAAC; (2) la formación del enlace amida entre los grupos aminos periféricos y el anillo β-lactámico de la AX. La CuAAC es una reacción sintética robusta que se utiliza habitualmente en la preparación de arquitecturas macromoleculares funcionalizadas [167]. El éxito de esta reacción "click" se atribuye a la

facilidad de realización, a las condiciones suaves de reacción y al uso eficiente de una amplia variedad de grupos funcionales y disolventes, incluyendo medios acuosos [244,245]. El método une regio-específicamente azidas y acetilenos terminales para dar sólo 1,2,3-triazoles 1,4-disustituidos con altos rendimientos utilizando una variedad de catalizadores de Cu(I) o precursores de estos catalizadores [246]. Para controlar la finalización de la reacción se utilizaron técnicas de RMN y de espectroscopia infrarrojo (IR). La Figura R20 muestra como ejemplo representativo de la aparición y desaparición de picos pertinentes en los espectros deRMN para la obtención del BiAn-dG2. Por otro lado, la Figura R21 muestra el espectro IR con la desaparición de las bandas correspondientes a la azida (absorción de estiramiento asimétrico a 2100 cm^{-1}) indicando el consumo completo de los grupos azida para la formación del anillo de triazol. De esta manera se obtuvo una librería de compuestos representado en la Tabla R1.

Tabla R1. Compuestos BiAn-dGn

Antígenos Sintéticos	Espaciador PEG MW(Da)	$(C_2H_4O)N$ donde N es	MW(Da) estimado	Valencia
	BiAn-dG0 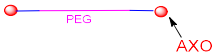			
BiAn-dG0(600)	600	14	1323.8	2
BiAn-dG0(1000)	1000	23	1723.8	2
BiAn-dG0(2000)	2000	45	2723.8	2
BiAn-dG0(4000)	4000	91	4723.8	2
BiAn-dG0(6000)	6000	136	6723.8	2
BiAn-dG0(8000)	8000	182	8723.8	2
BiAn-dG0(10000)	10000	227	10723.8	2
BiAn-dG0(12000)	12000	273	12723.8	2
	BiAn-dG1 			
BiAn-dG1(600)	600	14	2622.2	4
BiAn-dG1(1000)	1000	23	3022.2	4
BiAn-dG1(2000)	2000	45	4022.2	4
BiAn-dG1(4000)	4000	91	6022.2	4
BiAn-dG1(6000)	6000	136	8022.2	4
BiAn-dG1(8000)	8000	182	10022.2	4
BiAn-dG1(10000)	10000	227	12022.2	4
BiAn-dG1(12000)	12000	273	14022.2	4
	BiAn-dG2 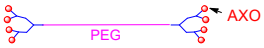			
BiAn-dG2(600)	600	14	4796.7	8
BiAn-dG2(1000)	1000	23	5196.7	8
BiAn-dG2(2000)	2000	45	6196.7	8
BiAn-dG2(4000)	4000	91	8196.7	8
BiAn-dG2(6000)	6000	136	10196.7	8
BiAn-dG2(8000)	8000	182	12196.7	8
BiAn-dG2(10000)	10000	227	14196.7	8
BiAn-dG2(12000)	12000	273	16196.7	8
	BiAn-dG3 			
BiAn-dG3(600)	600	14	9145.6	16
BiAn-dG3(1000)	1000	23	9545.6	16
BiAn-dG3(2000)	2000	45	10545.6	16
BiAn-dG234000)	4000	91	12545.6	16
BiAn-dG3(6000)	6000	136	14545.6	16
BiAn-dG238000)	8000	182	16545.6	16
BiAn-dG3(10000)	10000	227	18545.6	16
BiAn-dG3(12000)	12000	273	20545.6	16

Se realizaron inmunoensayos competitivos de inhibición de RAST utilizando sueros de pacientes alérgicos a AX (con niveles elevados de RAST, >7% de RAST utilizando discos de PLL-AXO) para estudiar el reconocimiento *in vitro* de las diferentes estructuras hacia los anticuerpos AX-sIgE. Para ello, se utilizaron en los experimentos discos de celulosa PLL-AXO (como fase sólida) y los diferentes inhibidores (BiAn-dG0, BiAn- dG1, BiAn- dG2, BiAn- dG3 y AXO-Bu) en la fase fluida. La Figura R22 muestra las curvas de inhibición de todos los BiAn-dGn en función de la concentración de las unidades AXO para comparar el patrón de reconocimiento molecular con IgE específico a AX de un pool de sueros alérgicos a AX.

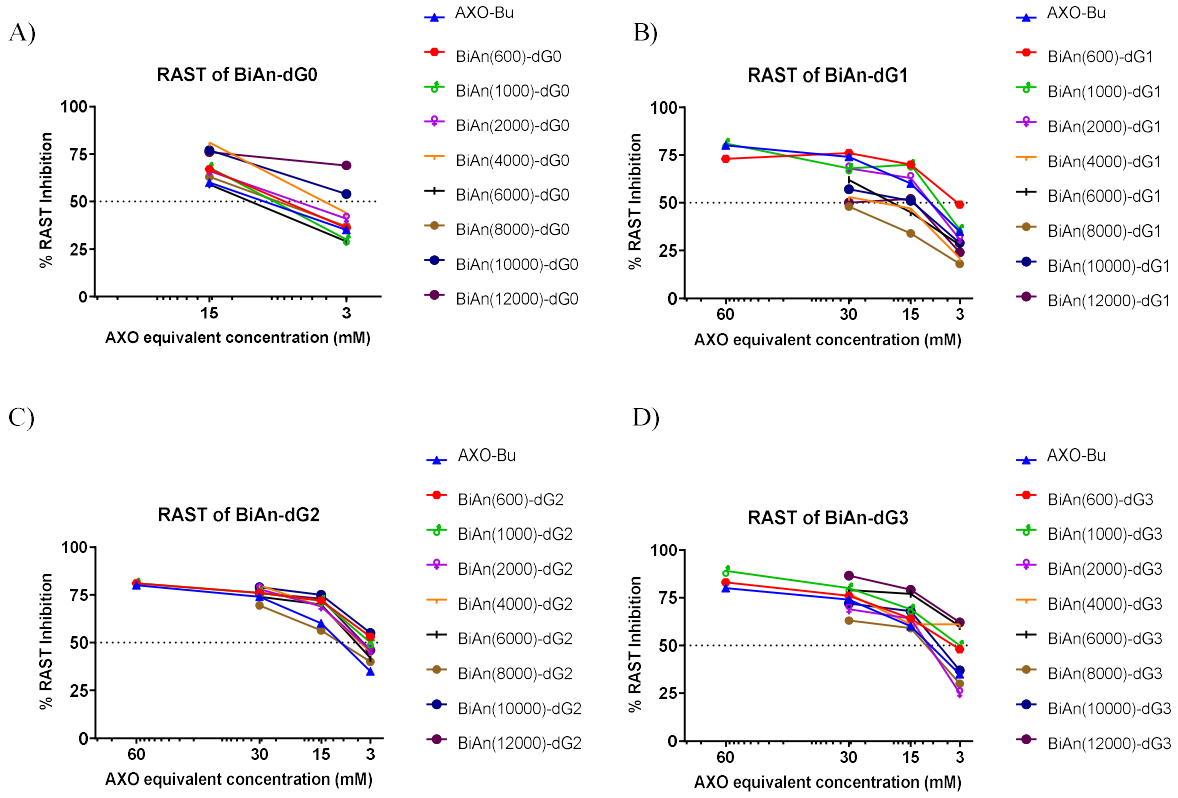

Figura R22. Ensayos de inhibición de RAST realizados con un pool de sueros de pacientes alérgicos a AX, utilizando BiAn-dG0 (A), BiAn- dG1(B), BiAn- dG2(C), BiAn- dG3 (D), construidos con espaciadores poliméricos de diferente longitud, y AXO-Bu como inhibidores. Los discos de celulosa modificados con PLL-AXO se utilizaron como fase sólida. El reconocimiento específico de la IgE se considera significativo con una inhibición ≥50%.

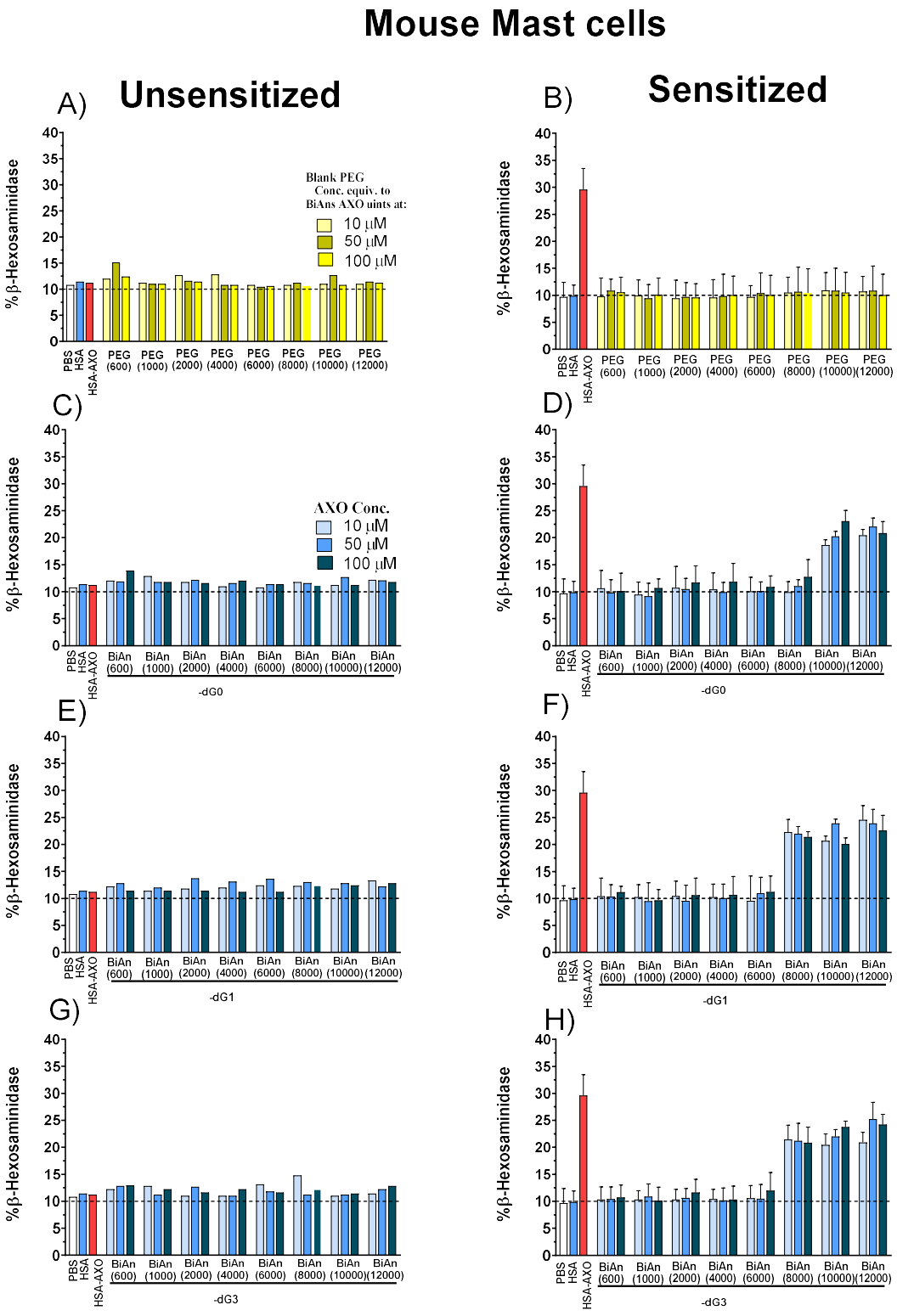

Figura R23. Ensayos de degranulación tras la incubación de las células con las series de BiAn-dGn a 10, 50 y 100 μM de equivalentes de AXO. Se utilizaron HSA y HSA-AXO (a 10 μM de AXO) como control negativo y positivo, respectivamente. A) Porcentaje de liberación de β-hexosaminidasa en MCs no sensibilizadas tratadas con estructuras PEG blanco, utilizando

concentraciones equivalentes a los BiAn-dGn con 10, 50 y 100 μM de AXO; B) Porcentaje de liberación de β-hexosaminidasa en MCs sensibilizadas tratadas con estructuras PEG blanco; C) Porcentaje de β-hexosaminidasa liberada por células no sensibilizadas tratadas con BiAn-dG0; D) Porcentaje de β-hexosaminidasa liberada por las células sensibilizadas tratadas con BiAn-dG0; E) Porcentaje de β-hexosaminidasa liberada por las células no sensibilizadas tratadas con BiAn-dG1; F) Porcentaje de β-hexosaminidasa liberada por las células sensibilizadas tratadas con BiAn-dG1; G) Porcentaje de β-hexosaminidasa liberada por las células no sensibilizadas tratadas con BiAn-dG3; H) Porcentaje de β-hexosaminidasa liberada por las células sensibilizadas con BiAn-dG3. Los datos se expresan como media ± S.D. La línea de base del porcentaje de liberación de β-hexosaminidasa está representada por la línea horizontal punteada.

Se evaluó la capacidad de los diferentes BiAn-dGn espaciados por polímeros con diversas multivalencias para estimular la degranulación de MCs derivadas de médula ósea sensibilizadas y tratadas con diferentes concentraciones (10, 50 y 100 μM de AXO) de BiAn-dGn (Figura R23). Debido a problemas técnicos, las estructuras basadas en BiAn-dG2 no pudieron evaluarse adecuadamente y los experimentos se realizarán próximamente. En condiciones de células sensibilizadas, en las que el HSA-AXO multivalente, a concentración de 10 μM de AXO, estimuló una respuesta máxima de aproximadamente un 28 % de liberación granular, ninguna de las estructuras BiAn-dGn que contenían los espaciadores más cortos ni las estructuras blanco de PEG indujeron la degranulación. Sin embargo, las estructuras BiAn-dGn que contenían los espaciadores más largos mostraron la capacidad de activar la degranulación celular. Sorprendentemente, independientemente de la diferencia en el número de determinantes antigénicos, todas las nanoestructuras probadas basadas en el espaciador polimérico más largo indujeron la degranulación celular: BiAn-dG0 (con 2 unidades AXO) que contenía PEG MW ≥ 10000 Da, así como tanto BiAn-dG1 (con 4 unidades AXO) como BiAn-dG3 (con 16 unidades AXO) basadas en PEG MW ≥ 8000 Da. Las MCs no sensibilizadas y tratadas con las estructuras de PEG blanco o con BiAn-dGn dieron lugar a una degranulación similar al control negativo. Esta ausencia de degranulación en las células no sensibilizadas excluye la activación por un mecanismo independiente de IgE.

Esto indica que las estructuras más simples, que son bivalentes, son capaces de unir dos IgE en los receptores FcεRI de las células dando lugar a la degranulación de las MCs. Los hallazgos muestran que las estructuras que llevan al menos dos unidades AXO con una distancia mínima

de ~18 nm dan lugar a la degranulación de las MCs (Figura 5.10 D). Dos factores podrían contribuir a que las estructuras BiAn-dGn (n=1,3) más cortas basadas en PEG MW 8000 Da se activen: (i) la contribución de las dimensiones del dendrón al tamaño total; (ii) la exposición de más unidades AXO.

En conclusión, este capítulo describe el desarrollo de estructuras bien definidas con variación simultánea tanto en el número de determinantes antigénicos como en la distancia entre haptenos definida por el espaciador polimérico, aportando un enfoque novedoso para estudiar la degranulación de las MCs en la reacción alérgica a AX. En resumen, el entrecruzamiento de FcεRI en la membrana celular de las células efectoras requiere de estructuras que posean mínimamente dos determinantes antigénicos cumpliendo el requisito de distancia mínima entre ellos.

Capítulo 6. **CONCLUSIONES**

1. Los dendrímeros PAMAM funcionalizados en su periferia con AXO, son reconocidos por la IgE específica de forma dependiente de la concentración, como conjugados antigénicos sintéticos, imitando los conjugados formados *in vivo* con proteínas naturales. Por lo tanto, el uso de dendrímeros de diferentes generaciones (de G1 a G5, que presentan de 8 a 128 AXO periféricos, junto con un tamaño linealmente creciente) permite la preparación de DeAns sintéticos con estructuras bien definidas desde el punto de vista químico.
2. Sólo los DeAns basados en la tercera generación (G3, con 32 AXO) y superiores pueden inducir la degranulación de las células efectoras. Estos resultados fueron consistentes en diferentes células efectoras (MCs derivadas de la médula ósea de ratón, RBL-2H3 y células LUVA) sensibilizadas con IgE específicas (monoclonal de ratón o policlonal de pacientes alérgicos), indicando que el mayor tamaño de la molécula portadora y la mayor valencia favorecen la activación celular.
3. Una serie de BiAns simétricos, basados en dos dendrones PAMAM de segunda generación (G2) funcionalizados con 8 AXO (por dendrón) y unidos entre sí con espaciadores PEG de diferentes longitudes (PEG 600 - PEG 12000) se han preparado como estructuras bien definidas desde el punto de vista químico, mediante la realización de una serie de reacciones sintéticas que incluyen "click" tiol-maleimida para el acoplamiento de los dendrones al PEG. Estas estructuras son reconocidas por la IgE específica a AX de forma dependiente de la concentración de equivalentes AXO, sin que haya diferencias en el grado de reconocimiento de la IgE entre los distintos BiAns.
4. Del estudio SAR de los BiAns, en su evaluación utilizando diferentes células efectoras (MCs derivadas de la médula ósea de ratón y RBL-2H3) sensibilizadas con IgE específica (monoclonal de ratón o policlonal de pacientes alérgicos), se puede deducir que sólo los BiAns basados en PEG MW $\geq$ 6000 estimulan la degranulación celular a través de un mecanismo dependiente de IgE. La estructura óptima es la BiAn basada en PEG MW $\geq$ 10000, lo que refleja la influencia del tamaño del conjugado fármaco-molécula portadora en el proceso de entrecruzamiento de la IgE. De hecho, los DeAn, basados en dendrímero PAMAM de segunda generación (G2), no activan a las células efectoras, pero pueden convertirse en activadores mediante la incorporación

únicamente de espaciadores poliméricos de tamaño adecuado, lo que pone de manifiesto la importancia de la distancia entre los determinantes antigénicos.

5. De los estudios realizados por TEM se deduce que la proporción de inmunocomplejos y el número de anticuerpos por complejo son mayores para las estructuras BiAn que mejor inducen respuestas celulares, en comparación con el resto de estructuras estudiadas (BiAn (10000) > BiAn (6000) > BiAn (600)).
6. Una librería de BiAns simétricos funcionalizados con AXO, BiAn-dGn, variando ambos parámetros: la generación del dendrón (Gn 0-3, mostrando 1, 2, 4 y 8 grupos de AXO por dendrón) y la longitud del espaciador (PEG MW 600-12000), puede lograrse eficientemente a través de un protocolo sencillo que implica la química "click" de CuAAC para el acoplamiento de bis-azida-PEG con dendrones de poliamida con núcleo acetileno. Estas estructuras BiAn-dGn son reconocidas por IgE específica a AX (de pacientes) de forma dependiente de la concentración de AXO.
7. Del estudio del SAR de BiAn-dGn, en su evaluación con MCs derivadas de la médula ósea sensibilizadas con IgE monoclonal de ratón contra AX, se puede deducir que de los BiAn-dGn (n=1,3) sólo aquellos basados en PEG MW ≥ 8000 estimulan la degranulación celular, mientras que para el BiAn-dG0 se necesita un espaciador más largo, basado en PEG MW ≥ 10000, para la activación celular.

Como observaciones finales, se resumen las siguientes afirmaciones generales:

- La evaluación inmunológica de diferentes antígenos sintéticos, basados en estructuras dendriméricas, con estructuras bien definidas han establecido los requisitos estructurales mínimos para que se produzca tanto el reconocimiento molecular de la IgE como la estimulación de las células efectoras en el contexto de la alergia a la AX.
- El reconocimiento de IgE específica a los determinantes de AX puede tener lugar en todas las estructuras sintéticas que presenten al menos una unidad de AXO accesible al anticuerpo. Este proceso de unión de la IgE se produce independientemente del tamaño de la estructura del antígeno, aunque una mayor proporción de inmunocomplejos y número de anticuerpos por complejo están implicados para las estructuras de mayor tamaño, que inducen mejor las respuestas celulares.
- La activación de la respuesta celular a AX puede producirse con una estructura de antígeno que contenga al menos dos grupos de AXO (determinantes antigénicos) separados entre ellos por la distancia mínima óptima, lo que pone de manifiesto la importancia del tamaño del antígeno para este proceso.

References

[1] *World Health Organization, International drug monitoring: the role of national centres., 1972.*

[2] *T. Bush, Adverse drug reactions in hospitalized patients., JAMA. 280 (1998).*

[3] *R. Warrington, F. Silviu-Dan, T. Wong, Drug allergy, Allergy, Asthma Clin. Immunol. 14 (2018) 129–139.*

[4] *B. Y-H Thong, T.-C. Tan, B. Yu-Hor Thong MBBS MRCP, Epidemiology and risk factors for drug allergy, (2011).*

[5] *D.A. Khan, R. Solensky, Drug allergy, J. Allergy Clin. Immunol. 125 (2010) S126–S137.*

[6] *P. Demoly, N.F. Adkinson, K. Brockow, M. Castells, A.M. Chiriac, P.A. Greenberger, D.A. Khan, D.M. Lang, H.-S. Park, W. Pichler, M. Sanchez-Borges, T. Shiohara, B.Y.-H. Thong, International Consensus on drug allergy, Allergy. 69 (2014) 420–437.*

[7] *C. Mayorga, T.D. Fernandez, M.I. Montañez, E. Moreno, M.J. Torres, Recent developments and highlights in drug hypersensitivity, Allergy. 74 (2019) 2368–2381.*

[8] *J.A. Anderson, Allergic Reactions to Drugs and Biological Agents, (2015).*

[9] *W.J. Pichler, Immune pathomechanism and classification of drug hypersensitivity, Allergy. 74 (2019) all.13765.*

[10] *W.J. Pichler, A. Beeler, M. Keller, M. Lerch, S. Posadas, D. Schmid, Z. Spanou, A. Zawodniak, B. Gerber, Pharmacological interaction of drugs with immune receptors: The p-i concept, Allergol. Int. 55 (2006) 17–25.*

[11] *B. Schnyder, W.J. Pichler, Mechanisms of drug-induced allergy, Mayo Clin. Proc. 84 (2009) 268–272.*

[12] *W.J. Pichler, Direct T-cell stimulations by drugs — bypassing the innate immune*

system, 209 (2005) 95–100.

[13] W.J. Pichler, O. Hausmann, Classification of Drug Hypersensitivity into Allergic, p-i, and Pseudo-Allergic Forms, Int. Arch. Allergy Immunol. 171 (2017) 166–179.

[14] T.V. Rajan, The Gell–Coombs classification of hypersensitivity reactions: a re-interpretation, Trends Immunol. 24 (2003) 376–379.

[15] W.J. Pichler, Division, Drug hypersensitivity reactions: Classification and relationship to T-Cell activation, Drug Hypersensitivity. (2007) 168–189.

[16] J.M. Paar, N.T. Harris, D. Holowka, B. Baird, Bivalent Ligands with Rigid Double-Stranded DNA Spacers Reveal Structural Constraints on Signaling by FcεRI, J. Immunol. 169 (2002) 856–864.

[17] M.W. Handlogten, T. Kiziltepe, N.J. Alves, B. Bilgicer, Synthetic Allergen Design Reveals the Significance of Moderate Affinity Epitopes in Mast Cell Degranulation, ACS Chem. Biol. 7 (2012) 1796–1801.

[18] J. Descotes, G. Choquet-Kastylevsky, Gell and Coombs's classification: Is it still valid?, Toxicology. 158 (2001) 43–49.

[19] I. Pali-schöll, E. Jensen-jarolim, Allergy Frontiers: Classification and Pathomechanisms, Springer Japan, Tokyo, 2009.

[20] I. Doña, M.J. Torres, M.I. Montañez, T.D. Fernández, In Vitro Diagnostic Testing for Antibiotic Allergy, Allergy. Asthma Immunol. Res. 9 (2017) 288.

[21] I. Doña, M.J. Torres, F. Gómez, M. Salas, C. Rondón, M.G. Canto, M. Blanca, Drug Hypersensitivity Reactions : Response Patterns , Drug Involved , and Temporal Variations in a Large Series of Patients, 22 (2012) 363–371.

[22] K.G. Blumenthal, J.G. Peter, J.A. Trubiano, E.J. Phillips, Antibiotic allergy, Lancet. 393 (2019) 183–198.

[23] P. Hei, L. Quok, C. Siew, I. Thomas, T.J. Watts, K. Loong, K. Rutkowski, C. Lau, Beta-lactam allergy in Chinese patients and factors predicting genuine allergy, World

Allergy Organ. J. 12 (2019) 100048.

[24] A. Romano, R. Warrington, Antibiotic Allergy, Immunol. Allergy Clin. North Am. 34 (2014) 489–506.

[25] M.J. Torres, M. Blanca, The Complex Clinical Picture of β-Lactam Hypersensitivity: Penicillins, Cephalosporins, Monobactams, Carbapenems, and Clavams, Med. Clin. North Am. 94 (2010) 805–820.

[26] M.J. Torres, N.F. Adkinson, J. Caubet, R. Gan, T. Aviv, W. Hartford, Controversies in Drug Allergy : Beta-Lactam Hypersensitivity Testing, J. Allergy Clin. Immunol. Pract. 7 (2018) 40–45.

[27] T. Su, B.D.L. Broekhuizen, T.J.M. Verheij, H. Rockmann, The impact of penicillin allergy labels on antibiotic and health care use in primary care: a retrospective cohort study, Clin. Transl. Allergy. 7 (2017) 18.

[28] M.A. Park, J.T.C. Li, Diagnosis and Management of Penicillin Allergy, Mayo Clin. Proc. 80 (2005) 405–410.

[29] S. Albin, S. Agarwal, Prevalence and characteristics of reported penicillin allergy in an urban outpatient adult population, Allergy Asthma Proc. 35 (2014) 489–494.

[30] M. Salas, J.J. Laguna, I. Doña, E. Barrionuevo, R. Fernandez-Santamaría, A. Ariza, E. Perez-Inestrosa, C. Mayorga, T.D. Fernández, M.J. Torres, Patients Taking Amoxicillin-Clavulanic Can Become Simultaneously Sensitized to Both Drugs, J. Allergy Clin. Immunol. Pract. 5 (2017) 694-702.e3.

[31] S.B. Chaudhry, M.P. Veve, J.L. Wagner, Cephalosporins: A Focus on Side Chains and β-Lactam Cross-Reactivity, Pharmacy. 7 (2019) 103.

[32] D.A. Khan, A. Banerji, J.A. Bernstein, B. Bilgicer, K. Blumenthal, M. Castells, D. Ein, D.M. Lang, E. Phillips, Cephalosporin Allergy: Current Understanding and Future Challenges, J. Allergy Clin. Immunol. Pract. 7 (2019) 2105–2114.

[33] H. Guvenir, E. Dibek Misirlioglu, M. Capanoglu, E. Vezir, M. Toyran, C.N. Kocabas, Proven Non-β-Lactam Antibiotic Allergy in Children, Int. Arch. Allergy Immunol. 169

(2016) 45–50.

[34] I. Doña, E. Moreno, N. Pérez-Sánchez, I. Andreu, D. Hernández Fernandez de Rojas, M.J. Torres, Update on Quinolone Allergy, Curr. Allergy Asthma Rep. 17 (2017) 56.

[35] E.U. McGee, E. Samuel, B. Boronea, N. Dillard, M.N. Milby, S.J. Lewis, Quinolone Allergy, Pharmacy. 7 (2019) 97.

[36] G.C. Wall, M.J. Taylor, H.L. Smith, Prevalence and characteristics of hospital inpatients with reported fluoroquinolone allergy, Int. J. Clin. Pharm. 40 (2018) 890–894.

[37] R. Solensky, Allergy to β-lactam antibiotics, J. Allergy Clin. Immunol. 130 (2012) 1442-1442.e5.

[38] N. Blanca-López, A. Ariza, I. Doña, C. Mayorga, M.I. Montañez, J. Garcia-Campos, F. Gomez, C. Rondón, M. Blanca, M.J. Torres, Hypersensitivity reactions to fluoroquinolones: analysis of the factors involved, Clin. Exp. Allergy. 43 (2013) 560–567.

[39] A. Aranda, C. Mayorga, A. Ariza, I. Doña, A. Rosado, N. Blanca-Lopez, I. Andreu, M.J. Torres, In vitro evaluation of IgE-mediated hypersensitivity reactions to quinolones, Allergy. 66 (2011) 247–254.

[40] B. Schnyder, W.J. Pichler, Allergy to sulfonamides, J. Allergy Clin. Immunol. 131 (2013) 256-257.e5.

[41] N.R. Wulf, K.A. Matuszewski, Sulfonamide cross-reactivity: Is there evidence to support broad cross-allergenicity?, Am. J. Heal. Pharm. 70 (2013) 1483–1494.

[42] A. Giles, J. Foushee, E. Lantz, G. Gumina, Sulfonamide Allergies, Pharmacy. 7 (2019) 132.

[43] M. Hwang, J. Do, E. Choi, J. Seo, Y. Nam, K. Yoon, J. Park, K. Cho, S. Kang, H. Jin, Immunoglobulin E-mediated hypersensitivity reaction after intraperitoneal administration of vancomycin, Kidney Res. Clin. Pract. 34 (2015) 57–59.

[44] J.S. Minhas, P.G. Wickner, A.A. Long, A. Banerji, K.G. Blumenthal, Immune-mediated reactions to vancomycin: A systematic case review and analysis., Ann. Allergy. Asthma Immunol. 116 (2016) 544–53.

[45] K.M. Krause, A.W. Serio, T.R. Kane, L.E. Connolly, Aminoglycosides: An Overview, Cold Spring Harb. Perspect. Med. 6 (2016) a027029.

[46] L.M. Childs-Kean, K.M. Shaeer, S. Varghese Gupta, J.C. Cho, Aminoglycoside Allergic Reactions, Pharmacy. 7 (2019) 124.

[47] M. Sánchez-Borges, B. Thong, M. Blanca, L.F.C. Ensina, S. González-Díaz, P.A. Greenberger, E. Jares, Y.K. Jee, L. Kase-Tanno, D. Khan, J.W. Park, W. Pichler, A. Romano, M.J.T. Jaén, Hypersensitivity reactions to non beta-lactam antimicrobial agents, a statement of the WAO special committee on drug allergy, World Allergy Organ. J. 6 (2013) 1–23.

[48] G.P. Dinos, The macrolide antibiotic renaissance, Br. J. Pharmacol. 174 (2017) 2967–2983.

[49] K.M. Shaeer, E.B. Chahine, S. Varghese Gupta, J.C. Cho, Macrolide Allergic Reactions, Pharmacy. 7 (2019) 135.

[50] R. Solensky, D.A. Khan, W.I. Contributors Leonard Bernstein, G.R. Bloomberg, M.C. Castells, L.M. Mendelson, M.E. Weiss, D.I. Bernstein, J. Blessing-Moore, L. Cox, D.M. Lang, R.A. Nicklas, J. Oppenheimer, J.M. Portnoy, C. Randolph, D.E. Schuller, S.L. Spector, S. Tilles, D. Wallace, R.J. Paul Dowling, -Kansas City, M. Mark Dykewicz, N.A. Paul Greenberger, I.M. Eric Macy, -San Diego, C.R. Kathleen May - Cumberland, M.T. Nguyen, C.B. Lawrence Schwartz, Drug allergy: An updated practice parameter, Ann. Allergy, Asthma Immunol. 105 (2010) 259-273.e78.

[51] A. Martin-Serrano, N. Barbero, J. Agundez, Y. Vida, E. Perez-Inestrosa, M. Montanez, New Advances in the Study of IgE Drug Recognition, Curr. Pharm. Des. 22 (2017) 6759–6772.

[52] J.L. Kishiyama, D.C. Adelman, The Cross-Reactivity and Immunology of ??-Lactam Antibiotics, Drug Saf. 10 (1994) 318–327.

[53] A. Ariza, C. Mayorga, T.D. Fernandez, N. Barbero, A. Martín-Serrano, D. Pérez-Sala, F.J. Sánchez-Gómez, M. Blanca, M.J. Torres, M.I. Montanez, Hypersensitivity reactions to β-lactams: relevance of hapten-protein conjugates., J. Investig. Allergol. Clin. Immunol. 25 (2015) 12–25. http://www.ncbi.nlm.nih.gov/pubmed/25898690 (accessed November 23, 2019).

[54] M.I. Montañez, A. Ariza, C. Mayorga, T.D. Fernandez, M.J. Torres, Cross-Reactivity in Betalactam Allergy: Alternative Treatments, Curr. Treat. Options Allergy. 2 (2015) 141–154.

[55] A. Ariza, C. Mayorga, M. Salas, I. Doña, Á. Martín-Serrano, E. Pérez-Inestrosa, D. Pérez-Sala, A.E. Guzmán, M.I. Montañez, M.J. Torres, The influence of the carrier molecule on amoxicillin recognition by specific IgE in patients with immediate hypersensitivity reactions to betalactams, Sci. Rep. 6 (2016) 35113.

[56] P.E. Deak, B. Kim, B. Koh, A.A. Qayum, T. Kiziltepe, M.H. Kaplan, B. Bilgicer, Covalent Heterobivalent Inhibitor Design for Inhibition of IgE-Dependent Penicillin Allergy in a Murine Model, J. Immunol. 203 (2019) 21–30.

[57] P.E. Deak, M.R. Vrabel, V.J. Pizzuti, T. Kiziltepe, B. Bilgicer, Nanoallergens: A multivalent platform for studying and evaluating potency of allergen epitopes in cellular degranulation, Exp. Biol. Med. 241 (2016) 996–1006.

[58] P.E. Deak, B. Kim, A. Abdul Qayum, J. Shin, G. Vitalpur, K.M. Kloepfer, M.J. Turner, N. Smith, W.G. Shreffler, T. Kiziltepe, M.H. Kaplan, B. Bilgicer, Designer covalent heterobivalent inhibitors prevent IgE-dependent responses to peanut allergen, Proc. Natl. Acad. Sci. 116 (2019) 8966–8974.

[59] E.B. Puffer, J.K. Pontrello, J.J. Hollenbeck, J.A. Kink, L.L. Kiessling, Activating B Cell Signaling with Defined Multivalent Ligands, ACS Chem. Biol. 2 (2007) 252–262.

[60] E.J. Baird, D. Holowka, G.W. Coates, B. Baird, Highly Effective Poly(Ethylene Glycol) Architectures for Specific Inhibition of Immune Receptor Activation †, Biochemistry. 42 (2003) 12739–12748.

[61] A. Gieras, B. Linhart, K.H. Roux, M. Dutta, M. Khodoun, D. Zafred, C.R. Cabauatan,

C. Lupinek, M. Weber, M. Focke-Tejkl, W. Keller, F.D. Finkelman, R. Valenta, IgE epitope proximity determines immune complex shape and effector cell activation capacity, J. Allergy Clin. Immunol. 137 (2016) 1557–1565.

[62] W.S. Hlavacek, R.G. Posner, A.S. Perelson, Steric Effects on Multivalent Ligand-Receptor Binding: Exclusion of Ligand Sites by Bound Cell Surface Receptors, Biophys. J. 76 (1999) 3031–3043.

[63] B.B. Levine, V.H. Price, Studies on the Immunological Mechanisms of Penicillin Allergy. II. Antigenic Specificities of Allergic Wheal-And-Flare Skin Responses in Patients with Histories of Penicillin Allergy., Immunology. 7 (1964) 542–56. http://www.ncbi.nlm.nih.gov/pubmed/14210764.

[64] F. Sánchez-Sancho, E. Perez-Inestrosa, R. Suau, M.I. Montañez, C. Mayorga, M.J. Torres, A. Romano, M. Blanca, Synthesis, characterization and immunochemical evaluation of cephalosporin antigenic determinants, J. Mol. Recognit. 16 (2003) 148–156.

[65] E. Perez-Inestrosa, R. Suau, M.I. Montañez, R. Rodriguez, C. Mayorga, M.J. Torres, M. Blanca, Cephalosporin chemical reactivity and its immunological implications, Curr. Opin. Allergy Clin. Immunol. 5 (2005) 323–330.

[66] M.I. Montañez, F. Najera, C. Mayorga, A.J. Ruiz-Sanchez, Y. Vida, D. Collado, M. Blanca, M.J. Torres, E. Perez-Inestrosa, Recognition of multiepitope dendrimeric antigens by human immunoglobulin E, Nanomedicine Nanotechnology, Biol. Med. 11 (2015) 579–588.

[67] C. Mayorga, M.J. Torres, A. Romano, F. Moreno, E. Sanchez-Sabater, C. Juarez, M. Blanca, Monoclonal antibodies to amoxicillin express different idiotypes determined by anti-idiotype antibodies production, Allergy. 57 (2002) 45–51.

[68] T.H. Sher, Penicillin hypersensitivity: A review, Pediatr. Clin. North Am. 30 (1983) 161–176.

[69] D.G. Harle, B.A. Baldo, Identification of penicillin allergenic determinants that bind IgE antibodies in the sera of subjects with penicillin allergy, Mol. Immunol. 27 (1990)

1063–1071.

[70] B.A. Baldo, Penicillins and cephalosporins as allergens — structural aspects of recognition and cross-reactions, 29 (1999) 744–749.

[71] M.J. Torres, M. Blanca, J. Fernandez, A. Romano, A. Weck, W. Aberer, K. Brockow, W.J. Pichler, P. Demoly, Diagnosis of immediate allergic reactions to beta-lactam antibiotics, Allergy. 58 (2003) 961–972.

[72] A. Ariza, D. Collado, Y. Vida, M.I. Montañez, E. Pérez-Inestrosa, M. Blanca, M.J. Torres, F.J. Cañada, D. Pérez-Sala, Study of protein haptenation by amoxicillin through the use of a biotinylated antibiotic, PLoS One. 9 (2014) 1–12.

[73] M.J. Torres, M.I. Montañez, A. Ariza, M. Salas, T.D. Fernandez, N. Barbero, C. Mayorga, M. Blanca, The role of IgE recognition in allergic reactions to amoxicillin and clavulanic acid, Clin. Exp. Allergy. 46 (2016) 264–274.

[74] M.J. Torres, A. Ariza, J. Fernández, E. Moreno, J.J. Laguna, M.I. Montañez, A.J. Ruiz-Sanchez, M. Blanca, Role of minor determinants of amoxicillin in the diagnosis of immediate allergic reactions to amoxicillin, Allergy. 65 (2010) 590–596.

[75] X. Meng, C.J. Earnshaw, A. Tailor, R.E. Jenkins, J.C. Waddington, P. Whitaker, N.S. French, D.J. Naisbitt, B.K. Park, Amoxicillin and Clavulanate Form Chemically and Immunologically Distinct Multiple Haptenic Structures in Patients, Chem. Res. Toxicol. 29 (2016) 1762–1772.

[76] C. Antunez, N. Blanca-Lopez, M.J. Torres, C. Mayorga, E. Perez-Inestrosa, M.I. Montañez, T. Fernandez, M. Blanca, Immediate allergic reactions to cephalosporins: Evaluation of cross-reactivity with a panel of penicillins and cephalosporins, J. Allergy Clin. Immunol. 117 (2006) 404–410.

[77] A. Romano, C. Mayorga, M.J. Torres, M.C. Artesani, R. Suau, F. Sánchez, E. Pérez, A. Venuti, M. Blanca, Immediate allergic reactions to cephalosporins: Cross-reactivity and selective responses, J. Allergy Clin. Immunol. 106 (2000) 1177–1183.

[78] M.I. Montañez, C. Mayorga, M.J. Torres, A. Ariza, M. Blanca, E. Perez-Inestrosa,

Synthetic approach to gain insight into antigenic determinants of cephalosporins: In vitro studies of chemical structure-IgE molecular recognition relationships, Chem. Res. Toxicol. 24 (2011) 706–717.

[79] A. Martín-Serrano, C. Mayorga, E. Barrionuevo, N. Pérez, A. Romano, E. Moreno, A. Ariza, E. Pérez-Inestrosa, M.J. Torres, M.I. Montañez, Design of an antigenic determinant of cefaclor: Chemical structure–IgE recognition relationship, J. Allergy Clin. Immunol. 145 (2020) 1301-1304.e4.

[80] G. Bogas, C. Mayorga, Á. Martín-Serrano, R. Fernández-Santamaría, I.M. Jiménez-Sánchez, A. Ariza, E. Barrionuevo, T. Posadas, M. Salas, T.D. Fernández, M.J. Torres, M.I. Montañez, Penicillin and cephalosporin cross-reactivity: role of side chain and synthetic cefadroxil epitopes, Clin. Transl. Allergy. 10 (2020) 57.

[81] K.M. Papp-Wallace, A. Endimiani, M.A. Taracila, R.A. Bonomo, Carbapenems: Past, Present, and Future, Antimicrob. Agents Chemother. 55 (2011) 4943–4960.

[82] R.G. Edwards, J.M. Dewdney, R.J. Dobrzanski, D. Lee, Immunogenicity and Allergenicity Studies on Two Beta-Lactam Structures, a Clavam, Clavulanic Acid, and a Carbapenem: Structure-Activity Relationships, Int. Arch. Allergy Immunol. 85 (1988) 184–189.

[83] N.F. Adkinson, E.A. Swabb, A.A. Sugerman, Immunology of the monobactam aztreonam, Antimicrob. Agents Chemother. 25 (1984) 93–97.

[84] L. Sánchez-Morillas, P.R. Pérez-Ezquerra, M. Reaño-Martos, J.J. Laguna-Martínez, M.L. Sanz, L.M. Martínez, Selective allergic reactions to clavulanic acid: A report of 9 cases, J. Allergy Clin. Immunol. 126 (2010) 177–179.

[85] P. Bonadonna, M. Schiappoli, G. Senna, G. Passalacqua, Delayed selective reaction to clavulanic acid: A case report, J. Investig. Allergol. Clin. Immunol. 15 (2005) 302–304.

[86] N. Blanca-Lopez, D. Perez-Alzate, F. Ruano, M. Garcimartin, V. de la Torre, C. Mayorga, M.L. Somoza, J. Perkins, M. Blanca, M.G. Canto, M.J. Torres, Selective immediate responders to amoxicillin and clavulanic acid tolerate penicillin derivative

administration after confirming the diagnosis, Allergy. 70 (2015) 1013–1019.

[87] N. Barbero, R. Fernández-Santamaría, C. Mayorga, Á. Martin-Serrano, M. Salas, G. Bogas, F. Nájera, D. Pérez-Sala, E. Pérez-Inestrosa, T.D. Fernandez, M.I. Montañez, M.J. Torres, Identification of an antigenic determinant of clavulanic acid responsible for IgE-mediated reactions, Allergy. 74 (2019) all.13761.

[88] D. Garzon, A. Ariza, L. Regazzoni, R. Clerici, A. Altomare, F.R. Sirtori, M. Carini, M.J. Torres, D. Pérez-Sala, G. Aldini, Mass Spectrometric Strategies for the Identification and Characterization of Human Serum Albumin Covalently Adducted by Amoxicillin: Ex Vivo Studies, Chem. Res. Toxicol. 27 (2014) 1566–1574.

[89] A. Ariza, D. Garzon, D.R. Abánades, V. de los Ríos, G. Vistoli, M.J. Torres, M. Carini, G. Aldini, D. Pérez-Sala, Protein haptenation by amoxicillin: High resolution mass spectrometry analysis and identification of target proteins in serum, J. Proteomics. 77 (2012) 504–520.

[90] A. Ariza, M.I. Montañez, D. Pérez-Sala, Proteomics in immunological reactions to drugs, Curr. Opin. Allergy Clin. Immunol. 11 (2011) 305–312.

[91] K. Yamasaki, V.T.G. Chuang, T. Maruyama, M. Otagiri, Albumin–drug interaction and its clinical implication, Biochim. Biophys. Acta - Gen. Subj. 1830 (2013) 5435–5443.

[92] U. Kragh-Hansen, V.T.G. Chuang, M. Otagiri, Practical Aspects of the Ligand-Binding and Enzymatic Properties of Human Serum Albumin., Biol. Pharm. Bull. 25 (2002) 695–704.

[93] C. Bertucci, E. Domenici, Reversible and Covalent Binding of Drugs to Human Serum Albumin: Methodological Approaches and Physiological Relevance, Curr. Med. Chem. 9 (2002) 1463–1481.

[94] M. Yvon, J.-M. Wal, Identification of lysine residue 199 of human serum albumin as a binding site for benzylpenicilloyl groups, FEBS Lett. 239 (1988) 237–240.

[95] M. Yvon, P. Anglade, J.-M. Wal, Identification of the binding sites of benzyl

penicilloyl, the allergenic metabolite of penicillin, on the serum albumin molecule, FEBS Lett. 263 (1990) 237–240.

[96] X. Meng, R.E. Jenkins, N.G. Berry, J.L. Maggs, J. Farrell, C.S. Lane, A. V. Stachulski, N.S. French, D.J. Naisbitt, M. Pirmohamed, B.K. Park, Direct Evidence for the Formation of Diastereoisomeric Benzylpenicilloyl Haptens from Benzylpenicillin and Benzylpenicillenic Acid in Patients, J. Pharmacol. Exp. Ther. 338 (2011) 841–849.

[97] M.E. Azoury, L. Filì, R. Bechara, N. Scornet, L. de Chaisemartin, R.J. Weaver, N. Claude, B. Maillere, P. Parronchi, D. Joseph, M. Pallardy, Identification of T-cell epitopes from benzylpenicillin conjugated to human serum albumin and implication in penicillin allergy, Allergy. 73 (2018) 1662–1672.

[98] R.E. Jenkins, X. Meng, V.L. Elliott, N.R. Kitteringham, M. Pirmohamed, B.K. Park, Characterisation of flucloxacillin and 5-hydroxymethyl flucloxacillin haptenated HSA in vitro and in vivo, Proteomics - Clin. Appl. 3 (2009) 720–729.

[99] P. Whitaker, X. Meng, S.N. Lavergne, S. El-Ghaiesh, M. Monshi, C. Earnshaw, D. Peckham, J. Gooi, S. Conway, M. Pirmohamed, R.E. Jenkins, D.J. Naisbitt, B.K. Park, Mass Spectrometric Characterization of Circulating and Functional Antigens Derived from Piperacillin in Patients with Cystic Fibrosis, J. Immunol. 187 (2011) 200–211.

[100] J. Gonzalez-Morena, M. Montanez, G. Aldini, F. Sanchez-Gomez, D. Perez-Sala, Adduct Formation and Context Factors in Drug Hypersensitivity: Insight from Proteomic Studies, Curr. Pharm. Des. 22 (2016) 6748–6758.

[101] P. Lafaye, C. Lapresle, Fixation of penicilloyl groups to albumin and appearance of anti-penicilloyl antibodies in penicillin-treated patients., J. Clin. Invest. 82 (1988) 7–12.

[102] B. Magi, B. Marzocchi, L. Bini, C. Cellesi, A. Rossolini, V. Pallini, Two-dimensional electrophoresis of human serum proteins modified by ampicillin during therapeutic treatment, Electrophoresis. 16 (1995) 1190–1192.

[103] Á. Martín-Serrano, J.M. Gonzalez-Morena, N. Barbero, A. Ariza, F.J. Sánchez Gómez, E. Pérez-Inestrosa, D. Pérez-Sala, M.J. Torres, M.I. Montañez, Biotin-Labelled

Clavulanic Acid to Identify Proteins Target for Haptenation in Serum: Implications in Allergy Studies, Front. Pharmacol. 11 (2020) 1–16.

[104] S. Ahlstedt, A. Kristofferson, P.O. Svärd, Ö. Strannegård, Immunological Properties of Ampicillin Polymers, Int. Arch. Allergy Immunol. 53 (1977) 247–253.

[105] A.C. Munro, J.M. Dewdney, H. Smith, A.W. Wheeler, Antigenic Properties of Polymers Formed by β-Lactam Antibiotics, Int. Arch. Allergy Immunol. 50 (1976) 192–205.

[106] E. V. Wairbrick, A.L. Thomas, V. Stejskal, J.W. Coleman, An analysis of β-lactam-derived antigens on spleen cell and serum proteins by ELISA and Western blotting, Allergy. 50 (1995) 910–917.

[107] L. Binderup, E. Arrigoni-Martelli, [14C]-d-penicillamine: Uptake and distribution in rat lymphocytes and macrophages, Biochem. Pharmacol. 28 (1979) 189–192.

[108] H. Watanabe, H. Kelly, R.L. Dawkins, Association of HLA DR1 with High D-Penicillamine Binding to Monocytes in Females, Microbiol. Immunol. 31 (1987) 83–88.

[109] H. Watanabe, G. Grimsley, G.A.C. Major, R.L. Dawkins, Increased binding of d-penicillamine to monocytes in rheumatoid arthritis, Clin. Immunol. Immunopathol. 39 (1986) 173–178.

[110] M.J. Torres, C. Mayorga, L. Leyva, A.E. Guzman, J.A. Cornejo-García, C. Juarez, M. Blanca, Controlled administration of penicillin to patients with a positive history but negative skin and specific serum IgE tests, Clin. Exp. Allergy. 32 (2002) 270–276.

[111] M. Blanca, A. Romano, M.J. Torres, J. Férnandez, C. Mayorga, J. Rodriguez, P. Demoly, P.J. Bousquet, H.F. Merk, M.L. Sanz, H. Ott, M. Atanasković-Marković, Update on the evaluation of hypersensitivity reactions to betalactams, Allergy. 64 (2009) 183–193.

[112] A. Romano, M. Blanca, M.J. Torres, A. Bircher, W. Aberer, K. Brockow, W.J. Pichler, P. Demoly, Diagnosis of nonimmediate reactions to beta-lactam antibiotics, Allergy. 59 (2004) 1153–1160.

[113] T.D. Fernandez, C. Mayorga, M. Salas, E. Barrionuevo, T. Posadas, A. Ariza, J.J. Laguna, E. Moreno, M.J. Torres, I. Doña, M.I. Montañez, Evolution of diagnostic approaches in betalactam hypersensitivity, Expert Rev. Clin. Pharmacol. 10 (2017) 671–683.

[114] J. Fernández, M.J. Torres, J. Campos, F. Arribas-Poves, M. Blanca, Prospective, multicenter clinical trial to validate new products for skin tests in the diagnosis of allergy to penicillin, J. Investig. Allergol. Clin. Immunol. 23 (2013) 398–408.

[115] J. Torres, A. Romano, C. Mayorga, M. Carmen, A.E. Guzman, M. Reche, C. Juarez, M. Blanca, Diagnostic evaluation of a large group of patients with immediate allergy to penicillins: The role of skin testing, Allergy Eur. J. Allergy Clin. Immunol. 56 (2001) 850–856.

[116] M.J. Torres, A. Ariza, C. Mayorga, I. Doña, N. Blanca-Lopez, C. Rondon, M. Blanca, Clavulanic acid can be the component in amoxicillin-clavulanic acid responsible for immediate hypersensitivity reactions, J. Allergy Clin. Immunol. 125 (2010) 502-505.e2.

[117] A.M. Chiriac, P. Demoly, Drug provocation tests: up-date and novel approaches, Allergy, Asthma Clin. Immunol. 9 (2013) 12.

[118] W. Aberer, A. Bircher, A. Romano, M. Blanca, P. Campi, J. Fernandez, K. Brockow, W.J. Pichler, P. Demoly, Drug provocation testing in the diagnosis of drug hypersensitivity reactions: general considerations, Allergy. 58 (2003) 854–863.

[119] M.J. Torres, G.E. Celik, P. Whitaker, M. Atanaskovic-Markovic, A. Barbaud, A. Bircher, M. Blanca, K. Brockow, J.-C. Caubet, J.R. Cernadas, A. Chiriac, P. Demoly, L.H. Garvey, H.F. Merk, H. Mosbech, A. Nakonechna, A. Romano, A EAACI drug allergy interest group survey on how European allergy specialists deal with β-lactam allergy, Allergy. 74 (2019) 1052–1062.

[120] C. Mayorga, G. Celik, P. Rouzaire, P. Whitaker, P. Bonadonna, J. Rodrigues-Cernadas, A. Vultaggio, K. Brockow, J.C. Caubet, J. Makowska, A. Nakonechna, A. Romano, M.I. Montañez, J.J. Laguna, G. Zanoni, J.L. Gueant, H. Oude Elberink, J. Fernandez, S. Viel, P. Demoly, M.J. Torres, In vitro tests for drug hypersensitivity

reactions: an ENDA/EAACI Drug Allergy Interest Group position paper, Allergy. 71 (2016) 1103–1134.

[121] C. Mayorga, D.G. Ebo, D.M. Lang, W.J. Pichler, V. Sabato, M.A. Park, J. Makowska, M. Atanaskovic-Markovic, P. Bonadonna, E. Jares, Controversies in drug allergy: In vitro testing, J. Allergy Clin. Immunol. 143 (2019) 56–65.

[122] G.J. Gleich, J.W. Yunginger, The radioallergosorbent test: a method to measure IgE antibodies, IgG blocking antibodies, and the potency of allergy extracts., Bull. N. Y. Acad. Med. 57 (1981) 559–67. http://www.ncbi.nlm.nih.gov/pubmed/6944131.

[123] E.C. McGowan, S. Saini, Update on the Performance and Application of Basophil Activation Tests, Curr. Allergy Asthma Rep. 13 (2013) 101–109.

[124] O. Hemmings, M. Kwok, R. McKendry, A.F. Santos, Basophil Activation Test: Old and New Applications in Allergy, Curr. Allergy Asthma Rep. 18 (2018) 77.

[125] M.J. Torres, A. Padial, C. Mayorga, T. Fernández, E. Sanchez-Sabate, J.A. Cornejo-Garcia, C. Antúnez, M. Blanca, The diagnostic interpretation of basophil activation test in immediate allergic reactions to betalactams, Clin. Exp. Allergy. 34 (2004) 1768–1775.

[126] A.L. De Week, M.L. Sanz, P.M. Gamboa, W. Aberer, G. Sturm, M.B. Bilo, M. Montroni, M. Blanca, M.J. Torres, L. Mayorga, P. Campi, M. Manfredi, M. Drouet, J. Sainte-Laudy, A. Romano, H. Merk, J.M. Weber, T.M. Jermann, ENDA (European Network for Drug Allergy), Diagnosis of immediate-type beta-lactam allergy in vitro by flow-cytometric basophil activation test and sulfidoleukotriene production: a multicenter study., J. Investig. Allergol. Clin. Immunol. 19 (2009) 91–109. http://www.ncbi.nlm.nih.gov/pubmed/19476013.

[127] M.L. Sanz, P.M. Gamboa, I. Antépara, C. Uasuf, L. Vila, C. Garcia-Avilés, M. Chazot, A.L. De Weck, Flow cytometric basophil activation test by detection of CD63 expression in patients with immediate-type reactions to betalactam antibiotics, Clin. Exp. Allergy. 32 (2002) 277–286.

[128] A.F. Santos, O. Alpan, H. Hoffmann, Basophil activation test: mechanisms and

considerations for use in clinical trials and clinical practice, Allergy. (2021) all.14747.

[129] K.J. Puan, A.K. Andiappan, B. Lee, D. Kumar, T.S. Lai, G. Yeo, D. Bercin, M. Starke, D. Haase, J. Lum, F.T. Chew, J. Connolly, S.C. Wong, F. Zolezzi, M. Poidinger, D.Y. Wang, Systematic characterization of basophil anergy, 72 (2017) 373–384.

[130] A.F. Santos, N. Couto-Francisco, N. Bécares, M. Kwok, H.T. Bahnson, G. Lack, A novel human mast cell activation test for peanut allergy, J. Allergy Clin. Immunol. 142 (2018) 689-691.e9.

[131] F. Pineda, A. Ariza, C. Mayorga, F. Arribas, R. González-Mendiola, N. Blanca-López, G. Davila, N. Cabañes, G. Canto, J.J. Laguna, C. Senent, P. Stahl-Skov, R. Palacios, M. Blanca, M.J. Torres, Role of Histamine Release Test for the Evaluation of Patients with Immediate Hypersensitivity Reactions to Clavulanic Acid, Int. Arch. Allergy Immunol. 168 (2016) 233–240.

[132] F. Arribas, S. Falkencrone, J. Sola, M. Gomez-Serranillos, J. Laguna, M. Montañez, T. Fernandez, D. Rodríguez, F. Pineda, P. Skov, C. Mayorga, M. Torres, Basophil Histamine Release Induced by Amoxicilloyl-poly-L-lysine Compared With Amoxicillin in Patients With IgE-Mediated Allergic Reactions to Amoxicillin, J. Investig. Allergol. Clin. Immunol. 27 (2017) 356–362.

[133] J. Elst, M.M. Van Der Poorten, M.A. Faber, A.L. Van Gasse, L.H. Garvey, C.H. Bridts, L.P. De Puysseleyr, C. Mertens, M.M. Hagendorens, V. Sabato, D.G. Ebo, Mast cell activation test in chlorhexidine allergy : a proof of concept, Br. J. Anaesth. 125 (2020) 970–975.

[134] P.E. Deak, B. Kim, A. Adnan, M. Labella, L. De las Vecillas, M. Castells, B. Bilgicer, Nanoallergen platform for detection of platin drug allergies, J. Allergy Clin. Immunol. 143 (2019) 1957-1960.e12.

[135] S. Bayda, M. Adeel, T. Tuccinardi, M. Cordani, F. Rizzolio, The History of Nanoscience and Nanotechnology: From Chemical–Physical Applications to Nanomedicine, Molecules. 25 (2019) 112.

[136] C. Mayorga, E. Perez-Inestrosa, N. Molina, M.I. Montañez, Development of nanostructures in the diagnosis of drug hypersensitivity reactions, Curr. Opin. Allergy Clin. Immunol. 16 (2016) 300–307.

[137] E.J. Cho, H. Holback, K.C. Liu, S.A. Abouelmagd, J. Park, Y. Yeo, Nanoparticle characterization: State of the art, challenges, and emerging technologies, Mol. Pharm. 10 (2013) 2093–2110.

[138] M. Nasrollahzadeh, Z. Issaabadi, M. Sajjadi, S.M. Sajadi, M. Atarod, Types of Nanostructures, in: Interface Sci. Technol., 1st ed., Elsevier Ltd., 2019: pp. 29–80.

[139] M.M. Bellah, S.M. Christensen, S.M. Iqbal, Nanostructures for Medical Diagnostics, J. Nanomater. 2012 (2012) 1–21.

[140] K. Khalid, X. Tan, H.F. Mohd Zaid, Y. Tao, C. Lye Chew, D.-T. Chu, M.K. Lam, Y.-C. Ho, J.W. Lim, L. Chin Wei, Advanced in developmental organic and inorganic nanomaterial: a review, Bioengineered. 11 (2020) 328–355.

[141] L. Wang, M. Feng, Q. Li, C. Qiu, R. Chen, Advances in nanotechnology and asthma, Ann. Transl. Med. 7 (2019) 180–180.

[142] P.V. Baptista, Nanodiagnostics: leaving the research lab to enter the clinics?, Diagnosis. 1 (2014) 305–309.

[143] S. Roethlisberger, O. Karoui, D. Mapelli, R. Audran, V. Aubert, L.D. Girard, F. Rebeaud, A. Leimgruber, G. Buss, J. Duc, F. Langner-Viviani, I. Maerki, F. Spertini, Novel Nanofluidic IgE Assay versus a Reference Method: A Real-World Comparison, Int. Arch. Allergy Immunol. 180 (2019) 28–36.

[144] M.I. Montañez, E. Perez-Inestrosa, R. Suau, C. Mayorga, M.J. Torres, M. Blanca, Dendrimerized Cellulose as a Scaffold for Artificial Antigens with Applications in Drug Allergy Diagnosis, Biomacromolecules. 9 (2008) 1461–1466.

[145] F. Sánchez-Sancho, E. Pérez-Inestrosa, R. Suau, C. Mayorga, M.J. Torres, M. Blanca, Dendrimers as Carrier Protein Mimetics for IgE Antibody Recognition. Synthesis and Characterization of Densely Penicilloylated Dendrimers, Bioconjug. Chem. 13 (2002)

647–653.

[146] M. Soler, P. Mesa-Antunez, M.-C. Estevez, A.J. Ruiz-Sanchez, M.A. Otte, B. Sepulveda, D. Collado, C. Mayorga, M.J. Torres, E. Perez-Inestrosa, L.M. Lechuga, Highly sensitive dendrimer-based nanoplasmonic biosensor for drug allergy diagnosis, Biosens. Bioelectron. 66 (2015) 115–123.

[147] Y. Vida, M.I. Montañez, D. Collado, F. Najera, A. Ariza, M. Blanca, M.J. Torres, C. Mayorga, E. Perez-Inestrosa, Dendrimeric antigen–silica particle composites: an innovative approach for IgE quantification, J. Mater. Chem. B. 1 (2013) 3044.

[148] A.J. Ruiz-Sanchez, M.I. Montanez, C. Mayorga, M.J. Torres, N.S. Kehr, Y. Vida, D. Collado, F. Najera, L. De Cola, E. Perez-Inestrosa, Dendrimer-Modified Solid Supports: Nanostructured Materials with Potential Drug Allergy Diagnostic Applications, Curr. Med. Chem. 19 (2012) 4942–4954.

[149] R.G. Posner, K. Subramanian, B. Goldstein, J. Thomas, T. Feder, D. Holowka, B. Baird, Simultaneous cross-linking by two nontriggering bivalent ligands causes synergistic signaling of IgE Fc epsilon RI complexes., J. Immunol. 155 (1995) 3601–9. http://www.ncbi.nlm.nih.gov/pubmed/7561059.

[150] D. Carmo, Synthesis and a Preliminary Characterization of Poly(Propylene)Imine Hexadecylamine Dendrimer (DAB-Am-16) Modified with Methyl Acrylate, Am. Chem. Sci. J. 3 (2013) 314–324.

[151] U. Gupta, O. Perumal, Dendrimers and Its Biomedical Applications, in: Nat. Synth. Biomed. Polym., 1st ed., Elsevier, 2014: pp. 243–257.

[152] A.K. Mandal, Dendrimers in targeted drug delivery applications: a review of diseases and cancer, Int. J. Polym. Mater. Polym. Biomater. 70 (2021) 287–297.

[153] E.N. Augustus, E.T. Allen, A. Nimibofa, W. Donbebe, A review of synthesis, characterization and applications of functionalized dendrimers, Am. J. Polym. Sci. 7 (2017) 8–14.

[154] A. Santos, F. Veiga, A. Figueiras, Dendrimers as Pharmaceutical Excipients:

Synthesis, Properties, Toxicity and Biomedical Applications, Materials (Basel). 13 (2019) 65.

[155] A.P. Sherje, M. Jadhav, B.R. Dravyakar, D. Kadam, Dendrimers: A versatile nanocarrier for drug delivery and targeting, Int. J. Pharm. 548 (2018) 707–720.

[156] C.M. Cardona, A.E. Kaifer, Asymmetric Redox-Active Dendrimers Containing a Ferrocene Subunit. Preparation, Characterization, and Electrochemistry, J. Am. Chem. Soc. 120 (1998) 4023–4024.

[157] C.B. Gorman, J.C. Smith, Effect of repeat unit flexibility on dendrimer conformation as studied by atomistic molecular dynamics simulations, Polymer (Guildf). 41 (2000) 675–683.

[158] M.A. Mintzer, M.W. Grinstaff, Biomedical applications of dendrimers: a tutorial, Chem. Soc. Rev. 40 (2011) 173–190.

[159] G.R. Newkome, Z. Yao, G.R. Baker, V.K. Gupta, Micelles. Part 1. Cascade molecules: a new approach to micelles. A [27]-arborol, J. Org. Chem. 50 (1985) 2003–2004.

[160] D.A. Tomalia, H. Baker, J. Dewald, M. Hall, G. Kallos, S. Martin, J. Roeck, J. Ryder, P. Smith, A New Class of Polymers : Starburst-Dendritic, Polym. J. 17 (1985) 117–132.

[161] D.A. Tomalia, Birth of a new macromolecular architecture: dendrimers as quantized building blocks for nanoscale synthetic polymer chemistry, Prog. Polym. Sci. 30 (2005) 294–324.

[162] A. Carlmark, E. Malmström, M. Malkoch, Dendritic architectures based on bis-MPA: Functional polymeric scaffolds for application-driven research, Chem. Soc. Rev. 42 (2013) 5858–5879.

[163] M. Sowinska, Z. Urbanczyk-Lipkowska, Advances in the chemistry of dendrimers, New J. Chem. 38 (2014) 2168–2203.

[164] E. Abbasi, S.F. Aval, A. Akbarzadeh, M. Milani, H.T. Nasrabadi, S.W. Joo, Y. Hanifehpour, K. Nejati-Koshki, R. Pashaei-Asl, Dendrimers: Synthesis, applications,

and properties, Nanoscale Res. Lett. 9 (2014) 1–10.

[165] C.J. Hawker, J.M.J. Fréchet, Preparation of Polymers with Controlled Molecular Architecture. A New Convergent Approach to Dendritic Macromolecules, J. Am. Chem. Soc. 112 (1990) 7638–7647.

[166] S.M. Grayson, J.M.J. Fréchet, Convergent Dendrons and Dendrimers: from Synthesis to Applications, Chem. Rev. 101 (2001) 3819–3868.

[167] A. Carlmark, C. Hawker, A. Hult, M. Malkoch, New methodologies in the construction of dendritic materials, Chem. Soc. Rev. 38 (2009) 352–362.

[168] C. Ornelas, Brief Timelapse on Dendrimer Chemistry: Advances, Limitations, and Expectations, Macromol. Chem. Phys. 217 (2016) 149–174.

[169] D.R. Vutukuri, P. Bharathi, Z. Yu, K. Rajasekaran, M.H. Tran, S. Thayumanavan, A mild deprotection strategy for allyl-protecting groups and its implications in sequence specific dendrimer synthesis, J. Org. Chem. 68 (2003) 1146–1149.

[170] A.P. Umali, H.L. Crampton, E.E. Simanek, Triazine dendrimers with orthogonally protected amines on the periphery. Masking amines with Dde and BOC groups provides an alternative to carrying protected alcohols and disulfides through an iterative synthesis, J. Org. Chem. 72 (2007) 9866–9874.

[171] C. Agami, F. Couty, The reactivity of the N-Boc protecting group: an underrated feature, Tetrahedron. 58 (2002) 2701–2724.

[172] N. Molina, F. Nájera, J.A. Guadix, J.M. Perez-Pomares, Y. Vida, E. Perez-Inestrosa, Synthesis of Amino Terminal Clicked Dendrimers. Approaches to the Application as a Biomarker, J. Org. Chem. 84 (2019) 10197–10208.

[173] A. Isidro-Llobet, M. Álvarez, F. Albericio, Amino Acid-Protecting Groups, Chem. Rev. 109 (2009) 2455–2504.

[174] P.G.M. Wuts, T.W. Greene, Protection for the Carboxyl Group, in: Greene's Prot. Groups Org. Synth., John Wiley & Sons, Inc., Hoboken, NJ, USA, 2006: pp. 533–646.

[175] J. Twibanire, T.B. Grindley, Polyester Dendrimers, Polymers (Basel). 4 (2012) 794–879.

[176] F. Grimm, K. Hartnagel, F. Wessendorf, A. Hirsch, Supramolecular self-assembly of dendrimers containing orthogonal binding motifs, Chem. Commun. (2009) 1331–1333.

[177] A. Lancelot, R. González-Pastor, R. Clavería-Gimeno, P. Romero, O. Abian, P. Martín-Duque, J.L. Serrano, T. Sierra, Cationic poly(ester amide) dendrimers: Alluring materials for biomedical applications, J. Mater. Chem. B. 6 (2018) 3956–3968.

[178] E. Ladd, A. Sheikhi, N. Li, T.G.M. Van De Ven, A. Kakkar, Design and synthesis of dendrimers with facile surface group functionalization, and an evaluation of their bactericidal efficacy, Molecules. 22 (2017).

[179] S. García-Gallego, O.C.J. Andrén, M. Malkoch, Accelerated Chemoselective Reactions to Sequence-Controlled Heterolayered Dendrimers, J. Am. Chem. Soc. 142 (2020) 1501–1509.

[180] G. Franc, A. Kakkar, Dendrimer design using CuI-catalyzed alkyne–azide "click-chemistry," Chem. Commun. (2008) 5267.

[181] E. Haldón, M.C. Nicasio, P.J. Pérez, Copper-catalysed azide–alkyne cycloadditions (CuAAC): an update, Org. Biomol. Chem. 13 (2015) 9528–9550.

[182] F. Himo, T. Lovell, R. Hilgraf, V. V. Rostovtsev, L. Noodleman, K.B. Sharpless, V. V. Fokin, Copper(I)-Catalyzed Synthesis of Azoles. DFT Study Predicts Unprecedented Reactivity and Intermediates, J. Am. Chem. Soc. 127 (2005) 210–216.

[183] H.C. Kolb, M.G. Finn, K.B. Sharpless, Click Chemistry: Diverse Chemical Function from a Few Good Reactions, Angew. Chemie Int. Ed. 40 (2001) 2004–2021.

[184] N. Li, T.-H. Tsoi, W.-S. Lo, Y.-J. Gu, H.-Y. Wan, W.-T. Wong, An efficient approach to synthesize glycerol dendrimers via thiol–yne "click" chemistry and their application in stabilization of gold nanoparticles with X-ray attenuation properties, Polym. Chem. 8 (2017) 6989–6996.

[185] A. Dondoni, A. Marra, Recent applications of thiol–ene coupling as a click process for glycoconjugation, Chem. Soc. Rev. 41 (2012) 573–586.

[186] A.B. Lowe, Thiol–ene "click" reactions and recent applications in polymer and materials synthesis: a first update, Polym. Chem. 5 (2014) 4820–4870.

[187] K.L. Killops, L.M. Campos, C.J. Hawker, Robust, Efficient, and Orthogonal Synthesis of Dendrimers via Thiol-ene "Click" Chemistry, J. Am. Chem. Soc. 130 (2008) 5062–5064.

[188] R. Hoogenboom, Thiol-yne chemistry: A powerful tool for creating highly functional materials, Angew. Chemie - Int. Ed. 49 (2010) 3415–3417.

[189] E.R. Gillies, J.M.J. Fréchet, Dendrimers and dendritic polymers in drug delivery, Drug Discov. Today. 10 (2005) 35–43.

[190] F. Abedi-Gaballu, G. Dehghan, M. Ghaffari, R. Yekta, S. Abbaspour-Ravasjani, B. Baradaran, J. Ezzati Nazhad Dolatabadi, M.R. Hamblin, PAMAM dendrimers as efficient drug and gene delivery nanosystems for cancer therapy, Appl. Mater. Today. 12 (2018) 177–190.

[191] A.K. Sharma, A. Gothwal, P. Kesharwani, H. Alsaab, A.K. Iyer, U. Gupta, Dendrimer nanoarchitectures for cancer diagnosis and anticancer drug delivery, Drug Discov. Today. 22 (2017) 314–326.

[192] E. Wiener, M.W. Brechbiel, H. Brothers, R.L. Magin, O.A. Gansow, D.A. Tomalia, P.C. Lauterbur, Dendrimer-based metal chelates: A new class of magnetic resonance imaging contrast agents, Magn. Reson. Med. 31 (1994) 1–8.

[193] L.D. Margerum, B.K. Campion, M. Koo, N. Shargill, J.J. Lai, A. Marumoto, P.C. Sontum, Gadolinium(III) DO3A macrocycles and polyethylene glycol coupled to dendrimers: Effect of molecular weight on physical and biological properties of macromolecular magnetic resonance imaging contrast agents, J. Alloys Compd. 249 (1997) 185–190.

[194] M.W. Grinstaff, Biodendrimers: New Polymeric Biomaterials for Tissue Engineering,

Chem. - A Eur. J. 8 (2002) 2838.

[195] M. Wathier, P.J. Jung, M.A. Carnahan, T. Kim, M.W. Grinstaff, Dendritic Macromers as in Situ Polymerizing Biomaterials for Securing Cataract Incisions, J. Am. Chem. Soc. 126 (2004) 12744–12745.

[196] A.J. Velazquez, New Dendritic Adhesives for Sutureless Ophthalmic Surgical Procedures, Arch. Ophthalmol. 122 (2004) 867.

[197] I.B. Rietveld, E. Kim, S.A. Vinogradov, Dendrimers with tetrabenzoporphyrin cores: Near infrared phosphors for in vivo oxygen imaging, Tetrahedron. 59 (2003) 3821–3831.

[198] S.M. Grist, L. Chrostowski, K.C. Cheung, Optical Oxygen Sensors for Applications in Microfluidic Cell Culture, Sensors. 10 (2010) 9286–9316.

[199] C.C. Lee, J.A. MacKay, J.M.J. Fréchet, F.C. Szoka, Designing dendrimers for biological applications, Nat. Biotechnol. 23 (2005) 1517–1526.

[200] S. Hecht, J.M.J. Fréchet, Dendritic Encapsulation of Function: Applying Nature's Site Isolation Principle from Biomimetics to Materials Science, Angew. Chemie Int. Ed. 40 (2001) 74–91.

[201] M.W. Handlogten, T. Kiziltepe, B. Bilgicer, Design of a heterotetravalent synthetic allergen that reflects epitope heterogeneity and IgE antibody variability to study mast cell degranulation, Biochem. J. 449 (2013) 91–99.

[202] N. Molina, A. Martin-Serrano, T.D. Fernandez, A. Tesfaye, F. Najera, M.J. Torres, C. Mayorga, Y. Vida, M.I. Monta ez, E. Perez-Inestrosa, Dendrimeric antigens for drug allergy diagnosis: A new approach for basophil activation tests, Molecules. 23 (2018) 1–13.

[203] M.I. Montañez, F. Najera, E. Perez-Inestrosa, NMR Studies and molecular dynamic simulation of synthetic dendritic antigens, Polymers (Basel). 3 (2011) 1533–1553.

[204] M.I. Montañez, C. Mayorga, M.J. Torres, M. Blanca, E. Perez-Inestrosa, Methodologies to anchor dendrimeric nanoconjugates to solid phase: Toward an

efficient in vitro detection of allergy to β-lactam antibiotics, Nanomedicine Nanotechnology, Biol. Med. 7 (2011) 682–685.

[205] A. Romano, M. Atanaskovic-Markovic, A. Barbaud, A.J. Bircher, K. Brockow, J. Caubet, G. Celik, J. Cernadas, A. Chiriac, P. Demoly, L.H. Garvey, C. Mayorga, A. Nakonechna, P. Whitaker, M.J. Torres, Towards a more precise diagnosis of hypersensitivity to beta-lactams — an EAACI position paper, Allergy. 75 (2020) 1300–1315.

[206] Y.-F. Huang, H. Liu, X. Xiong, Y. Chen, W. Tan, Nanoparticle-Mediated IgE−Receptor Aggregation and Signaling in RBL Mast Cells, J. Am. Chem. Soc. 131 (2009) 17328–17334.

[207] D. Sil, J.B. Lee, D. Luo, D. Holowka, B. Baird, Trivalent ligands with rigid DNA spacers reveal structural requirements for IgE receptor signaling in RBL mast cells, ACS Chem. Biol. 2 (2007) 674–684.

[208] M.W. Handlogten, T. Kiziltepe, A.P. Serezani, M.H. Kaplan, B. Bilgicer, Inhibition of weak-affinity epitope-IgE interactions prevents mast cell degranulation, Nat. Chem. Biol. 9 (2013) 789–795.

[209] S. Svenson, D.A. Tomalia, Dendrimers in biomedical applications - Reflections on the field, Adv. Drug Deliv. Rev. 57 (2005) 2106–2129.

[210] J. Kitaura, J. Song, M. Tsai, K. Asai, M. Maeda-Yamamoto, A. Mocsai, Y. Kawakami, F.T. Liu, C.A. Lowell, B.G. Barisas, S.J. Galli, T. Kawakami, Evidence that IgE molecules mediate a spectrum of effects on mast cell survival and activation via aggregation of the FcεRI, Proc. Natl. Acad. Sci. U. S. A. 100 (2003) 12911–12916.

[211] Y. Bakkour, V. Darcos, S. Li, J. Coudane, Diffusion ordered spectroscopy (DOSY) as a powerful tool for amphiphilic block copolymer characterization and for critical micelle concentration (CMC) determination, Polym. Chem. 3 (2012) 2006.

[212] A. Jerschow, N. Müller, Diffusion-Separated Nuclear Magnetic Resonance Spectroscopy of Polymer Mixtures, Macromolecules. 31 (1998) 6573–6578.

[213] N. Taghavi Pourianazar, P. Mutlu, U. Gunduz, Bioapplications of poly(amidoamine) (PAMAM) dendrimers in nanomedicine, J. Nanoparticle Res. 16 (2014) 2342.

[214] M.A. Van Dongen, B.G. Orr, M.M. Banaszak Holl, Diffusion NMR study of generation-five PAMAM dendrimer materials, J. Phys. Chem. B. 118 (2014) 7195–7202.

[215] V.A. Jiménez, J.A. Gavín, J.B. Alderete, Scaling trend in diffusion coefficients of low generation G0–G3 PAMAM dendrimers in aqueous solution at high and neutral pH, Struct. Chem. 23 (2012) 123–128.

[216] C. Mayorgaa, T. Obispo, L. Jimeno, M. Blanca, J.M. Del Prado, J. Carreira, J.J. Garcia, C. Juarez, Epitope mapping of β-lactam antibiotics with the use of monoclonal antibodies, Toxicology. 97 (1995) 225–234.

[217] S.G.A. Brown, Clinical features and severity grading of anaphylaxis, J. Allergy Clin. Immunol. 114 (2004) 371–376.

[218] E. Passante, N. Frankish, The RBL-2H3 cell line: its provenance and suitability as a model for the mast cell, Inflamm. Res. 58 (2009) 737–745.

[219] T.M. Laidlaw, J.W. Steinke, A.M. Tiñana, C. Feng, W. Xing, B.K. Lam, S. Paruchuri, J.A. Boyce, L. Borish, Characterization of a novel human mast cell line that responds to stem cell factor and expresses functional FcεRI, J. Allergy Clin. Immunol. 127 (2011) 815-822.e5.

[220] S. García-Gallego, G. Franci, A. Falanga, R. Gómez, V. Folliero, S. Galdiero, F.J. De La Mata, M. Galdiero, Function oriented molecular design: Dendrimers as novel antimicrobials, Molecules. 22 (2017) 1–29.

[221] D. Jishkariani, C.M. Macdermaid, Y.N. Timsina, S. Grama, S.S. Gillani, Self-interrupted synthesis of sterically hindered aliphatic polyamide dendrimers, (2017) 1–10.

[222] M. Huber, Activation/Inhibition of mast cells by supra-optimal antigen concentrations, Cell Commun. Signal. 11 (2013) 1–11.

[223] M.W. Handlogten, P.E. Deak, B. Bilgicer, Two-allergen model reveals complex relationship between IgE crosslinking and degranulation, Chem. Biol. 21 (2014) 1445–1451.

[224] T. Wang, Y. Zhang, L. Wei, Y.G. Teng, T. Honda, I. Ojima, Design, Synthesis, and Biological Evaluations of Asymmetric Bow-Tie PAMAM Dendrimer-Based Conjugates for Tumor-Targeted Drug Delivery, ACS Omega. 3 (2018) 3717–3736.

[225] L.N. Goswami, Z.H. Houston, S.J. Sarma, S.S. Jalisatgi, M.F. Hawthorne, Organic & Biomolecular Chemistry Efficient synthesis of diverse heterobifunctionalized clickable oligo(ethylene glycol) linkers: potential applications in bioconjugation and targeted drug delivery, Org. Biomol. Chem. 11 (2013) 1116.

[226] V. Biricova, A. Laznickova, Dendrimers: Analytical characterization and applications, Bioorg. Chem. 37 (2009) 185–192.

[227] A. CAMINADE, R. LAURENT, J. MAJORAL, Characterization of dendrimers, Adv. Drug Deliv. Rev. 57 (2005) 2130–2146.

[228] R. Müller, C. Laschober, W.W. Szymanski, G. Allmaier, Determination of Molecular Weight, Particle Size, and Density of High Number Generation PAMAM Dendrimers Using MALDI−TOF−MS and nES−GEMMA, Macromolecules. 40 (2007) 5599–5605.

[229] A. Lederer, D. Voigt, D. Appelhans, B. Voit, Molar mass characterization and solution behaviour of poly(ether amide) dendrimers, Polym. Bull. 57 (2006) 329–340.

[230] I.J. Majoros, B. Keszler, S. Woehler, T. Bull, J.R. Baker, Acetylation of Poly(amidoamine) Dendrimers, Macromolecules. 36 (2003) 5526–5529.

[231] M.A. van Dongen, A. Desai, B.G. Orr, J.R. Baker, M.M. Banaszak Holl, Quantitative analysis of generation and branch defects in G5 poly(amidoamine) dendrimer, Polymer (Guildf). 54 (2013) 4126–4133.

[232] J. Peterson, V. Allikmaa, J. Subbi, T. Pehk, M. Lopp, Structural deviations in poly(amidoamine) dendrimers: a MALDI-TOF MS analysis, Eur. Polym. J. 39 (2003) 33–42.

[233] M.S. Wendland, S.C. Zimmerman, Synthesis of Cored Dendrimers, J. Am. Chem. Soc. 121 (1999) 1389–1390.

[234] A. Sharma, D.K. Mohanty, A. Desai, R. Ali, A simple polyacrylamide gel electrophoresis procedure for separation of polyamidoamine dendrimers, Electrophoresis. 24 (2003) 2733–2739.

[235] H.M. Brothers II, L.T. Piehler, D.A. Tomalia, Slab-gel and capillary electrophoretic characterization of polyamidoamine dendrimers, J. Chromatogr. A. 814 (1998) 233–246.

[236] W. Zhang, J. Martinelli, J.A. Peters, J.M.A. Van Hengst, H. Bouwmeester, E. Kramer, C.S. Bonnet, F. Szeremeta, É. Tóth, K. Djanashvili, Surface PEG Grafting Density Determines Magnetic Relaxation Properties of Gd-Loaded Porous Nanoparticles for MR Imaging Applications, ACS Appl. Mater. Interfaces. 9 (2017) 23458–23465.

[237] M. Kusterle, S. Jevševar, V.G. Porekar, Size of pegylated protein conjugates studied by various methods, Acta Chim. Slov. 55 (2008) 594–601.

[238] K.L. Linegar, A.E. Adeniran, A.F. Kostko, M.A. Anisimov, Hydrodynamic radius of polyethylene glycol in solution obtained by dynamic light scattering, Colloid J. 72 (2010) 279–281.

[239] M. Lin, D. Krawitz, M.D. Callahan, G. Deperalta, A.T. Wecksler, Characterization of ELISA Antibody-Antigen Interaction using Footprinting-Mass Spectrometry and Negative Staining Transmission Electron Microscopy, J. Am. Soc. Mass Spectrom. 29 (2018) 961–971.

[240] M. Oda, S. Uchiyama, M. Noda, Y. Nishi, M. Koga, K. Mayanagi, C. V Robinson, K. Fukui, Y. Kobayashi, K. Morikawa, T. Azuma, Effects of antibody affinity and antigen valence on molecular forms of immune complexes, Mol. Immunol. 47 (2009) 357–364.

[241] F. Jönsson, M. Daëron, Mast Cells and Company, Front. Immunol. 3 (2012) 1–18.

[242] Z. Ma, D.N. LeBard, S.M. Loverde, K.A. Sharp, M.L. Klein, D.E. Discher, T.H. Finkel, TCR Triggering by pMHC Ligands Tethered on Surfaces via Poly(Ethylene Glycol)

Depends on Polymer Length, PLoS One. 9 (2014) e112292.

[243] E.F. Knol, Requirements for effective IgE cross-linking on mast cells and basophils, Mol. Nutr. Food Res. 50 (2006) 620–624.

[244] L. Liang, D. Astruc, The copper(I)-catalyzed alkyne-azide cycloaddition (CuAAC) "click" reaction and its applications. An overview, Coord. Chem. Rev. 255 (2011) 2933–2945.

[245] J.E. Hein, J.C. Tripp, L.B. Krasnova, K.B. Sharpless, V. V. Fokin, Copper(I)-Catalyzed Cycloaddition of Organic Azides and 1-Iodoalkynes, Angew. Chemie. 121 (2009) 8162–8165.

[246] V. V. Rostovtsev, L.G. Green, V. V. Fokin, K.B. Sharpless, A stepwise huisgen cycloaddition process: Copper(I)-catalyzed regioselective "ligation" of azides and terminal alkynes, Angew. Chemie - Int. Ed. 41 (2002) 2596–2599.

[247] J.F. Lutz, 1,3-Dipolar cycloadditions of azides and alkynes: A universal ligation tool in polymer and materials science, Angew. Chemie - Int. Ed. 46 (2007) 1018–1025.

[248] D. Canseco-González, J.L. Rodríguez De La O, J.E. Herbert-Pucheta, Combined XRD-paramagnetic 13C NMR spectroscopy of 1,2,3-triazoles for revealing copper traces in a Huisgen click-chemistry cycloaddition. A model case, Heterocycl. Commun. 25 (2019) 98–106.

[249] D. Pasini, The click reaction as an efficient tool for the construction of macrocyclic structures, Molecules. 18 (2013) 9512–9530.

[250] V. Castro, H. Rodríguez, F. Albericio, CuAAC: An Efficient Click Chemistry Reaction on Solid Phase, ACS Comb. Sci. 18 (2016) 1–14.

[251] M.F. Ebbesen, D. Itskalov, M. Baier, L. Hartmann, Cu Elimination from Cu-Coordinating Macromolecules, ACS Macro Lett. 6 (2017) 399–403.

[252] M.S. Diallo, L. Balogh, A. Shafagati, J.H. Johnson, W.A. Goddard, D.A. Tomalia, Poly(amidoamine) dendrimers: A new class of high capacity chelating agents for Cu(II) ions, Environ. Sci. Technol. 33 (1999) 820–824.

[253] M. Arseneault, C. Wafer, J.F. Morin, Recent advances in click chemistry applied to dendrimer synthesis, Molecules. 20 (2015) 9263–9294.

[254] C. Deraedt, N. Pinaud, D. Astruc, Recyclable catalytic dendrimer nanoreactor for part-per-million Cu I catalysis of "click" chemistry in water, J. Am. Chem. Soc. 136 (2014) 12092–12098.

[255] R.G. Posner, D. Geng, S. Haymore, J. Bogert, I. Pecht, A. Licht, P.B. Savage, Trivalent antigens for degranulation of mast cells, Org. Lett. 9 (2007) 3551–3554.

[256] A. Tesfaye, A. Rodríguez-Nogales, S. Benedé, T.D. Fernández, J.L. Paris, M.J. Rodriguez, I.M. Jiménez-Sánchez, G. Bogas, C. Mayorga, M.J. Torres, M.I. Montañez, Nanoarchitectures for Efficient IgE Cross-Linking on Effector Cells to Study Amoxicillin Allergy, Allergy. (2021) 1–11.

[257] R. Schweitzer-Stenner, A. Licht, I. Liischer, I. Pecht, Oligomerization and Ring Closure of Immunoglobulin E Class Antibodies by Divalent Haptens, Biochemistry. 26 (1987) 3602–3612.

[258] L. Zhang, J. Song, Y. Newhouse, S. Zhang, K.H. Weisgraber, G. Ren, An optimized negative-staining protocol of electron microscopy for apoE4•POPC lipoprotein, J. Lipid Res. 51 (2010) 1228–1236.

[259] N.A.A. Talib, F. Salam, Y. Sulaiman, Development of polyclonal antibody against clenbuterol for immunoassay application, Molecules. 23 (2018) 1–14.

[260] M. Blanca, C. Mayorga, F. Sanchez, J.M. Vega, J. Fernandez, C. Juarez, R. Suau, E. Perez, Differences in serum IgE antibody activity to benzylpenicillin and amoxicillin measured by RAST in a group of penicillin allergic patients, Allergy. 46 (1991) 632–638.

[261] S. Benedé, E. Cody, C. Agashe, M.C. Berin, Immune characterization of bone marrow-derived models of mucosal and connective tissue mast cells, Allergy, Asthma Immunol. Res. 10 (2018) 268–277.

[262] S. Benedé, J. Ramos-Soriano, F. Palomares, J. Losada, A. Mascaraque, J.C. López-

Rodríguez, J. Rojo, C. Mayorga, M. Villalba, E. Batanero, Peptide Glycodendrimers as Potential Vaccines for Olive Pollen Allergy, Mol. Pharm. 17 (2020) 827–836.

Appendix

Appendix

Spectra

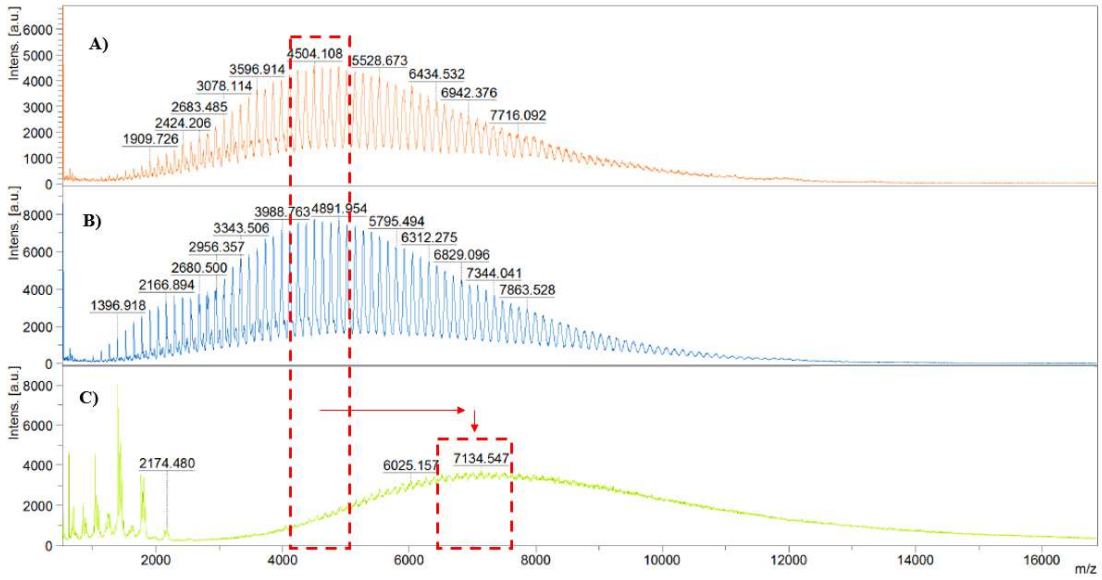

Figure S1. MALDI-TOF MS spectra of PLL control sample in PBS (A), commercial(B) and PLL-AXO conjugate (C).

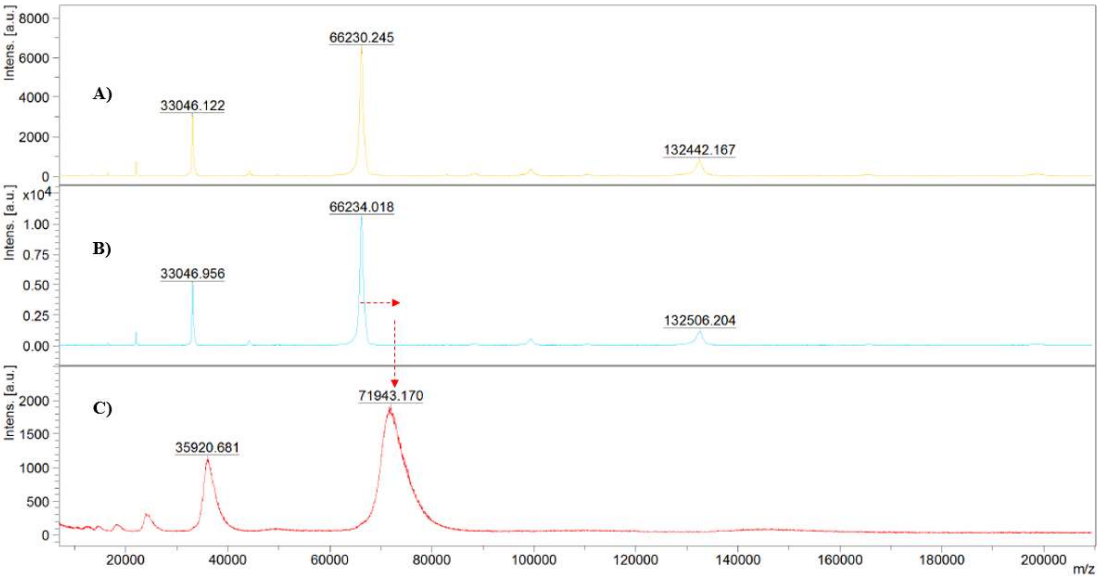

Figure S2. MALDI-TOF MS spectra of HSA control sample in PBS (A), commercial(B) and HSA-AXO conjugate (C).

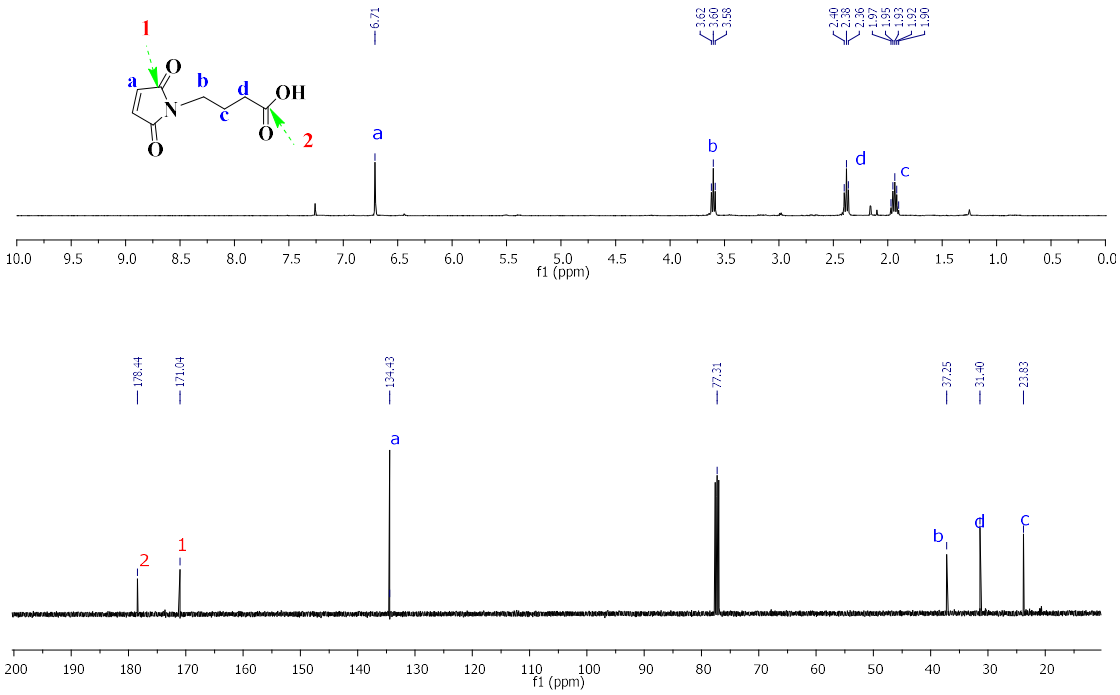

Figure S3. ^{1}H and ^{13}C NMR spectra of compound **1** in $CDCl_3$.

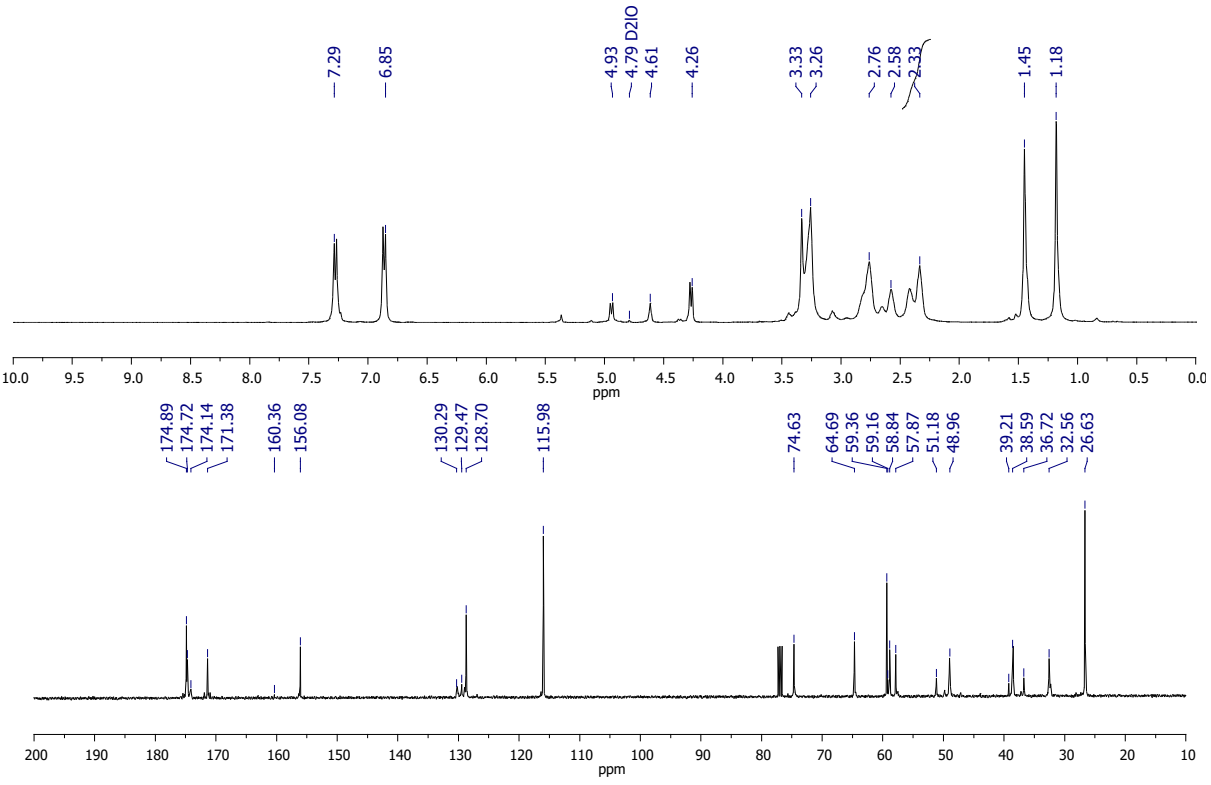

Figure S4. ^{1}H and ^{13}C NMR spectra of compound **2** in D_2O.

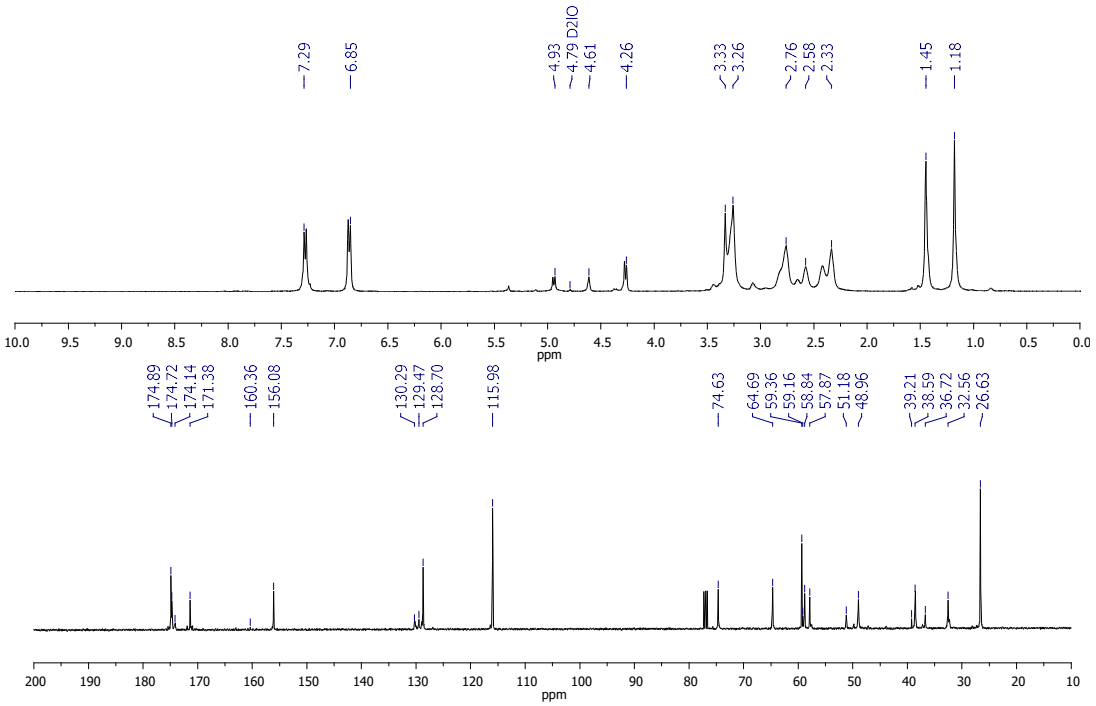

Figure S5. ^{1}H and ^{13}C NMR spectra of compound **3** in D_2O.

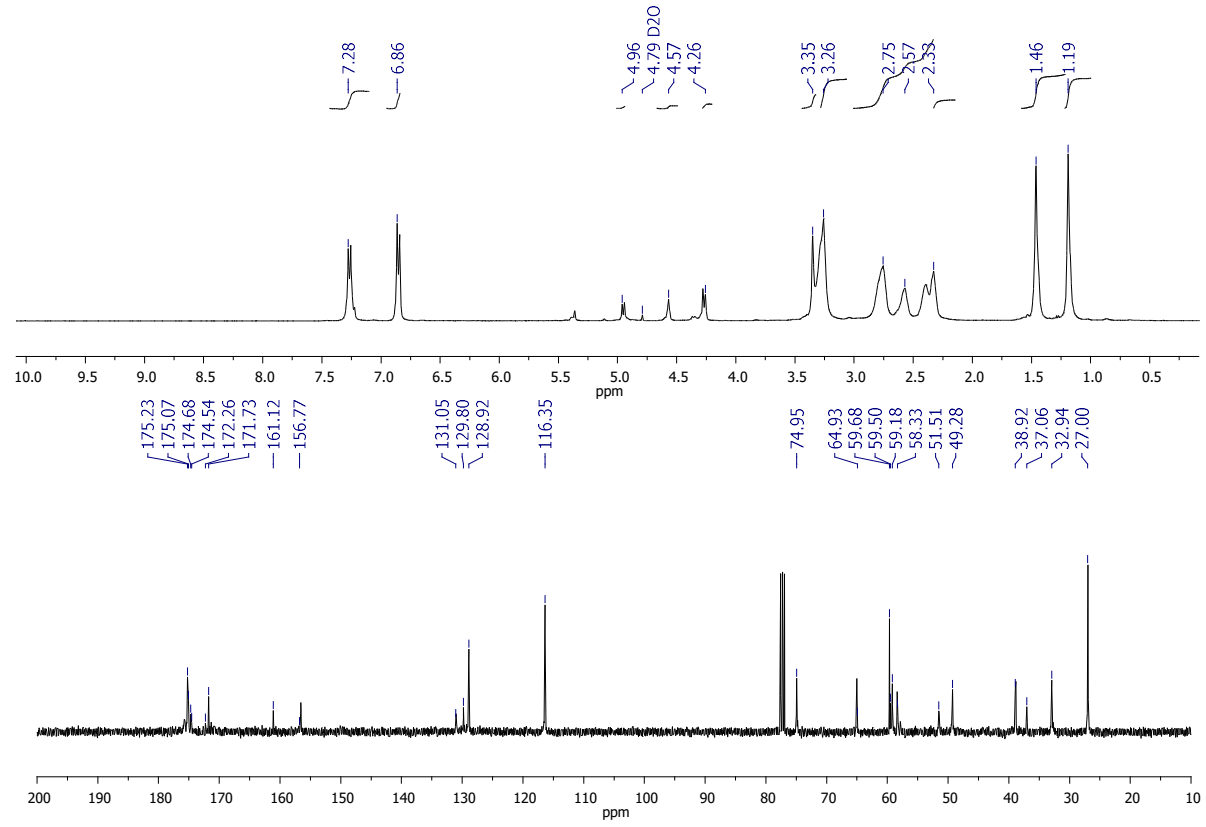

Figure S6. ^{1}H and ^{13}C NMR spectra of compound **4** in D_2O.

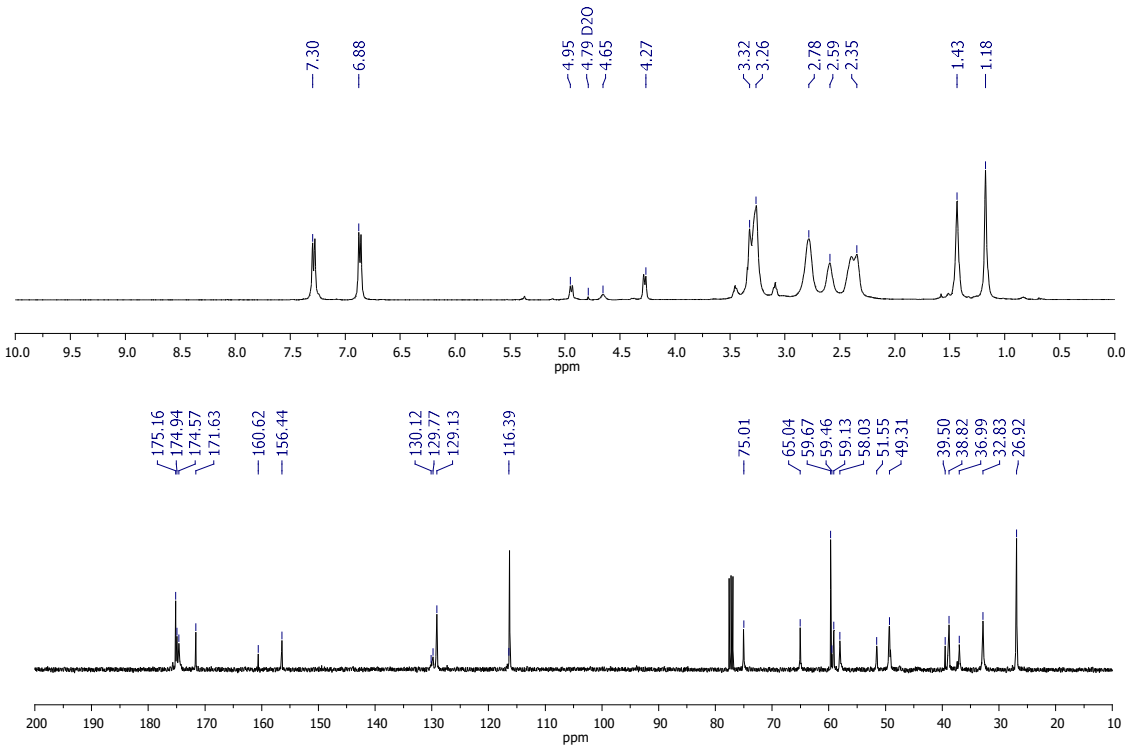

Figure S7. ^{1}H and ^{13}C NMR spectra of compound **5** in D_2O

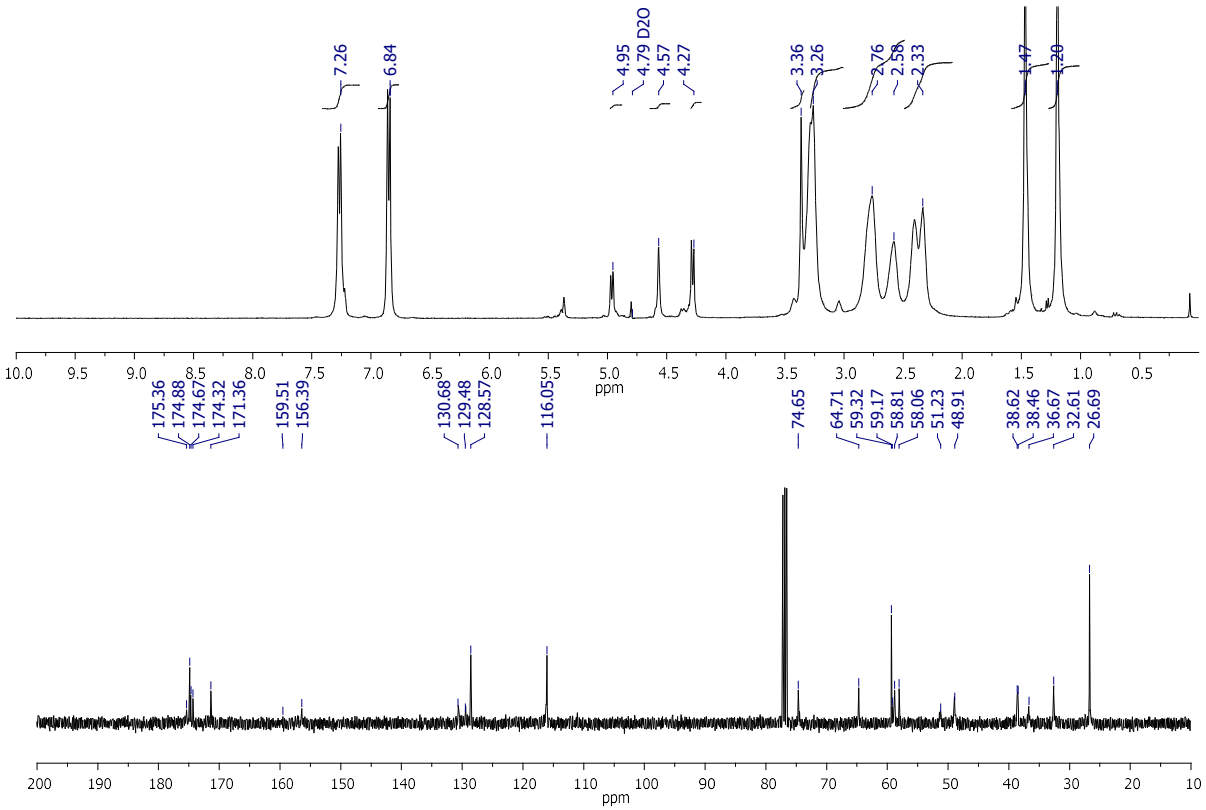

Figure S8. ^{1}H and ^{13}C NMR spectra of compound **6** in D_2O

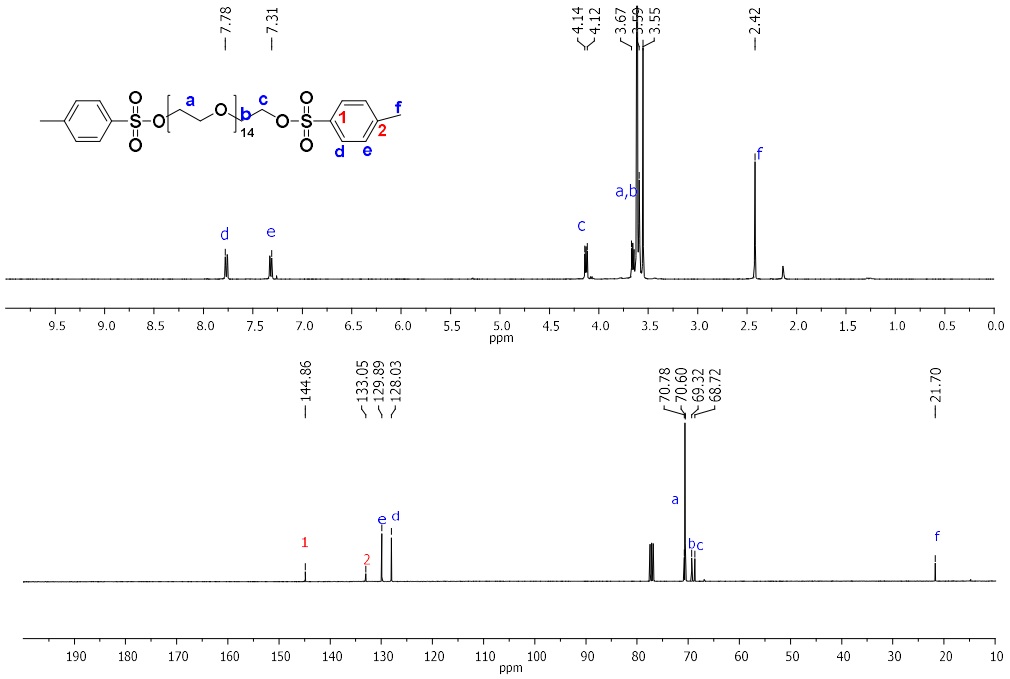

Figure S9. ^{1}H and ^{13}C NMR spectra of compound **7** in $CDCl_3$.

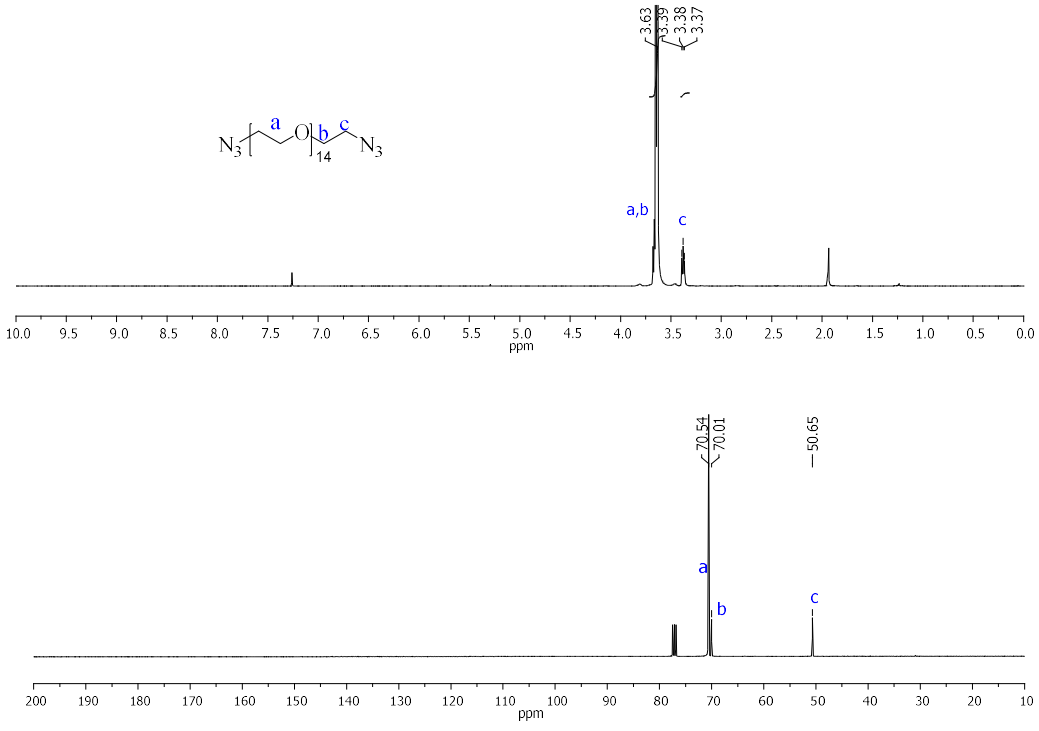

Figure S10. ^{1}H and ^{13}C NMR spectra of compound **8** in $CDCl_3$.

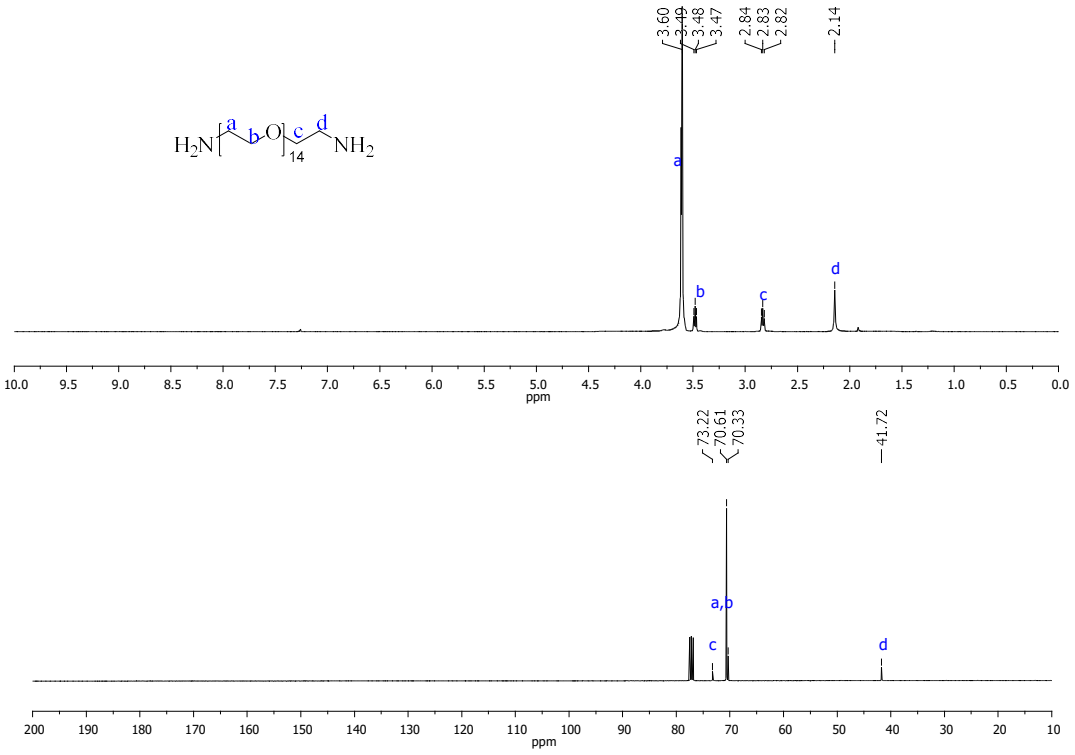

Figure S11. ^{1}H and ^{13}C NMR spectra of compound **9** in $CDCl_3$.

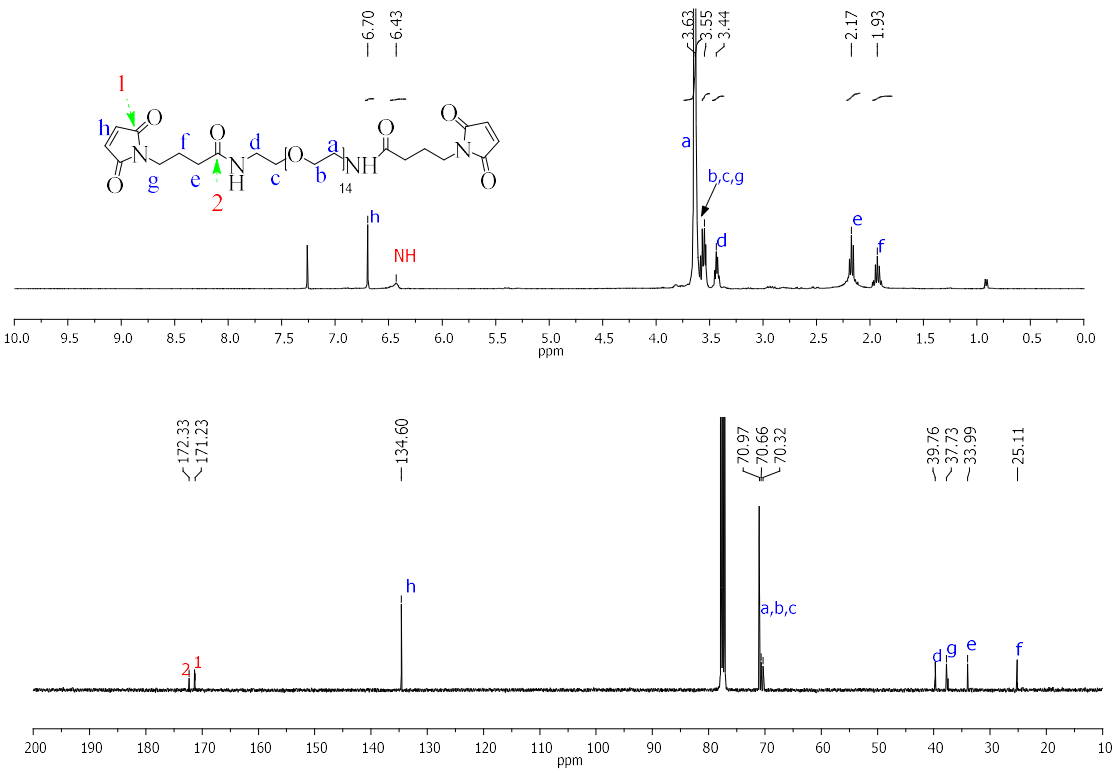

Figure S12. ^{1}H and ^{13}C NMR spectra of compound **10** in $CDCl_3$.

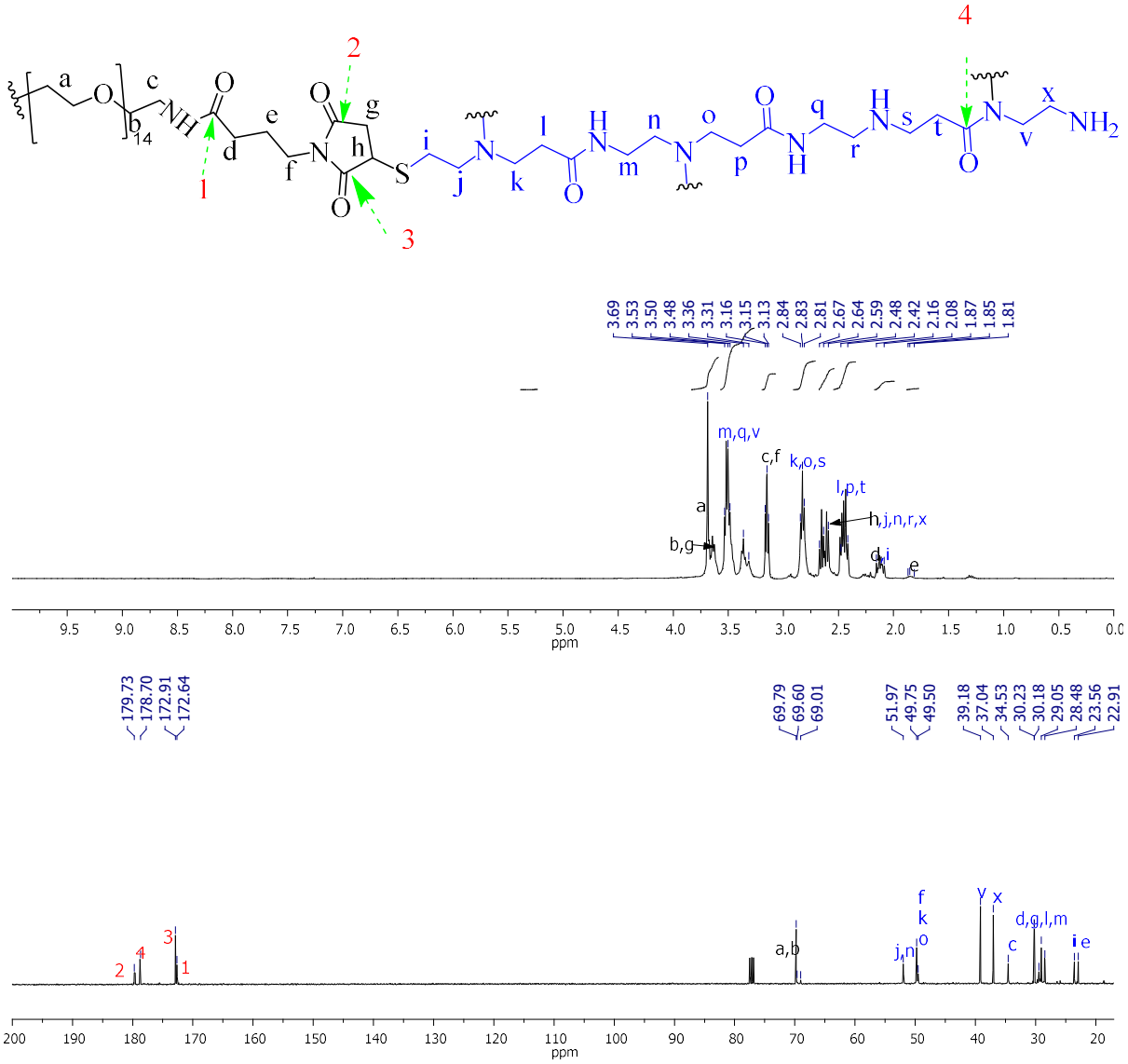

Figure S13. ^{1}H and ^{13}C NMR spectra of compound **11** in D_2O.

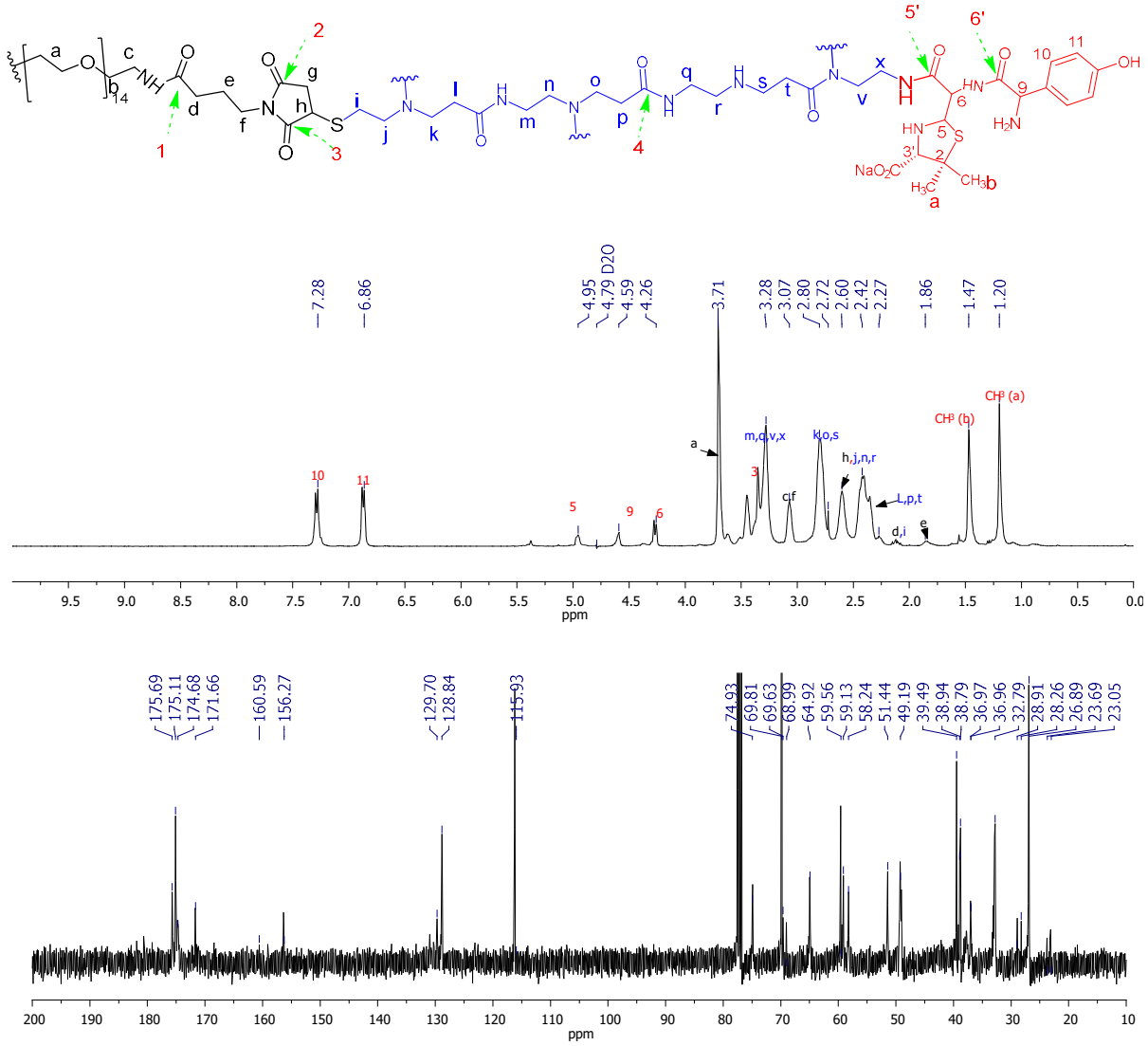

Figure S14. ^{1}H and ^{13}C NMR spectra of compound **12** in D_2O.

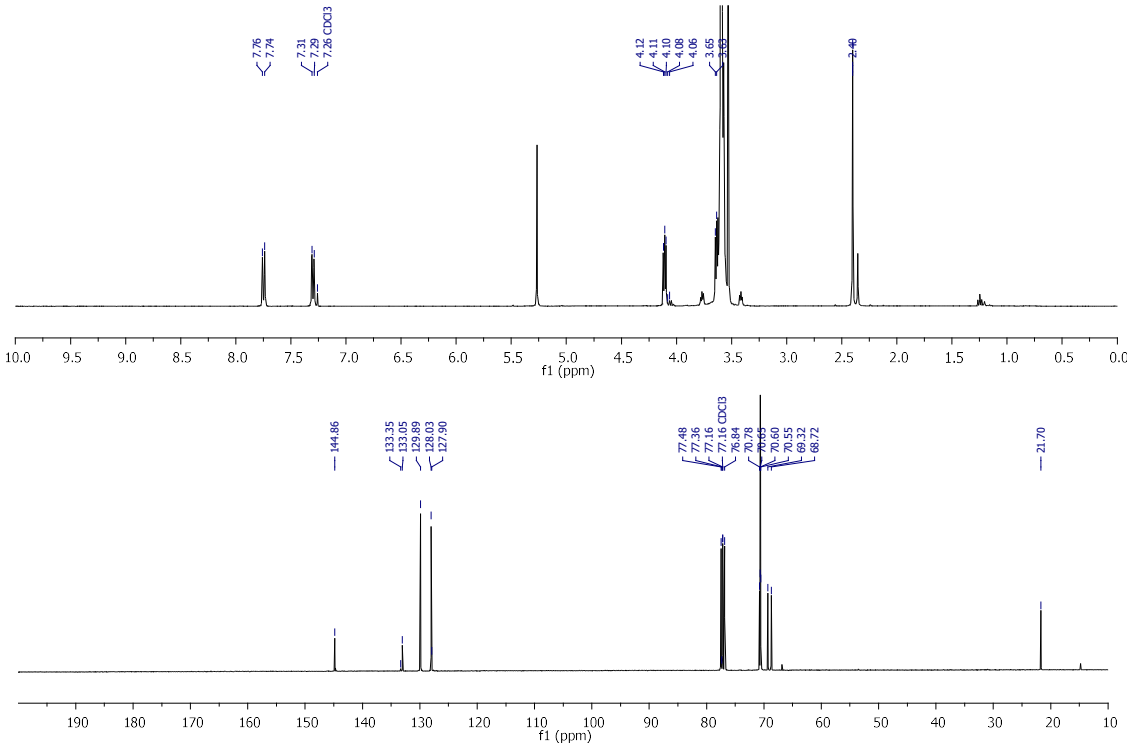

Figure S15. ^{1}H and ^{13}C NMR spectra of compound **13** in $CDCl_3$.

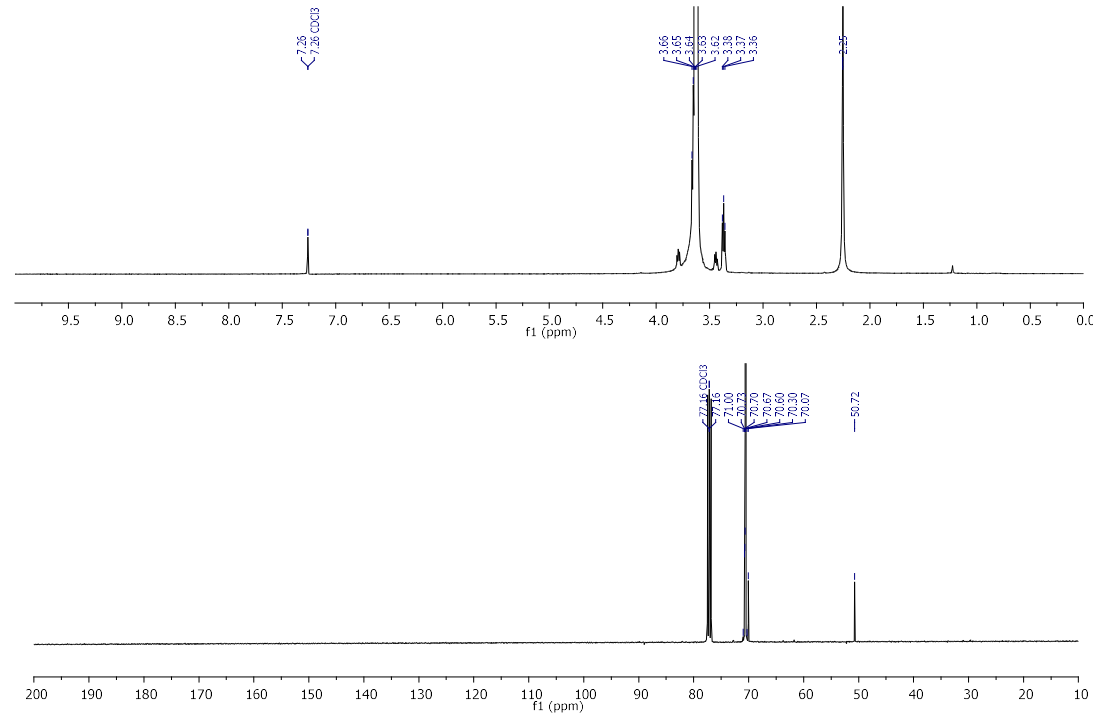

Figure S16. ^{1}H and ^{13}C NMR spectra of compound **14** in $CDCl_3$.

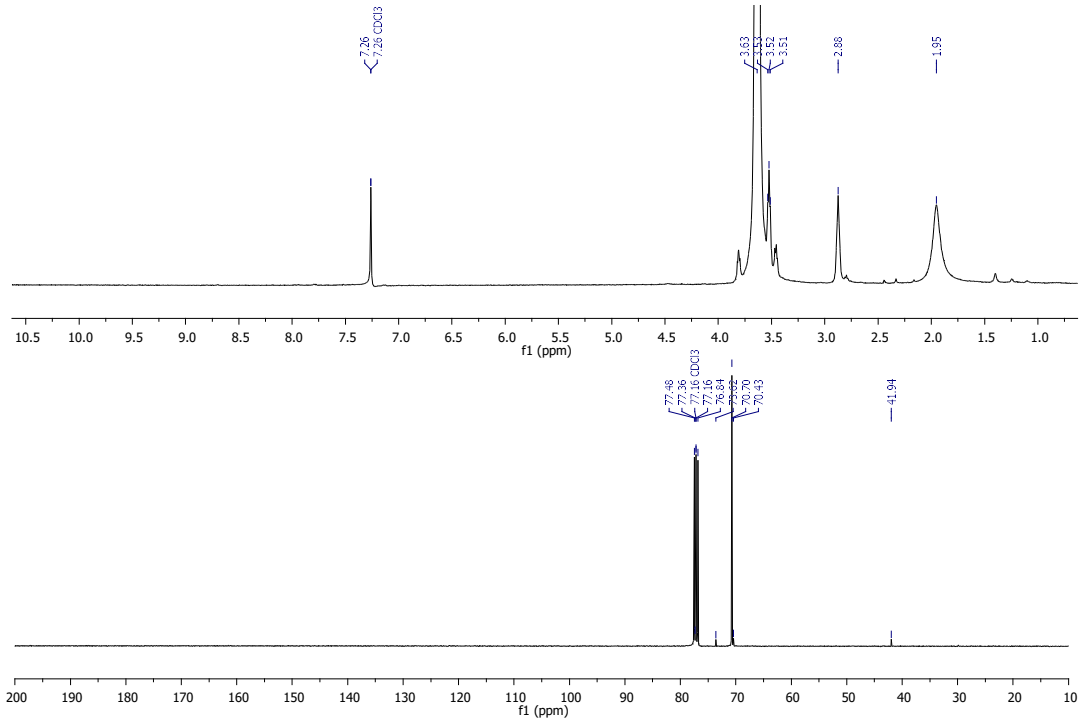

Figure S17. ^{1}H and ^{13}C NMR spectra of compound **15** in $CDCl_3$.

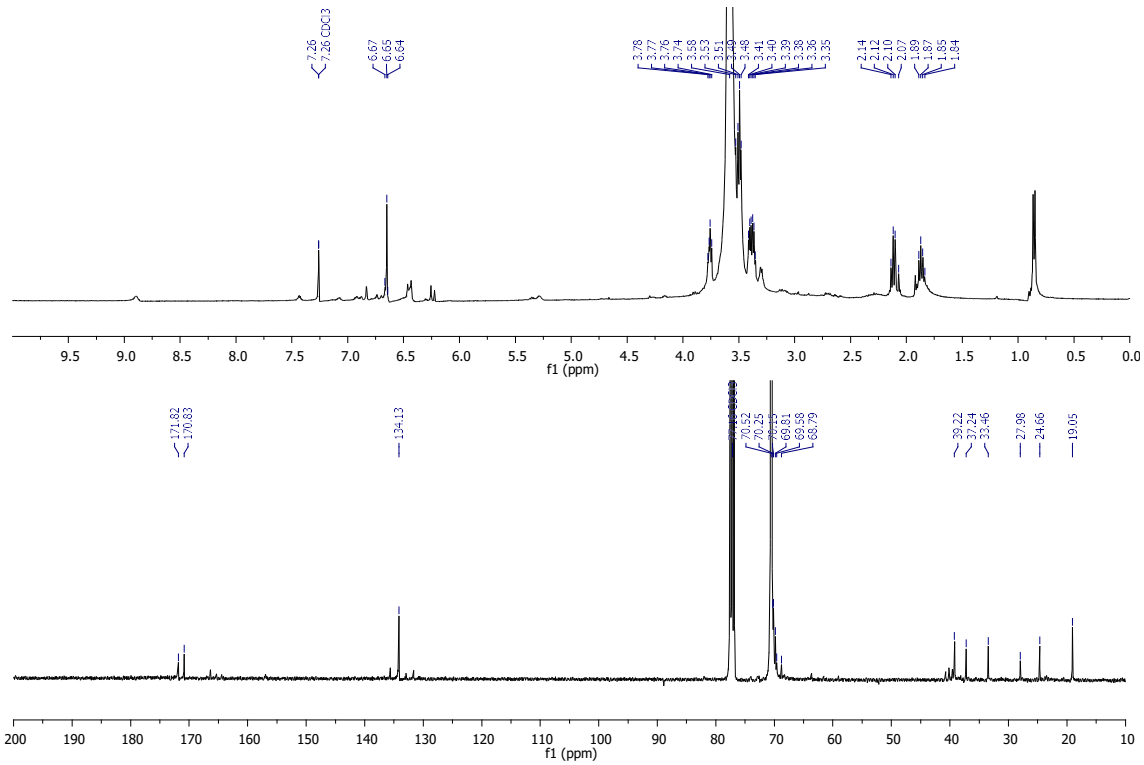

Figure S18. ^{1}H and ^{13}C NMR spectra of compound **16** in $CDCl_3$.

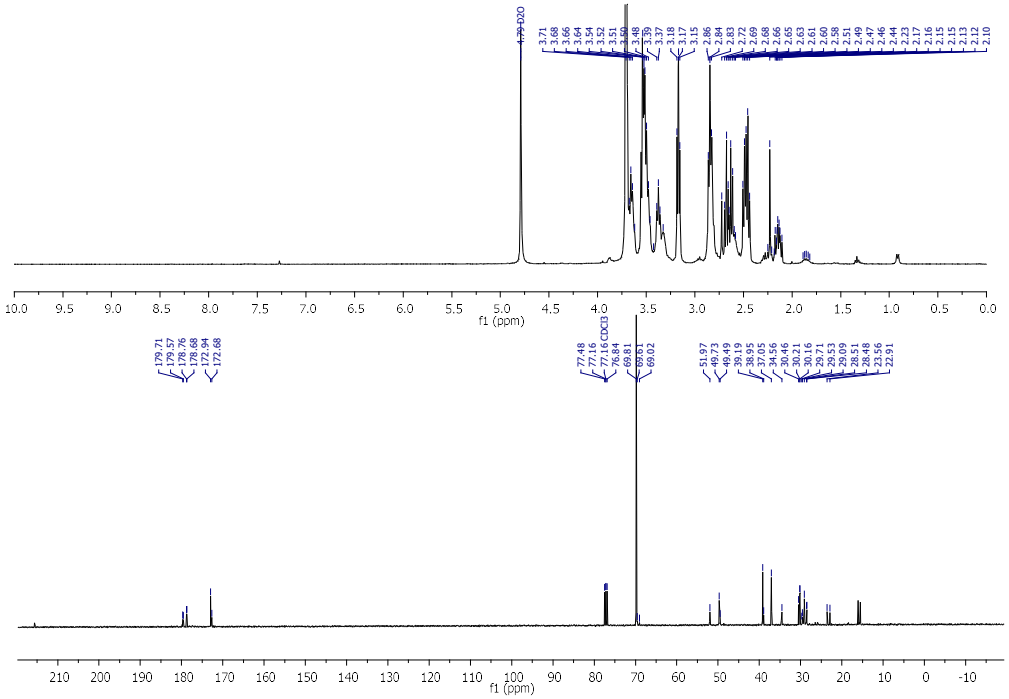

Figure S19. ^{1}H and ^{13}C NMR spectra of compound **17** in D_2O.

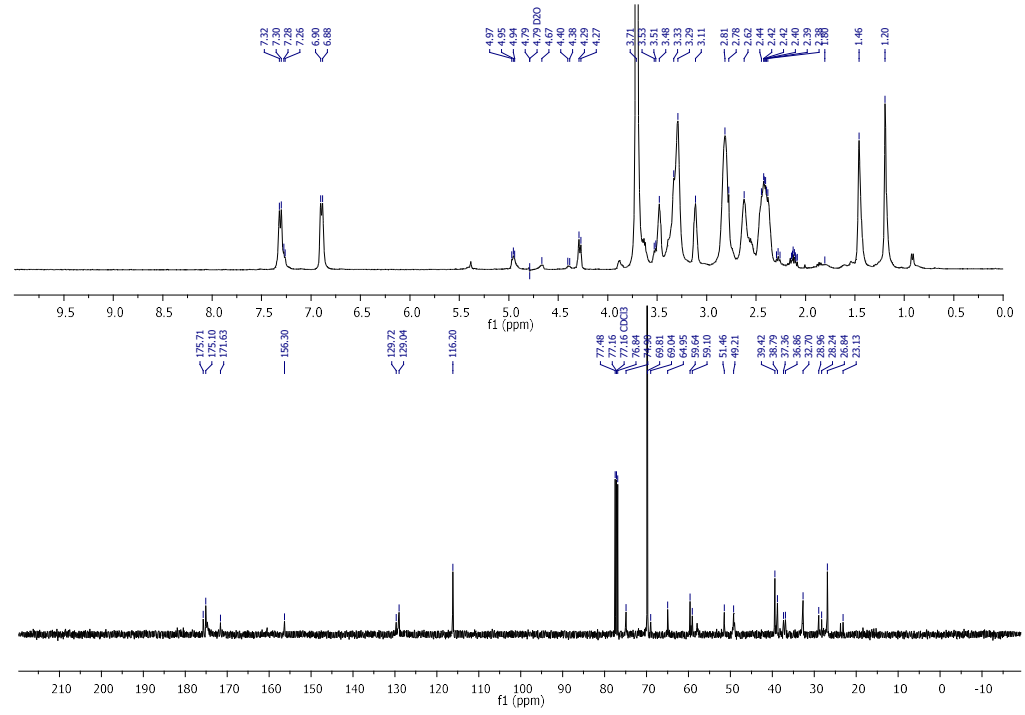

Figure S20. ^{1}H and ^{13}C NMR spectra of compound **18** in D_2O.

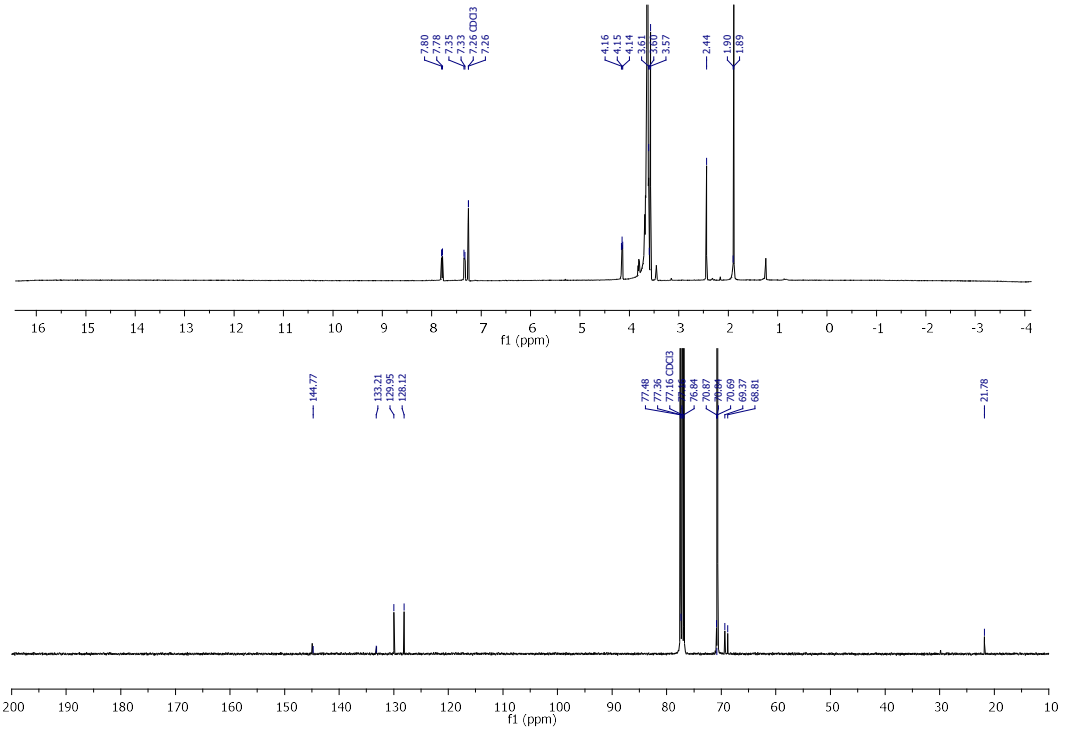

Figure S21. ^{1}H and ^{13}C NMR spectra of compound **19** in $CDCl_3$.

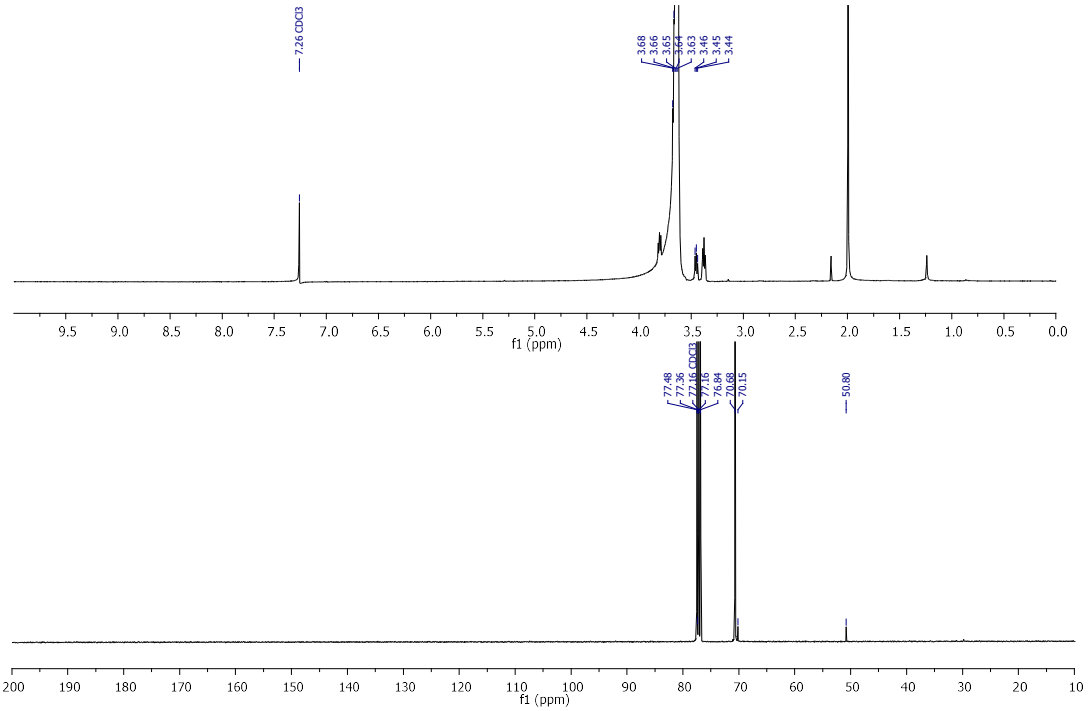

Figure S22. ^{1}H and ^{13}C NMR spectra of compound **20** in $CDCl_3$.

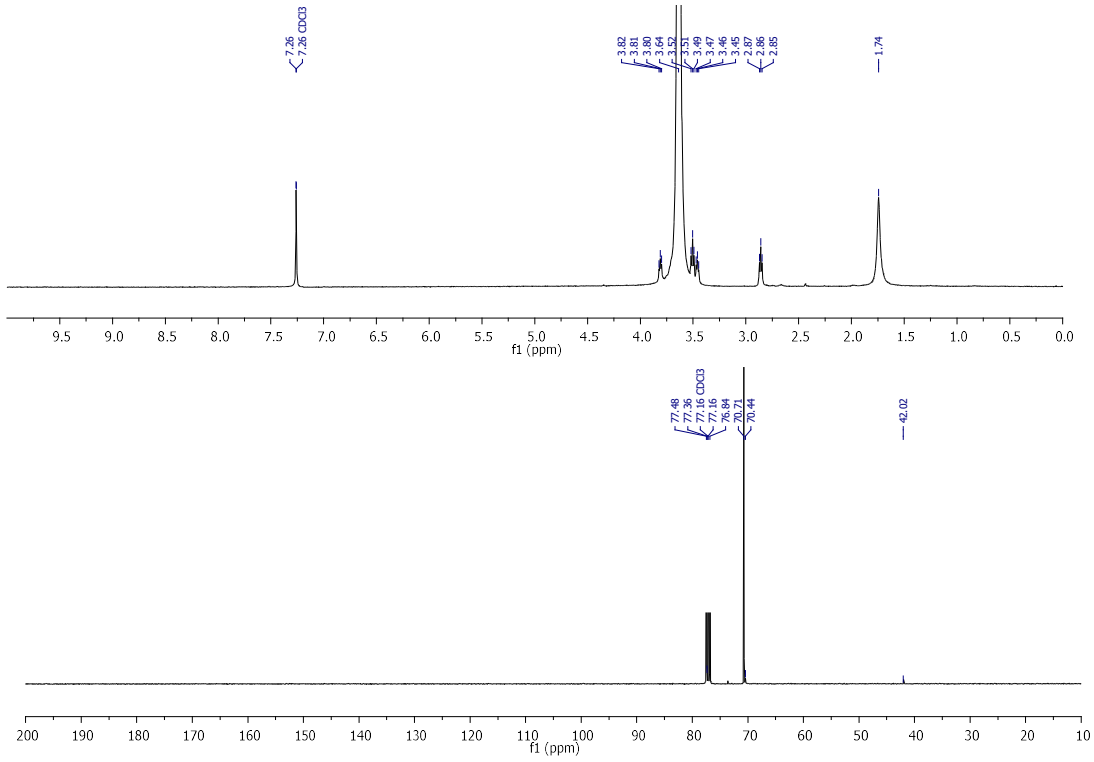

Figure S23. ^{1}H and ^{13}C NMR spectra of compound **21** in $CDCl_3$.

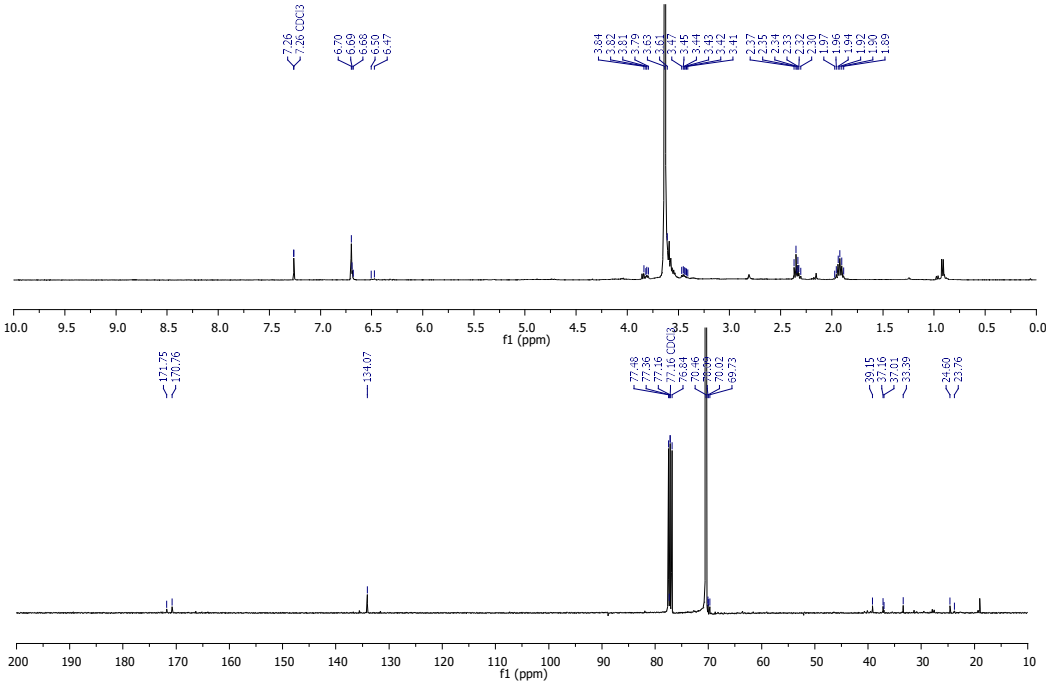

Figure S24. ^{1}H and ^{13}C NMR spectra of compound **22** in $CDCl_3$.

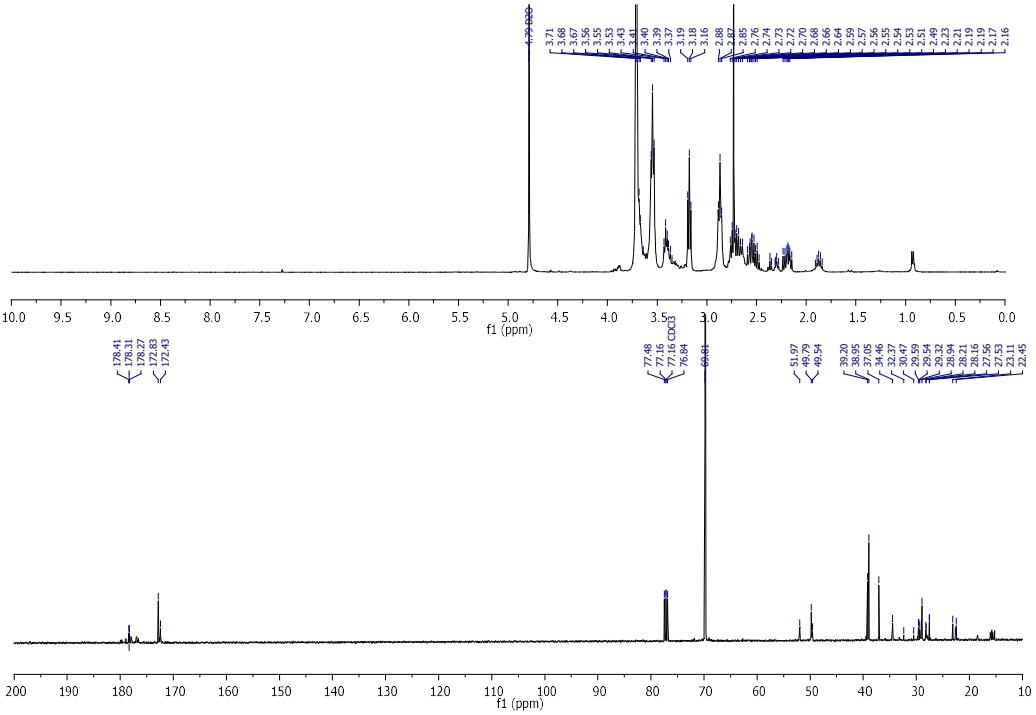

Figure S25. ^{1}H and ^{13}C NMR spectra of compound **23** in D_2O.

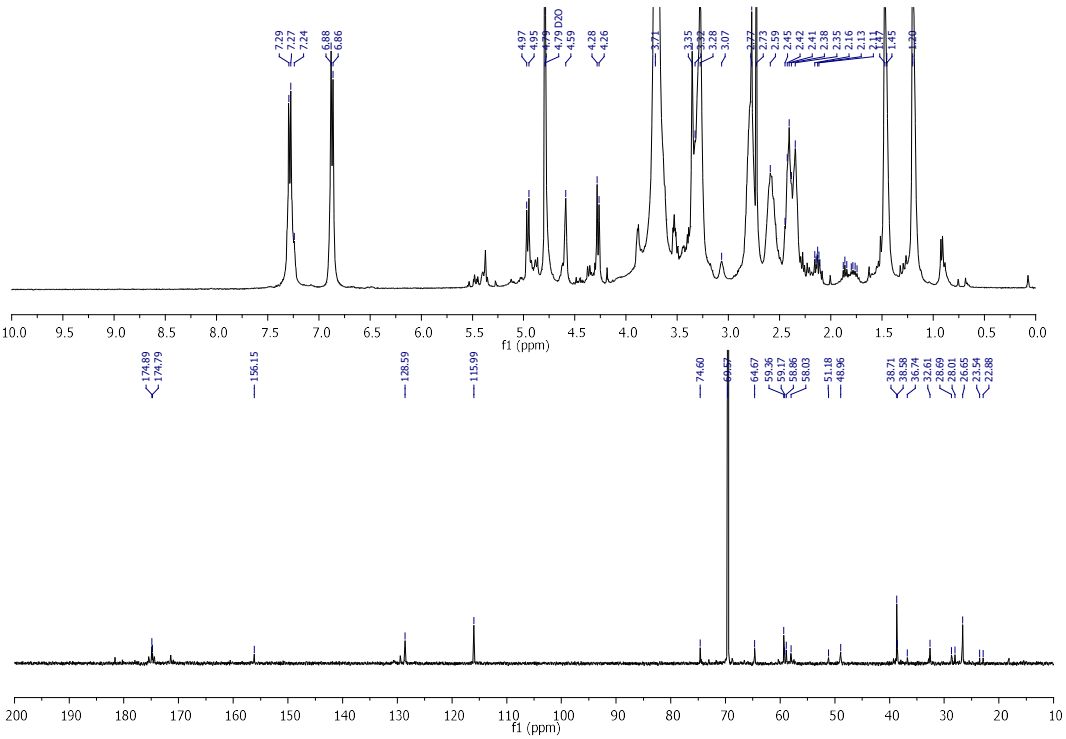

Figure S26. ^{1}H and ^{13}C NMR spectra of compound **24** in D_2O.

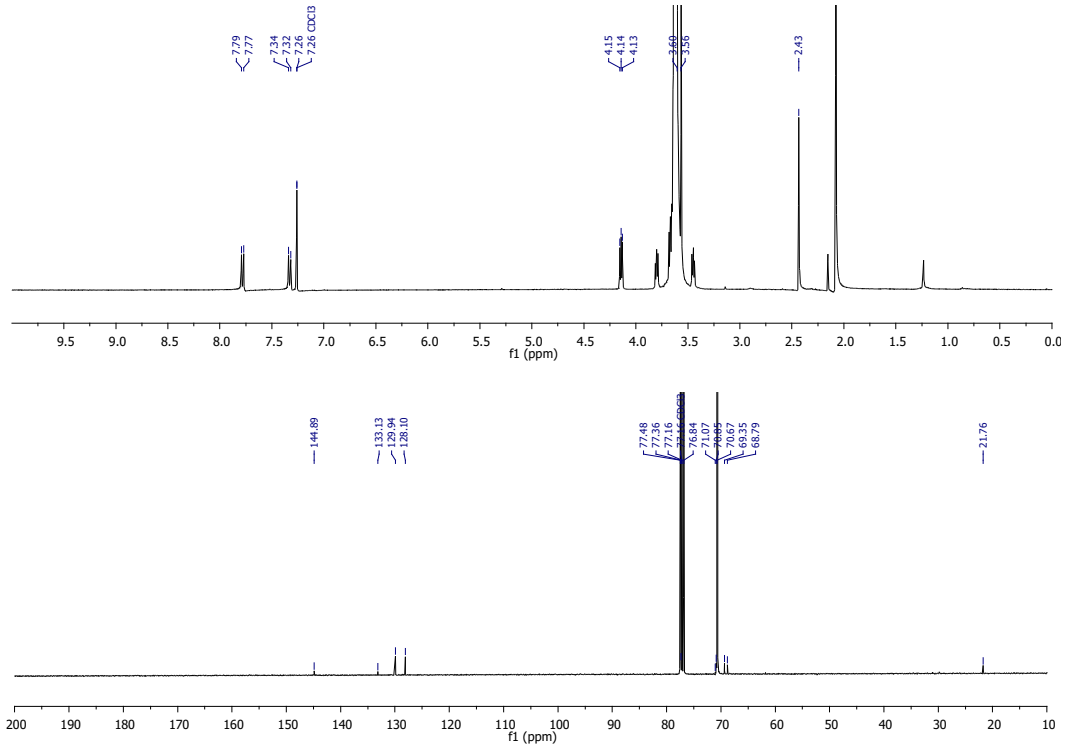

Figure S27. ^{1}H and ^{13}C NMR spectra of compound **25** in $CDCl_3$.

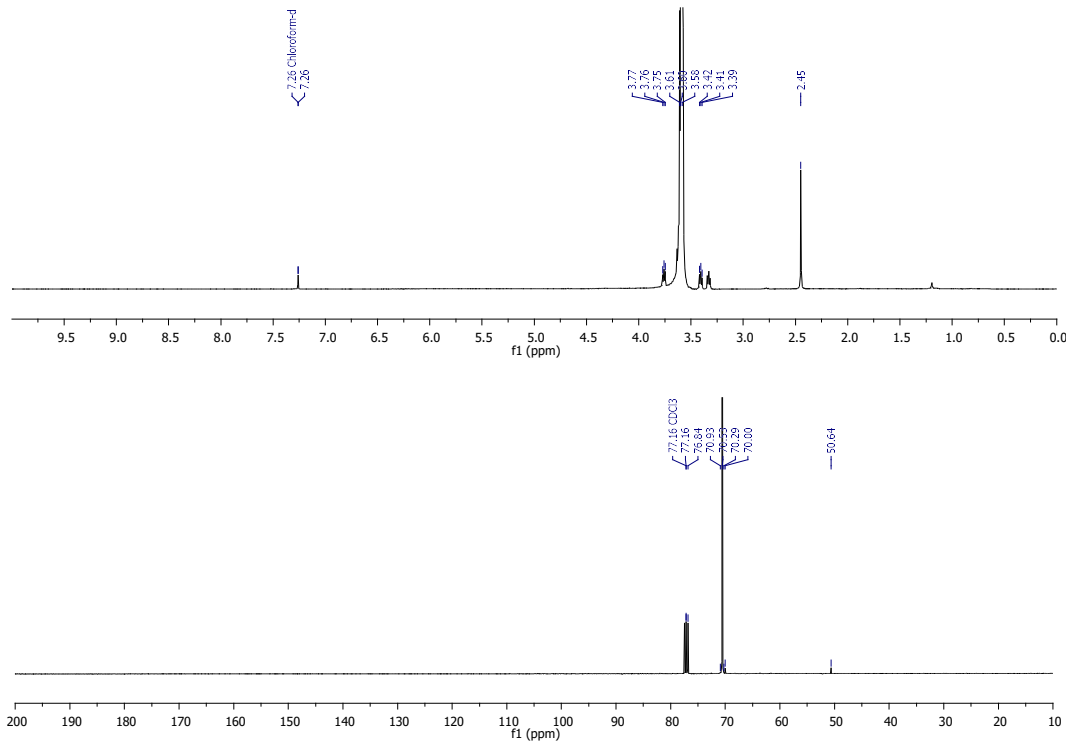

Figure S28. ^{1}H and ^{13}C NMR spectra of compound **26** in $CDCl_3$.

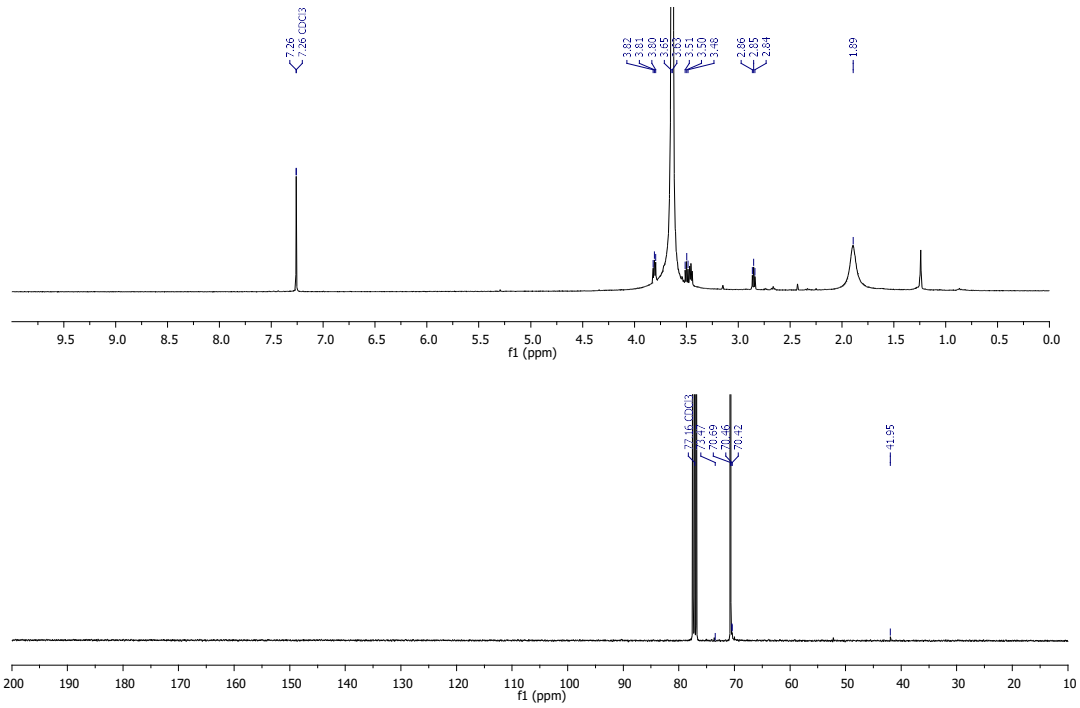

Figure S29. ^{1}H and ^{13}C NMR spectra of compound **27** in $CDCl_3$.

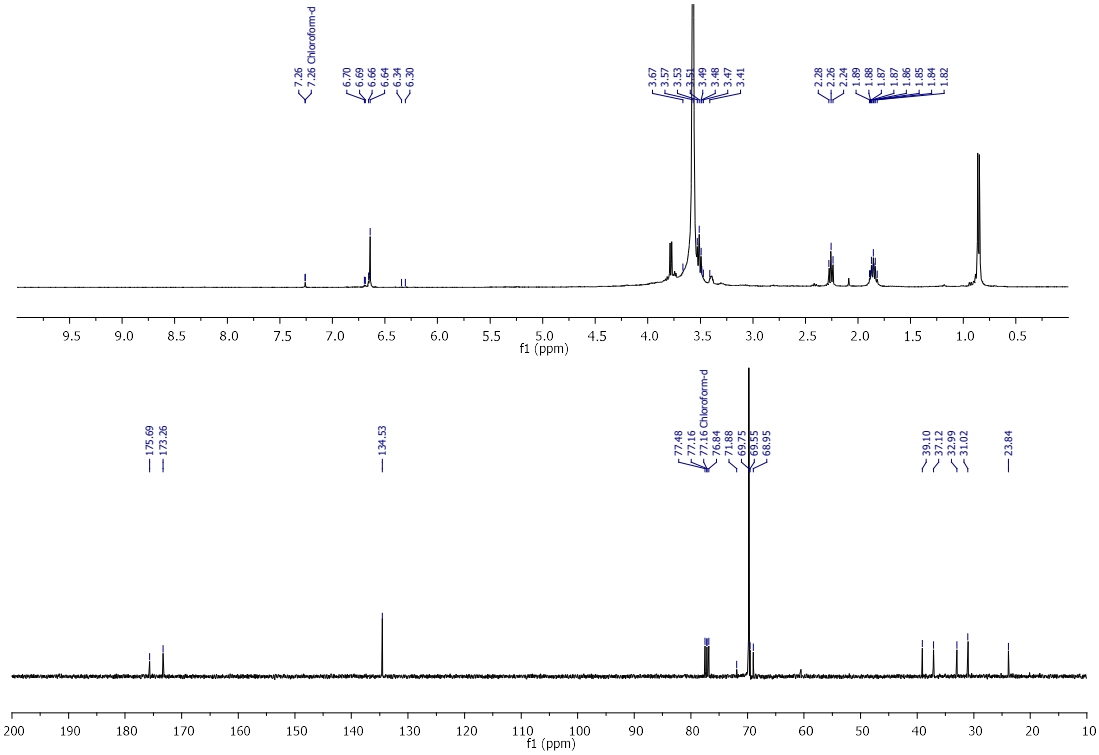

Figure S30. ^{1}H and ^{13}C NMR spectra of compound **28** in $CDCl_3$

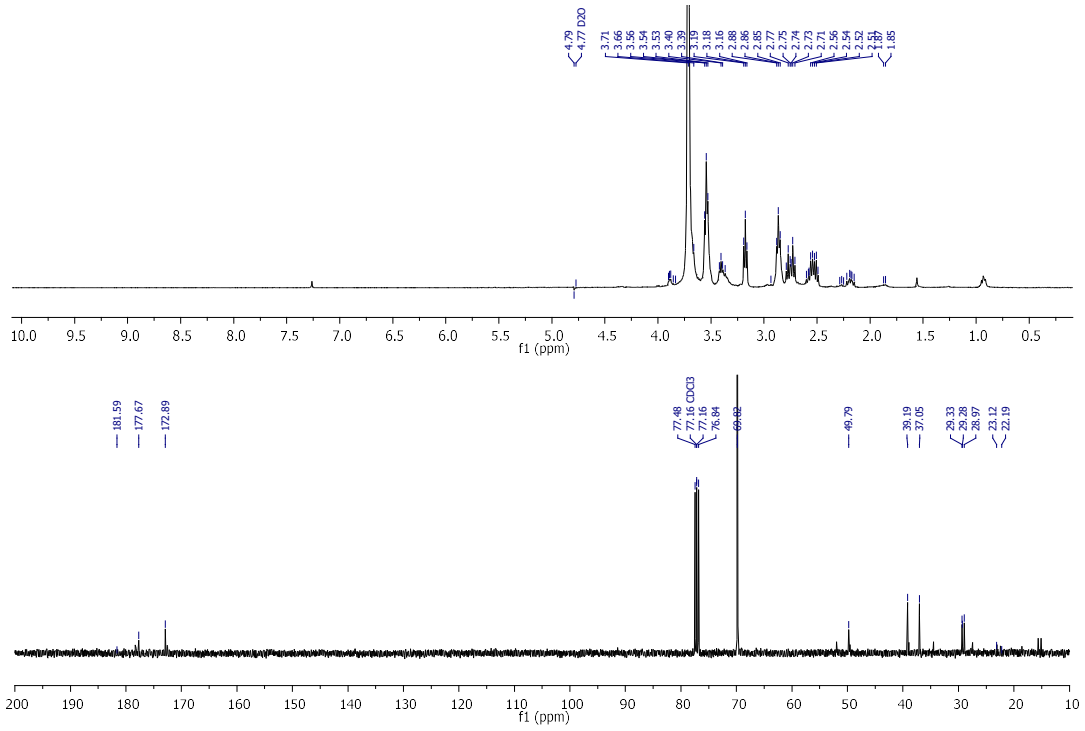

Figure S31. ^{1}H and ^{13}C NMR spectra of compound **29** in D_2O.

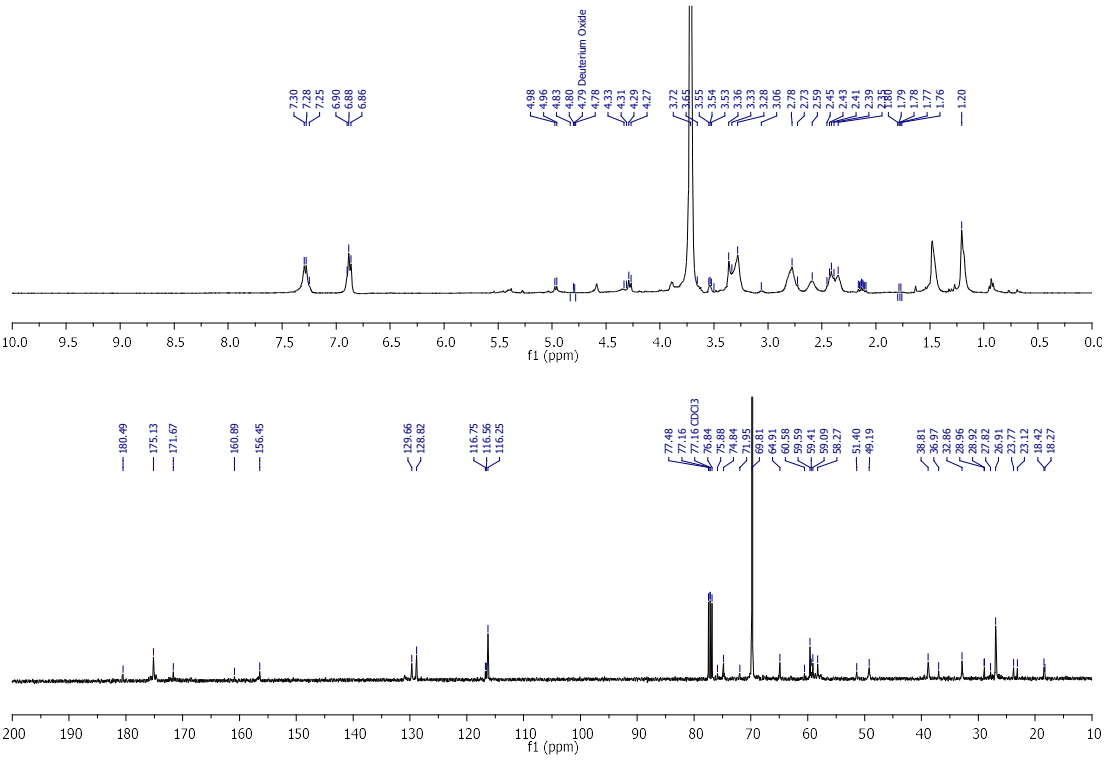

Figure S32. ^{1}H and ^{13}C NMR spectra of compound **30** in D_2O.

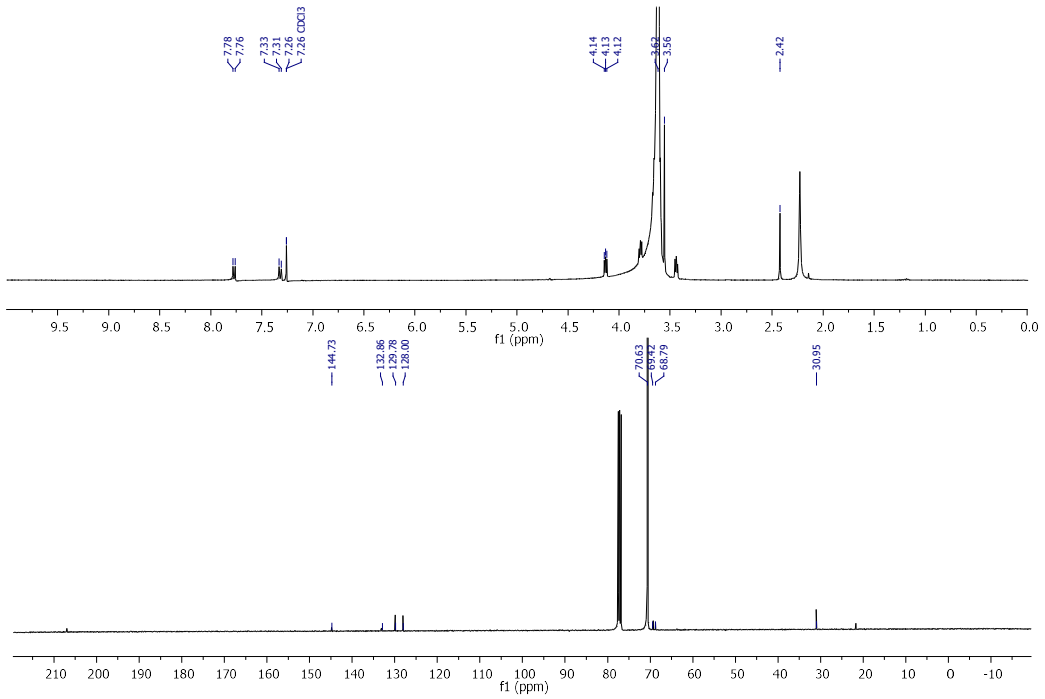

Figure S33. ^{1}H and ^{13}C NMR spectra of compound **31** in $CDCl_3$.

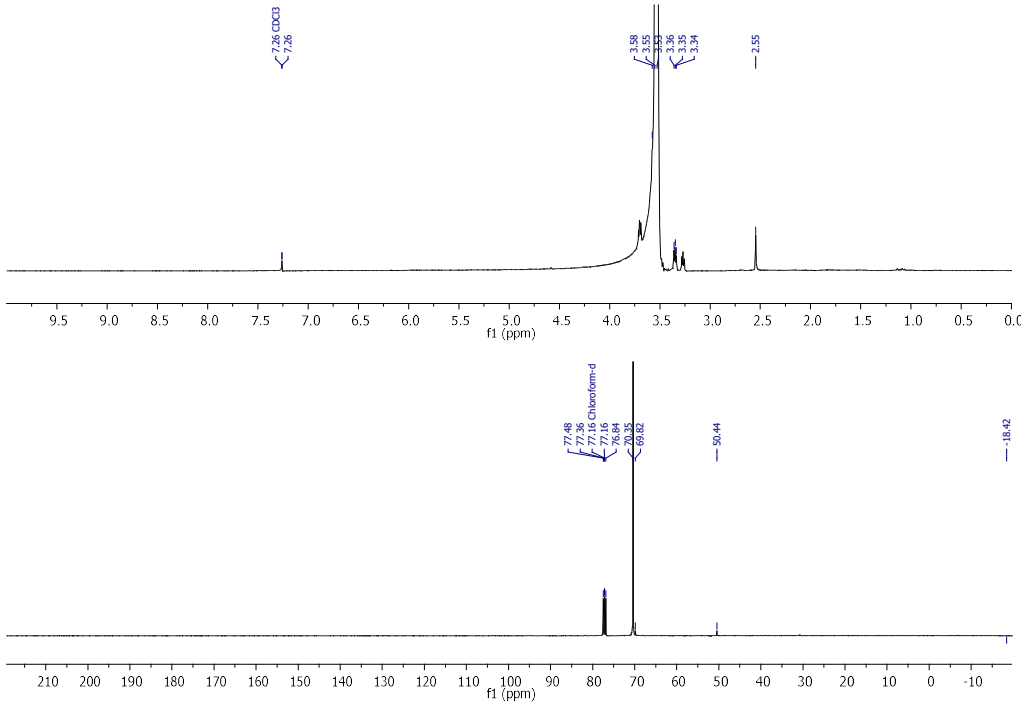

Figure S34. ^{1}H and ^{13}C NMR spectra of compound **32** in $CDCl_3$.

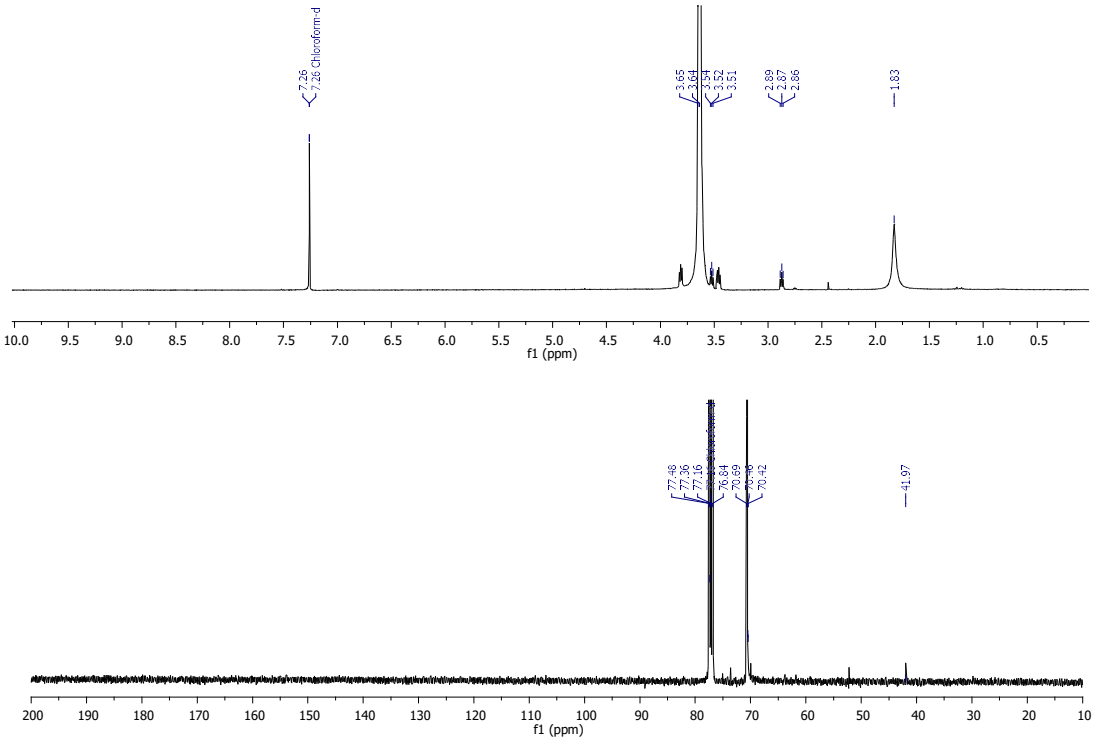

Figure S35. ^{1}H and ^{13}C NMR spectra of compound **33** in $CDCl_3$.

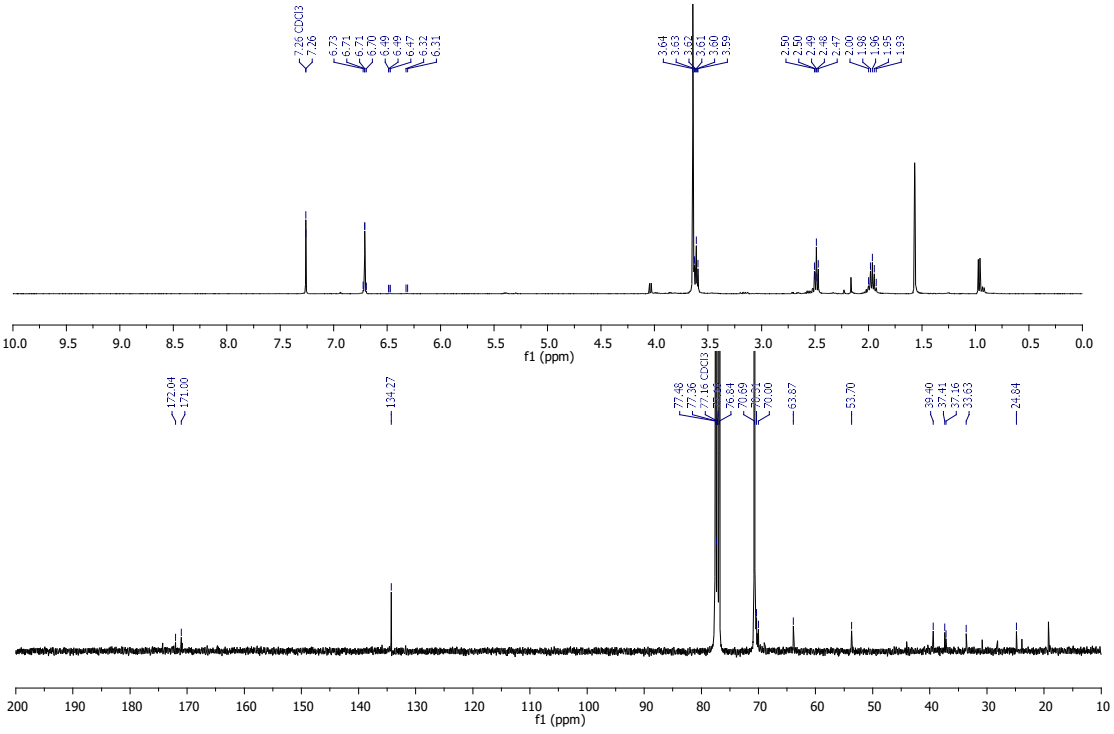

Figure S36. ^{1}H and ^{13}C NMR spectra of compound **34** in $CDCl_3$.

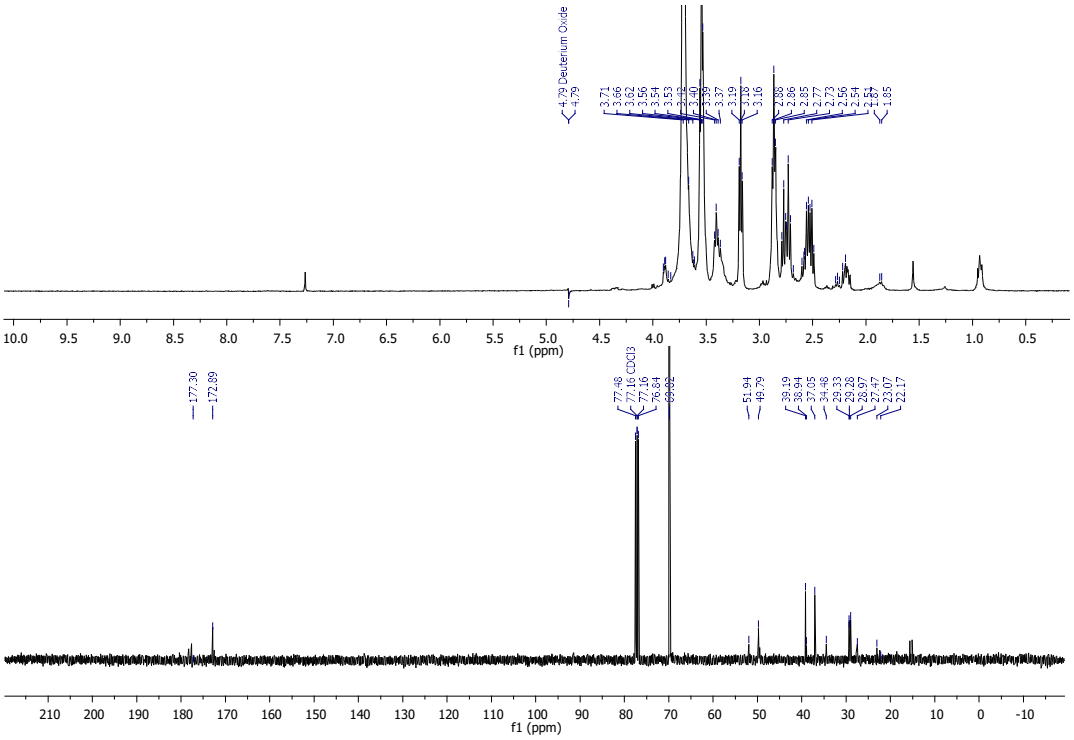

Figure S37. ^{1}H and ^{13}C NMR spectra of compound **35** in D_2O.

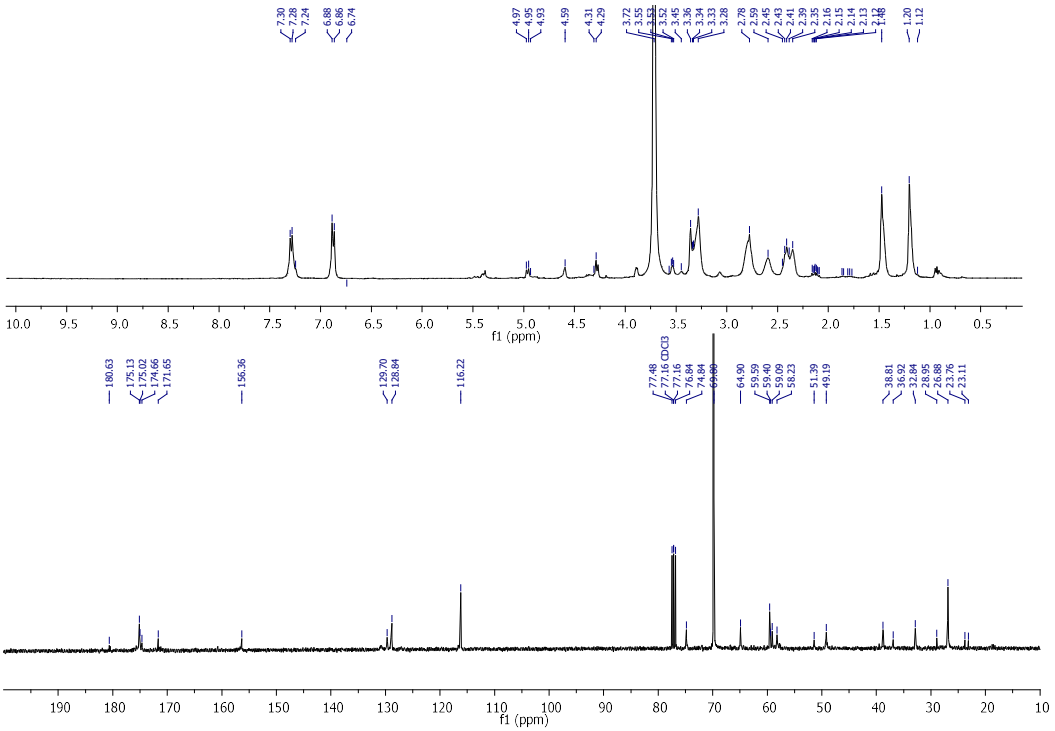

Figure S38. ^{1}H and ^{13}C NMR spectra of compound **36** in D_2O.

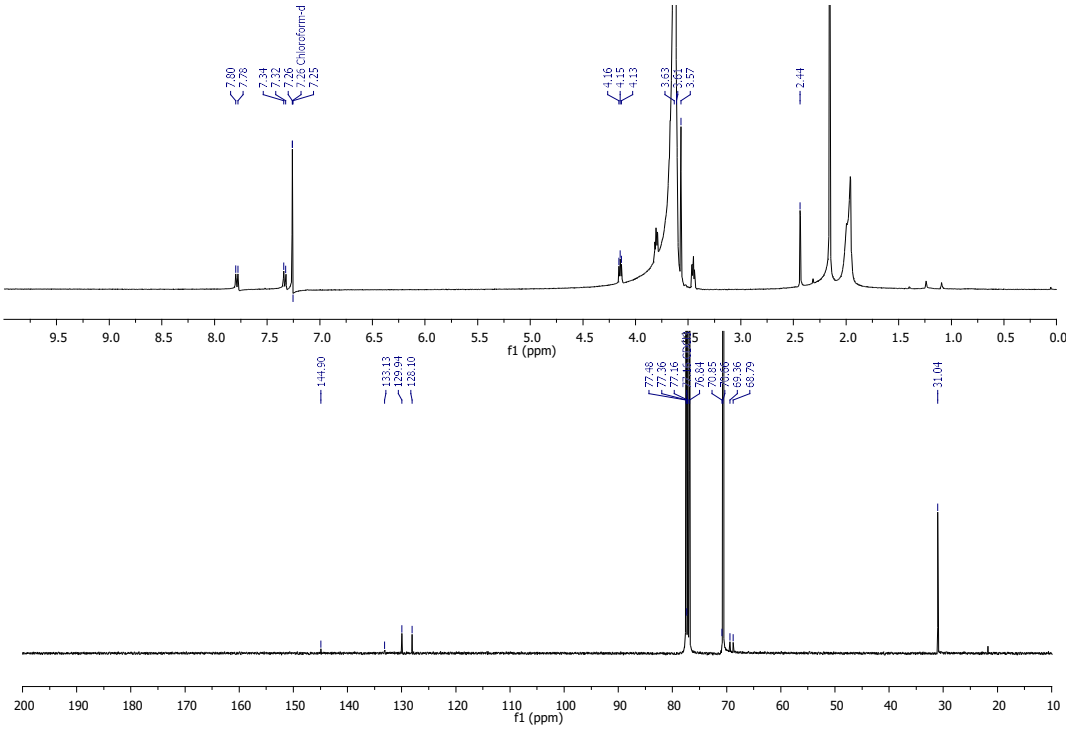

Figure S39. ^{1}H and ^{13}C NMR spectra of compound **37** in $CDCl_3$.

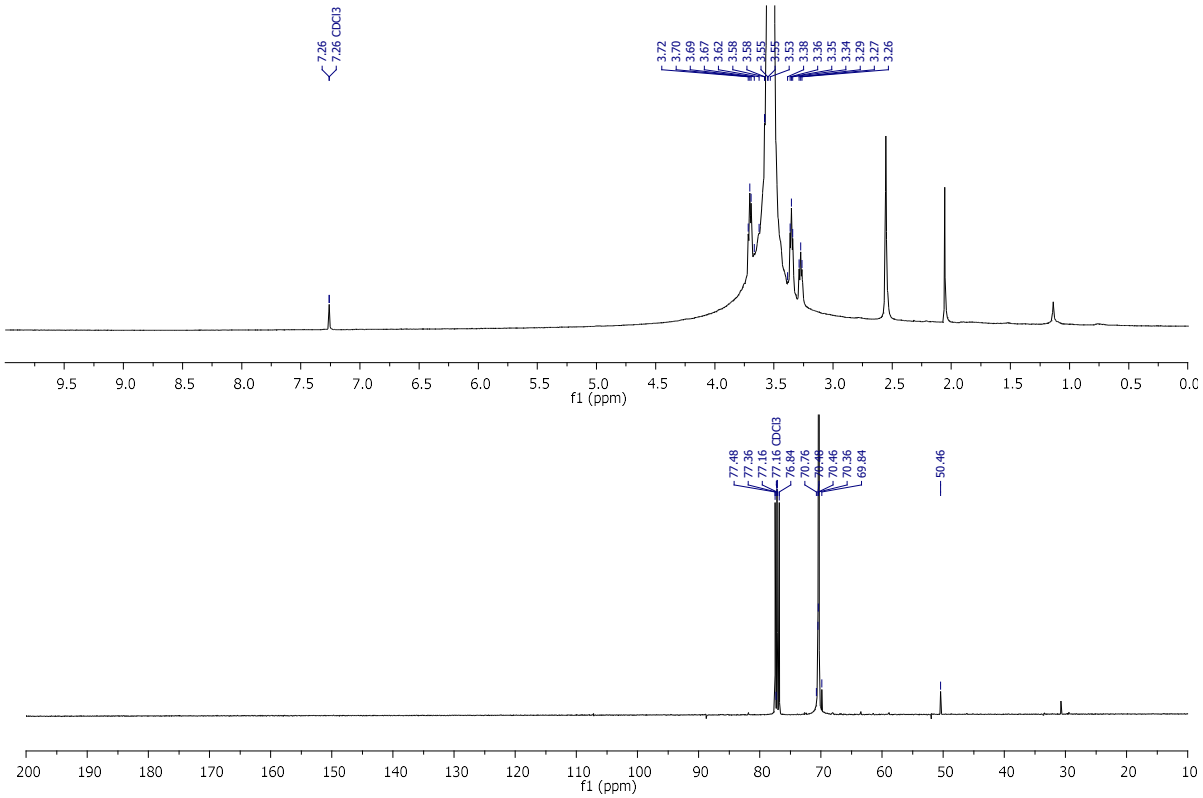

Figure S40. ^{1}H and ^{13}C NMR spectra of compound **38** in $CDCl_3$.

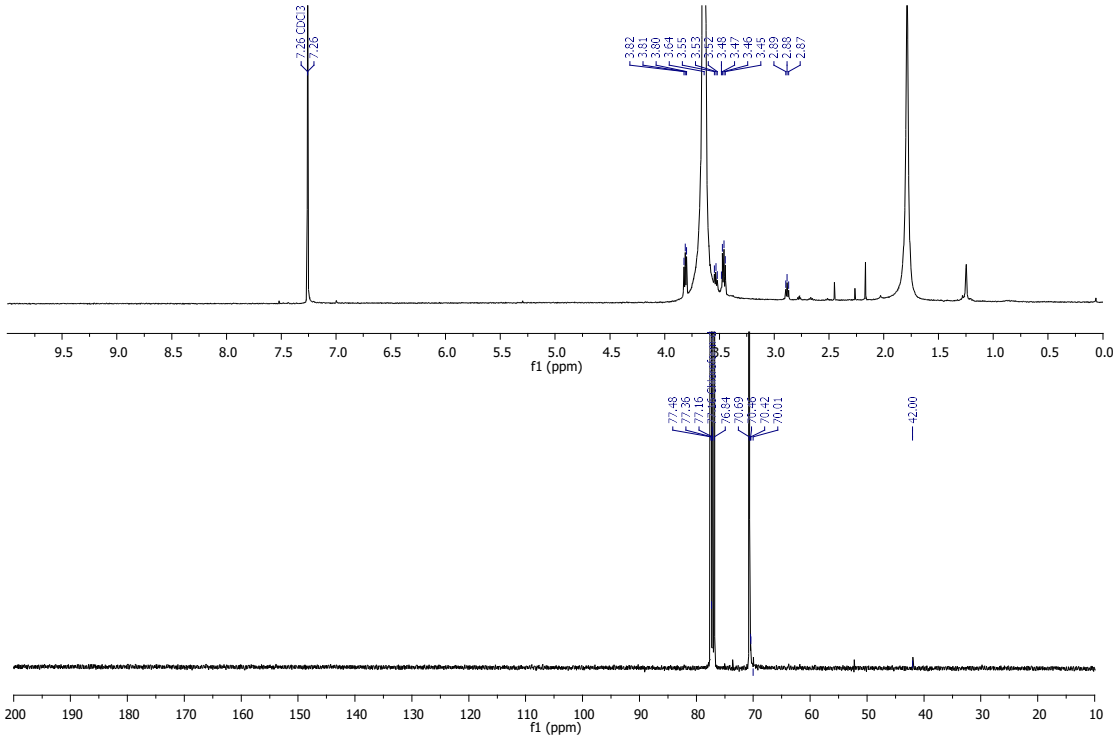

Figure S41. ^{1}H and ^{13}C NMR spectra of compound **39** in $CDCl_3$.

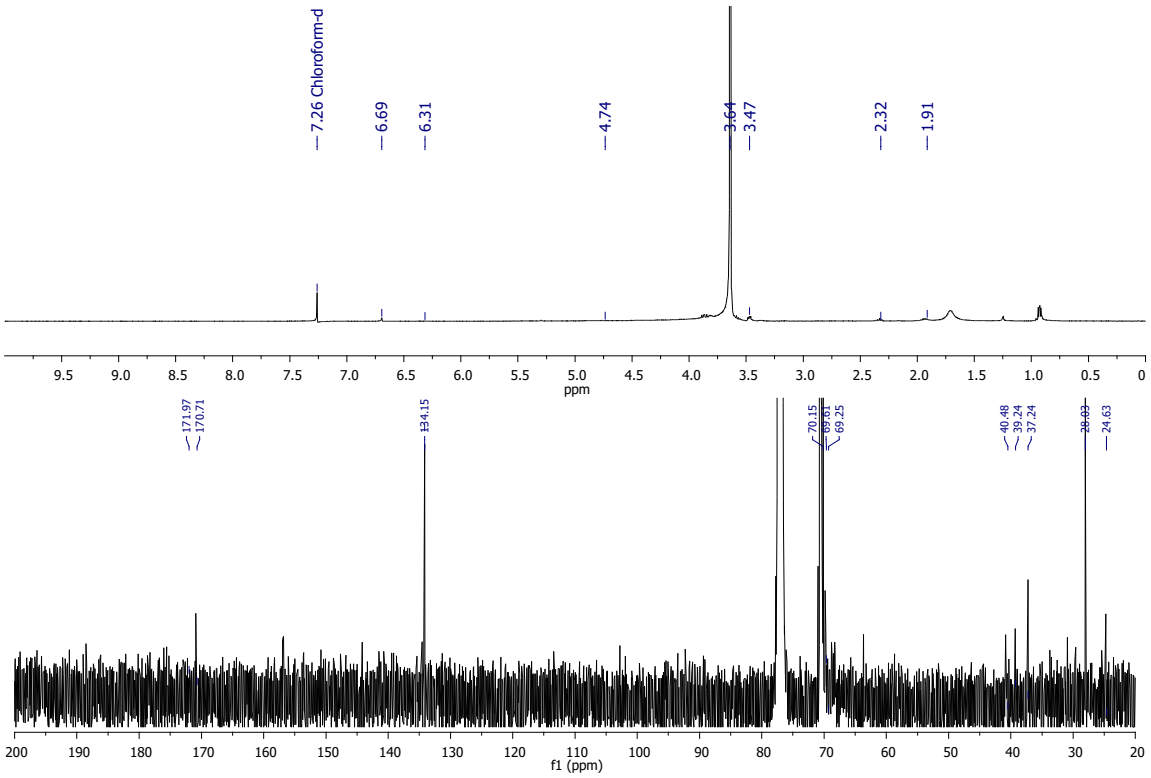

Figure S42. ^{1}H and ^{13}C NMR spectra of compound **40** in CDCl3.

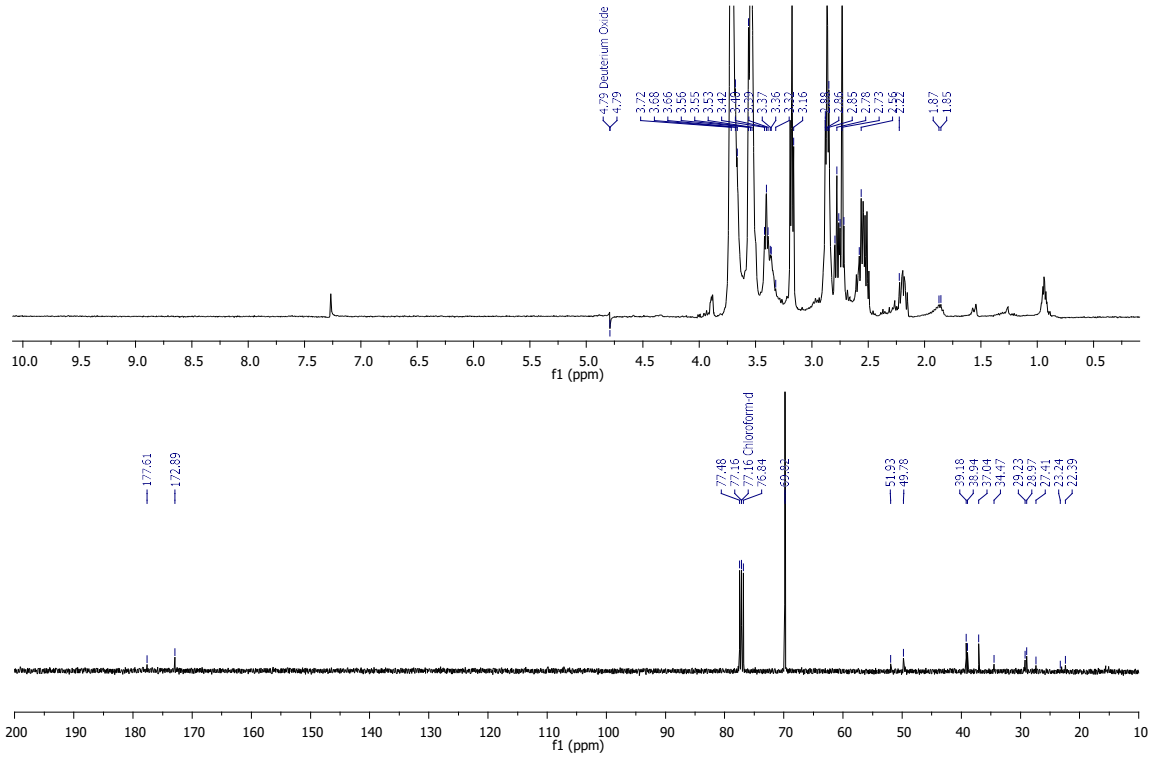

Figure S43. ^{1}H and ^{13}C NMR spectra of compound **41** in D_2O.

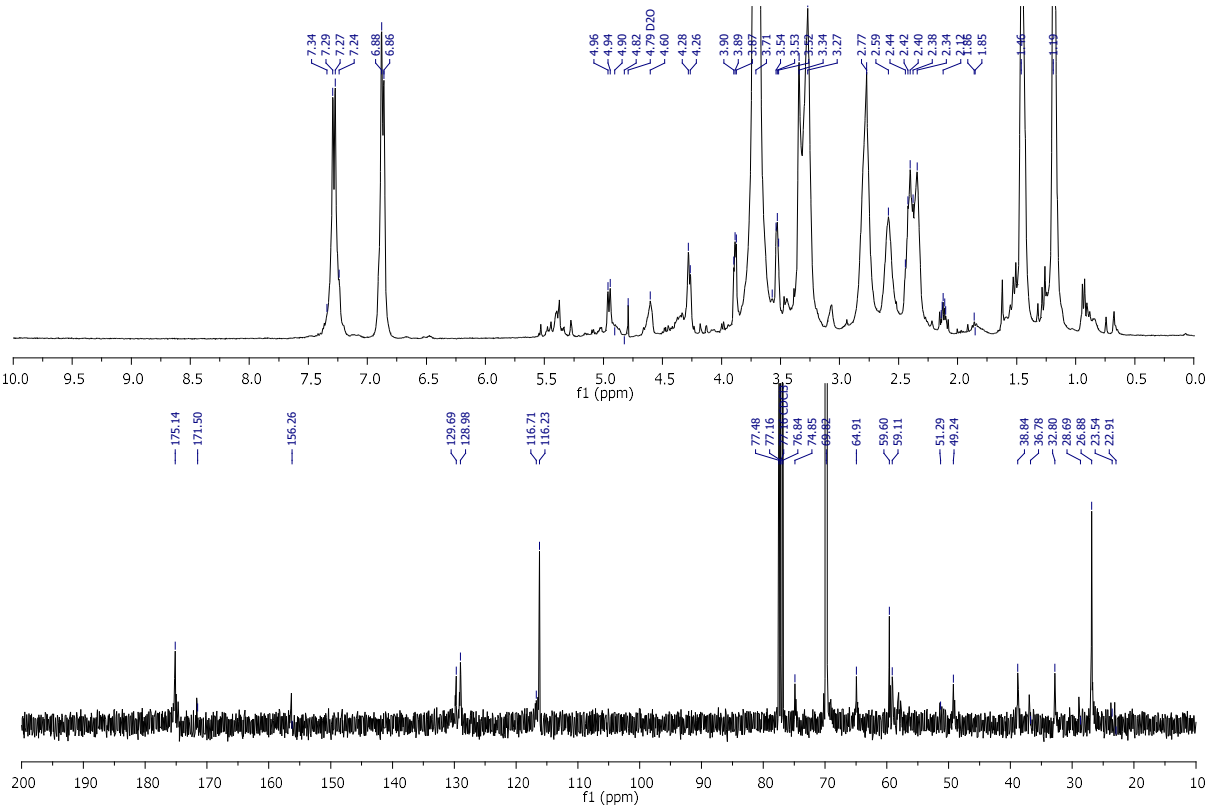

Figure S44. ^{1}H and ^{13}C NMR spectra of compound **42** in D_2O.

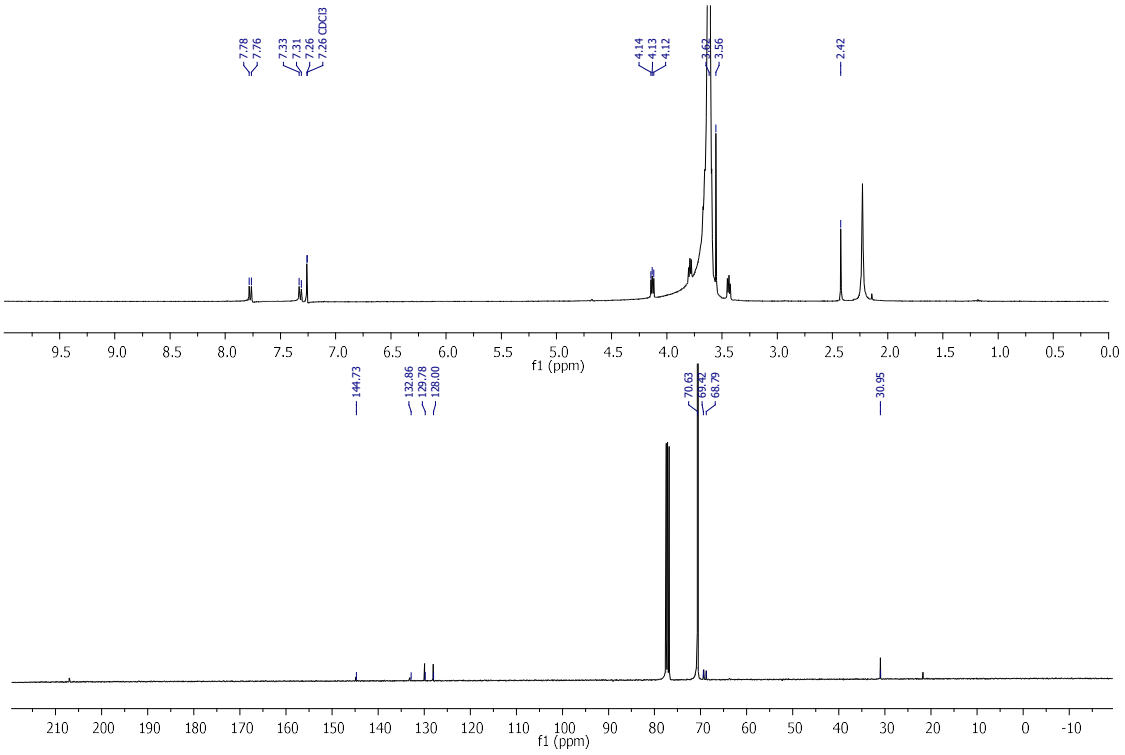

Figure S45. ^{1}H and ^{13}C NMR spectra of compound **43** in CDCl3

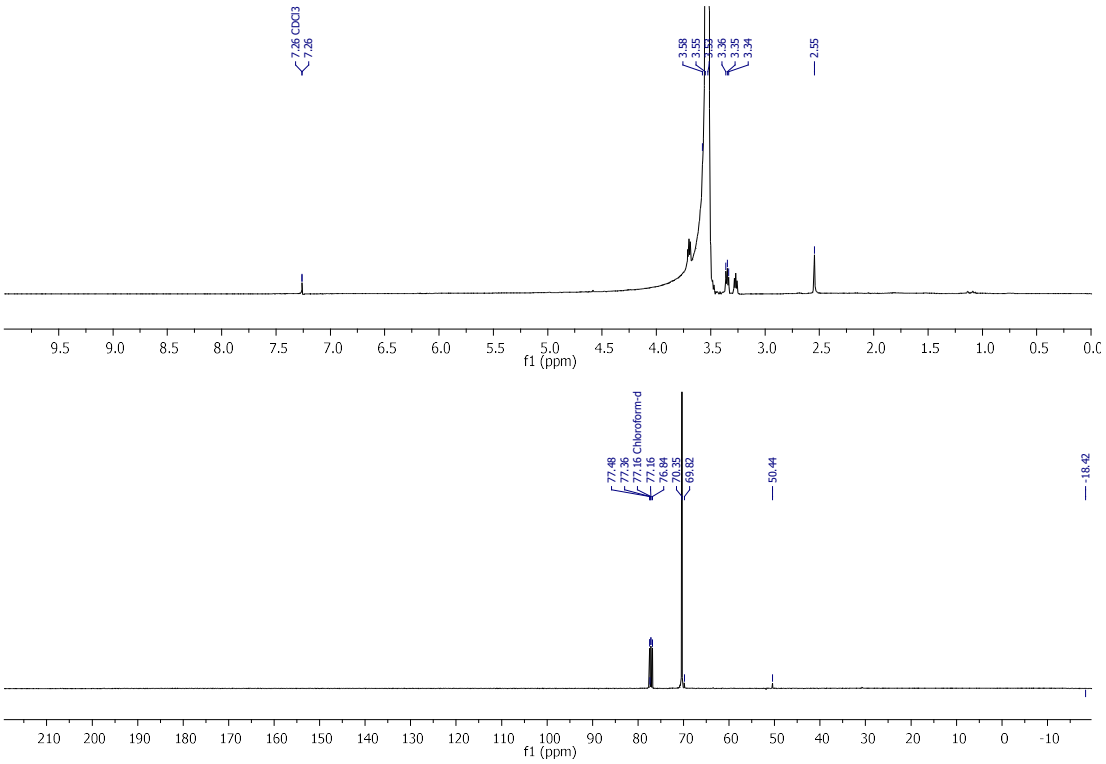

Figure S46. ^{1}H and ^{13}C NMR spectra of compound **44** in CDCl3.

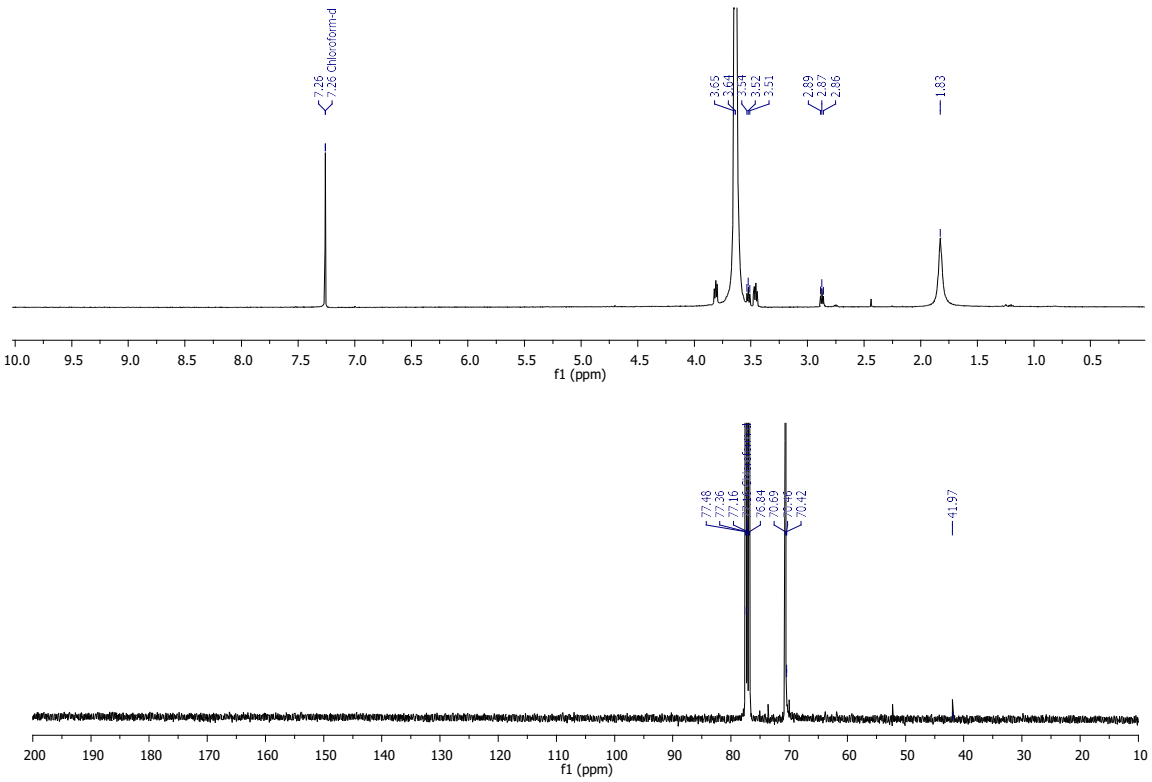

Figure S47. ^{1}H and ^{13}C NMR spectra of compound **45** in CDCl3

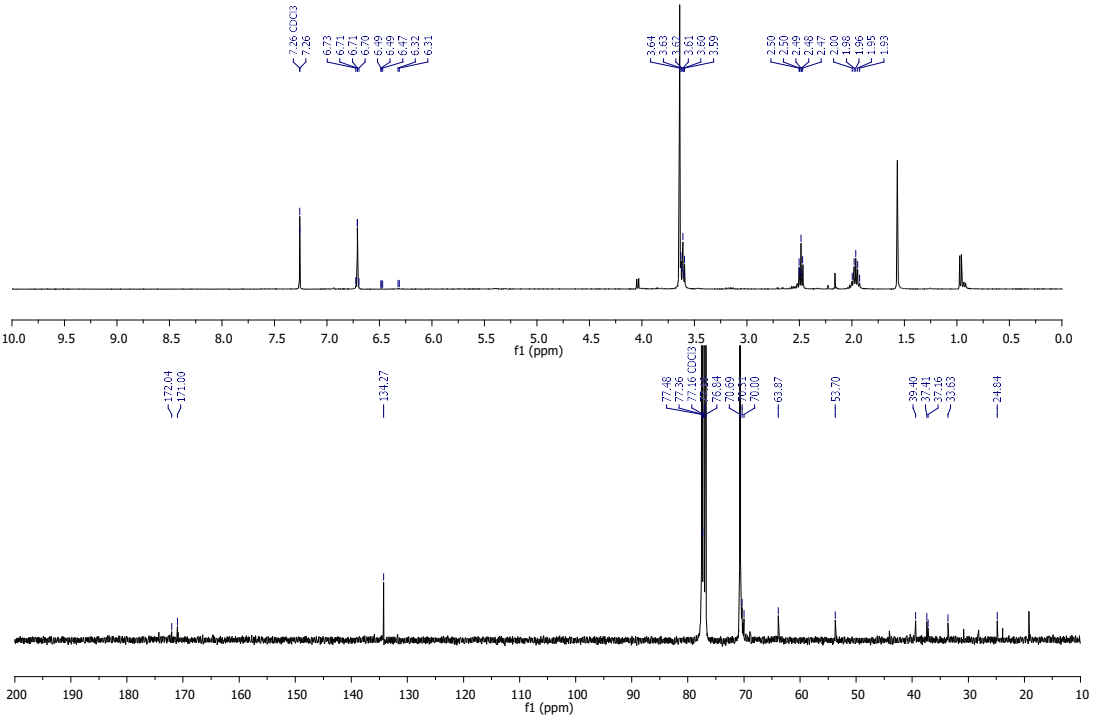

Figure S48. ^{1}H and ^{13}C NMR spectra of compound **46** in CDCl3

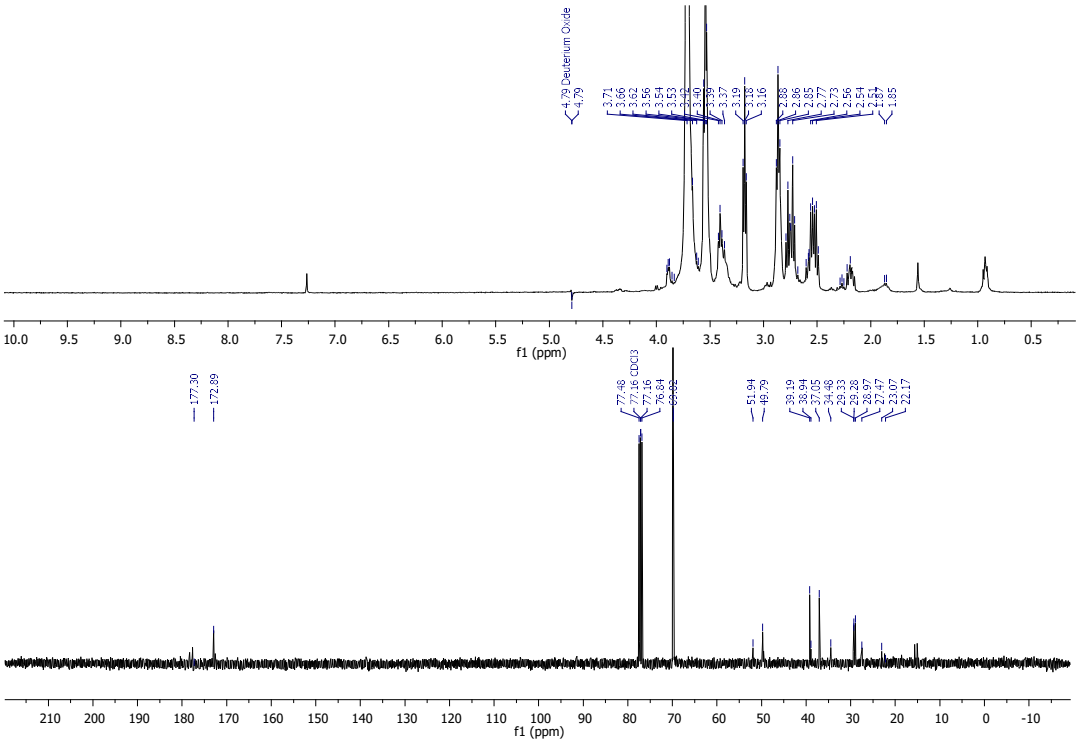

Figure S49. ^{1}H and ^{13}C NMR spectra of compound **47** in D_2O

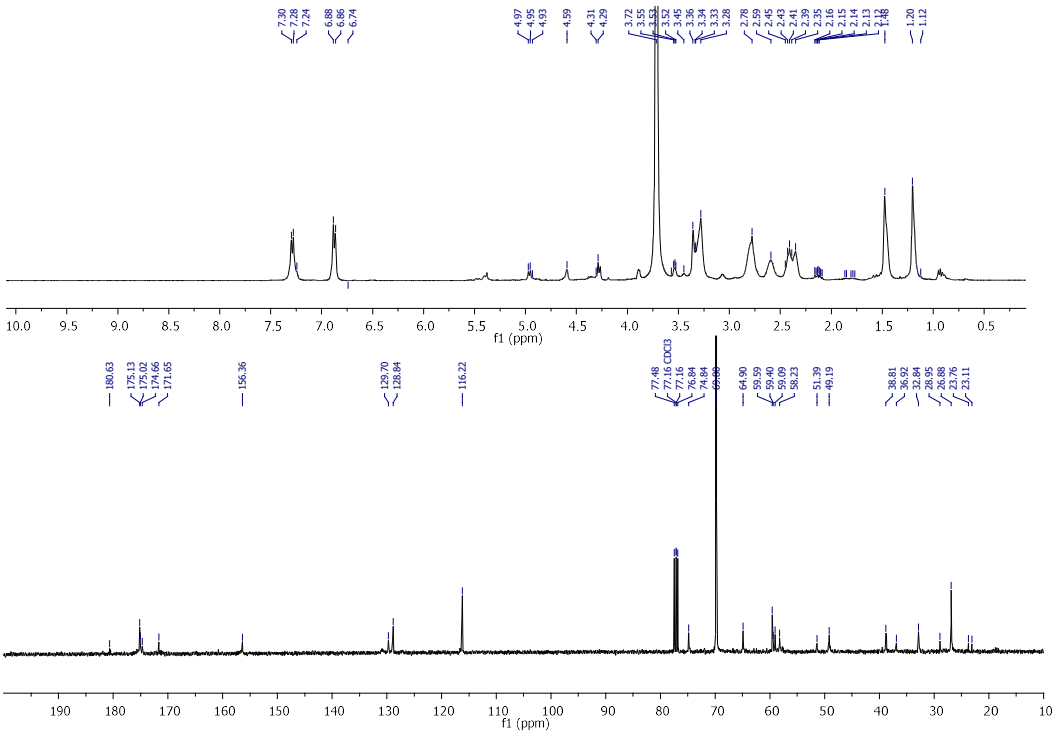

Figure S50. ^{1}H and ^{13}C NMR spectra of compound **48** in D_2O

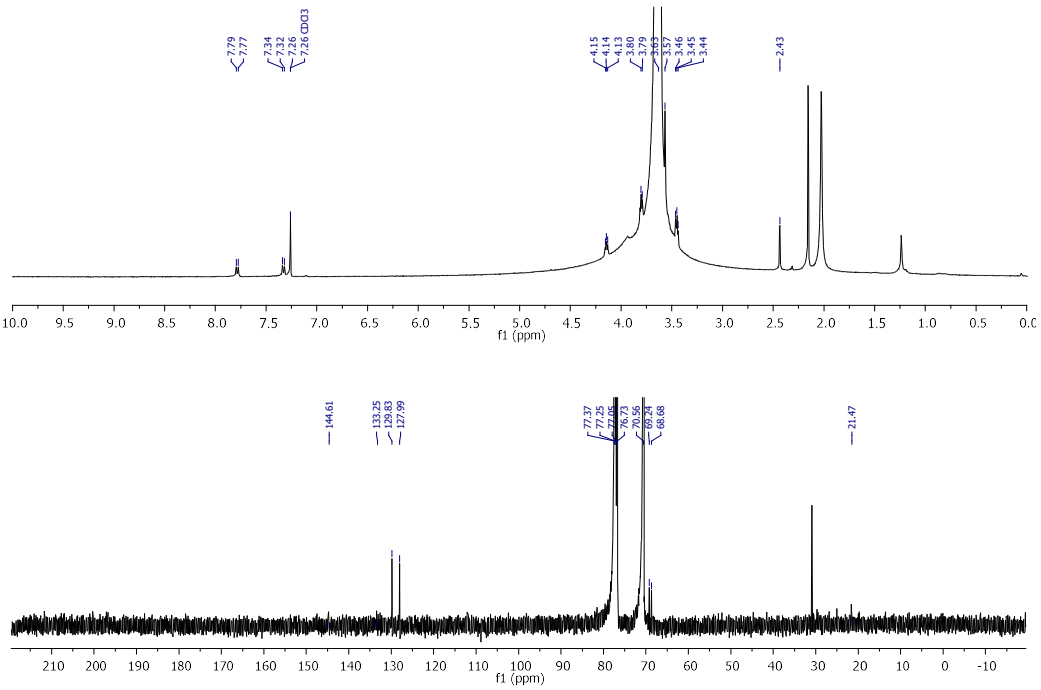

Figure S51. ^{1}H and ^{13}C NMR spectra of compound **49** in $CDCl_3$.

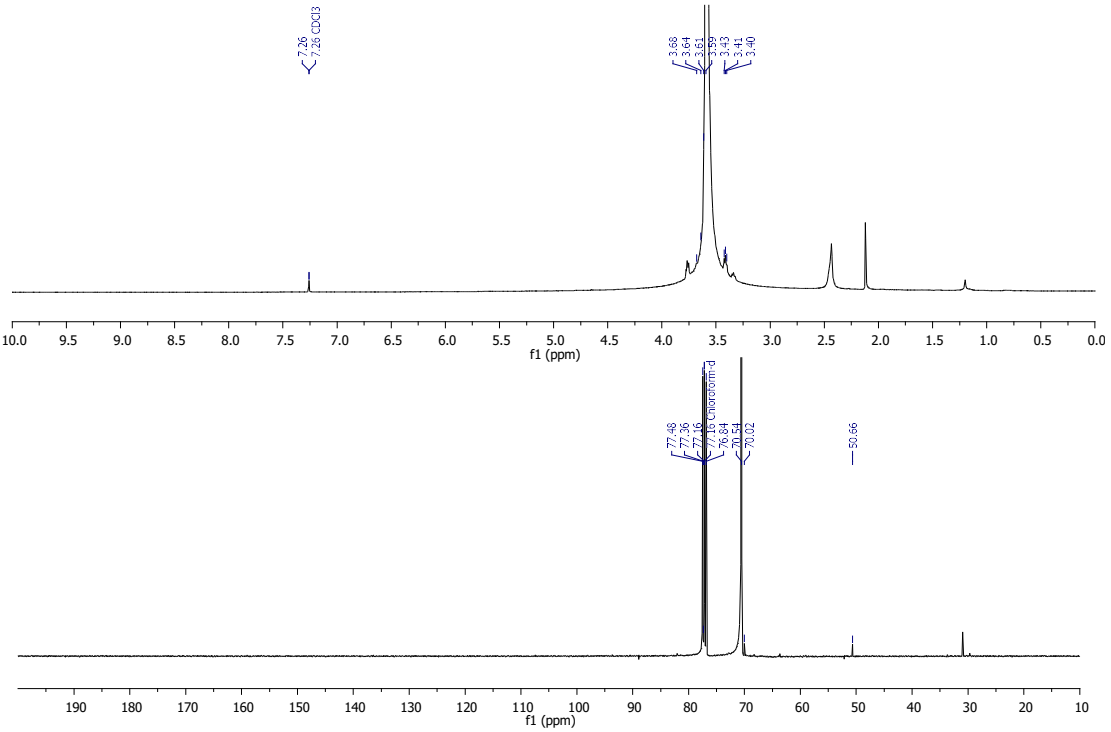

Figure S52. ^{1}H and ^{13}C NMR spectra of compound **50** in $CDCl_3$.

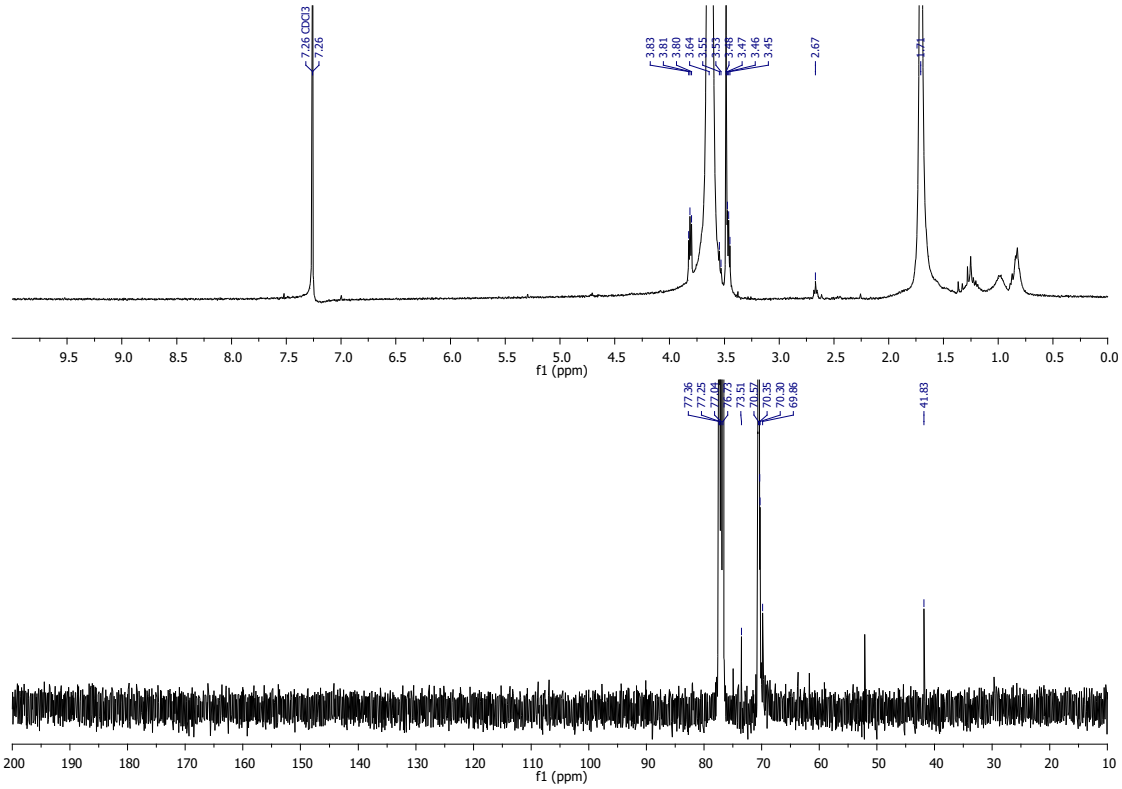

Figure S53. 1H and 13C NMR spectra of compound **51** in CDCl3.

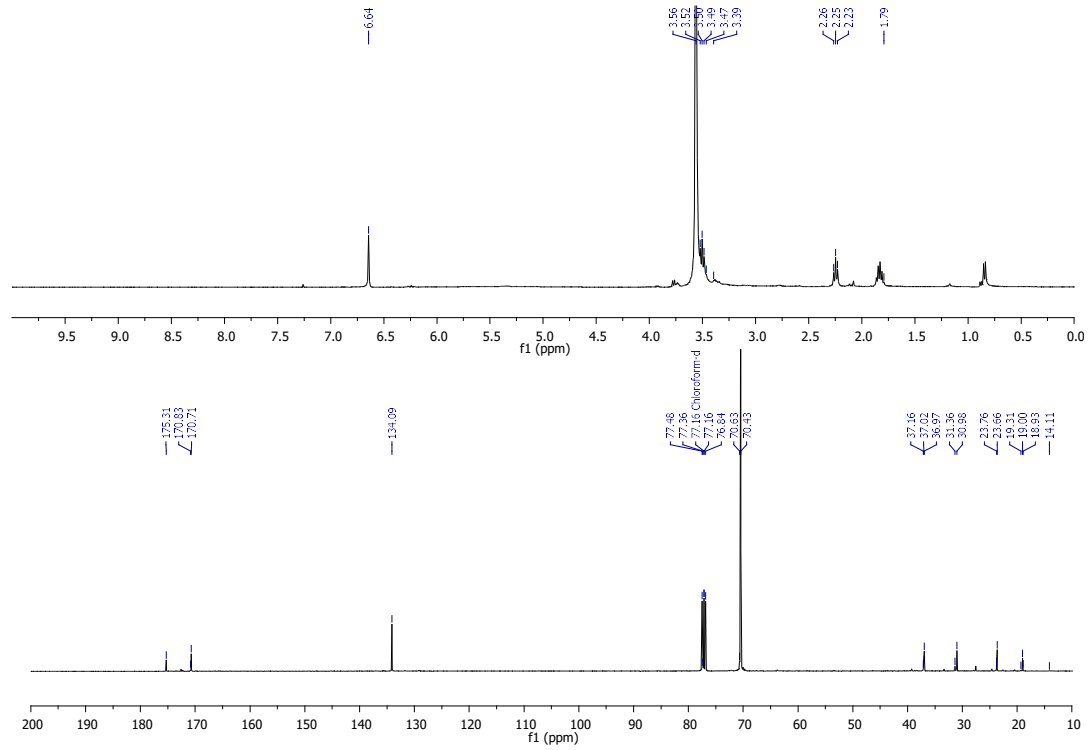

Figure S54. ^{1}H and ^{13}C NMR spectra of compound **52** in $CDCl_3$.

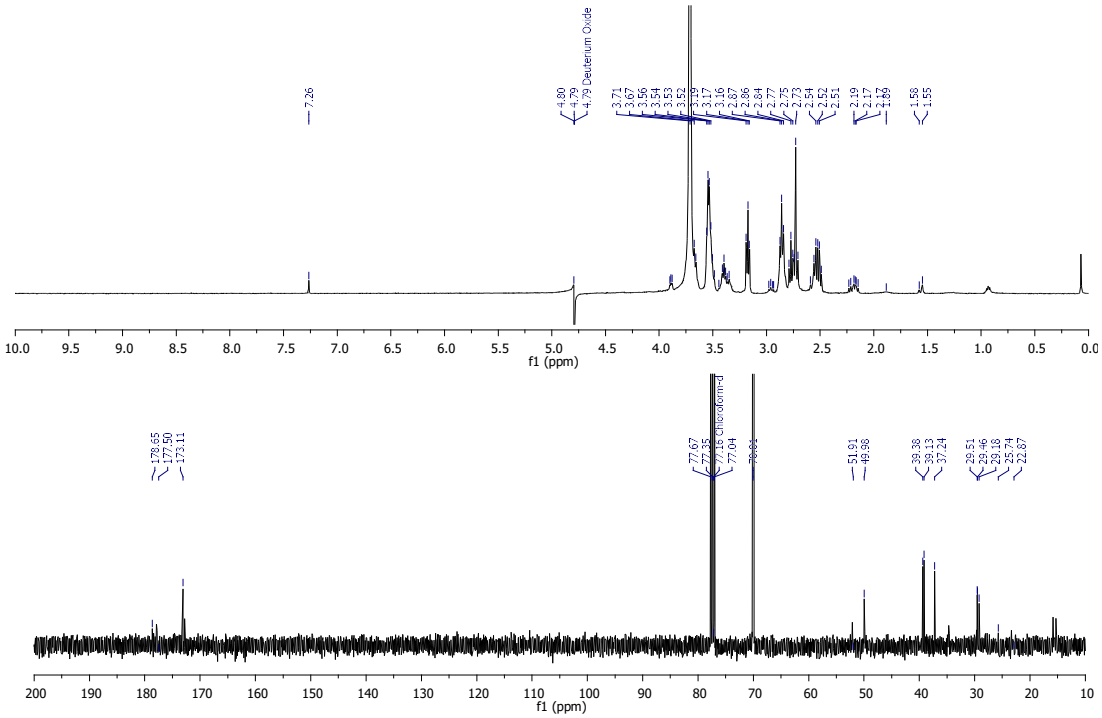

Figure S55. ^{1}H and ^{13}C NMR spectra of compound **53** in D_2O.

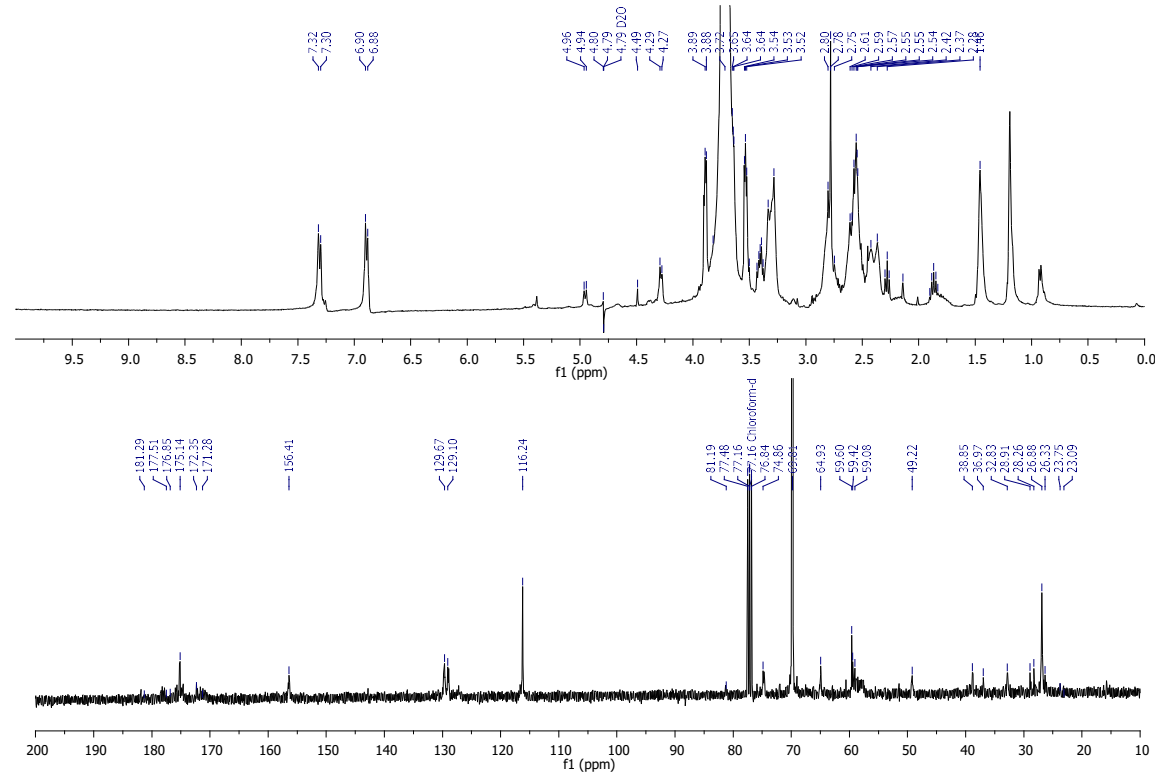

Figure S56. ^{1}H and ^{13}C NMR spectra of compound **54** in D_2O.

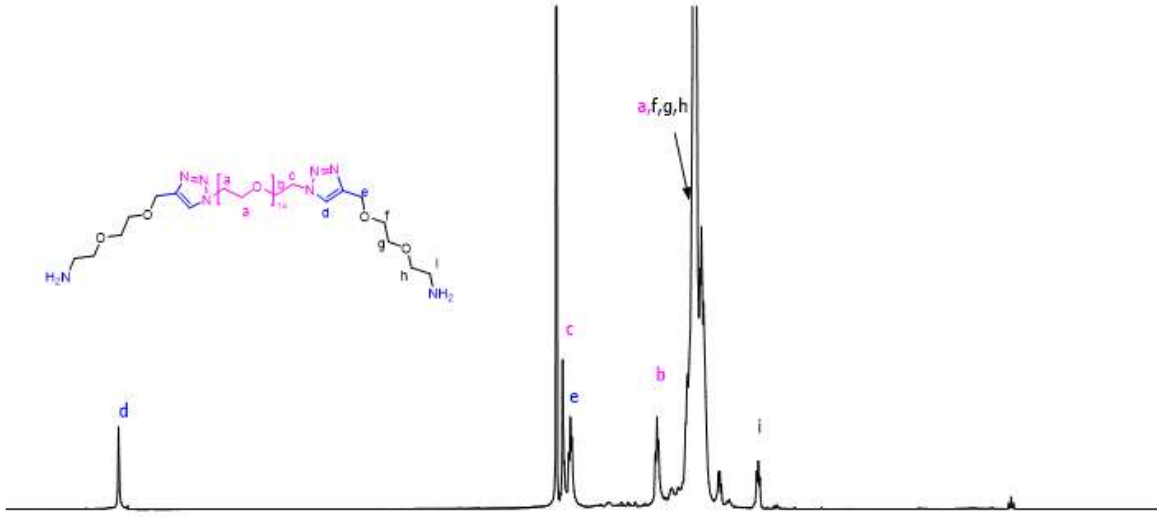

Figure S57. ^{1}H and ^{13}C NMR spectra of compound **55** in D_2O.

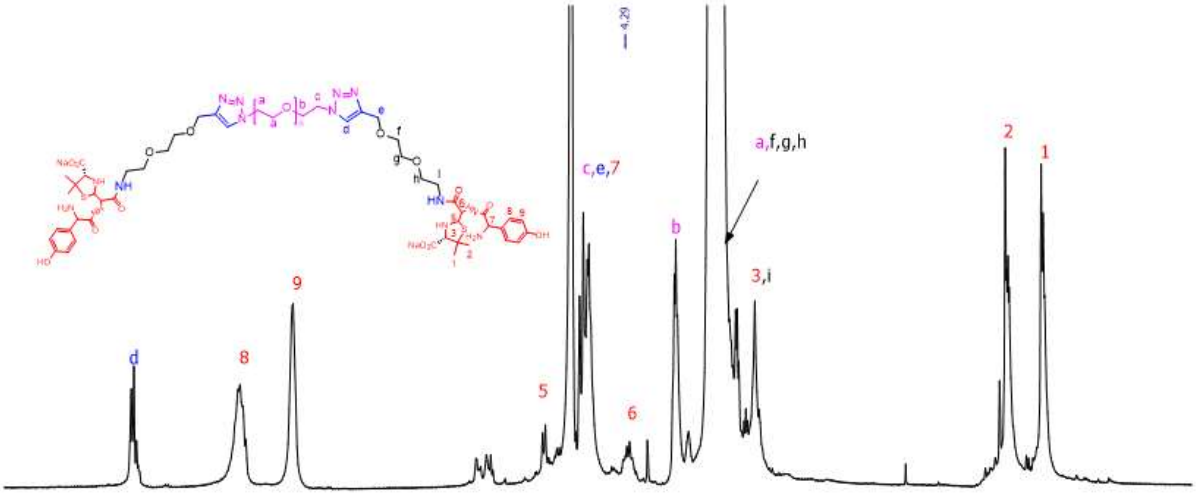

Figure S58. ^{1}H and ^{13}C NMR spectra of compound 56 in D_2O.

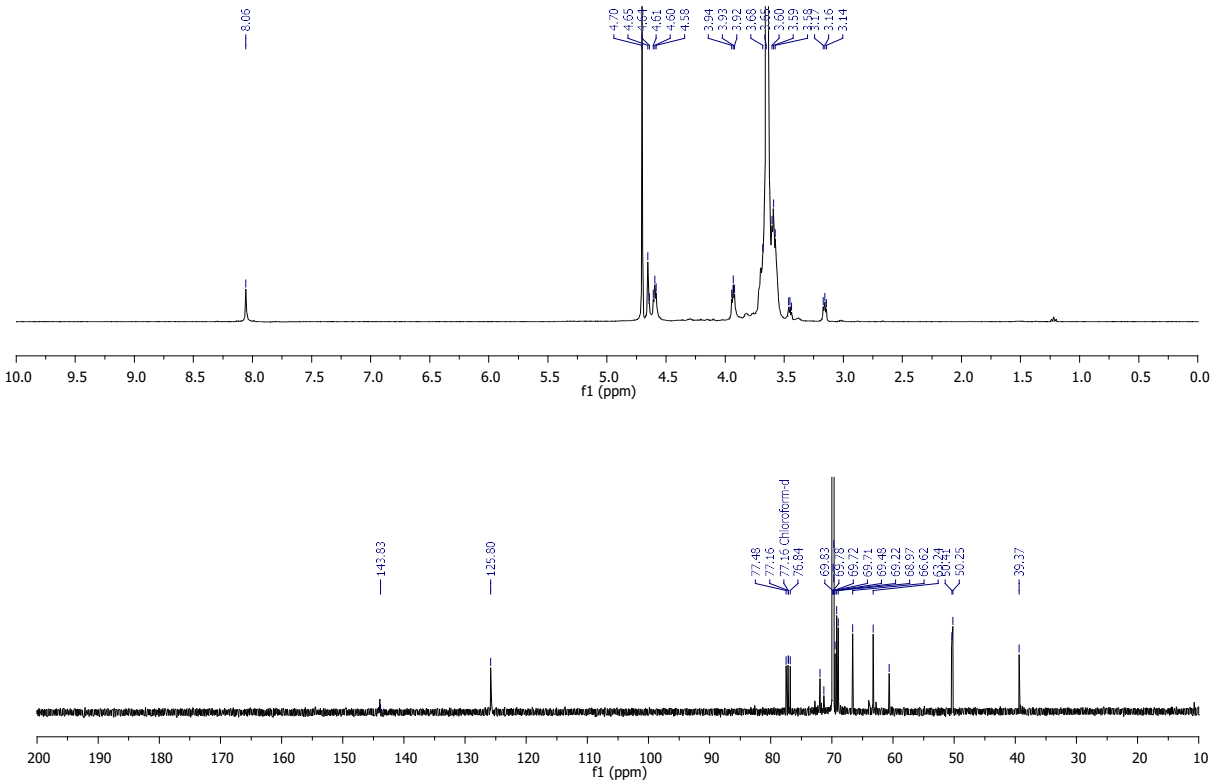

Figure S59. ^{1}H and ^{13}C NMR spectra of compound 57 in D_2O.

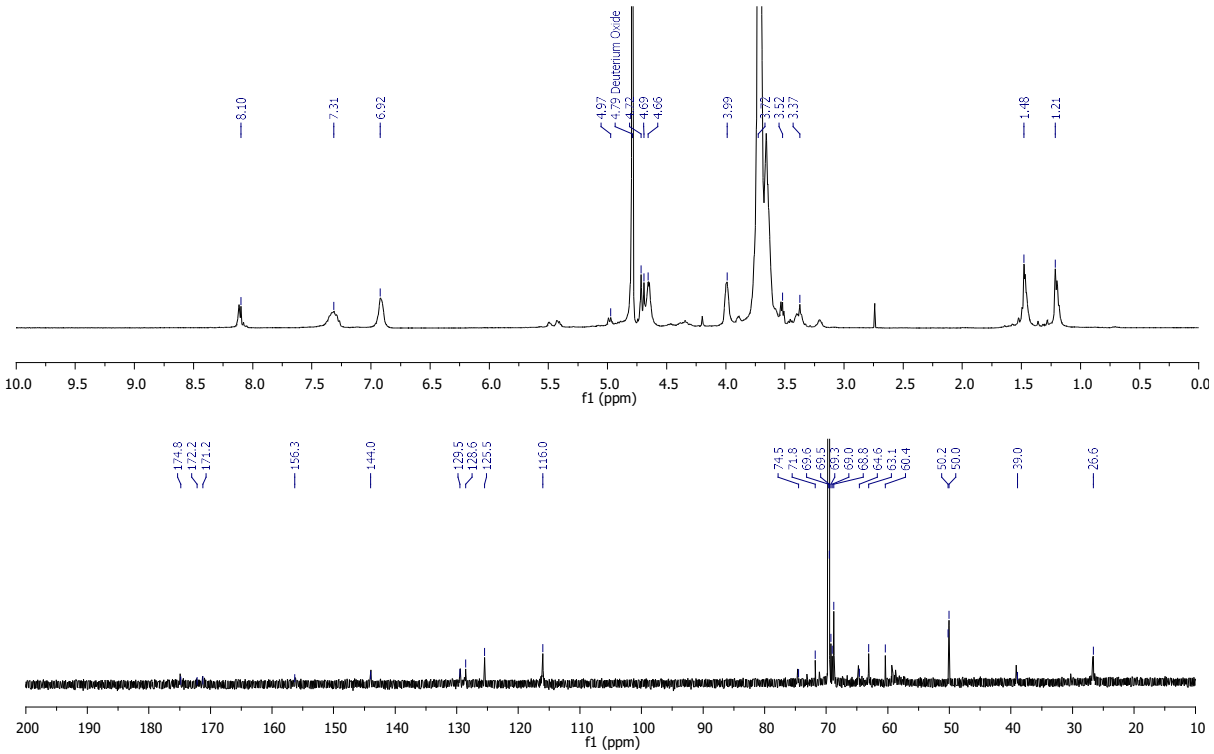

Figure S60. ^{1}H and ^{13}C NMR spectra of compound 58 in D_2O.

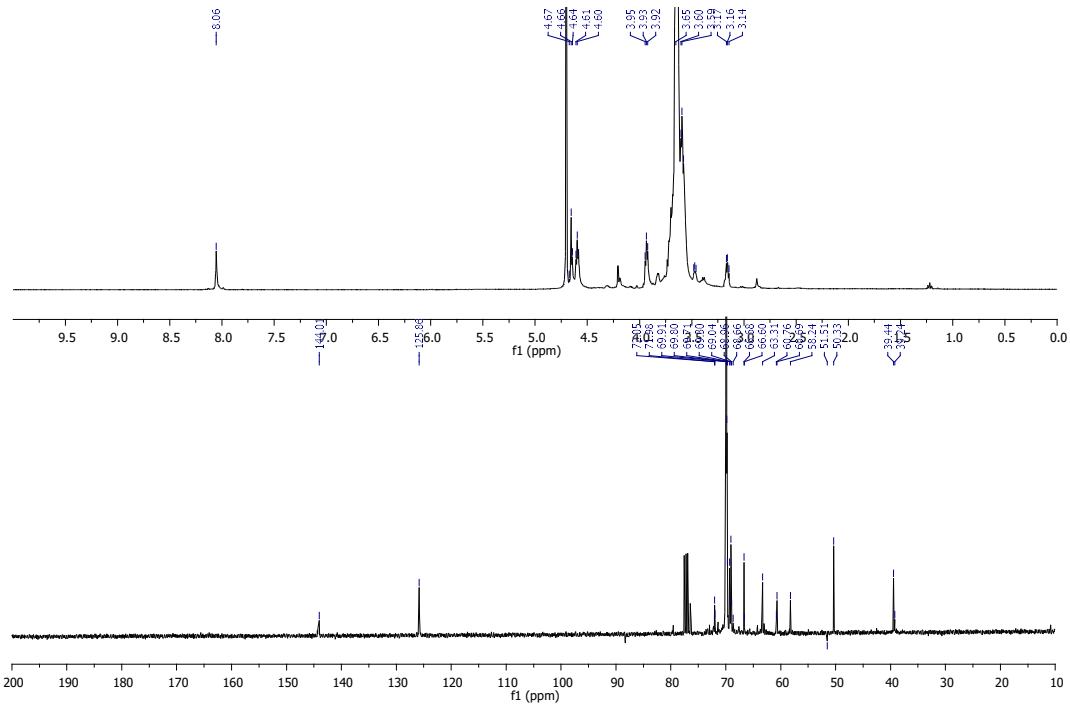

Figure S61. ^{1}H and ^{13}C NMR spectra of compound 59 in D_2O.

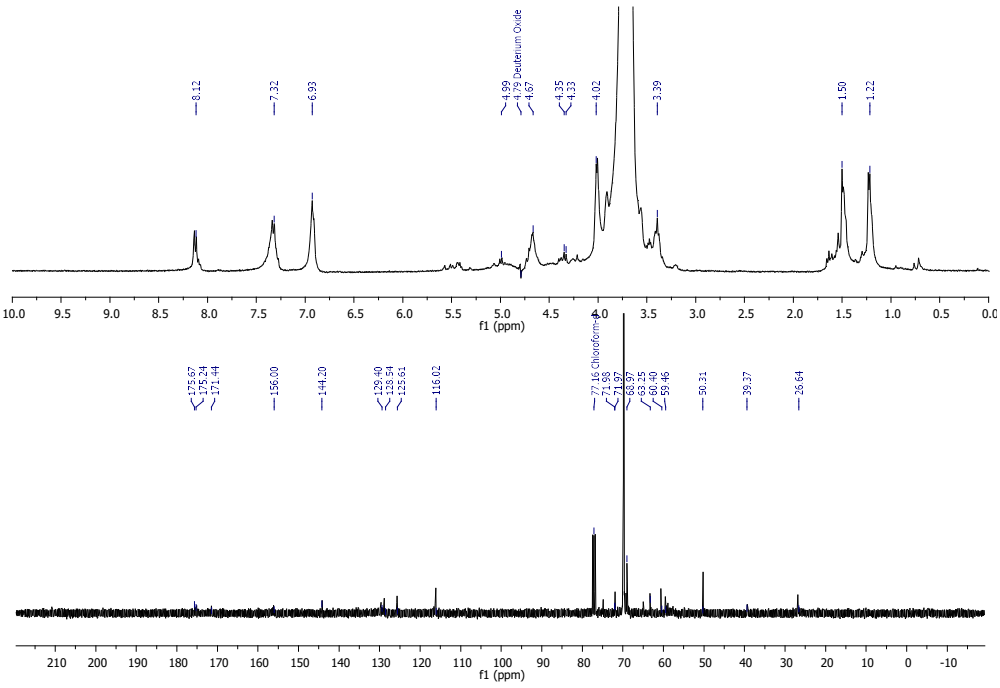

Figure S62. ^{1}H and ^{13}C NMR spectra of compound 60 in D_2O.

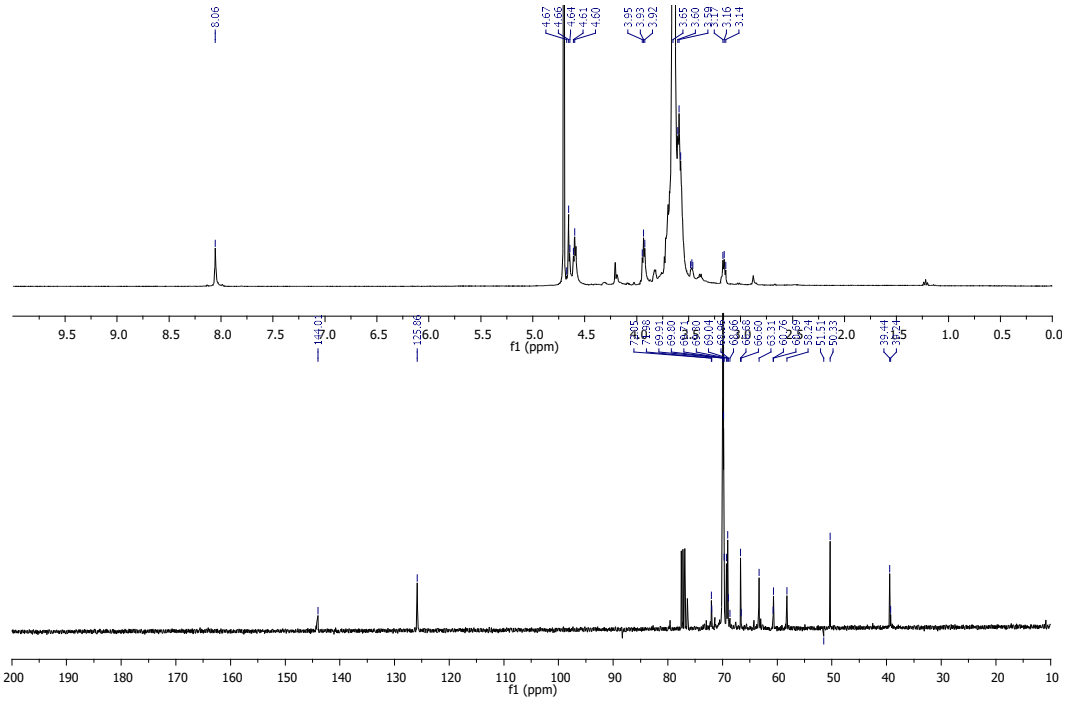

Figure S63. ^{1}H and ^{13}C NMR spectra of compound 61 in D_2O.

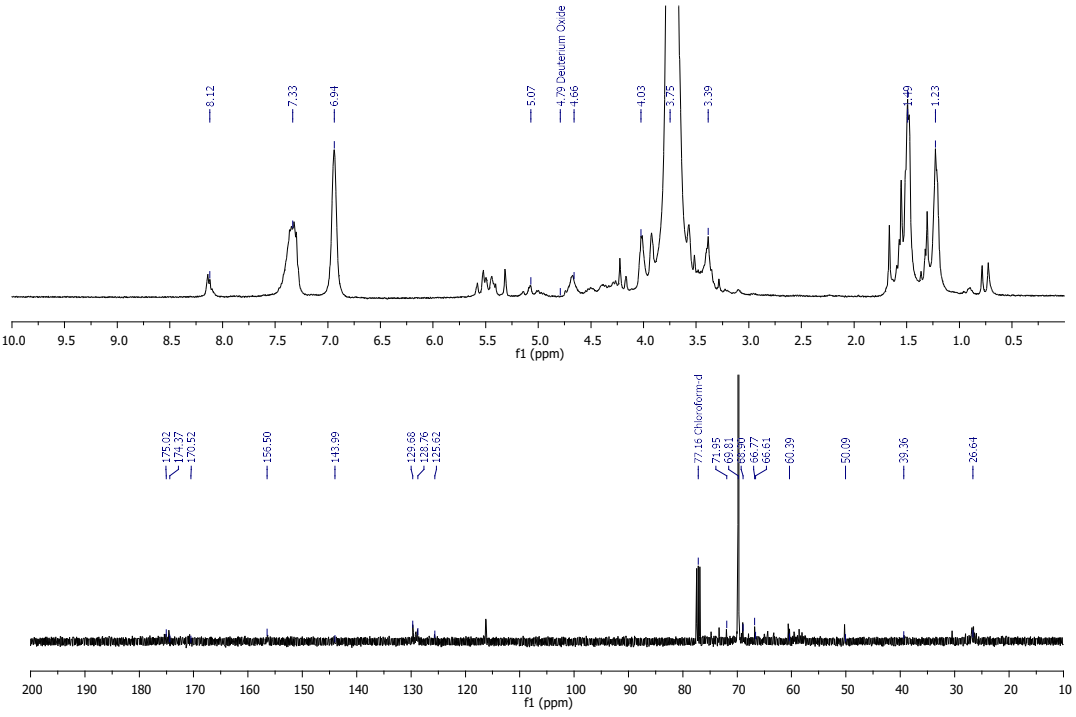

Figure S64. ^{1}H and ^{13}C NMR spectra of compound 62 in D_2O.

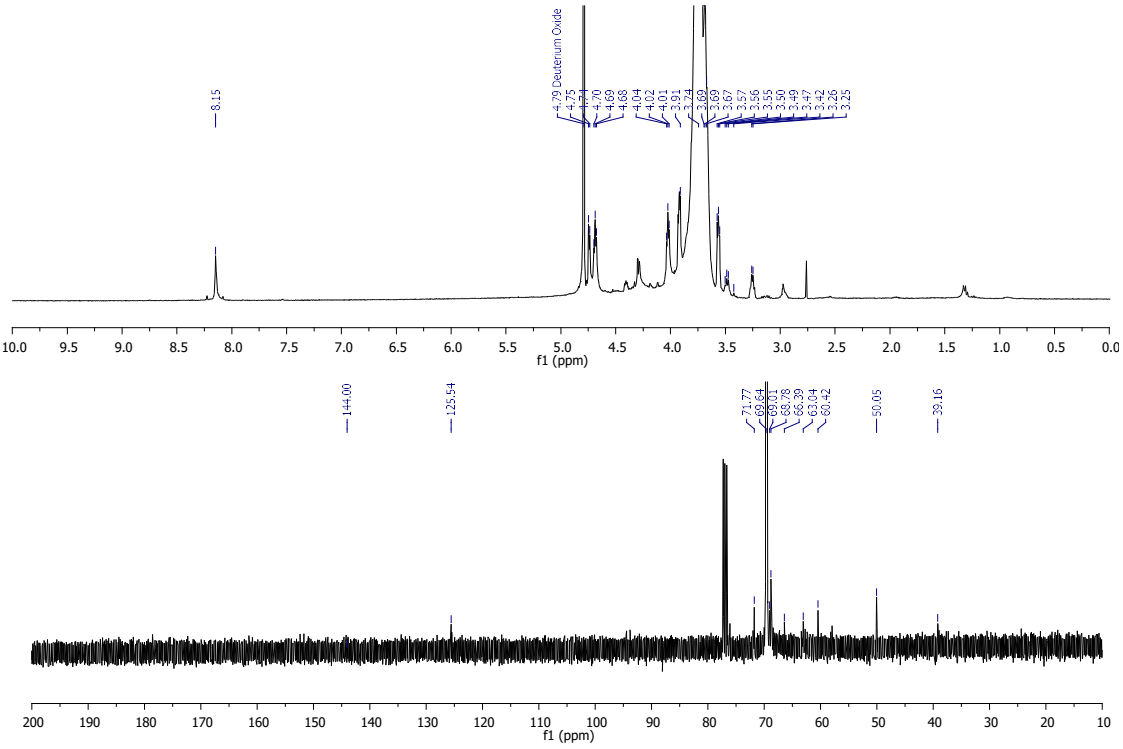

Figure S65. ^{1}H and ^{13}C NMR spectra of compound 63 in D_2O.

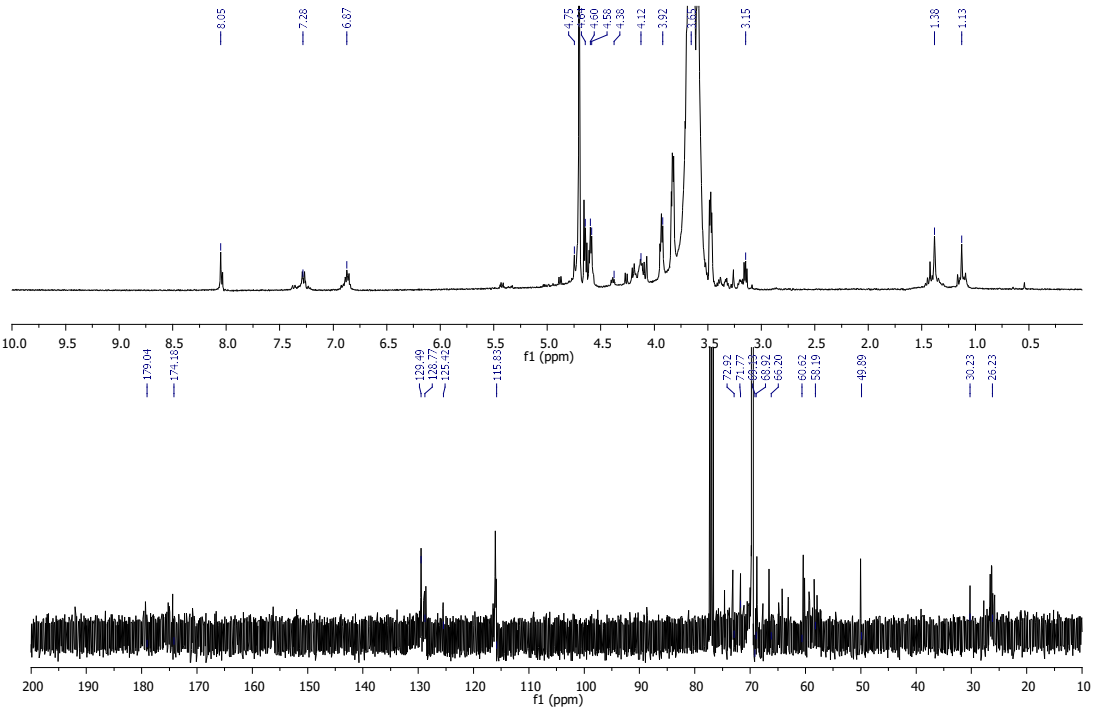

Figure S66. ^{1}H and ^{13}C NMR spectra of compound 64 in D_2O.

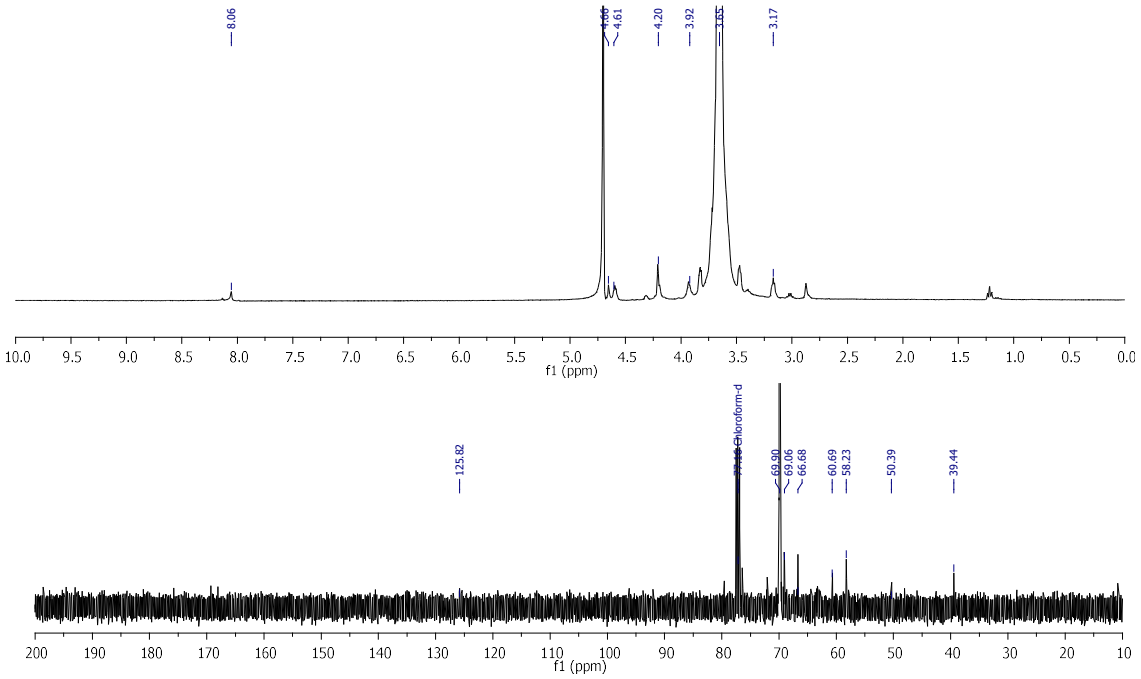

Figure S67. ^{1}H and ^{13}C NMR spectra of compound 65 in D_2O.

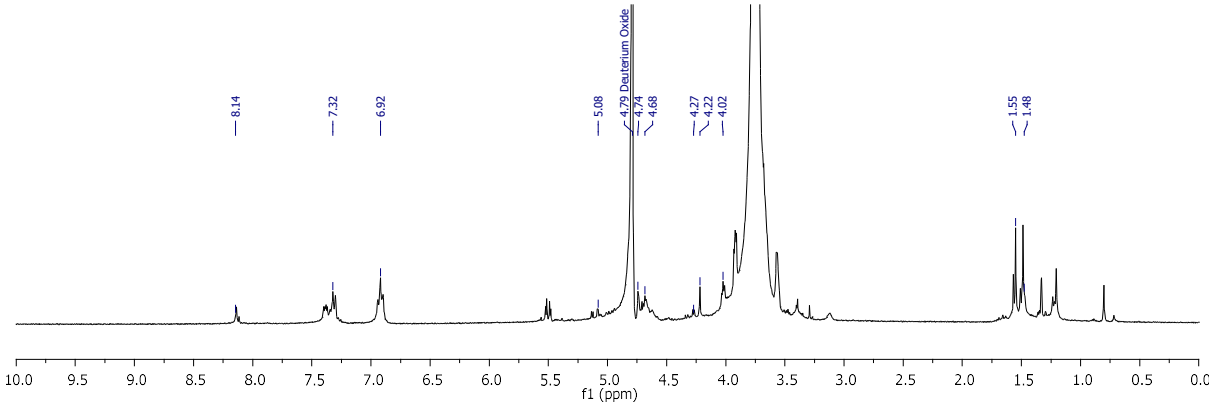

Figure S68. ^{1}H and ^{13}C NMR spectra of compound 66 in D_2O.

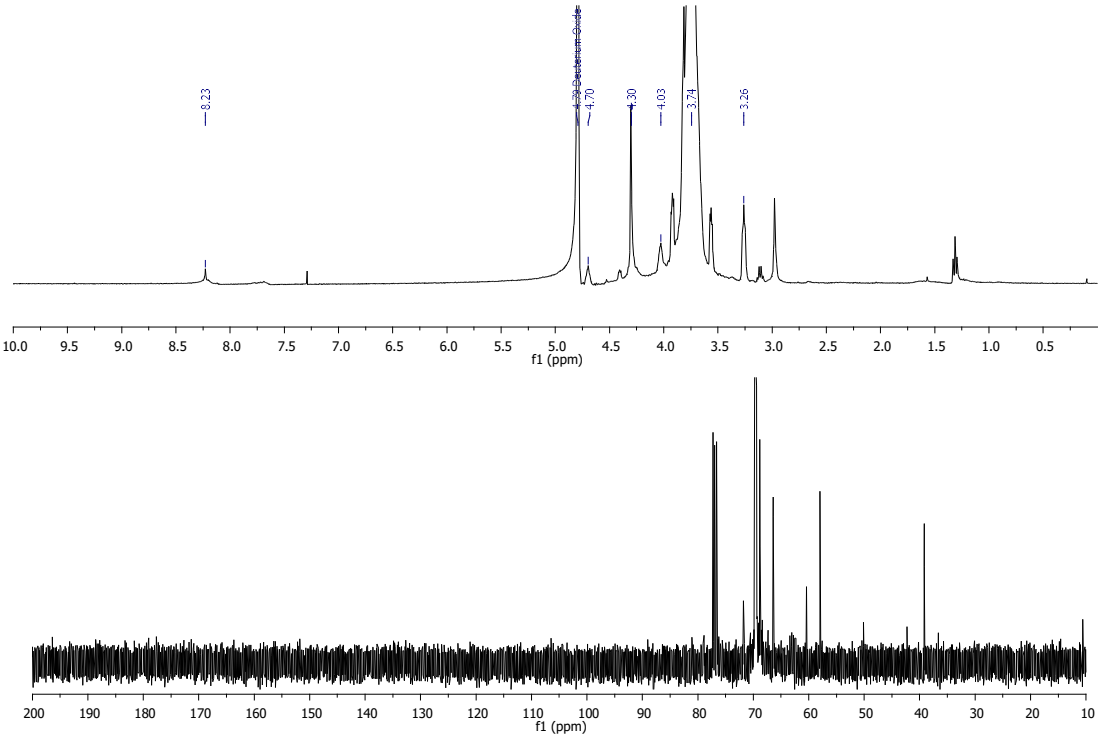

Figure S69. ^{1}H and ^{13}C NMR spectra of compound 67 in D_2O.

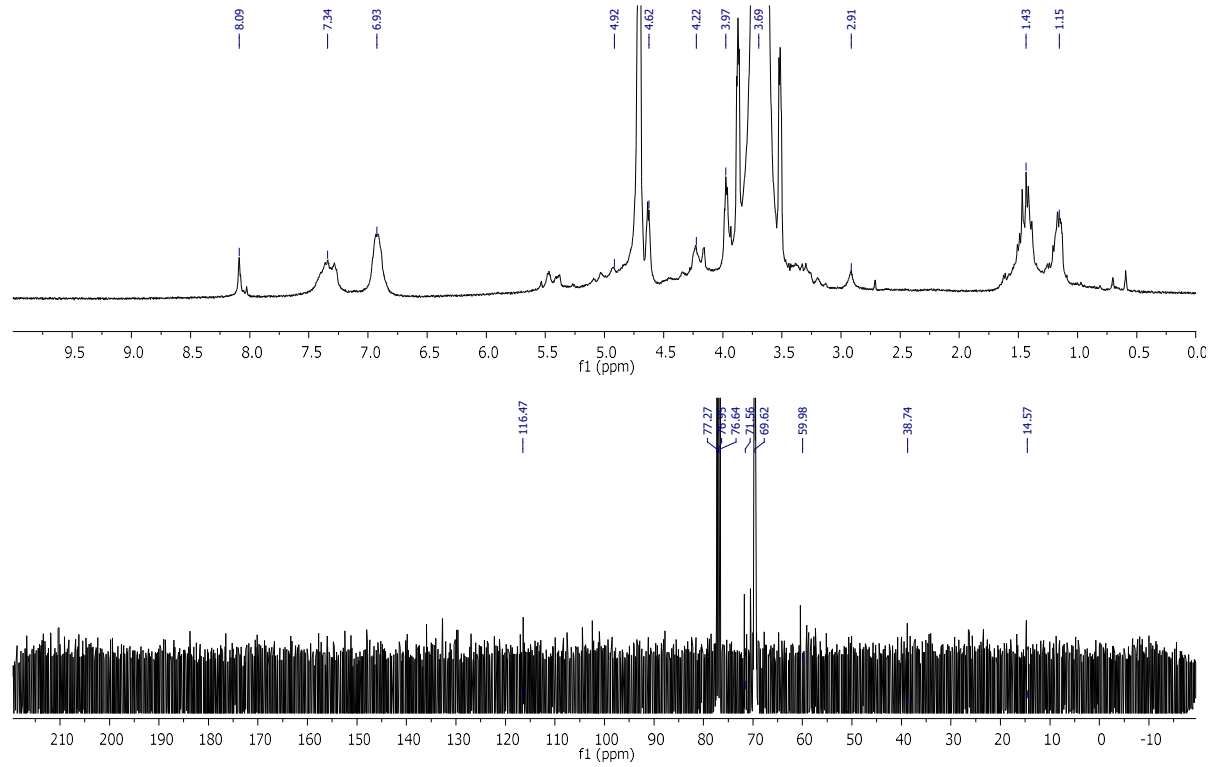

Figure S70. ^{1}H and ^{13}C NMR spectra of compound 68 in D_2O.

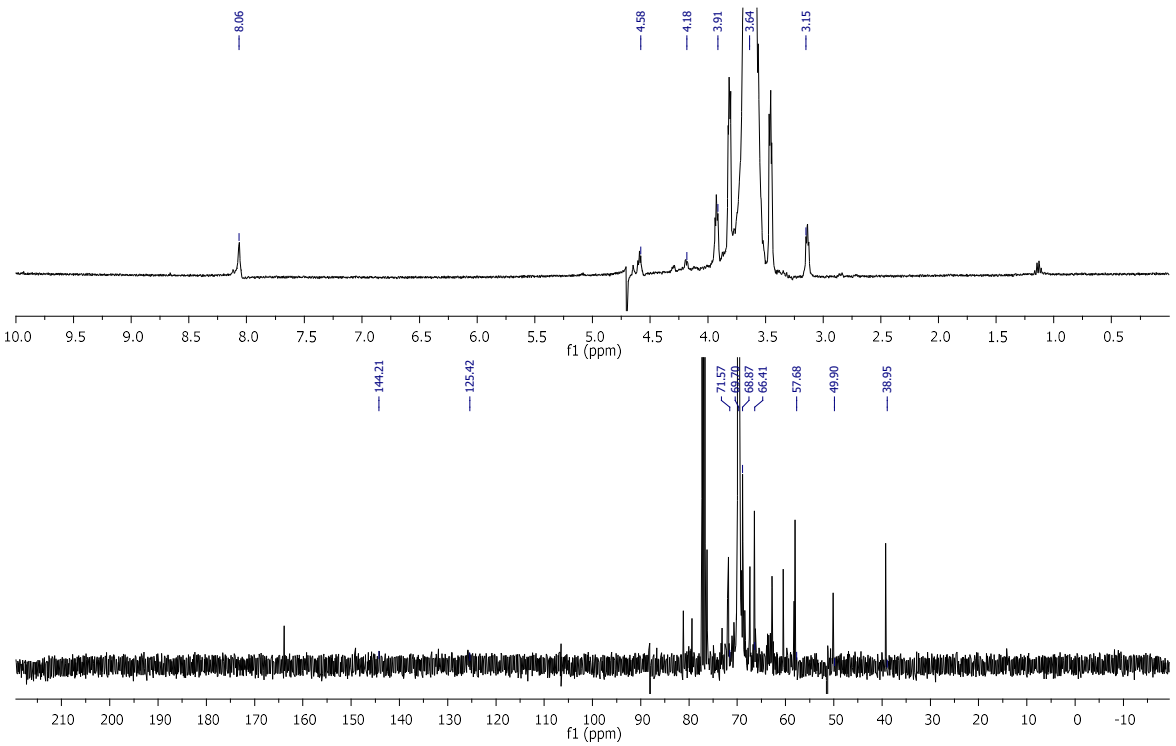

Figure S71. ^{1}H and ^{13}C NMR spectra of compound 69 in D_2O.

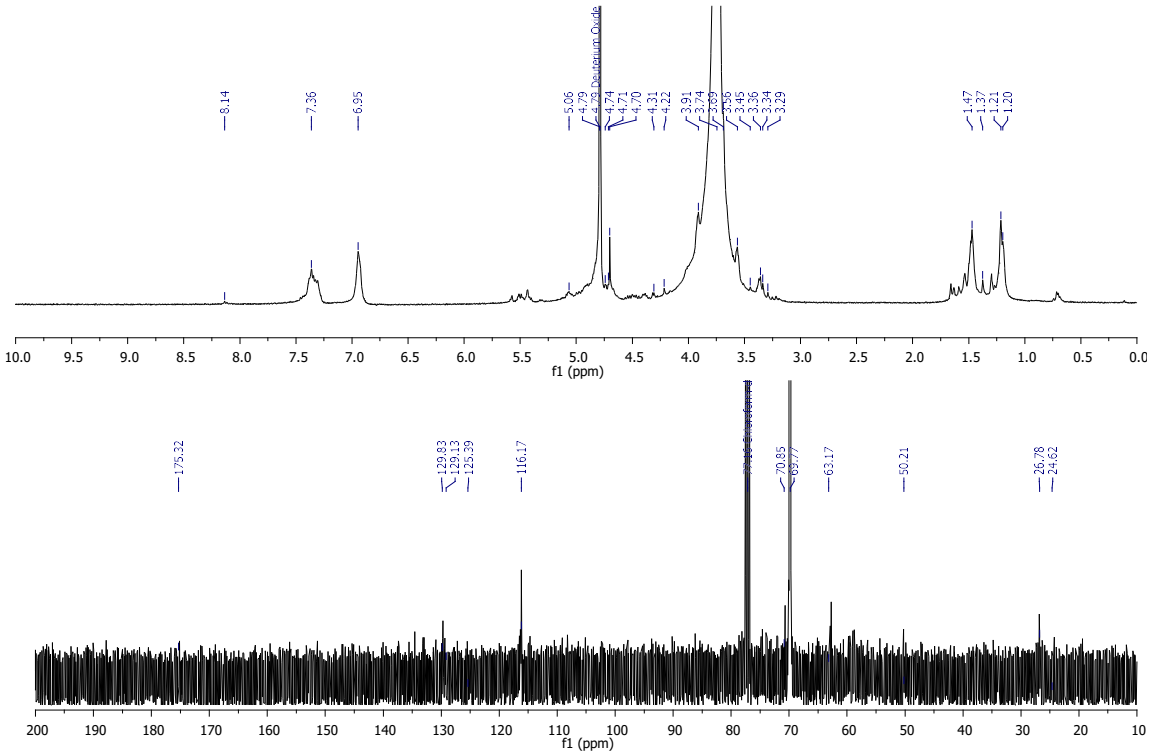

Figure S72. ^{1}H and ^{13}C NMR spectra of compound 70 in D_2O.

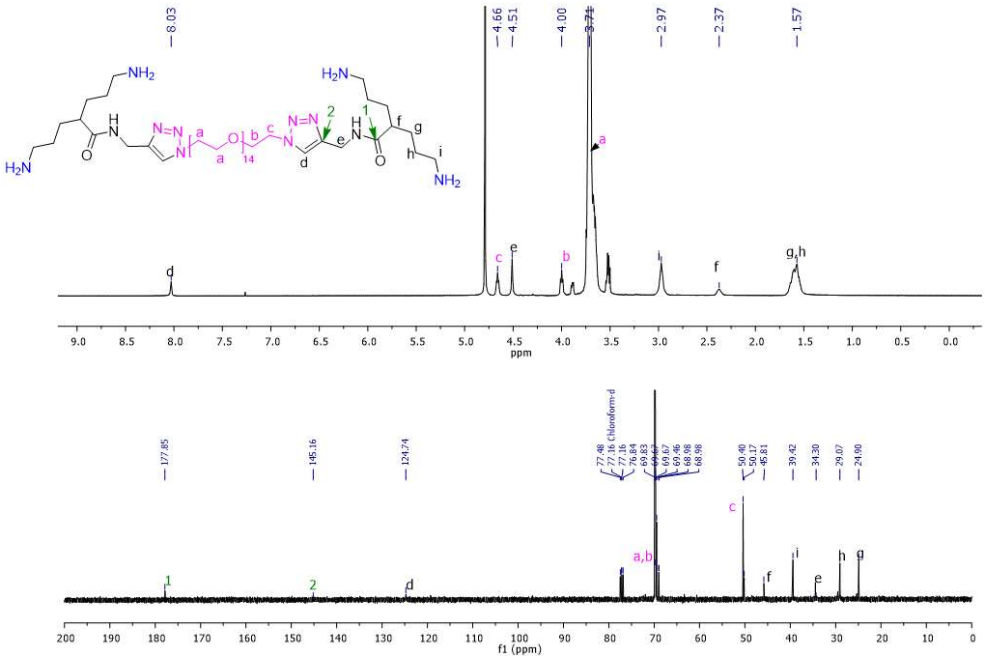

Figure S73. ^{1}H and ^{13}C NMR spectra of compound 71 in D_2O.

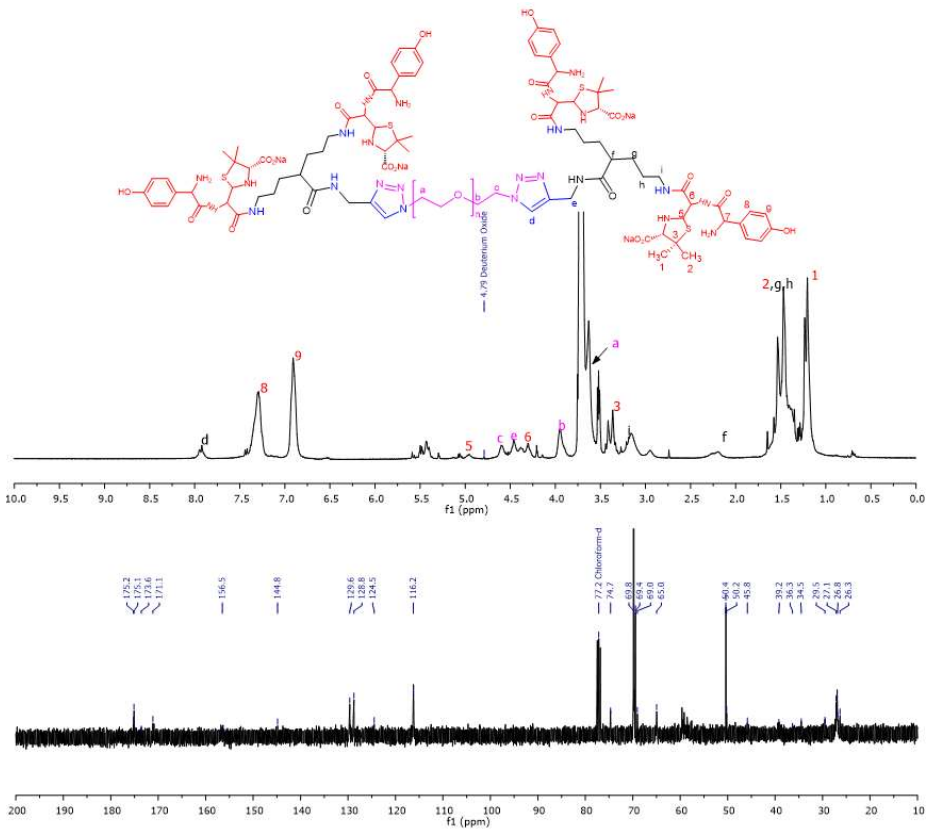

Figure S74. ^{1}H and ^{13}C NMR spectra of compound 72 in D_2O.

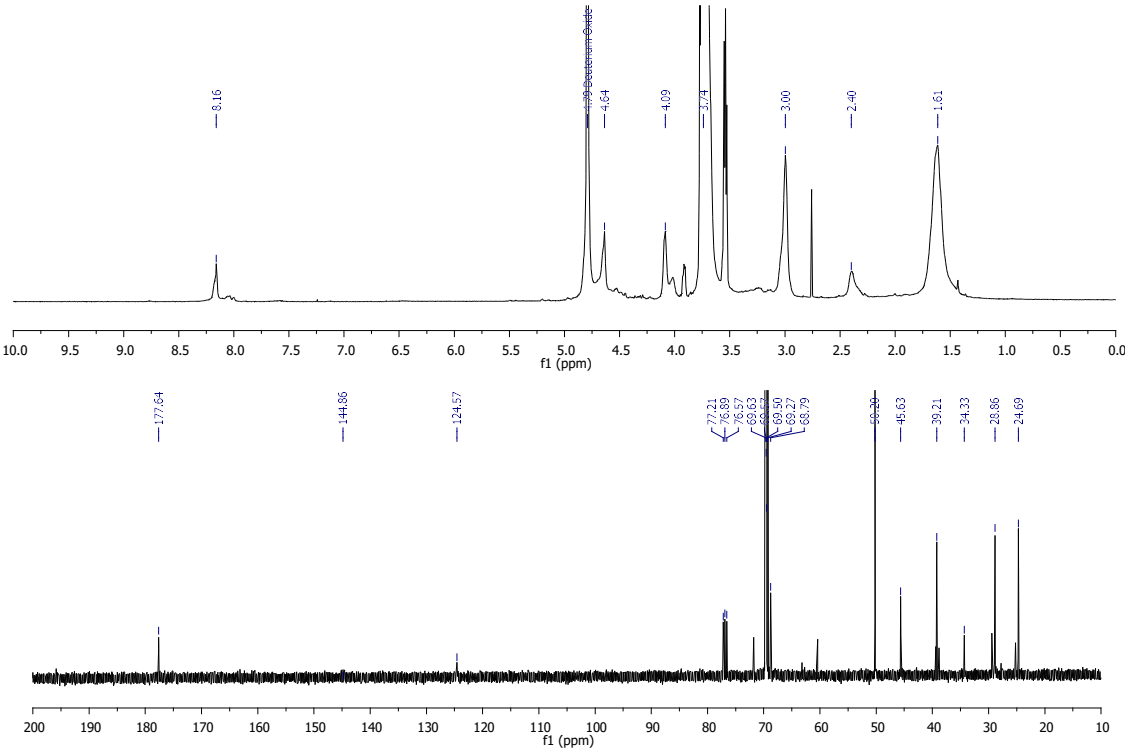

Figure S75. ^{1}H and ^{13}C NMR spectra of compound 73 in D_2O.

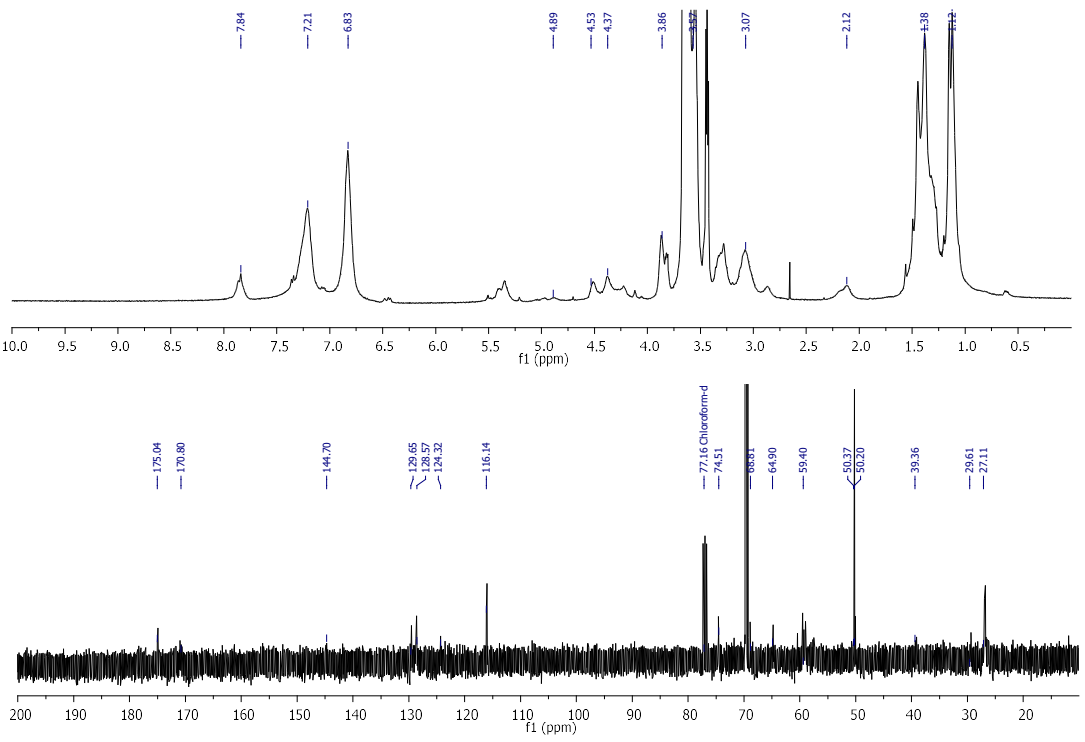

Figure S76. ^{1}H and ^{13}C NMR spectra of compound 74 in D_2O.

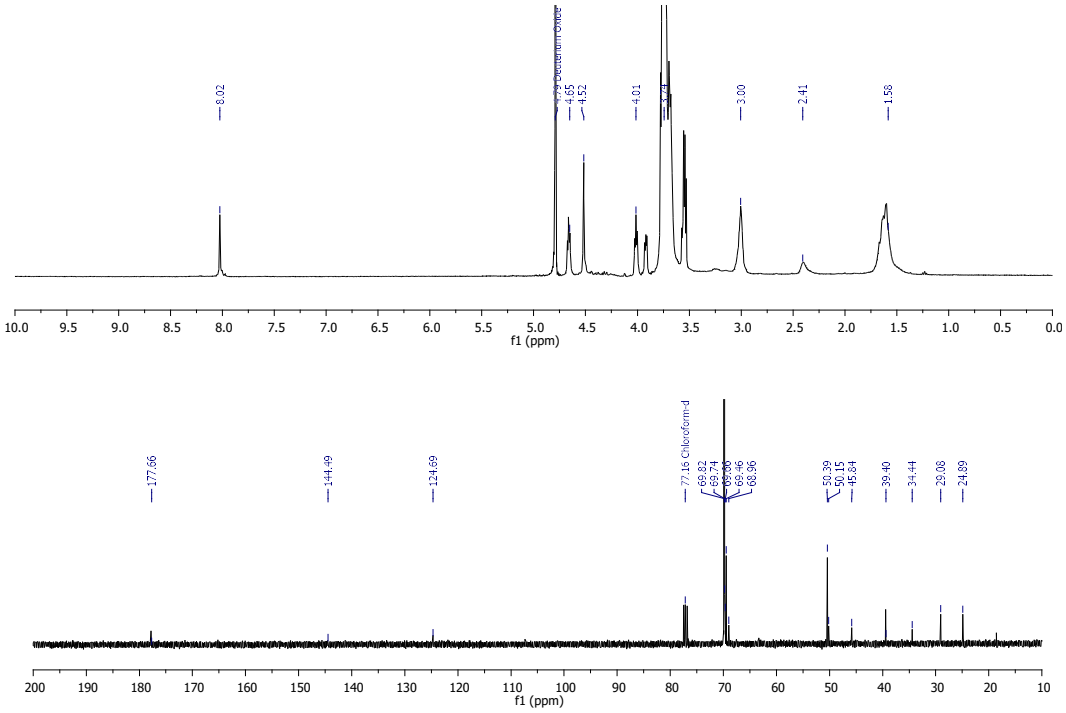

Figure S77. ^{1}H and ^{13}C NMR spectra of compound 75 in D_2O.

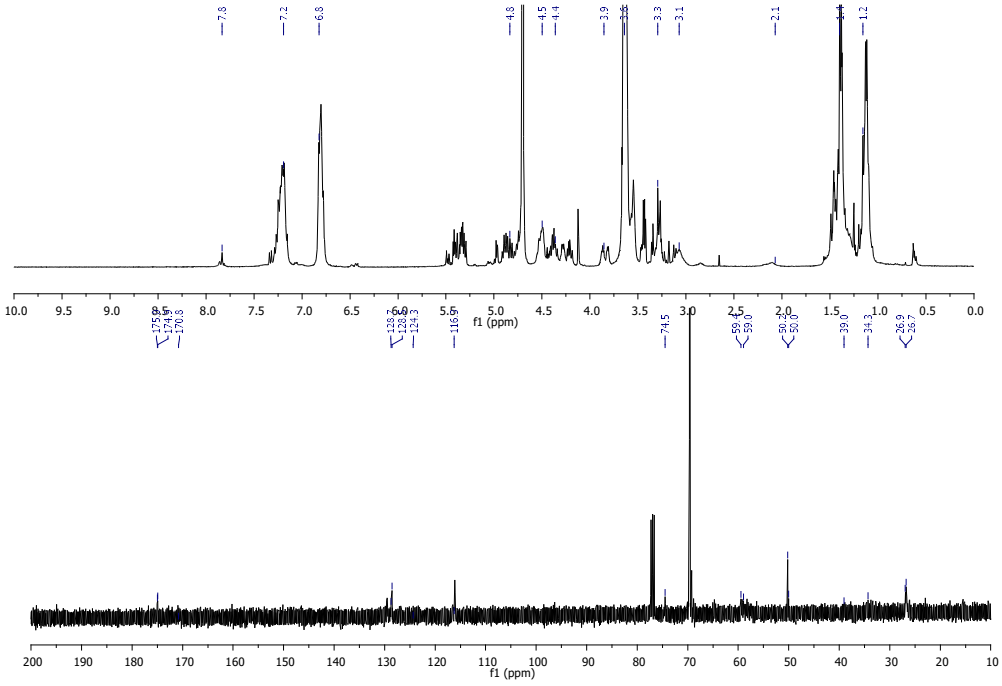

Figure S78. ^{1}H and ^{13}C NMR spectra of compound 76 in D_2O.

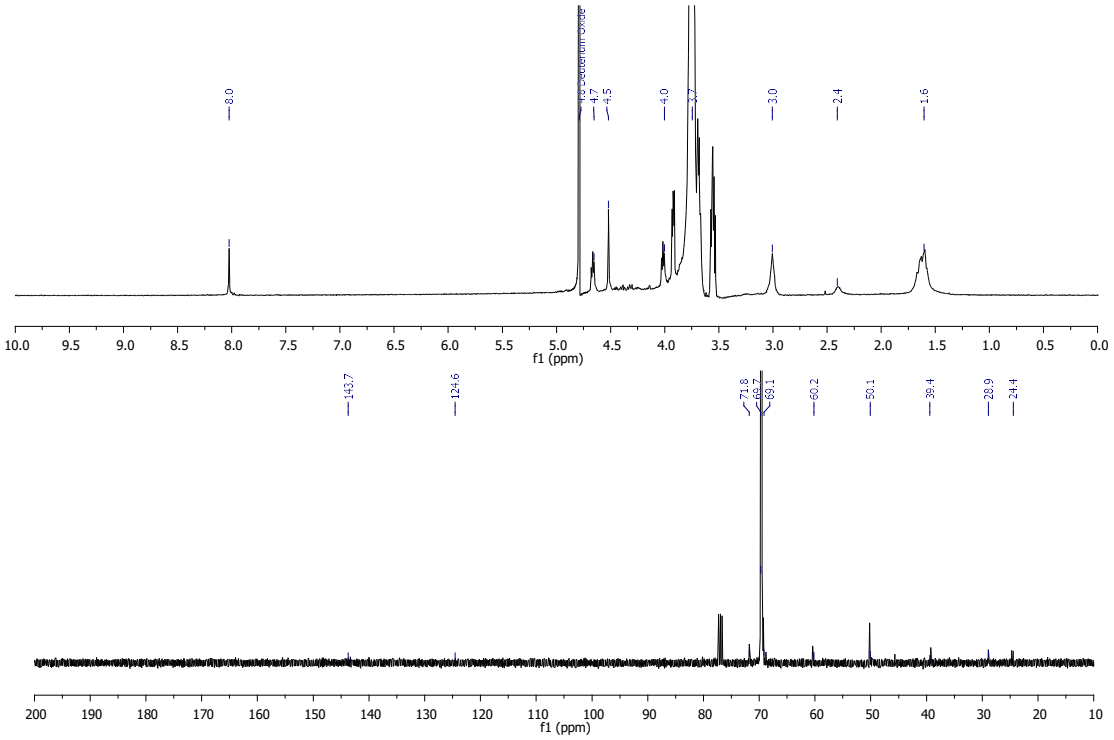

Figure S79. ^{1}H and ^{13}C NMR spectra of compound 77 in D_2O.

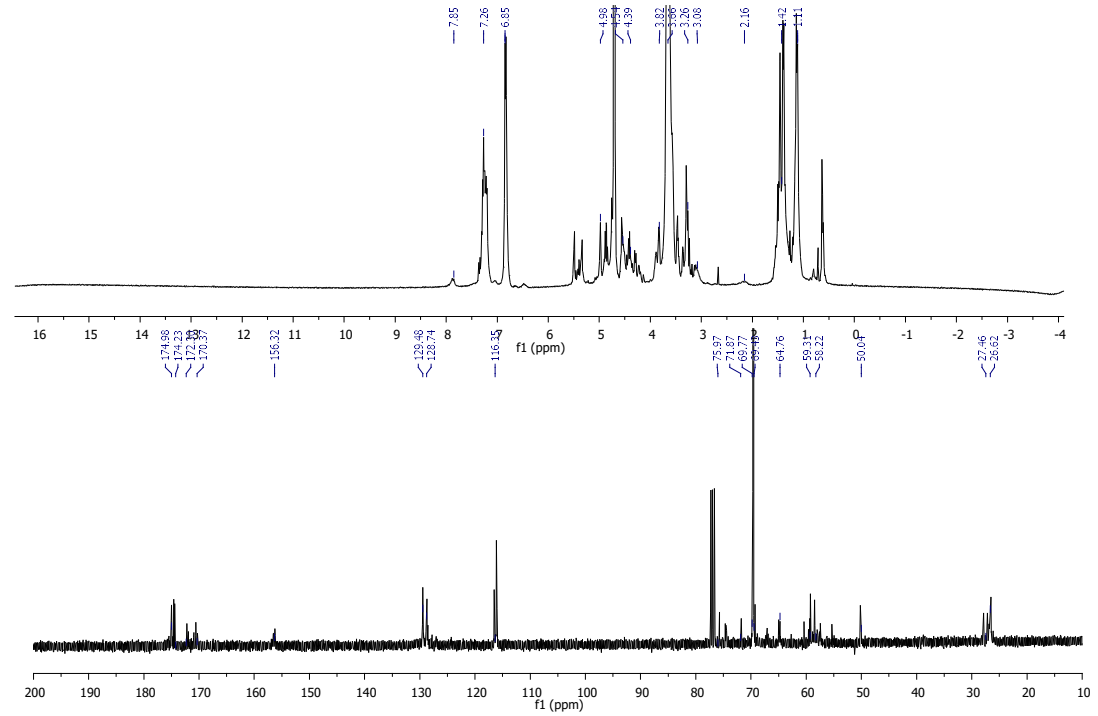

Figure S80. ^{1}H and ^{13}C NMR spectra of compound 78 in D_2O.

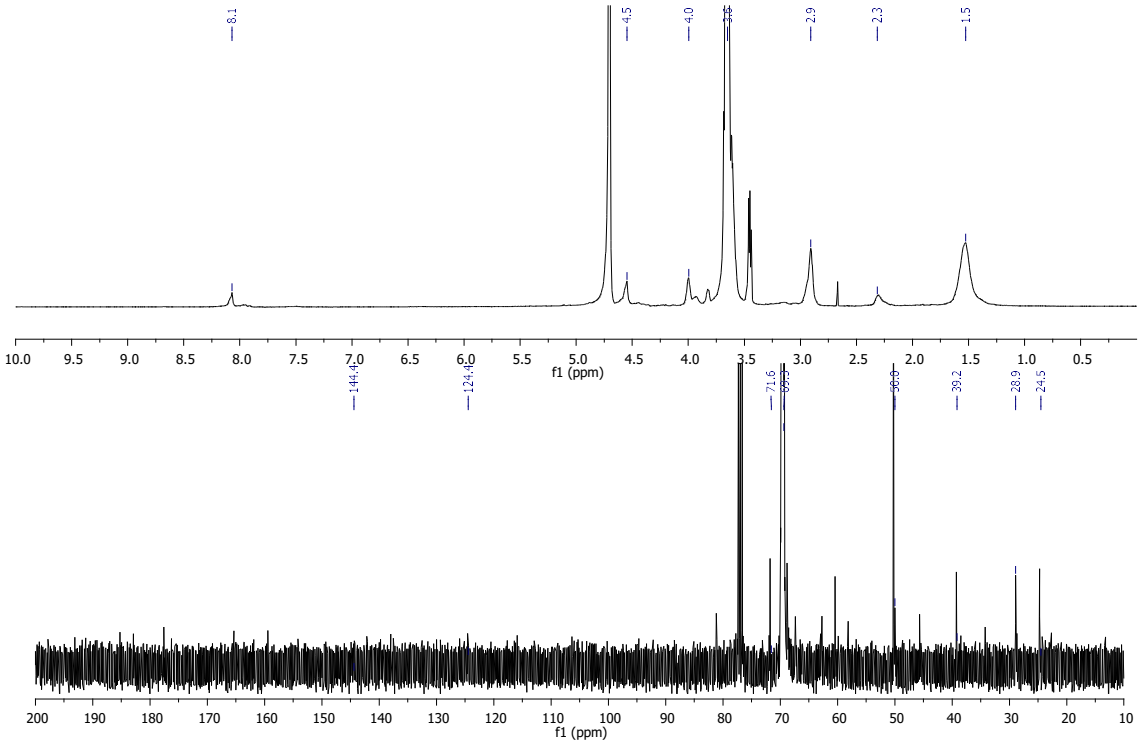

Figure S81. ^{1}H and ^{13}C NMR spectra of compound 79 in D_2O.

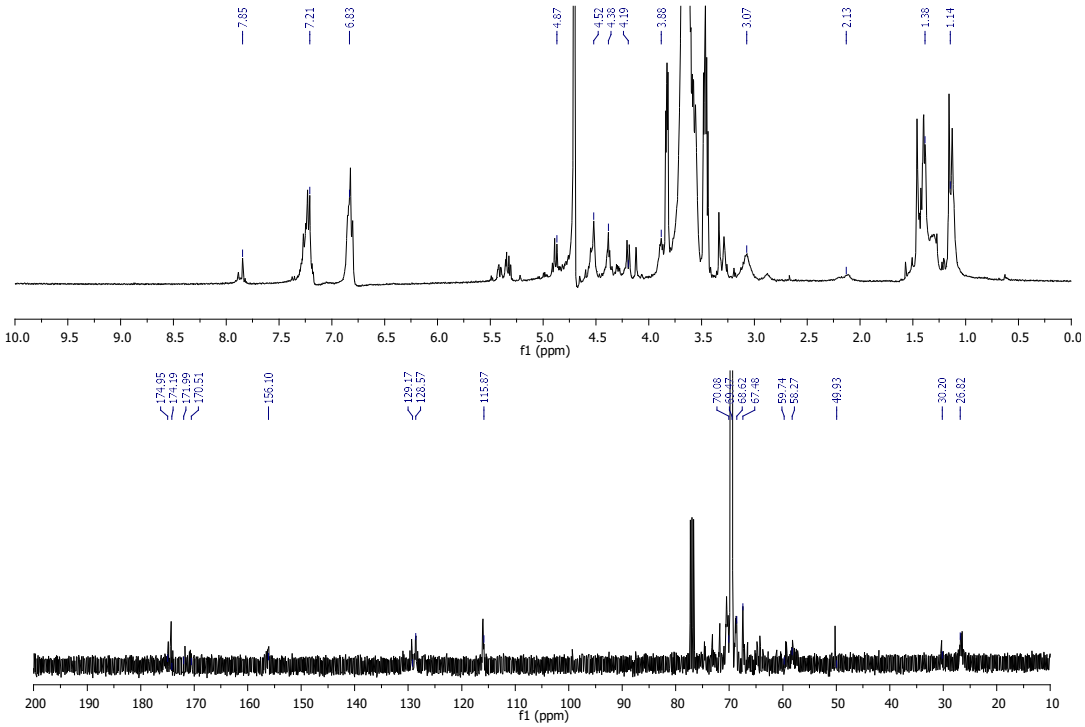

Figure S82. ^{1}H and ^{13}C NMR spectra of compound 80 in D_2O.

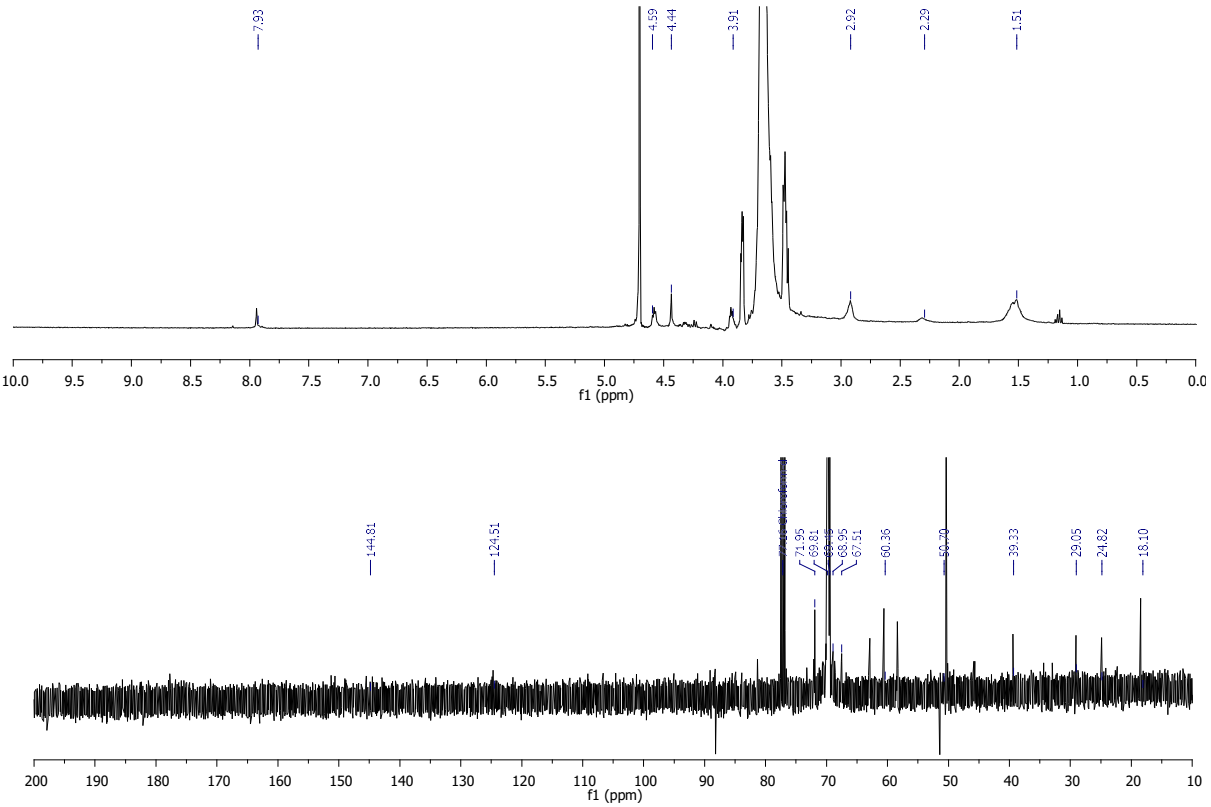

Figure S83. ^{1}H and ^{13}C NMR spectra of compound 81 in D_2O.

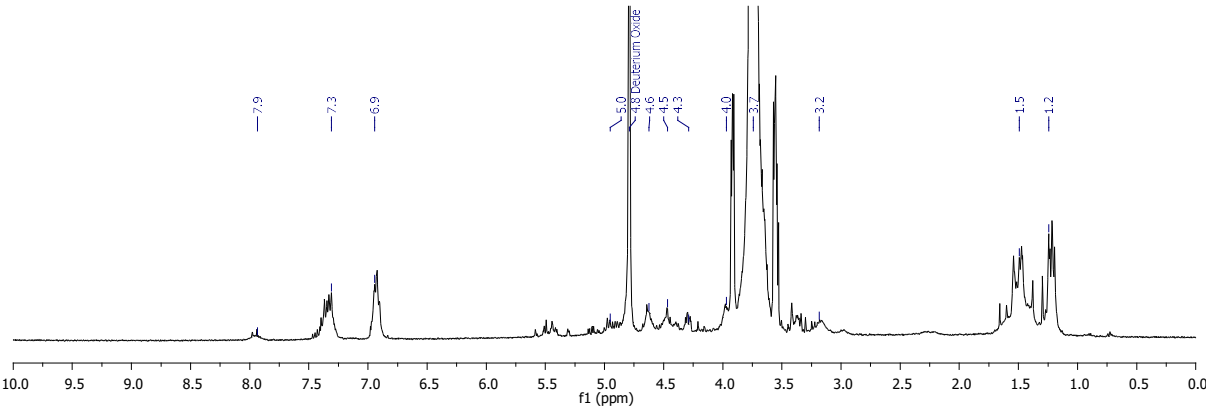

Figure S84. ^{1}H and ^{13}C NMR spectra of compound 82 in D_2O.

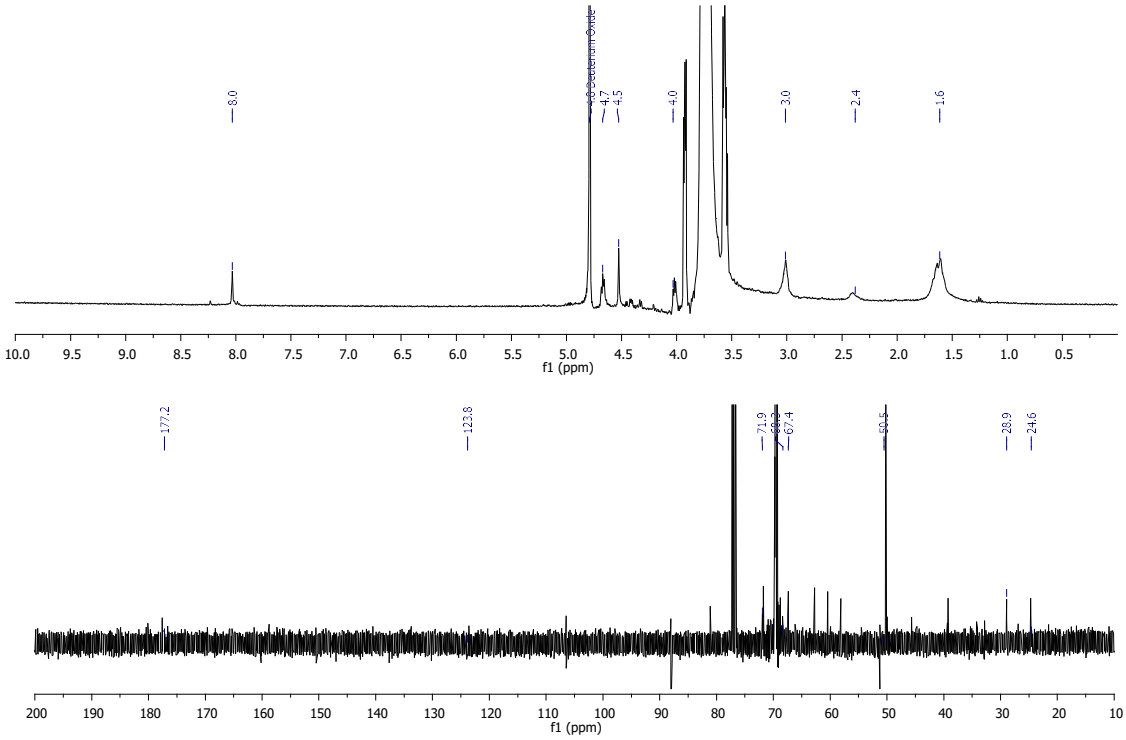

Figure S85. ^{1}H and ^{13}C NMR spectra of compound 83 in D_2O.

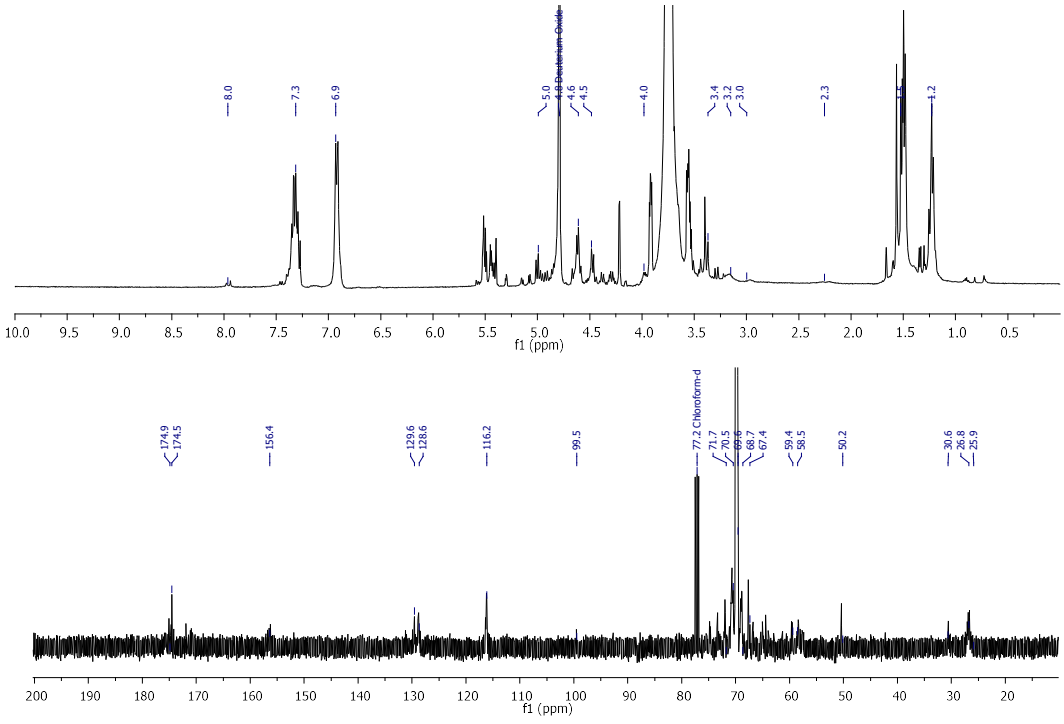

Figure S86. ^{1}H and ^{13}C NMR spectra of compound 84 in D_2O.

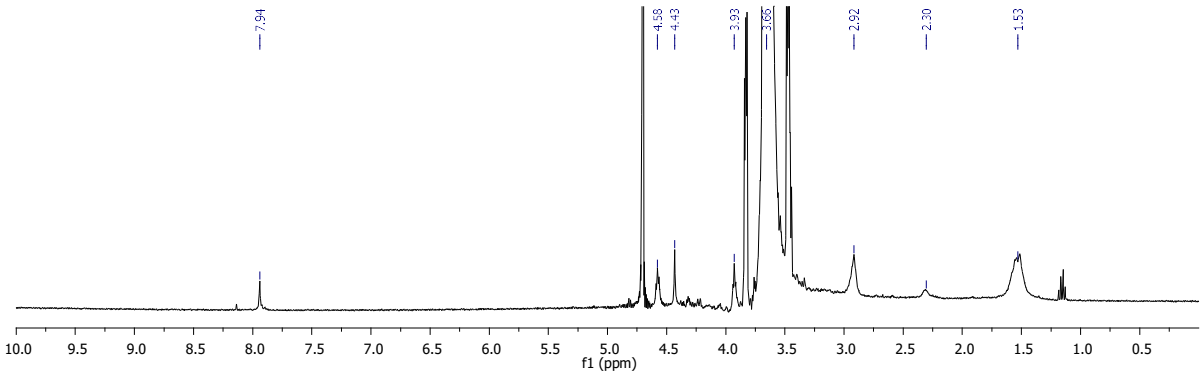

Figure S87. ^{1}H and ^{13}C NMR spectra of compound 85 in D_2O.

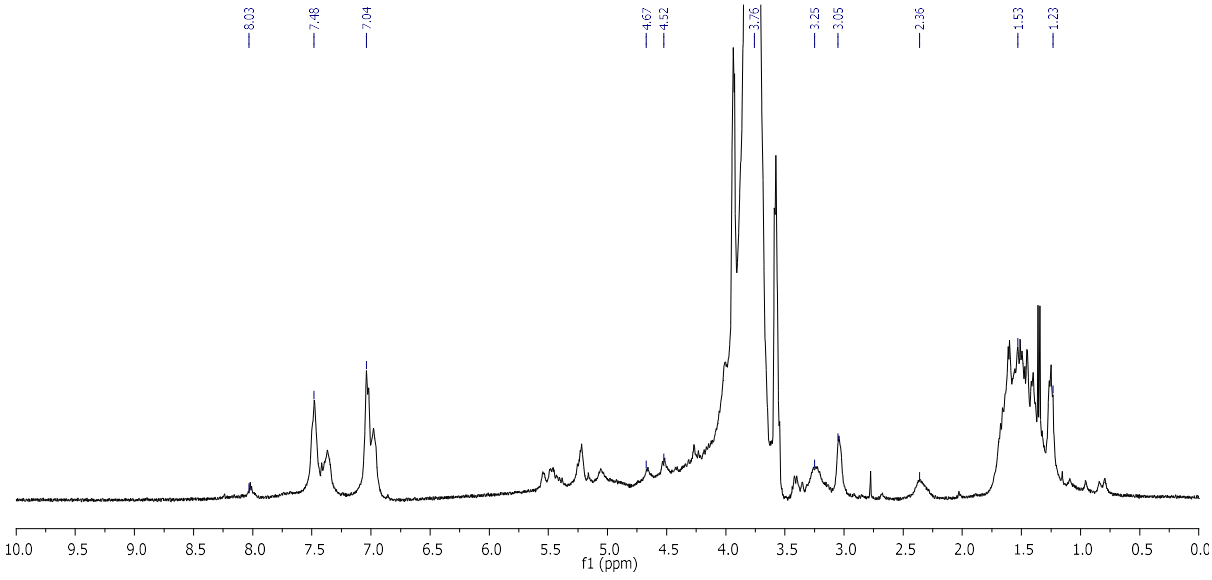

Figure S88. ^{1}H and ^{13}C NMR spectra of compound 86 in D_2O.

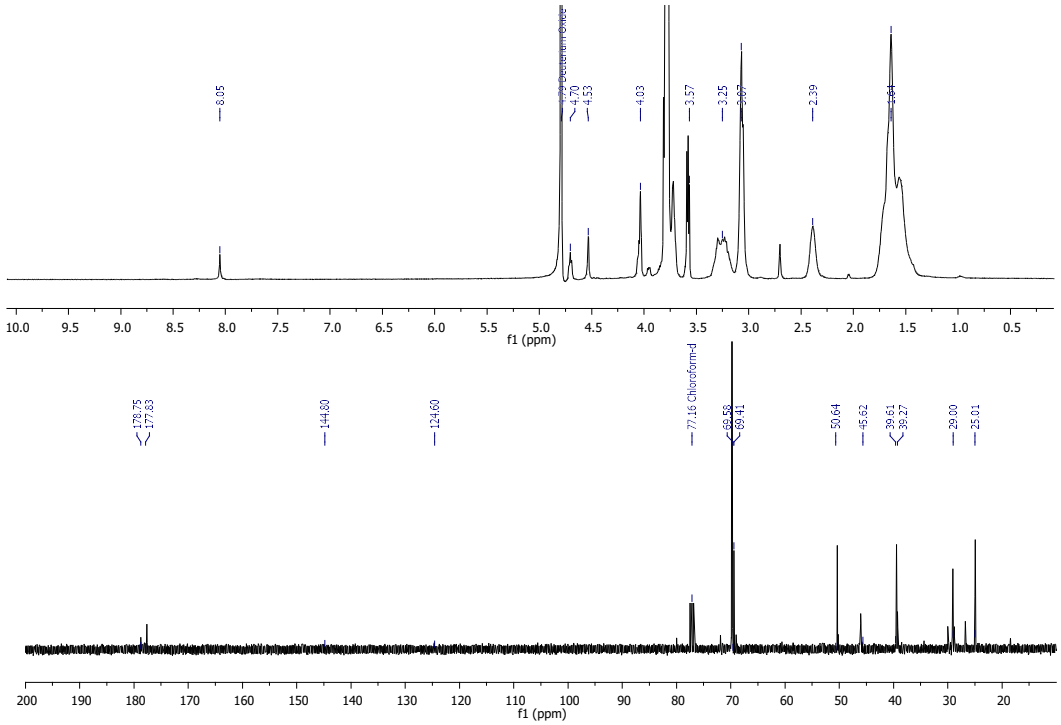

Figure S89. ^{1}H and ^{13}C NMR spectra of compound 87 in D_2O.

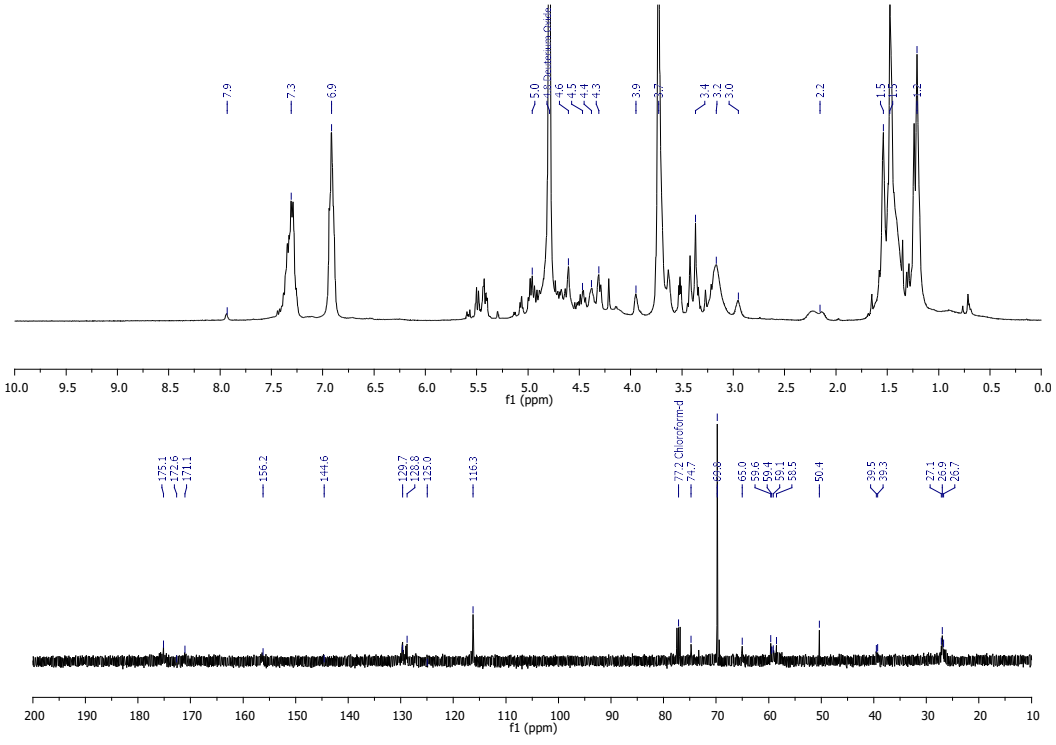

Figure S90. ^{1}H and ^{13}C NMR spectra of compound 88 in D_2O.

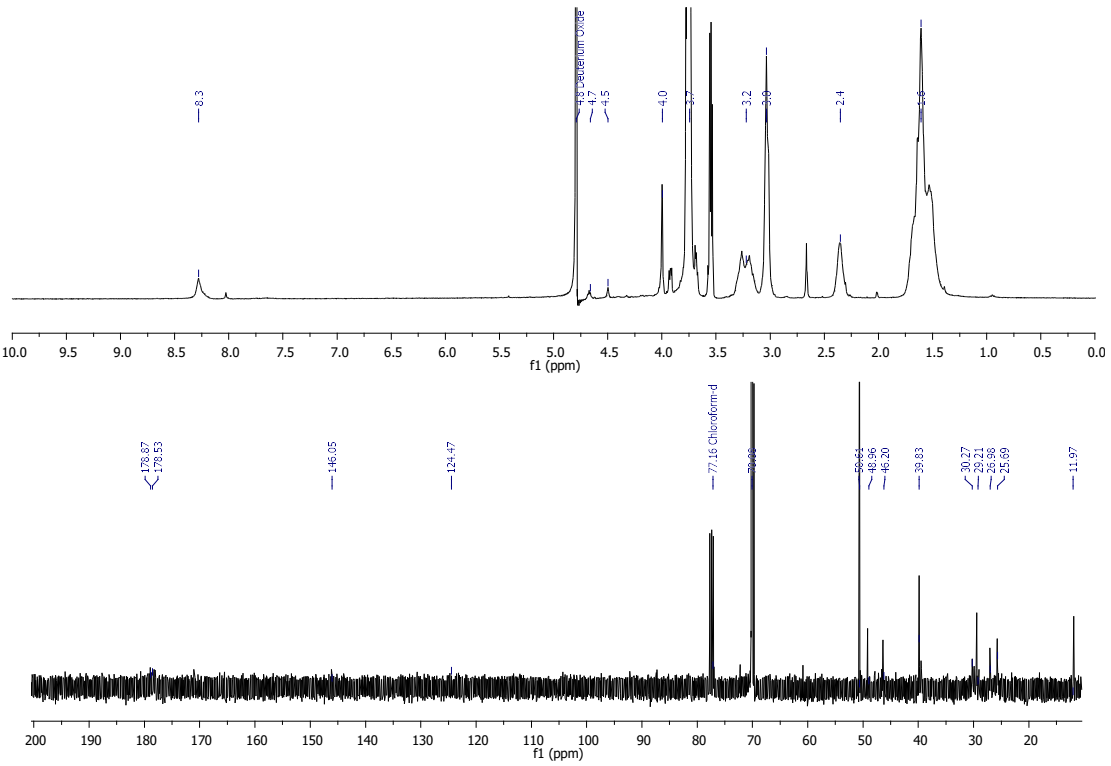

Figure S91. ^{1}H and ^{13}C NMR spectra of compound 89 in D_2O.

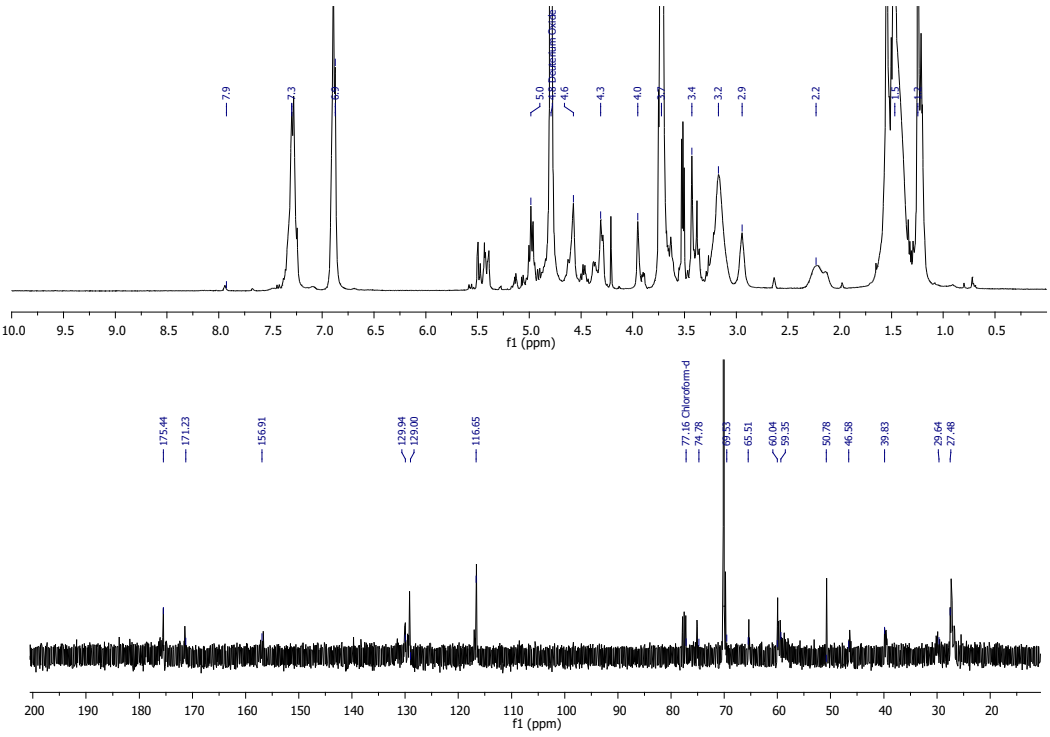

Figure S92. ^{1}H and ^{13}C NMR spectra of compound 90 in D_2O.

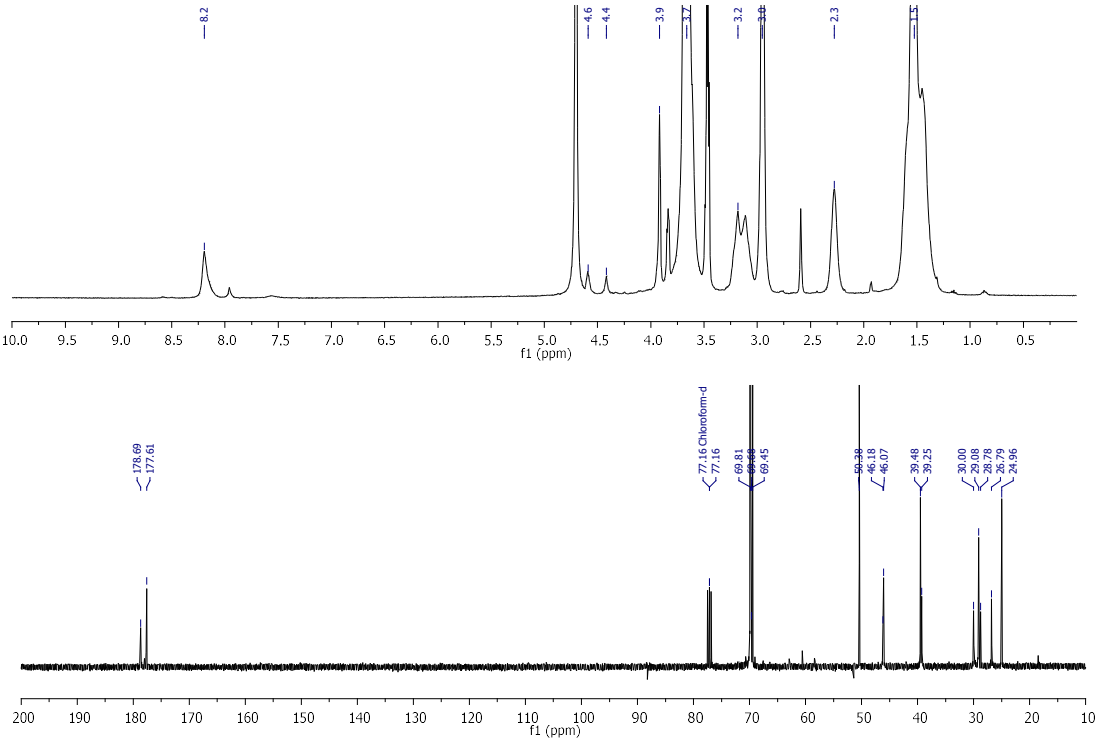

Figure S93. ^{1}H and ^{13}C NMR spectra of compound 91 in D_2O.

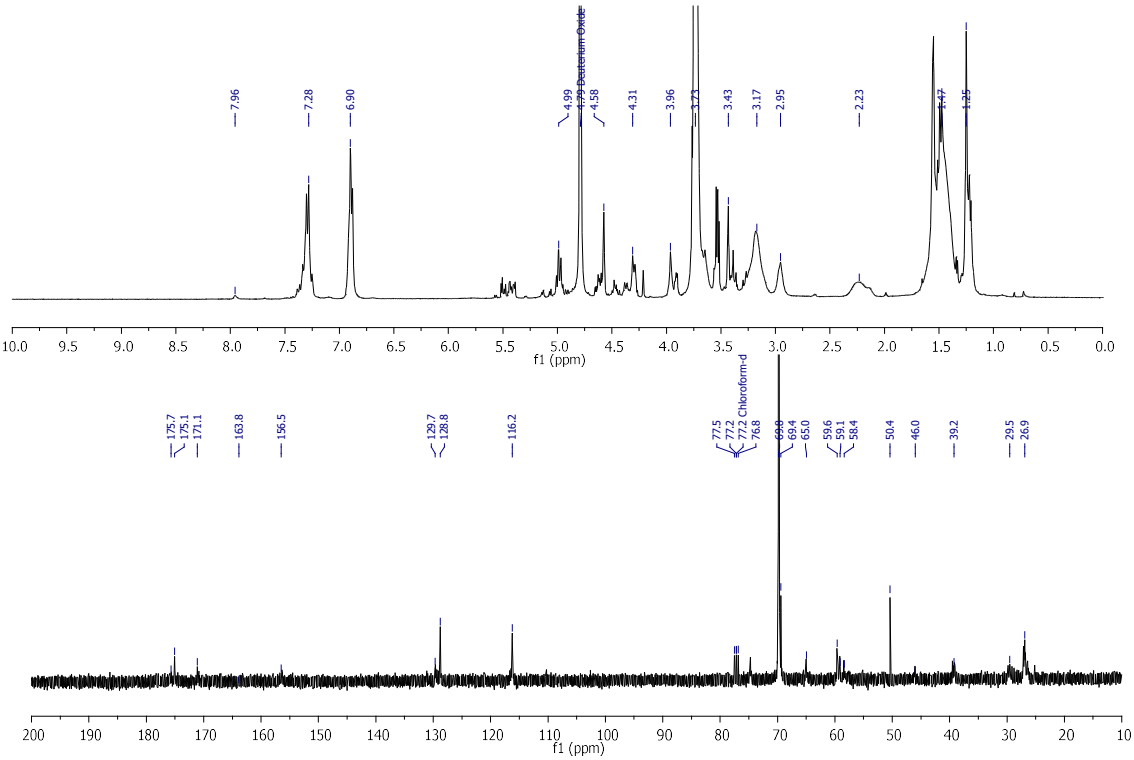

Figure S94. ^{1}H and ^{13}C NMR spectra of compound 92 in D_2O.

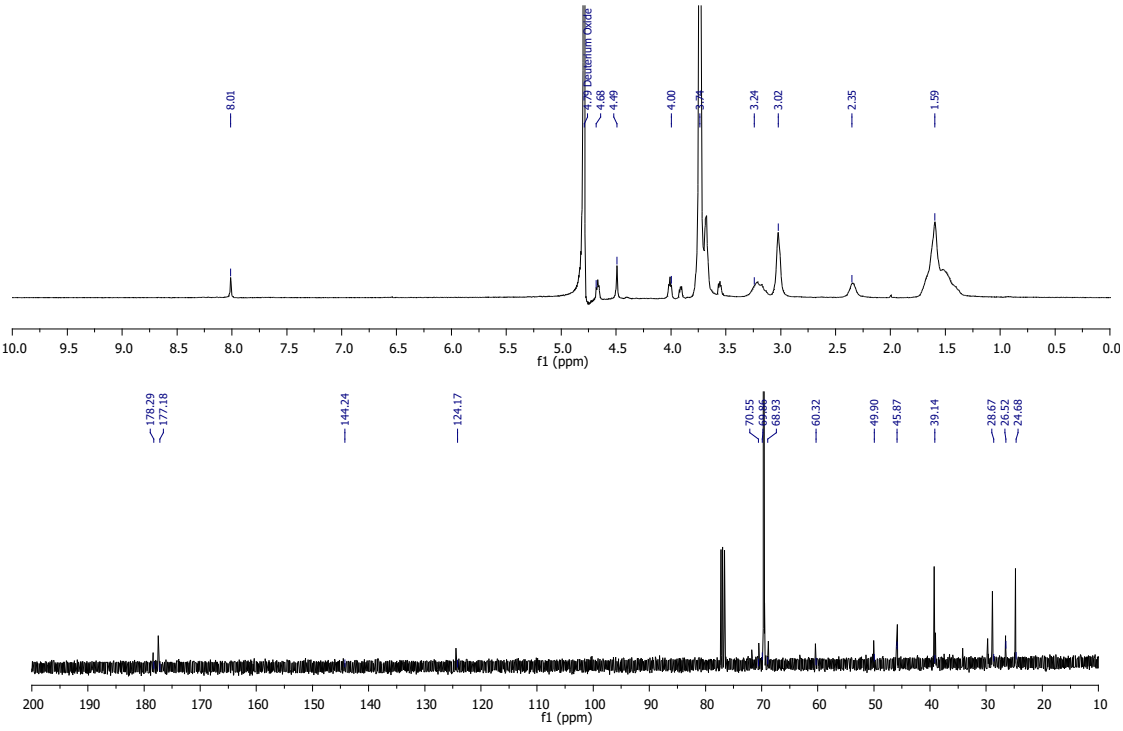

Figure S95. ^{1}H and ^{13}C NMR spectra of compound 93 in D_2O.

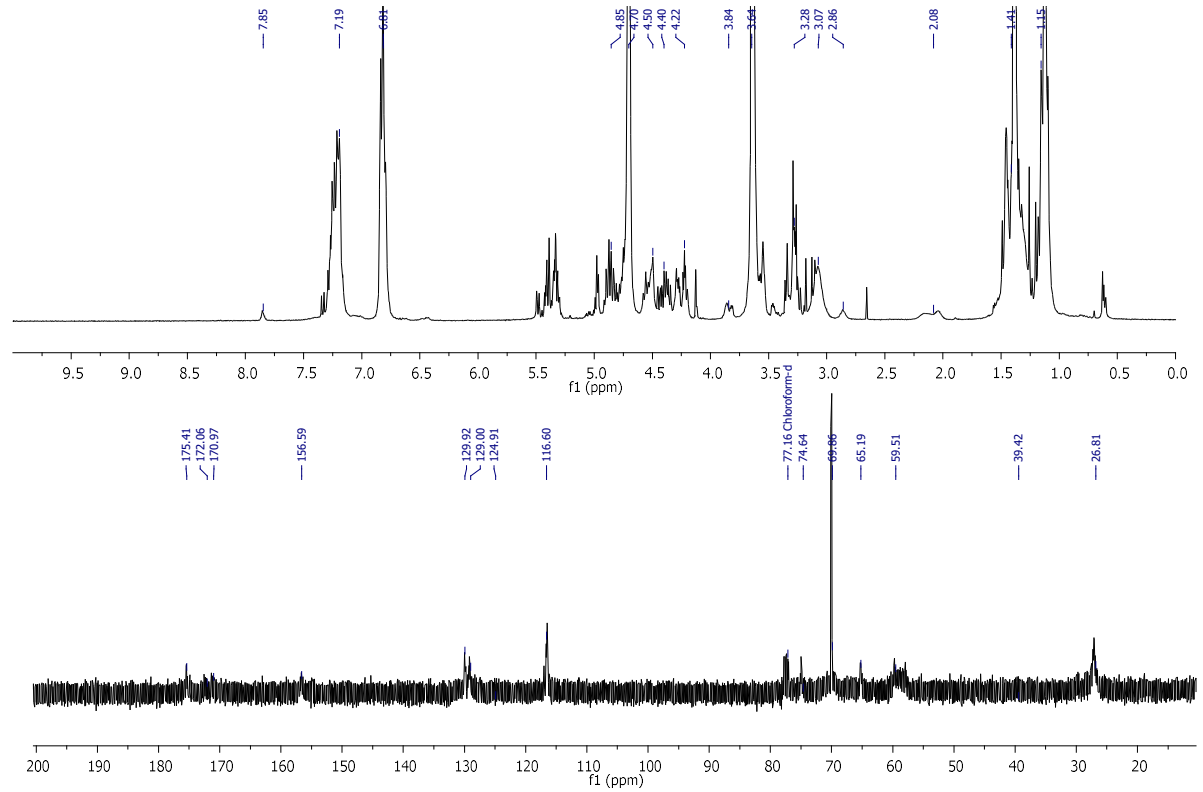

Figure S96. ^{1}H and ^{13}C NMR spectra of compound 94 in D_2O.

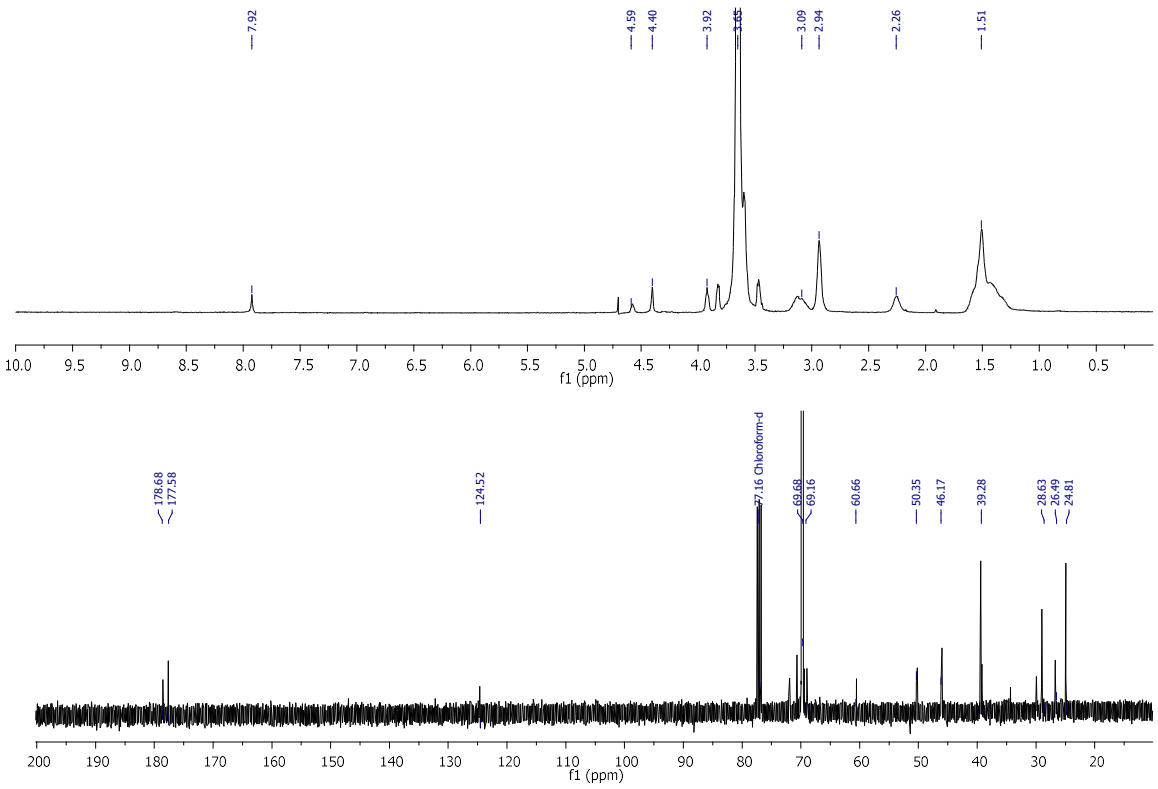

Figure S97. ^{1}H and ^{13}C NMR spectra of compound 95 in D_2O.

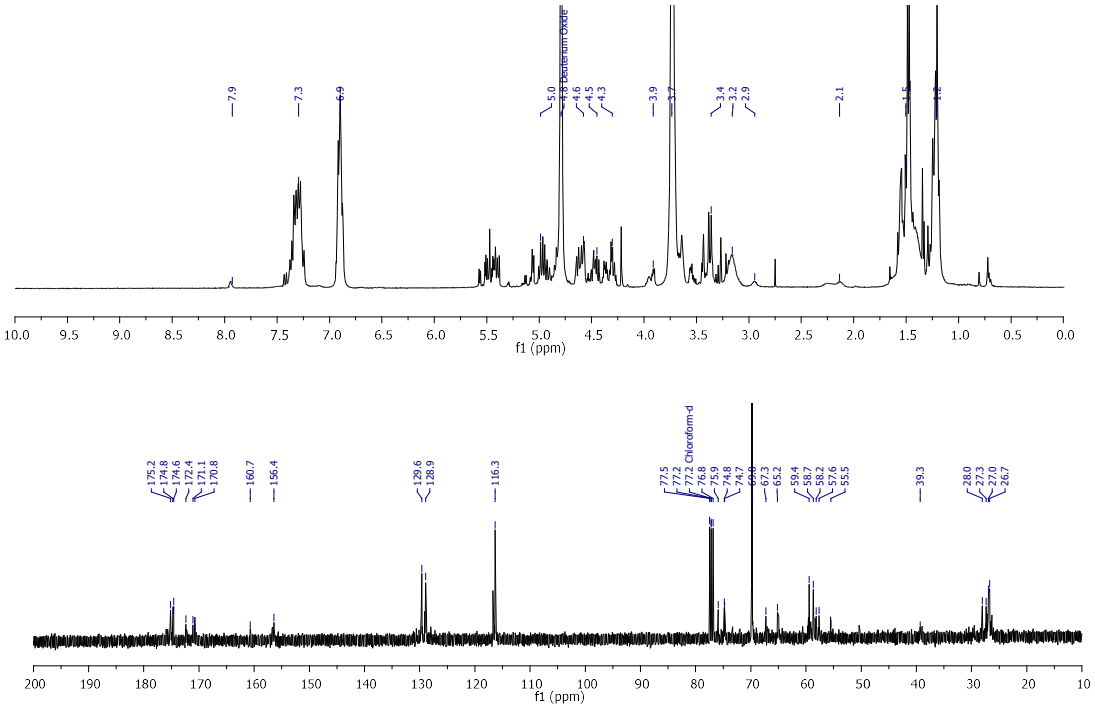

Figure S98. ^{1}H and ^{13}C NMR spectra of compound 96 in D_2O.

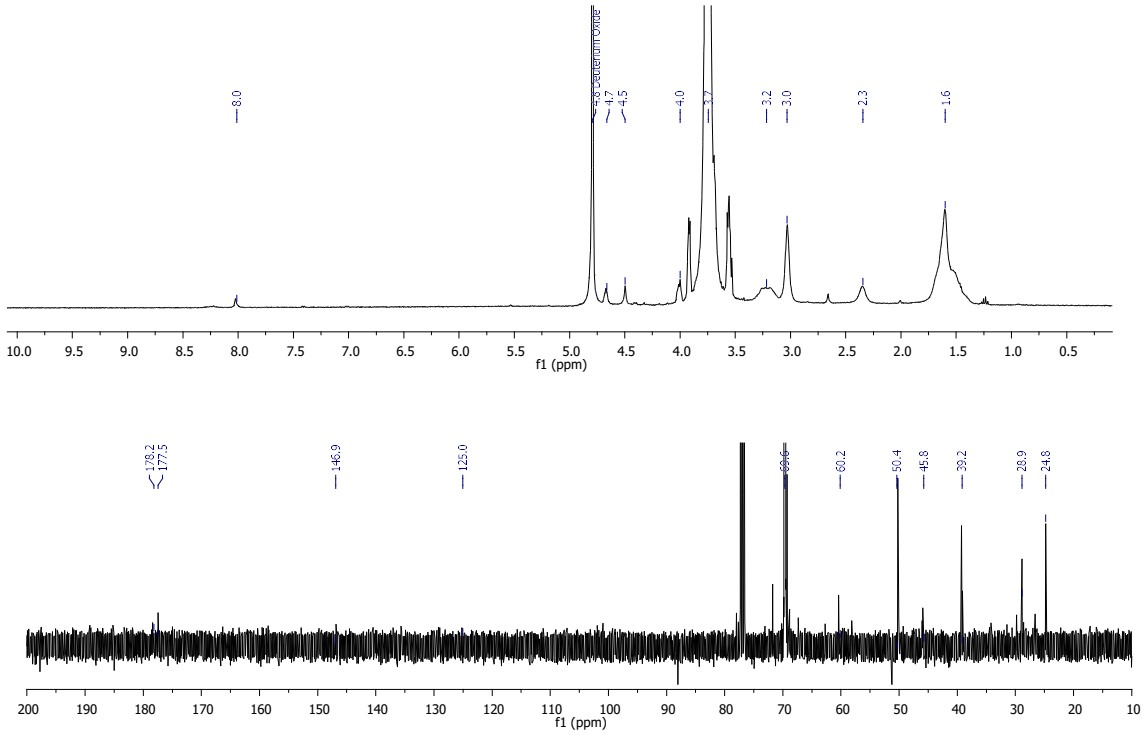

Figure S99. ^{1}H and ^{13}C NMR spectra of compound 97 in D_2O.

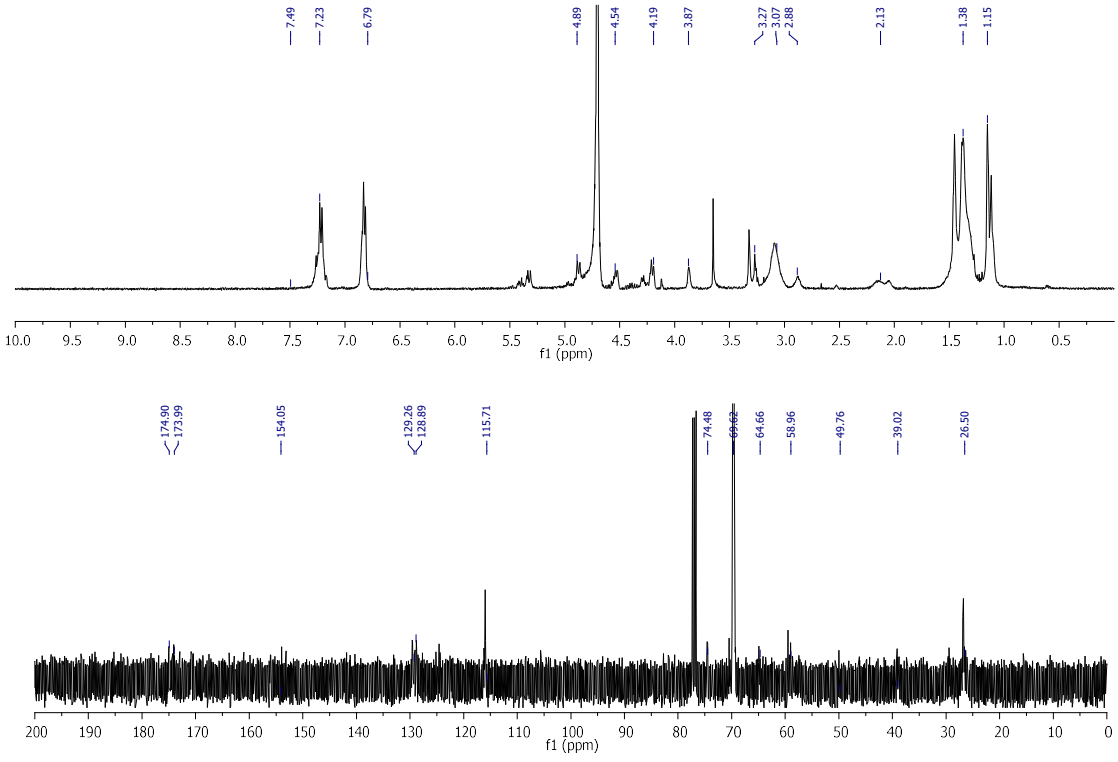

Figure S100. ^{1}H and ^{13}C NMR spectra of compound 98 in D_2O.

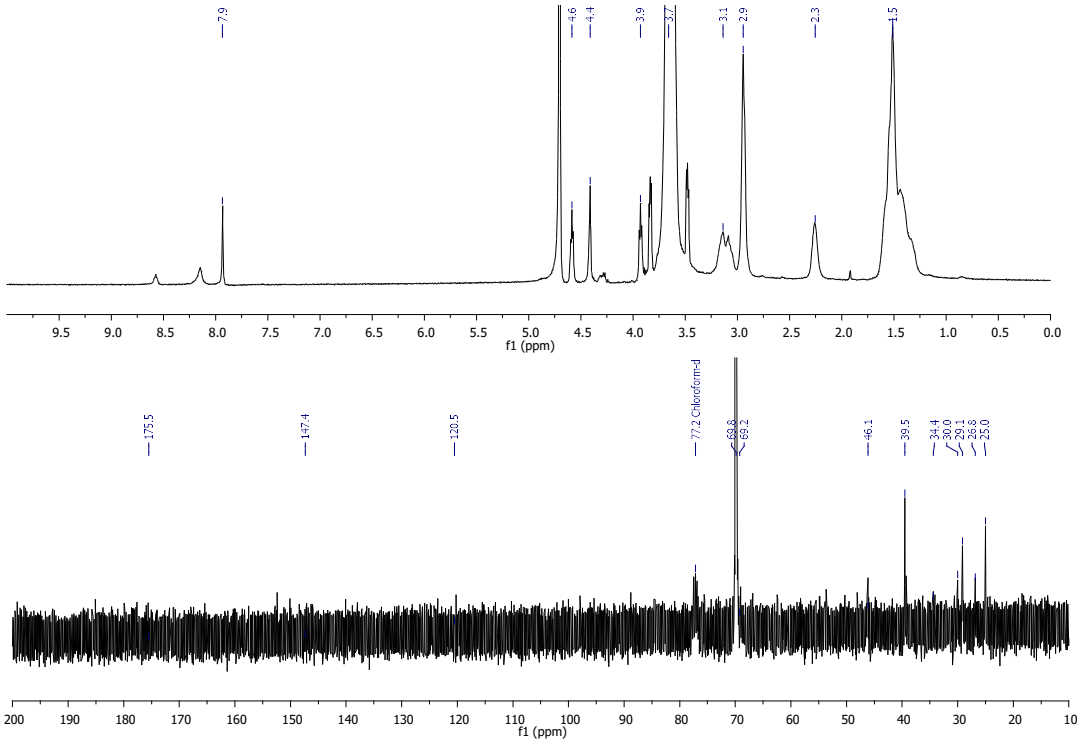

Figure S101. ^{1}H and ^{13}C NMR spectra of compound 99 in D_2O.

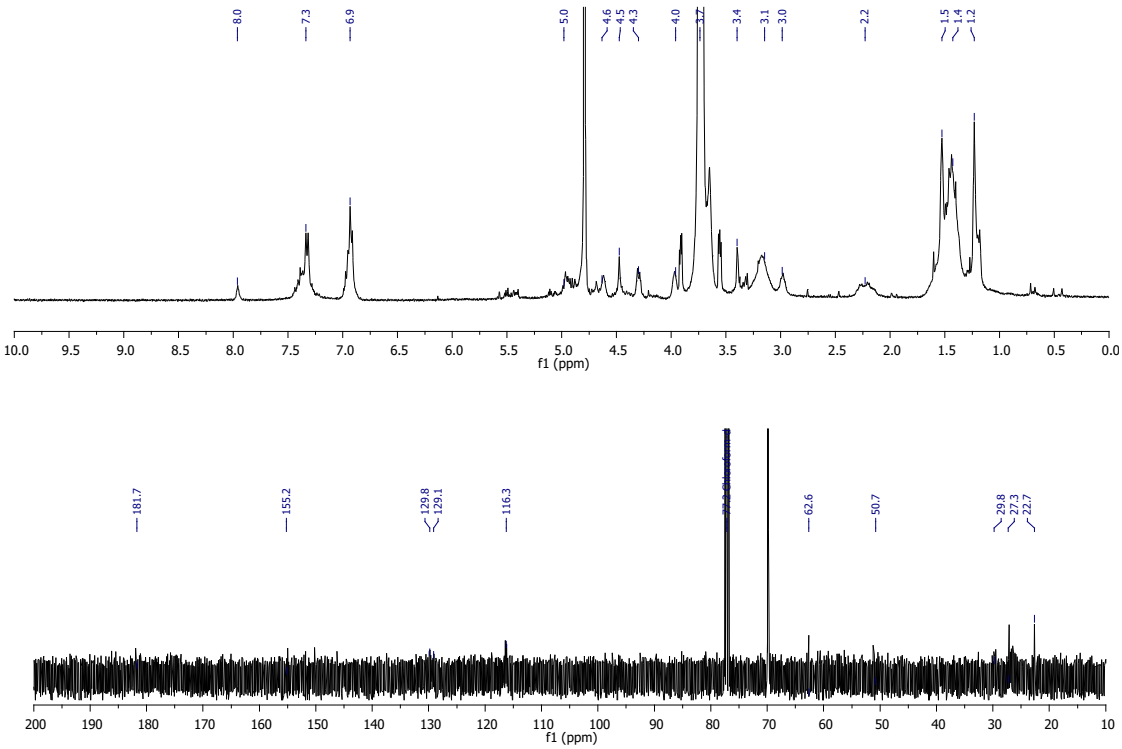

Figure S102. ^{1}H and ^{13}C NMR spectra of compound 100 in D_2O.

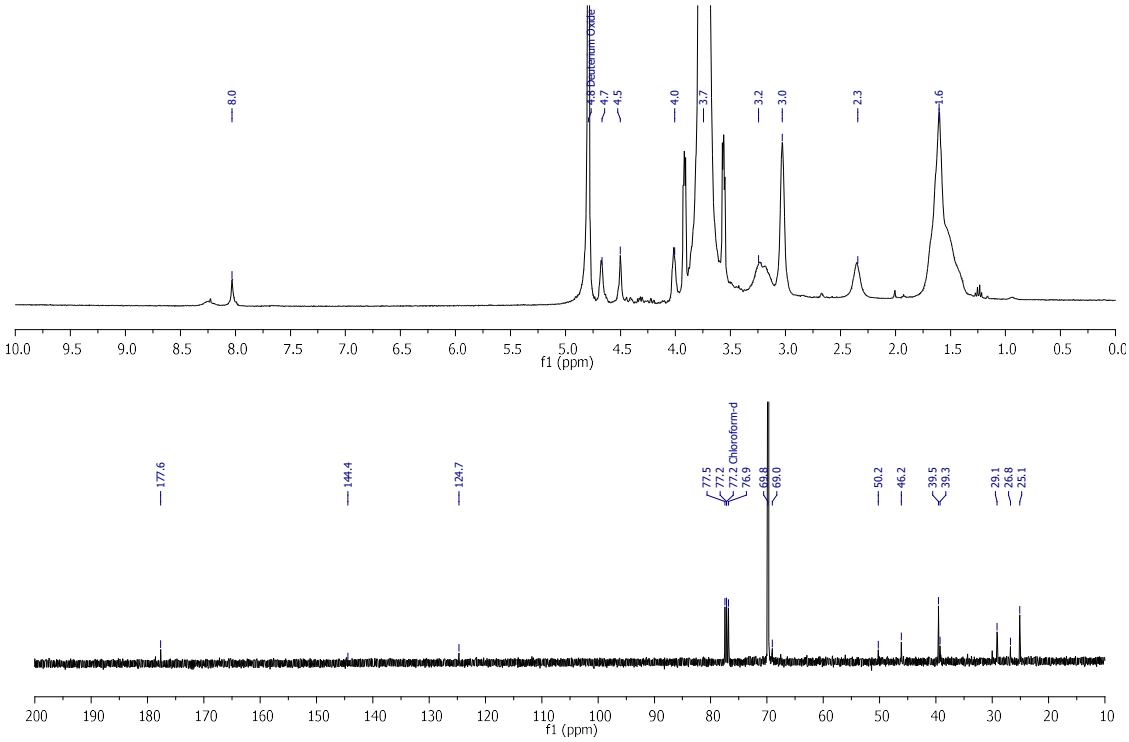

Figure S103. ^{1}H and ^{13}C NMR spectra of compound 101 in D_2O.

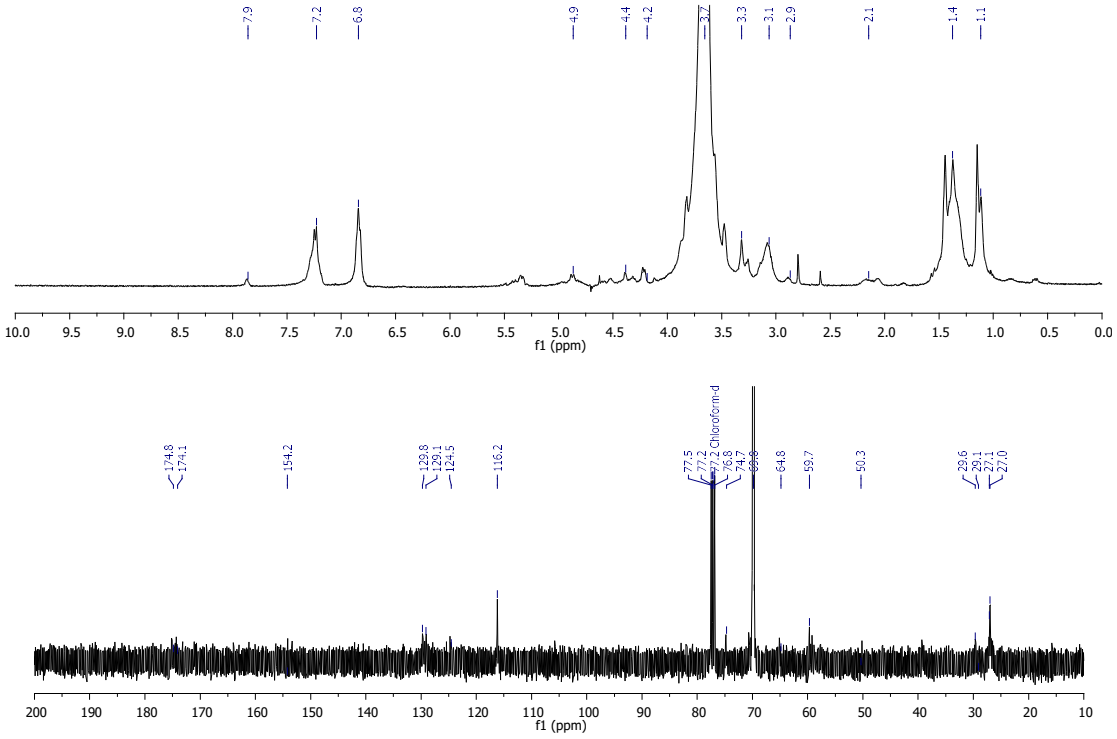

Figure S104. ^{1}H and ^{13}C NMR spectra of compound 102 in D_2O.

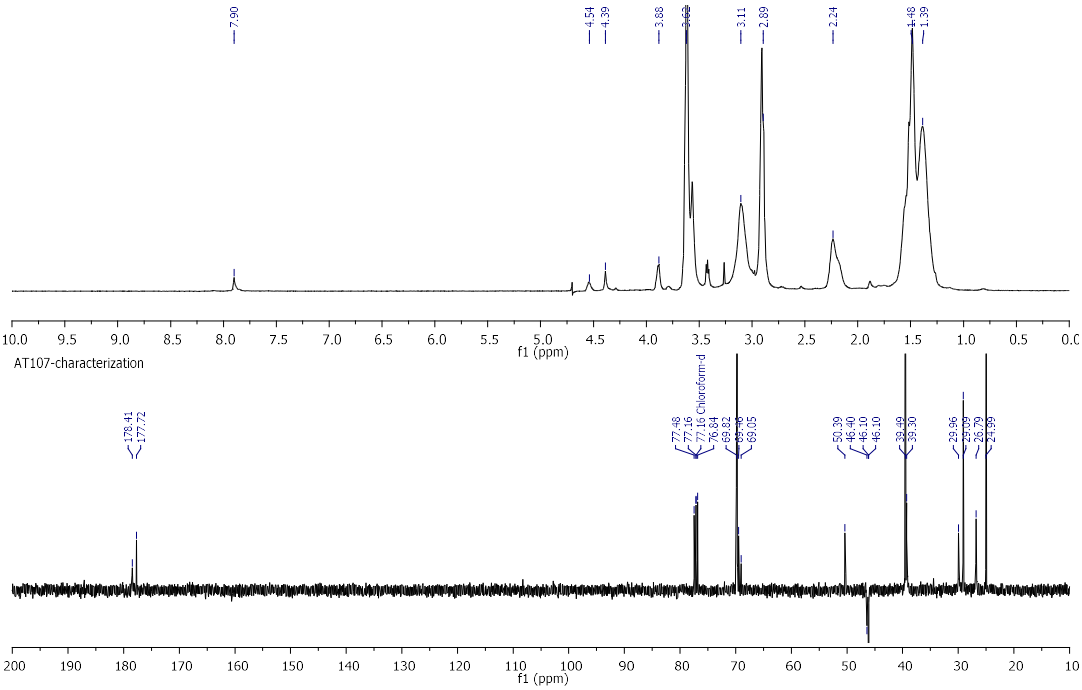

Figure S105. ^{1}H and ^{13}C(SEFT) NMR spectra of compound 103 in D_2O.

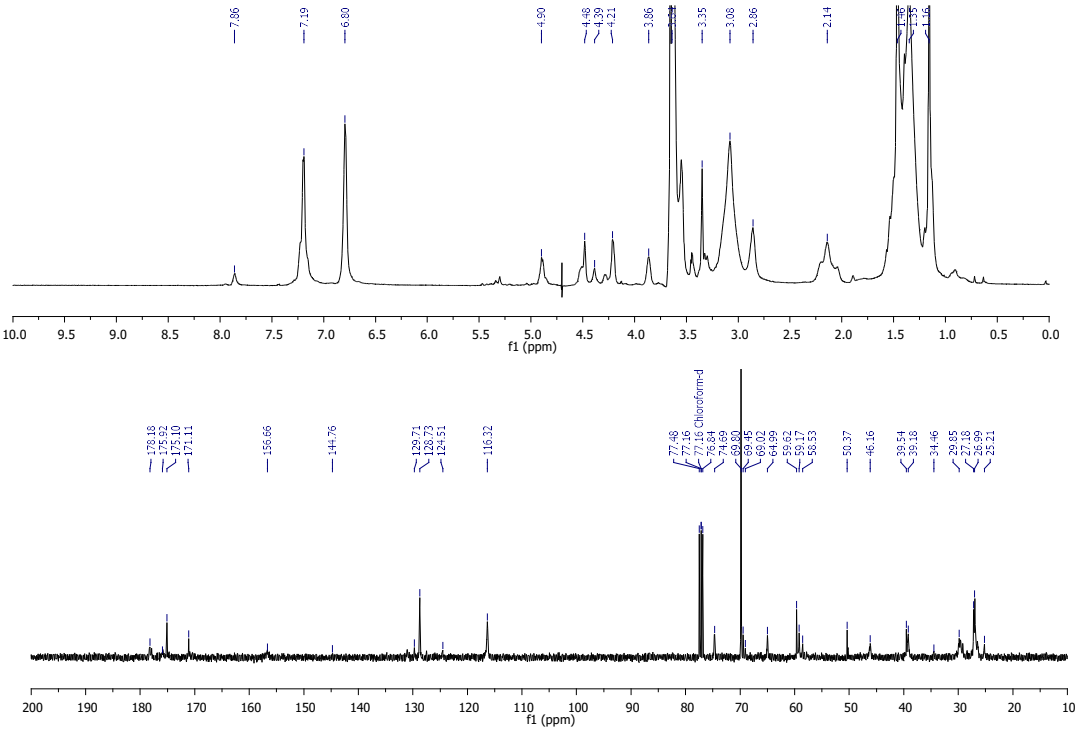

Figure S106. ^{1}H and ^{13}C NMR spectra of compound 104 in D_2O.

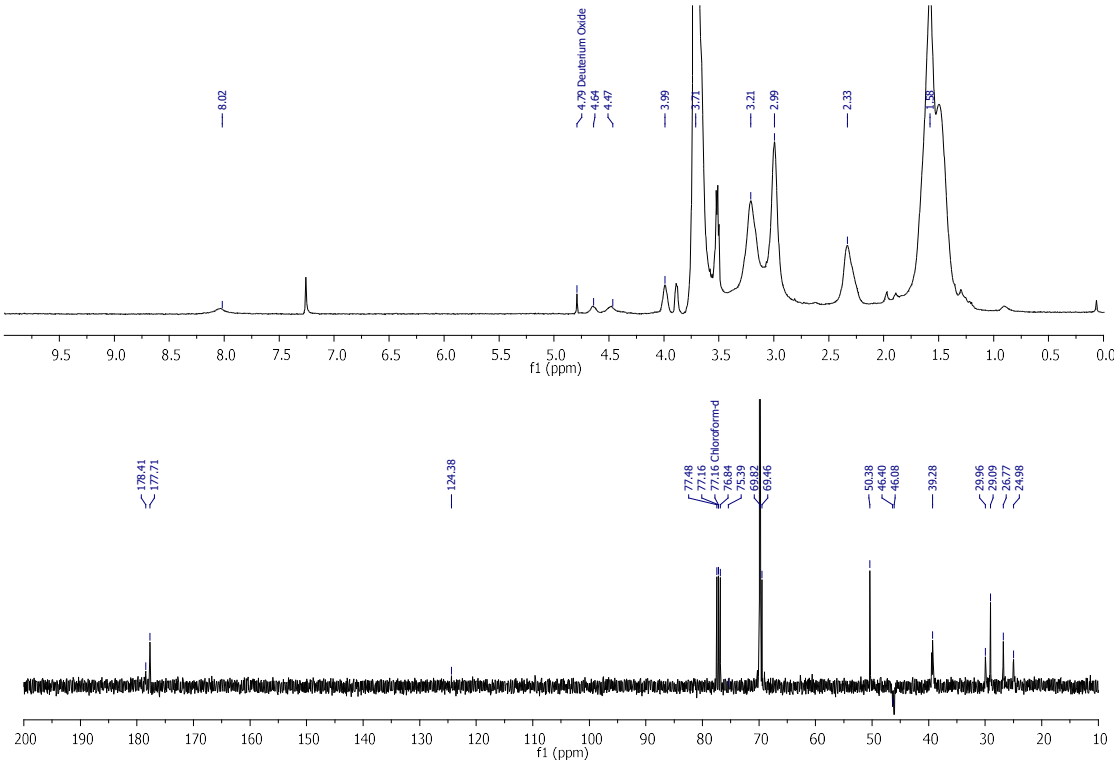

Figure S107. ^{1}H and ^{13}C(SEFT) NMR spectra of compound 105 in D_2O.

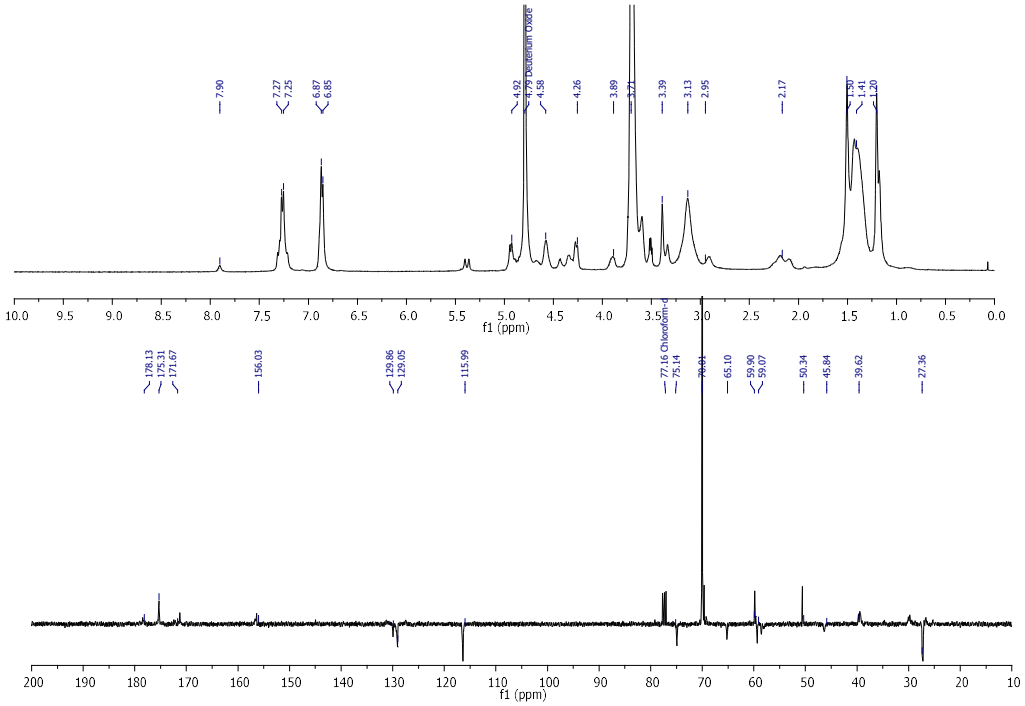

Figure S108. ^{1}H and ^{13}C(SEFT) NMR spectra of compound 106 in D_2O.

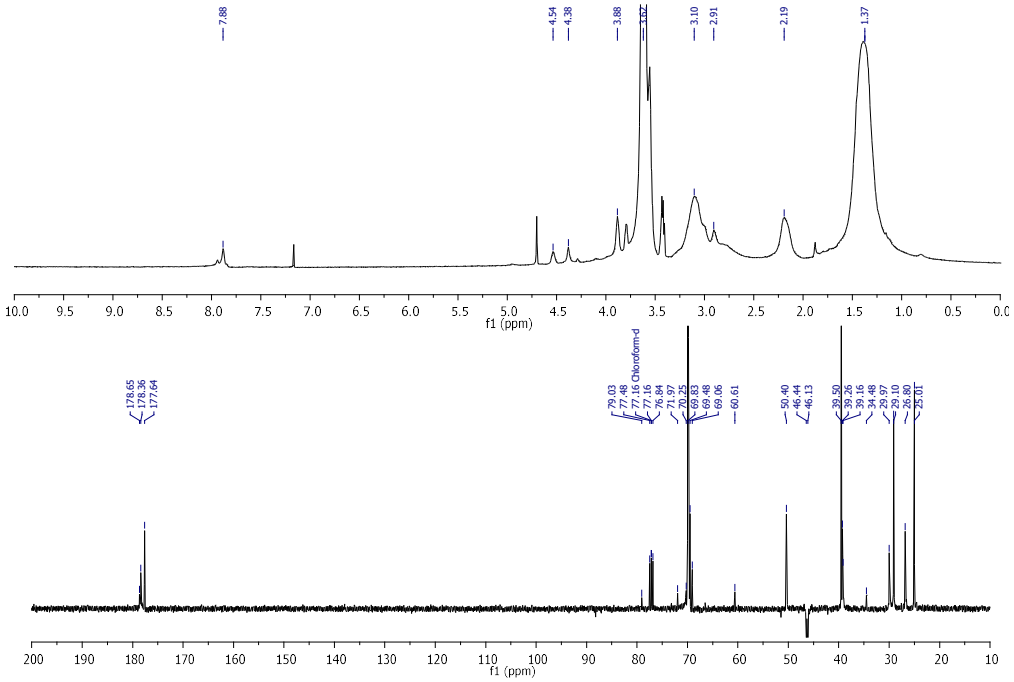

Figure S109. ^{1}H and ^{13}C(SEFT) NMR spectra of compound 107 in D_2O.

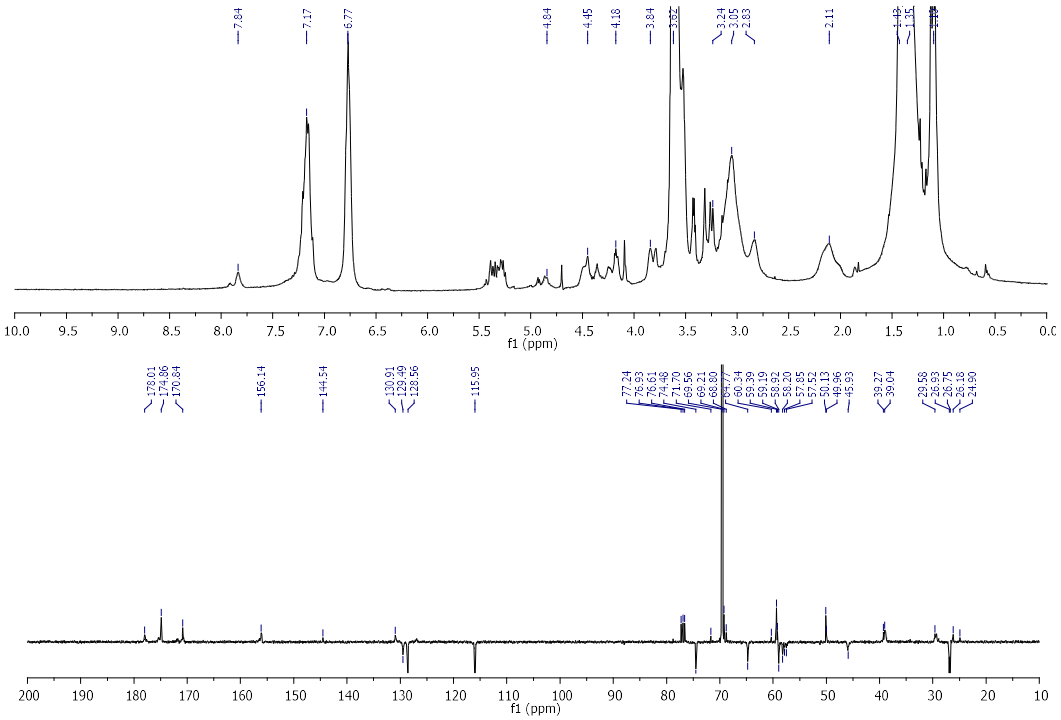

Figure S110. ^{1}H and ^{13}C(SEFT) NMR spectra of compound 108 in D_2O.

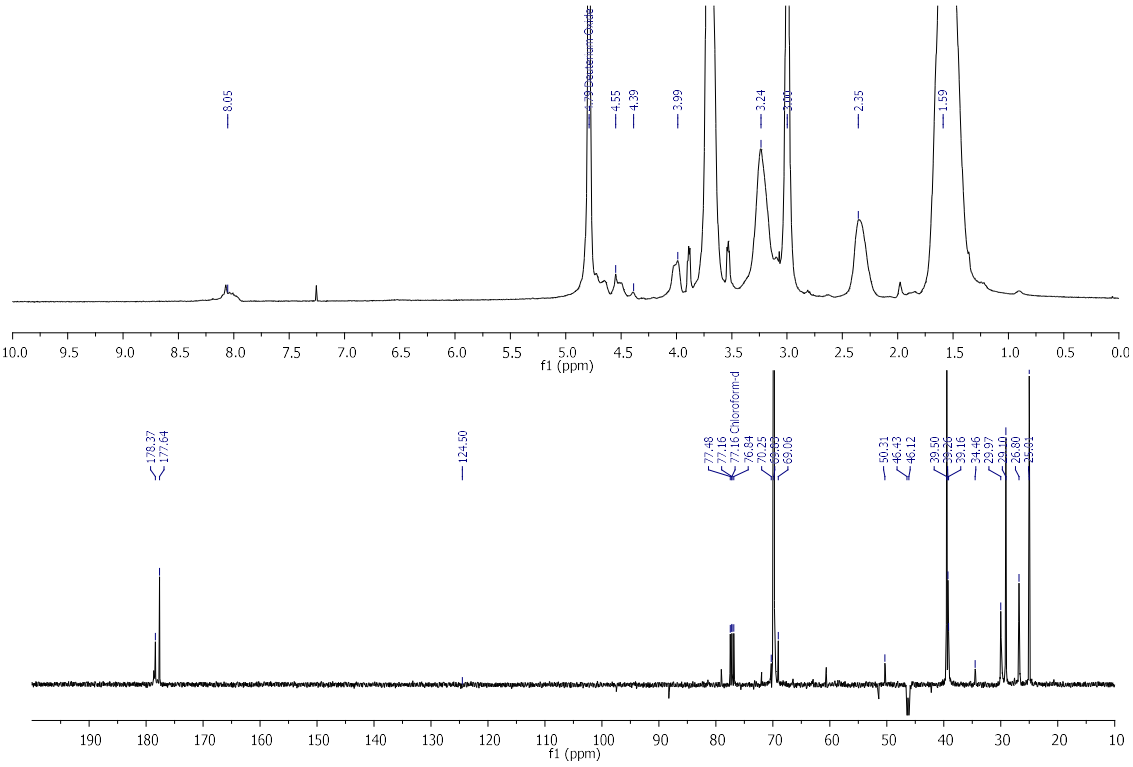

Figure S111. ^{1}H and ^{13}C(SEFT) NMR spectra of compound 109 in D_2O.

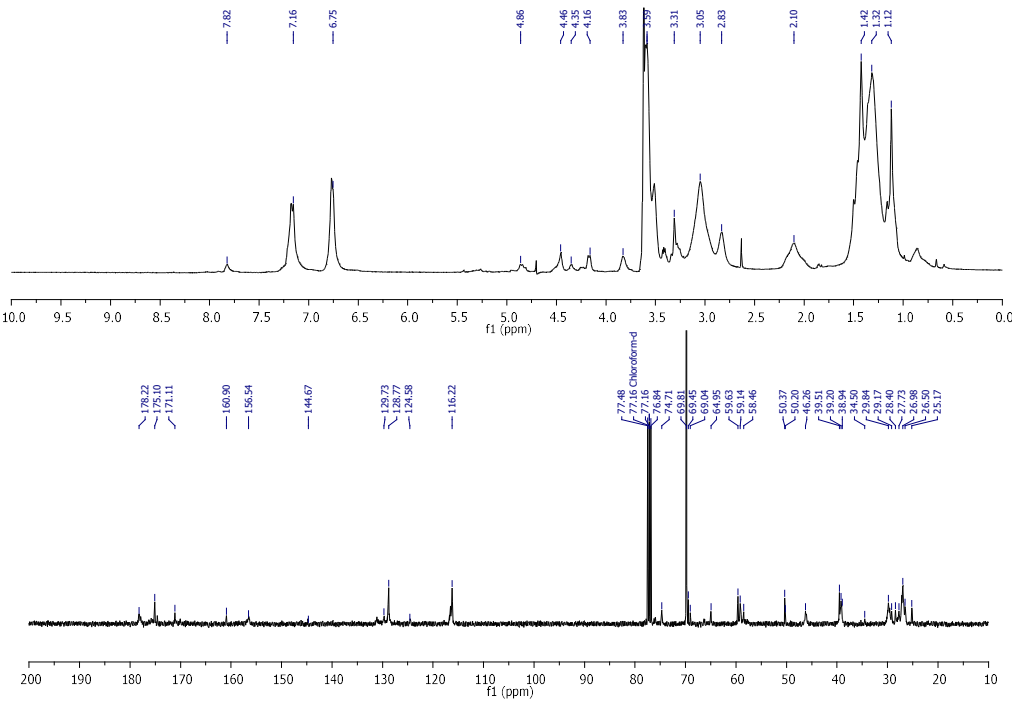

Figure S112. ^{1}H and ^{13}CNMR spectra of compound 110 in D_2O.

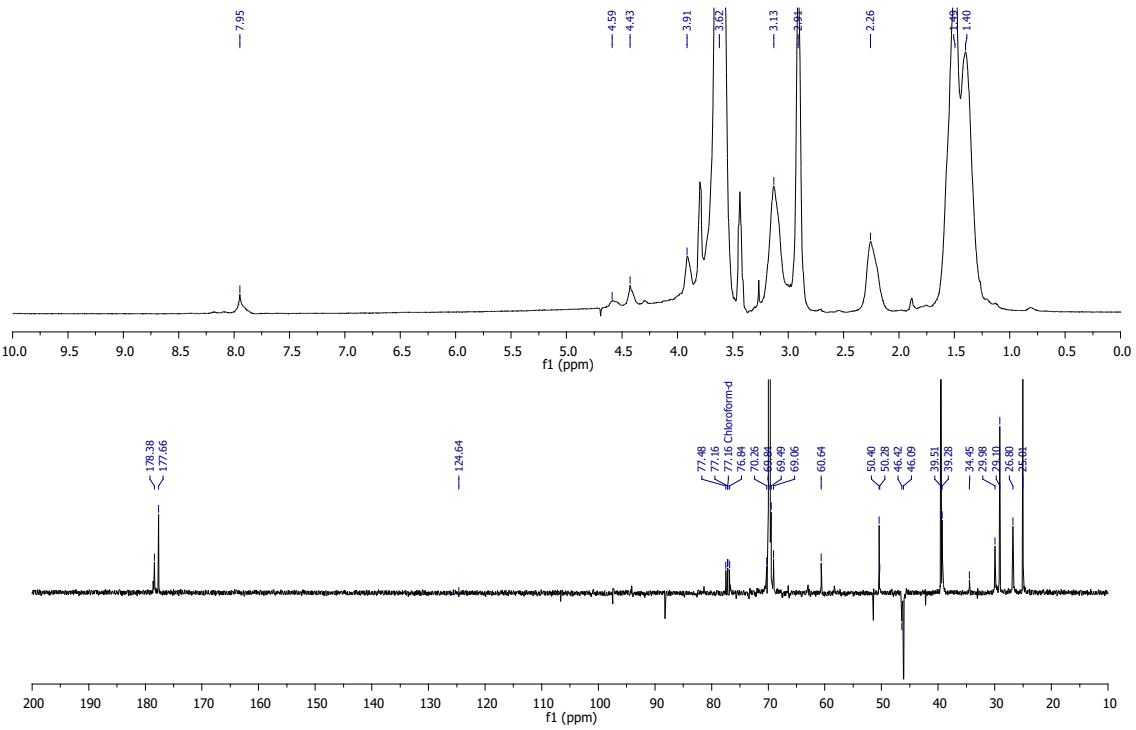

Figure S113. ^{1}H and ^{13}C(SEFT) NMR spectra of compound 111 in D_2O

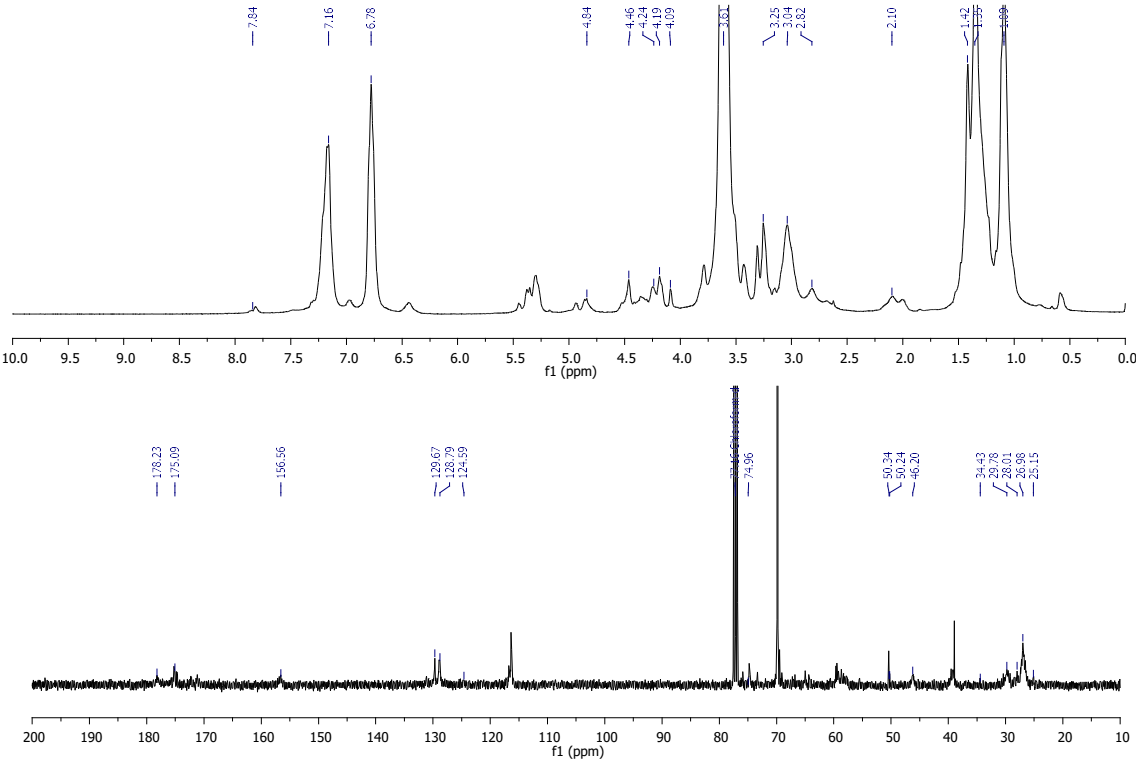

Figure S114. ^{1}H and ^{13}C NMR spectra of compound 112 in D_2O

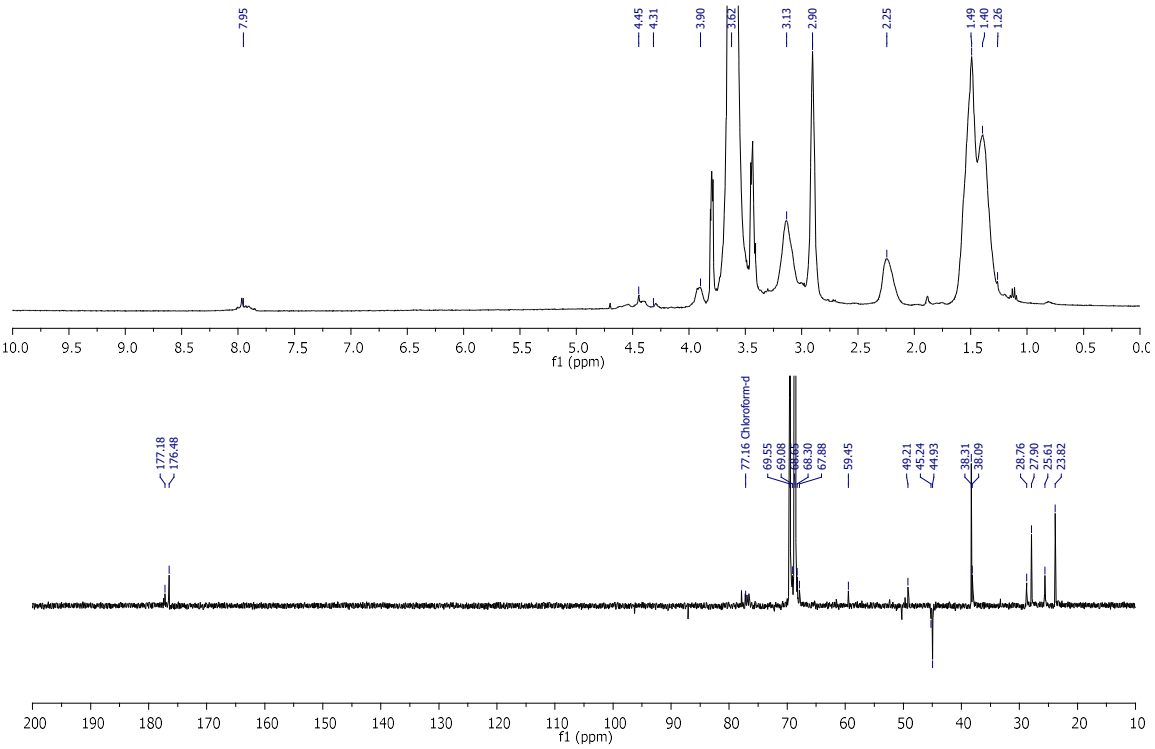

Figure S115. ^{1}H and ^{13}C NMR spectra of compound 113 in D_2O

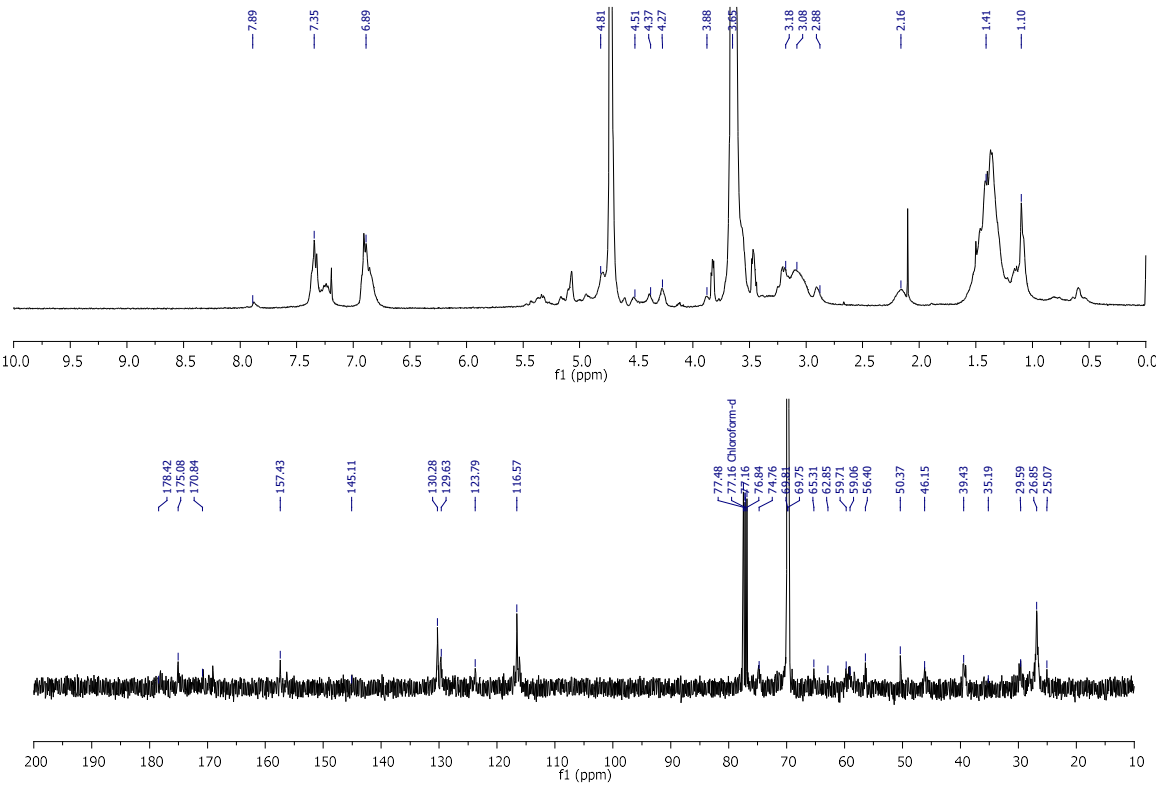

Figure S116. ^{1}H and ^{13}C NMR spectra of compound 114 in D_2O

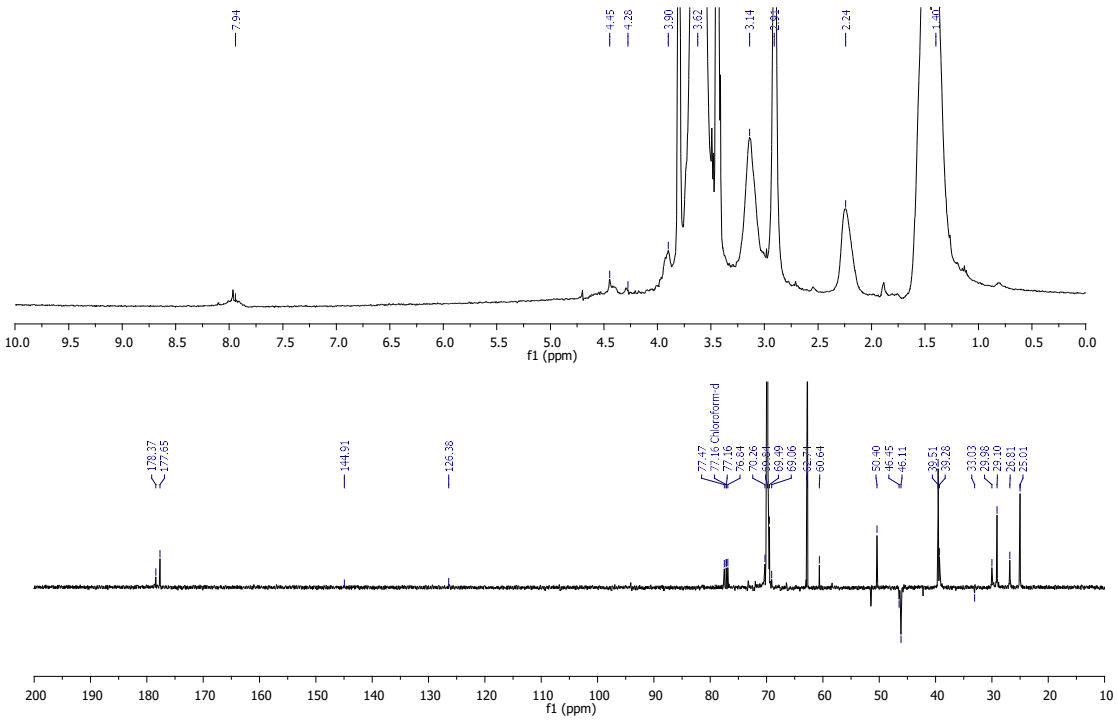

Figure S117. ^{1}H and ^{13}C NMR spectra of compound 115 in D_2O

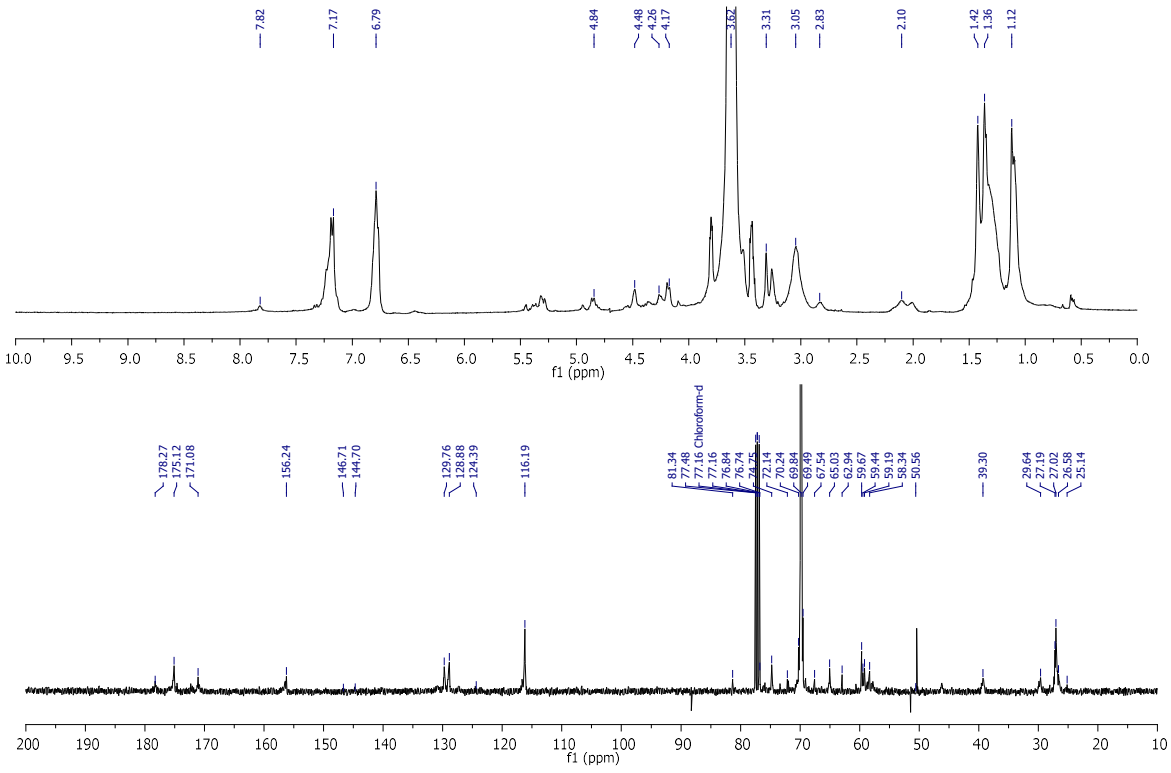

Figure S118. ^{1}H and ^{13}C NMR spectra of compound 116 in D_2O

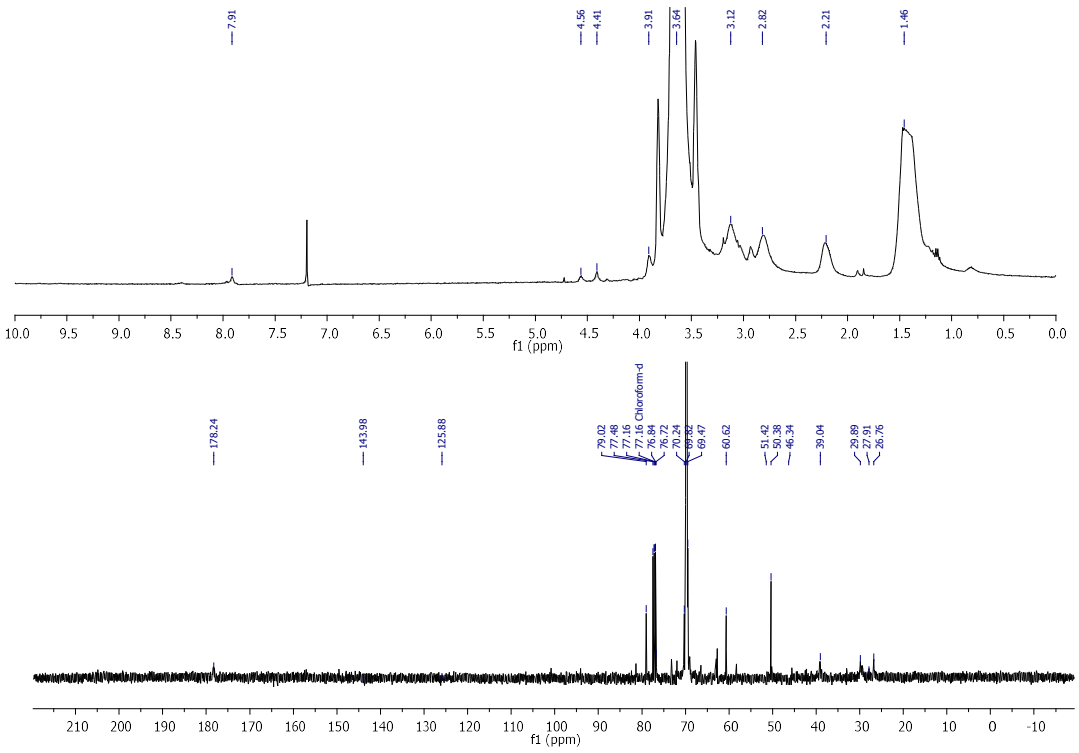

Figure S119. ^{1}H and ^{13}C NMR spectra of compound 117 in D_2O

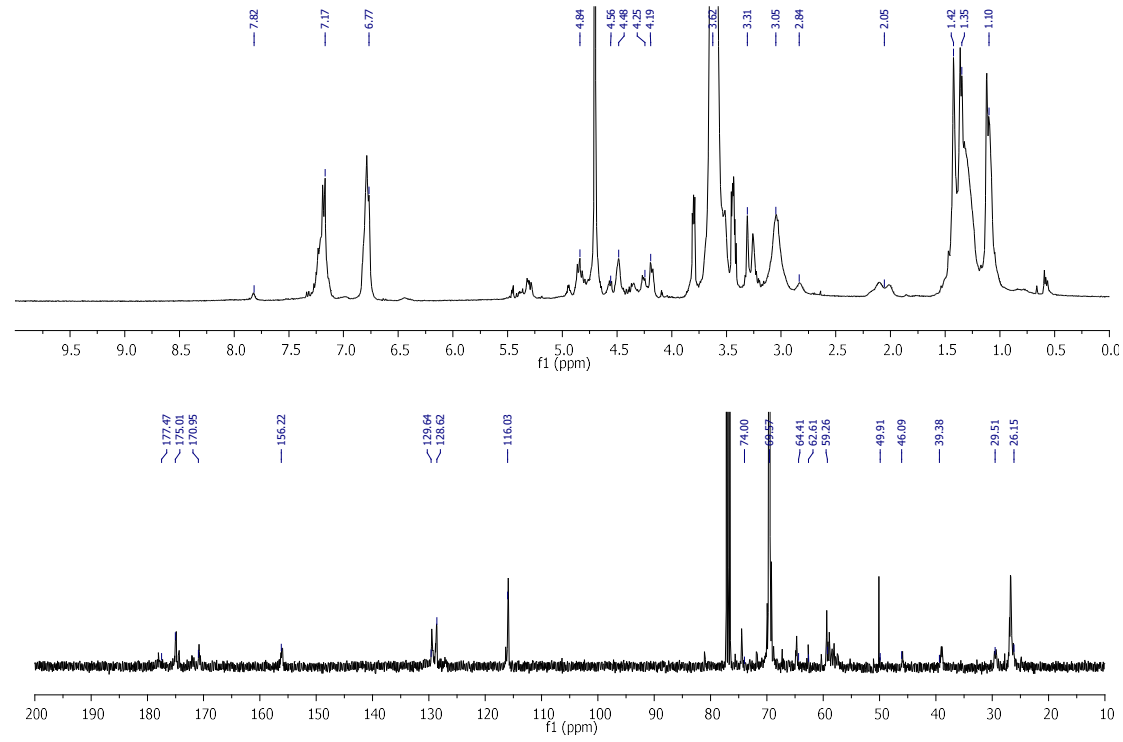

Figure S120. ^{1}H and ^{13}C NMR spectra of compound 118 in D_2O